BaBar Analysis Document #1586, Version 7
October 15, 2007

Global Fit for Branching Fractions of $B \to D^{(*)}\ell\nu$ Decays and Form Factor Slope of $B \to D\ell\nu$ Decays

Kenji Hamano (University of Victoria)
Robert V. Kowalewski (University of Victoria)

Abstract

We present details of our Global fit analysis in $B \to D^{(*,**)}(\pi)\ell\nu$ decays. We use 86×10^6 $B\bar{B}$ events collected by the Babar detector. The primary target of this analysis is to determine the branching fractions and form factor parameters of $B \to D\ell\nu$ and $B \to D^*\ell\nu$ decays and to extract $\mathcal{G}(1)|V_{cb}|$ and $\mathcal{F}(1)|V_{cb}|$.

Main changes from previous version

- More validation study.
  - Effect of Binning.
  - Effect of minimum candidates pere bin.
  - Effect of vertexing.
- In Discussion : Fit with ISGW2 $B \to D\ell\nu$ MC

To Do list

- Effect of $D_1 \to D\pi^+\pi^-$ decays.
- Effect of PHOTOS.
- Effect of Bremsstrahlung.
- Effect of higher X_c states.
  This is a comment from AWG reading "The only model we have until now for $B \to D\pi\pi\ell\nu$ (figure 91 BAD 1364) has a lepton momentum value which extends above 1.5 GeV/c. This is quite a delicate point. We have to understand if we can really extract BF."
- Reconsider PID systematics
- Unblind result on run 1-4 data.
- Quote complete covariance matrices for statistical and systematic errors.

Contents

List of Figures

List of Tables

1 Introduction

The Cabbibo-Kobayashi-Maskawa (CKM) Matrix [1][2] plays an important role in quark mixing and CP violation. The matrix elements of it are free parameters of the Standard Model of particle physics. They need to be determined by experiments. As a B-factory, Babar can measure some of the CKM matrix elements, such as $|V_{ub}|$ and $|V_{cb}|$, in a good precision. To extract $|V_{cb}|$, semileptonic $B \to X_c \ell \nu$ decays have been used. Here, X_c denotes a charmed meson or a particle system including a charmed meson, and ℓ an electron or a muon. Especially two exclusive decay modes, $B \to D^* \ell \nu$ and $B \to D \ell \nu$ have been very useful. A study of these decay modes are also important to measure $|V_{ub}|$ because these are the biggest background of $B \to X_u \ell \nu$ decays. However, there are still unresolved problems in these decay modes such as

- $B^0 \to D^{*-} \ell^+ \nu$ decay [1] branching fraction measurements disagreement.
- Discrepancy between inclusive and sum of exclusive branching fractions.
- $B \to D \ell \nu$ decay form factor slope is not well measured.
- HQET inspired model for $B \to D^{**} \ell \nu$ decays has not been used to evaluate the contribution from these decays.

In existing measurements, each decay mode is reconstructed exclusively to measure branching fractions or form factor parameters. However, the above problems are related with each other and cannot be easily solved by looking at a single decay mode. It is better to look at all semileptonic $B \to D^{(*,**)}(\pi) \ell \nu$ decay modes at the same time. We use a global fit method which simultaneously determine contributions from D, D^* and $D^{**}(D^{(*)}\pi)$. One analysis from Babar [3][4] has similar goals, and can also reconstruct the full set of $B \to D^{(*,**)}(\pi) \ell \nu$ decays. The analysis is complementary because the ability to distinguish among the different channels is better than in our work but the statistics are much lower since they use hadronic B-tag. Another important point of our fitting method is an ability to access form factor parameters. We implement this by Monte Carlo re-weighting method as explained later. Since it is not easy to determine a correct contribution from a decay mode without using a sufficient form factor, an ability to simultaneously measure branching fractions and form factor parameters is essential.

1.1 Problems in $B \to D^{(*,**)}(\pi) \ell \nu$ decays

There are still problems in semileptonic B to charmed meson decays even though many measurements have been done. We list important ones below.

- $B^0 \to D^{*-} \ell^+ \nu$ decay branching fraction measurements disagreement
  There ia s disagreement between $B^0 \to D^{*-} \ell^+ \nu$ decay branching fraction measurements. Those are summarized in Table 1. The results vary from 0.0459 (BELLE) to 0.0609 (CLEO), and those measurements are not consistent with each other.

[1] Charge conjugate modes are implied throughout this text

- Inclusive-exclusive disagreement
  There are mainly 10 exclusive decay modes of the type $B \to X_c \ell \nu$ (see Appendix A)
  - $B \to D\ell\nu$
  - $B \to D^*\ell\nu$
  - $B \to D_0^*\ell\nu$
  - $B \to D_1\ell\nu$
  - $B \to D_1'\ell\nu$
  - $B \to D_2^*\ell\nu$
  - $B \to D\pi^+\ell\nu$ (non-resonant)
  - $B \to D\pi^0\ell\nu$ (non-resonant)
  - $B \to D^*\pi^+\ell\nu$ (non-resonant)
  - $B \to D^*\pi^0\ell\nu$ (non-resonant)

  The D_0^*, D_1, D_1' and D_2^* are called D^{**} as a whole (see Appendix B).
  The sum of the branching fractions of these exclusive decays is supposed to be consistent with the inclusive $B \to X_c\ell\nu$ branching fractions (this X_c denotes a particle system including a charm quark such as D^* or $D\pi$ etc.). Those branching fractions are summarized in Table 2. In this table, non-resonant $B \to D^{(*)}\pi\ell\nu$ decays and $B \to D^{**}\ell\nu$ decays are combined (see Appendix D). The sum of exclusive modes is consistent with the inclusive branching fraction in case of B^+ decays. However, there is a disagreement in B^0 decays. If $\mathcal{B}(B^0 \to D^{*-}\ell^+\nu)$ is as large as to satisfy isospin symmetry with $\mathcal{B}(B^+ \to \bar{D}^{*0}\ell^+\nu)$, the inclusive and exclusive branching fractions agree. Note that the decay modes which include more than 2 pions such as $D^*\pi\pi\ell\nu$ mode or include D_s such as $D_sK\ell\nu$ mode are not included in the table; however, those contributions are expected to be too small [13] to explain the inclusive exclusive difference.

- $B \to D\ell\nu$ decay form factor slope and $G(1)|V_{cb}|$
  $B \to D\ell\nu$ decay form factor slope, ρ_D^2 (see Appendix H), has never been well measured. Existing measurements are listed in Table 3. The best measurement from BELLE has a 23 % uncertainty. Consequently, the uncertainty on $G(1)|V_{cb}|$ is much larger than $F(1)|V_{cb}|$. More precise measurement is necessary also to address the above issues.

- HQET inspired model for $B \to D^{**}\ell\nu$ decays.
  HQET inspired model for $B \to D^{**}\ell\nu$ decays (see Appendix H) is to describe these decays better. But, the HQET model has not been used in existing measurements.

In this analysis, we address these problems. We use a global fit technique to determine relative exclusive branching fractions, $\mathcal{B}(B \to D\ell\nu)$, $\mathcal{B}(B \to D^*\ell\nu)$ and

Branching Fraction	Experiment (year)	Decay mode
$0.0459 \pm 0.0023 \pm 0.0040$	BELLE (2002) [6]	$B^0 \to D^{*-}\ell^+\nu$
$0.0470 \pm 0.0013^{+0.0036}_{-0.0031}$	DELPHI (2001) [7]	$B^0 \to D^{*-}\ell^+\nu$
$0.0490 \pm 0.0007^{+0.0036}_{-0.0035}$	BABAR (2005) [8]	$B^0 \to D^{*-}\ell^+\nu$
$0.0526 \pm 0.0020 \pm 0.0046$	OPAL (2000) [9]	$B^0 \to D^{*-}\ell^+\nu$
$0.0553 \pm 0.0026 \pm 0.0052$	ALEPH (1997) [10]	$B^0 \to D^{*-}\ell^+\nu$
$0.0590 \pm 0.0022 \pm 0.0050$	DELPHI (2004) [11]	$B^0 \to D^{*-}\ell^+\nu$
$0.0609 \pm 0.0019 \pm 0.0040$	CLEO (2003) [12]	$B^0(B^+) \to D^{*-}(\bar{D}^{*0})\ell^+\nu$

Table 1: [$B^0 \to D^*\ell\nu$ **BF**] $B^0 \to D^{*-}\ell^+\nu$ branching fractions from different experiments. The first uncertainty is statistical and the second one is systematic. In the most right column, the decay modes measured in each analysis are listed. Only CLEO (2003) measured both $B^0 \to D^{*-}\ell^+\nu$ and $B^+ \to \bar{D}^{*0}\ell^+\nu$ modes.

$\mathcal{B}(B \to D^{**}\ell\nu) + \mathcal{B}(B \to D^{(*)}\pi\ell\nu)$, and form factor parameters of $B \to D\ell\nu$ and $B \to D^*\ell\nu$ decays. Using these results along with $\mathcal{G}(1)$ and $\mathcal{F}(1)$, we can also extract $|V_{cb}|$ as explained in section 16. We do not explicitly reconstruct D^* or D^{**}. Thus, we do not have to rely on slow pion reconstruction. We also do not have to determine the efficiency to reconstruct and detect a specific decay mode, wich is usually done by Monte Carlo simulation (MC). This is a different approach from the existing measurements listed above. We, however, depend on MC to construct the probability density functions (PDF) to be used in the fit. Details of our fit technique is explained in section 3. Since we use a different approach, our results are useful to address the above problems.

1.2 Structure of this document

- Section 2 : **Signals and Backgrounds**
  Events or decay modes in the signals and backgrounds are explained.

- Section 3 to 5 : **Fitting Method**
  Overview of our fitting method is described in section 3.
  Detailed description of the coefficients in our fit is in section 4.
  The constraints we apply in the fit is discussed in section 5.

- Section 6 : **Event Selection**
  The data set used in this analysis and selection methods to extract $B \to D^{(*,**)}(\pi)\ell\nu$ events are explained.

- Section 7 : **Tracking Efficiency and PID corrections**
  The effect of Tracking Efficiency and PID corrections are shown.

Decay mode (B^+)	Branching Fraction (%)	Reference
$B^+ \to \bar{D}^0\ell^+\nu$	2.15 ± 0.22	[13]
$B^+ \to \bar{D}^{*0}\ell^+\nu$	6.5 ± 0.5	[13]
$B^+ \to D^-\pi^+\ell^+\nu$	0.53 ± 0.10	[13]
$B^+ \to \bar{D}^0\pi^0\ell^+\nu$	0.265 ± 0.05	Isospin symmetry
$B^+ \to D^{*-}\pi^+\ell^+\nu$	0.64 ± 0.15	[13]
$B^+ \to \bar{D}^{*0}\pi^0\ell^+\nu$	0.32 ± 0.075	Isospin symmetry
Sum of exclusive modes	10.41 ± 0.61	
Inclusive $B^+ \to X_c\ell^+\nu$	10.97 ± 0.65	section 15
Decay mode (B^0)	Branching Fraction (%)	Reference
$B^0 \to D^-\ell^+\nu$	2.13 ± 0.18	[13]
$B^0 \to D^{*-}\ell^+\nu$	5.20 ± 0.24	[13]
$B^0 \to \bar{D}^0\pi^-\ell^+\nu$	0.32 ± 0.095	[13]
$B^0 \to D^-\pi^0\ell^+\nu$	0.16 ± 0.0475	Isospin symmetry
$B^0 \to \bar{D}^{*0}\pi^-\ell^+\nu$	0.65 ± 0.16	[13]
$B^0 \to D^{*-}\pi^0\ell^+\nu$	0.325 ± 0.08	Isospin symmetry
Sum of exclusive modes	8.79 ± 0.41	
Inclusive $B^0 \to X_c\ell^+\nu$	10.25 ± 0.60	section 15

Table 2: [**Exclusive-Inclusive comparison**] Branching fractions of $B \to X_c\ell\nu$ type of decays. $B \to D^{(*)}\pi\ell\nu$ decays include not only non-resonant $B \to D^{(*)}\pi\ell\nu$ decays but also $B \to D^{**}\ell\nu$ decays.

ρ_D^2	Experiment (year)	Decay mode
$0.97 \pm 0.98 \pm 0.38$	ALEPH (1997) [10]	$B^0 \to D^-\ell^+\nu$
$1.12 \pm 0.22 \pm 0.14$	BELLE (2002) [14]	$B^0 \to D^-\ell^+\nu$
$1.27 \pm 0.25 \pm 0.14$	CLEO (1999) [15]	$B^0 \to D^-\ell^+\nu$ and $B^+ \to \bar{D}^0\ell^+\nu$

Table 3: [$B \to D\ell\nu$ **FF slope**] Form factor slope ρ_D^2 from different experiments. The first uncertainty is statistic and the second one is systematic.

- Section 8 to 10 : **Monte Carlo Re-weighting**
  Overview of our Monte Carlo (MC) re-weighting method and Branching Fraction (BF) re-weighting is described in section 8.
  $B \to D^{(*,**)}(\pi)\ell\nu$ Form Factor (FF) re-weighting method is shown in section 9.
  The method to perform FF parameter fitting is explained in section 10.

- Section 13 : **Fit Result**
  Our fit result and discussion is given.

- Section 11 : **Fit Validation**
  Fit validation is done using MC. Validation fit results are shown.

- Section 15 : **Branching Fraction Re-normalization**
  The method to re-normalize fitted BFs to a measured inclusive BF is shown.

- Section 16 : **Calculation of $\mathcal{G}(1)|V_{cb}|$ and $\mathcal{F}(1)|V_{cb}|$**
  Calculation of $\mathcal{G}(1)|V_{cb}|$ and $\mathcal{F}(1)|V_{cb}|$ is shown.

- Section 17 : **Systematic Uncertainty**
  The results of systematic study is explained.

- Section 18 : **Full Covariance Matrix**
  We give full covariance matrix to keep track of correlations.

- Section 19 : **Discussions**
  We compare our results with previous Babar measurements.

- Section 20 : **Conclusion**
  We summarize our final results.

Appendix

- Appendix A : B decay modes
- Appendix B : Classification of D^{**}
- Appendix C : Isospin symmetry
- Appendix D : Values in MC and Fit
- Appendix E : BToDlnu skims
- Appendix F : $\cos\theta_{BY}$
- Appendix G : Velocity transfer w
- Appendix H : Form Factors of $B \to D^{(*,**)}X\ell\nu$ decays

2 Signal and Background Events

2.1 Signal

We are interested in $B \to D^{(*,**)}(\pi)\ell\nu$ decays. We reconstruct either D^0 or D^+ and a lepton (electron or muon) to form a Dl candidate as a candidate of a B meson. We do not explicitly reconstruct D^* or D^{**}. However, we can access those higher charmed meson states because, as described in Appendix A, D^* and D^{**} eventually decay into either D^0 or D^+. We separate decay modes into two categories: the decay modes to produce D^0 and the ones to produce D^+. Contributions of each component can be seen in Fig 1.

2.1.1 D^0 modes

The decay processes to produce D^0 are

- $B^+ \to \bar{D}^0\ell^+\nu$
- $B^+ \to \bar{D}^{*0}\ell^+\nu$ with $\bar{D}^{*0} \to \bar{D}^0\pi^0$ or $\bar{D}^{*0} \to \bar{D}^0\gamma$
- $B^0 \to D^{*-}\ell^+\nu$ with $D^{*-} \to \bar{D}^0\pi^-$
- $B^+ \to \bar{D}^{**0}\ell^+\nu$ with $\bar{D}^{**0} \to D^0\pi^0$
  $B^+ \to \bar{D}^{**0}\ell^+\nu$ with $\bar{D}^{**0} \to D^{*0}\pi^0$ and $D^{*0} \to \bar{D}^0\pi^0$ or $D^{*0} \to \bar{D}^0\gamma$
  $B^+ \to \bar{D}^{**0}\ell^+\nu$ with $\bar{D}^{**0} \to D^{*-}\pi^+$ and $D^{*-} \to \bar{D}^0\pi^-$
- $B^0 \to D^{**-}\ell^+\nu$ with $D^{**-} \to \bar{D}^0\pi^-$
  $B^0 \to D^{**-}\ell^+\nu$ with $D^{**-} \to \bar{D}^{*0}\pi^-$ and $\bar{D}^{*0} \to \bar{D}^0\pi^0$ or $\bar{D}^{*0} \to \bar{D}^0\gamma$
  $B^0 \to D^{**-}\ell^+\nu$ with $D^{**-} \to D^{*-}\pi^0$ and $D^{*-} \to \bar{D}^0\pi^-$
- $B^+ \to \bar{D}^0\pi^0\ell^+\nu$
- $B^0 \to \bar{D}^0\pi^-\ell^+\nu$
- $B^+ \to \bar{D}^{*0}\pi^0\ell^+\nu$ with $\bar{D}^{*0} \to \bar{D}^0\pi^0$ or $\bar{D}^{*0} \to \bar{D}^0\gamma$
  $B^+ \to D^{*-}\pi^+\ell^+\nu$ with $D^{*-} \to \bar{D}^0\pi^-$
- $B^0 \to \bar{D}^{*0}\pi^-\ell^+\nu$ with $\bar{D}^{*0} \to \bar{D}^0\pi^0$ or $\bar{D}^{*0} \to \bar{D}^0\gamma$
  $B^0 \to D^{*-}\pi^0\ell^+\nu$ with $D^{*-} \to \bar{D}^0\pi^-$

2.1.2 D^+ modes

The decay processes to produce D^+ are

- $B^0 \to D^-\ell^+\nu$
- $B^0 \to D^{*-}\ell^+\nu$ with $D^{*-} \to D^-\pi^0$ or $D^{*-} \to D^-\gamma$
- $B^0 \to D^{**-}\ell^+\nu$ with $D^{**-} \to D^-\pi^0$
  $B^0 \to D^{**-}\ell^+\nu$ with $D^{**-} \to D^{*-}\pi^0$ and $D^{*-} \to D^-\pi^0$ or $D^{*-} \to D^-\gamma$

- $B^+ \to \bar{D}^{**0}\ell^+\nu$ with $\bar{D}^{**0} \to D^-\pi^+$
  $B^+ \to \bar{D}^{**0}\ell^+\nu$ with $\bar{D}^{**0} \to D^{*-}\pi^+$ and $D^{*-} \to D^-\pi^0$ or $D^{*-} \to D^-\gamma$
- $B^0 \to D^-\pi^0\ell^+\nu$
- $B^+ \to D^-\pi^+\ell^+\nu$
- $B^0 \to D^{*-}\pi^0\ell^+\nu$ with $D^{*-} \to D^-\pi^0$ or $D^{*-} \to D^-\gamma$
- $B^+ \to D^{*-}\pi^+\ell^+\nu$ with $D^{*-} \to D^-\pi^0$ or $D^{*-} \to D^-\gamma$

2.2 Backgrounds

Backgrounds are categorized as described in the following subsections. Contributions of each component can be seen in Fig 1. Some of backgrounds are non-peaking backgrounds in D mass plots and almost disappear after D mass sideband subtraction. However, some are peaking backgrounds and remain after D mass sideband subtraction as can be seen in Figure 13 - 15 in section 6. D mass sidebands are defined in section 6.5.

2.2.1 UncorrDL : peaking background from $B\bar{B}$

D and ℓ come from different B (Uncorrelated), and ℓ come directly from B (DL = Direct Lepton).
For B^+, 80 % of this background is the following $B \to D\bar{D}$ type :

- $B^+ \to \bar{D}^0\ell^+\nu$
- $B^- \to D^{(*)0}D^{*-}K^0$ with $D^{*-} \to D^-\pi^0$ or $D^{*-} \to D^-\gamma$

These ℓ^+ from B^+ and D^- from B^- form a Dl candidate. 17 % is doubly Cabbibo suppressed D decays and this D is reconstructed as $\bar{D}$.
For B^0, there is another main contribution from $B^0\bar{B}^0$ mixing. Thus, for B^0, 40 % is the above $B \to D\bar{D}$ type and 50 % is $B^0\bar{B}^0$ mixing.

2.2.2 UncorrCL : peaking background from $B\bar{B}$

D and ℓ come from different B (Uncorrelated), and ℓ does not directly come from B (CL = Cascade Lepton).
90 % of this background is semileptonic D decays such as

- $B^+ \to \bar{D}^0 X_1$
- $B^- \to D^0 X_2$ with $D^0 \to K^-\ell^+\nu$

These $\bar{D}^0$ from B^+ and ℓ^+ from $B^-(D^0)$ form a Dl candidate.

2.2.3 CascL : peaking background from $B\bar{B}$

D and ℓ come from same B (Correlated), and ℓ does not directly come from B (Cascade Lepton)
50 % comes from the following type of decays

- $B^+ \to \bar{D}^0 D^{*0} K^+$
  with $\bar{D}^0 \to K^+ \ell^- \bar{\nu}$ and $D^{*0} \to D^0 \pi^0$

These ℓ^- and D^0 form a Dl candidate.
45 % of this background is $B \to X\tau\nu$ type. For example,

- $B^+ \to \bar{D}^0 \tau^+ \bar{\nu}$
  with $\tau^+ \to \mu^+ \bar{\nu}_\mu \nu_\tau$

These $\bar{D}^0$ and μ^+ form a Dl candidate.

2.2.4 FakeL : peaking background from $B\bar{B}$

The lepton in a Dl candidate is a mis-identified K, π or p.
90 % of mis identification is between μ and π.
We do not float this component in the fit.

2.2.5 CombRL : non-peaking background from $B\bar{B}$

Combinatorial background from $B\bar{B}$ events. This is the case that reconstructed D is not real. Typical mis-reconstructions are that the kaon and the pion do not come from same D or not directly come from D. In our analysis, D^0 has much less combinatorial background than D^+ because D^0 is reconstructed from two particles (one K and one π) whereas D^+ is reconstructed from three particles (one K and two π) (see section 6.1.1).
This component almost disappear after D mass sideband subtraction. Thus, we do not float this component in the fit.

2.2.6 CombFL : non-peaking background from $B\bar{B}$

D is mis-reconstructed (Combinatorial) and ℓ is mis-identified (Fake Lepton).
This component almost disappear after D mass sideband subtraction. Thus, we do not float this component in the fit.

2.2.7 OffPeak : OffPeak data

OffPeak data. The main contribution to OffPeak data is $c\bar{c}$, $s\bar{s}$, $u\bar{u}$, $d\bar{d}$ and $\tau^+\tau^-$ events. This can be separated into two category : continuum background and "$c\bar{c}$ with true D" background. Continuum background can be subtracted out by D mass sideband subtraction. "$c\bar{c}$ with true D" background is a peaking background in the D mass distribution and does not disappear after sideband subtraction.

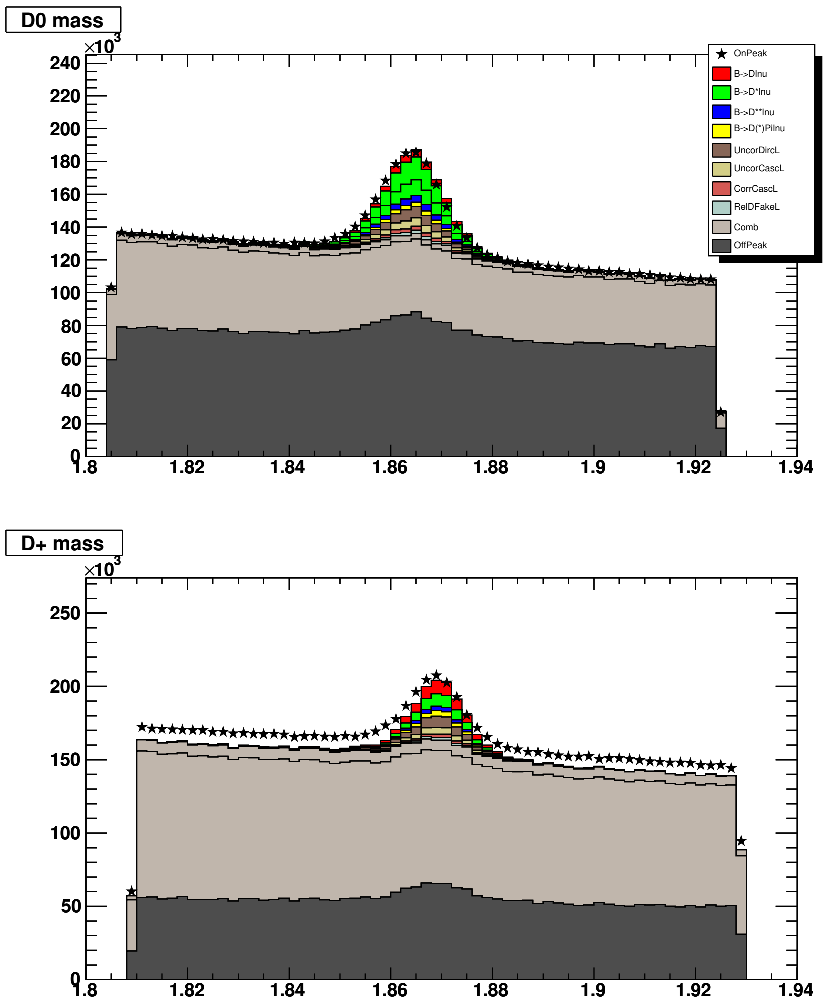

Figure 1: **(Run2 only)** [D **mass plot**] D mass plot before applying selection cuts. The top is D^0 and the bottom is D^+. Star is OnPeak data. Red is $B \to D\ell\nu$, green is $B \to D^*\ell\nu$, blue is $B \to D^{**}\ell\nu$, yellow is non-resonant $B \to D^{(*)}\pi\ell\nu$, and the rest is background. Dark brown is UncorrDL, light brown is UncorrCL, dark red is CascL, blue gray is FakeL, light gray is Comb, and dark gray is OffPeak. The data-MC difference in D^+ case is mainly because D^+ require one more chaged track to reconstruct. Details are in section 6.5

3 Fitting Method

We use binned χ^2 fitting.

3.1 Binning (i)

We use 3D binning by three variables :

- lepton momentum in the CM frame p^*_ℓ
  (7 bins (GeV)) : 0.8, 1.05, 1.3, 1.55, 1.8, 2.05, 2.3, 2.55
- D momentum in the CM frame p^*_D
  (5 bins (GeV)) : 0, 0.5, 1, 1.5, 2.0, 2.5
- $\cos\theta_{B-Dl}$ (see Appendix F)
  (5 bins) : -20, -5.5, -2, 0, 2, 10

The reason of this choice is the following :

- There are only three independent variables.
  In the $B \to D\ell\nu$ decays, there are only three independent kinematic variables. For example, in Figure 57, supposing D^* is D and does not decay, independent variables can be
  - The magnitude of lepton momentum
  - The magnitude of D momentum
  - The angle θ_ℓ

  because χ and θ_V are irrelevant. The same is true also in other decay modes when we reconstruct only $D\ell$. We chose three variables, p^*_ℓ, p^*_D and $\cos\theta_{B-Dl}$, because this combination is simple, well known and useful to separate each signal decay modes and backgrounds. As you can see from Figures 13-15 in section 6, the shape of the histogram of each MC mode is quite different. We also tried $\cos\theta_{D-\ell}$ (the cosine of the angle between D and ℓ in the CM frame) instead of $\cos\theta_{B-Dl}$ to assure that $\cos\theta_{B-Dl}$ is a better parameter.
- Choice of binning.
  The binning is decided in the valance of two opposing requirements :
  - It needs to be as fine as possible to preserve the shape of original distribution.
  - It needs to be as coarse as necessary to have a good statistics per bin.

  The binning of p^*_ℓ is finer to get finer lepton spectrum. Then we can compare our fit result with the lepton spectrum of existing measurements. Details of $\cos\theta_{B-Dl}$ binning are explained in section 14.4.1. The effect of binning on fit results are discussed in section 14.4.2.

3.2 χ^2

The χ^2 is given by

$$\chi^2 = \sum_{i=\text{bin}}^{D^0} \frac{(N_i^{OnPeak} - N_i^{OffPeak} - \sum_j C_j^{MC} N_{ij}^{MC})^2}{(\sigma_i^{OnPeak})^2 + (\sigma_i^{OffPeak})^2 + \sum_j (C_j^{MC}\sigma_{ij}^{MC})^2} + \sum_{i=\text{bin}}^{D^+} \frac{(N_i^{OnPeak} - N_i^{OffPeak} - \sum_j C_j^{MC} N_{ij}^{MC})^2}{(\sigma_i^{OnPeak})^2 + (\sigma_i^{OffPeak})^2 + \sum_j (C_j^{MC}\sigma_{ij}^{MC})^2} \quad (1)$$

where,

- i represents each bin
- j represents each MC mode.

MC modes are listed in section 4 separately for D^0 and D^+ modes. See also Appendix A and section 2.
Quantities in the χ^2 are:

- N_i^{OnPeak}
  The number of OnPeak data candidates in the i-th bin.
- $N_i^{OffPeak}$
  The number of OffPeak data candidates in the i-th bin, luminosity normalized to OnPeak data.
- N_{ij}^{MC}
  The number of j-th MC mode candidates in the i-th bin, luminosity normalized to OnPeak data. Details are in section 3.3. The effect of data MC differences from tracking and PID are corrected (see section 7). MC re-weighting is also done. We can fit for form factor parameters through MC re-weighting (see sections 8 and 9)
- C_j^{MC}
  The coefficient of each MC mode (j). These include branching fractions to be determined in the fit. Details are in section 4.
- σ_i^{OnPeak}
  The statistical uncertainty of N_i^{OnPeak}. $\sigma_i^{OnPeak} = \sqrt{N_i^{OnPeak}}$.
- $\sigma_i^{OffPeak}$
  The statistical uncertainty of $N_i^{OffPeak}$. Details are in section 3.4.
- σ_{ij}^{MC}
  The statistical uncertainty of N_{ij}^{MC}. Details are in section 3.4.

We use bins which have more than 10 expected candidates

$$\sum_j C_j^{MC} N_{ij}^{MC} > 10 \quad (2)$$

and neglect other bins. The number 10 can be changed for systematic study.

3.3 Number of MC Candidates N_{ij}^{MC}

We calculate the number of candidates from MC using MC truth information. We use five generic MC samples: BpBm, B0B0bar, ccbar, uds and tautau. Note that ccbar, uds and tautau MCs are used only for validation of the fit. Tracking efficiency and PID corrections are applied to adjust MC to OnPaek data (see section 7). MCs are also luminosity normalized to OnPeak data.

3.3.1 Luminosity normalization

All MC and OffPeak data are normalized to OnPeak data by luminosity. Supposing OnPeak luminosity is $\mathcal{L}^{OnPeak}$ and MC (mode j) luminosity is $\mathcal{L}_j^{MC}$, the normalization factor r_j^{Lumi} is given by

$$r_j^{Lumi} = \frac{\mathcal{L}^{OnPeak}}{\mathcal{L}_j^{MC}} \tag{3}$$

where the luminosity of $B\bar{B}$ MC is calculated by the generated number of events and B counting number from OnPeak data. For the luminosity of ccbar, uds and tautau MC, their cross sections are used. Details are in Appendix E. Note that depending on the given MC mode j, luminosity is given. For example, when j=1,2,6,8,etc., $\mathcal{L}_j^{MC}$ is the luminosity of BpBm MC and when j=3,5,7,9,etc., $\mathcal{L}_j^{MC}$ is the luminosity of B0B0bar MC (see section 4 for details of MC modes j).
Note that, the luminosity calculation was done based on the assumption that produced number of B^+B^- and $B^0\bar{B}^0$ are equal. The decay rate difference is taken into account in the coefficients (see section 4).
In case of OffPeak data, since OffPeak data is taken at 40 MeV lower energy than OnPeak data, we need to correct for $1/s$ dependence of cross section, where s is the square of CM energy :

$$\begin{aligned} s_{OnPeak} &= 10.58^2 \ \text{GeV} \\ s_{OffPeak} &= (10.58 - 0.04)^2 = 10.54^2 \ \text{GeV} \end{aligned} \tag{4}$$

Thus, correction factor is

$$r_{OffPeak}^{Lumi} = \frac{\mathcal{L}^{OnPeak} s_{OffPeak}}{\mathcal{L}^{OffPeak} s_{OnPeak}} \tag{5}$$

3.3.2 N_{ij}^{MC}

The number of MC candidates N_{ij}^{MC} is given by

$$N_{ij}^{MC} = r_j^{Lumi} \sum_k r_k^{Trk} r_k^{KPID} r_k^{LPID} W_{jk}^{MC} \tag{6}$$

where

- k represents the k-th candidate in i-th bin and MC mode j.

and

- r_k^{Trk} is the tracking efficiency correction factor (⇒ section 7)
- r_k^{KPID} is the kaon PID correction factor (⇒ section 7)
- r_k^{LPID} is the lepton PID correction factor (⇒ section 7)
- W_{jk}^{MC} is the MC weight (⇒ sections 8 and 9)

Tracking efficiency and PID corrections are described in section 7. MC weights are described in sections 8 and 9.

3.4 Statistical uncertainty $\sigma_i^{OffPeak}$ and σ_{ij}^{MC}

Statistical uncertainty of OnPeak data is given by

$$\sigma_i^{OnPeak} = \sqrt{N_i^{OnPeak}} \tag{7}$$

However, since statistical uncertainty of OffPeak data and MCs are luminosity normalized and re-weighted, statistical uncertainties are not simply given by $\sigma_i = \sqrt{N_i}$. In this section, we explain how the statistical uncertainty of OffPeak data and MCs are calculated.

3.4.1 Luminosity normalization and statistical uncertainty

OffPeak and MCs are luminosity normalized to OnPeak data. We take OffPeak data as an example. If the number of OffPeak candidate in i-th bin is N_i^0, the number of luminosity normalized candidate in the bin is given by

$$N_i^{OffPeak} = r_{OffPeak}^{Lumi} N_i^0 \tag{8}$$

and the statistical uncertainty of the bin is given by

$$\sigma_i^{OffPeak} = r_{OffPeak}^{Lumi} \sqrt{N_i^0} \tag{9}$$

3.4.2 MC re-weighting and statistical uncertainty

Supposing the total weight of the k-th candidate of MC mode j is

$$w_{jk}^T \equiv r_k^{Trk} r_k^{KPID} r_k^{LPID} W_{jk}^{MC} \tag{10}$$

The number of candidate in the i-th bin is given by

$$N_{ij}^{MC} = r_j^{Lumi} \sum_k w_{jk}^T \tag{11}$$

We add statistical uncertainty quadratically. Thus,

$$\sigma_{ij}^{MC} = r_j^{Lumi} \sqrt{\sum_k \left(w_{jk}^T\right)^2} \tag{12}$$

4 Coefficients in the fitting C_j^{MC}

Coefficients consist of branching fractions, some of which are to be determined by the fit. Coefficients are given by taking ratios between new branching fractions and the ones used in SP5/SP6 MC (the ones with superscript 0 in the following subsections). The decays contributing to each MC mode are shown in Appendix A and B. New measurements of branching fractions and constraints that we use in our fit are explained in section 5.

4.1 Number of produced B

Branching fractions of B^+B^- and $B^0\bar{B}^0$ of $\Upsilon(4S)$ resonance are denoted by

$$\begin{aligned} f_{+-} &= \mathcal{B}(\Upsilon(4S) \to B^+B^-) \\ f_{00} &= \mathcal{B}(\Upsilon(4S) \to B^0\bar{B}^0) \end{aligned} \tag{13}$$

We define the ratio of these two branching fractions

$$f_{+0} \equiv \frac{f_{+-}}{f_{00}} \tag{14}$$

In the first approximation, $f_{+-} = f_{00} = 0.5$ and $f_{+0} = 1$. In SP5/SP6 MC

$$f_{+0}^0 = 1 \tag{15}$$

is used [2]. The number of produced B is related to this ratio. Supposing $N_{B\bar{B}}$ of $B\bar{B}$-pairs are produced, the number of produced neutral B is

$$N_{neut}^{prod} = 2f_{00}N_{B\bar{B}} \tag{16}$$

and the number of produced charged B is

$$N_{chrg}^{prod} = 2f_{+-}N_{B\bar{B}} = f_{+0}N_{neut}^{prod} \tag{17}$$

Thus,

$$2N_{B\bar{B}} = N_{neut}^{prod} + N_{chrg}^{prod} = N_{neut}^{prod} + f_{+0}N_{neut}^{prod} \tag{18}$$

We get

$$N_{neut}^{prod} = \frac{2}{1+f_{+0}}N_{B\bar{B}} \tag{19}$$

and

$$N_{chrg}^{prod} = \frac{2f_{+0}}{1+f_{+0}}N_{B\bar{B}} \tag{20}$$

This f_{+0} can be floated in the fit.

[2] In this section the superscript "0" is used to denote SP5/SP6 values. For example, the BF that have a superscript "0" after the closing parenthesis are the values from the SP5/SP6 MC

4.2 $B\bar{B}$ luminosity correction

As explained in section 3.3.1, we assumed $f_{+0} = 1$, namely, the same number of B^+B^- and $B^0\bar{B}^0$ to calculate luminosity. We need to correct these. The correction factors are given by

$$C_{B^+} = \frac{2f_{+0}}{1+f_{+0}} \qquad \text{for BpBm MC}$$
$$C_{B^0} = \frac{2}{1+f_{+0}} \qquad \text{for B0B0bar MC} \tag{21}$$

The coefficients C_j^{MC} include the factor C_{B^+} if those are of BpBm MC and C_{B^0} if those are of B0B0bar MC.

4.3 D^0 MC modes

4.3.1 Coefficients for signals : $j = 1 - 15$

There are 15 signal MC modes.

- $j = 1 :\ B^+ \to \bar{D}^0\ell^+\nu$
  Number of produced events is

$$N = N_{chrg}^{prod}\mathcal{B}(B^+ \to \bar{D}^0\ell^+\nu)B_{D0} = N_{B\bar{B}}C_{B^+}\mathcal{B}(B^+ \to \bar{D}^0\ell^+\nu)B_{D0} \tag{22}$$

  As $N_{B\bar{B}}$ is common, it will be canceled by taking a ratio. Thus, the coefficient is given by

$$C_1^{MC} = \frac{C_{B^+}\mathcal{B}(B^+ \to \bar{D}^0\ell^+\nu)\mathcal{B}(D^0 \to K^-\pi^+)}{\mathcal{B}(B^+ \to \bar{D}^0\ell^+\nu)^0\mathcal{B}(D^0 \to K^-\pi^+)^0} \tag{23}$$

- $j = 2 :\ B^+ \to \bar{D}^{*0}\ell^+\nu$ with $\bar{D}^{*0} \to \bar{D}^0 + \gamma/\pi^0$
  Number of produced events is

$$\begin{aligned} N &= N_{chrg}^{prod}\mathcal{B}(B^+ \to \bar{D}^{*0}\ell^+\nu)[\mathcal{B}(D^{*0} \to D^0\pi^0) + \mathcal{B}(D^{*0} \to D^0\gamma)]\mathcal{B}(D^0 \to K^-\pi^+) \\ &= N_{B\bar{B}}C_{B^+}\mathcal{B}(B^+ \to \bar{D}^{*0}\ell^+\nu)\mathcal{B}(D^0 \to K^-\pi^+) \end{aligned} \tag{24}$$

  Thus

$$C_2^{MC} = \frac{C_{B^+}\mathcal{B}(B^+ \to \bar{D}^{*0}\ell^+\nu)\mathcal{B}(D^0 \to K^-\pi^+)}{\mathcal{B}(B^+ \to \bar{D}^{*0}\ell^+\nu)^0\mathcal{B}(D^0 \to K^-\pi^+)^0} \tag{25}$$

- $j = 3 :\ B^0 \to D^{*-}\ell^+\nu$ with $D^{*-} \to \bar{D}^0\pi^-$
  Number of produced events is

$$N = N_{B\bar{B}}C_{B^0}\mathcal{B}(B^0 \to D^{*-}\ell^+\nu)\mathcal{B}(D^{*+} \to D^0\pi^+)\mathcal{B}(D^0 \to K^-\pi^+) \tag{26}$$

  Thus

$$C_3^{MC} = \frac{C_{B^0}\mathcal{B}(B^0 \to D^{*-}\ell^+\nu)\mathcal{B}(D^{*+} \to D^0\pi^+)\mathcal{B}(D^0 \to K^-\pi^+)}{\mathcal{B}(B^0 \to D^{*-}\ell^+\nu)^0\mathcal{B}(D^{*+} \to D^0\pi^+)^0\mathcal{B}(D^0 \to K^-\pi^+)^0} \tag{27}$$

- $j = 4:\ B^+ \to \bar{D}_0^{*0}\ell^+\nu$ with $\bar{D}_0^{*0} \to \bar{D}^0\pi^0$
  The coefficient is

$$C_4^{MC} = \frac{C_{B^+}\mathcal{B}(B^+ \to \bar{D}_0^{*0}\ell^+\nu)\mathcal{B}(D_0^{*0} \to D^0\pi^0)\mathcal{B}(D^0 \to K^-\pi^+)}{\mathcal{B}(B^+ \to \bar{D}_0^{*0}\ell^+\nu)^0\mathcal{B}(D_0^{*0} \to D^0\pi^0)^0\mathcal{B}(D^0 \to K^-\pi^+)^0} \tag{28}$$

- $j = 5:\ B^0 \to D_0^{*-}\ell^+\nu$ with $D_0^{**-} \to \bar{D}^0\pi^-$
  The coefficient is

$$C_5^{MC} = \frac{C_{B^0}\mathcal{B}(B^0 \to D_0^{*-}\ell^+\nu)\mathcal{B}(D_0^{*+} \to D^0\pi^+)\mathcal{B}(D^0 \to K^-\pi^+)}{\mathcal{B}(B^0 \to D_0^{*-}\ell^+\nu)^0\mathcal{B}(D_0^{*+} \to D^0\pi^+)^0\mathcal{B}(D^0 \to K^-\pi^+)^0} \tag{29}$$

- $j = 6:\ B^+ \to \bar{D}_1^0\ell^+\nu$
  The decays contribute to this mode are
  $B^+ \to \bar{D}_1^0\ell^+\nu$ with $\bar{D}_1^0 \to D^{*-}\pi^+$ and $D^{*-} \to \bar{D}^0\pi^-$
  $B^+ \to \bar{D}_1^0\ell^+\nu$ with $\bar{D}_1^0 \to \bar{D}^{*0}\pi^0$ and $\bar{D}^{*0} \to \bar{D}^0 + \gamma/\pi^0$
  Number of produced events is

$$\begin{aligned}
N &= N_{B\bar{B}}C_{B^+}\mathcal{B}(B^+ \to \bar{D}_1^0\ell^+\nu)\mathcal{B}(D_1^0 \to D^{*+}\pi^-)\mathcal{B}(D^{*+} \to D^0\pi^+)\mathcal{B}(D^0 \to K^-\pi^+) \\
&\quad + N_{B\bar{B}}C_{B^+}\mathcal{B}(B^+ \to \bar{D}_1^0\ell^+\nu)\mathcal{B}(D_1^0 \to D^{*0}\pi^0) \\
&\qquad \times[\mathcal{B}(D^{*0} \to D^0\pi^0) + \mathcal{B}(D^{*0} \to D^0\gamma)]\mathcal{B}(D^0 \to K^-\pi^+) \\
&= N_{B\bar{B}}C_{B^+}\mathcal{B}(B^+ \to \bar{D}_1^0\ell^+\nu) \\
&\qquad \times[\mathcal{B}(D_1^0 \to D^{*+}\pi^-)\mathcal{B}(D^{*+} \to D^0\pi^+) + \mathcal{B}(D_1^0 \to D^{*0}\pi^0)]\mathcal{B}(D^0 \to K^-\pi^+)
\end{aligned} \tag{30}$$

  The coefficient is

$$C_6^{MC} = \frac{\begin{array}{l} C_{B^+}\mathcal{B}(B^+ \to \bar{D}_1^0\ell^+\nu)\times \\ {[\mathcal{B}(D_1^0 \to D^{*+}\pi^-)\mathcal{B}(D^{*+} \to D^0\pi^+) + \mathcal{B}(D_1^0 \to D^{*0}\pi^0)]\mathcal{B}(D^0 \to K^-\pi^+)} \end{array}}{\begin{array}{l} \mathcal{B}(B^+ \to \bar{D}_1^0\ell^+\nu)^0\times \\ {[\mathcal{B}(D_1^0 \to D^{*+}\pi^-)^0\mathcal{B}(D^{*+} \to D^0\pi^+)^0 + \mathcal{B}(D_1^0 \to D^{*0}\pi^0)^0]\mathcal{B}(D^0 \to K^-\pi^+)^0} \end{array}} \tag{31}$$

- $j = 7:\ B^0 \to D_1^-\ell^+\nu$
  The decays contribute to this mode are
  $B^0 \to D_1^-\ell^+\nu$ with $D_1^- \to D^{*-}\pi^0$ and $D^{*-} \to \bar{D}^0\pi^-$
  $B^0 \to D_1^-\ell^+\nu$ with $D_1^- \to \bar{D}^{*0}\pi^-$ and $\bar{D}^{*0} \to \bar{D}^0 + \gamma/\pi^0$
  Number of produced events is

$$\begin{aligned}
N &= N_{B\bar{B}}C_{B^0}\mathcal{B}(B^0 \to D_1^-\ell^+\nu)\mathcal{B}(D_1^+ \to D^{*+}\pi^0)\mathcal{B}(D^{*+} \to D^0\pi^+)\mathcal{B}(D^0 \to K^-\pi^+) \\
&\quad + N_{B\bar{B}}C_{B^0}\mathcal{B}(B^0 \to D_1^-\ell^+\nu)\mathcal{B}(D_1^+ \to D^{*0}\pi^+) \\
&\qquad \times[\mathcal{B}(D^{*0} \to D^0\pi^0) + \mathcal{B}(D^{*0} \to D^0\gamma)]\mathcal{B}(D^0 \to K^-\pi^+) \\
&= N_{B\bar{B}}C_{B^0}\mathcal{B}(B^0 \to D_1^-\ell^+\nu) \\
&\quad \times[\mathcal{B}(D_1^+ \to D^{*+}\pi^0)\mathcal{B}(D^{*+} \to D^0\pi^+) + \mathcal{B}(D_1^+ \to D^{*0}\pi^+)]\mathcal{B}(D^0 \to K^-\pi^+)
\end{aligned} \tag{32}$$

The coefficient is

$$C_7^{MC} = \frac{\begin{array}{l} C_{B^0}\mathcal{B}(B^0 \to D_1^-\ell^+\nu)\times \\ [\mathcal{B}(D_1^+ \to D^{*+}\pi^0)\mathcal{B}(D^{*+} \to D^0\pi^+) + \mathcal{B}(D_1^+ \to D^{*0}\pi^+)]\mathcal{B}(D^0 \to K^-\pi^+) \end{array}}{\begin{array}{l} \mathcal{B}(B^0 \to D_1^-\ell^+\nu)^0\times \\ [\mathcal{B}(D_1^+ \to D^{*+}\pi^0)^0\mathcal{B}(D^{*+} \to D^0\pi^+)^0 + \mathcal{B}(D_1^+ \to D^{*0}\pi^+)^0]\mathcal{B}(D^0 \to K^-\pi^+)^0 \end{array}} \tag{33}$$

- $j = 8 :\ B^+ \to \bar{D}_1'^0\ell^+\nu$
  The decays contribute to this mode are
  $B^+ \to \bar{D}_1'^0\ell^+\nu$ with $\bar{D}_1'^0 \to D^{*-}\pi^+$ and $D^{*-} \to \bar{D}^0\pi^-$
  $B^+ \to \bar{D}_1'^0\ell^+\nu$ with $\bar{D}_1'^0 \to \bar{D}^{*0}\pi^0$ and $\bar{D}^{*0} \to \bar{D}^0 + \gamma/\pi^0$
  Number of produced events is

$$\begin{aligned} N &= N_{B\bar{B}}C_{B^+}\mathcal{B}(B^+ \to \bar{D}_1'^0\ell^+\nu)\mathcal{B}(D_1'^0 \to D^{*+}\pi^-)\mathcal{B}(D^{*+} \to D^0\pi^+)\mathcal{B}(D^0 \to K^-\pi^+) \\ &\quad +N_{B\bar{B}}C_{B^+}\mathcal{B}(B^+ \to \bar{D}_1'^0\ell^+\nu)\mathcal{B}(D_1'^0 \to D^{*0}\pi^0) \\ &\qquad \times[\mathcal{B}(D^{*0} \to D^0\pi^0) + \mathcal{B}(D^{*0} \to D^0\gamma)]\mathcal{B}(D^0 \to K^-\pi^+) \\ &= N_{B\bar{B}}C_{B^+}\mathcal{B}(B^+ \to \bar{D}_1'^0\ell^+\nu) \\ &\quad \times[\mathcal{B}(D_1'^0 \to D^{*+}\pi^-)\mathcal{B}(D^{*+} \to D^0\pi^+) + \mathcal{B}(D_1'^0 \to D^{*0}\pi^0)]\mathcal{B}(D^0 \to K^-\pi^+) \end{aligned} \tag{34}$$

The coefficient is

$$C_8^{MC} = \frac{\begin{array}{l} C_{B^+}\mathcal{B}(B^+ \to \bar{D}_1'^0\ell^+\nu)\times \\ [\mathcal{B}(D_1'^0 \to D^{*+}\pi^-)\mathcal{B}(D^{*+} \to D^0\pi^+) + \mathcal{B}(D_1'^0 \to D^{*0}\pi^0)]\mathcal{B}(D^0 \to K^-\pi^+) \end{array}}{\begin{array}{l} \mathcal{B}(B^+ \to \bar{D}_1'^0\ell^+\nu)^0\times \\ [\mathcal{B}(D_1'^0 \to D^{*+}\pi^-)^0\mathcal{B}(D^{*+} \to D^0\pi^+)^0 + \mathcal{B}(D_1'^0 \to D^{*0}\pi^0)^0]\mathcal{B}(D^0 \to K^-\pi^+)^0 \end{array}} \tag{35}$$

- $j = 9 :\ B^0 \to D_1'^-\ell^+\nu$
  The decays contribute to this mode are
  $B^0 \to D_1'^-\ell^+\nu$ with $D_1'^- \to D^{*-}\pi^0$ and $D^{*-} \to \bar{D}^0\pi^-$
  $B^0 \to D_1'^-\ell^+\nu$ with $D_1'^- \to \bar{D}^{*0}\pi^-$ and $\bar{D}^{*0} \to \bar{D}^0 + \gamma/\pi^0$
  Number of produced events is

$$\begin{aligned} N &= N_{B\bar{B}}C_{B^0}\mathcal{B}(B^0 \to D_1'^-\ell^+\nu)\mathcal{B}(D_1'^+ \to D^{*+}\pi^0)\mathcal{B}(D^{*+} \to D^0\pi^+)\mathcal{B}(D^0 \to K^-\pi^+) \\ &\quad +N_{B\bar{B}}C_{B^0}\mathcal{B}(B^0 \to D_1'^-\ell^+\nu)\mathcal{B}(D_1'^+ \to D^{*0}\pi^+) \\ &\qquad \times[\mathcal{B}(D^{*0} \to D^0\pi^0) + \mathcal{B}(D^{*0} \to D^0\gamma)]\mathcal{B}(D^0 \to K^-\pi^+) \\ &= N_{B\bar{B}}C_{B^0}\mathcal{B}(B^0 \to D_1'^-\ell^+\nu) \\ &\quad \times[\mathcal{B}(D_1'^+ \to D^{*+}\pi^0)\mathcal{B}(D^{*+} \to D^0\pi^+) + \mathcal{B}(D_1'^+ \to D^{*0}\pi^+)]\mathcal{B}(D^0 \to K^-\pi^+) \end{aligned} \tag{36}$$

$$C_9^{MC} = \frac{\begin{array}{l} C_{B^0}\mathcal{B}(B^0 \to D_1'^{-}\ell^+\nu)\times \\ [\mathcal{B}(D_1'^{+} \to D^{*+}\pi^0)\mathcal{B}(D^{*+} \to D^0\pi^+) + \mathcal{B}(D_1'^{+} \to D^{*0}\pi^+)]\mathcal{B}(D^0 \to K^-\pi^+) \end{array}}{\begin{array}{l} \mathcal{B}(B^0 \to D_1'^{-}\ell^+\nu)^0\times \\ [\mathcal{B}(D_1'^{+} \to D^{*+}\pi^0)^0\mathcal{B}(D^{*+} \to D^0\pi^+)^0 + \mathcal{B}(D_1'^{+} \to D^{*0}\pi^+)^0]\mathcal{B}(D^0 \to K^-\pi^+)^0 \end{array}} \tag{37}$$

- $j = 10:\ B^+ \to \bar{D}_2^{*0}\ell^+\nu$
  The decays contribute to this mode are
  $B^+ \to \bar{D}_2^{*0}\ell^+\nu$ with $\bar{D}_2^{*0} \to D^{*-}\pi^+$ and $D^{*-} \to \bar{D}^0\pi^-$
  $B^+ \to \bar{D}_2^{*0}\ell^+\nu$ with $\bar{D}_2^{*0} \to \bar{D}^{*0}\pi^0$ and $\bar{D}^{*0} \to \bar{D}^0 + \gamma/\pi^0$
  $B^+ \to \bar{D}_2^{*0}\ell^+\nu$ with $\bar{D}_2^{*0} \to \bar{D}^0\pi^0$
  Number of produced events is

$$\begin{aligned} N &= N_{B\bar{B}}C_{B^+}\mathcal{B}(B^+ \to \bar{D}_2^{*0}\ell^+\nu)\mathcal{B}(D_2^{*0} \to D^{*+}\pi^-)\mathcal{B}(D^{*+} \to D^0\pi^+)\mathcal{B}(D^0 \to K^-\pi^+) \\ &\quad +N_{B\bar{B}}C_{B^+}\mathcal{B}(B^+ \to \bar{D}_2^{*0}\ell^+\nu)\mathcal{B}(D_2^{*0} \to D^{*0}\pi^0) \\ &\qquad \times[\mathcal{B}(D^{*0} \to D^0\pi^0) + \mathcal{B}(D^{*0} \to D^0\gamma)]\mathcal{B}(D^0 \to K^-\pi^+) \\ &\quad +N_{B\bar{B}}C_{B^+}\mathcal{B}(B^+ \to \bar{D}_2^{*0}\ell^+\nu)\mathcal{B}(D_2^{*0} \to D^0\pi^0)\mathcal{B}(D^0 \to K^-\pi^+) \\ &= N_{B\bar{B}}C_{B^+}\mathcal{B}(B^+ \to \bar{D}_2^{*0}\ell^+\nu) \\ &\quad \times[\mathcal{B}(D_2^{*0} \to D^{*+}\pi^-)\mathcal{B}(D^{*+} \to D^0\pi^+) + \mathcal{B}(D_2^{*0} \to D^{*0}\pi^0) + \mathcal{B}(D_2^{*0} \to D^0\pi^0)] \\ &\quad \times\mathcal{B}(D^0 \to K^-\pi^+) \end{aligned} \tag{38}$$

  The coefficient is

$$C_{10}^{MC} = \frac{\begin{array}{l} C_{B^+}\mathcal{B}(B^+ \to \bar{D}_2^{*0}\ell^+\nu)\times \\ [\mathcal{B}(D_2^{*0} \to D^{*+}\pi^-)\mathcal{B}(D^{*+} \to D^0\pi^+) + \mathcal{B}(D_2^{*0} \to D^{*0}\pi^0) + \mathcal{B}(D_2^{*0} \to D^0\pi^0)] \\ \times\mathcal{B}(D^0 \to K^-\pi^+) \end{array}}{\begin{array}{l} \mathcal{B}(B^+ \to \bar{D}_2^{*0}\ell^+\nu)^0\times \\ [\mathcal{B}(D_2^{*0} \to D^{*+}\pi^-)^0\mathcal{B}(D^{*+} \to D^0\pi^+)^0 + \mathcal{B}(D_2^{*0} \to D^{*0}\pi^0)^0 + \mathcal{B}(D_2^{*0} \to D^0\pi^0)^0] \\ \times\mathcal{B}(D^0 \to K^-\pi^+)^0 \end{array}} \tag{39}$$

- $j = 11:\ B^0 \to D_2^{*-}\ell^+\nu$
  The decays contribute to this mode are
  $B^0 \to D_2^{*-}\ell^+\nu$ with $D_2^{*-} \to D^{*-}\pi^0$ and $D^{*-} \to \bar{D}^0\pi^-$
  $B^0 \to D_2^{*-}\ell^+\nu$ with $D_2^{*-} \to \bar{D}^{*0}\pi^-$ and $\bar{D}^{*0} \to \bar{D}^0 + \gamma/\pi^0$
  $B^0 \to D_2^{*-}\ell^+\nu$ with $D_2^{*-} \to \bar{D}^0\pi^-$

Number of produced events is

$$\begin{aligned}
N &= N_{B\bar{B}} C_{B^0} \mathcal{B}(B^0 \to D_2^{*-}\ell^+\nu)\mathcal{B}(D_2^{*+} \to D^{*+}\pi^0)\mathcal{B}(D^{*+} \to D^0\pi^+)\mathcal{B}(D^0 \to K^-\pi^+) \\
&\quad + N_{B\bar{B}} C_{B^0} \mathcal{B}(B^0 \to D_2^{*-}\ell^+\nu)\mathcal{B}(D_2^{*+} \to D^{*0}\pi^+) \\
&\qquad \times[\mathcal{B}(D^{*0} \to D^0\pi^0) + \mathcal{B}(D^{*0} \to D^0\gamma)]\mathcal{B}(D^0 \to K^-\pi^+) \\
&\quad + N_{B\bar{B}} C_{B^0} \mathcal{B}(B^0 \to D_2^{*-}\ell^+\nu)\mathcal{B}(D_2^{*+} \to D^0\pi^+)\mathcal{B}(D^0 \to K^-\pi^+) \\
&= N_{B\bar{B}} C_{B^0} \mathcal{B}(B^0 \to D_2^{*-}\ell^+\nu) \\
&\quad \times[\mathcal{B}(D_2^{*+} \to D^{*+}\pi^0)\mathcal{B}(D^{*+} \to D^0\pi^+) + \mathcal{B}(D_2^{*+} \to D^{*0}\pi^+) + \mathcal{B}(D_2^{*+} \to D^0\pi^+)] \\
&\quad \times\mathcal{B}(D^0 \to K^-\pi^+)
\end{aligned} \tag{40}$$

The coefficient is

$$C_{11}^{MC} = \frac{\begin{array}{l} C_{B^0}\mathcal{B}(B^0 \to D_2^{*-}\ell^+\nu)\times \\ {[\mathcal{B}(D_2^{*+} \to D^{*+}\pi^0)\mathcal{B}(D^{*+} \to D^0\pi^+) + \mathcal{B}(D_2^{*+} \to D^{*0}\pi^+) + \mathcal{B}(D_2^{*+} \to D^0\pi^+)]} \\ \times\mathcal{B}(D^0 \to K^-\pi^+) \end{array}}{\begin{array}{l} \mathcal{B}(B^0 \to D_2^{*-}\ell^+\nu)^0\times \\ {[\mathcal{B}(D_2^{*+} \to D^{*+}\pi^0)^0\mathcal{B}(D^{*+} \to D^0\pi^+)^0 + \mathcal{B}(D_2^{*+} \to D^{*0}\pi^+)^0 + \mathcal{B}(D_2^{*+} \to D^0\pi^+)^0)} \\ \times\mathcal{B}(D^0 \to K^-\pi^+)^0 \end{array}} \tag{41}$$

- $j = 12: \ B^+ \to \bar{D}^0\pi^0\ell^+\nu$
  The coefficient is

$$C_{12}^{MC} = \frac{C_{B^+}\mathcal{B}(B^+ \to \bar{D}^0\pi^0\ell^+\nu)\mathcal{B}(D^0 \to K^-\pi^+)}{\mathcal{B}(B^+ \to \bar{D}^0\pi^0\ell^+\nu)^0\mathcal{B}(D^0 \to K^-\pi^+)^0} \tag{42}$$

- $j = 13: \ B^0 \to \bar{D}^0\pi^-\ell^+\nu$
  The coefficient is

$$C_{13}^{MC} = \frac{C_{B^0}\mathcal{B}(B^0 \to \bar{D}^0\pi^-\ell^+\nu)\mathcal{B}(D^0 \to K^-\pi^+)}{\mathcal{B}(B^0 \to \bar{D}^0\pi^-\ell^+\nu)^0\mathcal{B}(D^0 \to K^-\pi^+)^0} \tag{43}$$

- $j = 14: \ B^+ \to D^*\pi\ell^+\nu$
  The decays contribute to this mode are
  $B^+ \to D^{*-}\pi^+\ell^+\nu$ with $D^{*-} \to \bar{D}^0 + \pi^-$
  $B^+ \to \bar{D}^{*0}\pi^0\ell^+\nu$ with $\bar{D}^{*0} \to \bar{D}^0 + \gamma/\pi^0$
  Number of produced events is

$$\begin{aligned}
N &= N_{B\bar{B}} C_{B^+} \mathcal{B}(B^+ \to D^{*-}\pi^+\ell^+\nu)\mathcal{B}(D^{*+} \to D^0\pi^+)\mathcal{B}(D^0 \to K^-\pi^+) \\
&\quad + N_{B\bar{B}} C_{B^+} \mathcal{B}(B^+ \to \bar{D}^{*0}\pi^0\ell^+\nu)[\mathcal{B}(D^{*0} \to D^0\pi^0) + \mathcal{B}(D^{*0} \to D^0\gamma)]\mathcal{B}(D^0 \to K^-\pi^+) \\
&= N_{B\bar{B}} C_{B^+}[\mathcal{B}(B^+ \to D^{*-}\pi^+\ell^+\nu)\mathcal{B}(D^{*+} \to D^0\pi^+) + \mathcal{B}(B^+ \to \bar{D}^{*0}\pi^0\ell^+\nu)] \\
&\quad \times\mathcal{B}(D^0 \to K^-\pi^+)
\end{aligned} \tag{44}$$

The coefficient is

$$C_{14}^{MC} = \frac{\begin{array}{l} C_{B^+}[\mathcal{B}(B^+ \to D^{*-}\pi^+\ell^+\nu)\mathcal{B}(D^{*+} \to D^0\pi^+) + \mathcal{B}(B^+ \to \bar{D}^{*0}\pi^0\ell^+\nu)] \\ \times\mathcal{B}(D^0 \to K^-\pi^+) \end{array}}{\begin{array}{l} [\mathcal{B}(B^+ \to D^{*-}\pi^+\ell^+\nu)^0\mathcal{B}(D^{*+} \to D^0\pi^+)^0 + \mathcal{B}(B^+ \to \bar{D}^{*0}\pi^0\ell^+\nu)^0] \\ \times\mathcal{B}(D^0 \to K^-\pi^+)^0 \end{array}} \tag{45}$$

- $j = 15: \ B^0 \to D^*\pi\ell^+\nu$
  The decays contribute to this mode are
  $B^0 \to D^{*-}\pi^0\ell^+\nu$ with $D^{*-} \to \bar{D}^0 + \pi^-$
  $B^0 \to \bar{D}^{*0}\pi^-\ell^+\nu$ with $\bar{D}^{*0} \to \bar{D}^0 + \gamma/\pi^0$
  Number of produced events is

$$\begin{aligned} N &= N_{B\bar{B}}C_{B^0}\mathcal{B}(B^0 \to D^{*-}\pi^0\ell^+\nu)\mathcal{B}(D^{*+} \to D^0\pi^+)\mathcal{B}(D^0 \to K^-\pi^+) \\ &\quad +N_{B\bar{B}}C_{B^0}\mathcal{B}(B^0 \to \bar{D}^{*0}\pi^-\ell^+\nu)[\mathcal{B}(D^{*0} \to D^0\pi^0) + \mathcal{B}(D^{*0} \to D^0\gamma)]\mathcal{B}(D^0 \to K^-\pi^+) \\ &= N_{B\bar{B}}C_{B^0}[\mathcal{B}(B^0 \to D^{*-}\pi^0\ell^+\nu)\mathcal{B}(D^{*+} \to D^0\pi^+) + \mathcal{B}(B^0 \to \bar{D}^{*0}\pi^-\ell^+\nu)] \\ &\quad \times\mathcal{B}(D^0 \to K^-\pi^+) \end{aligned} \tag{46}$$

  The coefficient is

$$C_{15}^{MC} = \frac{\begin{array}{l} C_{B^0}[\mathcal{B}(B^0 \to D^{*-}\pi^0\ell^+\nu)\mathcal{B}(D^{*+} \to D^0\pi^+) + \mathcal{B}(B^0 \to \bar{D}^{*0}\pi^-\ell^+\nu)] \\ \times\mathcal{B}(D^0 \to K^-\pi^+) \end{array}}{\begin{array}{l} [\mathcal{B}(B^0 \to D^{*-}\pi^0\ell^+\nu)^0\mathcal{B}(D^{*+} \to D^0\pi^+)^0 + \mathcal{B}(B^0 \to \bar{D}^{*0}\pi^-\ell^+\nu)^0] \\ \times\mathcal{B}(D^0 \to K^-\pi^+)^0 \end{array}} \tag{47}$$

4.3.2 Coefficients for backgrounds : $j = 16 - 27$

There are 12 background MC modes. The coefficient of each mode is

- $j = 16$, UncorrDL from B^+B^-

$$C_{16}^{MC} = C_{UncorDL}^{D^0}\frac{C_{B^+}\mathcal{B}(D^0 \to K^-\pi^+)}{\mathcal{B}(D^0 \to K^-\pi^+)^0} \tag{48}$$

- $j = 17$, UncorrDL from $B^0\bar{B}^0$

$$C_{17}^{MC} = C_{UncorDL}^{D^0}\frac{C_{B^0}\mathcal{B}(D^0 \to K^-\pi^+)}{\mathcal{B}(D^0 \to K^-\pi^+)^0} \tag{49}$$

- $j = 18$, UncorrCL from B^+B^-

$$C_{18}^{MC} = C_{UncorCL}^{D^0}\frac{C_{B^+}\mathcal{B}(D^0 \to K^-\pi^+)}{\mathcal{B}(D^0 \to K^-\pi^+)^0} \tag{50}$$

- $j = 19$, UncorrCL from $B^0\bar{B}^0$

$$C_{19}^{MC} = C_{UncorCL}^{D^0} \frac{C_{B^0}\mathcal{B}(D^0 \to K^-\pi^+)}{\mathcal{B}(D^0 \to K^-\pi^+)^0} \tag{51}$$

- $j = 20$, CascL from B^+B^-

$$C_{20}^{MC} = C_{CascL}^{D^0} \frac{C_{B^+}\mathcal{B}(D^0 \to K^-\pi^+)}{\mathcal{B}(D^0 \to K^-\pi^+)^0} \tag{52}$$

- $j = 21$, CascL from $B^0\bar{B}^0$

$$C_{21}^{MC} = C_{CascL}^{D^0} \frac{C_{B^0}\mathcal{B}(D^0 \to K^-\pi^+)}{\mathcal{B}(D^0 \to K^-\pi^+)^0} \tag{53}$$

- $j = 22$, FakeL from B^+B^-

$$C_{22}^{MC} = C_{FakeL}^{D^0} \frac{C_{B^+}\mathcal{B}(D^0 \to K^-\pi^+)}{\mathcal{B}(D^0 \to K^-\pi^+)^0} \tag{54}$$

- $j = 23$, FakeL from $B^0\bar{B}^0$

$$C_{23}^{MC} = C_{FakeL}^{D^0} \frac{C_{B^0}\mathcal{B}(D^0 \to K^-\pi^+)}{\mathcal{B}(D^0 \to K^-\pi^+)^0} \tag{55}$$

- $j = 24$, CombRL from B^+B^-

$$C_{24}^{MC} = \frac{C_{B^+}\mathcal{B}(D^0 \to K^-\pi^+)}{\mathcal{B}(D^0 \to K^-\pi^+)^0} \tag{56}$$

- $j = 25$, CombRL from $B^0\bar{B}^0$

$$C_{25}^{MC} = \frac{C_{B^0}\mathcal{B}(D^0 \to K^-\pi^+)}{\mathcal{B}(D^0 \to K^-\pi^+)^0} \tag{57}$$

- $j = 26$, CombFL from B^+B^-

$$C_{26}^{MC} = \frac{C_{B^+}\mathcal{B}(D^0 \to K^-\pi^+)}{\mathcal{B}(D^0 \to K^-\pi^+)^0} \tag{58}$$

- $j = 27$, CombFL from $B^0\bar{B}^0$

$$C_{27}^{MC} = \frac{C_{B^0}\mathcal{B}(D^0 \to K^-\pi^+)}{\mathcal{B}(D^0 \to K^-\pi^+)^0} \tag{59}$$

The factors such as $C_{UncorDL}^{D^0}$ are free parameters to be floated with constraints in the fit. See section 5.3 for details of constraints.

4.4 D^+ MC modes

4.4.1 Coefficients for signals : $j = 1 - 14$

There are 14 signal MC modes.

- $j = 1$: $B^0 \to D^-\ell^+\nu$
  The coefficient is

$$C_1^{MC} = \frac{C_{B^0}\mathcal{B}(B^0 \to D^-\ell^+\nu)\mathcal{B}(D^+ \to K^-\pi^+\pi^+)}{\mathcal{B}(B^0 \to D^-\ell^+\nu)^0\mathcal{B}(D^+ \to K^-\pi^+\pi^+)^0} \tag{60}$$

- $j = 2$: $B^0 \to D^{*-}\ell^+\nu$ with $D^{*-} \to D^- + \gamma/\pi^0$
  The coefficient is

$$C_2^{MC} = \frac{\begin{array}{l} C_{B^0}\mathcal{B}(B^0 \to D^{*-}\ell^+\nu)\times \\ [\mathcal{B}(D^{*+} \to D^+\pi^0) + \mathcal{B}(D^{*+} \to D^+\gamma)]\mathcal{B}(D^+ \to K^-\pi^+\pi^+) \end{array}}{\begin{array}{l} \mathcal{B}(B^0 \to D^{*-}\ell^+\nu)^0\times \\ [\mathcal{B}(D^{*+} \to D^+\pi^0)^0 + \mathcal{B}(D^{*+} \to D^+\gamma)^0]\mathcal{B}(D^+ \to K^-\pi^+\pi^+)^0 \end{array}} \tag{61}$$

- $j = 3$: $B^+ \to \bar{D}_0^{*0}\ell^+\nu$ with $\bar{D}_0^{*0} \to D^- + \pi^+$
  The coefficient is

$$C_3^{MC} = \frac{C_{B^+}\mathcal{B}(B^+ \to \bar{D}_0^{*0}\ell^+\nu)\mathcal{B}(D_0^{*0} \to D^+\pi^-)\mathcal{B}(D^+ \to K^-\pi^+\pi^+)}{\mathcal{B}(B^+ \to \bar{D}_0^{*0}\ell^+\nu)^0\mathcal{B}(D_0^{*0} \to D^+\pi^-)^0\mathcal{B}(D^+ \to K^-\pi^+\pi^+)^0} \tag{62}$$

- $j = 4$: $B^0 \to D_0^{*-}\ell^+\nu$ with $D_0^{*-} \to D^-\pi^0$
  The coefficient is

$$C_4^{MC} = \frac{C_{B^0}\mathcal{B}(B^0 \to D_0^{*-}\ell^+\nu)\mathcal{B}(D_0^{*+} \to D^+\pi^0)\mathcal{B}(D^+ \to K^-\pi^+\pi^+)}{\mathcal{B}(B^0 \to D_0^{*-}\ell^+\nu)^0\mathcal{B}(D_0^{*+} \to D^+\pi^0)^0\mathcal{B}(D^+ \to K^-\pi^+\pi^+)^0} \tag{63}$$

- $j = 5$: $B^+ \to \bar{D}_1^0\ell^+\nu$ with $\bar{D}_1^0 \to D^{*-} + \pi^+$ and $D^{*-} \to D^- + \pi^0/\gamma$
  The coefficient is

$$C_5^{MC} = \frac{\begin{array}{l} C_{B^+}\mathcal{B}(B^+ \to \bar{D}_1^0\ell^+\nu)\mathcal{B}(D_1^0 \to D^{*+}\pi^-)\times \\ [\mathcal{B}(D^{*+} \to D^+\pi^0) + \mathcal{B}(D^{*+} \to D^+\gamma)]\mathcal{B}(D^+ \to K^-\pi^+\pi^+) \end{array}}{\begin{array}{l} \mathcal{B}(B^+ \to \bar{D}_1^0\ell^+\nu)^0\mathcal{B}(D_1^0 \to D^{*+}\pi^-)^0\times \\ [\mathcal{B}(D^{*+} \to D^+\pi^0)^0 + \mathcal{B}(D^{*+} \to D^+\gamma)^0]\mathcal{B}(D^+ \to K^-\pi^+\pi^+)^0 \end{array}} \tag{64}$$

- $j = 6$: $B^0 \to D_1^-\ell^+\nu$ with $D_1^- \to D^{*-}\pi^0$ and $D^{*-} \to D^- + \pi^0/\gamma$
  The coefficient is

$$C_6^{MC} = \frac{\begin{array}{l} C_{B^0}\mathcal{B}(B^0 \to D_1^-\ell^+\nu)\mathcal{B}(D_1^+ \to D^{*+}\pi^0)\times \\ [\mathcal{B}(D^{*+} \to D^+\pi^0) + \mathcal{B}(D^{*+} \to D^+\gamma)]\mathcal{B}(D^+ \to K^-\pi^+\pi^+) \end{array}}{\begin{array}{l} \mathcal{B}(B^0 \to D_1^-\ell^+\nu)^0\mathcal{B}(D_1^+ \to D^{*+}\pi^0)^0\times \\ [\mathcal{B}(D^{*+} \to D^+\pi^0)^0 + \mathcal{B}(D^{*+} \to D^+\gamma)^0]\mathcal{B}(D^+ \to K^-\pi^+\pi^+)^0 \end{array}} \tag{65}$$

- $j = 7:\ B^+ \to \bar{D}_1'^0 \ell^+\nu$ with $\bar{D}_1'^0 \to D^{*-} + \pi^+$ and $D^{*-} \to D^- + \pi^0/\gamma$
  The coefficient is

$$C_7^{MC} = \frac{\begin{array}{l} C_{B^+}\mathcal{B}(B^+ \to \bar{D}_1'^0\ell^+\nu)\mathcal{B}(D_1'^0 \to D^{*+}\pi^-)\times \\ {[\mathcal{B}(D^{*+} \to D^+\pi^0) + \mathcal{B}(D^{*+} \to D^+\gamma)]}\mathcal{B}(D^+ \to K^-\pi^+\pi^+) \end{array}}{\begin{array}{l} \mathcal{B}(B^+ \to \bar{D}_1'^0\ell^+\nu)^0\mathcal{B}(D_1'^0 \to D^{*+}\pi^-)^0\times \\ {[\mathcal{B}(D^{*+} \to D^+\pi^0)^0 + \mathcal{B}(D^{*+} \to D^+\gamma)^0]}\mathcal{B}(D^+ \to K^-\pi^+\pi^+)^0 \end{array}} \tag{66}$$

- $j = 8:\ B^0 \to D_1'^- \ell^+\nu$ with $D_1'^- \to D^{*-}\pi^0$ and $D^{*-} \to D^- + \pi^0/\gamma$
  The coefficient is

$$C_8^{MC} = \frac{\begin{array}{l} C_{B^0}\mathcal{B}(B^0 \to D_1'^-\ell^+\nu)\mathcal{B}(D_1'^+ \to D^{*+}\pi^0)\times \\ {[\mathcal{B}(D^{*+} \to D^+\pi^0) + \mathcal{B}(D^{*+} \to D^+\gamma)]}\mathcal{B}(D^+ \to K^-\pi^+\pi^+) \end{array}}{\begin{array}{l} \mathcal{B}(B^0 \to D_1'^-\ell^+\nu)^0\mathcal{B}(D_1'^+ \to D^{*+}\pi^0)^0\times \\ {[\mathcal{B}(D^{*+} \to D^+\pi^0)^0 + \mathcal{B}(D^{*+} \to D^+\gamma)^0]}\mathcal{B}(D^+ \to K^-\pi^+\pi^+)^0 \end{array}} \tag{67}$$

- $j = 9:\ B^+ \to \bar{D}_2^{*0}\ell^+\nu$
  The decays contribute to this mode are
  $B^+ \to \bar{D}_2^{*0}\ell^+\nu$ with $\bar{D}_2^{*0} \to D^{*-} + \pi^+$ and $D^{*-} \to D^- + \pi^0/\gamma$
  $B^+ \to \bar{D}_2^{*0}\ell^+\nu$ with $\bar{D}_2^{*0} \to D^- + \pi^+$
  The coefficient is

$$C_9^{MC} = \frac{\begin{array}{l} C_{B^+}\mathcal{B}(B^+ \to \bar{D}_2^{*0}\ell^+\nu)\times \\ \{\mathcal{B}(D_2^{*0} \to D^{*+}\pi^-)[\mathcal{B}(D^{*+} \to D^+\pi^0) + \mathcal{B}(D^{*+} \to D^+\gamma)] + \mathcal{B}(D_2^{*0} \to D^+\pi^-)\} \\ \times\mathcal{B}(D^+ \to K^-\pi^+\pi^+) \end{array}}{\begin{array}{l} \mathcal{B}(B^+ \to \bar{D}_2^{*0}\ell^+\nu)^0\times \\ \{\mathcal{B}(D_2^{*0} \to D^{*+}\pi^-)^0[\mathcal{B}(D^{*+} \to D^+\pi^0)^0 + \mathcal{B}(D^{*+} \to D^+\gamma)^0] + \mathcal{B}(D_2^{*0} \to D^+\pi^-)^0)\} \\ \times\mathcal{B}(D^+ \to K^-\pi^+\pi^+)^0 \end{array}} \tag{68}$$

- $j = 10:\ B^0 \to D_2^{*-}\ell^+\nu$
  The decays contribute to this mode are
  $B^0 \to D_2^{*-}\ell^+\nu$ with $D_2^{*-} \to D^{*-}\pi^0$ and $D^{*-} \to D^- + \pi^0/\gamma$
  $B^0 \to D_2^{*-}\ell^+\nu$ with $D_2^{*-} \to D^-\pi^0$

The coefficient is

$$C_{10}^{MC} = \frac{\begin{array}{l} C_{B^0}\mathcal{B}(B^0 \to D_2^{*-}\ell^+\nu)\times \\ \{\mathcal{B}(D_2^{*+} \to D^{*+}\pi^0)[\mathcal{B}(D^{*+} \to D^+\pi^0) + \mathcal{B}(D^{*+} \to D^+\gamma)] + \mathcal{B}(D_2^{*+} \to D^+\pi^0)\} \\ \times\mathcal{B}(D^+ \to K^-\pi^+\pi^+) \end{array}}{\begin{array}{l} \mathcal{B}(B^0 \to D_2^{*-}\ell^+\nu)^0\times \\ \{\mathcal{B}(D_2^{*+} \to D^{*+}\pi^0)^0[\mathcal{B}(D^{*+} \to D^+\pi^0)^0 + \mathcal{B}(D^{*+} \to D^+\gamma)^0] + \mathcal{B}(D_2^{*+} \to D^+\pi^0)^0)\} \\ \times\mathcal{B}(D^+ \to K^-\pi^+\pi^+)^0 \end{array}} \tag{69}$$

- $j = 11 : \ B^+ \to D^-\pi^+\ell^+\nu$
  The coefficient is

$$C_{11}^{MC} = \frac{C_{B^+}\mathcal{B}(B^+ \to D^-\pi^+\ell^+\nu)\mathcal{B}(D^+ \to K^-\pi^+\pi^+)}{\mathcal{B}(B^+ \to D^-\pi^+\ell^+\nu)^0\mathcal{B}(D^+ \to K^-\pi^+\pi^+)^0} \tag{70}$$

- $j = 12 : \ B^0 \to D^-\pi^0\ell^+\nu$
  The coefficient is

$$C_{12}^{MC} = \frac{C_{B^0}\mathcal{B}(B^0 \to D^-\pi^0\ell^+\nu)\mathcal{B}(D^+ \to K^-\pi^+\pi^+)}{\mathcal{B}(B^0 \to D^-\pi^0\ell^+\nu)^0\mathcal{B}(D^+ \to K^-\pi^+\pi^+)^0} \tag{71}$$

- $j = 13 : \ B^+ \to D^{*-}\pi^+\ell^+\nu$ with $D^{*-} \to D^- + \gamma/\pi^0$
  The coefficient is

$$C_{13}^{MC} = \frac{\begin{array}{l} C_{B^+}\mathcal{B}(B^+ \to D^{*-}\pi^+\ell^+\nu)\times \\ [\mathcal{B}(D^{*+} \to D^+\pi^0) + \mathcal{B}(D^{*+} \to D^+\gamma)]\mathcal{B}(D^+ \to K^-\pi^+\pi^+) \end{array}}{\begin{array}{l} \mathcal{B}(B^+ \to D^{*-}\pi^+\ell^+\nu)^0\times \\ [\mathcal{B}(D^{*+} \to D^+\pi^0)^0 + \mathcal{B}(D^{*+} \to D^+\gamma)^0]\mathcal{B}(D^+ \to K^-\pi^+\pi^+)^0 \end{array}} \tag{72}$$

- $j = 14 : \ B^0 \to D^{*-}\pi^0\ell^+\nu$ with $D^{*-} \to D^- + \gamma/\pi^0$
  The coefficient is

$$C_{14}^{MC} = \frac{\begin{array}{l} C_{B^0}\mathcal{B}(B^0 \to D^{*-}\pi^0\ell^+\nu)\times \\ [\mathcal{B}(D^{*+} \to D^+\pi^0) + \mathcal{B}(D^{*+} \to D^+\gamma)]\mathcal{B}(D^+ \to K^-\pi^+\pi^+) \end{array}}{\begin{array}{l} \mathcal{B}(B^0 \to D^{*-}\pi^0\ell^+\nu)^0\times \\ [\mathcal{B}(D^{*+} \to D^+\pi^0)^0 + \mathcal{B}(D^{*+} \to D^+\gamma)^0]\mathcal{B}(D^+ \to K^-\pi^+\pi^+)^0 \end{array}} \tag{73}$$

4.4.2 Coefficients for backgrounds : $j = 15 - 26$

There are 16 background MC modes (j). The coefficient of each mode is

- $j = 15$, UncorrDL B^+B^-

$$C_{15}^{MC} = C_{UncorDL}^{D^+} \frac{C_{B^+}\mathcal{B}(D^+ \to K^-\pi^+\pi^+)}{\mathcal{B}(D^+ \to K^-\pi^+\pi^+)^0} \tag{74}$$

- $j = 16$, UncorrDL from $B^0\bar{B}^0$

$$C_{16}^{MC} = C_{UncorDL}^{D^+} \frac{C_{B^0}\mathcal{B}(D^+ \to K^-\pi^+\pi^+)}{\mathcal{B}(D^+ \to K^-\pi^+\pi^+)^0} \tag{75}$$

- $j = 17$, UncorrCL from B^+B^-

$$C_{17}^{MC} = C_{UncorCL}^{D^+} \frac{C_{B^+}\mathcal{B}(D^+ \to K^-\pi^+\pi^+)}{\mathcal{B}(D^+ \to K^-\pi^+\pi^+)^0} \tag{76}$$

- $j = 18$, UncorrCL from $B^0\bar{B}^0$

$$C_{18}^{MC} = C_{UncorCL}^{D^+} \frac{C_{B^0}\mathcal{B}(D^+ \to K^-\pi^+\pi^+)}{\mathcal{B}(D^+ \to K^-\pi^+\pi^+)^0} \tag{77}$$

- $j = 19$, CascL from B^+B^-

$$C_{19}^{MC} = C_{CascL}^{D^+} \frac{C_{B^+}\mathcal{B}(D^+ \to K^-\pi^+\pi^+)}{\mathcal{B}(D^+ \to K^-\pi^+\pi^+)^0} \tag{78}$$

- $j = 20$, CascL from $B^0\bar{B}^0$

$$C_{20}^{MC} = C_{CascL}^{D^+} \frac{C_{B^0}\mathcal{B}(D^+ \to K^-\pi^+\pi^+)}{\mathcal{B}(D^+ \to K^-\pi^+\pi^+)^0} \tag{79}$$

- $j = 21$, FakeL from B^+B^-

$$C_{21}^{MC} = C_{FakeL}^{D^+} \frac{C_{B^+}\mathcal{B}(D^+ \to K^-\pi^+\pi^+)}{\mathcal{B}(D^+ \to K^-\pi^+\pi^+)^0} \tag{80}$$

- $j = 22$, FakeL from $B^0\bar{B}^0$

$$C_{22}^{MC} = C_{FakeL}^{D^+} \frac{C_{B^0}\mathcal{B}(D^+ \to K^-\pi^+\pi^+)}{\mathcal{B}(D^+ \to K^-\pi^+\pi^+)^0} \tag{81}$$

- $j = 23$, CombRL from B^+B^-

$$C_{23}^{MC} = \frac{C_{B^+}\mathcal{B}(D^+ \to K^-\pi^+\pi^+)}{\mathcal{B}(D^+ \to K^-\pi^+\pi^+)^0} \tag{82}$$

- $j = 24$, CombRL from $B^0\bar{B}^0$

$$C_{24}^{MC} = \frac{C_{B^0}\mathcal{B}(D^+ \to K^-\pi^+\pi^+)}{\mathcal{B}(D^+ \to K^-\pi^+\pi^+)^0} \tag{83}$$

- $j = 25$, CombFL from B^+B^-

$$C_{25}^{MC} = \frac{C_{B^+}\mathcal{B}(D^+ \to K^-\pi^+\pi^+)}{\mathcal{B}(D^+ \to K^-\pi^+\pi^+)^0} \tag{84}$$

- $j = 26$, CombFL from $B^0\bar{B}^0$

$$C_{26}^{MC} = \frac{C_{B^0}\mathcal{B}(D^+ \to K^-\pi^+\pi^+)}{\mathcal{B}(D^+ \to K^-\pi^+\pi^+)^0} \tag{85}$$

5 Constraints on variables in the fit

5.1 $B \to D^{**}\ell\nu$ and $B \to D^{(*)}\pi\ell\nu$ decay branching fractions

[Note] The calculated results in this subsection are not used in our fit as explained later. We keep this section for the following purposes :

- **to show the origin of our parametrization.**
- **to keep the original numbers for a reference.**

Our fitting method does not have the sensitivity to determine all 16 branching fractions of $B \to D^{**}\ell\nu$ and $B \to D^{(*)}\pi\ell\nu$ (non-resonant) decays. Thus, we need constraints to reduce free parameters. Available measurements of these decay modes are very limited. Currently we have only four usable results. The first is from PDG [13]

$$\mathcal{B}(B^+ \to \bar{D}_1^0\ell^+\nu) = 0.0056 \pm 0.0013 \pm 0.0009 = 0.0056 \pm 0.00158 \tag{86}$$

The next is from the most recent Babar measurement [16]

$$\begin{aligned}
\mathcal{B}(B^+ \to \bar{D}_1^0\ell^+\nu) &= 0.00448 \pm 0.00026 \pm 0.00035 = 0.00448 \pm 0.000436 \\
\mathcal{B}(B^+ \to \bar{D}_2^{*0}\ell^+\nu) &= 0.00354 \pm 0.00032 \pm 0.00054 = 0.00354 \pm 0.000627 \\
\mathcal{B}(B^0 \to D_1^-\ell^+\nu) &= 0.00364 \pm 0.00032 \pm 0.00049 = 0.00364 \pm 0.000585 \\
\mathcal{B}(B^0 \to D_2^{*-}\ell^+\nu) &= 0.00270 \pm 0.00035 \pm 0.00043 = 0.00270 \pm 0.000554
\end{aligned} \tag{87}$$

The third is from the most recent DELPHI measurement [17]

$$\begin{aligned}
&\mathcal{B}(B^0 \to D_0^{*-}\ell^+\nu) = 0.0042 \pm 0.0033 \pm 0.0022 = 0.0042 \pm 0.0040 \\
&\mathcal{B}(B^0 \to D_1'^-\ell^+\nu) = 0.0124 \pm 0.0025 \pm 0.0027 = 0.0124 \pm 0.0037 \\
&\mathcal{BT}(B^0 \to D^{**-}\ell^+\nu) \\
&\equiv \mathcal{B}(B^0 \to D_0^{*-}\ell^+\nu) + \mathcal{B}(B^0 \to D_1'^-\ell^+\nu) + \mathcal{B}(B^0 \to D_1^-\ell^+\nu) + \mathcal{B}(B^0 \to D_2^{*-}\ell^+\nu) \\
&= 0.027 \pm 0.007 \pm 0.002 = 0.027 \pm 0.073
\end{aligned} \tag{88}$$

The last is also from PDG [13]

$$\begin{aligned}
\mathcal{BT}(B^+ \to D^-\pi^+\ell^+\nu) &= 0.0053 \pm 0.0009 \pm 0.0005 = 0.0053 \pm 0.0010 \\
\mathcal{BT}(B^+ \to D^{*-}\pi^+\ell^+\nu) &= 0.0064 \pm 0.0015 \pm 0.0002 = 0.0064 \pm 0.0015 \\
\mathcal{BT}(B^0 \to \bar{D}^0\pi^-\ell^+\nu) &= 0.0032 \pm 0.0009 \pm 0.0003 = 0.0032 \pm 0.00095 \\
\mathcal{BT}(B^0 \to \bar{D}^{*0}\pi^-\ell^+\nu) &= 0.0065 \pm 0.0015 \pm 0.0005 = 0.0065 \pm 0.0016
\end{aligned} \tag{89}$$

These values are based on a BELLE measurement [18] and $B \to D^{**}\ell\nu$ decays are included in these branching fractions.
As we show in the following sections, it is convenient to divide $B \to D^{**}\ell\nu$ and $B \to D^{(*)}\pi\ell\nu$ (non-resonant) decay branching fractions into three categories : "$B \to D_1\ell\nu$ and $B \to D_2^*\ell\nu$", "$B \to D_0^*\ell\nu$ and $B \to D\pi\ell\nu$", and "$B \to D_1'\ell\nu$ and $B \to D^*\pi\ell\nu$".

5.1.1 $B \to D_1 \ell\nu$ and $B \to D_2^* \ell\nu$

There are 4 branching fractions in these decay modes : $\mathcal{B}(B^+ \to \bar{D}_1^0 \ell^+ \nu)$, $\mathcal{B}(B^0 \to D_1^- \ell^+ \nu)$, $\mathcal{B}(B^+ \to \bar{D}_2^{*0} \ell^+ \nu)$ and $\mathcal{B}(B^0 \to D_2^{*-} \ell^+ \nu)$. We define two parameters, one total branching fraction and one branching fraction ratio, and relate the 4 branching fractions to the parameters. Based on isospin symmetry

$$\begin{aligned}\mathcal{B}(B^+ \to \bar{D}_1^0 \ell^+ \nu) &= t_{+0} \mathcal{B}(B^0 \to D_1^- \ell^+ \nu) \\ \mathcal{B}(B^+ \to \bar{D}_2^{*0} \ell^+ \nu) &= t_{+0} \mathcal{B}(B^0 \to D_2^{*-} \ell^+ \nu)\end{aligned} \tag{90}$$

The Babar results (Equation (87)) show that isospin symmetry holds. Thus, we take averages. As we do not know the correlation between these branching fractions, we take a conservative side and assume the maximum correlation

$$\begin{aligned}\mathcal{B}(B^+ \to \bar{D}_1^0 \ell^+ \nu) &= \tfrac{1}{2} \left[(0.00448 \pm 0.000436) + (0.00364 \pm 0.000585) \times (1.071 \pm 0.009)\right] \\ &= \tfrac{1}{2} \left[(0.00448 \pm 0.000436) + (0.003898 \pm 0.0006274)\right] \\ &= 0.00419 \pm 0.000532\end{aligned} \tag{91}$$

and

$$\begin{aligned}\mathcal{B}(B^+ \to \bar{D}_2^{*0} \ell^+ \nu) &= \tfrac{1}{2} \left[(0.00354 \pm 0.000627) + (0.00270 \pm 0.000554) \times (1.071 \pm 0.009)\right] \\ &= \tfrac{1}{2} \left[(0.00354 \pm 0.000627) + (0.002892 \pm 0.0005938)\right] \\ &= 0.003215 \pm 0.0006104\end{aligned} \tag{92}$$

Thus, if we define a total branching fraction

$$\begin{aligned}\mathcal{BT}(B^+ \to \bar{D}_1^0/\bar{D}_2^{*0} \ell^+ \nu) &\equiv \mathcal{B}(B^+ \to \bar{D}_1^0 \ell^+ \nu) + \mathcal{B}(B^+ \to \bar{D}_2^{*0} \ell^+ \nu) \\ &= (0.00419 \pm 0.000532) + (0.003215 \pm 0.0006104) \\ &= 0.007405 \pm 0.0011874\end{aligned} \tag{93}$$

and a branching fraction ratio

$$\begin{aligned}f_{D_2^*/D_1} \equiv \frac{\mathcal{B}(B^+ \to \bar{D}_2^{*0} \ell^+ \nu)}{\mathcal{B}(B^+ \to \bar{D}_1^0 \ell^+ \nu)} &= \frac{0.003215 \pm 0.0006104}{0.00419 \pm 0.000532} \\ &= 0.767 \pm 0.243\end{aligned} \tag{94}$$

We can relate 4 branching fractions to $f_{D_2^*/D_1}$ and $\mathcal{BT}(B^+ \to \bar{D}_1^0/\bar{D}_2^{*0} \ell^+ \nu)$

$$\mathcal{B}(B^+ \to \bar{D}_1^0 \ell^+ \nu) = \frac{1}{1 + f_{D_2^*/D_1}} \mathcal{BT}(B^+ \to \bar{D}_1^0/\bar{D}_2^{*0} \ell^+ \nu) \tag{95}$$

$$\begin{aligned}\mathcal{B}(B^0 \to D_1^- \ell^+ \nu) &= \frac{\mathcal{B}(B^+ \to \bar{D}_1^0 \ell^+ \nu)}{t_{+0}} \\ &= \frac{1}{t_{+0}(1 + f_{D_2^*/D_1})} \mathcal{BT}(B^+ \to \bar{D}_1^0/\bar{D}_2^{*0} \ell^+ \nu)\end{aligned} \tag{96}$$

$$\begin{aligned}
\mathcal{B}(B^+ \to \bar{D}_2^{*0}\ell^+\nu) &= f_{D_2^*/D_1}\mathcal{B}(B^+ \to \bar{D}_1^0\ell^+\nu) \\
&= \frac{f_{D_2^*/D_1}}{1+f_{D_2^*/D_1}}\mathcal{BT}(B^+ \to \bar{D}_1^0/\bar{D}_2^{*0}\ell^+\nu)
\end{aligned} \tag{97}$$

$$\begin{aligned}
\mathcal{B}(B^0 \to D_2^{*-}\ell^+\nu) &= \frac{\mathcal{B}(B^+ \to \bar{D}_2^{*0}\ell^+\nu)}{t_{+0}} \\
&= \frac{\mathcal{B}(B^+ \to \bar{D}_2^{*0}\ell^+\nu)}{t_{+0}(1+f_{D_2^*/D_1})}\mathcal{BT}(B^+ \to \bar{D}_1^0/\bar{D}_2^{*0}\ell^+\nu)
\end{aligned} \tag{98}$$

5.1.2 $B \to D_0^*\ell\nu$ and non-resonant $B \to D\pi\ell\nu$

There are 6 branching fractions in this category : $\mathcal{B}(B^+ \to \bar{D}_0^{*0}\ell^+\nu)$, $\mathcal{B}(B^0 \to D_0^{*-}\ell^+\nu)$, $\mathcal{B}(B^+ \to D^-\pi^+\ell^+\nu)$, $\mathcal{B}(B^0 \to \bar{D}^0\pi^-\ell^+\nu)$, $\mathcal{B}(B^+ \to \bar{D}^0\pi^0\ell^+\nu)$ and $\mathcal{B}(B^0 \to D^-\pi^0\ell^+\nu)$. As in the previous section, we define two parameters, one total branching fraction and one branching fraction ratio, and relate the 6 branching fractions to the parameters. Isospin symmetry gives

$$\begin{aligned}
&\mathcal{B}(B^+ \to \bar{D}_0^{*0}\ell^+\nu) = t_{+0}\mathcal{B}(B^0 \to D_0^{*-}\ell^+\nu) \\
&\mathcal{B}(B^+ \to D^-\pi^+\ell^+\nu) = 2\mathcal{B}(B^+ \to \bar{D}^0\pi^0\ell^+\nu) \\
&\quad = t_{+0}\mathcal{B}(B^0 \to \bar{D}^0\pi^-\ell^+\nu) = 2t_{+0}\mathcal{B}(B^0 \to D^-\pi^0\ell^+\nu) \\
&\mathcal{BT}(B^+ \to D^-\pi^+\ell^+\nu) = t_{+0}\mathcal{BT}(B^0 \to \bar{D}^0\pi^-\ell^+\nu)
\end{aligned} \tag{99}$$

Note that $\mathcal{BT}(B^+ \to D^-\pi^+\ell^+\nu)$ is what is given in Equation (89). This includes not only non-resonant $D^-\pi^+$ mode but also relevant D^{**} modes. Thus,

$$\begin{aligned}
&\mathcal{BT}(B^+ \to D^-\pi^+\ell^+\nu) \\
&= \mathcal{B}(B^+ \to \bar{D}_0^{*0}\ell^+\nu)\mathcal{B}(\bar{D}_0^{*0} \to D^-\pi^+) + \mathcal{B}(B^+ \to \bar{D}_2^{*0}\ell^+\nu)\mathcal{B}(\bar{D}_2^{*0} \to D^-\pi^+) \\
&\quad +\mathcal{B}(B^+ \to D^-\pi^+\ell^+\nu)
\end{aligned} \tag{100}$$

Using the above isospin condition, we can take an average of Equation (89). Here, we also take the maximum correlation

$$\begin{aligned}
&\mathcal{BT}(B^+ \to D^-\pi^+\ell^+\nu) \\
&= \tfrac{1}{2}\left[(0.0053 \pm 0.0010) + (0.00323 \pm 0.00095) \times (1.071 \pm 0.009)\right] \\
&= \tfrac{1}{2}\left[(0.0053 \pm 0.0010) + (0.00346 \pm 0.001018)\right] \\
&= 0.00438 \pm 0.00101
\end{aligned} \tag{101}$$

From Equation (100),

$$\begin{aligned}
&\mathcal{BT}(B^+ \to D^-\pi^+\ell^+\nu) \\
&= \mathcal{B}(B^+ \to \bar{D}_0^{*0}\ell^+\nu) \times \tfrac{2}{3} + \mathcal{B}(B^+ \to \bar{D}_2^{*0}\ell^+\nu)\mathcal{B}(\bar{D}_2^{*0} \to D^-\pi^+) \\
&\quad +\mathcal{B}(B^+ \to D^-\pi^+\ell^+\nu)
\end{aligned} \tag{102}$$

Using equations (186) (in section 8) and (92),

$$\begin{aligned}
&\mathcal{B}(B^+ \to D^-\pi^+\ell^+\nu) + \tfrac{2}{3}\mathcal{B}(B^+ \to \bar{D}_0^{*0}\ell^+\nu) \\
&= \mathcal{BT}(B^+ \to D^-\pi^+\ell^+\nu) - \mathcal{B}(B^+ \to \bar{D}_2^{*0}\ell^+\nu)\mathcal{B}(\bar{D}_2^{*0} \to D^-\pi^+) \\
&= (0.00438 \pm 0.00101) - (0.003215 \pm 0.0006104) \times (0.452 \pm 0.167) \\
&= (0.00438 \pm 0.00101) - (0.001453 \pm 0.0006036) \\
&= 0.00293 \pm 0.00118
\end{aligned} \tag{103}$$

Thus, if we define a total branching fraction

$$\begin{aligned}
&\mathcal{BT}(B^+ \to \bar{D}_0^{*0}/(D\pi)^0\ell^+\nu) \\
&\equiv \mathcal{B}(B^+ \to \bar{D}_0^{*0}\ell^+\nu) + \mathcal{B}(B^+ \to D^-\pi^+\ell^+\nu) + \mathcal{B}(B^+ \to \bar{D}^0\pi^0\ell^+\nu) \\
&= \mathcal{B}(B^+ \to \bar{D}_0^{*0}\ell^+\nu) + \tfrac{3}{2}\mathcal{B}(B^+ \to D^-\pi^+\ell^+\nu) \\
&= \tfrac{3}{2}(0.00293 \pm 0.00118) = 0.0044 \pm 0.0018
\end{aligned} \tag{104}$$

and a branching fraction ratio

$$f_{D\pi/D_0^*} \equiv \frac{\mathcal{B}(B^+ \to D^-\pi^+\ell^+\nu)}{\mathcal{B}(B^+ \to \bar{D}_0^{*0}\ell^+\nu)} \tag{105}$$

we can relate 6 branching fractions to $\mathcal{BT}(B^+ \to \bar{D}_0^{*0}/(D\pi)^0\ell^+\nu)$ and $f_{D\pi/D_0^*}$.

$$\mathcal{B}(B^+ \to \bar{D}_0^{*0}\ell^+\nu) = \frac{2}{2+3f_{D\pi/D_0^*}}\mathcal{BT}(B^+ \to \bar{D}_0^{*0}/(D\pi)^0\ell^+\nu) \tag{106}$$

$$\begin{aligned}
\mathcal{B}(B^+ \to D^-\pi^+\ell^+\nu) &= f_{D\pi/D_0^*}\mathcal{B}(B^+ \to \bar{D}_0^{*0}\ell^+\nu) \\
&= \frac{2f_{D\pi/D_0^*}}{2+3f_{D\pi/D_0^*}}\mathcal{BT}(B^+ \to \bar{D}_0^{*0}/(D\pi)^0\ell^+\nu)
\end{aligned} \tag{107}$$

$$\begin{aligned}
\mathcal{B}(B^+ \to \bar{D}^0\pi^0\ell^+\nu) &= \frac{\mathcal{B}(B^+ \to D^-\pi^+\ell^+\nu)}{2} \\
&= \frac{f_{D\pi/D_0^*}}{2+3f_{D\pi/D_0^*}}\mathcal{BT}(B^+ \to \bar{D}_0^{*0}/(D\pi)^0\ell^+\nu)
\end{aligned} \tag{108}$$

$$\begin{aligned}
\mathcal{B}(B^0 \to D_0^{*-}\ell^+\nu) &= \frac{\mathcal{B}(B^+ \to \bar{D}_0^{*0}\ell^+\nu)}{t_{+0}} \\
&= \frac{2}{t_{+0}(2+3f_{D\pi/D_0^*})}\mathcal{BT}(B^+ \to \bar{D}_0^{*0}/(D\pi)^0\ell^+\nu)
\end{aligned} \tag{109}$$

$$\begin{aligned}
\mathcal{B}(B^0 \to \bar{D}^0\pi^-\ell^+\nu) &= \frac{\mathcal{B}(B^+ \to D^-\pi^+\ell^+\nu)}{t_{+0}} \\
&= \frac{2f_{D\pi/D_0^*}}{t_{+0}(2+3f_{D\pi/D_0^*})}\mathcal{BT}(B^+ \to \bar{D}_0^{*0}/(D\pi)^0\ell^+\nu)
\end{aligned} \tag{110}$$

$$\begin{aligned}
\mathcal{B}(B^0 \to D^-\pi^0\ell^+\nu) &= \frac{\mathcal{B}(B^+ \to \bar{D}^0\pi^0\ell^+\nu)}{t_{+0}} \\
&= \frac{f_{D\pi/D_0^*}}{t_{+0}(2+3f_{D\pi/D_0^*})}\mathcal{BT}(B^+ \to \bar{D}_0^{*0}/(D\pi)^0\ell^+\nu)
\end{aligned} \tag{111}$$

Now, let us calculate $f_{D\pi/D_0^*}$. Using Equation (88)

$$\begin{aligned}&\mathcal{B}(B^+ \to \bar{D}_0^{*0}\ell^+\nu) = t_{+0}\mathcal{B}(B^0 \to D_0^{*-}\ell^+\nu)\\&= (1.071 \pm 0.009)(0.0042 \pm 0.0040) = 0.0045 \pm 0.0043\end{aligned} \tag{112}$$

Thus, from Equation (103),

$$\begin{aligned}\mathcal{B}(B^+ \to D^-\pi^+\ell^+\nu) &= (0.00293 \pm 0.00118) - \tfrac{2}{3}(0.0045 \pm 0.0043)\\&= -0.00007 \pm 0.00310\end{aligned} \tag{113}$$

Then, $f_{D\pi/D_0^*}$ is given by

$$f_{D\pi/D_0^*} = \frac{-0.00007 \pm 0.00310}{0.0045 \pm 0.0043} = -0.016 \pm 0.689 \tag{114}$$

The ratio $f_{D\pi/D_0^*}$ cannot be negative. Thus, we take a positive number as described below.

5.1.3 $B \to D_1'\ell\nu$ and non-resonant $B \to D^*\pi\ell\nu$.

There are also 6 branching fractions in this category : $\mathcal{B}(B^+ \to \bar{D}_1'^0\ell^+\nu)$, $\mathcal{B}(B^0 \to D_1'^-\ell^+\nu)$, $\mathcal{B}(B^+ \to D^{*-}\pi^+\ell^+\nu)$, $\mathcal{B}(B^0 \to \bar{D}^{*0}\pi^-\ell^+\nu)$, $\mathcal{B}(B^+ \to \bar{D}^{*0}\pi^0\ell^+\nu)$ and $\mathcal{B}(B^0 \to D^{*-}\pi^0\ell^+\nu)$. Again, we define two parameters, one total branching fraction and one branching fraction ratio, and relate the 6 branching fractions to the parameters. From isospin symmetry

$$\begin{aligned}&\mathcal{B}(B^+ \to \bar{D}_1'^0\ell^+\nu) = t_{+0}\mathcal{B}(B^0 \to D_1'^-\ell^+\nu)\\&\mathcal{B}(B^+ \to D^{*-}\pi^+\ell^+\nu) = 2\mathcal{B}(B^+ \to \bar{D}^{*0}\pi^0\ell^+\nu)\\&\quad = t_{+0}\mathcal{B}(B^0 \to \bar{D}^{*0}\pi^-\ell^+\nu) = 2t_{+0}\mathcal{B}(B^0 \to D^{*-}\pi^0\ell^+\nu)\\&\mathcal{BT}(B^+ \to D^{*-}\pi^+\ell^+\nu) = t_{+0}\mathcal{BT}(B^0 \to \bar{D}^{*0}\pi^-\ell^+\nu)\end{aligned} \tag{115}$$

Note that $\mathcal{BT}(B^+ \to D^{*-}\pi^+\ell^+\nu)$ is what is given in Equation (89). This includes not only non-resonant $D^{*-}\pi^+$ mode but also relevant D^{**} modes. Thus,

$$\begin{aligned}&\mathcal{BT}(B^+ \to D^{*-}\pi^+\ell^+\nu)\\&= \mathcal{B}(B^+ \to \bar{D}_1^0\ell^+\nu)\mathcal{B}(D_1^0 \to D^{*+}\pi^-) + \mathcal{B}(B^+ \to \bar{D}_1'^0\ell^+\nu)\mathcal{B}(D_1'^0 \to D^{*+}\pi^-)\\&\quad +\mathcal{B}(B^+ \to \bar{D}_2^{*0}\ell^+\nu)\mathcal{B}(D_2^{*0} \to D^{*+}\pi^-) + \mathcal{B}(B^+ \to D^{*-}\pi^+\ell^+\nu)\end{aligned} \tag{116}$$

Using the above isospin condition, we can take an average of Equation (89). Again, assuming the maximum correlation,

$$\begin{aligned}&\mathcal{BT}(B^+ \to D^{*-}\pi^+\ell^+\nu)\\&= \tfrac{1}{2}\left[(0.0064 \pm 0.0015) + (0.0065 \pm 0.0016) \times (1.071 \pm 0.009)\right]\\&= \tfrac{1}{2}\left[(0.0064 \pm 0.0015) + (0.00696 \pm 0.00171)\right]\\&= 0.00668 \pm 0.00161\end{aligned} \tag{117}$$

From Equation (116),

$$\begin{aligned}
&\mathcal{BT}(B^+ \to D^{*-}\pi^+\ell^+\nu) \\
&= \tfrac{2}{3}\mathcal{B}(B^+ \to \bar{D}_1^0\ell^+\nu) + \tfrac{2}{3}\mathcal{B}(B^+ \to \bar{D}_1^{\prime 0}\ell^+\nu) \\
&\quad +\mathcal{B}(B^+ \to \bar{D}_2^{*0}\ell^+\nu)\mathcal{B}(D_2^{*+} \to D^{*0}\pi^+) + \mathcal{B}(B^+ \to D^{*-}\pi^+\ell^+\nu)
\end{aligned} \tag{118}$$

Using equations (91), (188) (in section 8) and (92),

$$\begin{aligned}
&\mathcal{B}(B^+ \to D^{*-}\pi^+\ell^+\nu) + \tfrac{2}{3}\mathcal{B}(B^+ \to \bar{D}_1^{\prime 0}\ell^+\nu) \\
&= \mathcal{BT}(B^+ \to D^{*-}\pi^+\ell^+\nu) - \tfrac{2}{3}\mathcal{B}(B^+ \to \bar{D}_1^0\ell^+\nu) - \mathcal{B}(B^+ \to \bar{D}_2^{*0}\ell^+\nu)\mathcal{B}(D_2^{*+} \to D^{*0}\pi^+) \\
&= (0.00668 \pm 0.00161) - \tfrac{2}{3} \times (0.00419 \pm 0.000532) \\
&\qquad -(0.003215 \pm 0.0006104) \times (0.215 \pm 0.045) \\
&= (0.00668 \pm 0.00161) - (0.00279 \pm 0.0003547) - (0.000691 \pm 0.0001953) \\
&= 0.00319 \pm 0.00166
\end{aligned} \tag{119}$$

Thus, if we define a total branching fraction

$$\begin{aligned}
&\mathcal{BT}(B^+ \to \bar{D}_1^{*0}/(D^*\pi)^0\ell^+\nu) \\
&\equiv \mathcal{B}(B^+ \to \bar{D}_1^{\prime 0}\ell^+\nu) + \mathcal{B}(B^+ \to D^{*-}\pi^+\ell^+\nu) + \mathcal{B}(B^+ \to \bar{D}^{*0}\pi^0\ell^+\nu) \\
&= \mathcal{B}(B^+ \to \bar{D}_1^{\prime 0}\ell^+\nu) + \tfrac{3}{2}\mathcal{B}(B^+ \to D^{*-}\pi^+\ell^+\nu) \\
&= \tfrac{3}{2}(0.00319 \pm 0.00166) = 0.0048 \pm 0.0025
\end{aligned} \tag{120}$$

and a branching fraction ratio

$$f_{D^*\pi/D_1'} \equiv \frac{\mathcal{B}(B^+ \to D^{*-}\pi^+\ell^+\nu)}{\mathcal{B}(B^+ \to \bar{D}_1^{\prime 0}\ell^+\nu)} \tag{121}$$

We can relate the 6 branching fractions to $\mathcal{BT}(B^+ \to \bar{D}_1^{*0}/(D^*\pi)^0\ell^+\nu)$ and $f_{D^*\pi/D_1'}$

$$\mathcal{B}(B^+ \to \bar{D}_1^{\prime 0}\ell^+\nu) = \frac{2}{2+3f_{D^*\pi/D_1'}}\mathcal{BT}(B^+ \to \bar{D}_1^{*0}/(D^*\pi)^0\ell^+\nu) \tag{122}$$

$$\begin{aligned}
\mathcal{B}(B^+ \to D^{*-}\pi^+\ell^+\nu) &= f_{D^*\pi/D_1'}\mathcal{B}(B^+ \to \bar{D}_1^{\prime 0}\ell^+\nu) \\
&= \frac{2f_{D^*\pi/D_1'}}{2+3f_{D^*\pi/D_1'}}\mathcal{BT}(B^+ \to \bar{D}_1^{*0}/(D^*\pi)^0\ell^+\nu)
\end{aligned} \tag{123}$$

$$\begin{aligned}
\mathcal{B}(B^+ \to \bar{D}^{*0}\pi^0\ell^+\nu) &= \frac{\mathcal{B}(B^+ \to D^{*-}\pi^+\ell^+\nu)}{2} \\
&= \frac{f_{D^*\pi/D_1'}}{2+3f_{D^*\pi/D_1'}}\mathcal{BT}(B^+ \to \bar{D}_1^{*0}/(D^*\pi)^0\ell^+\nu)
\end{aligned} \tag{124}$$

$$\begin{aligned}
\mathcal{B}(B^0 \to D_1^{\prime -}\ell^+\nu) &= \frac{\mathcal{B}(B^+ \to \bar{D}_1^{\prime 0}\ell^+\nu)}{t_{+0}} \\
&= \frac{2}{t_{+0}(2+3f_{D^*\pi/D_1'})}\mathcal{BT}(B^+ \to \bar{D}_1^{*0}/(D^*\pi)^0\ell^+\nu)
\end{aligned} \tag{125}$$

$$\begin{aligned}\mathcal{B}(B^0 \to \bar{D}^{*0}\pi^-\ell^+\nu) &= \frac{\mathcal{B}(B^+ \to D^{*-}\pi^+\ell^+\nu)}{t_{+0}} \\ &= \frac{2f_{D^*\pi/D_1'}}{t_{+0}(2+3f_{D^*\pi/D_1'})}\mathcal{BT}(B^+ \to \bar{D}_1^{*0}/(D^*\pi)^0\ell^+\nu) \end{aligned} \tag{126}$$

$$\begin{aligned}\mathcal{B}(B^0 \to D^{*-}\pi^0\ell^+\nu) &= \frac{\mathcal{B}(B^+ \to \bar{D}^{*0}\pi^0\ell^+\nu)}{t_{+0}} \\ &= \frac{f_{D^*\pi/D_1'}}{t_{+0}(2+3f_{D^*\pi/D_1'})}\mathcal{BT}(B^+ \to \bar{D}_1^{*0}/(D^*\pi)^0\ell^+\nu) \end{aligned} \tag{127}$$

Now, let us calculate $f_{D^*\pi/D_1'}$. Using Equation (88)

$$\begin{aligned}&\mathcal{B}(B^+ \to \bar{D}_1'^0\ell^+\nu) = t_{+0}\mathcal{B}(B^0 \to D_1'^-\ell^+\nu) \\ &= (1.071 \pm 0.009)(0.0124 \pm 0.0037) = 0.0133 \pm 000725\end{aligned} \tag{128}$$

Thus, by Equation (119),

$$\begin{aligned}&\mathcal{B}(B^+ \to D^{*-}\pi^+\ell^+\nu) = (0.00319 \pm 0.00166) - \tfrac{2}{3}(0.0133 \pm 0.00725) \\ &\quad = -0.005677 \pm 0.00511\end{aligned} \tag{129}$$

Then, $f_{D\pi/D_0^*}$ is

$$f_{D^*\pi/D_1'} = \frac{-0.005677 \pm 0.00511}{0.0133 \pm 0.00725} = -0.427 \pm 0.449 \tag{130}$$

The ratio $f_{D^*\pi/D_1'}$ cannot be negative. Thus, we take a positive number as described below.

5.1.4 $B \to D^{**}\ell\nu$ and non-resonant $B \to D^{(*)}\pi\ell\nu$

We define a total branching fraction

$$\begin{aligned}&\mathcal{BT}(B^+ \to \bar{D}^{**0}/(D\pi)^0\ell^+\nu) \\ &\equiv \mathcal{BT}(B^+ \to \bar{D}_1^0/\bar{D}_2^{*0}\ell^+\nu) + \mathcal{BT}(B^+ \to \bar{D}_0^{*0}/(D\pi)^0\ell^+\nu) + \mathcal{BT}(B^+ \to \bar{D}_1^{*0}/(D^*\pi)^0\ell^+\nu)\end{aligned} \tag{131}$$

We also define two ratios

$$\begin{aligned}f_{D_0^*D\pi T/D_1D_2^*T} &\equiv \frac{\mathcal{BT}(B^+ \to \bar{D}_0^{*0}/(D\pi)^0\ell^+\nu)}{\mathcal{BT}(B^+ \to \bar{D}_1^0/\bar{D}_2^{*0}\ell^+\nu)} = \frac{3}{2}\frac{0.00293 \pm 0.00118}{0.007405 \pm 0.0011874} \\ &= 0.59 \pm 0.26\end{aligned} \tag{132}$$

and

$$\begin{aligned}f_{D_1'D^*\pi T/D_1D_2^*T} &\equiv \frac{\mathcal{BT}(B^+ \to \bar{D}_1^{*0}/(D^*\pi)^0\ell^+\nu)}{\mathcal{BT}(B^+ \to \bar{D}_1^0/\bar{D}_2^{*0}\ell^+\nu)} = \frac{3}{2}\frac{0.00319 \pm 0.00166}{0.007405 \pm 0.0011874} \\ &= 0.65 \pm 0.35\end{aligned} \tag{133}$$

Then, we can relate all 16 branching fractions of $B \to D^{**}\ell\nu$ and non-resonant $B \to D^{(*)}\pi\ell\nu$ decays to $\mathcal{BT}(B^+ \to \bar{D}^{**0}/(D\pi)^0\ell^+\nu)$ and five ratios. First, we have

$$\mathcal{BT}(B^+ \to \bar{D}_1^0/\bar{D}_2^{*0}\ell^+\nu) = \frac{\mathcal{BT}(B^+ \to \bar{D}^{**0}/(D\pi)^0\ell^+\nu)}{1 + f_{D_0^* D\pi T/D_1 D_2^* T} + f_{D_1' D^*\pi T/D_1 D_2^* T}} \tag{134}$$

$$\begin{aligned}\mathcal{BT}(B^+ \to \bar{D}_0^{*0}/(D\pi)^0\ell^+\nu) &= f_{D_0^* D\pi T/D_1 D_2^* T}\mathcal{BT}(B^+ \to \bar{D}_1^0/\bar{D}_2^{*0}\ell^+\nu) \\ &= \frac{f_{D_0^* D\pi T/D_1 D_2^* T}\mathcal{BT}(B^+ \to \bar{D}^{**0}/(D\pi)^0\ell^+\nu)}{1 + f_{D_0^* D\pi T/D_1 D_2^* T} + f_{D_1' D^*\pi T/D_1 D_2^* T}}\end{aligned} \tag{135}$$

$$\begin{aligned}\mathcal{BT}(B^+ \to \bar{D}_1^{*0}/(D^*\pi)^0\ell^+\nu) &= f_{D_1' D^*\pi T/D_1 D_2^* T}\mathcal{BT}(B^+ \to \bar{D}_1^0/\bar{D}_2^{*0}\ell^+\nu) \\ &= \frac{f_{D_1' D^*\pi T/D_1 D_2^* T}\mathcal{BT}(B^+ \to \bar{D}^{**0}/(D\pi)^0\ell^+\nu)}{1 + f_{D_0^* D\pi T/D_1 D_2^* T} + f_{D_1' D^*\pi T/D_1 D_2^* T}}\end{aligned} \tag{136}$$

Substituting these into equations (95)-(98), (106)-(111) and (122)-(127),

$$\mathcal{B}(B^+ \to \bar{D}_1^0\ell^+\nu) = \frac{\mathcal{BT}(B^+ \to \bar{D}^{**0}/(D\pi)^0\ell^+\nu)}{(1 + f_{D_2^*/D_1})(1 + f_{D_0^* D\pi T/D_1 D_2^* T} + f_{D_1' D^*\pi T/D_1 D_2^* T})} \tag{137}$$

$$\mathcal{B}(B^+ \to \bar{D}_2^{*0}\ell^+\nu) = f_{D_2^*/D_1}\mathcal{B}(B^+ \to \bar{D}_1^0\ell^+\nu) \tag{138}$$

$$\mathcal{B}(B^+ \to \bar{D}_0^{*0}\ell^+\nu) = \frac{2f_{D_0^* D\pi T/D_1 D_2^* T}\mathcal{BT}(B^+ \to \bar{D}^{**0}/(D\pi)^0\ell^+\nu)}{(2 + 3f_{D\pi/D_0^*})(1 + f_{D_0^* D\pi T/D_1 D_2^* T} + f_{D_1' D^*\pi T/D_1 D_2^* T})} \tag{139}$$

$$\mathcal{B}(B^+ \to \bar{D}_1'^0\ell^+\nu) = \frac{2f_{D_1' D^*\pi T/D_1 D_2^* T}\mathcal{BT}(B^+ \to \bar{D}^{**0}/(D\pi)^0\ell^+\nu)}{(2 + 3f_{D^*\pi/D_1'})(1 + f_{D_0^* D\pi T/D_1 D_2^* T} + f_{D_1' D^*\pi T/D_1 D_2^* T})} \tag{140}$$

$$\mathcal{B}(B^+ \to D^-\pi^+\ell^+\nu) = f_{D\pi/D_0^*}\mathcal{B}(B^+ \to \bar{D}_0^{*0}\ell^+\nu) \tag{141}$$

$$\mathcal{B}(B^+ \to \bar{D}^0\pi^0\ell^+\nu) = \frac{\mathcal{B}(B^+ \to D^-\pi^+\ell^+\nu)}{2} \tag{142}$$

$$\mathcal{B}(B^+ \to D^{*-}\pi^+\ell^+\nu) = f_{D^*\pi/D_1'}\mathcal{B}(B^+ \to \bar{D}_1'^0\ell^+\nu) \tag{143}$$

$$\mathcal{B}(B^+ \to \bar{D}^{*0}\pi^0\ell^+\nu) = \frac{\mathcal{B}(B^+ \to D^{*-}\pi^+\ell^+\nu)}{2} \tag{144}$$

and

$$\mathcal{B}(B^0 \to D_1^-\ell^+\nu) = \frac{\mathcal{B}(B^+ \to \bar{D}_1^0\ell^+\nu)}{t_{+0}} \tag{145}$$

$$\mathcal{B}(B^0 \to D_2^{*-}\ell^+\nu) = \frac{\mathcal{B}(B^+ \to \bar{D}_2^{*0}\ell^+\nu)}{t_{+0}} \tag{146}$$

$$\mathcal{B}(B^0 \to D_0^{*-}\ell^+\nu) = \frac{\mathcal{B}(B^+ \to \bar{D}_0^{*0}\ell^+\nu)}{t_{+0}} \tag{147}$$

$$\mathcal{B}(B^0 \to D_1'^-\ell^+\nu) = \frac{\mathcal{B}(B^+ \to \bar{D}_1'^0\ell^+\nu)}{t_{+0}} \tag{148}$$

$$\mathcal{B}(B^0 \to \bar{D}^0\pi^-\ell^+\nu) = \frac{\mathcal{B}(B^+ \to D^-\pi^+\ell^+\nu)}{t_{+0}} \tag{149}$$

$$\mathcal{B}(B^0 \to D^-\pi^0\ell^+\nu) = \frac{\mathcal{B}(B^+ \to \bar{D}^0\pi^0\ell^+\nu)}{t_{+0}} \tag{150}$$

$$\mathcal{B}(B^0 \to \bar{D}^{*0}\pi^-\ell^+\nu) = \frac{\mathcal{B}(B^+ \to D^{*-}\pi^+\ell^+\nu)}{t_{+0}} \tag{151}$$

$$\mathcal{B}(B^0 \to D^{*-}\pi^0\ell^+\nu) = \frac{\mathcal{B}(B^+ \to \bar{D}^{*0}\pi^0\ell^+\nu)}{t_{+0}} \tag{152}$$

Thus, we have only one branching fraction, $\mathcal{BT}(B^+ \to \bar{D}^{**0}/(D\pi)^0\ell^+\nu)$, to be determined by the fit. We also have five ratios. Three of them are determined from measurements as described above (Equations (94), (132) and (133)).

$$f_{D_2^*/D_1} = 0.767 \pm 0.243 \tag{153}$$

$$f_{D_0^* D\pi T/D_1 D_2^* T} = 0.59 \pm 0.26 \tag{154}$$

$$f_{D_1' D^*\pi T/D_1 D_2^* T} = 0.65 \pm 0.35 \tag{155}$$

and the other two have negative central numbers (Equations (114) and (130))

$$f_{D\pi/D_0^*} = -0.016 \pm 0.689 \tag{156}$$

$$f_{D^*\pi/D_1'} = -0.427 \pm 0.449 \tag{157}$$

In our fit, we set

$$f_{D\pi/D_0^*} = 0.2 \tag{158}$$

$$f_{D^*\pi/D_1'} = 0.1 \tag{159}$$

and we vary these values from 0 to 2 to get the systematic uncertainty from these ratios.
It is worth noting that our fit does not have the sensitivity to determine these ratios. We tried to float these ratios in our fit, but the results give large statistical uncertainties, for example, values larger than 100 %. Thus, we decided to fix these ratios in our fit.

5.2 New standard branching fractions from Semileotonic AWG

The following are the new branching fraction values recommended by the Semileptonic AWG [19]. We use these values in our fit, instead of the values shown above.

- B^+ decays
  - $\mathcal{B}(B^+ \to \bar{D}_0^{*0}\ell^+\nu) = 0.0045 \pm 0.0009$
  - $\mathcal{B}(B^+ \to \bar{D}_1^{0}\ell^+\nu) = 0.0054 \pm 0.0006$
  - $\mathcal{B}(B^+ \to \bar{D}_1^{\prime 0}\ell^+\nu) = 0.0085 \pm 0.0020$
  - $\mathcal{B}(B^+ \to \bar{D}_2^{*0}\ell^+\nu) = 0.0042 \pm 0.0008$
  - $\mathcal{B}(B^+ \to D^{-}\pi^+\ell^+\nu) = 0.0019 \pm 0.0012$
  - $\mathcal{B}(B^+ \to \bar{D}^{0}\pi^0\ell^+\nu) = 0.0010 \pm 0.0006$
  - $\mathcal{B}(B^+ \to D^{*-}\pi^+\ell^+\nu) = 0.0006 \pm 0.0004$

- $\mathcal{B}(B^+ \to \bar{D}^{*0}\pi^0\ell^+\nu) = 0.0003 \pm 0.0002$

- B^0 decays
  - $\mathcal{B}(B^0 \to D_0^{*-}\ell^+\nu) = 0.0043 \pm 0.0009$
  - $\mathcal{B}(B^0 \to D_1^{-}\ell^+\nu) = 0.0050 \pm 0.0008$
  - $\mathcal{B}(B^0 \to D_1'^{-}\ell^+\nu) = 0.0080 \pm 0.0020$
  - $\mathcal{B}(B^0 \to D_2^{*-}\ell^+\nu) = 0.0039 \pm 0.0007$
  - $\mathcal{B}(B^0 \to \bar{D}^0\pi^-\ell^+\nu) = 0.0019 \pm 0.0012$
  - $\mathcal{B}(B^0 \to D^-\pi^0\ell^+\nu) = 0.0009 \pm 0.0006$
  - $\mathcal{B}(B^0 \to \bar{D}^{*0}\pi^-\ell^+\nu) = 0.0006 \pm 0.0004$
  - $\mathcal{B}(B^0 \to D^{*-}\pi^0\ell^+\nu) = 0.0003 \pm 0.0004$

Here, isospin symmetry is assumed. We calculate the branching fraction ratios by assuming the above branching fractions are independent.

$$\begin{aligned}
&f_{D_2^*/D_1} \equiv \frac{\mathcal{B}(B^+\to\bar{D}_2^{*0}\ell^+\nu)}{\mathcal{B}(B^+\to\bar{D}_1^0\ell^+\nu)} = 0.78 \pm 0.17\\
&f_{D_0^*D\pi T/D_1D_2^*T} \equiv \frac{\mathcal{BT}(B^+\to\bar{D}_0^{*0}/(D\pi)^0\ell^+\nu)}{\mathcal{BT}(B^+\to\bar{D}_1^0/\bar{D}_2^{*0}\ell^+\nu)} = 0.77 \pm 0.19\\
&f_{D_1'D^*\pi T/D_1D_2^*T} \equiv \frac{\mathcal{BT}(B^+\to\bar{D}_1^{*0}/(D^*\pi)^0\ell^+\nu)}{\mathcal{BT}(B^+\to\bar{D}_1^0/\bar{D}_2^{*0}\ell^+\nu)} = 0.98 \pm 0.24\\
&f_{D\pi/D_0^*} \equiv \frac{\mathcal{B}(B^+\to D^-\pi^+\ell^+\nu)}{\mathcal{B}(B^+\to\bar{D}_0^{*0}\ell^+\nu)} = 0.42 \pm 0.28\\
&f_{D^*\pi/D_1'} \equiv \frac{\mathcal{B}(B^+\to D^{*-}\pi^+\ell^+\nu)}{\mathcal{B}(B^+\to\bar{D}_1^{*0}\ell^+\nu)} = 0.071 \pm 0.050
\end{aligned} \tag{160}$$

5.3 Backgrounds

In our fit there are 8 background coefficients for peaking backgrounds: $C^{D^0}_{UncorDL}$, $C^{D^0}_{UncorCL}$, $C^{D^0}_{CascL}$, $C^{D^0}_{FakeL}$, $C^{D^+}_{UncorDL}$, $C^{D^+}_{UncorCL}$, $C^{D^+}_{CascL}$ and $C^{D^+}_{FakeL}$. We would like to float all 8 coefficients, but as it turned out, our fit is not sensitive to $C^{D^0}_{FakeL}$ and $C^{D^+}_{FakeL}$. As a result, if we float $C^{D^0}_{FakeL}$ and/or $C^{D^+}_{FakeL}$, uncertainties on the fit results become large. Thus, we fix $C^{D^0}_{FakeL}$ and $C^{D^+}_{FakeL}$

$$\begin{aligned}
C^{D^+}_{FakeL} &= 1\\
C^{D^0}_{FakeL} &= 1
\end{aligned} \tag{161}$$

and float other 6 coefficients. Note that combinatorial backgrounds are always fixed.

5.4 Summary of fitting parameters and constraints

As a summary, we are trying to fit for three branching fractions and $\Upsilon(4S)$ decay BF ratio

- $\mathcal{B}(B^+ \to \bar{D}^0\ell^+\nu)$
- $\mathcal{B}(B^+ \to \bar{D}^{*0}\ell^+\nu)$

- $\mathcal{BT}(B^+ \to \bar{D}^{**0}/(D\pi)^0\ell^+\nu)$
- f_{+0}

with isospin constraints

- $\mathcal{B}(B^+ \to \bar{D}^0\ell^+\nu) = t_{+0}\mathcal{B}(B^0 \to D^-\ell^+\nu)$
- $\mathcal{B}(B^+ \to \bar{D}^{*0}\ell^+\nu) = t_{+0}\mathcal{B}(B^0 \to D^{*-}\ell^+\nu)$
- $\mathcal{B}(B^+ \to \bar{D}_0^{*0}\ell^+\nu) = t_{+0}\mathcal{B}(B^0 \to D_0^{*-}\ell^+\nu)$
- $\mathcal{B}(B^+ \to \bar{D}_1^0\ell^+\nu) = t_{+0}\mathcal{B}(B^0 \to D_1^-\ell^+\nu)$
- $\mathcal{B}(B^+ \to \bar{D}_1^{*0}\ell^+\nu) = t_{+0}\mathcal{B}(B^0 \to D_1'^-\ell^+\nu)$
- $\mathcal{B}(B^+ \to \bar{D}_2^{*0}\ell^+\nu) = t_{+0}\mathcal{B}(B^0 \to D_2^{*-}\ell^+\nu)$
- $\mathcal{B}(B^+ \to D^-\pi^+\ell^+\nu) = 2\mathcal{B}(B^+ \to \bar{D}^0\pi^0\ell^+\nu)$
  $= t_{+0}\mathcal{B}(B^0 \to \bar{D}^0\pi^-\ell^+\nu) = 2t_{+0}\mathcal{B}(B^0 \to D^-\pi^0\ell^+\nu)$
- $\mathcal{B}(B^+ \to D^{*-}\pi^+\ell^+\nu) = 2\mathcal{B}(B^+ \to \bar{D}^{*0}\pi^0\ell^+\nu)$
  $= t_{+0}\mathcal{B}(B^0 \to \bar{D}^{*0}\pi^-\ell^+\nu) = 2t_{+0}\mathcal{B}(B^0 \to D^{*-}\pi^0\ell^+\nu)$

and constraints on relative branching fractions

- $f_{D_2^*/D_1} \equiv \frac{\mathcal{B}(B^+\to\bar{D}_2^{*0}\ell^+\nu)}{\mathcal{B}(B^+\to\bar{D}_1^0\ell^+\nu)} = 0.78 \pm 0.17$
- $f_{D_0^*D\pi T/D_1D_2^*T} \equiv \frac{\mathcal{BT}(B^+\to\bar{D}_0^{*0}/(D\pi)^0\ell^+\nu)}{\mathcal{BT}(B^+\to\bar{D}_1^0/\bar{D}_2^{*0}\ell^+\nu)} = 0.77 \pm 0.19$
- $f_{D_1'D^*\pi T/D_1D_2^*T} \equiv \frac{\mathcal{BT}(B^+\to\bar{D}_1^{*0}/(D^*\pi)^0\ell^+\nu)}{\mathcal{BT}(B^+\to\bar{D}_1^0/\bar{D}_2^{*0}\ell^+\nu)} = 0.98 \pm 0.24$
- $f_{D\pi/D_0^*} \equiv \frac{\mathcal{B}(B^+\to D^-\pi^+\ell^+\nu)}{\mathcal{B}(B^+\to\bar{D}_0^{*0}\ell^+\nu)} = 0.42 \pm 0.28$
- $f_{D^*\pi/D_1'} \equiv \frac{\mathcal{B}(B^+\to D^{*-}\pi^+\ell^+\nu)}{\mathcal{B}(B^+\to\bar{D}_1^{*0}\ell^+\nu)} = 0.071 \pm 0.050$

and by floating background components

- $C^{D^0}_{UncorDL}$
- $C^{D^0}_{UncorCL}$
- $C^{D^0}_{CascL}$
- $C^{D^+}_{UncorDL}$
- $C^{D^+}_{UncorCL}$
- $C^{D^+}_{CascL}$

but fixing background components

- $C^{D^0}_{FakeL} = 1$
- $C^{D^+}_{FakeL} = 1$

We also fit for form factor parameters of $B \to D^{(*)}\ell\nu$ decays. See details in section 9.

6 Event Selection

We use the data sample of approximately 230 million $B\bar{B}$-pairs, collected by the BaBar detector. This corresponds to the integrated luminosity of 207 fb^{-1}. A description of the BaBar detector can be found elsewhere [20]. The $B\bar{B}$-pairs are produced from $\Upsilon(4S)$ resonance created by the asymmetric e^+e^- collider, PEP-II [21], at the Stanford Linear Accelerator Center (SLAC). We also use 21.5 fb^{-1} of off-resonance data collected 40 MeV below the resonance. This can be used to subtract non-$B\bar{B}$ background. The package EvtGen [22] is used to generate events and to model decays, and the GEANT4 software [23] is used to simulate the Babar detector in our Monte Carlo simulation. We use analysis-26 (release 16.1.5) to analyze Run1-4 data and SP5/SP6 MC.

We consider the uncertainty on signal to optimize our cuts. We use generic MC (BpBm, B0B0bar, ccbar, uds and tautau) to model OnPeak data. Since we apply D mass sideband subtraction to reduce combinatorial and continuum backgrounds, we need to consider signal yields and background yields in the D mass peak and the D mass sideband regions. We denote those as N^{Sig}_{peak}, N^{Bkg}_{peak}, N^{Sig}_{side} and N^{Bkg}_{side}. We can determine these numbers using MC truth information and luminosity normalization to OnPeak data. The definition of sidebands are given in section 6.5. Since sidebands are larger than peak region, the number of candidates in the sidebands is scaled down to the peak region. The scale factor is

$$\begin{aligned} r^{D^0}_{side} &= \tfrac{1.888-1.840}{(1.840-1.806)+(1.922-1.888)} = 0.7059 \\ r^{D^+}_{side} &= \tfrac{1.890-1.848}{(1.848-1.810)+(1.928-1.890)} = 0.5526 \end{aligned} \tag{162}$$

Expected OnPeak yields, which are determined by MC, are given by

$$\begin{aligned} N^{OnPeak}_{peak} &= N^{Sig}_{peak} + N^{Bkg}_{peak} \\ N^{OnPeak}_{side} &= r_{side}(N^{Sig}_{side} + N^{Bkg}_{side}) \end{aligned} \tag{163}$$

In actual fit, we are interested in (OnPeak - OffPeak) data. The number of events, $N^{OffPeak}$, and uncertainty, $\sigma^{OffPeak}$, of OffPeak data after luminosity normalization to OnPeak data are given by

$$\begin{aligned} N^{OffPeak}_{peak} &= r^{Lumi}_{OffPeak} N^{OffOrg}_{peak} \\ \sigma^{OffPeak}_{peak} &= r^{Lumi}_{OffPeak} \sqrt{N^{OffOrg}_{peak}} \\ N^{OffPeak}_{side} &= r^{Lumi}_{OffPeak} r_{side} N^{OffOrg}_{side} \\ \sigma^{OffPeak}_{side} &= r^{Lumi}_{OffPeak} r_{side} \sqrt{N^{OffOrg}_{side}} \end{aligned} \tag{164}$$

where N^{OffOrg} is the actual yield of OffPeak data before normalization and $r^{Lumi}_{OffPeak}$ is the normalization factor (see section 3.3.1). We do not need to model OffPeak data by MC. This is because we do not need MC truth information to separate OffPaek candidates into signal and background. The signal yield, S, after sideband subtraction (and OffPeak subtraction) is given by

$$S = N^{Sig}_{peak} - r_{side} N^{Sig}_{side} \tag{165}$$

The variance by performing D mass sideband subtraction and OffPeak subtraction is expected to be

$$\begin{aligned}\sigma_S^2 &= (N_{peak}^{OnPeak} + N_{side}^{OnPeak}) + [(\sigma_{peak}^{OffPeak})^2 + (\sigma_{side}^{OffPeak})^2] \\ &= N_{peak}^{Sig} + N_{peak}^{Bkg} + r_{side}^2(N_{side}^{Sig} + N_{side}^{Bkg}) + \left(r_{OffPeak}^{Lumi}\right)^2 (N_{peak}^{OffOrg} + r_{side}^2 N_{side}^{OffOrg})\end{aligned} \tag{166}$$

Therefore, the uncertainty on signal is given by

$$\frac{\sigma_S}{S} = \frac{\sqrt{N_{peak}^{Sig} + N_{peak}^{Bkg} + r_{side}^2(N_{side}^{Sig} + N_{side}^{Bkg}) + \left(r_{OffPeak}^{Lumi}\right)^2 (N_{peak}^{OffOrg} + r_{side}^2 N_{side}^{OffOrg})}}{N_{peak}^{Sig} - r_{side} N_{side}^{Sig}} \tag{167}$$

6.1 BToDlnu skim

First, the collected data is precessed to select only $B \to D^{(*)}\ell\nu$ candidates. This process is done by BaBar collaboration and the produced data set is called BToDlnu skim. In this subsection, we summarize the selection criteria of BToDlnu skim. See also Appendix E.

6.1.1 Reconstruction of D^0 and D^+

D^0 is reconstructed by the following 4 modes:

- $D^0 \to K^-\pi^+$
- $D^0 \to K^-\pi^+\pi^+\pi^-$
- $D^0 \to K^-\pi^+\pi^0$
- $D^0 \to \bar{K}^0\pi^+\pi^-$

D^+ is reconstructed by the following 2 modes:

- $D^+ \to K^-\pi^+\pi^+$
- $D^+ \to \bar{K}^0\pi^+$

Figure 2 is the D^0 mass plots corresponding to four D^0 reconstruction modes. From top to bottom, $D^0 \to K^-\pi^+$, $D^0 \to K^-\pi^+\pi^+\pi^-$, $D^0 \to K^-\pi^+\pi^0$, $D^0 \to \bar{K}^0\pi^+\pi^-$. Figure 3 is the D^+ mass plots corresponding to two D^+ reconstruction modes. From top to bottom, $D^+ \to K^-\pi^+\pi^+$ and $D^+ \to \bar{K}^0\pi^+$. In these plots, star is the On Peak data, green is the B^+B^- MC, yellow is the $B^0\bar{B}^0$ MC, blue is the Off Peak data, magenta is the $c\bar{c}$ MC, cyan is the uds MC, and gray is the $\tau^+\tau^-$ MC. From these plots, we can observe clear peaks only in the top plots. Thus,

- We use only $D^0 \to K^-\pi^+$ and $D^+ \to K^-\pi^+\pi^+$ modes.

For K^- tracks in the skim,

- GoodTracksLoose (GTL) is used to reconstruct D^0
- KLHNotPion selector is used to reconstruct D^+

We apply the same KLHNotPion to D^0 as described in subsection 6.2.
In BToDlnu skim, D^* is also reconstructed, but we do not use them in our analysis. This avoids the problems in the reconstruction of soft pions from D^* decays.

6.1.2 Reconstruction of Dl candidates

Electrons and muons are are selected by PID selectors.

- PidLHElectron selector for electrons
- muNNTight selector for muons

are used in the BToDlnu skims. These leptons are combined with D^0 or D^+ to form Dl candidates. Since neutrinos cannot be detected, we cannot reconstruct B mesons. Thus, these Dl candidates are the candidates of B mesons. Only one true Dl-pair can be produced from one B meson. However, tens of Dl candidates are usually reconstructed in a event. Most of them are combinatorial backgrounds with a misreconstructed D.
The following cuts are also applied

- Lepton momentum cut
  $0.8 < p^* < 3.0$ GeV, where p^* is the lepton momentum in the $\Upsilon(4S)$ rest frame.
- Lepton and kaon charge correlation cut
  The kaon and lepton from the same B meson must have the same sign of charge. See Appendix A.

6.2 Kaon Selection

In BToDlnu skim, for K^-, GoodTracksLoose (GTL) is used to reconstruct D^0, but KLHNotPion is used to reconstruct D^+. We apply KLHNotPion to D^0 reconstruction as well to reduce kaon misidentification. Signal and background yield and the uncertainty on signal in both before and after KLHNotPion are given in Table 4. We can reduce the uncertainty on signal by 41 %, keeping 98 % of signal candidates. There is no cahnge in D^+ mode because KLHNotPion selector was already applied in the BToDlnu skims.

6.3 Vertexing

No vertexing is done in BToDlnu skim, hence, we apply TreeFitter [24] to D vertex and B vertex. By B vertex, we mean the vertex of Dl combination. We cut on the probability value, $P(\chi^2, dof)$, calculated by the χ^2 and the number of degrees of

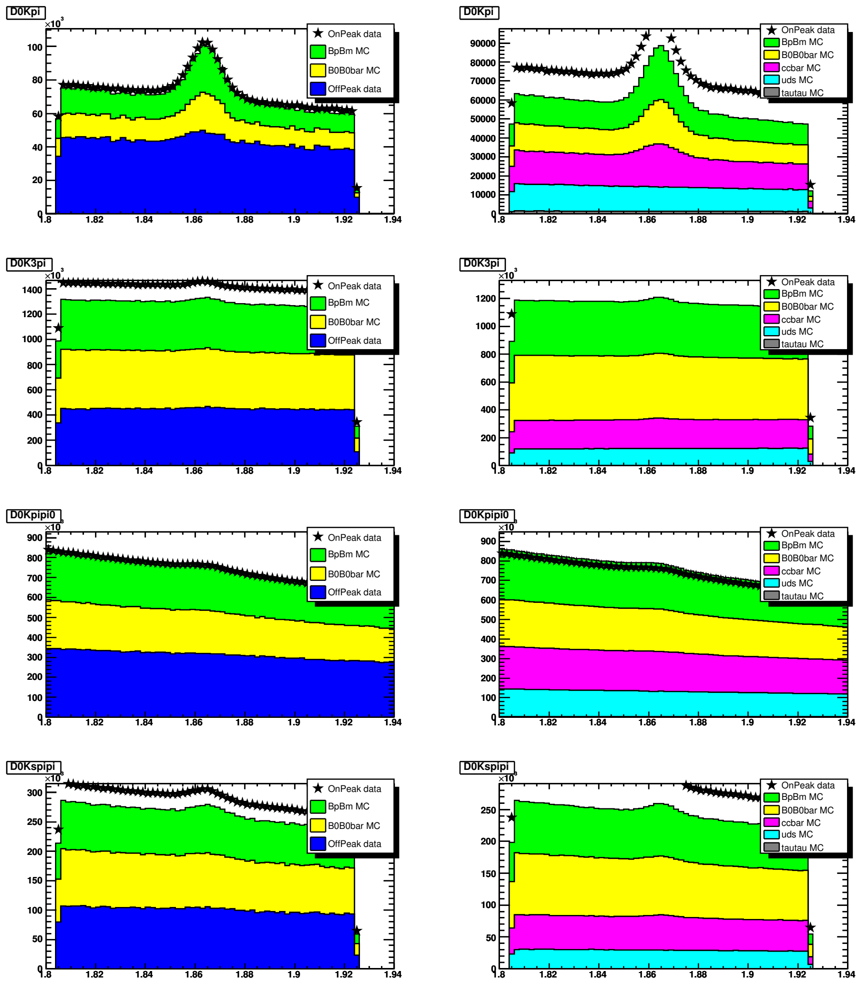

Figure 2: [D^0 **mass plots with 4 reconstruction modes**] D^0 mass plots. From top to bottom, $D^0 \to K^-\pi^+$, $D^0 \to K^-\pi^+\pi^+\pi^-$, $D^0 \to K^-\pi^+\pi^0$, $D^0 \to \bar{K}^0\pi^+$. Star is the On Peak data, green is the B^+B^- MC, yellow is the $B^0\bar{B}^0$ MC, blue is the Off Peak data, magenta is the $c\bar{c}$ MC, cyan is the uds MC, and gray is the $\tau^+\tau^-$ MC.

D^0	Before KLHNotPion	After KLHNotPion
$\frac{\sigma_S}{S}$	0.01952	0.01154
N^{Sig}_{paek}	300194	292993
D^+	Before KLHNotPion	After KLHNotPion
$\frac{\sigma_S}{S}$	0.0269	0.0269
N^{Sig}_{paek}	177725	177725

Table 4: [**KLHNotPion selection**] The uncertainty on signal Signal (σ_S/S) and signal yield in D mass peak region (N^{Sig}_{paek}) before and after KLHNotPion

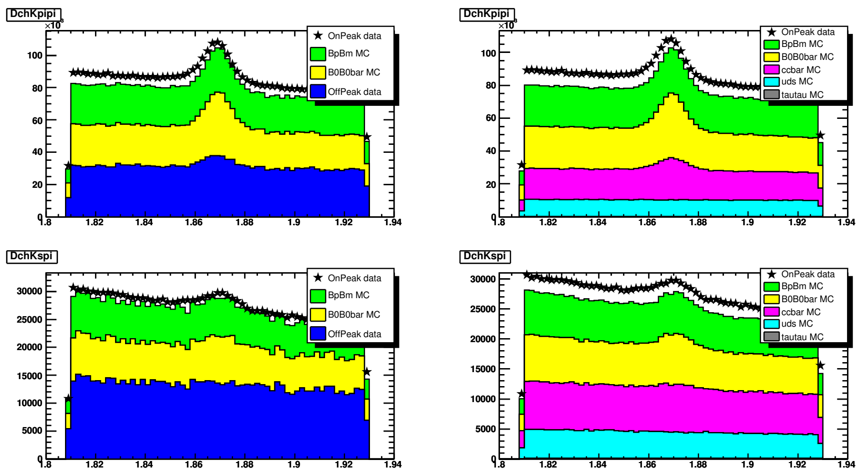

Figure 3: [D^+ **mass plots with 2 reconstruction modes**] D^+ mass plots. From top to bottom, $D^+ \to K^-\pi^+\pi^+$ and $D^+ \to \bar{K}^0\pi^+$. Star is the On Peak data, green is the B^+B^- MC, yellow is the $B^0\bar{B}^0$ MC, blue is the Off Peak data, magenta is the $c\bar{c}$ MC, cyan is the uds MC, and gray is the $\tau^+\tau^-$ MC.

freedom (dof) of the vertex fitting. Table 5 shows the uncertainty on signal with variety of $P(\chi^2, dof)$ cuts of D and B vertexing. Tighter cuts give better uncertainties. However, since there is no big difference on uncertainties, we chose looser cuts :

$$P^D(\chi^2, dof) > 0.001, \quad P^B(\chi^2, dof) > 0.01, \tag{168}$$

These cuts improve the uncertainty by 19 % for D^0 mode and 22 % for D^+ mode, and we loose 6 % and 9 % of signal candidates respectively.

6.4 Thrust cut

$B\bar{B}$ events are isotropic and other $q\bar{q}$ events tend to go back to back in the $\Upsilon(4S)$ rest frame. This is because the mass difference between $\Upsilon(4S)$ and, for example, $D\bar{D}$-pair is big and produced D mesons carry rather large momentum. Thus, we can separate $q\bar{q}$ events from $B\bar{B}$ events using thrust axis. We calculate thrust axis of Dl candidate and "non-Dl" particles in each event. Here, "non-Dl" particles mean all charged tracks and calorimeter energy deposits other than the ones used to reconstruct the Dl candidate. Dl is supposed to be one B in the event; thus, non-Dl should be the other B in the event. However, since we do not reconstruct D^* or D^{**}, soft pions from Dl side are included in non-Dl side. Nevertheless we can achieve a good separation between $B\bar{B}$ events and $q\bar{q}$ events as you can see in the following. We then calculate $|\cos\theta_{Dl-nonDl}|$, which is the cosine of the angle between thrust axis of Dl candidate and non-Dl particles. Those are shown in Figure 4 for D^0 and Figure 5 for D^+. It is almost flat for signal events but peaked at $|\cos\theta_{Dl-nonDl}| = 1$ for $q\bar{q}$ events as expected.

To optimize the cut, we calculate the uncertainty on signal by changing cuts. Table 6

D^0	no cut	$P^D(\chi^2, dof) > 0.0001$	0.001	0.01	0.1
no cut	0.01154	0.01055	0.01043	0.01027	0.01031
$P^B > 0.0001$	0.00974	0.00973	0.00968	0.00959	0.00969
0.001	0.00955	0.00955	0.00953	0.00947	0.00959
0.01	0.00929	0.00929	**0.00929**	0.00928	0.00943
0.1	0.00911	0.00911	0.00911	0.00911	0.00925
D^+	no cut	$P^D(\chi^2, dof) > 0.0001$	0.001	0.01	0.1
no cut	0.02689	0.02275	0.02252	0.0223	0.02226
$P^B > 0.0001$	0.02168	0.02165	0.02152	0.02131	0.02139
0.001	0.02131	0.02131	0.02127	0.02112	0.02124
0.01	0.02079	0.02079	**0.02079**	0.02077	0.02099
0.1	0.02038	0.02038	0.02038	0.02038	0.02056

Table 5: [**Vertex cuts**] The change in the uncertainty on signal, σ_S/S, with variety of $P(\chi^2, dof)$ cuts of D and B vertexing. D^0 , D^+ are shown separately.

show the result. The lowest uncertainty is at $|\cos\theta_{Dl-nonDl}| < 0.80$. However, since no big difference between 0.80 and 0.92, we choose looser cut

$$\cos\theta_{Dl-nonDl} < 0.92 \tag{169}$$

With this cut, we can reduce the uncertainty by 18 % for D^0 and 15 % for D^+, and we can keeep 91 % of signal candidates.

6.5 Summary of event selection cuts

The cuts we applied, the uncertainty on signal and the number of selected signal candidates in the D mass peak region are summarized in Table 7. We reduced uncertainty by 61 % for D^0 and 34 % for D^+ in total. We also lose 16 % and 18 % of signal candidates by these selection cuts. Tables 8 and 9 are cut-flow tables for D^0 and D^+ respectively. (OnPeak - OffPeak) data and $B\bar{B}$ MC are compared in these tables. Efficiencies show a good agreement.
After event selection cuts, number of candidates per event are

- Signal
  - $B^+ \to D^0/\bar{D}^0 X \ell^+ \nu$ mode : 1.0015
  - $B^+ \to D^+/D^- X \ell^+ \nu$ mode : 1.0012
  - $B^0 \to D^0/\bar{D}^0 X \ell^+ \nu$ mode : 1.0010
  - $B^0 \to D^+/D^- X \ell^+ \nu$ mode : 1.0020

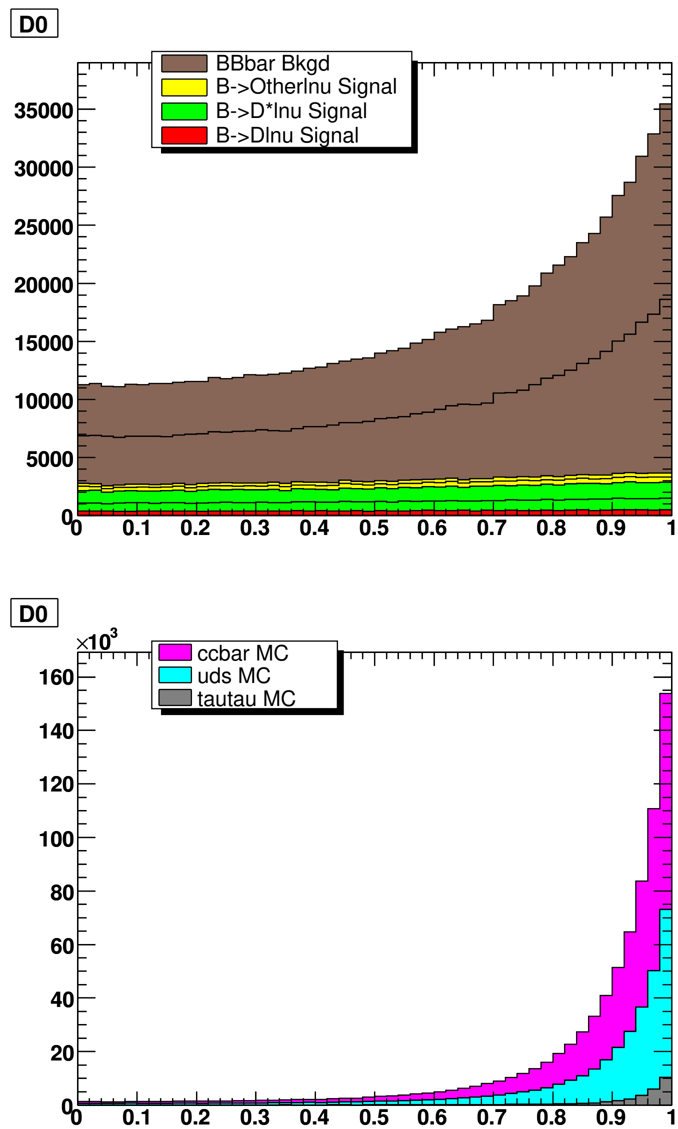

Figure 4: [$|\cos\theta_{Dl-nonDl}|$, D^0] $|\cos\theta_{Dl-nonDl}|$ plot for D^0 case. In the top plot, red is $B \to D\ell\nu$, green is $B \to D^*\ell\nu$, yellow is $B \to D^{**}/(D^{(*)}\pi)\ell\nu$ and brown is $B\bar{B}$ backgrounds. In the bottom plot, magenta is $c\bar{c}$, light blue is uds and gray is $\tau^+\tau^-$.

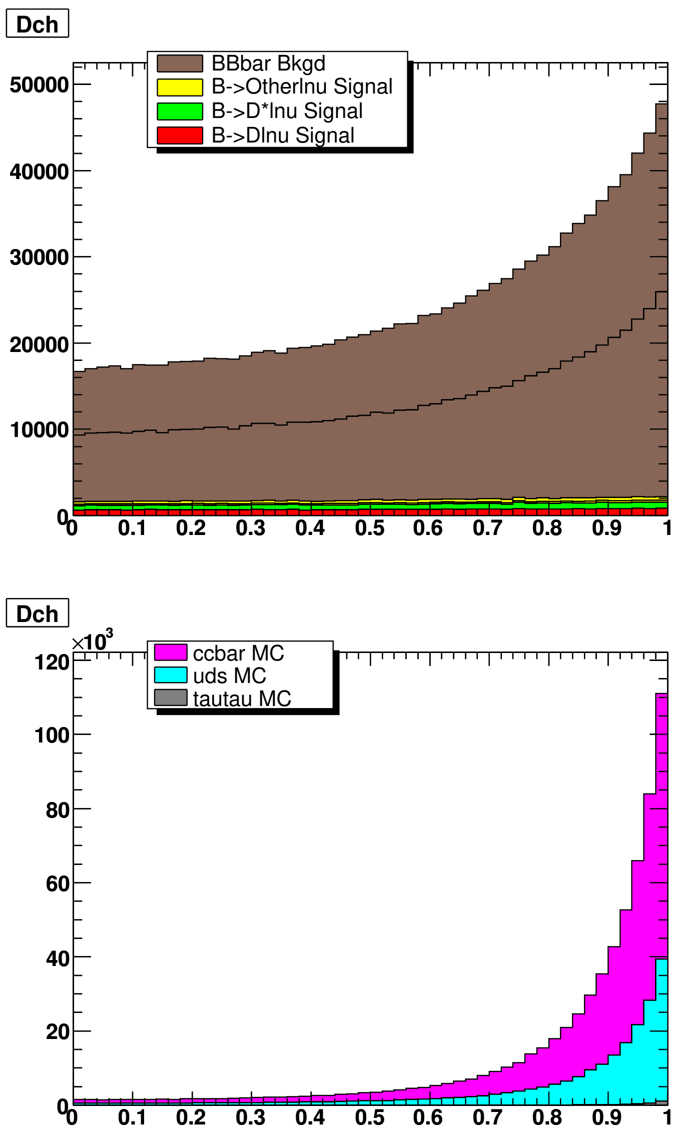

Figure 5: [$|\cos\theta_{Dl-nonDl}|$, D^+] $|\cos\theta_{Dl-nonDl}|$ plot for D^+ case. In the top plot, red is $B \to D\ell\nu$, green is $B \to D^*\ell\nu$, yellow is $B \to D^{**}/(D^{(*)}\pi)\ell\nu$ and brown is $B\bar{B}$ backgrounds. In the bottom plot, magenta is $c\bar{c}$, light blue is uds and gray is $\tau^+\tau^-$.

cuts	D^0	D^+
no cut	0.00929	0.02079
$\lvert\cos\theta_{Dl-nonDl}\rvert < 0.96$	0.00823	0.01889
0.92	**0.00764**	**0.01770**
0.88	0.00725	0.01690
0.84	0.00697	0.01635
0.80	0.00680	0.01600

Table 6: [**Thrust cuts**] The change in the uncertainty on signal, $\frac{\sigma_S}{S}$, with variety of $\lvert\cos\theta_{Dl-nonDl}\rvert$ cuts.

- Backgrounds
  - $B^0 \to D^+/D^- X\ell^+\nu$ Uncorrelated Direct Lepton : 1.0038
  - $B^+ \to D^0/\bar{D}^0 X\ell^+\nu$ Uncorrelated Cascade Lepton : 1.0038
  - $B^0 \to D^0/\bar{D}^0 X\ell^+\nu$ Correlated Cascade Lepton : 1.0038

To understand these numbers, we try to estimate the rate to reconstruct $D\ell$ candidate in the $B^+ \to D^0/\bar{D}^0$ case.

$$\begin{aligned}&\mathcal{B}(B^+ \to X_c\ell^+\nu)\mathcal{B}(X_c \to D^0/\bar{D}^0 X)\mathcal{B}(D^0 \to K^+\pi^-) \times (\text{acceptance} \times \text{efficiency})\\&\simeq 0.1 \times 1 \times 0.04 \times 0.4 = 0.0016\end{aligned} \tag{170}$$

where we assumed $\mathcal{B}(X_c \to D^0/\bar{D}^0 X) = 1$, but this number can be lower than 1. Thus, the above number 1.0015 shows that we just reconstructed true $D\ell$ candidate from both B^+ and B^-.
Figure 6 shows the D mass plot before selection cuts are applied. Figure 7 - 9 shows the D mass plot after all cuts with all leptons (= electrons + muons), electrons only, and muons only, respectively. There is a significant data-MC disagreement especially in the D^+ case. This is mailnly because D^+ require more chaged tracks to reconstruct than D^0. If you look at Figures 2 and 3, $D^0 \to K^-\pi^+\pi^+\pi^+$ mode shows more data-MC disagreement than $D^+ \to K^-\pi^+\pi^+$ mode. It is understandable that combinatrial bcakground is less well modeled in MC when it requires more tracks. However, since the data-MC difference for combinatrial bckground is flat throughout the D mass region, this difference disappear after D mass sideband subtraction.
From these D mass plots, we decided the range of D mass peak and sidebands as follows

- D^0 mass
  Peak : 1.840 - 1.888 GeV
  Side bands : 1.806 - 1.840 and 1.888 - 1.922 GeV

	D^0		D^+	
cuts	$\frac{\sigma_S}{S}$	N_{peak}^{Sig}	$\frac{\sigma_S}{S}$	N_{peak}^{Sig}
BToDlnu skim	0.01952	300194	0.0269	177725
KLHNotPion selector	0.01154	292993	0.0269	177725
$P^D(\chi^2, dof) > 0.001$ $P^B(\chi^2, dof) > 0.01$	0.00929	276669	0.0208	161267
$\lvert \cos\theta_{Dl-nonDl}\rvert < 0.92$	0.00764	250420	0.0177	146269

Table 7: [**Event selection cuts**] The summary of event selection cuts.

- D^+ mass
  Peak : 1.848 - 1.890 GeV
  Side bands : 1.810 - 1.848 and 1.890 - 1.928 GeV

Approximately 4.6 % of signal candidates goes into sideband.
Figure 10 - 12 and 13 - 15 show the lepton momentum, D momentum and $\cos\theta_{B-Dl}$ before and after all selection cuts, and after D mass sideband subtraction. These are the projections of 3D histograms. Data-MC agreement is better than the D mass plot, but still there are visible disagreements. We will correct them by MC corrections and re-weighting. See sections 7, 8, and 9 for details. See also section 7.3 for bin by bin effects.

OnPeak - OffPeak	Yield	Efficiency	Cumulative efficiency
BToDlnu skim	381377		
KLHNotPion selector	379722	0.9957	0.9957
$P^D(\chi^2, dof) > 0.001$ $P^B(\chi^2, dof) > 0.01$	340517	0.8968	0.8929
$\lvert\cos\theta_{Dl-nonDl}\rvert < 0.92$	302788	0.8892	0.7939
$B\bar{B}$ MC	Yield	Efficiency	Cumulative efficiency
BToDlnu skim	411274		
KLHNotPion selector	405898	0.9869	0.9869
$P^D(\chi^2, dof) > 0.001$ $P^B(\chi^2, dof) > 0.01$	372283	0.9172	0.9052
$\lvert\cos\theta_{Dl-nonDl}\rvert < 0.92$	332782	0.8939	0.8091

Table 8: [**Cut-flow Table,** D^0] The cut-flow table for D^0. Yield = number of candidates after D mass sideband subtraction.

OnPeak - OffPeak	Yield	Efficiency	Cumulative efficiency
BToDlnu skim	232505		
KLHNotPion selector	232509	1.0000	1.0000
$P^D(\chi^2, dof) > 0.001$ $P^B(\chi^2, dof) > 0.01$	199994	0.8602	0.8602
$\lvert\cos\theta_{Dl-nonDl}\rvert < 0.92$	178595	0.8930	0.7681
$B\bar{B}$ MC	Yield	Efficiency	Cumulative efficiency
BToDlnu skim	283572		
KLHNotPion selector	283572	1.0000	1.0000
$P^D(\chi^2, dof) > 0.001$ $P^B(\chi^2, dof) > 0.01$	246511	0.8693	0.8693
$\lvert\cos\theta_{Dl-nonDl}\rvert < 0.92$	217339	0.8817	0.7664

Table 9: [**Cut-flow Table,** D^+] The cut-flow table for D^+. Yield = number of candidates after D mass sideband subtraction.

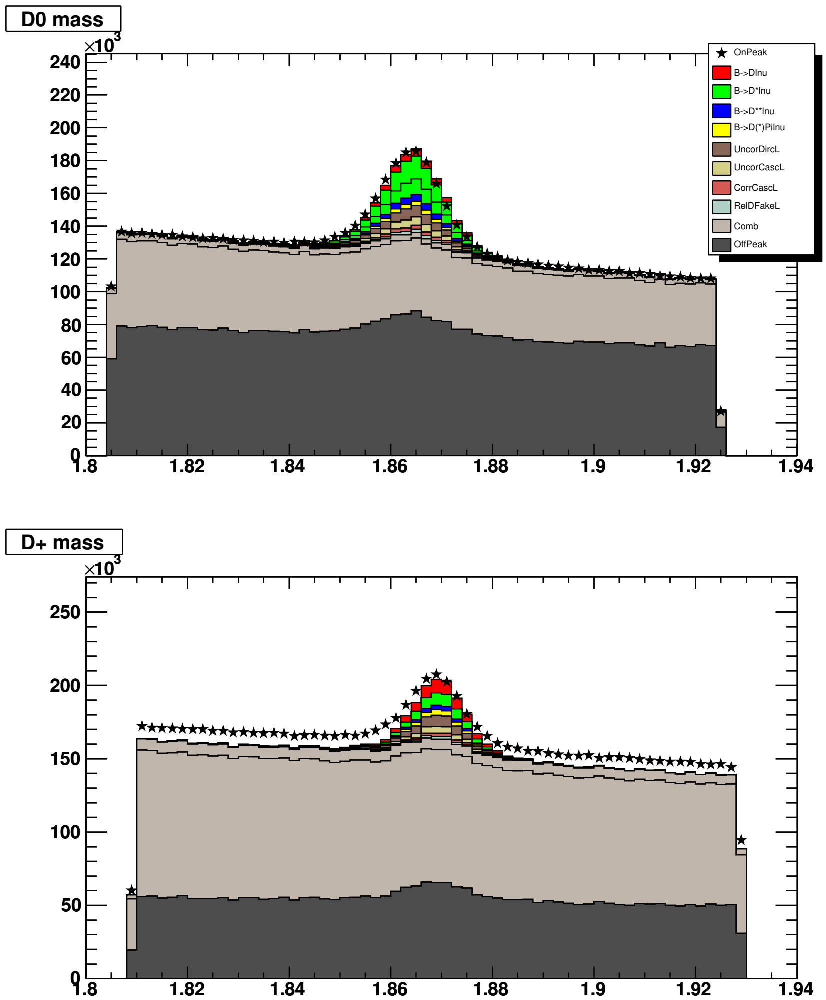

Figure 6: [D **mass before event selection**] D mass plot before applying selection cuts. The top is D^0 and the bottom is D^+. Star is OnPeak data. Red is $B \to D\ell\nu$, green is $B \to D^*\ell\nu$, blue is $B \to D^{**}\ell\nu$, yellow is non-resonant $B \to D^{(*)}\pi\ell\nu$, and the rest is background. Dark brown is UncorrDL, light brown is UncorrCL, dark red is CascL, blue gray is FakeL, light gray is Comb, and dark gray is OffPeak.

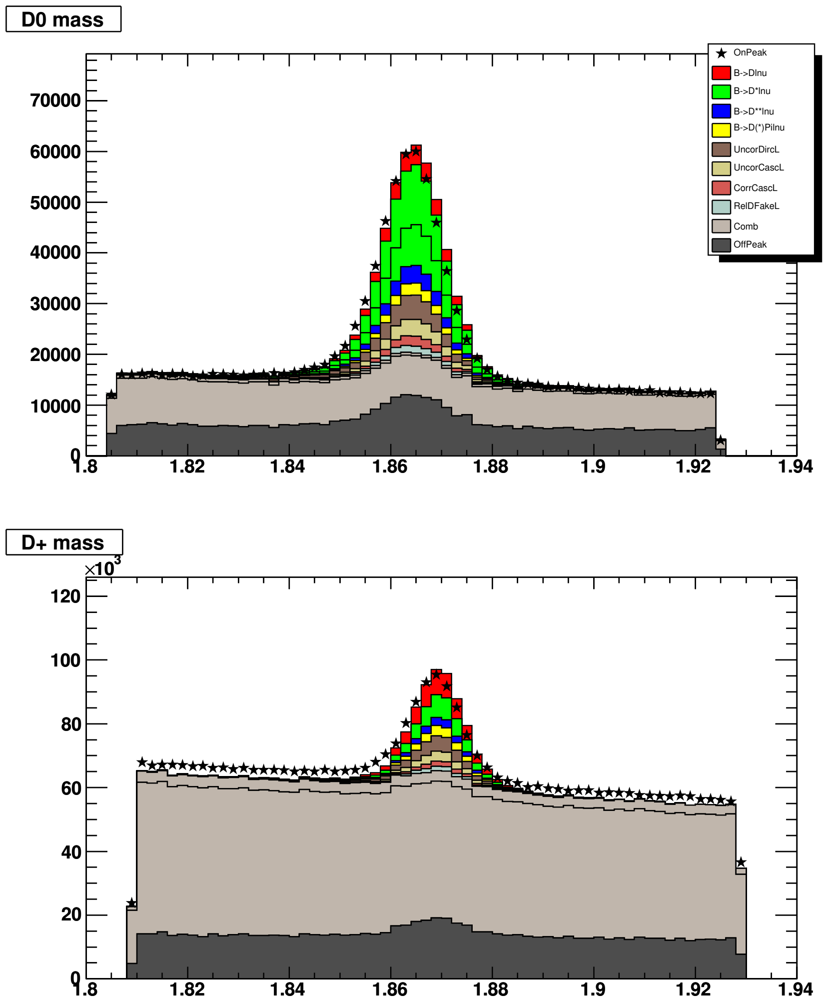

Figure 7: [D **mass after event selection**] D mass plot after all cuts. The top is D^0 and the bottom is D^+. Star is OnPeak data. Red is $B \to D\ell\nu$, green is $B \to D^*\ell\nu$, blue is $B \to D^{**}\ell\nu$, yellow is non-resonant $B \to D^{(*)}\pi\ell\nu$, and the rest is background. Dark brown is UncorrDL, light brown is UncorrCL, dark red is CascL, blue gray is FakeL, light gray is Comb, and dark gray is OffPeak.

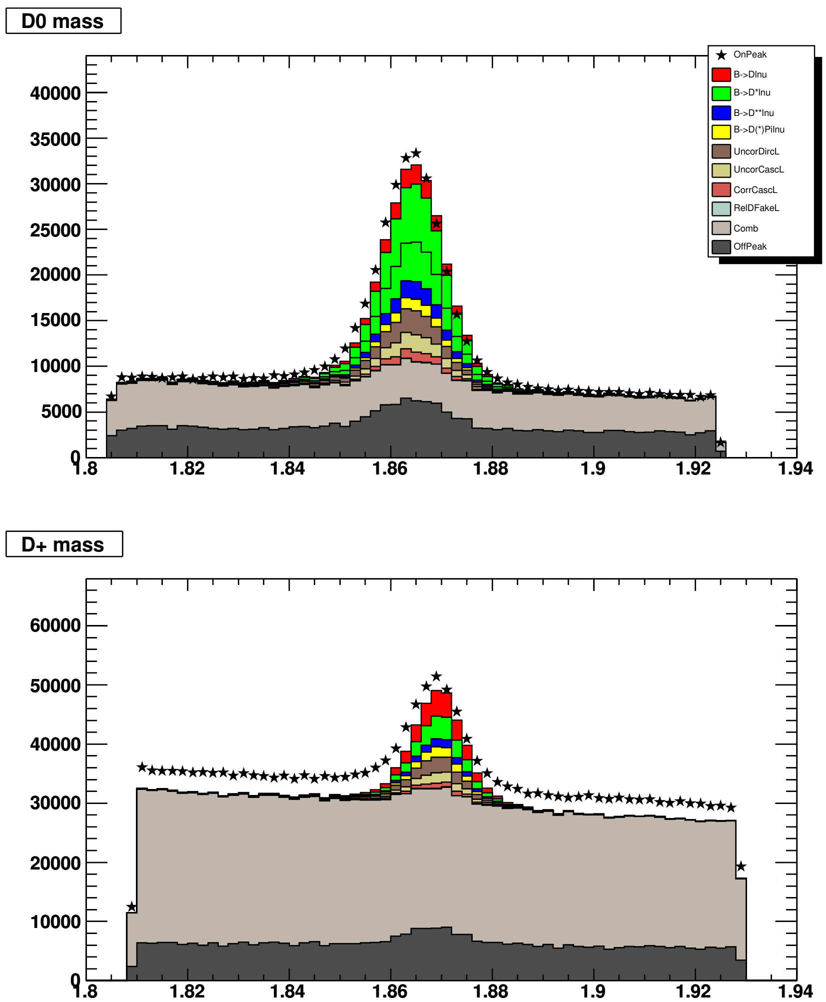

Figure 8: [D **mass after event selection, electron**] D mass plot after all cuts. Only **electrons** are selected. The top is D^0 and the bottom is D^+. Star is OnPeak data. Red is $B \to D\ell\nu$, green is $B \to D^*\ell\nu$, blue is $B \to D^{**}\ell\nu$, yellow is non-resonant $B \to D^{(*)}\pi\ell\nu$, and the rest is background. Dark brown is UncorrDL, light brown is UncorrCL, dark red is CascL, blue gray is FakeL, light gray is Comb, and dark gray is OffPeak.

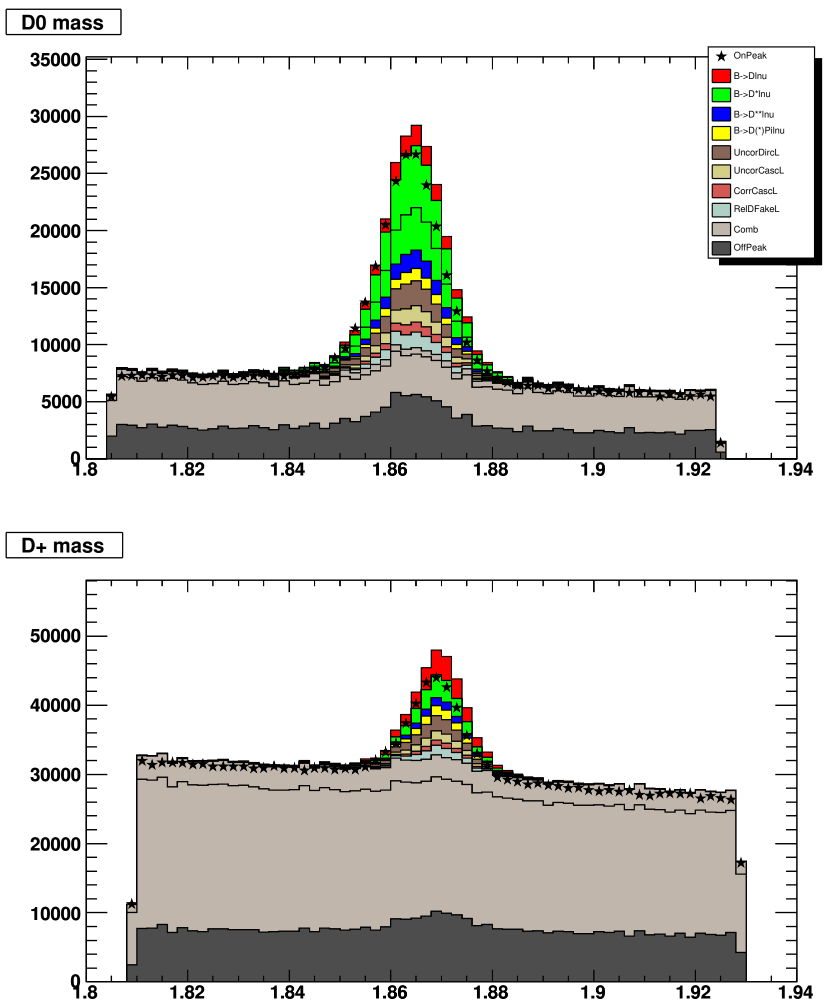

Figure 9: [D **mass after event selection, muon**] D mass plot after all cuts. Only **muons** are selected. The top is D^0 and the bottom is D^+. Star is OnPeak data. Red is $B \to D\ell\nu$, green is $B \to D^*\ell\nu$, blue is $B \to D^{**}\ell\nu$, yellow is non-resonant $B \to D^{(*)}\pi\ell\nu$, and the rest is background. Dark brown is UncorrDL, light brown is UncorrCL, dark red is CascL, blue gray is FakeL, light gray is Comb, and dark gray is OffPeak.

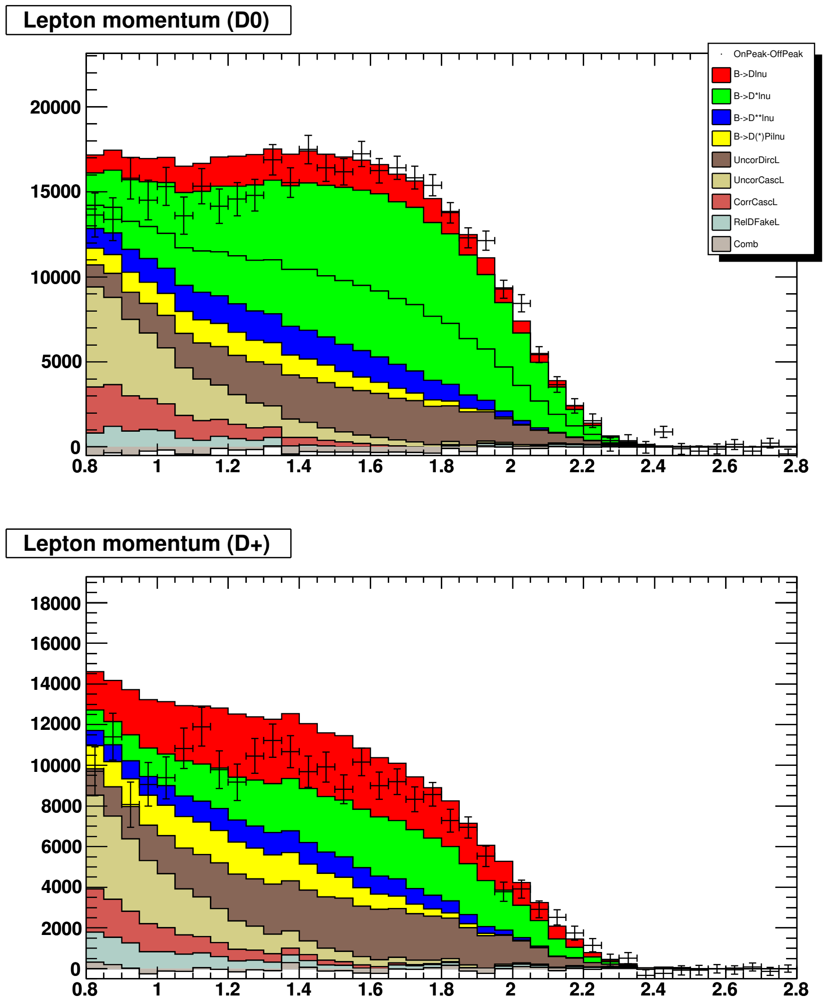

Figure 10: [p_ℓ **before event selection**] Lepton momentum plot before selection cuts and after D mass sideband subtraction. The top is D^0 and the bottom is D^+. Black is OnPeak - OffPeak data. Red is $B \to D\ell\nu$, green is $B \to D^*\ell\nu$, blue is $B \to D^{**}\ell\nu$, yellow is non-resonant $B \to D^{(*)}\pi\ell\nu$, and the rest is background. Dark brown is UncorrDL, light brown is UncorrCL, dark red is CascL, blue gray is FakeL, and light gray is Comb. Comb is almost disappeared after D mass sideband subtraction. This plot has larger statistical uncertainty than Figure 13 due to D mass sideband subtraction with larger combinatorial and continuum backgrounds. Figure 6 and 7 show the difference of those backgrounds.

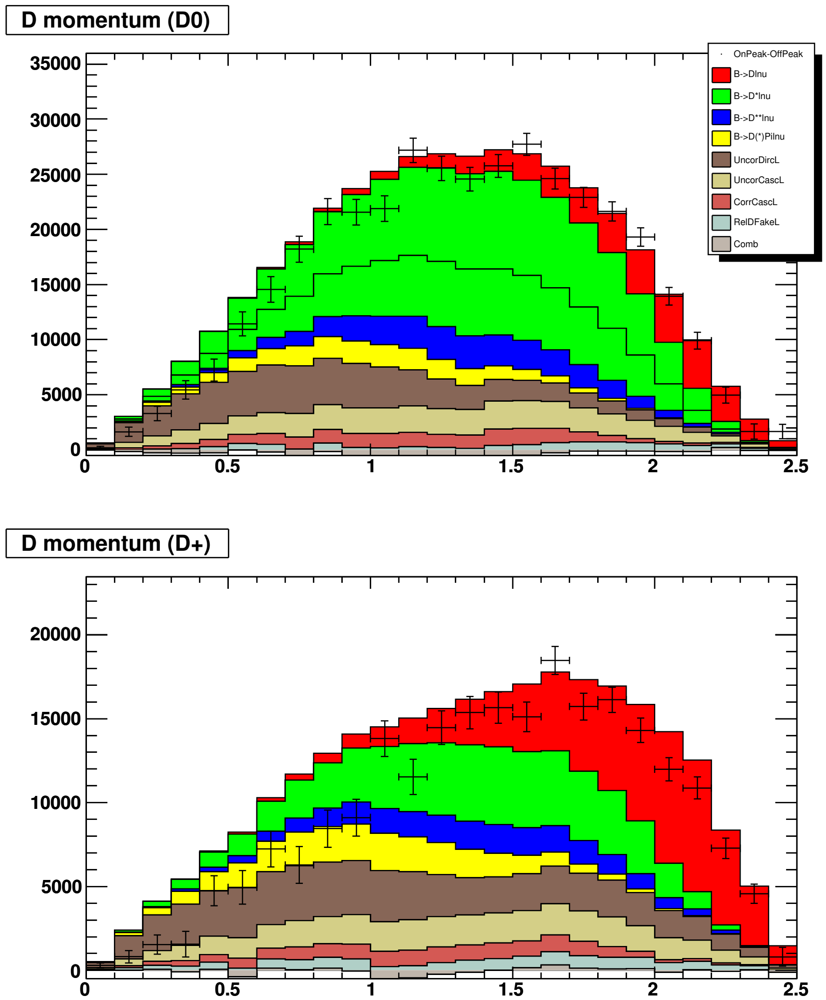

Figure 11: [p_D **before event selection**] D momentum plot before selection cuts and after D mass sideband subtraction. The top is D^0 and the bottom is D^+. Black is OnPeak - OffPeak data. Red is $B \to D\ell\nu$, green is $B \to D^*\ell\nu$, blue is $B \to D^{**}\ell\nu$, yellow is non-resonant $B \to D^{(*)}\pi\ell\nu$, and the rest is background. Dark brown is UncorrDL, light brown is UncorrCL, dark red is CascL, blue gray is FakeL, and light gray is Comb. Comb is almost disappeared after D mass sideband subtraction. This plot has larger statistical uncertainty than Figure 14 due to D mass sideband subtraction with larger combinatorial and continuum backgrounds. Figure 6 and 7 show the difference of those backgrounds.

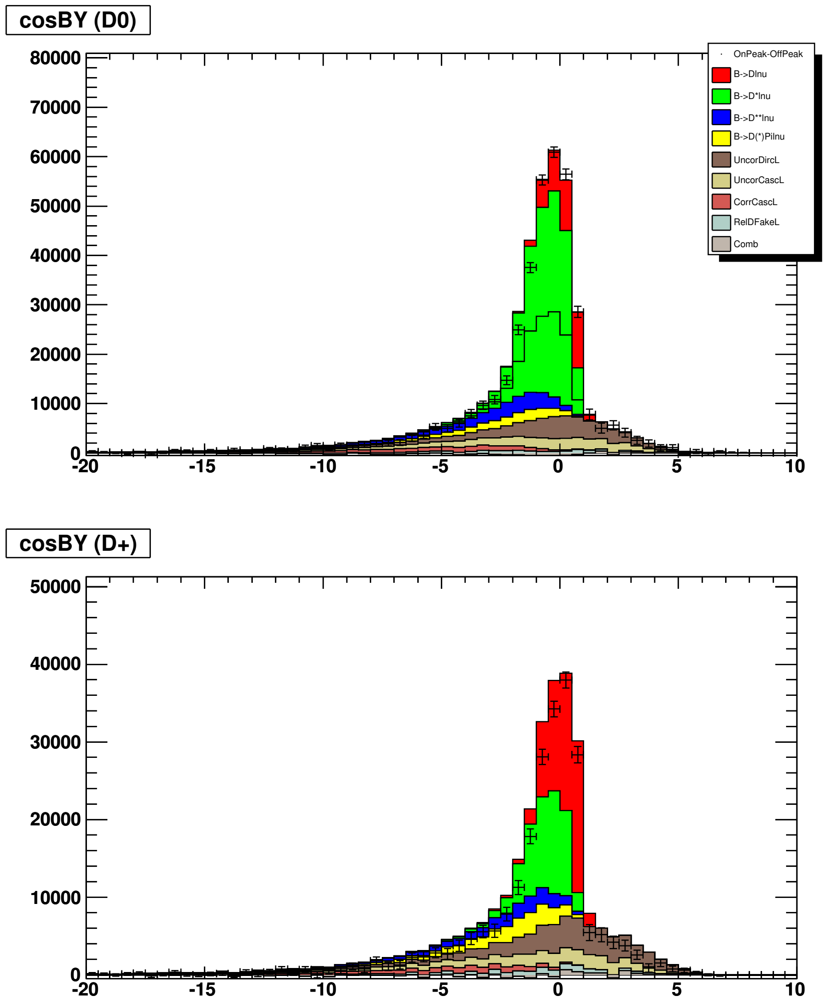

Figure 12: [$\cos\theta_{B-Dl}$ **before event selection**] $\cos\theta_{B-Dl}$ plot before selection cuts and after D mass sideband subtraction. The top is D^0 and the bottom is D^+. Black is OnPeak - OffPeak data. Red is $B \to D\ell\nu$, green is $B \to D^*\ell\nu$, blue is $B \to D^{**}\ell\nu$, yellow is non-resonant $B \to D^{(*)}\pi\ell\nu$, and the rest is background. Dark brown is UncorrDL, light brown is UncorrCL, dark red is CascL, blue gray is FakeL, and light gray is Comb. Comb is almost disappeared after D mass sideband subtraction. This plot has larger statistical uncertainty than Figure 15 due to D mass sideband subtraction with larger combinatorial and continuum backgrounds. Figure 6 and 7 show the difference of those backgrounds.

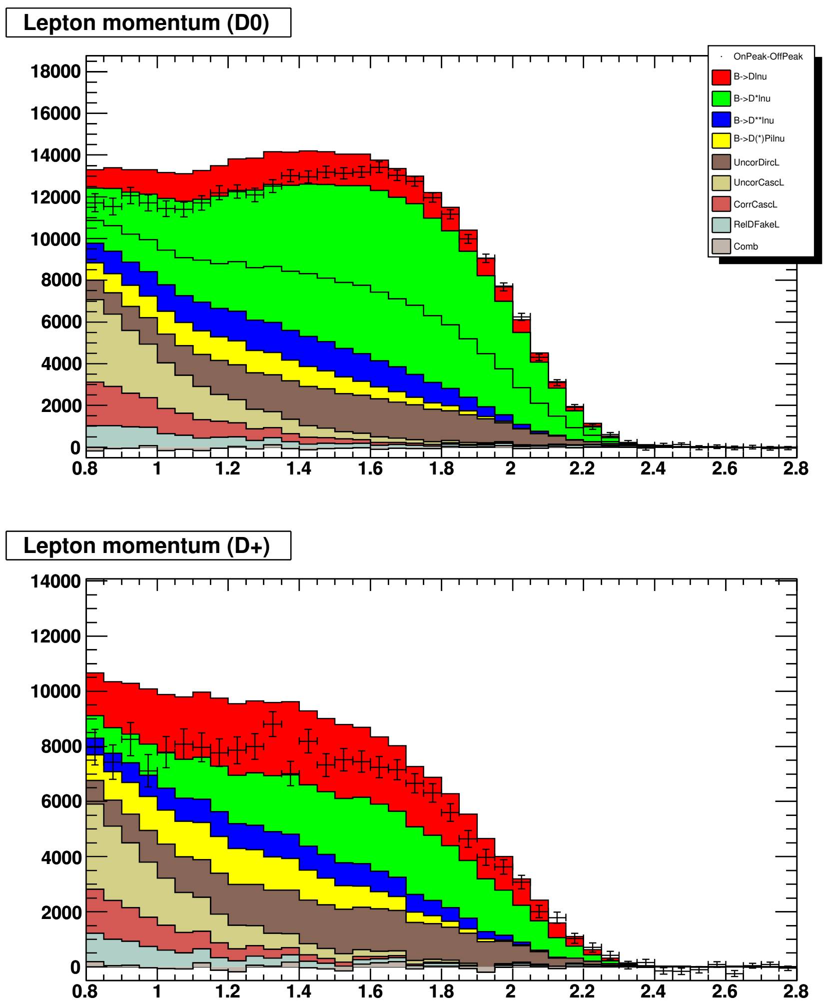

Figure 13: [p_ℓ **after event selection**] Lepton momentum plot after all cuts and D mass sideband subtraction. The top is D^0 and the bottom is D^+. Black is OnPeak - OffPeak data. Red is $B \to D\ell\nu$, green is $B \to D^*\ell\nu$, blue is $B \to D^{**}\ell\nu$, yellow is non-resonant $B \to D^{(*)}\pi\ell\nu$, and the rest is background. Dark brown is UncorrDL, light brown is UncorrCL, dark red is CascL, blue gray is FakeL, and light gray is Comb. Comb is almost disappeared after D mass sideband subtraction.

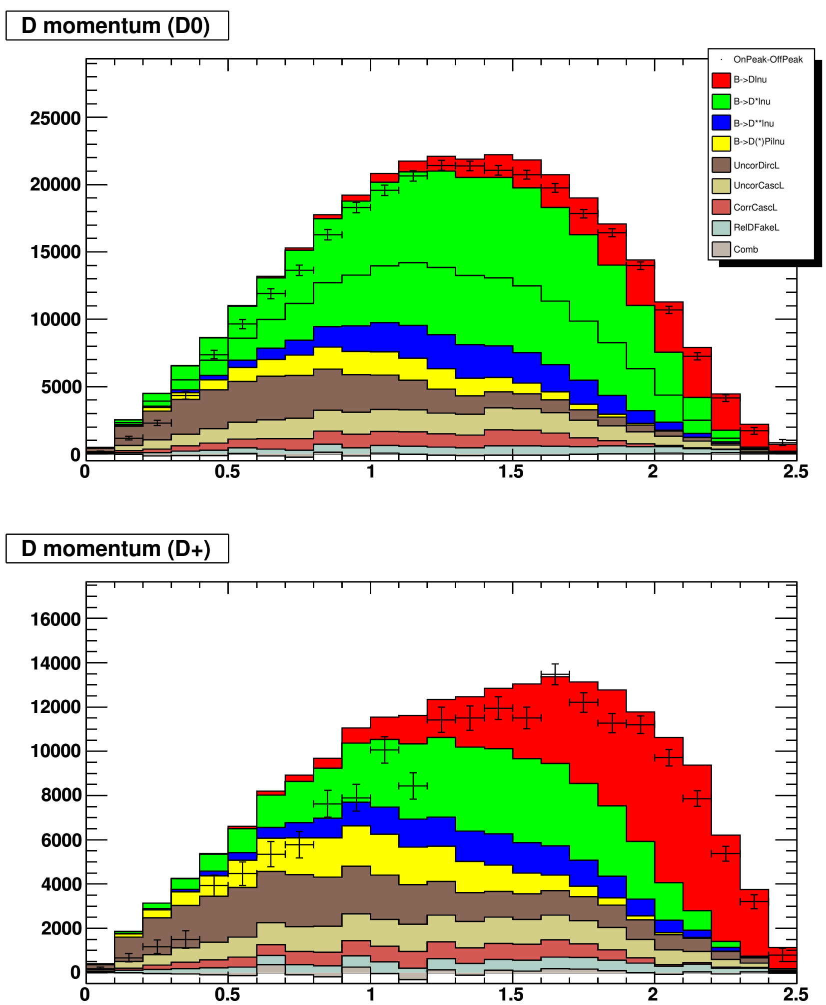

Figure 14: [p_D **after event selection**] D momentum plot after all cuts and D mass sideband subtraction. The top is D^0 and the bottom is D^+. Black is OnPeak - OffPeak data. Red is $B \to D\ell\nu$, green is $B \to D^*\ell\nu$, blue is $B \to D^{**}\ell\nu$, yellow is non-resonant $B \to D^{(*)}\pi\ell\nu$, and the rest is background. Dark brown is UncorrDL, light brown is UncorrCL, dark red is CascL, blue gray is FakeL, and light gray is Comb. Comb is almost disappeared after D mass sideband subtraction.

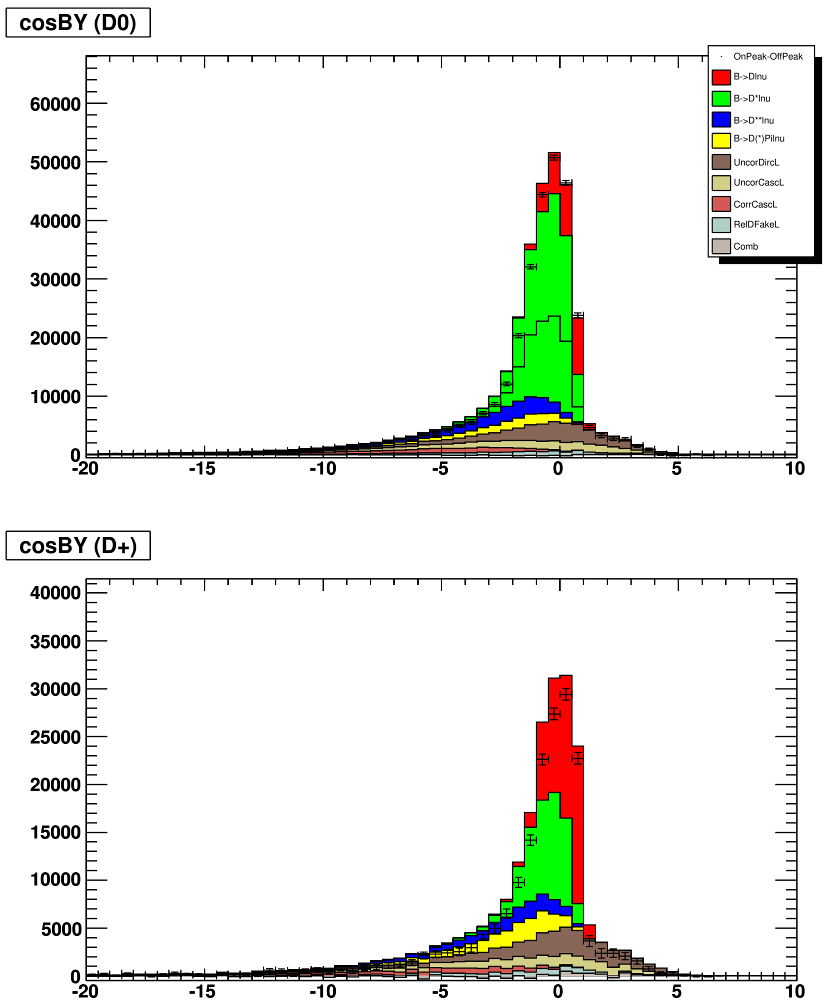

Figure 15: [$\cos\theta_{B-Dl}$ **after event selection**] $\cos\theta_{B-Dl}$ plot after all cuts and D mass sideband subtraction. The top is D^0 and the bottom is D^+. Black is OnPeak - OffPeak data. Red is $B \to D\ell\nu$, green is $B \to D^*\ell\nu$, blue is $B \to D^{**}\ell\nu$, yellow is non-resonant $B \to D^{(*)}\pi\ell\nu$, and the rest is background. Dark brown is UncorrDL, light brown is UncorrCL, dark red is CascL, blue gray is FakeL, and light gray is Comb. Comb is almost disappeared after D mass sideband subtraction.

7 Tracking Efficiency and PID correction

Tracking efficiency and PID efficiency are not completely equal in both data and MC. There is always a difference no matter how sophisticated the codes to reconstruct charged tracks and to identify particles are. Tracking efficiency and PID corrections are the corrections to account for the residual difference between data and MC. Both corrections are done in similar way. The correction factors are read out from correction tables stored in the condition database. We use R16 correction tables since we use R16b skims.

7.1 Tracking efficiency correction : r_k^{Trk}

Tracking efficiency correction factors are given for each charged track, depending on its transverse momentum, direction in the LAB frame and the multiplicity of the event. There are 3 charged tracks to reconstruct a $D^0(K\pi)l$ candidate, and 4 charged tracks to reconstruct a $D^+(K\pi\pi)l$ candidate. We multiply those correction factors of charged tracks to get a correction factor r_k^{Trk} for each candidate (k). The distribution of r_k^{Trk} for BpBm MC is shown in Figure 16.

7.2 PID correction : r_k^{LPID} and r_k^{KPID}

PID correction factors (called weights) are given one for each PID selector. Thus, we have one factor r_k^{LPID} for lepton (PidLHElectron for electrons and muNNTight for muons) and another factor r_k^{KPID} for kaon (KLHNotPion) for each candidate (k). When the identified particles are real, r_k^{LPID} and r_k^{KPID} are the factor to correct identification efficiency difference. When the identified particles are fake, r_k^{LPID} and r_k^{KPID} give the factor to correct fake rate difference. The distribution of electron r_k^{LPID} for BpBm MC is shown in Figure 17 and muon r_k^{LPID} in Figure 18. r_k^{KPID} is shown in Figure 19.

7.3 Effect of efficiency correction

Figure 20 and 21 show the D mass plots before and after tracking efficiency and PID corrections. At the bottom of each D^0 and D^+ plot, (number of OnPaek) - (number of MC + OffPeak) plot is given. The effect of corrections is small. Figure 22 - 24 show the lepton momentum, D momentum and $\cos\theta_{B-Dl}$ after tracking efficiency and PID correction. These are the projections of 3D histograms. If you compare these with Figure 13 - 15, you can see improvements of data-MC agreement.

Figure 25 - 30 show all bins of the 3D histograms of before event selection, after event selection, and after efficiency correction, respectively. Binning are described in section 3. These plots show that the event selection cuts and tracking efficiency and PID correction did not introduce unwanted bias to the histograms.

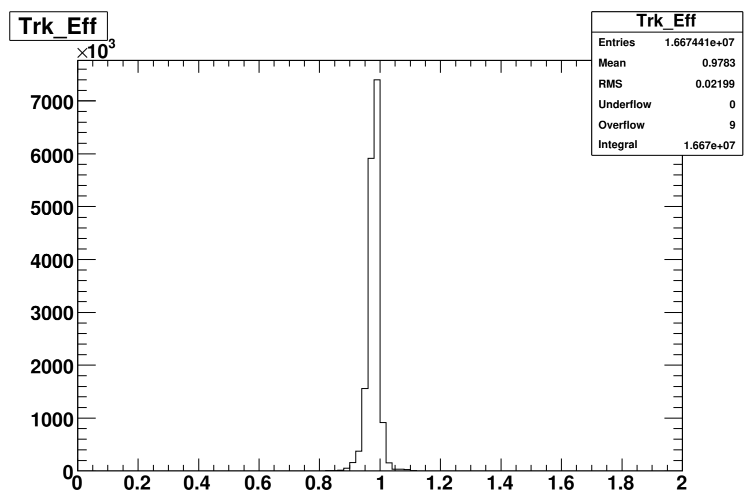

Figure 16: **(Run2 only)** [**TrkEff correction factor**] Tracking efficiency correction factor for each candidate. BpBm MC is used to make this plot.

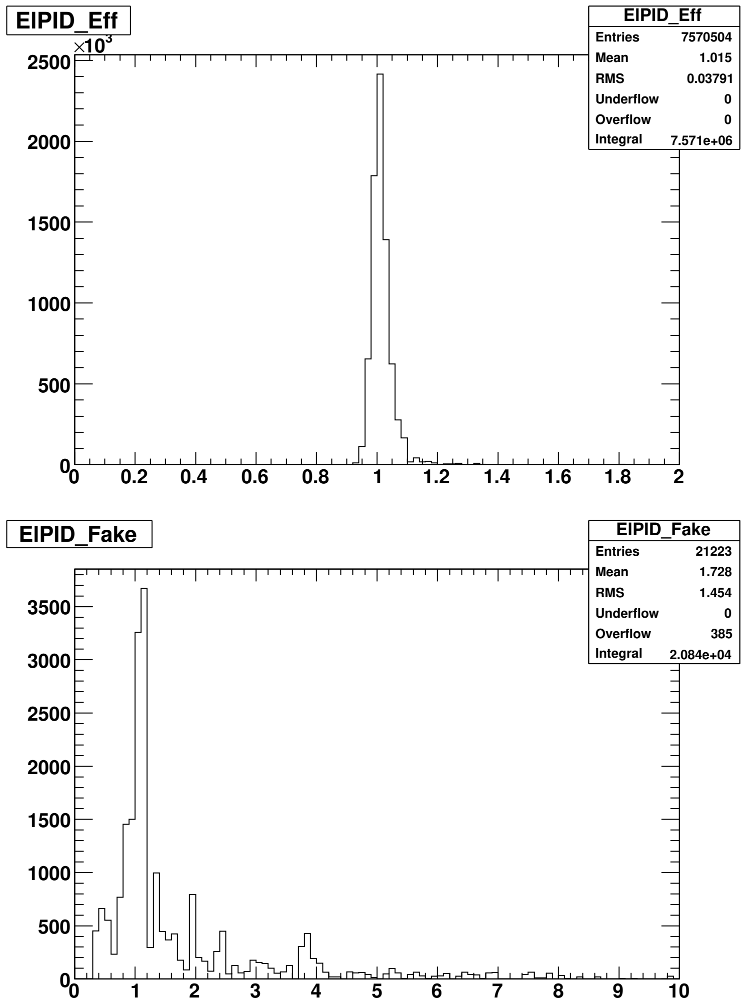

Figure 17: **(Run2 only)** [**Electron PID weight**] Electron PID correction factor for each candidate. BpBm MC is used to make this plot. The top is the efficiency correction factors and the bottom is the fake rate correction factors.

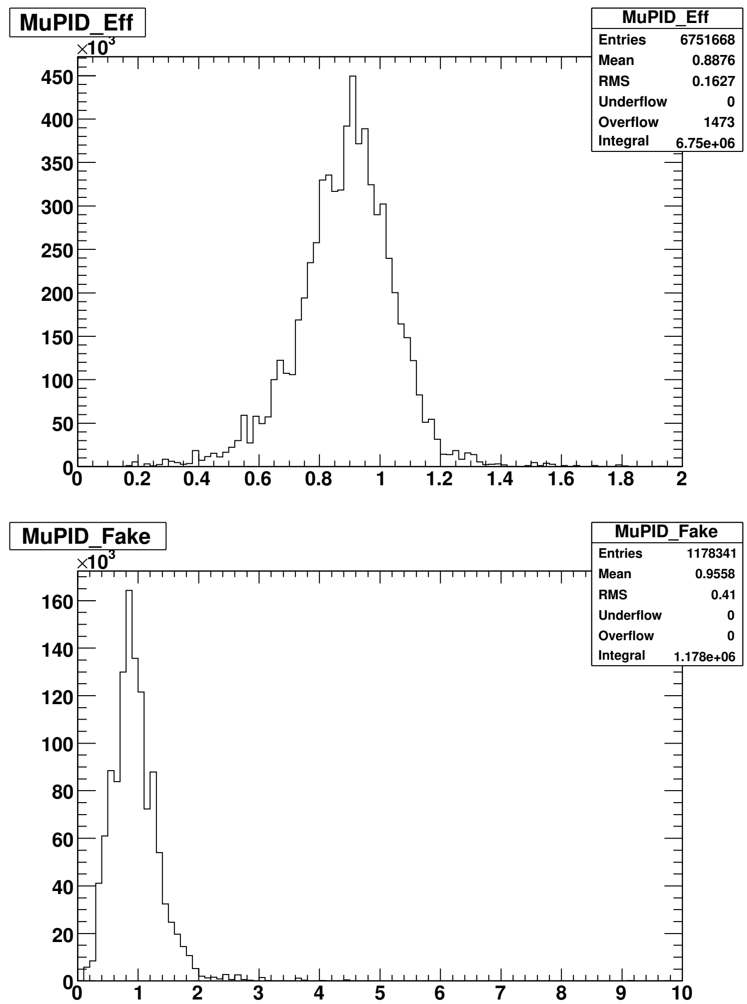

Figure 18: **(Run2 only)** [**Muon PID weight**] Muon PID correction factor for each candidate. BpBm MC is used to make this plot. The top is the efficiency correction factors and the bottom is the fake rate correction factors.

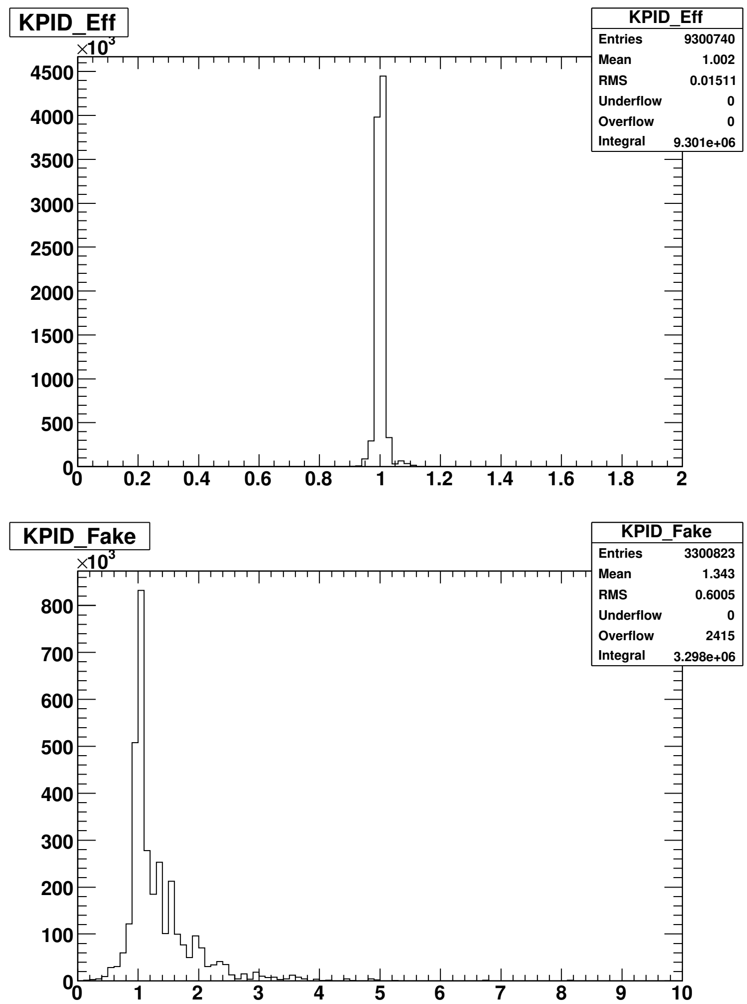

Figure 19: **(Run2 only)** [**Kaon PID weight**] Kaon PID correction factor for each candidate. BpBm MC is used to make this plot. The top is the efficiency correction factors and the bottom is the fake rate correction factors.

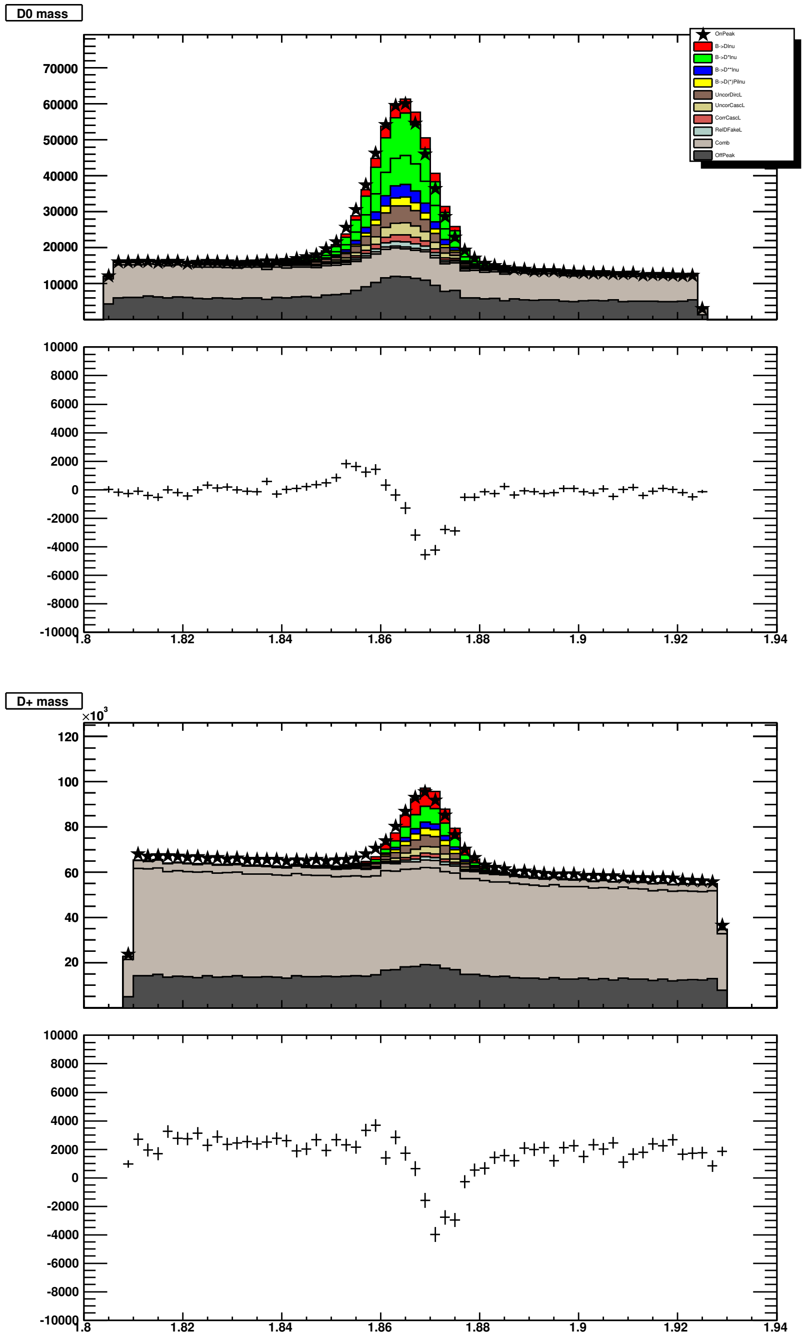

Figure 20: **(Run2 only)** [D **mass before Trk PID correction**] D mass plot before tracking efficiency and PID corrections. The top is D^0 and the bottom is D^+. Star is OnPeak data. Red is $B \to D\ell\nu$, green is $B \to D^*\ell\nu$, blue is $B \to D^{**}\ell\nu$, yellow is non-resonant $B \to D^{(*)}\pi\ell\nu$, and the rest is background. Dark brown is UncorrDL, light brown is UncorrCL, dark red is CascL, blue gray is FakeL, light gray is Comb, and dark gray is OffPeak. At the bottom of each D^0 and D^+ plot, (number of OnPaek) - (number of MC + OffPeak) plot is given.

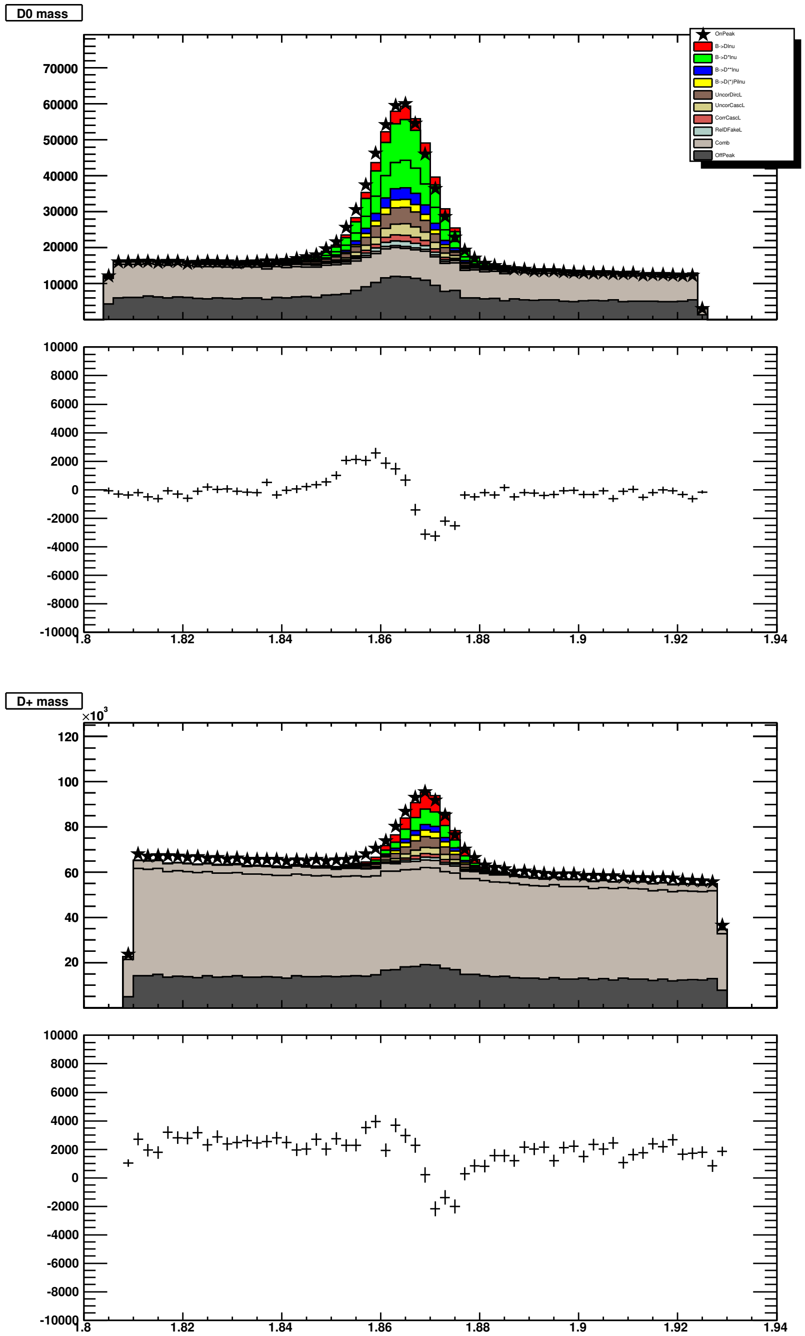

Figure 21: **(Run2 only)** [D **mass after Trk PID correction**] D mass plot after tracking efficiency and PID corrections. The top is D^0 and the bottom is D^+. Star is OnPeak data. Red is $B \to D\ell\nu$, green is $B \to D^*\ell\nu$, blue is $B \to D^{**}\ell\nu$, yellow is non-resonant $B \to D^{(*)}\pi\ell\nu$, and the rest is background. Dark brown is UncorrDL, light brown is UncorrCL, dark red is CascL, blue gray is FakeL, light gray is Comb, and dark gray is OffPeak. At the bottom of each D^0 and D^+ plot, (number of OnPaek) - (number of MC + OffPeak) plot is given.

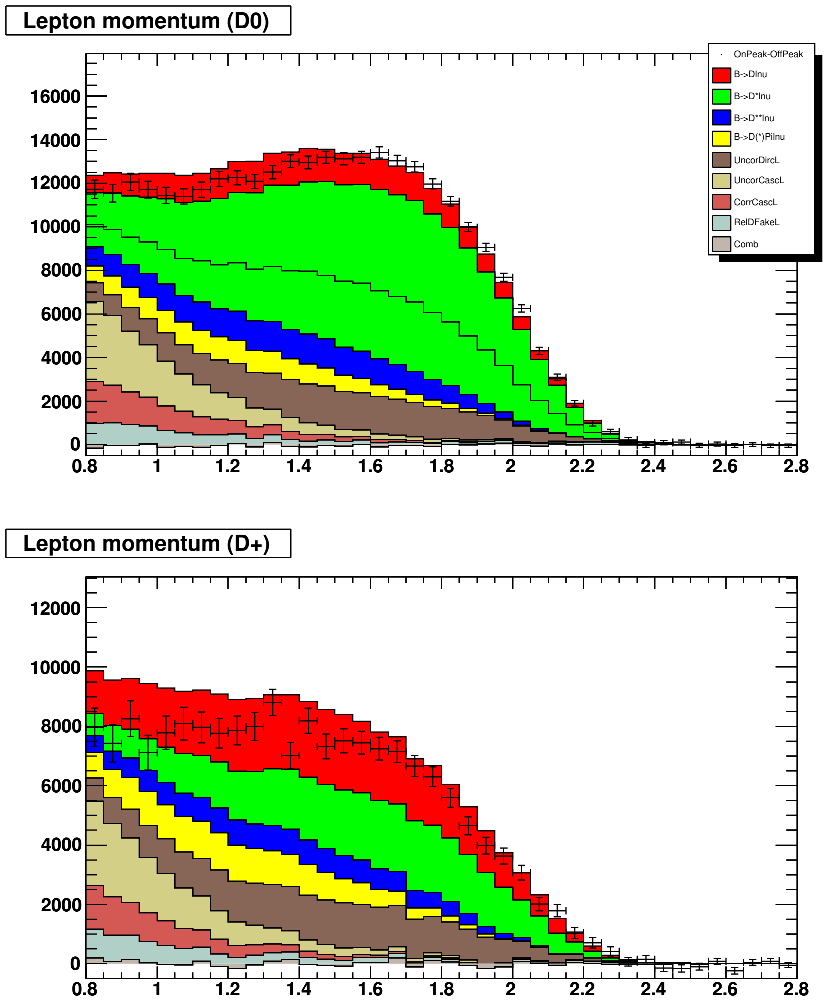

Figure 22: **(Run2 only)** [p_ℓ **after Trk PID**] Lepton momentum plot after PID and tracking corrected and D mass sideband subtracted. The top is D^0 and the bottom is D^+. Black is OnPeak - OffPeak data. Red is $B \to D\ell\nu$, green is $B \to D^*\ell\nu$, blue is $B \to D^{**}\ell\nu$, yellow is non-resonant $B \to D^{(*)}\pi\ell\nu$, and the rest is background. Dark brown is UncorrDL, light brown is UncorrCL, dark red is CascL, blue gray is FakeL, and light gray is Comb. Comb is almost disappeared after D mass sideband subtraction.

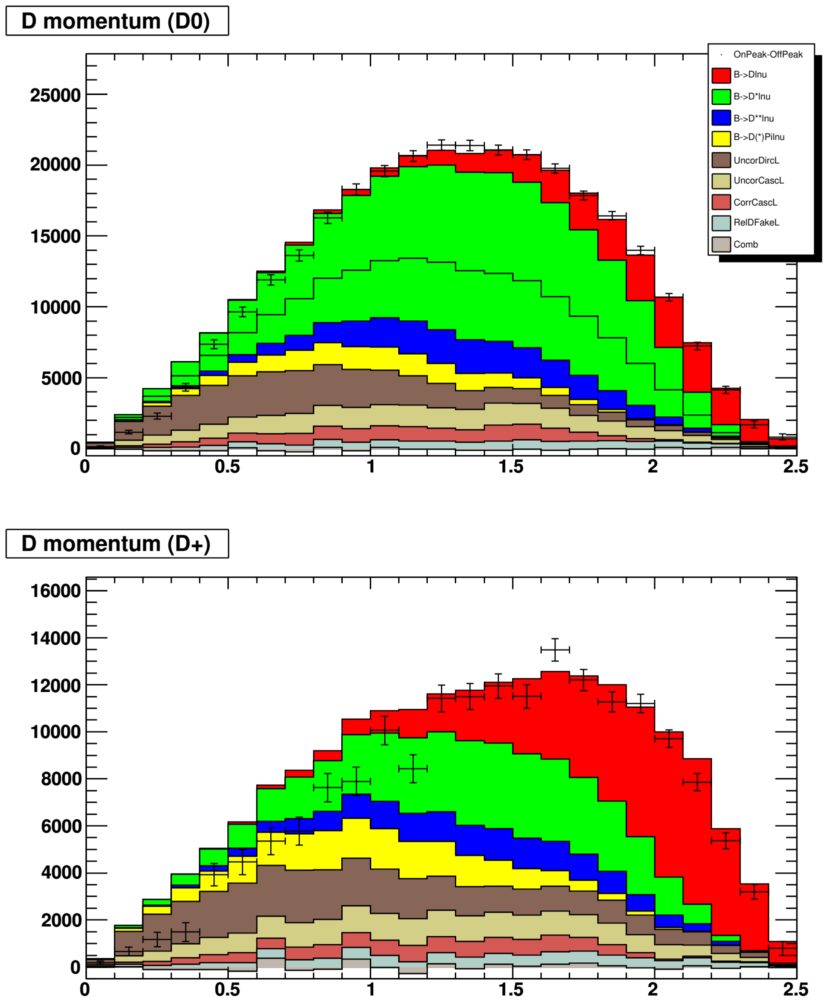

Figure 23: **(Run2 only)** [p_D **after Trk PID**] D momentum plot after PID and tracking corrected and D mass sideband subtracted. The top is D^0 and the bottom is D^+. Black is OnPeak - OffPeak data. Red is $B \to D\ell\nu$, green is $B \to D^*\ell\nu$, blue is $B \to D^{**}\ell\nu$, yellow is non-resonant $B \to D^{(*)}\pi\ell\nu$, and the rest is background. Dark brown is UncorrDL, light brown is UncorrCL, dark red is CascL, blue gray is FakeL, and light gray is Comb. Comb is almost disappeared after D mass sideband subtraction.

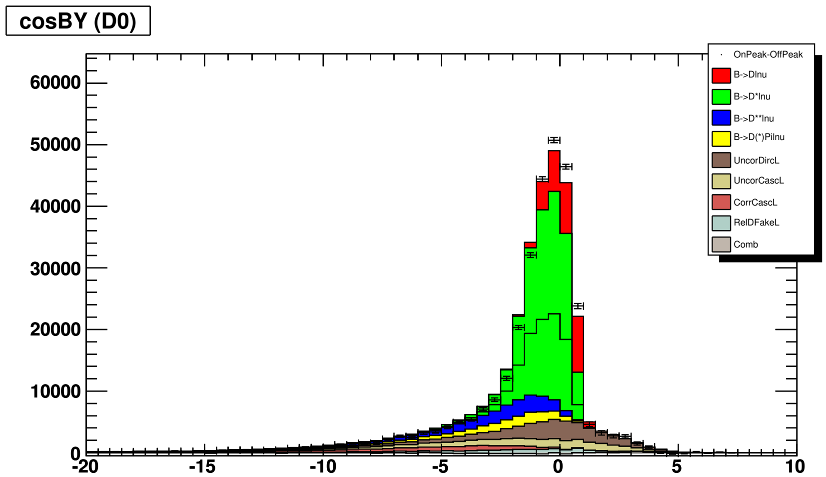

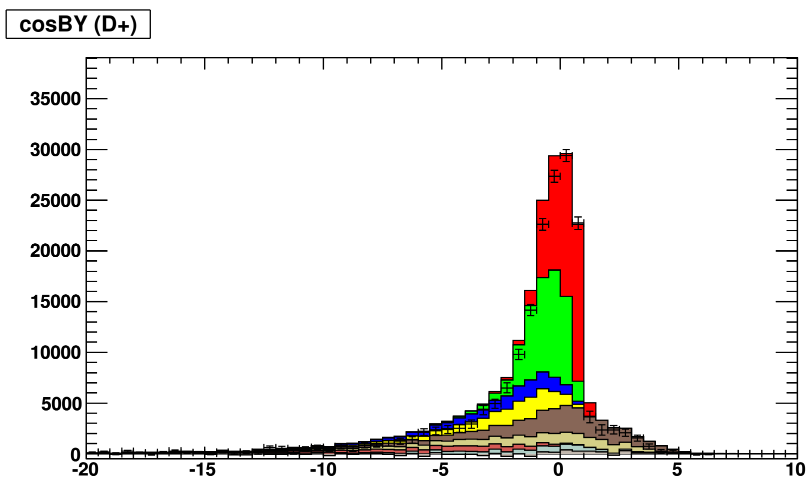

Figure 24: **(Run2 only)** [$\cos\theta_{B-Dl}$ **after Trk PID**] $\cos\theta_{B-Dl}$ plot after PID and tracking corrected and D mass sideband subtracted. The top is D^0 and the bottom is D^+. Black is OnPeak - OffPeak data. Red is $B \to D\ell\nu$, green is $B \to D^*\ell\nu$, blue is $B \to D^{**}\ell\nu$, yellow is non-resonant $B \to D^{(*)}\pi\ell\nu$, and the rest is background. Dark brown is UncorrDL, light brown is UncorrCL, dark red is CascL, blue gray is FakeL, and light gray is Comb. Comb is almost disappeared after D mass sideband subtraction.

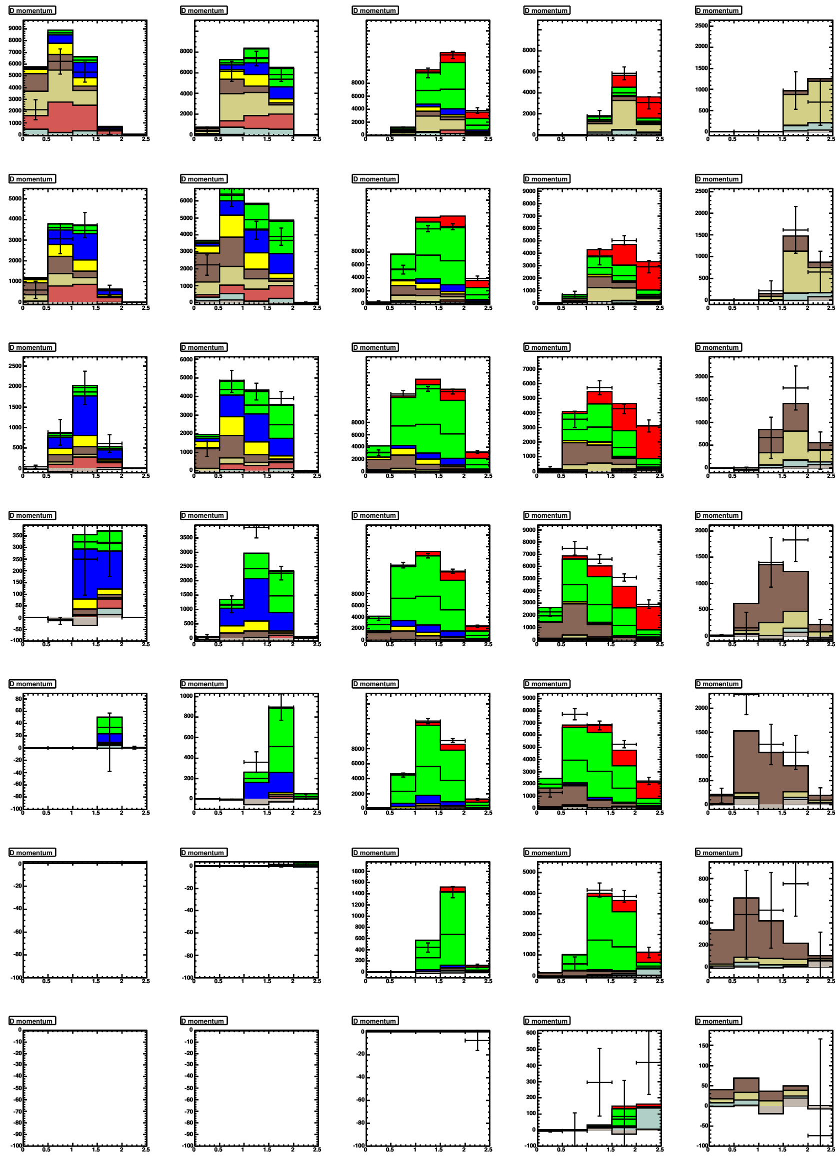

Figure 25: **(Run2 only)** [**Bin by bin plot** (D^0) **before event selection**] D^0 momentum plots showing all bins before event selection cuts and D mass sideband subtraction. From top to bottom, lepton momentum bin changes from the lowest to the highest, and from left to right, cosBY bin changes from negative to positive. In each plots, colors are the same as other plots. Black is OnPeak - OffPeak data. Red is $B \to D\ell\nu$, green is $B \to D^*\ell\nu$, blue is $B \to D^{**}\ell\nu$, yellow is non-resonant $B \to D^{(*)}\pi\ell\nu$, and the rest is background. Dark brown is UncorrDL, light brown is UncorrCL, dark red is CascL, blue gray is FakeL, and light gray is Comb. Comb is almost disappeared after D mass sideband subtraction.

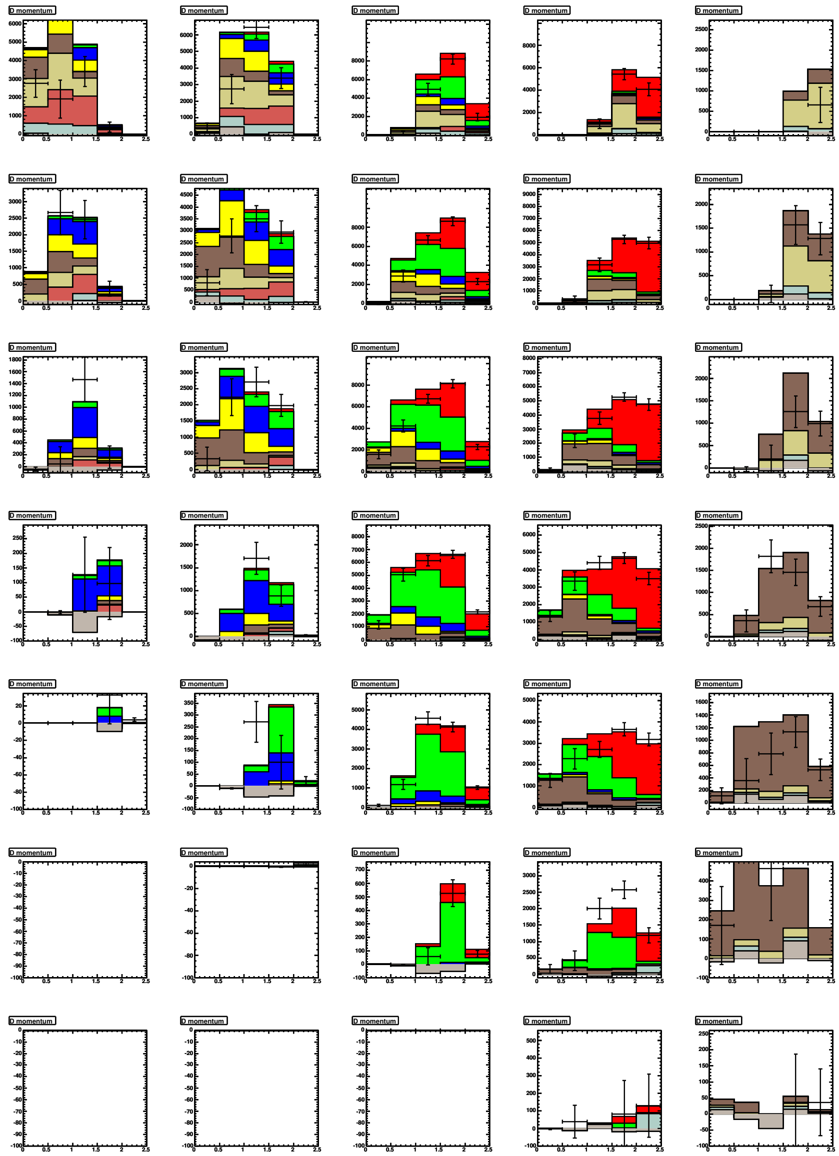

Figure 26: **(Run2 only)** [**Bin by bin plot** (D^+) **before event selection**] D^+ momentum plots showing all bins before event selection cuts and D mass sideband subtraction. From top to bottom, lepton momentum bin changes from the lowest to the highest, and from left to right, cosBY bin changes from negative to positive. In each plots, colors are the same as other plots. Black is OnPeak - OffPeak data. Red is $B \to D\ell\nu$, green is $B \to D^*\ell\nu$, blue is $B \to D^{**}\ell\nu$, yellow is non-resonant $B \to D^{(*)}\pi\ell\nu$, and the rest is background. Dark brown is UncorrDL, light brown is UncorrCL, dark red is CascL, blue gray is FakeL, and light gray is Comb. Comb is almost disappeared after D mass sideband subtraction.

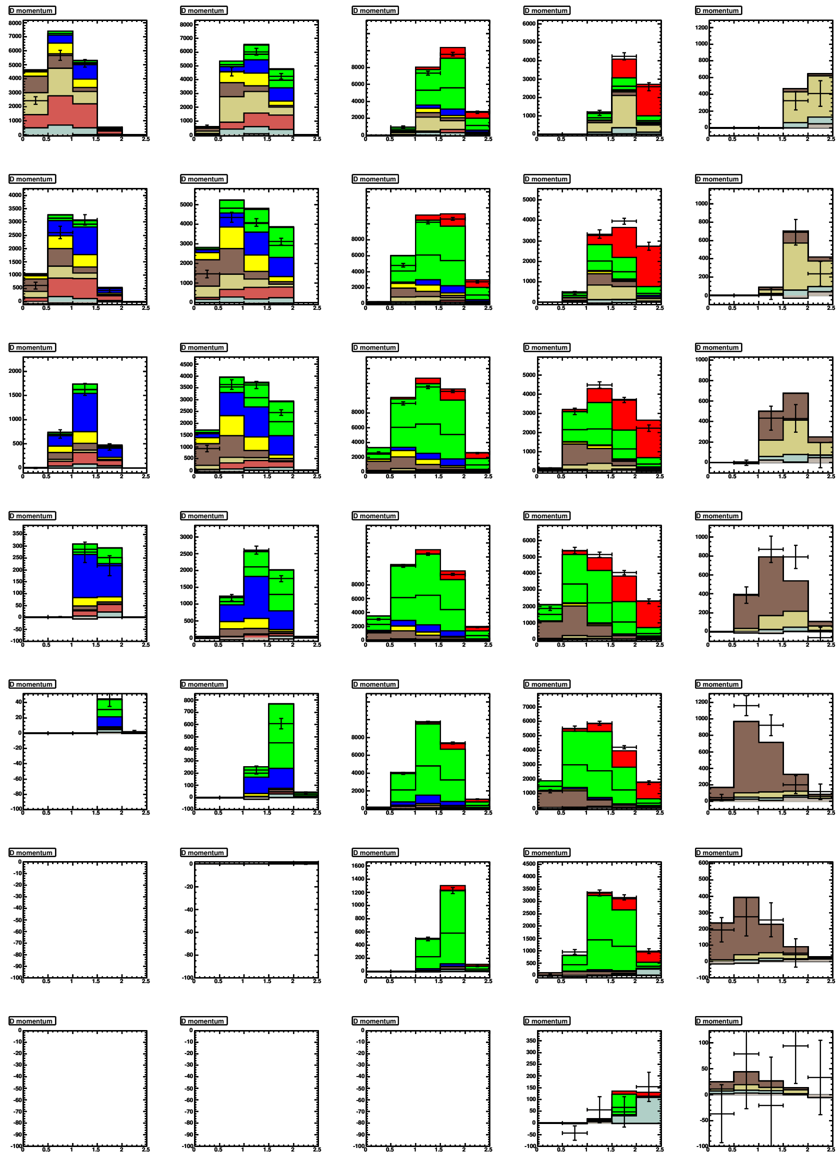

Figure 27: **(Run2 only)** [**Bin by bin plot** (D^0) **after event selection**] D^0 momentum plots showing all bins after event selection cuts and D mass sideband subtraction. From top to bottom, lepton momentum bin changes from the lowest to the highest, and from left to right, cosBY bin changes from negative to positive. In each plots, colors are the same as other plots. Black is OnPeak - OffPeak data. Red is $B \to D\ell\nu$, green is $B \to D^*\ell\nu$, blue is $B \to D^{**}\ell\nu$, yellow is non-resonant $B \to D^{(*)}\pi\ell\nu$, and the rest is background. Dark brown is UncorrDL, light brown is UncorrCL, dark red is CascL, blue gray is FakeL, and light gray is Comb. Comb is almost disappeared after D mass sideband subtraction.

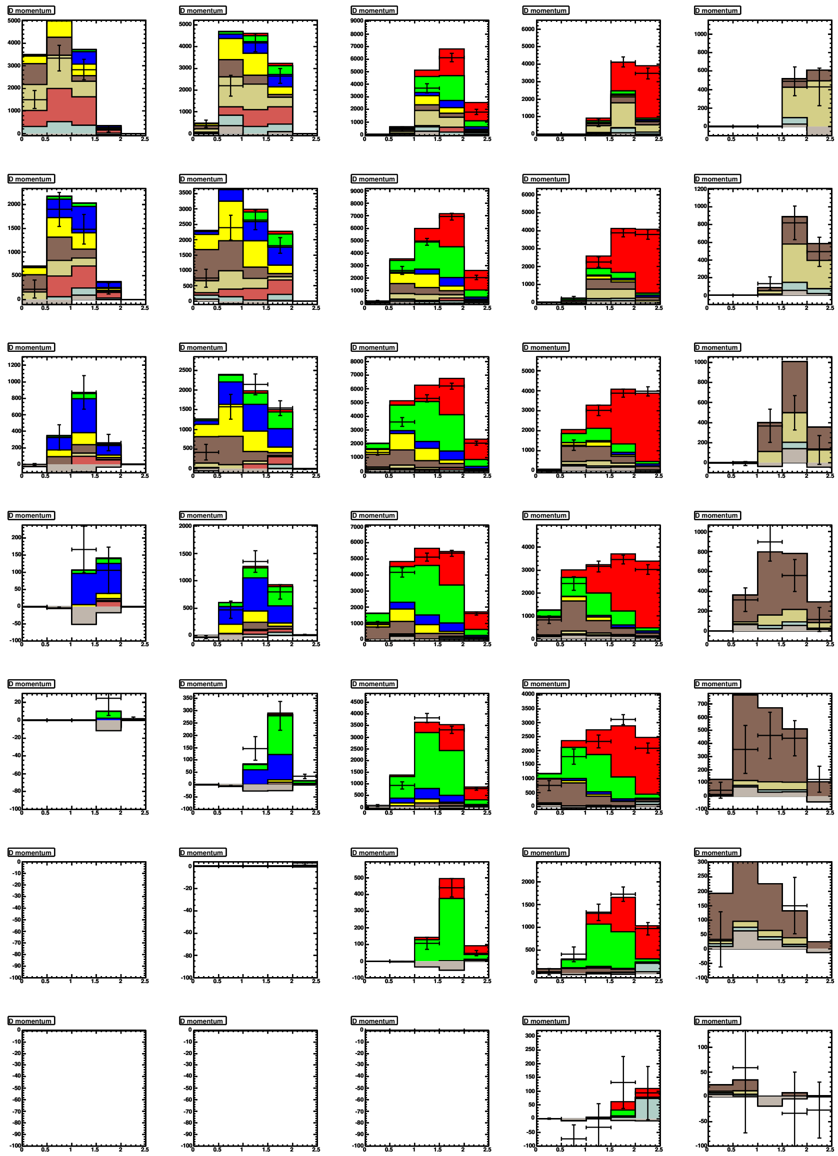

Figure 28: **(Run2 only)** [**Bin by bin plot** **(D^+) after event selection**] D^+ momentum plots showing all bins after event selection cuts and D mass sideband subtraction. From top to bottom, lepton momentum bin changes from the lowest to the highest, and from left to right, cosBY bin changes from negative to positive. In each plots, colors are the same as other plots. Black is OnPeak - OffPeak data. Red is $B \to D\ell\nu$, green is $B \to D^*\ell\nu$, blue is $B \to D^{**}\ell\nu$, yellow is non-resonant $B \to D^{(*)}\pi\ell\nu$, and the rest is background. Dark brown is UncorrDL, light brown is UncorrCL, dark red is CascL, blue gray is FakeL, and light gray is Comb. Comb is almost disappeared after D mass sideband subtraction.

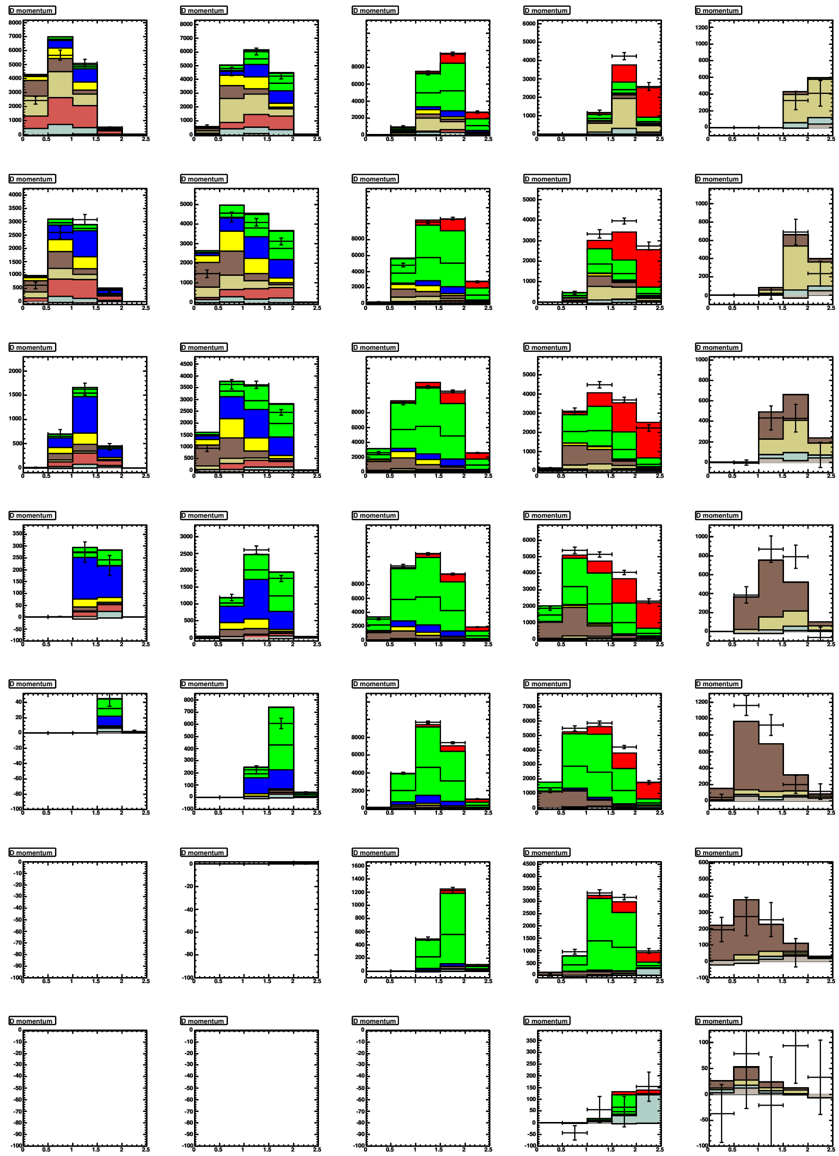

Figure 29: **(Run2 only)** [**Bin by bin plot** (D^0) **after Trk PID**] D^0 momentum plots showing all bins after tracking efficiency and PID correction and D mass sideband subtraction. From top to bottom, lepton momentum bin changes from the lowest to the highest, and from left to right, cosBY bin changes from negative to positive. In each plots, colors are the same as other plots. Black is OnPeak - OffPeak data. Red is $B \to D\ell\nu$, green is $B \to D^*\ell\nu$, blue is $B \to D^{**}\ell\nu$, yellow is non-resonant $B \to D^{(*)}\pi\ell\nu$, and the rest is background. Dark brown is UncorrDL, light brown is UncorrCL, dark red is CascL, blue gray is FakeL, and light gray is Comb. Comb is almost disappeared after D mass sideband subtraction.

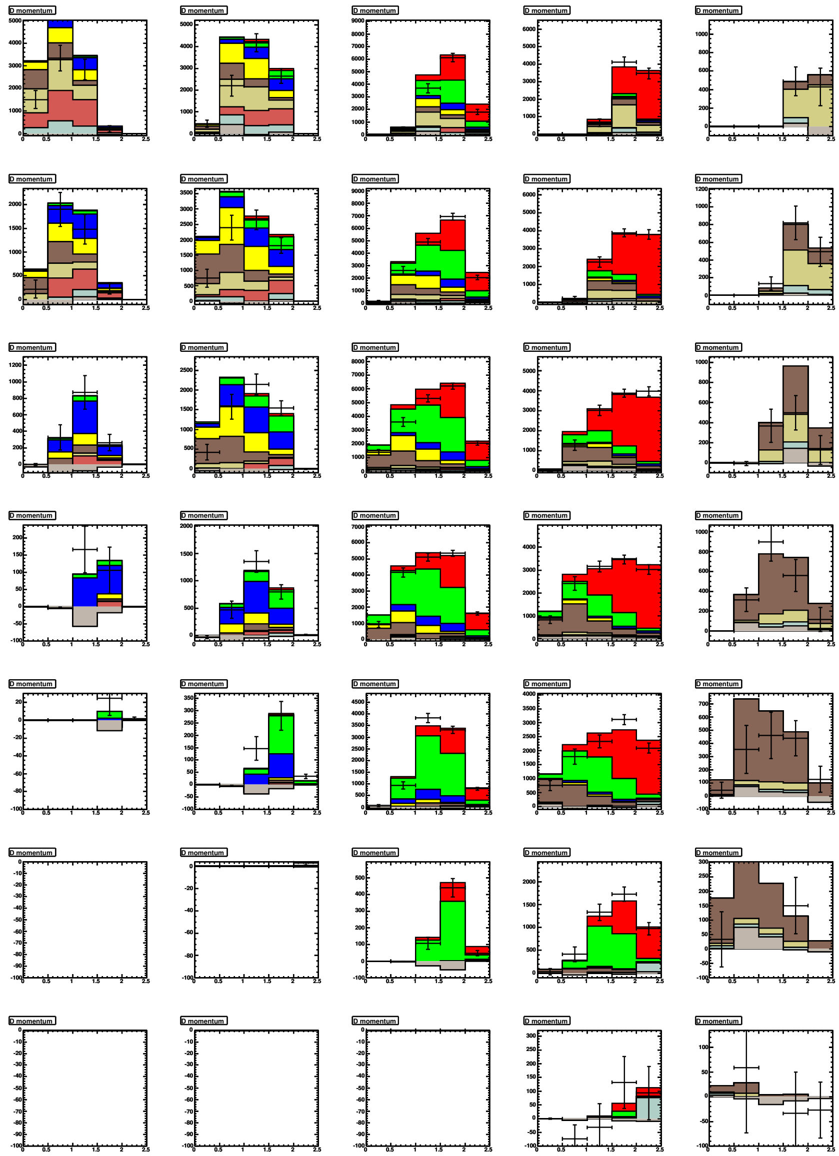

Figure 30: **(Run2 only)** [**Bin by bin plot** (D^{+}) **after Trk PID**] D^{+} momentum plots showing all bins after tracking efficiency and PID correction and D mass sideband subtraction. From top to bottom, lepton momentum bin changes from the lowest to the highest, and from left to right, cosBY bin changes from negative to positive. In each plots, colors are the same as other plots. Black is OnPeak - OffPeak data. Red is $B \to D\ell\nu$, green is $B \to D^{*}\ell\nu$, blue is $B \to D^{**}\ell\nu$, yellow is non-resonant $B \to D^{(*)}\pi\ell\nu$, and the rest is background. Dark brown is UncorrDL, light brown is UncorrCL, dark red is CascL, blue gray is FakeL, and light gray is Comb. Comb is almost disappeared after D mass sideband subtraction.

8 Monte Carlo Re-weighting (W^{MC}_{jk})

Because of theoretical and experimental improvements, some of numbers and formulas used in our MC are obsolete. In order to take new results into account, we need to re-wight MC. In this analysis, we re-weight decay branching fractions and form factors. In this section, details of branching fraction re-weighting is presented. Form factor re-weighting is described in section 9

8.1 Background components

As described in section 2, a few specific decay modes dominate the backgrounds. We need to update some of decay branching fraction to get better description of data.

8.1.1 Semileptonic D decay branching fractions

In case of CascL and UncrorrCL backgrounds, we correct the branching fractions of semileptonic D decays. The values used in SP5/SP6 MC and in PDG [13] are listed in Table 10 along with the weights. The weight is given by the ratio of new and old branching fractions. See section 8.1.5 for an example.

8.1.2 $B \to D^{(*)}\tau\nu$ decay branching fractions

In case of CascL and UncrorrCL backgrounds, we correct $B \to D^{(*)}\tau\nu$ decay branching fractions. For the decays $B^+ \to \bar{D}^0\tau^+\nu$, $B^+ \to \bar{D}^{*0}\tau^+\nu$ and $B^0 \to D^-\tau^+\nu$ we use Babar results [25]. For the decay $B^0 \to D^{*-}\tau^+\nu$ we take an average of Babar [25]

$$B^0 \to D^{*-}\tau^+\nu = 0.0162 \pm 0.0031 \pm 0.0010 \pm 0.005 \tag{171}$$

and Belle [26] results.

$$B^0 \to D^{*-}\tau^+\nu = 0.0202 \pm 0.004 \pm 0.0037 \pm 0.005 \tag{172}$$

Averaged BF and weights are given in Table 11

8.1.3 Inclusive $B \to X\ell\nu$ decay branching fractions

In case of UncorrDL and CombRL backgrounds, we correct the branching fraction of inclusive $B \to X\ell\nu$ decays. In SP5/SP6 MC, the following values are used :

$$\begin{aligned}
&\mathcal{B}(B^+ \to X_c\ell\nu) = \mathcal{B}(B^0 \to X_c\ell\nu) = 0.104 \\
&\mathcal{B}(B^+ \to X_u\ell\nu) = 0.002088 \\
&\mathcal{B}(B^0 \to X_u\ell\nu) = 0.002100
\end{aligned} \tag{173}$$

Thus

$$\begin{aligned}
&\mathcal{B}(B^+ \to X\ell\nu) = 0.106088 \\
&\mathcal{B}(B^0 \to X\ell\nu) = 0.106100
\end{aligned} \tag{174}$$

Weights are given by the ratios of new and old branching fractions as summarized in Table 12. These weights are applied to lepton side of each candidate.

Decay mode	SP5/SP6	PDG [13]	Weight
$D^0 \to K^{*-} e\nu$	0.0202	0.0216 ± 0.0016	1.0693 ± 0.0792
$D^0 \to K^- e\nu$	0.0364	0.0350 ± 0.0009	0.9315 ± 0.0247
$D^0 \to \pi^- e\nu$	0.0037	0.0028 ± 0.0002	0.7568 ± 0.0459
$D^0 \to \rho^- e\nu$	0.0029	0.0019 ± 0.0004	0.6552 ± 0.1379
$D^0 \to K^{*-} \mu\nu$	0.0198	0.0194 ± 0.0025	0.9798 ± 0.1263
$D^0 \to K^- \mu\nu$	0.0322	0.0327 ± 0.0013	1.0155 ± 0.0404
$D^0 \to \pi^- \mu\nu$	0.0037	0.0024 ± 0.0002	0.6378 ± 0.0649
$D^0 \to \rho^- \mu\nu$	0.0029	0.0019 ± 0.0004	0.6552 ± 0.1379
$D^+ \to K^{*0} e\nu$	0.0480	0.0556 ± 0.0032	1.1583 ± 0.0667
$D^+ \to K^0 e\nu$	0.0670	0.0860 ± 0.0050	1.2836 ± 0.0667
$D^+ \to \pi^0 e\nu$	0.0031	0.0044 ± 0.0007	1.4194 ± 0.2258
$D^+ \to \rho^0 e\nu$	0.0022	0.0022 ± 0.0004	1.000 ± 0.1818
$D^+ \to \omega e\nu$	0.0029	0.0016 ± 0.0007	0.5517 ± 0.2414
$D^+ \to K^{*0} \mu\nu$	0.0430	0.0550 ± 0.0050	1.2791 ± 0.1163
$D^+ \to K^0 \mu\nu$	0.0700	0.0960 ± 0.0080	1.3714 ± 0.1143
$D^+ \to \pi^0 \mu\nu$	0.0064	0.0044 ± 0.0007	0.6875 ± 0.1094
$D^+ \to \rho^0 \mu\nu$	0.0027	0.0025 ± 0.0005	0.9259 ± 0.1852
$D^+ \to \omega \mu\nu$	0.0029	0.0016 ± 0.0007	0.5517 ± 0.2222
$D_s^+ \to \phi \ell\nu$	0.0200	0.0249 ± 0.0028	1.2450 ± 0.2400
$D_s^+ \to \eta \ell\nu$	0.0260	0.0320 ± 0.0060	1.2308 ± 0.2308
$D_s^+ \to \eta' \ell\nu$	0.0089	0.0111 ± 0.0034	1.2472 ± 0.3820

Table 10: [**Semileptonic D decay BF weight**] D semileptonic decay branching fractions and weights.

Decay mode	SP5/SP6	Measured [25][26]	Weight
$B^+ \to \bar{D}^0 \tau^+ \nu$	0.0070	$0.0092 \pm 0.0026 \pm 0.0011 \pm 0.006$	1.3142 ± 0.4123
$B^+ \to \bar{D}^{*0} \tau^+ \nu$	0.0160	$0.0174 \pm 0.0033 \pm 0.0010 \pm 0.006$	1.0875 ± 0.2188
$B^0 \to D^- \tau^+ \nu$	0.0070	$0.0086 \pm 0.0024 \pm 0.0011 \pm 0.006$	1.2286 ± 0.3868
$B^0 \to D^{*-} \tau^+ \nu$	0.0160	0.0173 ± 0.0028	1.0795 ± 0.1762

Table 11: [$B \to D^{(*)}\tau\nu$ **decay BF weight**] $B \to D^{(*)}\tau\nu$ decay branching fractions and weights.

Decay mode	SP5/SP6	PDG [13]	Weight
$B^+ \to \bar{X}^0 \ell^+ \nu$	0.106088	0.1099 ± 0.0028	1.0359 ± 0.0264
$B^0 \to X^- \ell^+ \nu$	0.106100	0.1033 ± 0.0028	0.9736 ± 0.0264

Table 12: [$B \to \ell$ **decay BF weight**] Inclusive $B \to x\ell\nu$ branching fractions.

p_D (GeV)	$B^- \to D^0$	$\bar{B}^0 \to D^0$
0.00 - 0.15	0.0600 ± 0.1217	0.0275 ± 0.3010
0.15 - 0.30	0.4667 ± 0.1217	0.6083 ± 0.2374
0.30 - 0.45	0.9800 ± 0.1241	0.7300 ± 0.2080
0.45 - 0.60	0.8600 ± 0.1040	0.9036 ± 0.1863
0.60 - 0.75	1.1022 ± 0.1014	1.0000 ± 0.1779
0.75 - 0.90	1.2491 ± 0.1005	1.0125 ± 0.1677
0.90 - 1.05	1.1431 ± 0.0904	1.1791 ± 0.1516
1.05 - 1.20	1.1770 ± 0.0879	1.2500 ± 0.1519
1.20 - 1.35	1.1306 ± 0.0839	1.1738 ± 0.1451
1.35 - 1.50	1.1324 ± 0.0760	1.3902 ± 0.1516
1.50 - 1.65	1.0128 ± 0.0680	1.1245 ± 0.1214
1.65 - 1.80	1.1371 ± 0.0788	0.9500 ± 0.1538
1.80 - 1.95	0.9544 ± 0.0676	1.0423 ± 0.1600
1.95 - 2.10	0.9673 ± 0.0708	1.0850 ± 0.1789
2.10 - 2.25	0.8850 ± 0.0765	1.4500 ± 0.5274
2.25 - 2.40	0.8154 ± 0.1101	

Table 13: [p_D **dependent** $B \to D^0$ **weight (Correlated)**] D^0 momentum dependent, inclusive $B \to D^0$ branching fraction weights (Correlated). These are based on the branching fractions given in [27][28].

p_D (GeV)	$B^+ \to D^0$	$B^0 \to D^0$
0.00 - 0.15	0.1333 ± 0.1374	0.0938 ± 0.2519
0.15 - 0.30	0.4500 ± 0.1521	0.5114 ± 0.2636
0.30 - 0.45	0.7143 ± 0.1738	0.5172 ± 0.2695
0.45 - 0.60	0.9391 ± 0.1962	1.2000 ± 0.3265
0.60 - 0.75	1.2833 ± 0.2083	1.2214 ± 0.3465
0.75 - 0.90	1.4182 ± 0.2186	1.2424 ± 0.3601
0.90 - 1.05	2.3733 ± 0.3206	0.8182 ± 0.3961
1.05 - 1.20	1.1077 ± 0.2837	0.5647 ± 0.4759
1.20 - 1.35	0.8571 ± 0.4247	1.6000 ± 0.8412
1.35 - 1.50	2.9000 ± 1.1180	-3.5333 ± 1.9887
1.50 - 1.65	0.0833 ± 0.8580	3.4615 ± 2.6315
1.65 - 1.80	0.4000 ± 0.1844	6.3333 ± 8.3333

Table 14: [p_D **dependent** $B \to D^0$ **weight (Uncorrelated)**] D^0 momentum dependent, inclusive $B \to D^0$ branching fraction weights (Uncorrelated). These are based on the branching fractions given in [27][28].

p_D (GeV)	$B^- \to D^+$	$\bar{B}^0 \to D^+$
0.00 - 0.20	0.5588 ± 0.2712	0.1333 ± 0.2007
0.02 - 0.40	0.6484 ± 0.2190	0.6790 ± 0.2351
0.40 - 0.60	1.0438 ± 0.2285	0.3702 ± 0.1820
0.60 - 0.80	1.0402 ± 0.2032	0.6823 ± 0.1581
0.80 - 1.00	0.6615 ± 0.1655	0.6279 ± 0.1347
1.00 - 1.20	0.7929 ± 0.1585	0.7489 ± 0.1286
1.20 - 1.40	0.7056 ± 0.1557	1.0468 ± 0.1417
1.40 - 1.60	0.5414 ± 0.1762	1.0208 ± 0.1027
1.60 - 1.80	0.8313 ± 0.2642	1.0036 ± 0.1241
1.80 - 2.00	0.7500 ± 0.4413	1.0453 ± 0.1255
2.00 - 2.20	0.3333 ± 0.5429	0.8105 ± 0.1175
2.20 - 2.40		0.8490 ± 0.1514

Table 15: [p_D **dependent** $B \to D^+$ **weight (Correlated)**] D^+ momentum dependent, inclusive $B \to D^+$ branching fraction weights (Correlated). These are based on the branching fractions given in [27][28].

p_D (GeV)	$B^+ \to D^+$	$B^0 \to D^+$
0.00 - 0.20	0.1935 ± 0.1962	0.1613 ± 0.1962
0.20 - 0.40	0.2273 ± 0.2293	0.6462 ± 0.4440
0.40 - 0.60	1.0400 ± 0.3078	0.9315 ± 0.5156
0.60 - 0.80	0.0789 ± 0.2654	0.1143 ± 0.5157
0.80 - 1.00	0.8088 ± 0.3175	-0.0984 ± 0.5590
1.00 - 1.20	1.3400 ± 0.3795	1.7674 ± 0.9047
1.20 - 1.40	0.0800 ± 0.4948	-0.6667 ± 1.4414
1.40 - 1.60	0.5000 ± 1.3463	2.0000 ± 5.2100
1.60 - 1.80	2.1429 ± 1.4070	5.5000 ± 5.2633
1.80 - 2.00	2.0000 ± 2.2361	-8.0000 ± 6.4275

Table 16: [p_D **dependent** $B \to D^+$ **weight (Uncorrelated)**] D^+ momentum dependent, inclusive $B \to D^+$ branching fraction weights (Uncorrelated). These are based on the branching fractions given in [27][28].

Decay mode	SP5/SP6	Measured	Updated	Weight
$B^- \to D_s^+$	0.0130	0.0110 ± 0.0041	0.0100 ± 0.0038	0.7692 ± 0.2942
$B^+ \to D_s^+$	0.1380	0.1070 ± 0.0094	0.0943 ± 0.0113	0.7049 ± 0.0819
$\bar{B}^0 \to D_s^+$	0.0150	0.0180 ± 0.0102	0.0164 ± 0.0094	1.0909 ± 0.6236
$B^0 \to D_s^+$	0.1310	0.1390 ± 0.0158	0.1264 ± 0.0173	0.9646 ± 0.1318

Table 17: [$B \to D_s$ **decay BF weight**] Inclusive $B \to D_s$ branching fractions. The measured value from [27][28] are updated using newer $D_s \to \phi\pi$ branching fractions from PDG [13].

8.1.4 Inclusive $B \to D$ decay branching fractions

In case of UncorrDL, UncorrCL, CascL and FakeL, we correct the branching fraction of inclusive $B \to D$ decays using measured branching fractions from [27][28]. The D momentum dependent weights are given in Tables 13 - 16. If we apply these weights to, for example, UncorrDL ($B^+B^- \to D^0$), we get a distribution shown in Figure 31. The corrected histogram is fluctuated because of the statistical fluctuation of the weights. To smooth up the fluctuation, we use a Gaussian plus a 3rd order polynomial to approximate the weights as a function of D momentum. We use a Gaussian to account for the contribution from two body decays such as $B \to D\bar{D}$. We set the mean of the Gaussian to

$$\frac{m_B - m_D - m_{\bar{D}}}{2} = \frac{5.3 - 1.9 - 2.0}{2} = 0.7 \tag{175}$$

because one of the D is likely to be D_s or D^*. Since mass difference of D and D_s or D^* and the momentum of initial B are small, we asuum that D and $\bar{D}$ go back to back with the same momentum in the CM frame. The distributions of weights and fit results are given in Figures 32 - 39. Using the fitted coefficients and the normalization and width, the weight w is given by

$$\begin{aligned} w = &(\text{Coefficient0}) + (\text{Coefficient1})p_D + (\text{Coefficient2})p_D^2 + (\text{Coefficient3})p_D^3 \\ &+ \frac{(\text{normalization})}{\sqrt{2\pi(\text{width})}} e^{-\frac{(p_D - 0.7)^2}{2(\text{width})^2}} \end{aligned} \tag{176}$$

where p_D is the D momentum. In Figure 40, the same UncorrDL ($B^+B^- \to D^0$) using this fit resut is given. The corrected distribution is much smoother and retains similar character as the original distribution. For a comparison, we show the fit results when we use only a 3rd order polynomial in Figures 41 - 48. In this case, using the fitted coefficients, the weight w is given by

$$w = (\text{Coefficient0}) + (\text{Coefficient1})p_D + (\text{Coefficient2})p_D^2 + (\text{Coefficient3})p_D^3 \tag{177}$$

If you compare Figures 32 - 35 with 41 - 35, in the $B \to D^0$ case, there is a significant contribution from two body decays (Gaussian), but in the $B \to D^+$ case (Figures 33 - 39 and 46 - 39), the contribution is small except for the $B^- \to D^+$ (Figures 36 and 45). Note tat the weights are the ratio between data and MC. Thus no Gaussian contribution, such as in case of $B \to D^0$, means that two body decays are well modeled and no significant difference between data and MC.

We also correct the branching fractions of inclusive $B \to D_s$ decays using measured branching fractions from [27][28]. In [27][28], older branching fraction of $D_s \to \phi\pi$ are used. We use the numbers in PDG [13] to update the inclusive branching fractions. Weights are given in Table 17.

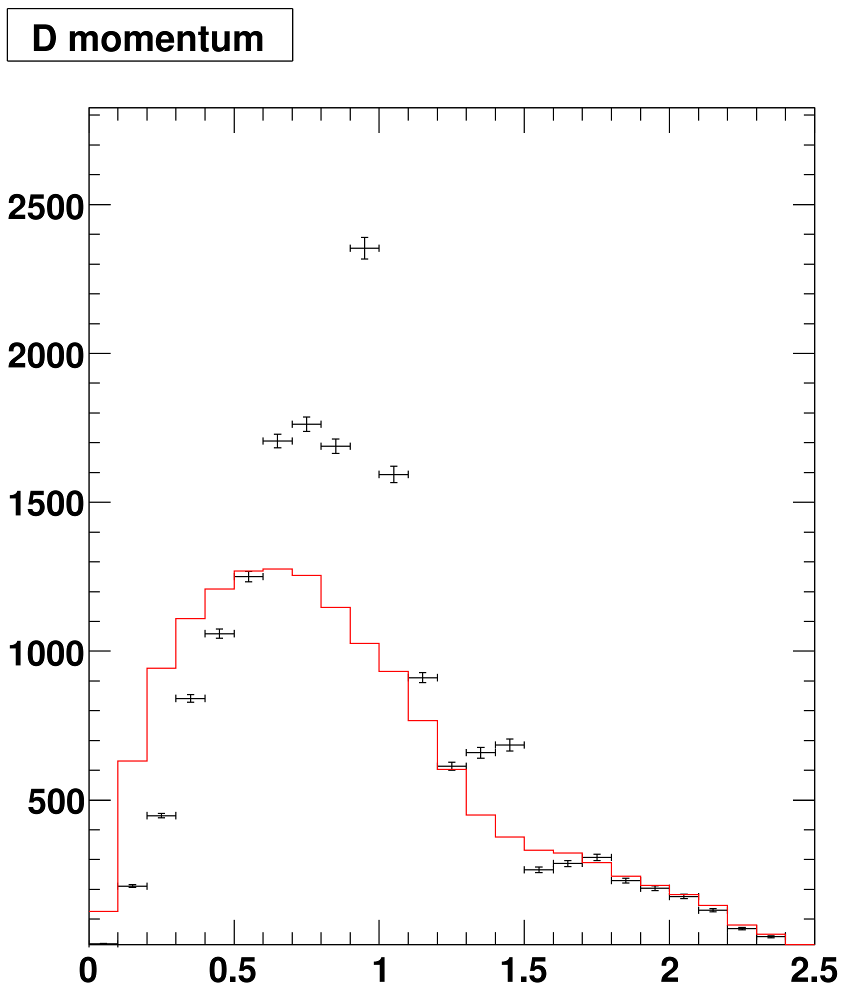

Figure 31: [**UncorrDL BF correction - Table**] Effect of BpBm UncorrDL background BF correction using weights given in tables. The red histogram is before correction, and the black lines with error bars are after correction.

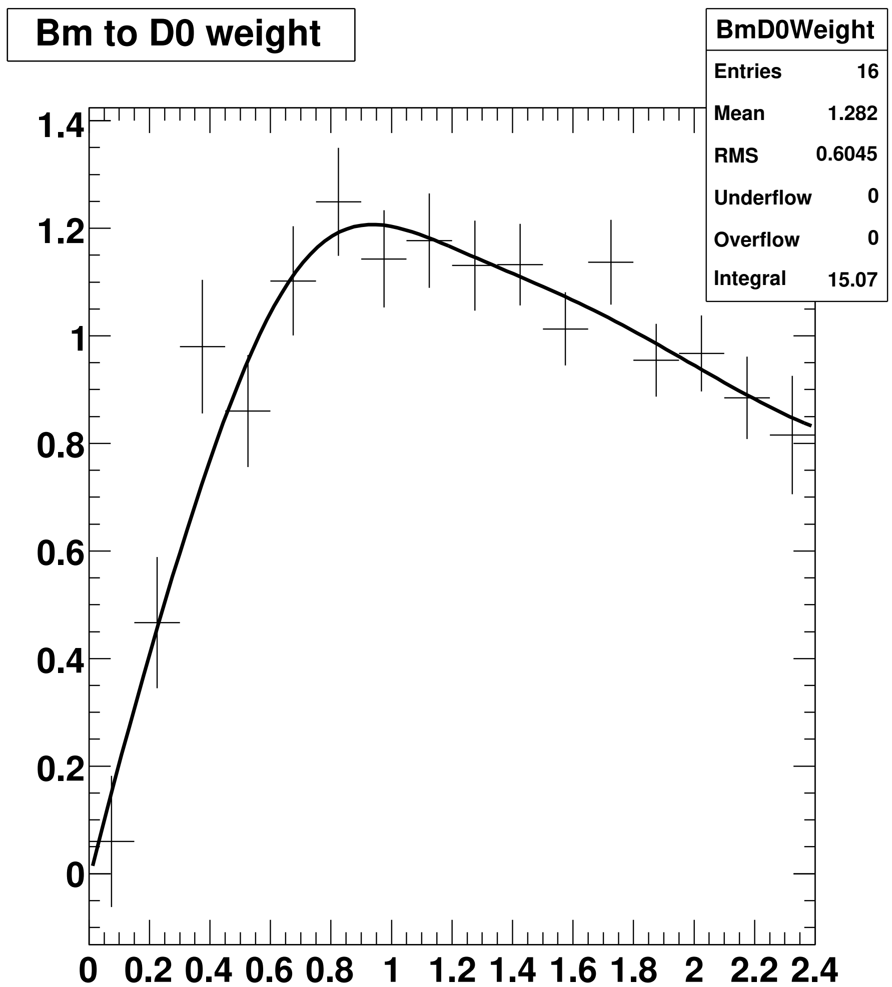

Figure 32: [**Fit for** $B^- \to D^0$ **weight : G+P**] Gaussian plus 3rd order polynomial fit for $B^- \to D^0$ weight.

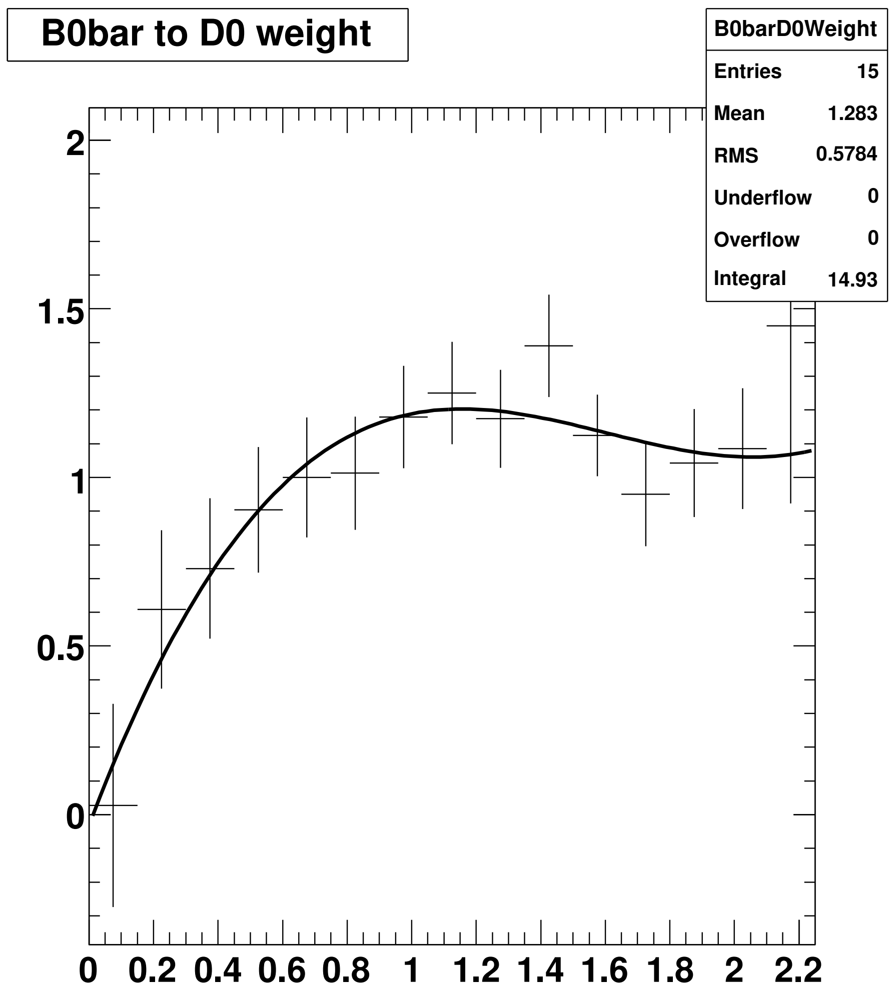

Figure 33: [**Fit for $\bar{B}^0 \to D^0$ weight : G+P**] Gaussian plus 3rd order polynomial fit for $\bar{B}^0 \to D^0$ weight.

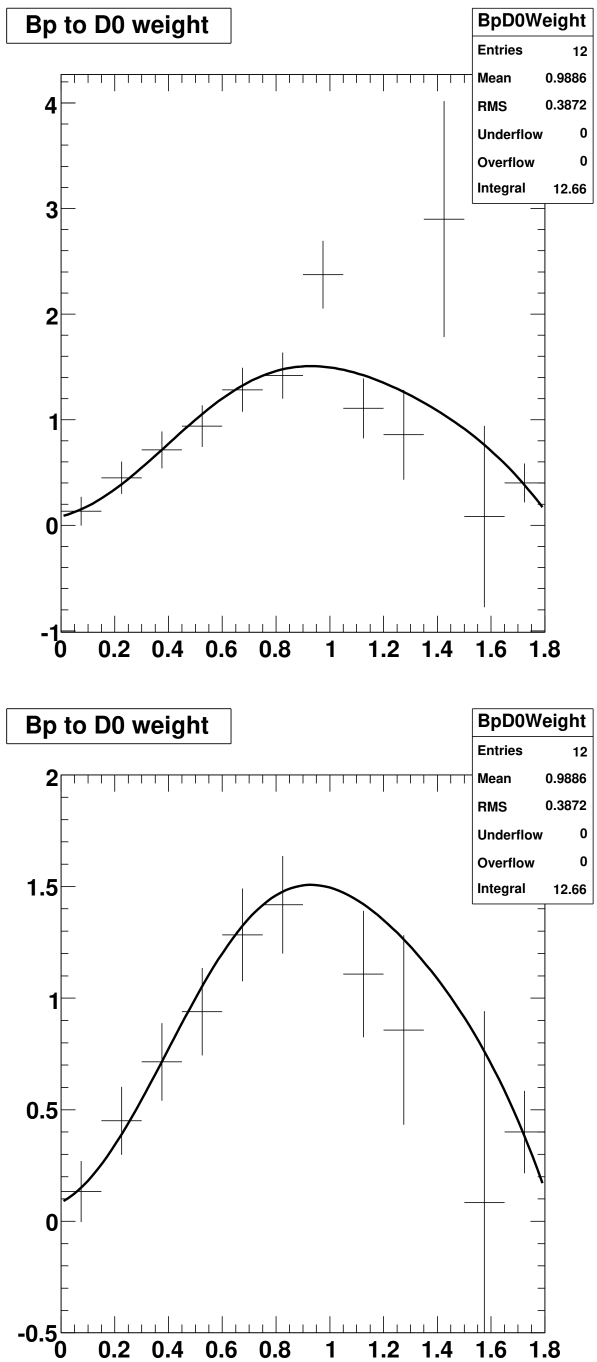

Figure 34: [**Fit for $B^+ \to D^0$ weight : G+P**] Gaussian plus 3rd order polynomial fit for $B^+ \to D^0$ weight. The bottom plot is a close up of the above plot.

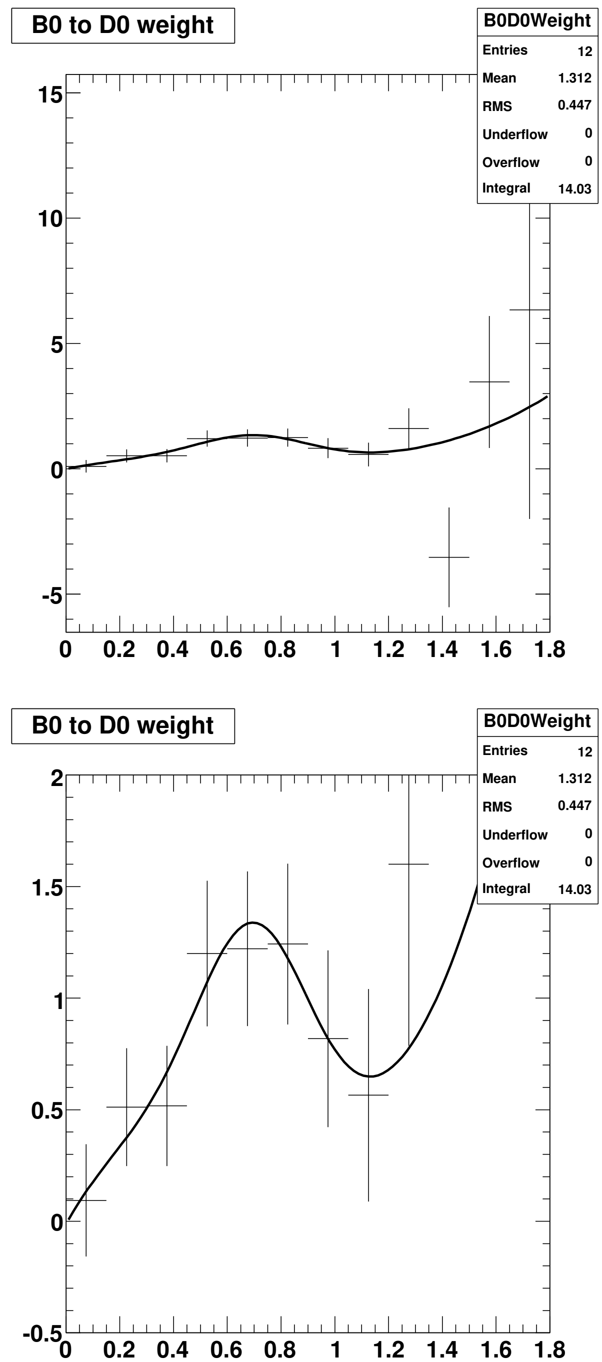

Figure 35: [**Fit for $B^0 \to D^0$ weight : G+P**] Gaussian plus 3rd order polynomial fit for $B^0 \to D^0$ weight. The bottom plot is a close up of the above plot.

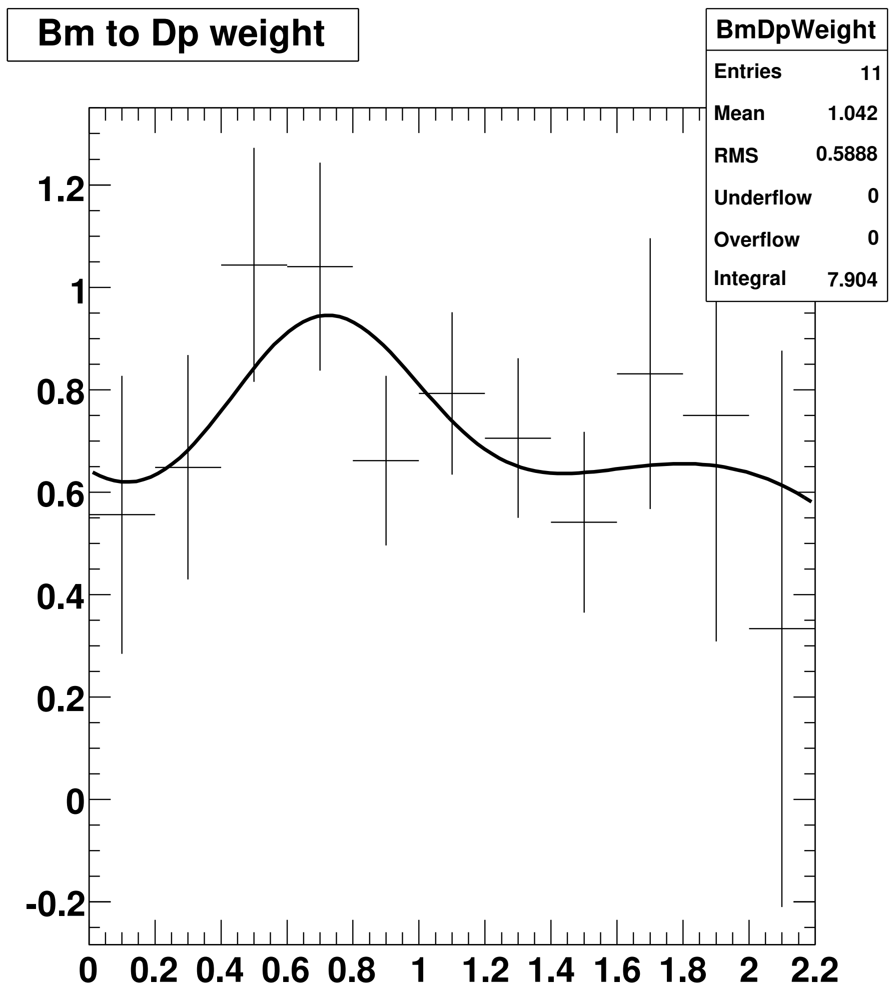

Figure 36: [**Fit for** $B^- \rightarrow D^+$ **weight : G+P**] Gaussian plus 3rd order polynomial fit for $B^- \rightarrow D^+$ weight.

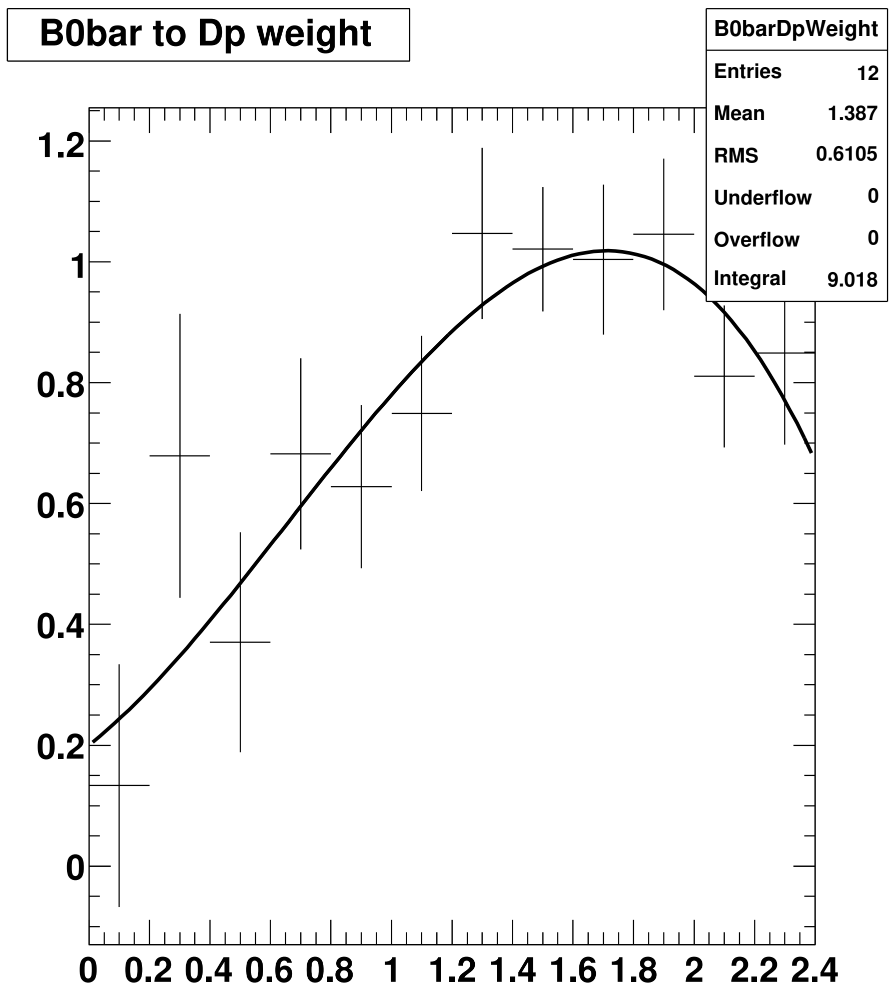

Figure 37: [**Fit for $\bar{B}^0 \to D^+$ weight : G+P**] Gaussian plus 3rd order polynomial fit for $\bar{B}^0 \to D^+$ weight.

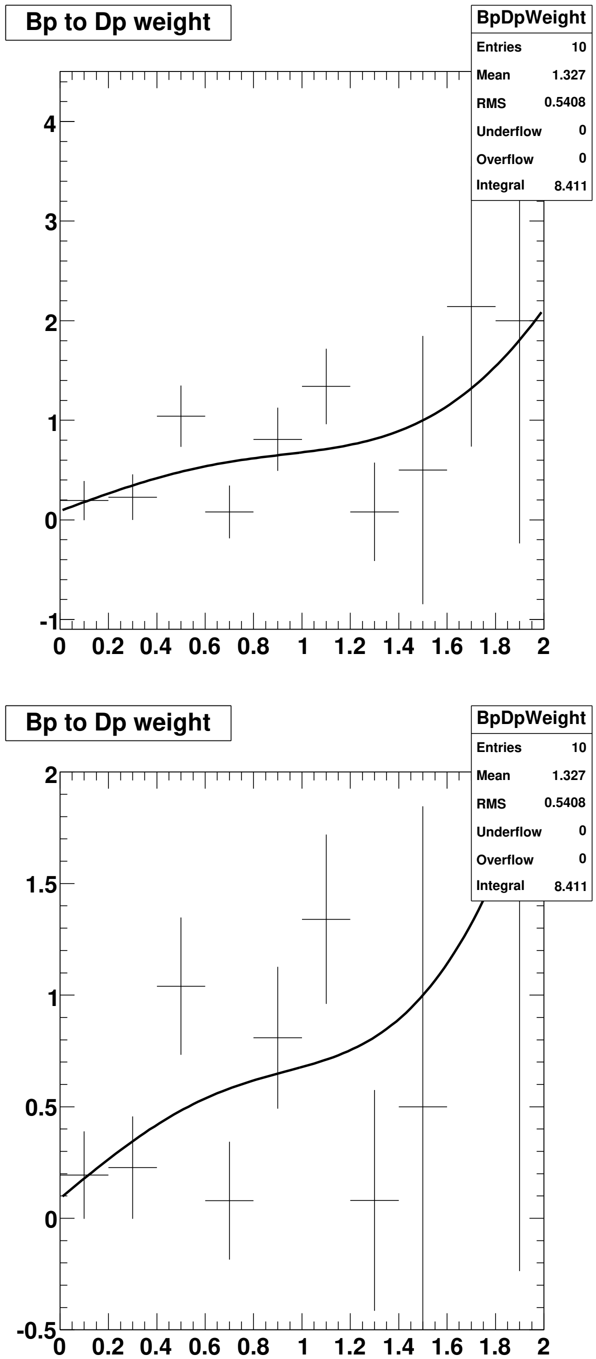

Figure 38: [**Fit for $B^+ \rightarrow D^+$ weight : G+P**] Gaussian plus 3rd order polynomial fit for $B^+ \rightarrow D^+$ weight. The bottom plot is a close up of the above plot.

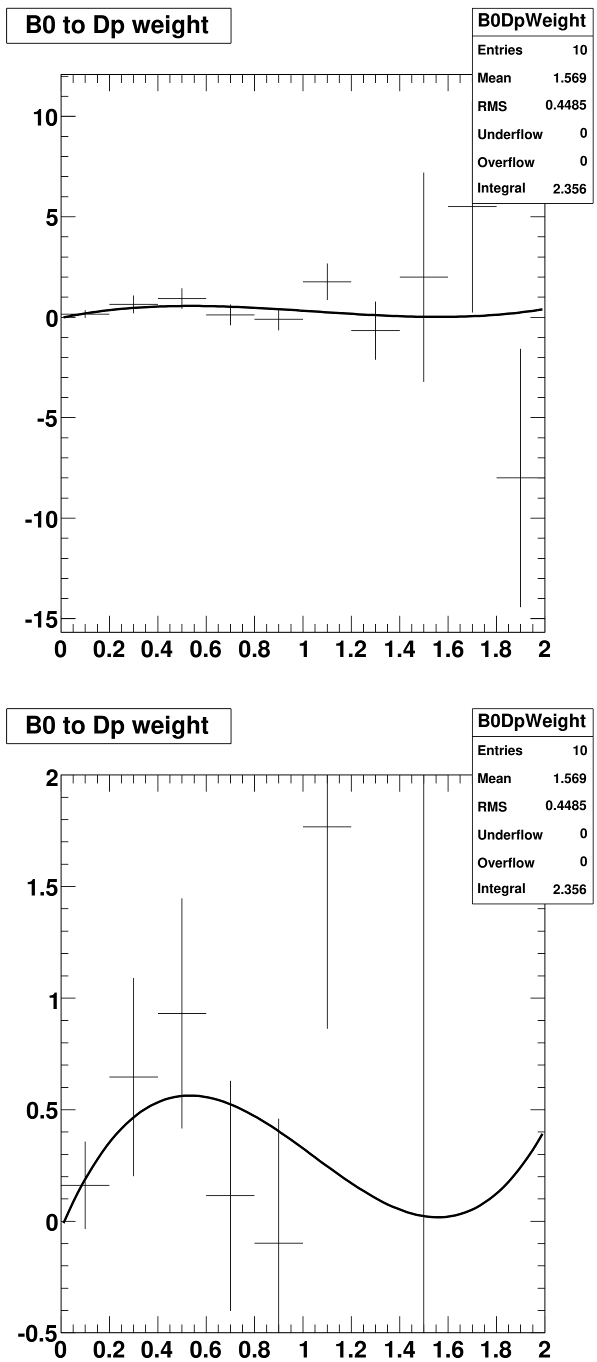

Figure 39: [**Fit for $B^0 \to D^+$ weight : G+P**] Gaussian plus 3rd order polynomial fit for $B^0 \to D^+$ weight. The bottom plot is a close up of the above plot.

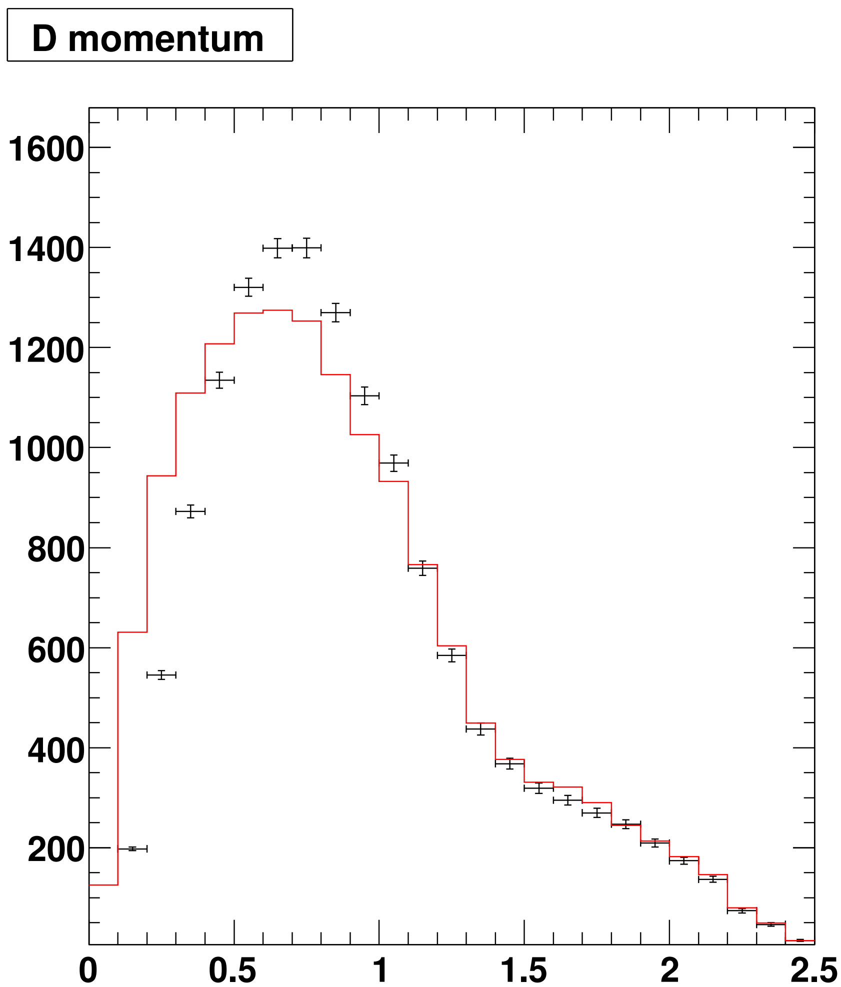

Figure 40: [**UncorrDL BF correction - Fitted**] Effect of BpBm UncorrDL background BF correction using a Gaussian and a 3rd order polynomial. The red histogram is before correction, and the black lines with error bars are after correction.

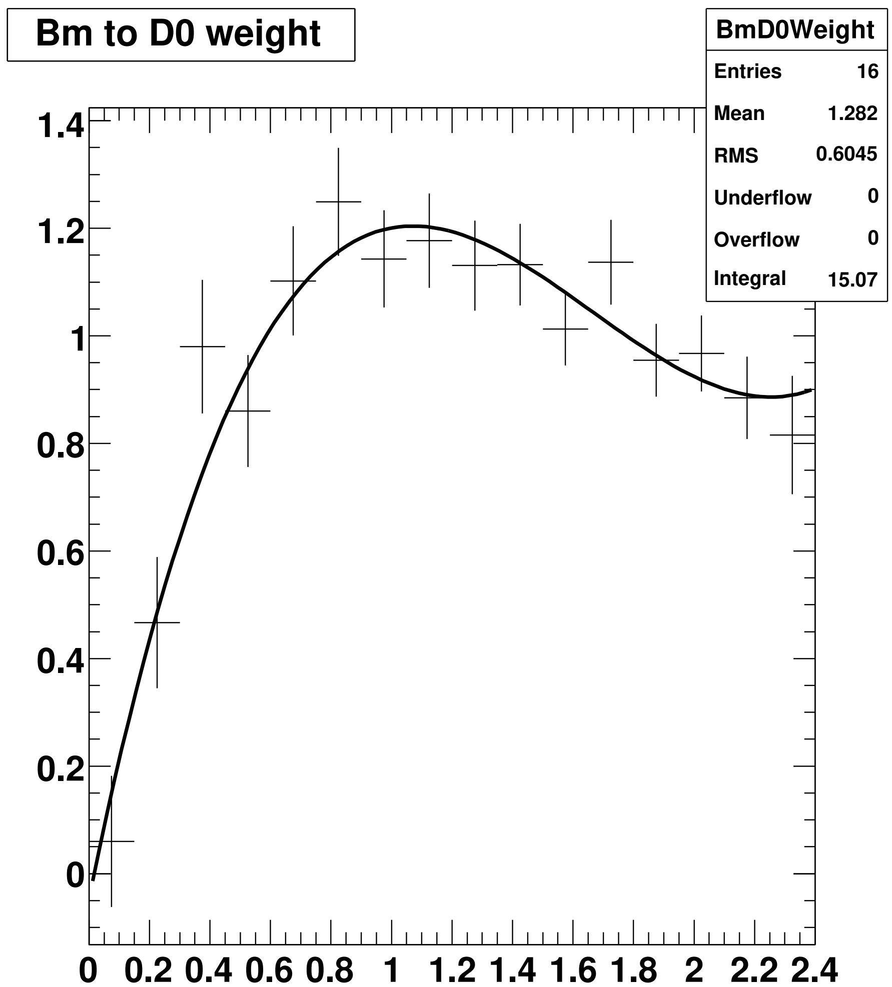

Figure 41: [**Fit for** $B^- \to D^0$ **weight : P**] 3rd order polynomial fit for $B^- \to D^0$ weight.

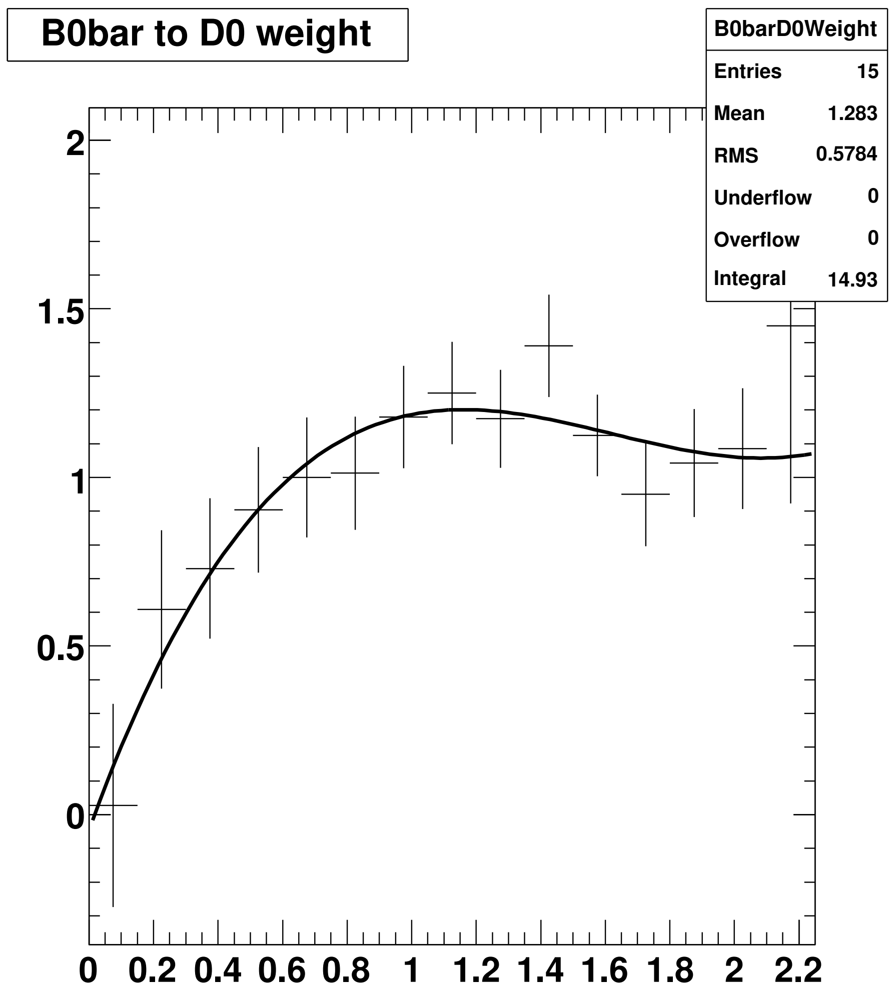

Figure 42: [**Fit for $\bar{B}^0 \rightarrow D^0$ weight : P**] 3rd order polynomial fit for $\bar{B}^0 \rightarrow D^0$ weight.

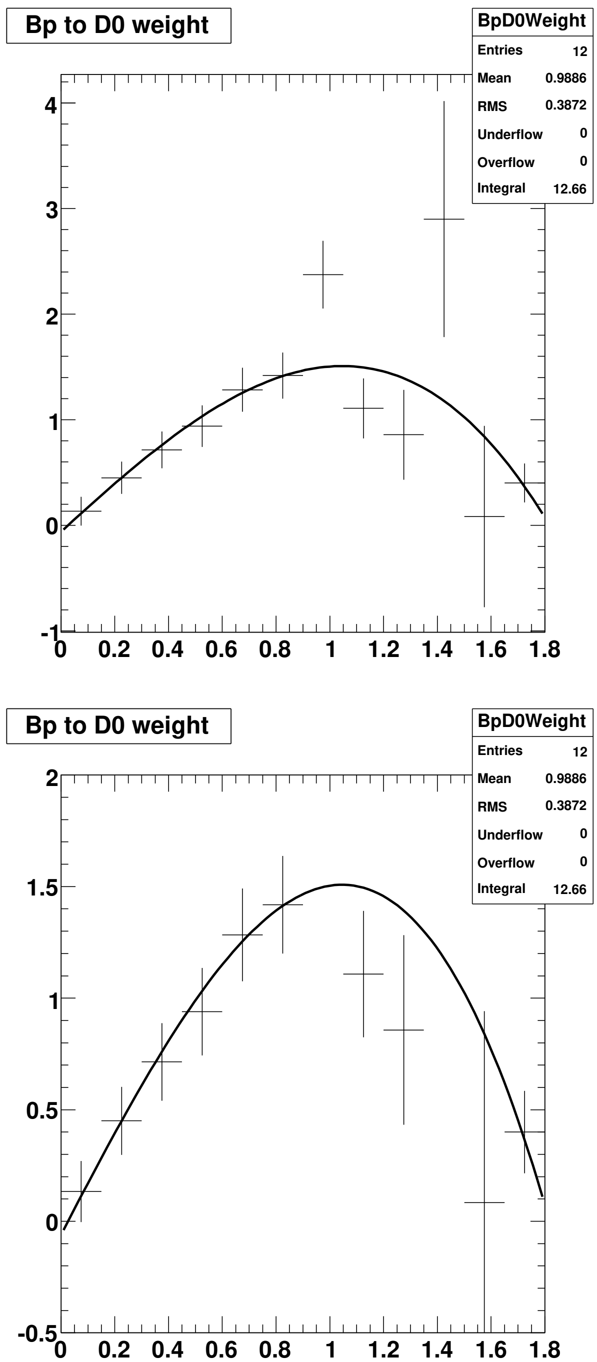

Figure 43: [**Fit for** $B^+ \to D^0$ **weight : P**] 3rd order polynomial fit for $B^+ \to D^0$ weight. The bottom plot is a close up of the above plot.

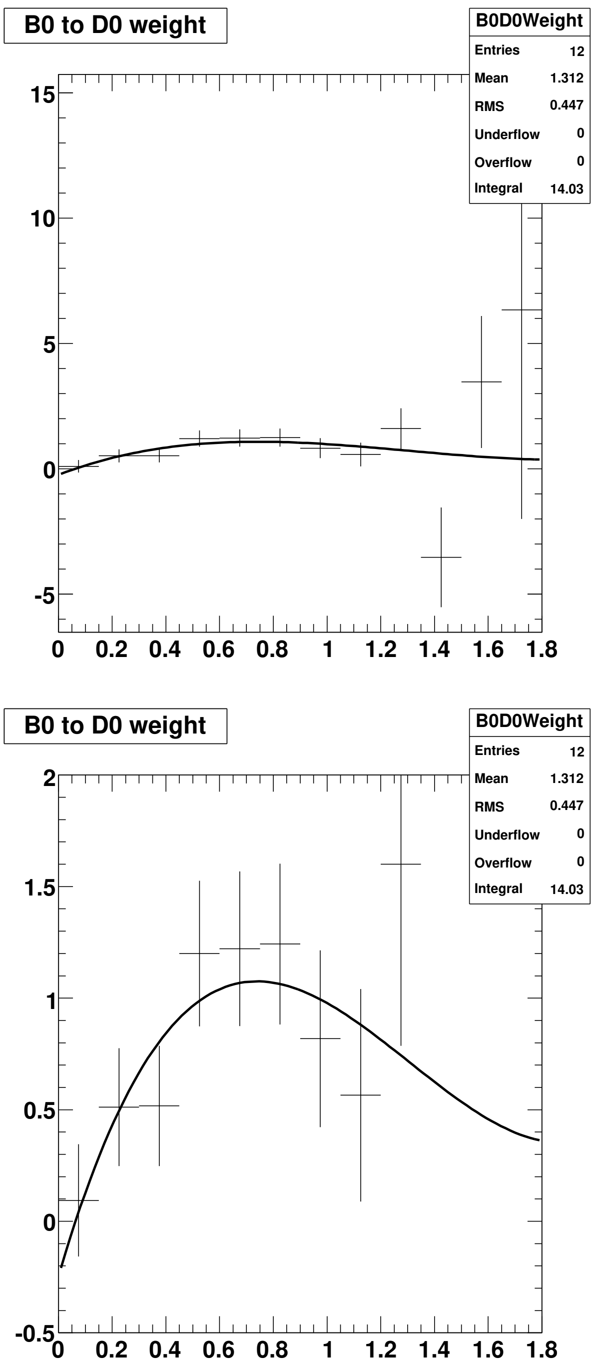

Figure 44: [**Fit for** $B^0 \rightarrow D^0$ **weight : P**] 3rd order polynomial fit for $B^0 \rightarrow D^0$ weight. The bottom plot is a close up of the above plot.

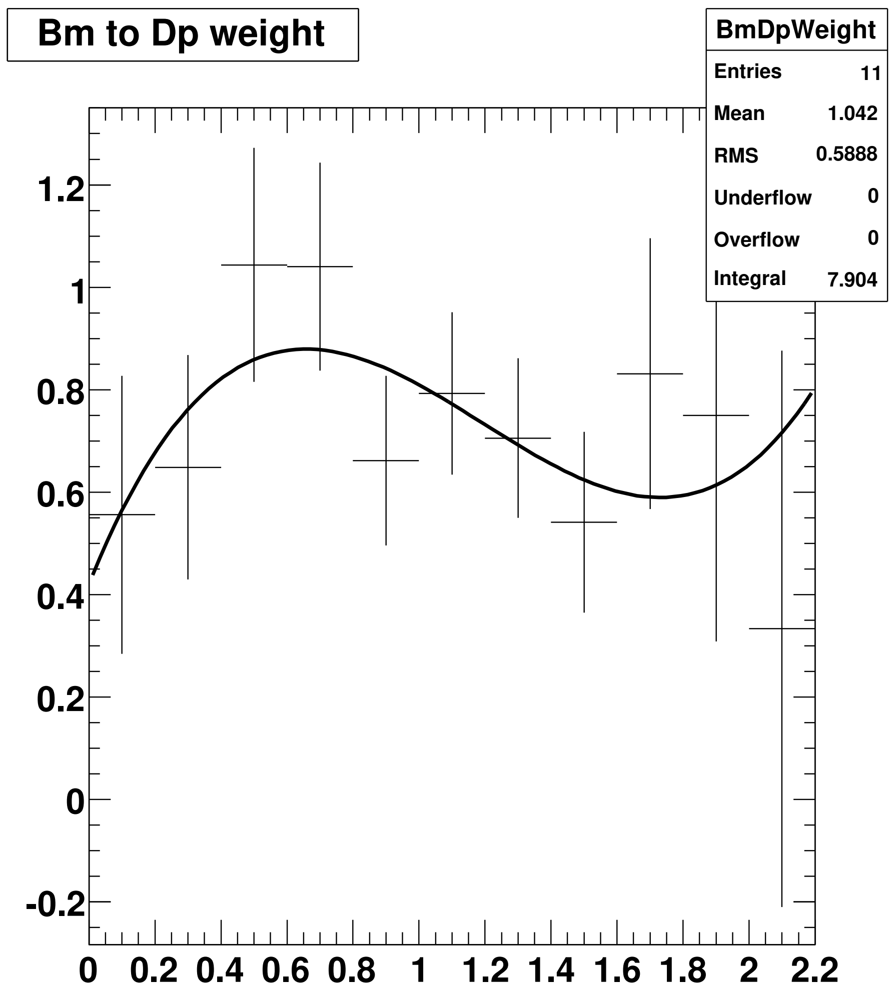

Figure 45: [**Fit for** $B^- \to D^+$ **weight : P**] 3rd order polynomial fit for $B^- \to D^+$ weight.

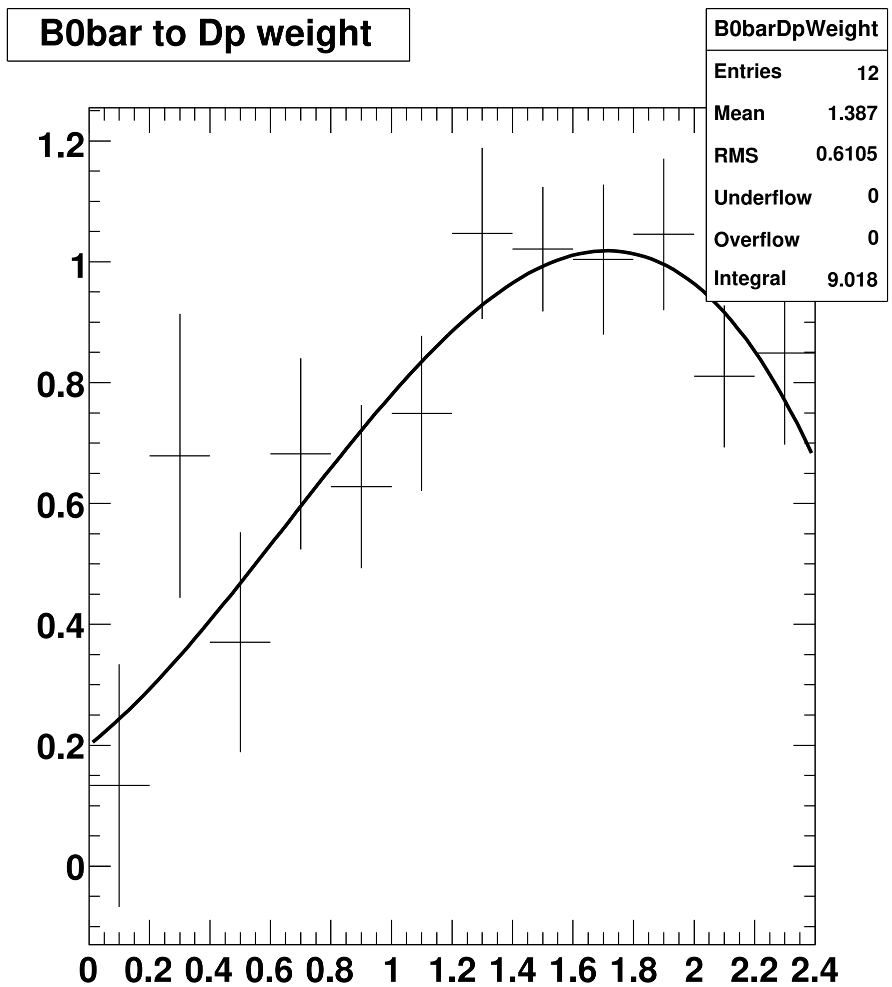

Figure 46: [**Fit for** $\bar{B}^0 \to D^+$ **weight : P**] 3rd order polynomial fit for $\bar{B}^0 \to D^+$ weight.

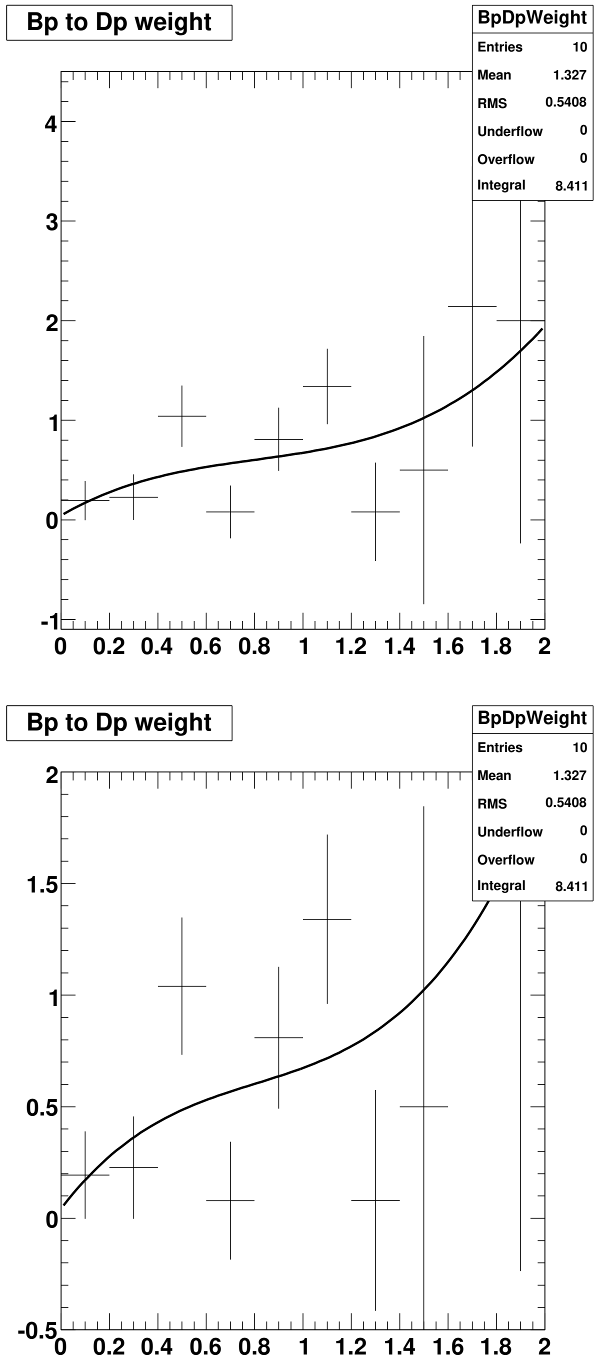

Figure 47: [**Fit for** $B^+ \to D^+$ **weight : P**] 3rd order polynomial fit for $B^+ \to D^+$ weight. The bottom plot is a close up of the above plot.

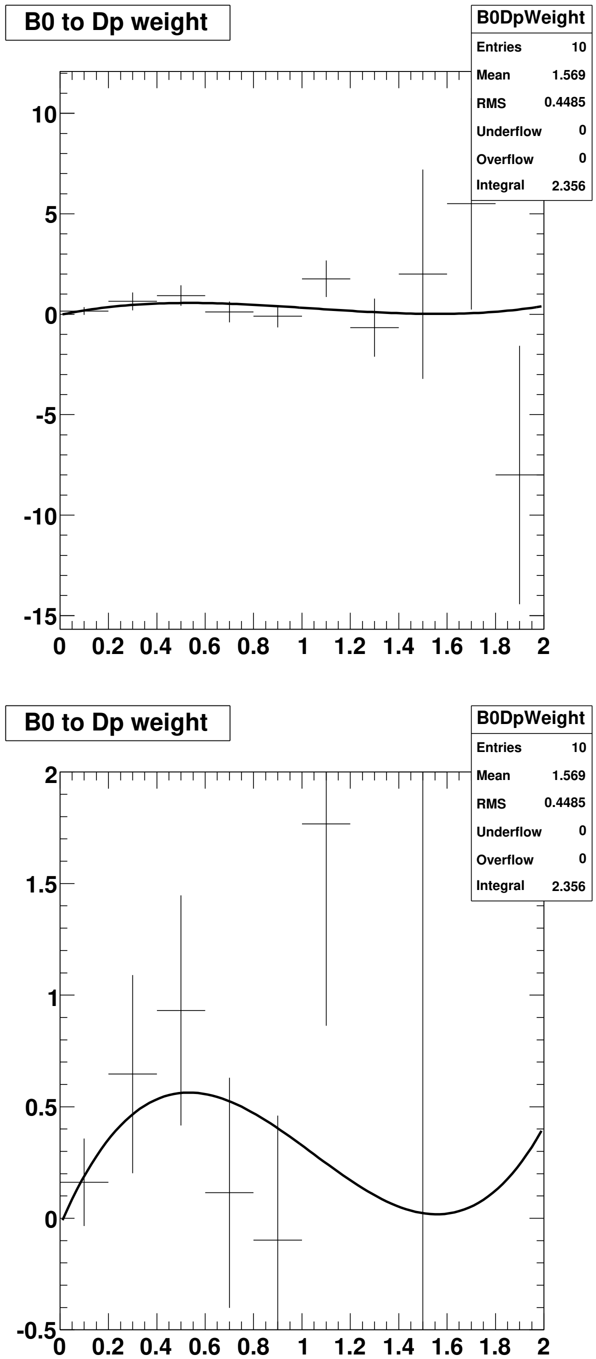

Figure 48: [**Fit for** $B^0 \to D^+$ **weight : P**] 3rd order polynomial fit for $B^0 \to D^+$ weight. The bottom plot is a close up of the above plot.

8.1.5 An example

Here we give a specific example to illustrate BF re-weighting. In the case of

- $B^+ \to D^{*-}D^+K^+$
  with $D^{*-} \to \bar{D}^0\pi^-$ and $D^+ \to \bar{K}^0e^+\nu$
  and these $\bar{D}^0$ and e^+ form a Dl candidate as if $B^+ \to \bar{D}^0e^+\nu$

The number of this background is given by

$$\begin{aligned} &N = (\text{number of produced } B^+B^- \text{ pairs})\times \\ &\mathcal{B}(B^+ \to D^{*-}D^+K^+)\mathcal{B}(D^{*-} \to \bar{D}^0\pi^-)\mathcal{B}(D^+ \to \bar{K}^0e^+\nu)\mathcal{B}(D^0 \to K^-\pi^+) \end{aligned} \tag{178}$$

Thus, it is proportional to all branching fractions. This means that the weight is given by the ratio of new and old branching fractions. This also means that even if you do not know the details of the decay chain, if you know, for example, $D^+ \to \bar{K}^0e^+\nu$ is included in the chain, you can still apply a weight only for the known part.

8.2 D^{**} decay branching fractions

The values used in SP5/SP6 MC are summarized in Appendix D. We adopt the following new values in our fit. These are not applied in candidate level. Thus, these values goes into the coefficients in the fit. See details in section 4. For D_0^*, D_1 and D_1', based on isospin symmetry

$$\begin{aligned} \mathcal{B}(D_0^{*+} \to D^0\pi^+) &= 2\mathcal{B}(D_0^{*+} \to D^+\pi^0) \\ \mathcal{B}(D_0^{*0} \to D^+\pi^-) &= 2\mathcal{B}(D_0^{*0} \to D^0\pi^0) \\ \mathcal{B}(D_1^+ \to D^{*0}\pi^+) &= 2\mathcal{B}(D_1^+ \to D^{*+}\pi^0) \\ \mathcal{B}(D_1^0 \to D^{*+}\pi^-) &= 2\mathcal{B}(D_1^0 \to D^{*0}\pi^0) \\ \mathcal{B}(D_1'^+ \to D^{*0}\pi^+) &= 2\mathcal{B}(D_1'^+ \to D^{*+}\pi^0) \\ \mathcal{B}(D_1'^0 \to D^{*+}\pi^-) &= 2\mathcal{B}(D_1'^0 \to D^{*0}\pi^0) \end{aligned} \tag{179}$$

Thus, we use

$$\begin{aligned} &\mathcal{B}(D_0^{*+} \to D^0\pi^+) = \mathcal{B}(D_0^{*0} \to D^+\pi^-) = \mathcal{B}(D_1^+ \to D^{*0}\pi^+) = \mathcal{B}(D_1^0 \to D^{*+}\pi^-) \\ &= \mathcal{B}(D_1'^+ \to D^{*0}\pi^+) = \mathcal{B}(D_1'^0 \to D^{*+}\pi^-) = 0.6667 \end{aligned} \tag{180}$$

and

$$\begin{aligned} &\mathcal{B}(D_0^{*+} \to D^+\pi^0) = \mathcal{B}(D_0^{*0} \to D^0\pi^0) = \mathcal{B}(D_1^+ \to D^{*+}\pi^0) = \mathcal{B}(D_1^0 \to D^{*0}\pi^0) \\ &= \mathcal{B}(D_1'^+ \to D^{*+}\pi^0) = \mathcal{B}(D_1'^0 \to D^{*0}\pi^0) = 0.3333 \end{aligned} \tag{181}$$

Here we asuumed that D^{**} decays 100 % into $D^{(*)}\pi$. However there is an observation of $D_1 \to D\pi^+\pi^-$ decays [29]. We consider this in the next version.

For D_2^*, from isospin symmetry

$$\begin{aligned}
\mathcal{B}(D_2^{*+} \to D^0\pi^+) &= 2\mathcal{B}(D_2^{*+} \to D^+\pi^0) \\
\mathcal{B}(D_2^{*+} \to D^{*0}\pi^+) &= 2\mathcal{B}(D_2^{*+} \to D^{*+}\pi^0) \\
\mathcal{B}(D_2^{*0} \to D^+\pi^-) &= 2\mathcal{B}(D_2^{*0} \to D^0\pi^0) \\
\mathcal{B}(D_2^{*0} \to D^{*+}\pi^-) &= 2\mathcal{B}(D_2^{*0} \to D^{*0}\pi^0)
\end{aligned} \tag{182}$$

From PDG [13]

$$\frac{\mathcal{B}(D_2^{*+} \to D^0\pi^+)}{\mathcal{B}(D_2^{*+} \to D^{*0}\pi^+)} = 1.9 \pm 1.1 \pm 0.3 \tag{183}$$

$$\frac{\mathcal{B}(D_2^{*0} \to D^+\pi^-)}{\mathcal{B}(D_2^{*0} \to D^{*+}\pi^-)} = 2.3 \pm 0.6 \tag{184}$$

By isospin symmetry, these two numbers are supposed to be same. Thus, we take an average and get

$$\begin{aligned}
f_{D_2^*} \equiv \frac{\mathcal{B}(D_2^{*+} \to D^0\pi^+)}{\mathcal{B}(D_2^{*+} \to D^{*0}\pi^+)} &= \frac{\mathcal{B}(D_2^{*0} \to D^+\pi^-)}{\mathcal{B}(D_2^{*0} \to D^{*+}\pi^-)} \\
&= 2.1 \pm 0.644
\end{aligned} \tag{185}$$

Hence, branching fractions are

$$\mathcal{B}(D_2^{*+} \to D^0\pi^+) = \mathcal{B}(D_2^{*0} \to D^+\pi^-) = \frac{2f_{D_2^*}}{3(1+f_{D_2^*})} = 0.452 \pm 0.167 \tag{186}$$

$$\mathcal{B}(D_2^{*+} \to D^+\pi^0) = \mathcal{B}(D_2^{*0} \to D^0\pi^0) = \frac{f_{D_2^*}}{3(1+f_{D_2^*})} = 0.226 \pm 0.084 \tag{187}$$

$$\mathcal{B}(D_2^{*+} \to D^{*0}\pi^+) = \mathcal{B}(D_2^{*0} \to D^{*+}\pi^-) = \frac{2}{3(1+f_{D_2^*})} = 0.215 \pm 0.045 \tag{188}$$

$$\mathcal{B}(D_2^{*+} \to D^{*+}\pi^0) = \mathcal{B}(D_2^{*0} \to D^{*0}\pi^0) = \frac{1}{3(1+f_{D_2^*})} = 0.107 \pm 0.022 \tag{189}$$

$$\tag{190}$$

8.3 $D^{(*)}$ decay branching fractions

The values used in SP5/SP6 MC are summarized in Appendix D. We adopt the following new values in our fit. These are not applied in candidate level. Thus, these values goes into the coefficients in the fit. See details in section 4.

8.3.1 $\mathcal{B}(D^0 \to K^-\pi^+)$

PDG uses five measurements to make an average [13]. One of them is a CLEO-c result. Since we use updated CLEO-c result, we remove the CLEO-c result from

PDG average. The rests used in PDG are

$$\begin{aligned}
\mathcal{B}(D^0 \to K^-\pi^+) &= 0.0382 \pm 0.0007 \pm 0.0012 \\
\mathcal{B}(D^0 \to K^-\pi^+) &= 0.039 \pm 0.0009 \pm 0.0012 \\
\mathcal{B}(D^0 \to K^-\pi^+) &= 0.0341 \pm 0.0012 \pm 0.0028 \\
\mathcal{B}(D^0 \to K^-\pi^+) &= 0.0362 \pm 0.0034 \pm 0.0044
\end{aligned} \tag{191}$$

We take an average of these four measurements and get

$$\mathcal{B}(D^0 \to K^-\pi^+) = 0.03806 \pm 0.00095 \tag{192}$$

Babar measured [30]

$$\mathcal{B}(D^0 \to K^-\pi^+) = 0.04007 \pm 0.00037 \pm 0.00070 \tag{193}$$

CLEO-c also measured [31]

$$\mathcal{B}(D^0 \to K^-\pi^+) = 0.03891 \pm 0.00035 \pm 0.00059 \pm 0.00035 \tag{194}$$

We take an average of these three numbers. The error of the average of these is given by

$$\frac{1}{\sigma^2} = \frac{1}{0.00095^2} + \frac{1}{0.00037^2 + 0.00070^2} + \frac{1}{0.00035^2 + 0.00059^2 + 0.00035^2} \tag{195}$$

Thus

$$\sigma = 0.00048 \tag{196}$$

The average value is given by

$$\left(\frac{0.03806}{0.00095^2} + \frac{0.04007}{0.00037^2 + 0.00070^2} + \frac{0.03891}{0.00035^2 + 0.00059^2 + 0.00035^2}\right)\sigma^2 = 0.03912 \tag{197}$$

Thus, the averaged BF is

$$\mathcal{B}(D^0 \to K^-\pi^+) = 0.03912 \pm 0.00048 \tag{198}$$

8.3.2 $\mathcal{B}(D^+ \to K^-\pi^+\pi^+)$

PDG uses three measurements to make an average [13]. One of them is a CLEO-c result. Since we use updated CLEO-c result, we remove the CLEO-c result from PDG average. The rests used in PDG are

$$\begin{aligned}
\mathcal{B}(D^+ \to K^-\pi^+\pi^+) &= 0.093 \pm 0.006 \pm 0.008 \\
\mathcal{B}(D^+ \to K^-\pi^+\pi^+) &= 0.091 \pm 0.013 \pm 0.004
\end{aligned} \tag{199}$$

We take an average of these four measurements and get

$$\mathcal{B}(D^+ \to K^-\pi^+\pi^+) = 0.09230 \pm 0.00806 \tag{200}$$

CLEO-c measured [31]

$$\mathcal{B}(D^+ \to K^-\pi^+\pi^+) = 0.0915 \pm 0.0010 \pm 0.0016 \pm 0.0007 \tag{201}$$

We take an average of these numbers. The error of the average of these is given by

$$\frac{1}{\sigma^2} = \frac{1}{0.00806^2} + \frac{1}{0.0010^2 + 0.0016^2 + 0.0007^2} \tag{202}$$

Thus

$$\sigma = 0.0020 \tag{203}$$

The average value is given by

$$\left(\frac{0.09230}{0.00806^2} + \frac{0.0915}{0.0019^2 + 0.0016^2 + 0.0007^2}\right)\sigma^2 = 0.0915 \tag{204}$$

Thus, the averaged BF is

$$\mathcal{B}(D^+ \to K^-\pi^+\pi^+) = 0.0915 \pm 0.0020 \tag{205}$$

8.3.3 D^{*+} decay BF

From PDG [13]

$$\begin{aligned}\mathcal{B}(D^{*+} \to D^0\pi^+) &= 0.677 \pm 0.005\\ \mathcal{B}(D^{*+} \to D^+\pi^0) &= 0.307 \pm 0.005\\ \mathcal{B}(D^{*+} \to D^+\gamma) &= 0.016 \pm 0.004\end{aligned} \tag{206}$$

We use

$$\begin{aligned}&\mathcal{B}(D^{*+} \to D^0\pi^+) = 0.677 \pm 0.005\\ &\mathcal{B}(D^{*+} \to D^+\pi^0) + \mathcal{B}(D^{*+} \to D^+\gamma) = 1 - \mathcal{B}(D^{*+} \to D^0\pi^+)\end{aligned} \tag{207}$$

8.4 $\cos\theta_{B-Dl}$ beam energy correction

As can be seen in Figure 24, $\cos\theta_{B-Dl}$ peak of OnPeak - OffPeak data is narrower than MC. This is because average beam energy of data is higher than MC due to the beam energy fluctuation of data. The average beam energy of Run2 is 10.5802 GeV and the SP5/SP6 MC beam energy is

$$\sqrt{s}^{\text{Nom}} = 10.5782\text{GeV} \tag{208}$$

Thus, the difference is small, but still affect on $\cos\theta_{B-Dl}$. The $\cos\theta_{B-Dl}$ is given by (see Appendix F)

$$\cos\Theta_{B-Dl} = \frac{2E_B E_{Dl} - m_B^2 - m_{Dl}^2}{2|\vec{p}_B||\vec{p}_{Dl}|} \tag{209}$$

where E_B and $p_B = |\vec{p}_B|$ are calculated from beam energy :

$$\begin{aligned} E_B &= E_{beam} \equiv \sqrt{s}/2 \\ p_B &= \sqrt{E_{beam}^2 - m_B^2} \end{aligned} \tag{210}$$

A small change in beam energy won't affect the numerator of $\cos\theta_{B-Dl}$ but will affect p_B because

$$\frac{\Delta(p_B)}{p_B} = \left(\frac{E_{beam}}{p_B}\right)^2 \left(\frac{\Delta(E_{beam})}{E_{beam}}\right) \tag{211}$$

The bem energy is given in EventInfo list; thus, we apply event-by-event weight to OnPeak data to correct the effect of beam energy fluctuation on $\cos\theta_{B-Dl}$. We take $\sqrt{s} = 10.5802$GeV as an example to show how we calculate weights. Using $m_B = 5.279$ GeV,

$$p_B = \sqrt{\left(\frac{\sqrt{s}}{2}\right)^2 - m_B^2} = \sqrt{\left(\frac{10.5802}{2}\right)^2 - 5.279^2} = 0.342516 \text{ GeV} \tag{212}$$

and

$$p_B^{\text{Nom}} = \sqrt{\left(\frac{\sqrt{s}^{\text{Nom}}}{2}\right)^2 - m_B^2} = \sqrt{\left(\frac{10.5782}{2}\right)^2 - 5.279^2} = 0.326701 \text{ GeV} \tag{213}$$

Thus, the weight is

$$w_{cosBY} = \frac{p_B}{p_B^{\text{Nom}}} = 1.0484 \tag{214}$$

This is a 4.8 % correction and is not small.

8.5 Effect of MC branching fraction re-weighting

Figure 49 - 51 show the lepton momentum, D momentum and $\cos\theta_{B-Dl}$ after branching fraction re-weighting. These are the projections of 3D histograms. If you compare these with figure 22 - 24, you can see improvements of data-MC agreement.
Note that, $\cos\theta_{B-Dl}$ correction is not yet included in these plots.

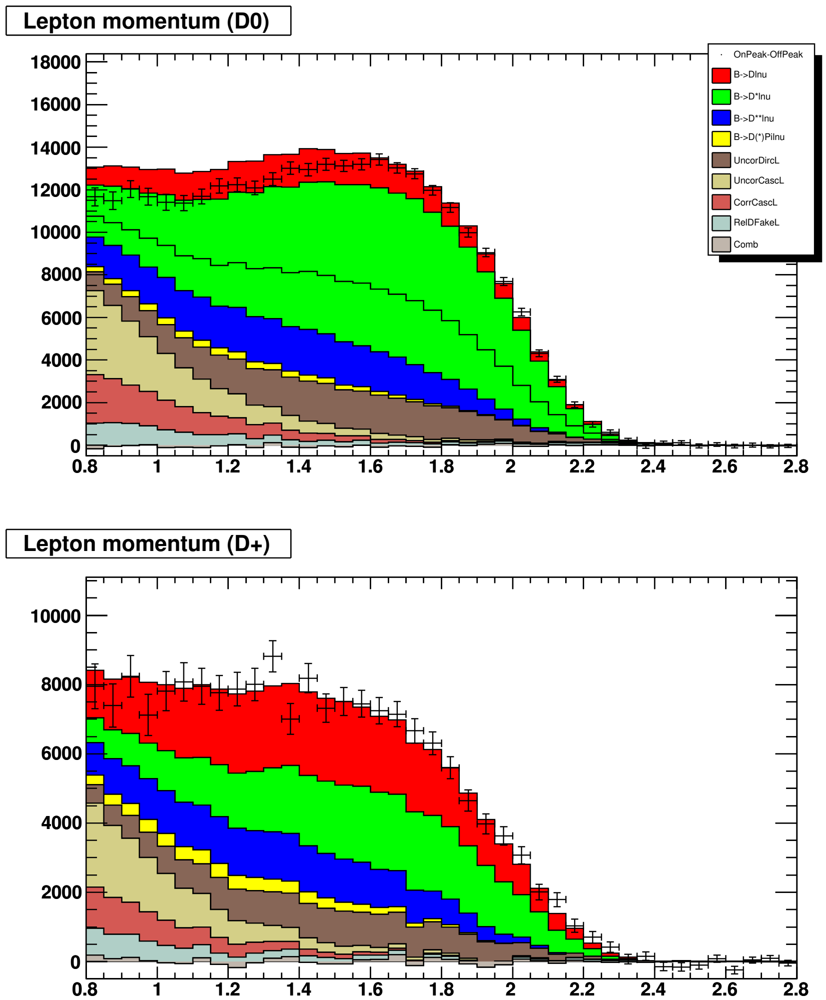

Figure 49: **(Run2 only)** [p_ℓ **after MC re-weighting**] Lepton momentum plot after branching fraction re-weighting and D mass sideband subtraction. The top is D^0 and the bottom is D^+. Black is OnPeak - OffPeak data. Red is $B \to D\ell\nu$, green is $B \to D^*\ell\nu$, blue is $B \to D^{**}\ell\nu$, yellow is non-resonant $B \to D^{(*)}\pi\ell\nu$, and the rest is background. Dark brown is UncorrDL, light brown is UncorrCL, dark red is CascL, blue gray is FakeL, and light gray is Comb. Comb is almost disappeared after D mass sideband subtraction.

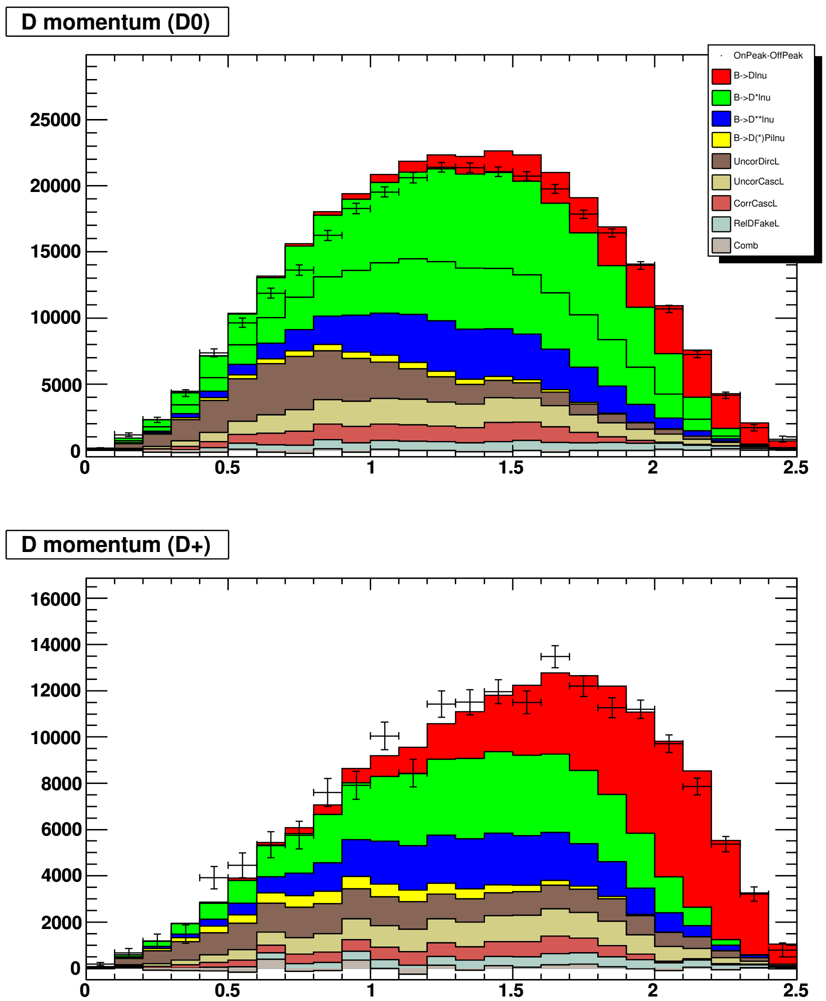

Figure 50: **(Run2 only)** [p_D **after MC re-weighting**] D momentum plot after branching fraction re-weighting and D mass sideband subtraction. The top is D^0 and the bottom is D^+. Black is OnPeak - OffPeak data. Red is $B \to D\ell\nu$, green is $B \to D^*\ell\nu$, blue is $B \to D^{**}\ell\nu$, yellow is non-resonant $B \to D^{(*)}\pi\ell\nu$, and the rest is background. Dark brown is UncorrDL, light brown is UncorrCL, dark red is CascL, blue gray is FakeL, and light gray is Comb. Comb is almost disappeared after D mass sideband subtraction.

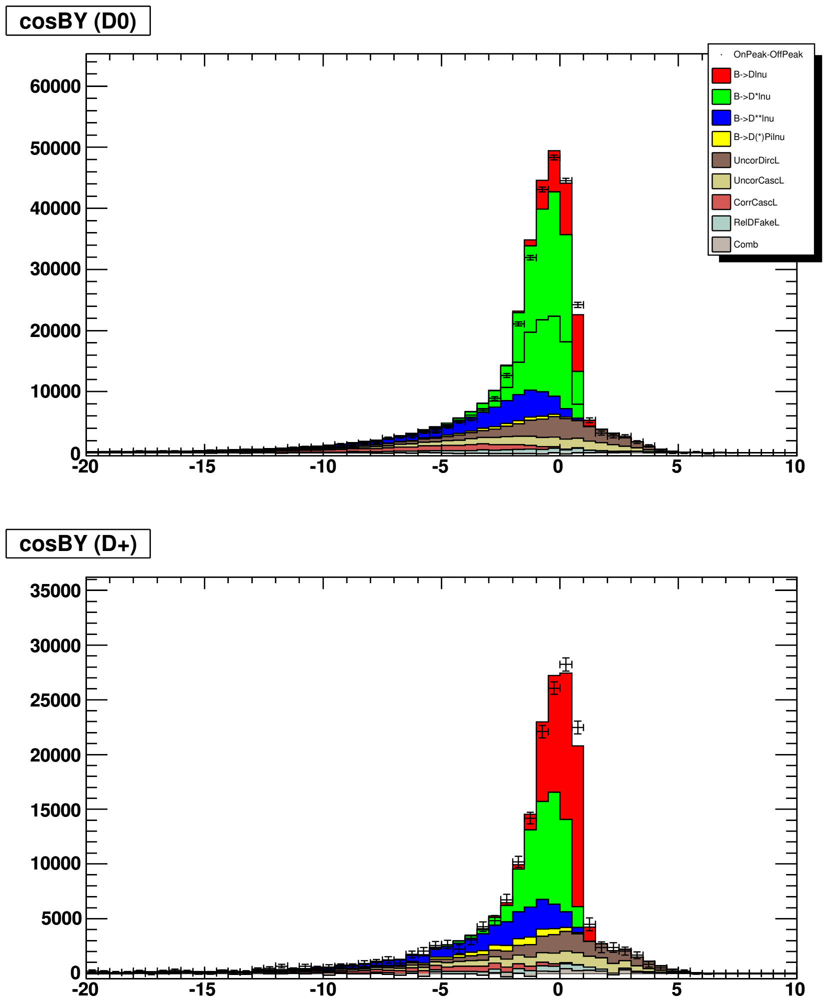

Figure 51: **(Run2 only)** [$\cos\theta_{B-Dl}$ **after MC re-weighting**] $\cos\theta_{B-Dl}$ plot after branching fraction re-weighting and D mass sideband subtraction. The top is D^0 and the bottom is D^+. Black is OnPeak - OffPeak data. Red is $B \to D\ell\nu$, green is $B \to D^*\ell\nu$, blue is $B \to D^{**}\ell\nu$, yellow is non-resonant $B \to D^{(*)}\pi\ell\nu$, and the rest is background. Dark brown is UncorrDL, light brown is UncorrCL, dark red is CascL, blue gray is FakeL, and light gray is Comb. Comb is almost disappeared after D mass sideband subtraction.

9 Form Factor (FF) Re-weighting (W_{jk}^{MC})

We use SP5/SP6 MC for our analysis. However, there have been some improvements of form factors (FF) since SP5/SP6 MC were generated. To take those improvements into account, form factor re-weighting is necessary. See also Appendix H for details of form factors.

9.1 Normalization

When we change parameters of form factors, we need to make sure that total rates stay same. Thus, we need a normalization factor, R_N, such that

$$\Gamma = \int \frac{d\Gamma(\text{old FF})}{dw} dw = R_N \int \frac{d\Gamma(\text{new FF})}{dw} dw \tag{215}$$

In actual integration the Gaussian quadrature method is used.

9.2 $B \to D\ell\nu$

In this mode, ISGW2 model [32][33] is used in MC. ISGW2 is a type of constituent quark models. We need to change it to HQET (Heavy Quark Effective Theory) model [34][35]. The ISGW2 model gives form factors $f_+(q^2)$ and $f_-(q^2)$, and the HQET model gives $h_+(w)$ and $h_-(w)$, where w is the velocity transfer (see Appendix G). These form factors are related by

$$h_+ = \frac{1}{R}\left(f_+ + \frac{1-r}{1+r} f_-\right) \tag{216}$$

$$h_- = \frac{1}{R}\left(\frac{1-r}{1+r} f_+ + f_-\right) \tag{217}$$

where

$$R = \frac{2\sqrt{m_B m_D}}{m_B + m_D} \tag{218}$$

and

$$r = \frac{m_D}{m_B} \tag{219}$$

q^2 is related to w by

$$w = \frac{m_B^2 + m_D^2 - q^2}{2 m_B m_D} \quad \text{or} \quad q^2 = m_B^2 + m_D^2 - 2 m_B m_D w \tag{220}$$

The differential decay rate is given by

$$\frac{d\Gamma(B \to D\ell\nu)}{dw} = \frac{G_F^2 |V_{cb}|^2 m_B^5}{48\pi^3} r^3 (w^2-1)^{3/2}\, \mathcal{J}_D(w) \tag{221}$$

where

$$\mathcal{J}_D(w) = [(1+r)h_+(w) - (1-r)h_-(w)]^2 \tag{222}$$

In the ISGW2 model,

$$\begin{aligned}
&(1+r)h_+ - (1-r)h_- \\
&\quad = (1+r)\frac{1}{R}\left(f_+ + \frac{1-r}{1+r}f_-\right) - (1-r)\frac{1}{R}\left(\frac{1-r}{1+r}f_+ + f_-\right) \\
&\quad = \frac{1+r}{R}\frac{(1+r)^2-(1-r)^2}{(1+r)^2}f_+ = \frac{1+r}{R}\frac{4r}{(1+r)^2}f_+ = \frac{1+r}{R}R^2 f_+ \\
&\quad = (1+r)Rf_+
\end{aligned} \tag{223}$$

Thus

$$\mathcal{J}_D^{ISGW2} = [(1+r)Rf_+]^2 \tag{224}$$

In HQET model, we can set

$$\begin{aligned}
h_+(w) &= h_+(1)[1-\rho_D^2(w-1)] \\
h_-(w) &= 0
\end{aligned} \tag{225}$$

where ρ_D^2 is the slope. $h_+(1)$ can be given by a Lattice QCD calculation [36]

$$h_+(1) = 1.074 \pm 0.018 \pm 0.016 = 1.074 \pm 0.024 \tag{226}$$

Thus

$$\mathcal{J}_D^{HQET} = (1+r)^2[h_+(1)]^2[1-\rho_D^2(w-1)]^2 \tag{227}$$

By using Equation (220), we can express f_+ as a function of w. Then, the weight is given by

$$W_{jk}^{MC}(w_k) = \frac{\mathcal{J}_D^{HQET}}{\mathcal{J}_D^{ISGW2}}R_N = \frac{[h_+(1)]^2[1-\rho_D^2(w-1)]^2}{[Rf_+]^2}R_N \tag{228}$$

where, the normalization factor, R_N, is given by

$$\begin{aligned}
&\int_0^{1.590}(w^2-1)^{3/2}\,[Rf_+]^2\,dw \\
&\quad = R_N\int_1^{1.590}(w^2-1)^{3/2}[h_+(1)]^2[1-\rho_D^2(w-1)]^2 dw
\end{aligned} \tag{229}$$

Or, we can use the CLN parametrization proposed by Caprini, Lellouch and Neubert [37]

$$h_+(w) = h_+(1)[1-8\rho_D^2 z + (51\rho_D^2-10)z^2 - (252\rho_D^2-84)z^3] \tag{230}$$

where

$$z = \frac{\sqrt{w+1}-\sqrt{2}}{\sqrt{w+1}+\sqrt{2}} \tag{231}$$

In this case, the weight is given by

$$W_{jk}^{MC}(w_k) = \frac{[h_+(1)]^2[1-8\rho_D^2 z + (51\rho_D^2-10)z^2 - (252\rho_D^2-84)z^3]^2}{[Rf_+]^2}R_N \tag{232}$$

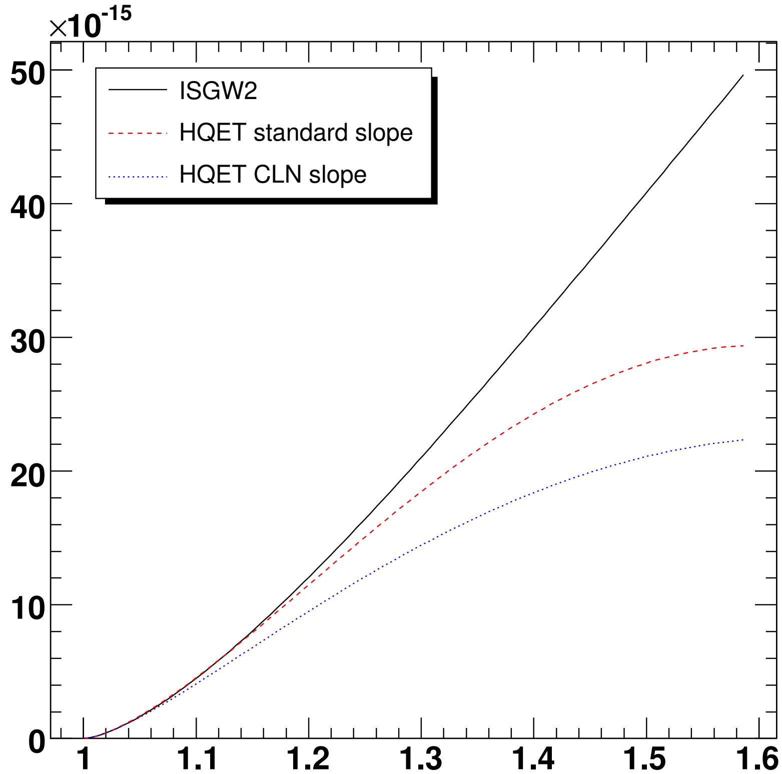

Figure 52: [$B \to D\ell\nu$ **FF**] The differential decay rate $d\Gamma(B \to D\ell\nu)/dw$ as a function of w. This is in case that the standard slope is $\rho_D^2 = 0.8$ and the CLN slope is $\rho_D^2 = 1.4$

where, the normalization factor, R_N, is given by

$$\begin{aligned}&\int_0^{1.590} dw\ \ (w^2-1)^{3/2}\,[Rf_+]^2 \\ &= R_N \int_1^{1.590} dw\ \ (w^2-1)^{3/2}[h_+(1)]^2 \times \\ &\qquad \left[1 - 8\rho_D^2 z + (51\rho_D^2 - 10)z^2 - (252\rho_D^2 - 84)z^3\right]^2 \end{aligned} \tag{233}$$

Figure 52 shows the differential decay rate $d\Gamma(B \to D\ell\nu)/dw$ as a function of w. The black line shows the ISGW2 model, the red dashed line shows the HQET model with the standard slope in case of $\rho_D^2 = 0.8$, and the blue dotted line shows the HQET model with the CLN slope in case of $\rho_D^2 = 1.4$. Figure 53 shows the distribution of weight W_{jk}^{MC} in the case of the CLN slope of $\rho_D^2 = 1.4$, corresponding to the normalization factor $R_N = 1.686$. BpBm MC is used to create the plot. The change in the spectrum of lepton momentum, D momentum and $\cos\theta_{B-Dl}$ is given in Figure 54 - 56.

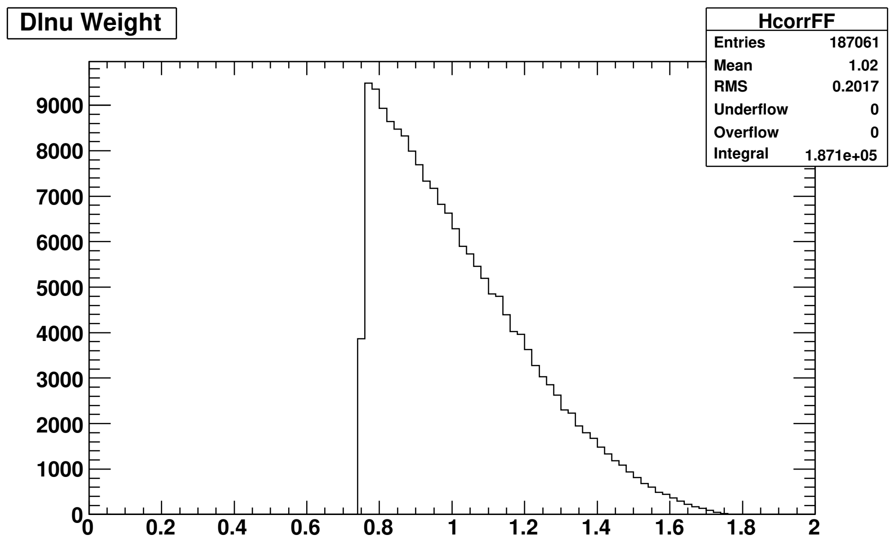

Figure 53: [$B \to D\ell\nu$ **FF weight**] The distribution of weight W_{jk}^{MC} for $B \to D\ell\nu$ decays This is made from BpBm MC.

9.3 $B \to D^*\ell\nu$

We need three kinematic variables to describe this decay. We usually chose $\cos\theta_\ell$, $\cos\theta_V$ and χ as shown in the figure 57. The definition of these variables are

- $\cos\theta_\ell$: the cosine of the angle between the directions of "the ℓ in the W rest frame" and "the W in the B rest frame".
- $\cos\theta_V$: the cosine of the angle between the directions of "the D in the D^* rest frame" and "the D^* in the B rest frame".
- χ : the azimuthal angle between the planes formed by "W-ℓ system' ' and "$D^* - D$ system".

HQET model is used and the differential decay rate is given by [34][35]

$$\begin{aligned}\frac{d\Gamma(B\to D^*\ell\nu)}{dwd\cos\theta_V d\cos\theta_\ell d\chi} \quad = \quad & \frac{3G_F^2}{4(4\pi)^4}|V_{cb}|^2 m_B m_{D^*}^2\sqrt{w^2-1}(1-2wr+r^2)\times \\ & [(1-\cos\theta_\ell)^2\sin^2\theta_V|H_+(w)|^2 \\ & +(1+\cos\theta_\ell)^2\sin^2\theta_V|H_-(w)|^2 \\ & +4\sin^2\theta_\ell\cos^2\theta_V|H_0(w)|^2 \\ & -4\sin\theta_\ell(1-\cos\theta_\ell)\sin\theta_V\cos\theta_V\cos\chi H_+(w)H_0(w) \\ & +4\sin\theta_\ell(1+\cos\theta_\ell)\sin\theta_V\cos\theta_V\cos\chi H_-(w)H_0(w) \\ & -2\sin^2\theta_\ell\sin^2\theta_V\cos 2\chi H_+(w)H_-(w)]\end{aligned} \tag{234}$$

where r is the mass ratio

$$r = \frac{m_{D^*}}{m_B} \tag{235}$$

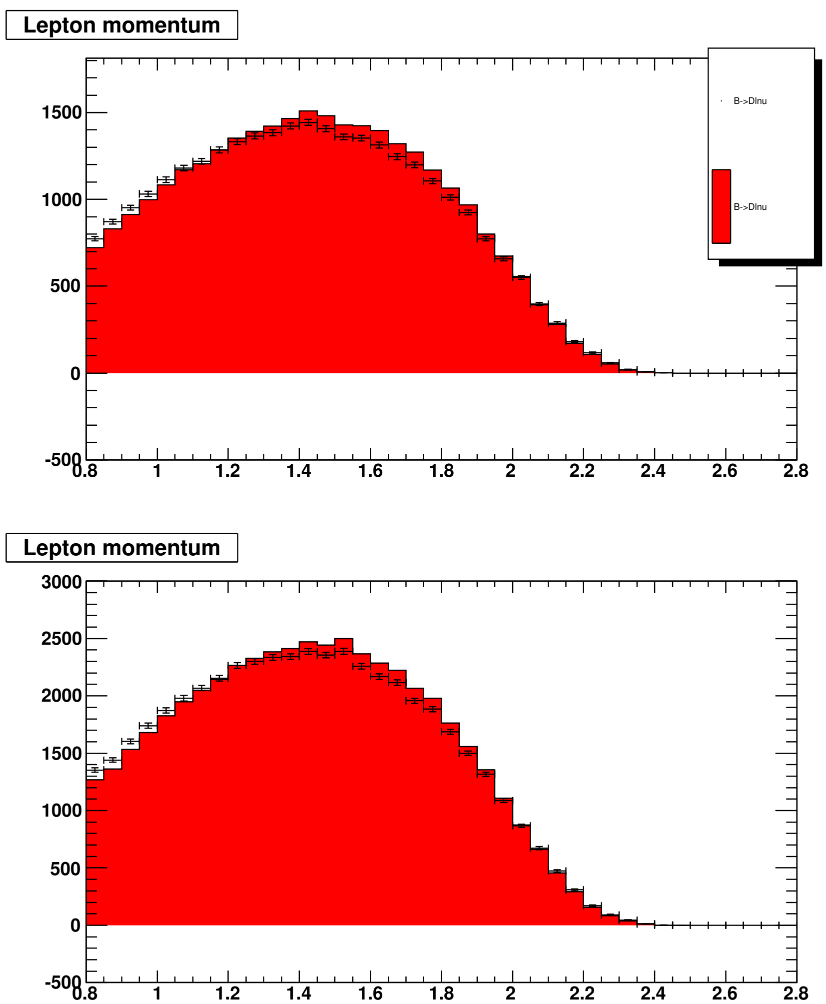

Figure 54: [p_ℓ **after** $B \to D\ell\nu$ **re-weighting**] Lepton momentum spectrum of $B^+ \to \bar{D}^0\ell\nu$ decays (top) and $B^0 \to D^-\ell\nu$ decays (bottom). Black line is ISGW2 model and red histogram is HQET model with CLN slope $\rho_D^2 = 1.4$

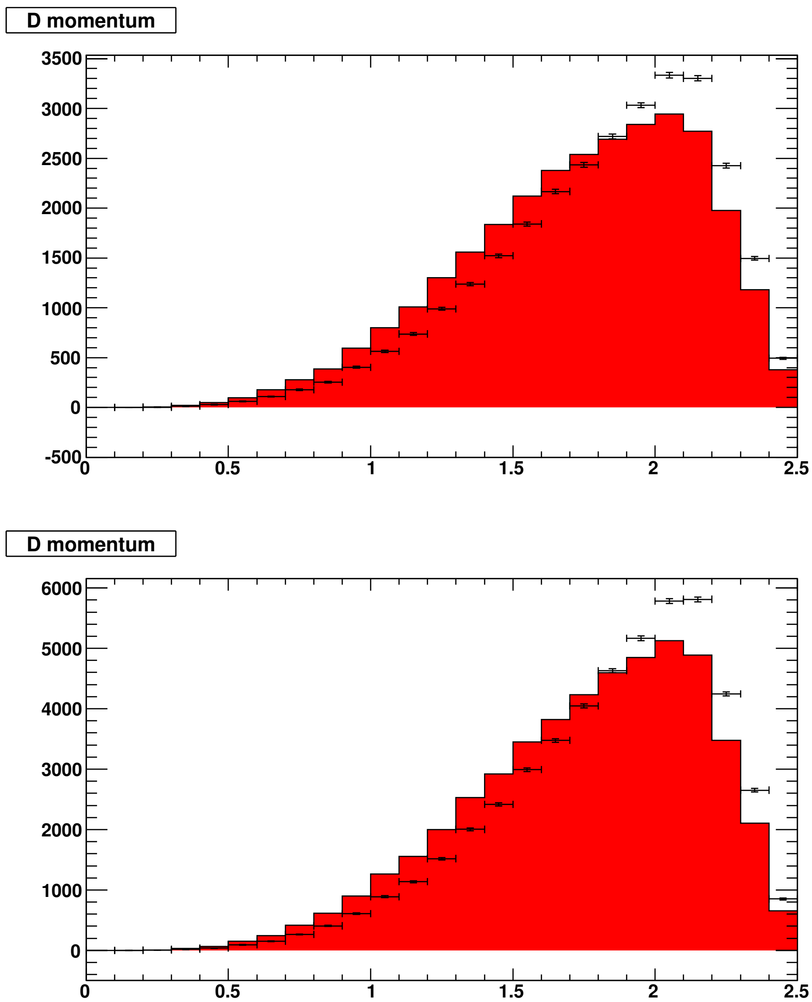

Figure 55: [p_D **after** $B \to D\ell\nu$ **re-weighting**] D momentum spectrum of $B^+ \to \bar{D}^0\ell\nu$ decays (top) and $B^0 \to D^-\ell\nu$ decays (bottom). Black line is ISGW2 model and red histogram is HQET model with CLN slope $\rho_D^2 = 1.4$

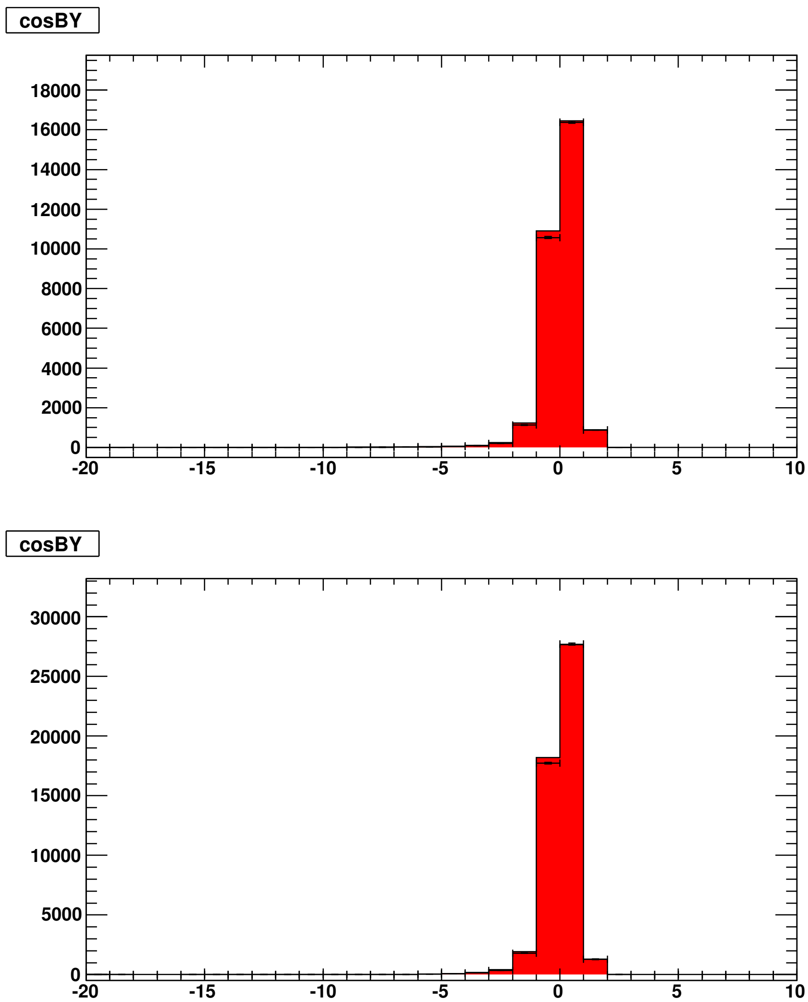

Figure 56: [$\cos\theta_{B-Dl}$ **after** $B \to D\ell\nu$ **re-weighting**] $\cos\theta_{B-Dl}$ of $B^+ \to \bar{D}^0\ell\nu$ decays (top) and $B^0 \to D^-\ell\nu$ decays (bottom). Black line is ISGW2 model and red histogram is HQET model with CLN slope $\rho_D^2 = 1.4$

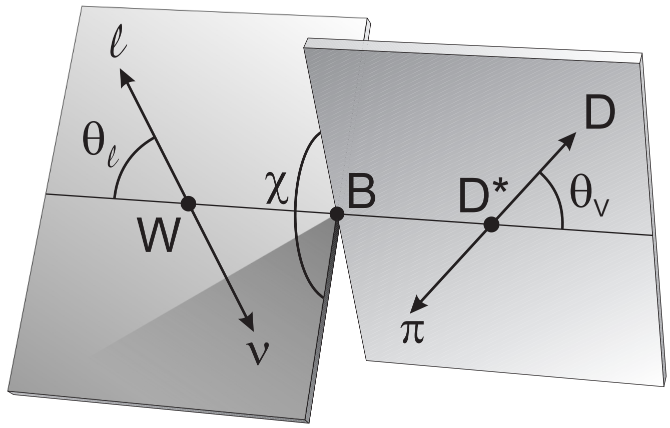

Figure 57: [$B \to D^*\ell\nu$ **decay geometry**] Geometry of $B \to D^*\ell\nu$ decays.

$H_i(w)$ are

$$H_i = -m_B \frac{R^*(1-r^2)(w+1)}{2\sqrt{1-2wr+r^2}} h_{A_1}(w)\widetilde{H}_i(w) \tag{236}$$

where R^* is

$$R^* = \frac{2\sqrt{m_B m_{D^*}}}{m_B + m_{D^*}} \tag{237}$$

and $\widetilde{H}_i(w)$ are

$$\begin{aligned} \widetilde{H}_\pm(w) &= \tfrac{\sqrt{1-2wr+r^2}}{1-r}\left(1 \mp \sqrt{\tfrac{w-1}{w+1}} R_1(w)\right) \\ \widetilde{H}_0(w) &= 1 + \tfrac{w-1}{1-r}\left(1 - R_2(w)\right) \end{aligned} \tag{238}$$

were R_1 and R_2 are the form factor ratios. To make the notation simple, we define

$$\begin{aligned} c_L &\equiv \cos\theta_\ell \\ c_V &\equiv \cos\theta_V \\ c_\chi &\equiv \cos\chi \\ \tilde{h}_\pm(w) &\equiv (1-r)\widetilde{H}_\pm(w) = \sqrt{1-2wr+r^2}\left(1 \mp \sqrt{\tfrac{w-1}{w+1}} R_1(w)\right) \\ \tilde{h}_0(w) &\equiv (1-r)\widetilde{H}_0(w) = (1-r) + (w-1)\left(1 - R_2(w)\right) = (w-r) - (w-1)R_2(w) \end{aligned} \tag{239}$$

then (see Appendix H.4)

$$\frac{d\Gamma(B \to D^*\ell\nu)}{dw\,dc_V\,dc_L\,d\chi} = \frac{G_F^2|V_{cb}|^2 m_B^5}{48\pi^3} r^3 (w^2-1)^{1/2} \times \frac{9}{64\pi}(w+1)^2\ \mathcal{J}_{FF} \tag{240}$$

where

$$\begin{aligned}
\mathcal{J}_{FF}(R_1, R_2, \rho^2) \;=\;& [h_{A_1}(w)]^2 \times \\
& [(1-c_L)^2(1-c_V^2)\tilde{h}_+^2 + (1+c_L)^2(1-c_V^2)\tilde{h}_-^2 \\
& +4(1-c_L^2)c_V^2\tilde{h}_0^2 - 2(1-c_L^2)(1-c_V^2)(2c_\chi^2-1)\tilde{h}_+\tilde{h}_- \\
& -4\sqrt{1-c_L^2}(1-c_L)\sqrt{1-c_V^2}c_V c_\chi \tilde{h}_+\tilde{h}_0 \\
& +4\sqrt{1-c_L^2}(1+c_L)\sqrt{1-c_V^2}c_V c_\chi \tilde{h}_-\tilde{h}_0]
\end{aligned} \tag{241}$$

In SP5/SP6 MC, the values of parameters are

$$\begin{aligned}
R_1^{MC} &= 1.18 \\
R_2^{MC} &= 0.72 \\
(\rho^2)^{MC} &= 0.92
\end{aligned} \tag{242}$$

with

$$\begin{aligned}
R_1(w) &= R_1^{MC} \\
R_2(w) &= R_2^{MC} \\
h_{A_1}(w) &= h_{A_1}(1)\left[1-(\rho^2)^{MC}(w-1)\right]
\end{aligned} \tag{243}$$

The values from a recent Babar measurement [38] are

$$\begin{aligned}
R_1 &= 1.396 \pm 0.060 \pm 0.035 \pm 0.027 = 1.396 \pm 0.0745 \\
R_2 &= 0.885 \pm 0.040 \pm 0.022 \pm 0.013 = 0.885 \pm 0.0474 \\
\rho^2 &= 1.145 \pm 0.059 \pm 0.030 \pm 0.035 = 1.145 \pm 0.075
\end{aligned} \tag{244}$$

where the CLN parametrization [37] is used only for the slope

$$\begin{aligned}
R_1(w) &= R_1 \\
R_2(w) &= R_2 \\
h_{A_1}(w) &= h_{A_1}(1)\left[1-8\rho^2 z + (53\rho^2-15)z^2 - (231\rho^2-91)z^3\right]
\end{aligned} \tag{245}$$

We also use CLN parametrization [37] in our fit including w dependence of $R_1(w)$ and $R_2(w)$

$$\begin{aligned}
R_1(w) &= R_1 - 0.12(w-1) + 0.05(w-1)^2 \\
R_2(w) &= R_2 + 0.11(w-1) - 0.06(w-1)^2 \\
h_{A_1}(w) &= h_{A_1}(1)\left[1-8\rho^2 z + (53\rho^2-15)z^2 - (231\rho^2-91)z^3\right]
\end{aligned} \tag{246}$$

where

$$z = \frac{\sqrt{w+1}-\sqrt{2}}{\sqrt{w+1}+\sqrt{2}} \tag{247}$$

The weight is given by

$$W_{jk}^{MC}(w_k) = \frac{\mathcal{J}_{FF}(R_1, R_2, \rho^2)}{\mathcal{J}_{FF}(R_1^0, R_2^0, \rho_0^2)} \tag{248}$$

To calculate the normalization factor R_N, we need to integrate over c_V, c_L and χ. Thus, it is easier to use $d\Gamma/dw$ (see Appendix H.4)

$$\frac{d\Gamma(B \to D^*\ell\nu)}{dw} = \frac{G_F^2|V_{cb}|^2 m_B^5}{48\pi^3} r^3 (w^2-1)^{1/2} \mathcal{J}_{WD}(R_1, R_2, \rho^2) \tag{249}$$

where

$$\mathcal{J}_{WD}(R_1, R_2, \rho^2) = (w+1)^2 [h_{A_1}]^2 (\tilde{h}_+^2 + \tilde{h}_-^2 + \tilde{h}_0^2) \tag{250}$$

Thus, the normalization factor is given by

$$\begin{aligned} &\int_1^{1.504} dw \;\; (w^2-1)^{1/2} \mathcal{J}_{WD}(R_1^0, R_2^0, \rho_0^2) \\ &= R_N \int_1^{1.504} dw \;\; (w^2-1)^{1/2} \mathcal{J}_{WD}(R_1, R_2, \rho^2) \end{aligned} \tag{251}$$

Figure 58 shows the differential decay rate $d\Gamma(B \to D^*\ell\nu)/dw$ as a function of w. The red dashed line shows the HQET model with the old parameters of R_1, R_2 and ρ^2, and the blue dotted line shows the HQET model with new parameters. Figure 59 shows the distribution of weight W_{jk}^{MC} for BpBm MC corresponding to the normalization factor $R_N = 1.033$. The change in the spectrum of lepton momentum, D momentum and $\cos\theta_{B-Dl}$ is given in Figure 60 - 62.

9.4 $B \to D^{**}\ell\nu$

In SP5/SP6 MC, ISGW2 model is used. We would like to use HQET based LLSW model [41][42]. Details of LLSW model is given in Appendix H. We use the Approximation B1 to calculate the form factors and the Approximation B2 to estimate systematic uncertainties. The differential decay rates are given as functions of w and θ. This θ is the angle between the charged lepton and the charmed meson in the rest frame of the virtual W boson. Thus $\theta = \pi - \theta_\ell$, e.g.,

$$\cos\theta = \cos(\pi - \theta_\ell) = -\cos\theta_\ell \tag{252}$$

9.4.1 $B \to D_0^*\ell\nu$

The ISGW2 form factors $u_+(q^2)$ and $u_-(q^2)$ are related to the LLSW form factors $g_+(w)$ and $g_-(w)$

$$g_+ = \frac{1}{R}\left(u_+ + \frac{1-r}{1+r}u_-\right), \;\; g_- = \frac{1}{R}\left(\frac{1-r}{1+r}u_+ + u_-\right) \tag{253}$$

where

$$R = \frac{2\sqrt{m_B m_{D_0^*}}}{m_B + m_{D_0^*}}, \;\; r = \frac{m_{D_0^*}}{m_B} \tag{254}$$

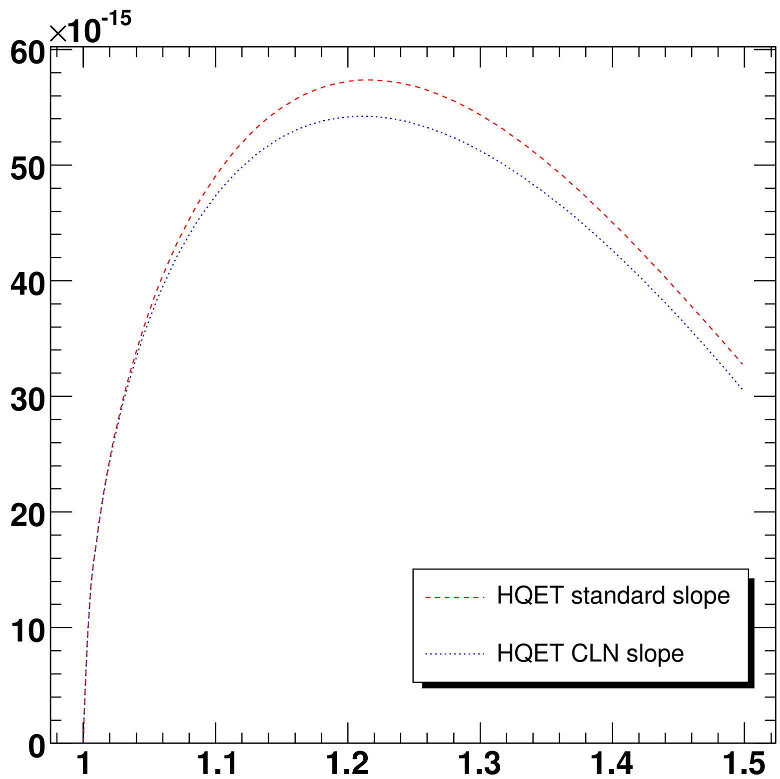

Figure 58: [$B \to D^* \ell \nu$ **FF**] The differential decay rate $d\Gamma(B \to D^* \ell \nu)/dw$ as a function of w.

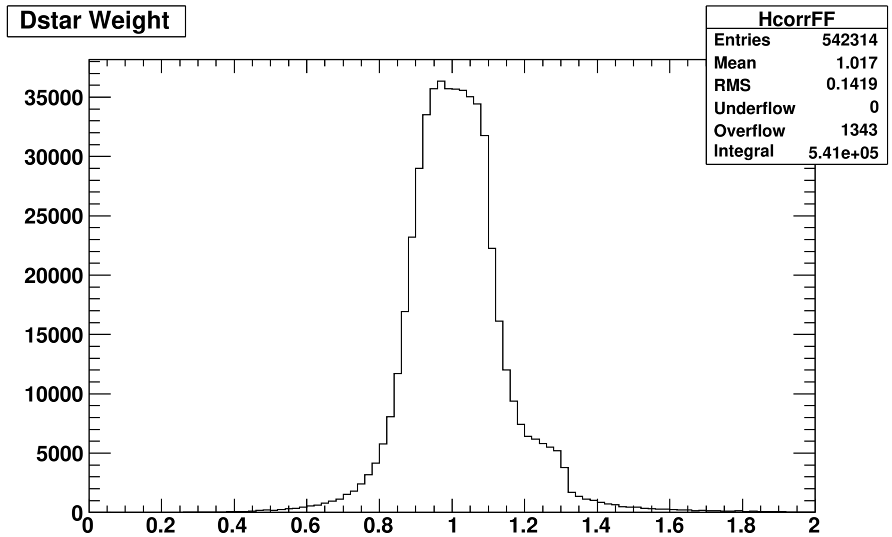

Figure 59: [$B \to D^*\ell\nu$ **FF weight**] The distribution of weight W^{MC}_{jk} for $B \to D^*\ell\nu$ decays This is made from BpBm MC.

The differential decay rate is given by

$$\frac{d^2\Gamma_{D_0^*}}{dw\,d\cos\theta} = \frac{G_F^2|V_{cb}|^2 m_B^5}{64\pi^3} r^3(w^2-1)^{3/2}\,\mathcal{I}_{D_0^*}(w,\theta) \tag{255}$$

where

$$\mathcal{I}_{D_0^*}(w,\theta) = (1-\cos^2\theta)[(1+r)g_+ - (1-r)g_-]^2 \tag{256}$$

The weight is given by the ratio of $\mathcal{I}_{D_0^*}$ part.

$$W^{MC}_{jk}(w_k) = \frac{\mathcal{I}^{LLSW}_{D_0^*}}{\mathcal{I}^{ISGW2}_{D_0^*}} R_N \tag{257}$$

Integrated by θ, the differential decay rate is

$$\frac{d\Gamma(B\to D_0^*\ell\nu)}{dw} = \frac{G_F^2|V_{cb}|^2 m_B^5}{48\pi^3} r^3(w^2-1)^{3/2}\,\mathcal{J}_{D_0^*}(w) \tag{258}$$

where

$$\mathcal{J}_{D_0^*}(w) = [(1+r)g_+ - (1-r)g_-]^2 \tag{259}$$

Thus, the normalization factor, R_N, is given by

$$\int_0^{1.327}(w^2-1)^{3/2}\mathcal{J}^{ISGW2}_{D_0^*}dw = R_N\int_1^{1.327}(w^2-1)^{3/2}\mathcal{J}^{LLSW}_{D_0^*}dw \tag{260}$$

Figure 63 shows the differential decay rate $d\Gamma(B\to D_0^*\ell\nu)/dw$ as a function of w. The black line shows the ISGW2 model, the other lines show the LLSW model; the green

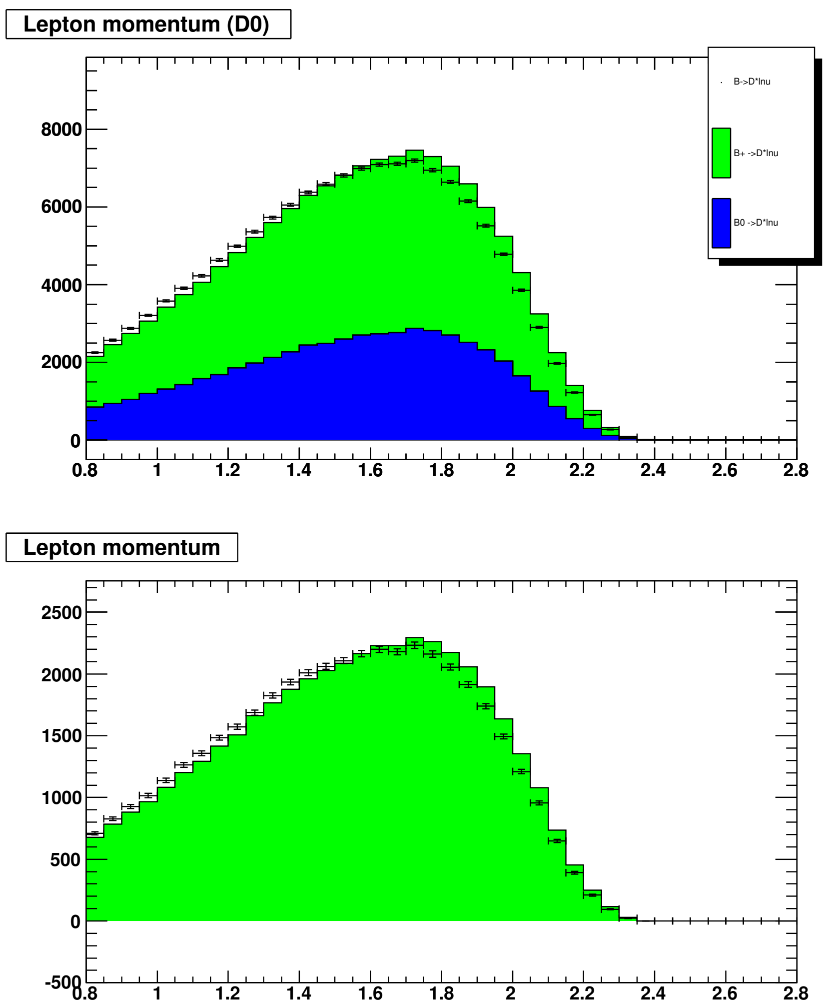

Figure 60: [p_ℓ **after** $B \to D^*\ell\nu$ **re-weighting**] Lepton momentum spectrum of $B \to D^*\ell\nu$ decays. The top is D^0 and the bottom is D^+. Black line is with old FF parameters and histogram is with new FF parameters. Green is the contribution from B^+ and blue is from B^0.

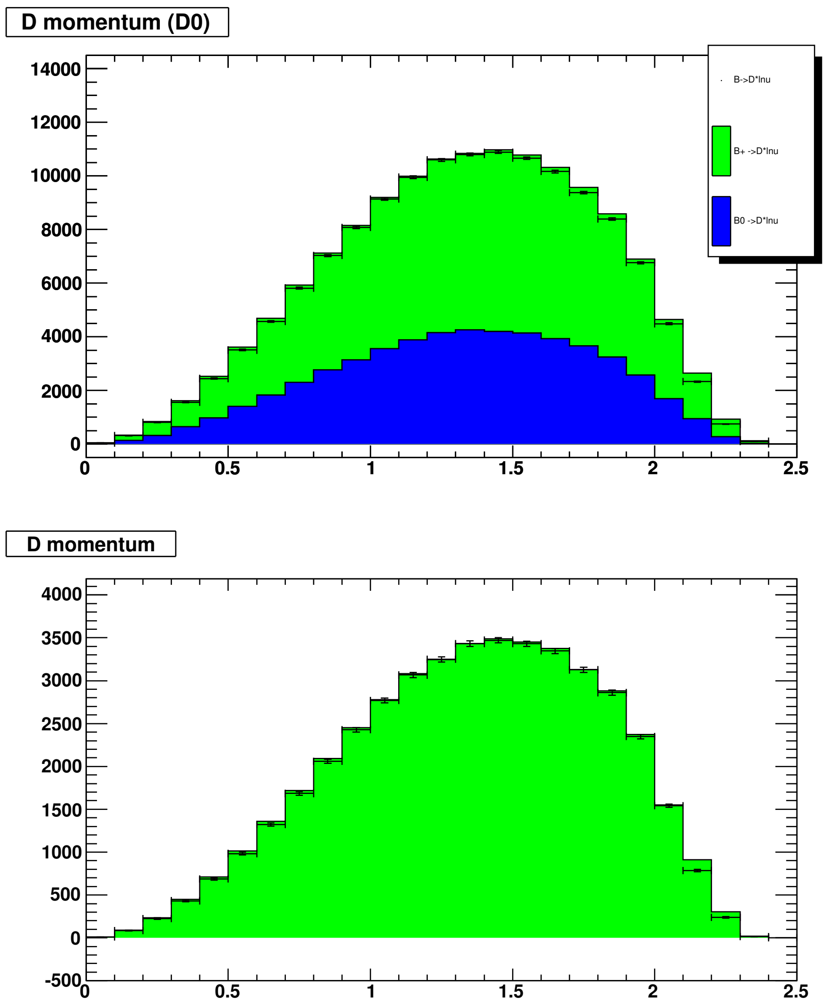

Figure 61: [p_D **after** $B \to D^*\ell\nu$ **re-weighting**] D momentum spectrum of $B \to D^*\ell\nu$ decays. The top is D^0 and the bottom is D^+. Black line is with old FF parameters and histogram is with new FF parameters. Green is the contribution from B^+ and blue is from B^0.

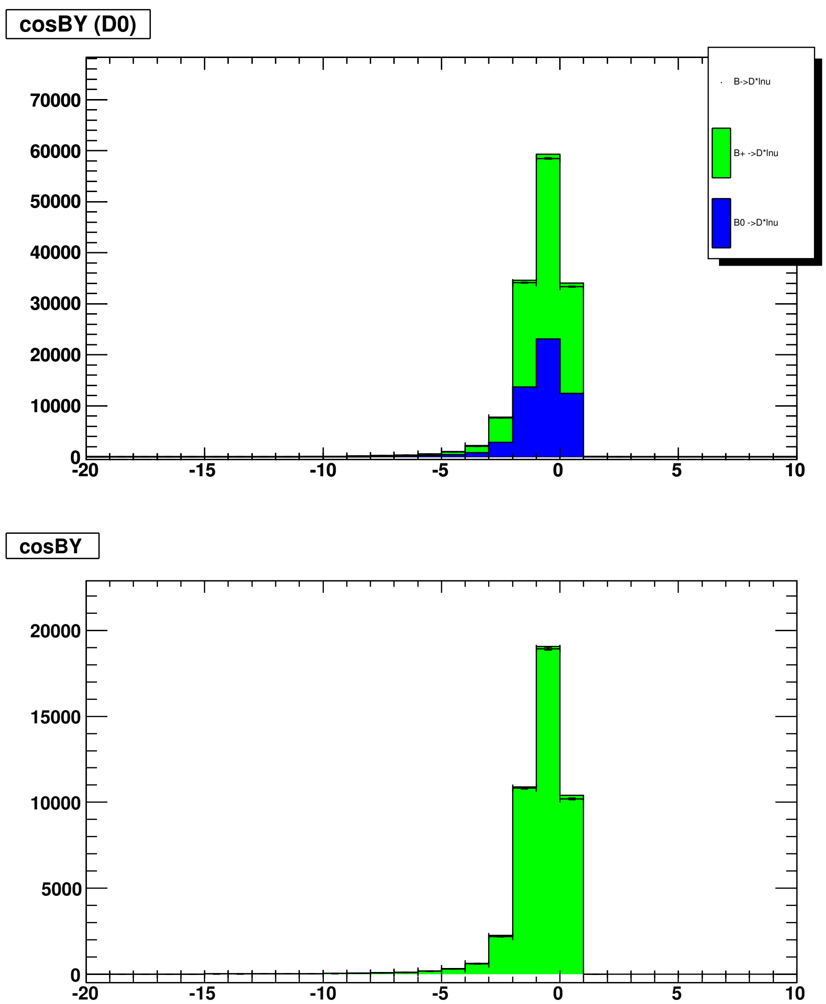

Figure 62: [$\cos\theta_{B-Dl}$ **after** $B \to D^*\ell\nu$ **re-weighting**] $\cos\theta_{B-Dl}$ of $B \to D^*\ell\nu$ decays. The top is D^0 and the bottom is D^+. Black line is with old FF parameters and histogram is with new FF parameters. Green is the contribution from B^+ and blue is from B^0.

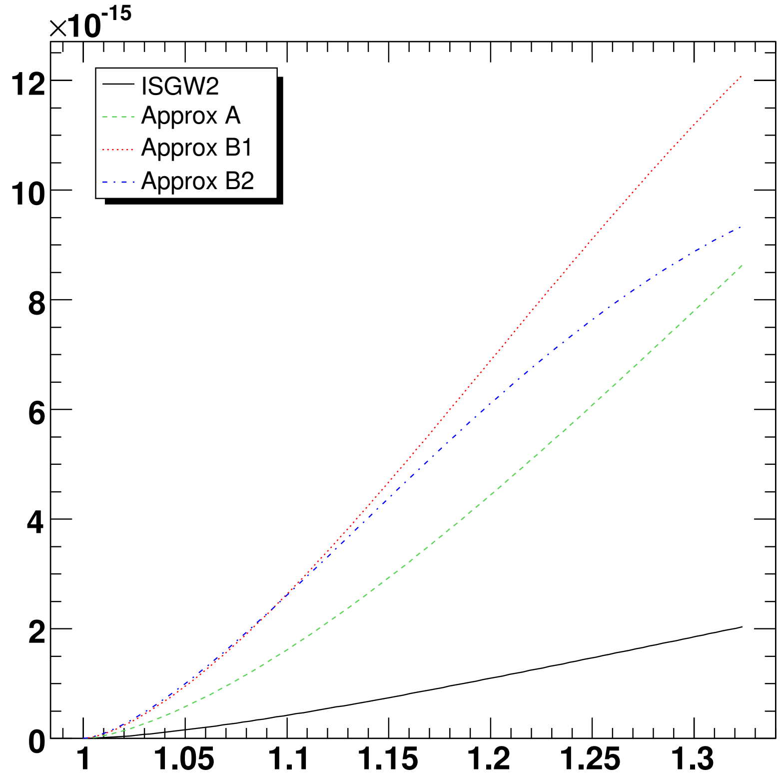

Figure 63: [$B \to D_0^* \ell \nu$ **FF**] The differential decay rate $d\Gamma(B \to D_0^* \ell \nu)/dw$ as a function of w.

dashed line is the Approximation A, the red dotted line is the Approximation B1 and the blue dot-dashed line is the Approximation B2. We use the Approximation B1 in our fit. Figure 64 shows the distribution of weight W_{jk}^{MC} in the case of the Approximation B1, corresponding to the normalization factor $R_N = 0.1624$. BpBm MC is used to create the plot.

9.4.2 $B \to D_1' \ell \nu$

The ISGW2 form factors q, l and c_+ are related to the LLSW form factors g_A, g_{V_1}, g_{V_2} and g_{V_3}.

$$g_A = R m_B (1+r) q \tag{261}$$

$$g_{V_1} = \frac{2}{R m_B (1+r)} l \tag{262}$$

$$g_{V_3} + r g_{V_2} = R m_B (1+r) c_+ \tag{263}$$

where

$$R = \frac{2\sqrt{m_B m_{D_1'}}}{m_B + m_{D_1'}}, \quad r = \frac{m_{D_1'}}{m_B} \tag{264}$$

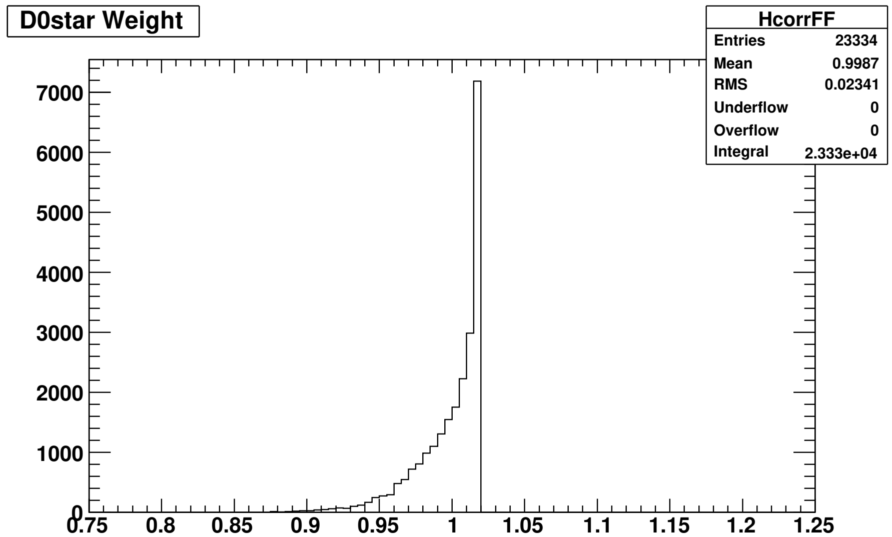

Figure 64: [$B \to D_0^* \ell\nu$ **FF weight**] The distribution of weight W_{jk}^{MC} for $B \to D_0^* \ell\nu$ decays This is made from BpBm MC.

The differential decay rate is given by

$$\frac{d^2\Gamma_{D_1'}}{dw d\cos\theta} = \frac{G_F^2 |V_{cb}|^2 m_B^5}{64\pi^3} r^3 (w^2-1)^{1/2}\, \mathcal{I}_{D_1'}(w,\theta) \tag{265}$$

where

$$\begin{aligned}\mathcal{I}_{D_1'}(w,\theta) &= (1-\cos^2\theta)[(w-r)g_{V_1} + (w^2-1)(g_{V_3}+rg_{V_2})]^2 \\ &+ (1-2rw+r^2)[(1+\cos^2\theta)(g_{V_1}^2 + (w^2-1)g_A^2) - 4\cos\theta\sqrt{w^2-1}g_{V_1}g_A]\end{aligned} \tag{266}$$

The weight is given by the ratio of $\mathcal{I}_{D_1'}$ part.

$$W_{jk}^{MC}(w_k) = \frac{\mathcal{I}_{D_1'}^{LLSW}}{\mathcal{I}_{D_1'}^{ISGW2}} R_N \tag{267}$$

Integrated by θ, the differential decay rate is

$$\frac{d\Gamma(B \to D_1 \ell\nu)}{dw} = \frac{G_F^2 |V_{cb}|^2 m_B^5}{48\pi^3} r^3 (w^2-1)^{1/2}\, \mathcal{J}_{D_1'}(w) \tag{268}$$

where

$$\begin{aligned}\mathcal{J}_{D_1'}(w) &= \left[(w-r)g_{V_1} + (w^2-1)(g_{V_3}+rg_{V_2})\right]^2 \\ &+ 2(1-2rw+r^2)[g_{V_1}^2 + (w^2-1)g_A^2]\end{aligned} \tag{269}$$

Thus, the normalization factor, R_N, is given by

$$\int_0^{1.316} dw (w^2-1)^{1/2} \mathcal{J}_{D_1'}^{ISGW2} = R_N \int_1^{1.316} dw (w^2-1)^{1/2} \mathcal{J}_{D_1'}^{LLSW} \tag{270}$$

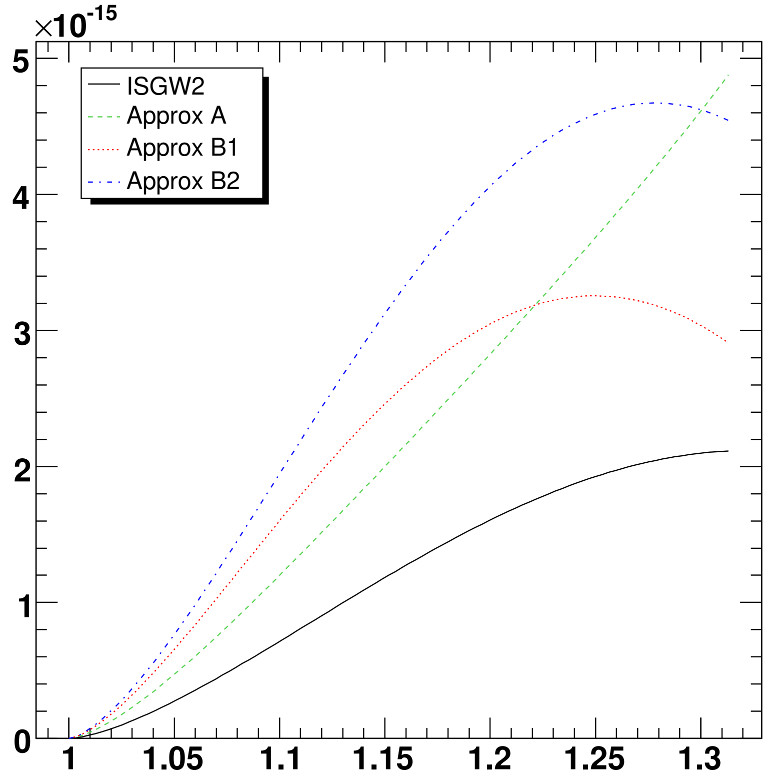

Figure 65: [$B \to D_1'\ell\nu$ **FF**] The differential decay rate $d\Gamma(B \to D_1'\ell\nu)/dw$ as a function of w.

Figure 65 shows the differential decay rate $d\Gamma(B \to D_1'\ell\nu)/dw$ as a function of w. The black line shows the ISGW2 model, the other lines show the LLSW model; the green dashed line is the Approximation A, the red dotted line is the Approximation B1 and the blue dot-dashed line is the Approximation B2. We use the Approximation B1 in our fit. Figure 66 shows the distribution of weight W^{MC}_{jk} in the case of the Approximation B1, corresponding to the normalization factor $R_N = 0.5488$. BpBm MC is used to create the plot.

9.4.3 $B \to D_1\ell\nu$

The ISGW2 form factors v, r and s_+ are related to the LLSW form factor f_A, f_{V_1}, f_{V_2} and f_{V_3}.

$$f_A = Rm_B(1+r)v \tag{271}$$

$$f_{V_1} = \frac{2}{Rm_B(1+r)}r \tag{272}$$

$$f_{V_3} + rf_{V_2} = Rm_B(1+r)s_+ \tag{273}$$

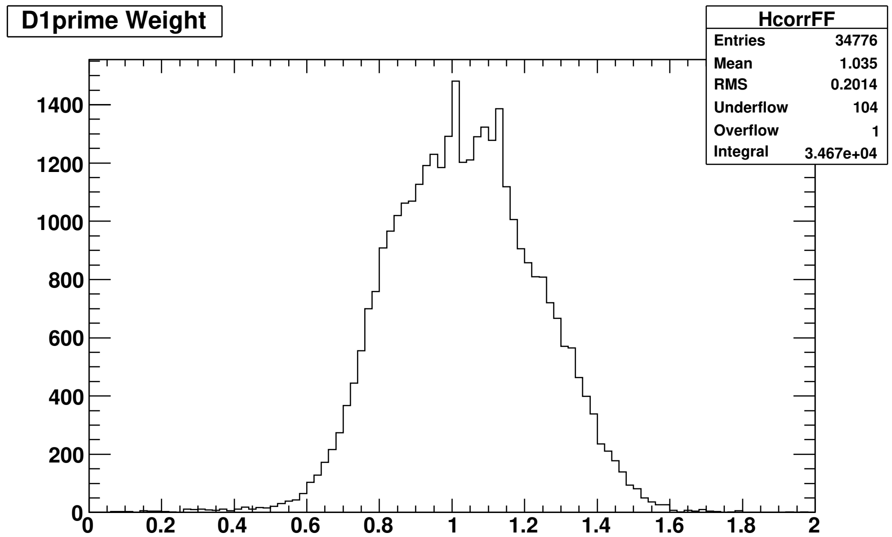

Figure 66: [$B \to D_1' \ell \nu$ **FF weight**] The distribution of weight W_{jk}^{MC} for $B \to D_1' \ell \nu$ decays This is made from BpBm MC.

where

$$R = \frac{2\sqrt{m_B m_{D_1}}}{m_B + m_{D_1}}, \quad r = \frac{m_{D_1}}{m_B} \tag{274}$$

The differential decay rate is given by

$$\frac{d^2\Gamma_{D_1}}{dw d\cos\theta} = \frac{G_F^2 |V_{cb}|^2 m_B^5}{64\pi^3} r^3 (w^2-1)^{1/2}\, \mathcal{I}_{D_1}(w,\theta) \tag{275}$$

where

$$\begin{aligned}\mathcal{I}_{D_1}(w,\theta) = &(1-\cos^2\theta)[(w-r)f_{V_1} + (w^2-1)(f_{V_3} + r f_{V_2})]^2 \\ &+(1-2rw+r^2)[(1+\cos^2\theta)(f_{V_1}^2 + (w^2-1)f_A^2) - 4\cos\theta\sqrt{w^2-1} f_{V_1} f_A]\end{aligned} \tag{276}$$

The weight is given by the ratio of $\mathcal{I}_{D_1}$ part.

$$W_{jk}^{MC}(w_k) = \frac{\mathcal{I}_{D_1}^{LLSW}}{\mathcal{I}_{D_1}^{ISGW2}} R_N \tag{277}$$

Integrated by θ, the differential decay rate is

$$\frac{d\Gamma(B \to D_1 \ell \nu)}{dw} = \frac{G_F^2 |V_{cb}|^2 m_B^5}{48\pi^3} r^3 (w^2-1)^{1/2}\, \mathcal{J}_{D_1}(w) \tag{278}$$

where

$$\begin{aligned}\mathcal{J}_{D_1}(w) = &\left[(w-r)f_{V_1} + (w^2-1)(f_{V_3} + r f_{V_2})\right]^2 \\ &+2(1-2rw+r^2)[f_{V_1}^2 + (w^2-1)f_A^2]\end{aligned} \tag{279}$$

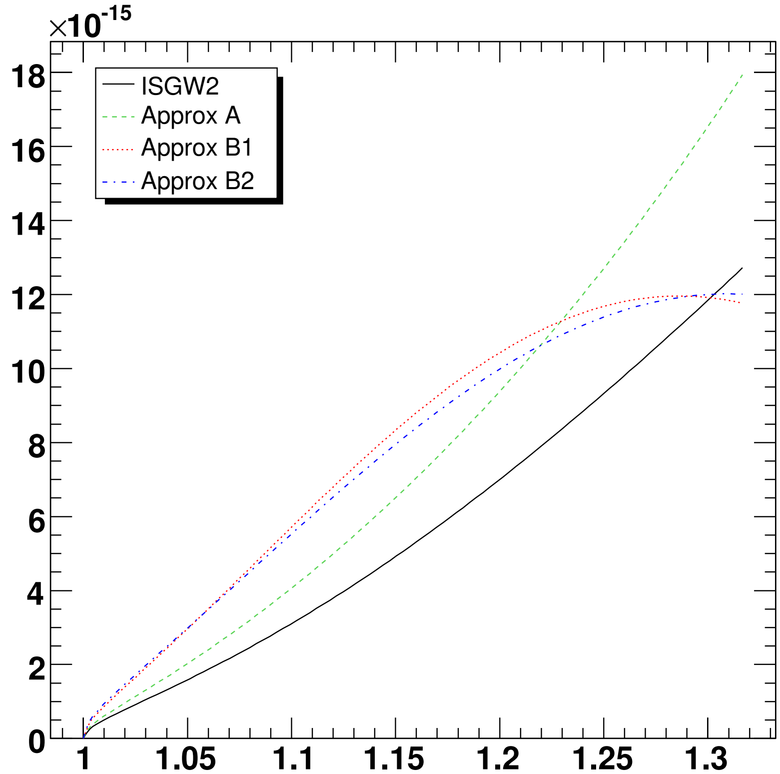

Figure 67: [$B \to D_1 \ell \nu$ **FF**] The differential decay rate $d\Gamma(B \to D_1 \ell \nu)/dw$ as a function of w.

Thus, the normalization factor, R_N, is given by

$$\int_0^{1.320} dw(w^2-1)^{1/2} \mathcal{J}_{D_1}^{ISGW2} = R_N \int_1^{1.320} dw(w^2-1)^{1/2} \mathcal{J}_{D_1}^{LLSW} \tag{280}$$

Figure 67 shows the differential decay rate $d\Gamma(B \to D_1 \ell \nu)/dw$ as a function of w. The black line shows the ISGW2 model, the other lines show the LLSW model; the green dashed line is the Approximation A, the red dotted line is the Approximation B1 and the blue dot-dashed line is the Approximation B2. We use the Approximation B1 in our fit. Figure 68 shows the distribution of weight W_{jk}^{MC} in the case of the Approximation B1, corresponding to the normalization factor $R_N = 0.7330$. BpBm MC is used to create the plot.

9.4.4 $B \to D_2^* \ell \nu$

The ISGW2 form factors h, k and b_+ are related to the LLSW form factor k_V, k_{A_1}, k_{A_2} and k_{A_3}.

$$k_V = R m_B^2 (1-r) h \tag{281}$$

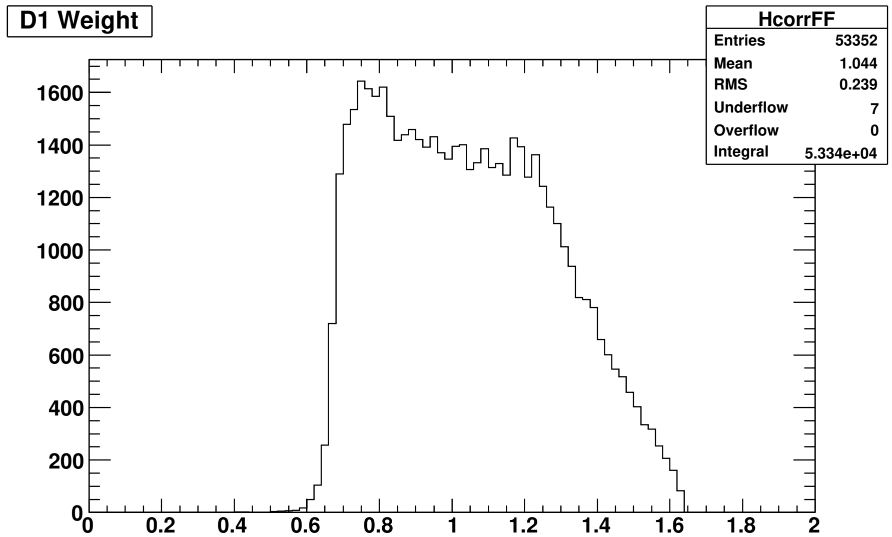

Figure 68: [$B \to D_1 \ell \nu$ **FF weight**] The distribution of weight W_{jk}^{MC} for $B \to D_1 \ell \nu$ decays This is made from BpBm MC.

$$k_{A_1} = \frac{2}{R(1-r)} k \tag{282}$$

$$k_{A_3} + r k_{A_2} = R m_B^2 (1-r) b_+ \tag{283}$$

where

$$R = \frac{2\sqrt{m_B m_{D_2^*}}}{m_B + m_{D_2^*}}, \quad r = \frac{m_{D_2^*}}{m_B} \tag{284}$$

The differential decay rate is given by

$$\frac{d^2 \Gamma_{D_2^*}}{dw d\cos\theta} = \frac{G_F^2 |V_{cb}|^2 m_B^5}{64\pi^3} r^3 (w^2-1)^{3/2} \, \frac{1}{2} \, \mathcal{I}_{D_2^*}(w,\theta) \tag{285}$$

where

$$\begin{aligned}\mathcal{I}_{D_2^*}(w,\theta) = {} & \frac{4}{3}(1-\cos^2\theta)[(w-r)k_{A_1} + (w^2-1)(k_{A_3} + r k_{A_2})]^2 \\ & + (1-2rw+r^2)[(1+\cos^2\theta)(k_{A_1}^2 + (w^2-1)k_V^2) - 4\cos\theta\sqrt{w^2-1}k_{A_1}k_V]\end{aligned} \tag{286}$$

The weight is given by the ratio of $\mathcal{I}_{D_2^*}$ part

$$W_{jk}^{MC}(w_k) = \frac{\mathcal{I}_{D_2^*}^{LLSW}}{\mathcal{I}_{D_2^*}^{ISGW2}} R_N \tag{287}$$

Integrated by θ, decay rate is

$$\frac{d\Gamma(B \to D_2^* \ell \nu)}{dw} = \frac{G_F^2 |V_{cb}|^2 m_B^5}{48\pi^3} r^3 (w^2-1)^{3/2} \, \mathcal{J}_{D_2^*}(w) \tag{288}$$

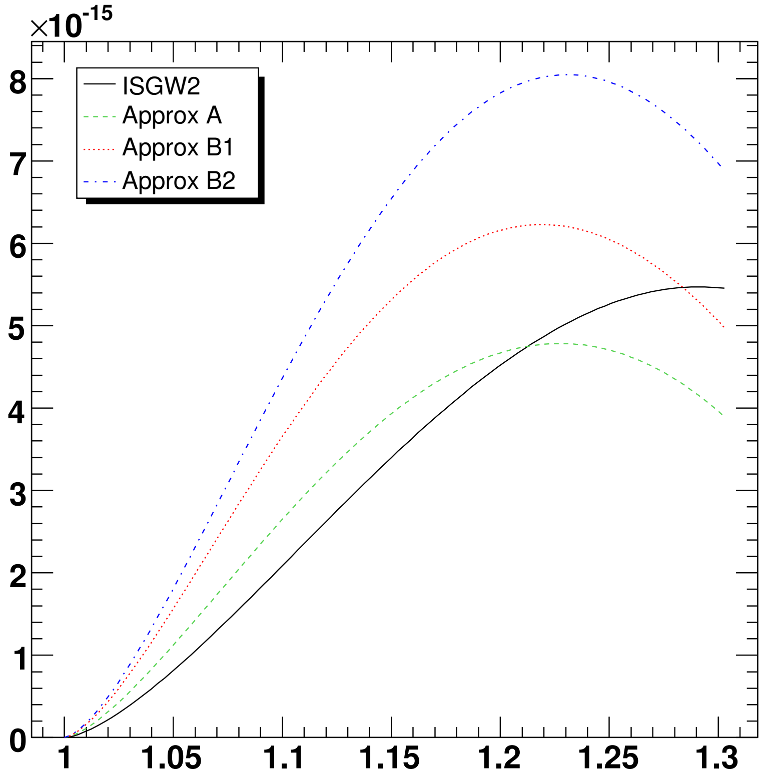

Figure 69: [$B \to D_2^* \ell\nu$ **FF**] The differential decay rate $d\Gamma(B \to D_2^* \ell\nu)/dw$ as a function of w.

where

$$\mathcal{J}_{D_2^*}(w) = \frac{2}{3}\left[(w-r)k_{A_1} + (w^2-1)(k_{A_3} + rk_{A_2})\right]^2 \\ +2(1-2rw+r^2)[k_{A_1}^2 + (w^2-1)k_V^2] \tag{289}$$

Thus, the normalization factor, R_N, is given by

$$\int_0^{1.306} dw(w^2-1)^{3/2}\mathcal{J}_{D_2^*}^{ISGW2} = R_N \int_1^{1.306} dw(w^2-1)^{3/2}\mathcal{J}_{D_2^*}^{LLSW} \tag{290}$$

Figure 69 shows the differential decay rate $d\Gamma(B \to D_2^* \ell\nu)/dw$ as a function of w. The black line shows the ISGW2 model, the other lines show the LLSW model; the green dashed line is the Approximation A, the red dotted line is the Approximation B1 and the blue dot-dashed line is the Approximation B2. We use the Approximation B1 in our fit. Figure 70 shows the distribution of weight W_{jk}^{MC} in the case of the Approximation B1, corresponding to the normalization factor $R_N = 0.7490$. BpBm MC is used to create the plot.

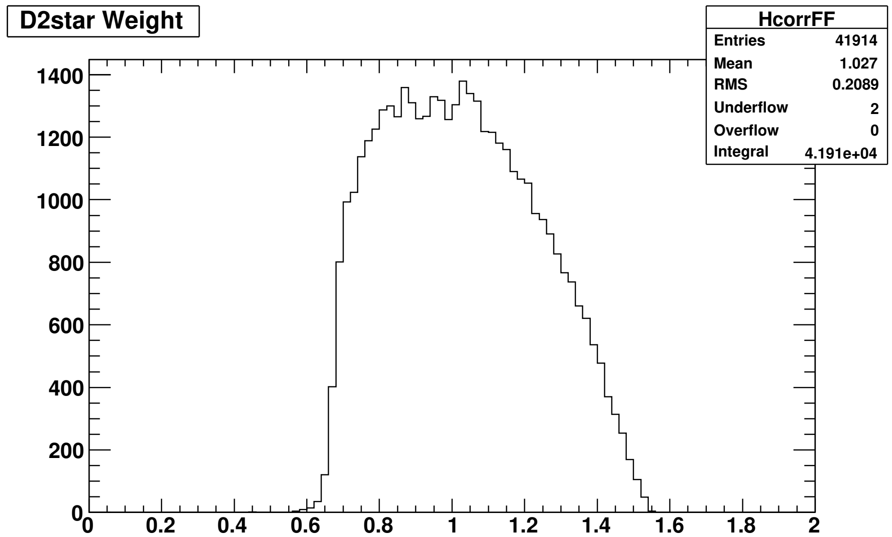

Figure 70: [$B \to D_2^* \ell \nu$ **FF weight**] The distribution of weight W_{jk}^{MC} for $B \to D_2^* \ell \nu$ decays This is made from BpBm MC.

9.4.5 Effect on kinematic variables

The change in the spectrum of lepton momentum, D momentum and $\cos\theta_{B-Dl}$ is given in Figure 71 - 73.

9.5 $B \to D^{(*)} \pi \ell \nu$ (non-resonant)

In SP5/SP6 Goiry-Roberts model [43][44] is used. We keep this model because these is no better alternative.

9.5.1 $B \to D \pi \ell \nu$

$$W_{jk}^{Sig}(w_k) = 1 \tag{291}$$

9.5.2 $B \to D^* \pi \ell \nu$

$$W_{jk}^{Sig}(w_k) = 1 \tag{292}$$

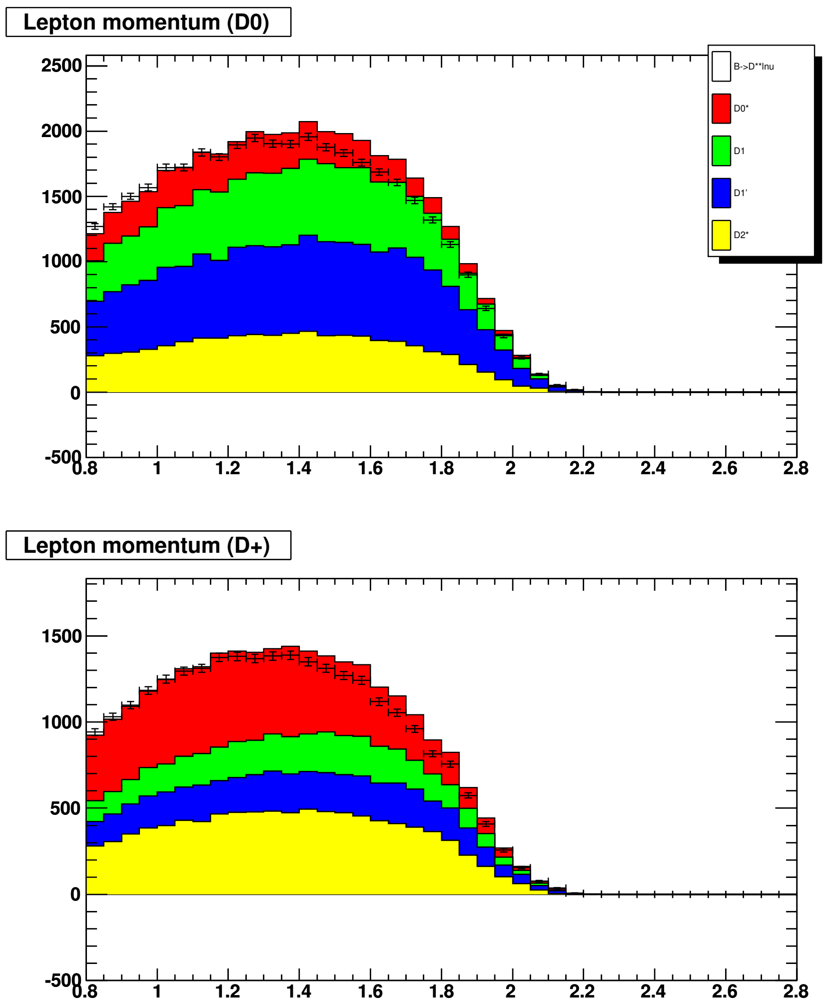

Figure 71: [p_ℓ **after** $B \rightarrow D^{**}\ell\nu$ **re-weighting**] Lepton momentum spectrum of $B \rightarrow D^{**}\ell\nu$ decays. Black line is ISGW2 model and colored histogram is HQET model. Red is D_0^*, green is D_1, blue is D_1' and yellow is D_2^*.

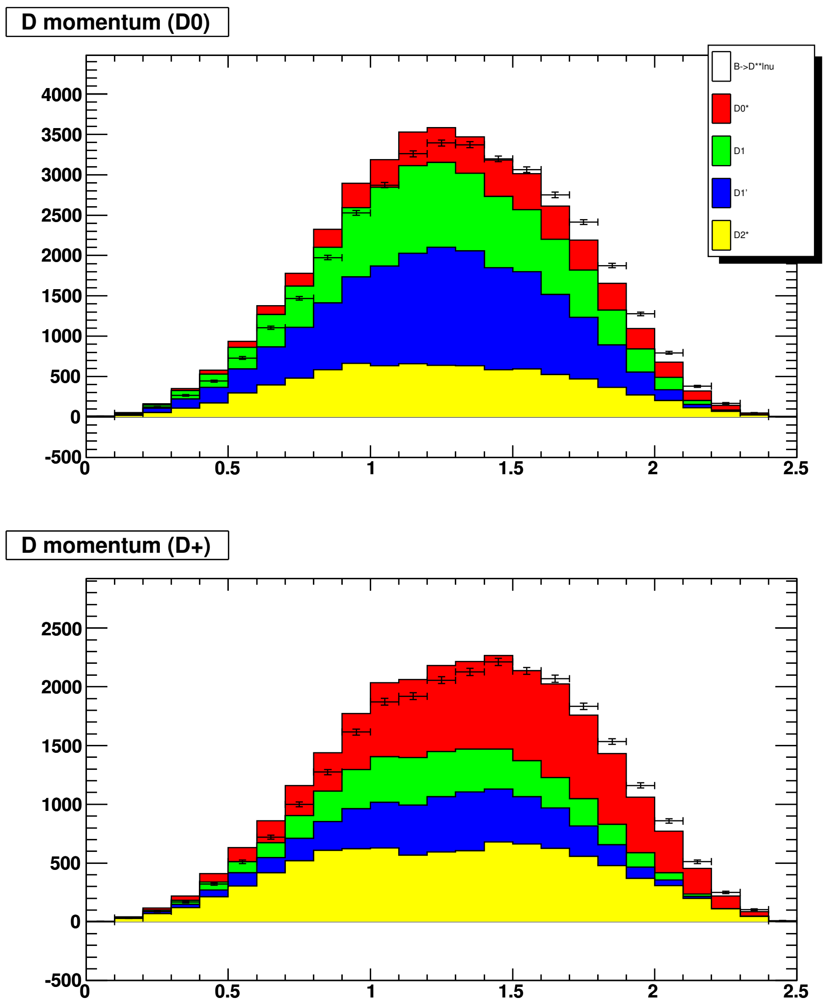

Figure 72: [p_D **after** $B \to D^{**}\ell\nu$ **re-weighting**] D momentum spectrum of $B \to D^{**}\ell\nu$ decays. Black line is ISGW2 model and colored histogram is HQET model. Red is D_0^*, green is D_1, blue is D_1' and yellow is D_2^*.

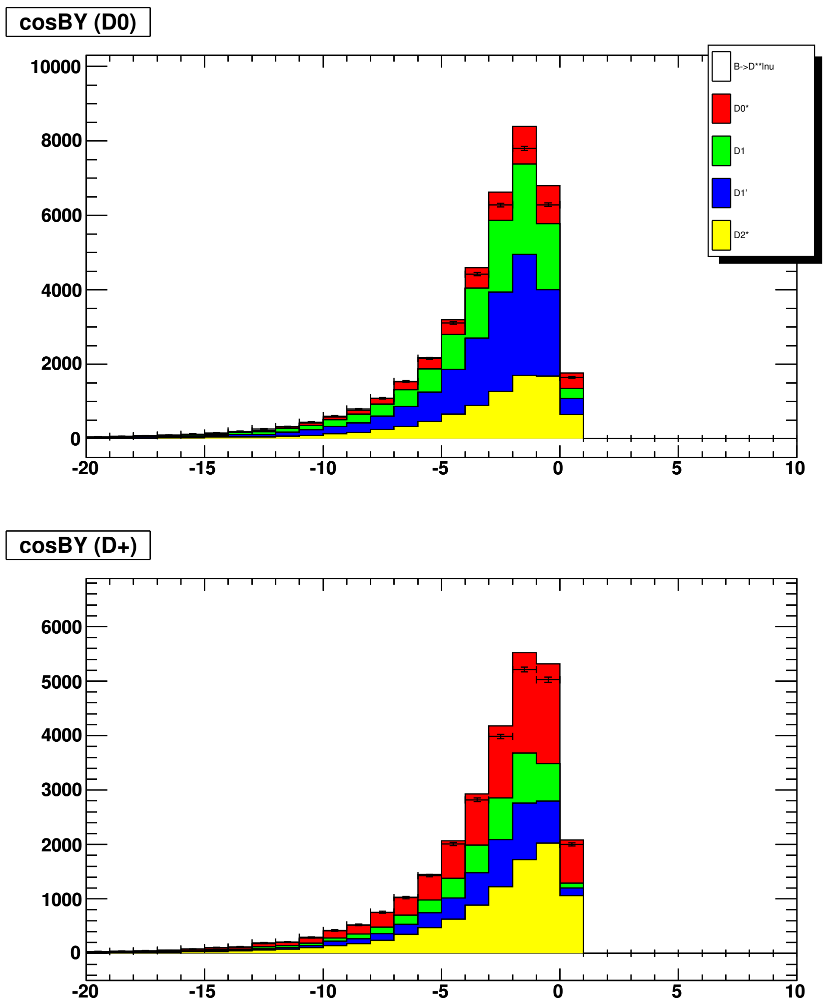

Figure 73: [$\cos\theta_{B-Dl}$ **after** $B \to D^{**}\ell\nu$ **re-weighting**] $\cos\theta_{B-Dl}$ of $B \to D^{**}\ell\nu$ decays. Black line is ISGW2 model and colored histogram is HQET model. Red is D_0^*, green is D_1, blue is D_1' and yellow is D_2^*.

10 FF parameter fitting technique

10.1 $B \to D\ell\nu$ slope fitting

To fit for $B \to D\ell\nu$ slope, it is not computationally efficient to go through the calculation of the weight event by event. The following is a better way to do fitting.

10.1.1 Number of events

We may rewrite the weight (Equation (228))

$$W_{jk}^{MC}(w_k) = \left[\frac{[h_+(1)]^2}{[Rf_+]^2} - \frac{2(w-1)[h_+(1)]^2}{[Rf_+]^2}\rho_D^2 + \frac{(w-1)^2[h_+(1)]^2}{[Rf_+]^2}\left(\rho_D^2\right)^2\right] R_N \quad (293)$$

Hence, we define

$$W_{jk}^{MC}(w_k) \equiv \left[W_{jk}^0(w_k) - W_{jk}^1(w_k)\rho_D^2 + W_{jk}^2(w_k)\left(\rho_D^2\right)^2\right] R_N \quad (294)$$

Then, the number of events is

$$\begin{aligned} N_{ij}^{MC} = \Bigg[&\sum_l \left(r_l^{Lumi} \sum_{k\in i,j,l} r_k^{Trk} r_k^{KPID} r_k^{LPID} W_{jk}^0\right) \\ &- \sum_l \left(r_l^{Lumi} \sum_{k\in i,j,l} r_k^{Trk} r_k^{KPID} r_k^{LPID} W_{jk}^1\right)\rho_D^2 \\ &+ \sum_l \left(r_l^{Lumi} \sum_{k\in i,j,l} r_k^{Trk} r_k^{KPID} r_k^{LPID} W_{jk}^2\right)\left(\rho_D^2\right)^2\Bigg] R_N \end{aligned} \quad (295)$$

Hence

$$N_{ij}^{MC} \equiv \left[N_{ij}^{MC0} - N_{ij}^{MC1}\rho_D^2 + N_{ij}^{MC2}\left(\rho_D^2\right)^2\right] R_N \quad (296)$$

Instead of going through event by event in fitting, first we create these three histograms (N_{ij}^{MC0}, N_{ij}^{MC1} and N_{ij}^{MC2}), and then use those histograms in fitting.
In another parametrization (Equation (230)).

$$\begin{aligned} &1 - 8\rho_D^2 z + (51\rho_D^2 - 10)z^2 - (252\rho_D^2 - 84)z^3 \\ &= (1 - 10z^2 + 84z^3) - (8z - 51z^2 + 252z^3)\rho_D^2 \end{aligned} \quad (297)$$

Thus, by replacing

$$\begin{aligned} &1 \to (1 - 10z^2 + 84z^3) \\ &(w-1) \to (8z - 51z^2 + 252z^3) \end{aligned} \quad (298)$$

we can use the same method

10.1.2 Weighted events and statistical uncertainty

Sine our events are weighted, calculation of statistical uncertainty is a little bit tricky. Suppose the weight of the k-th event or candidate is W_k and it is given by

$$W_k = F_{1k} - F_{2k}\rho_D^2 + F_{3k}\left(\rho_D^2\right)^2 \tag{299}$$

The number of events after D mass sideband subtraction is given by

$$\begin{aligned}\sum_k^{peak} W_k - \sum_k^{sideband} W_k = &\left(\sum_k^{peak} F_{1k} - \sum_k^{sideband} F_{1k}\right)\\ &- \left(\sum_k^{peak} F_{2k} - \sum_k^{sideband} F_{2k}\right)\rho_D^2 + \left(\sum_k^{peak} F_{3k} - \sum_k^{sideband} F_{3k}\right)\left(\rho_D^2\right)^2\end{aligned} \tag{300}$$

Thus, the number of events is still given by

$$N = \left[N_1 - N_2\rho_D^2 + N_3\left(\rho_D^2\right)^2\right] R_N \tag{301}$$

The square of statistical uncertainty is calculated by

$$\begin{aligned}\sum_k^{peak} W_k^2 + \sum_k^{sideband} W_k^2 = &\sum_k^{peak}\left(F_{1k} - F_{2k}\rho_D^2 + F_{3k}\left(\rho_D^2\right)^2\right)^2\\ &+ \sum_k^{sideband}\left(F_{1k} - F_{2k}\rho_D^2 + F_{3k}\left(\rho_D^2\right)^2\right)^2\end{aligned} \tag{302}$$

Thus, no need to sum peak and sideband separately

$$\begin{aligned}\sum_k W_k^2 &= \sum_k \left(F_{1k} - F_{2k}\rho_D^2 + F_{3k}\left(\rho_D^2\right)^2\right)^2\\ &= \sum_k F_{1k}^2 - \sum_k 2F_{1k}F_{2k}\rho_D^2 + \sum_k\left(2F_{1k}F_{3k} + F_{2k}^2\right)\left(\rho_D^2\right)^2\\ &\quad - \sum_k 2F_{2k}F_{3k}\left(\rho_D^2\right)^3 + \sum_k F_{3k}^2\left(\rho_D^2\right)^4\end{aligned} \tag{303}$$

Hence, we need 5 histograms to calculate the square of statistical uncertainty

$$\sigma^2 = \left[N_1 - N_2\rho_D^2 + N_3\left(\rho_D^2\right)^2 - N_4\left(\rho_D^2\right)^3 + N_5\left(\rho_D^2\right)^4\right] R_N^2 \tag{304}$$

Note that in the above argumant, the sideband scale factor introduced in section 6 Equation (162), is included in the weight W_k (F_{nk}).

10.2 $B \to D^* \ell \nu$ parameter fitting

We may rewrite the $\mathcal{J}_{FF}(R_1, R_2, \rho^2)$. From equation (241),

$$\begin{aligned}
&\mathcal{J}_{FF}(R_1, R_2, \rho^2) \\
&= [F_1 - F_2\rho^2 + F_3(\rho^2)^2]\,[G_1 + G_2R_1 + G_3R_2 + G_4R_1^2 + G_5R_2^2 + G_6R_1R_2] \\
&= F_1G_1 - F_2G_1\rho^2 + F_3G_1(\rho^2)^2 \\
&\quad +F_1G_2R_1 - F_2G_2R_1\rho^2 + F_3G_2R_1(\rho^2)^2 \\
&\quad +F_1G_3R_2 - F_2G_3R_2\rho^2 + F_3G_3R_2(\rho^2)^2 \\
&\quad +F_1G_4R_1^2 - F_2G_4R_1^2\rho^2 + F_3G_4R_1^2(\rho^2)^2 \\
&\quad +F_1G_5R_2^2 - F_2G_5R_2^2\rho^2 + F_3G_5R_2^2(\rho^2)^2 \\
&\quad +F_1G_6R_1R_2 - F_2G_6R_1R_2\rho^2 + F_3G_6R_1R_2(\rho^2)^2
\end{aligned} \tag{305}$$

where, using the CLN parametrization of the slope,

$$
\begin{aligned}
F_1 &= (1-15z^2+91z^3)^2\\
F_2 &= 2(1-15z^2+91z^3)(8z-53z^2+231z^3)\\
F_3 &= (8z-53z^2+231z^3)^2\\
G_6 &= (-4)\sqrt{1-c_L^2}(1-c_L)\sqrt{1-c_V^2}c_Vc_\chi\sqrt{1-2wr+r^2}(w-1)\sqrt{\tfrac{w-1}{w+1}}\\
&\quad+4\sqrt{1-c_L^2}(1+c_L)\sqrt{1-c_V^2}c_Vc_\chi\sqrt{1-2wr+r^2}(-1)(w-1)\sqrt{\tfrac{w-1}{w+1}}\\
G_4 &= (1-c_L)^2(1-c_V^2)(1-2wr+r^2)\tfrac{w-1}{w+1}\\
&\quad+(1+c_L)^2(1-c_V^2)(1-2wr+r^2)\tfrac{w-1}{w+1}\\
&\quad+(-2)(1-c_L^2)(1-c_V^2)(2c_\chi^2-1)(1-2wr+r^2)(-1)\tfrac{w-1}{w+1}\\
G_2 &= (1-c_L)^2(1-c_V^2)(1-2wr+r^2)(-2)\sqrt{\tfrac{w-1}{w+1}}\\
&\quad+(1+c_L)^2(1-c_V^2)(1-2wr+r^2)(+2)\sqrt{\tfrac{w-1}{w+1}}\\
&\quad+(-4)\sqrt{1-c_L^2}(1-c_L)\sqrt{1-c_V^2}c_Vc_\chi\sqrt{1-2wr+r^2}(-1)(w-r)\sqrt{\tfrac{w-1}{w+1}}\\
&\quad+4\sqrt{1-c_L^2}(1+c_L)\sqrt{1-c_V^2}c_Vc_\chi\sqrt{1-2wr+r^2}(w-r)\sqrt{\tfrac{w-1}{w+1}}\\
&\quad+2G_4A_1+G_6A_2\\
G_5 &= 4(1-c_L^2)c_V^2(w-1)^2\\
G_3 &= 4(1-c_L^2)c_V^2(-2)(w-r)(w-1)\\
&\quad+(-4)\sqrt{1-c_L^2}(1-c_L)\sqrt{1-c_V^2}c_Vc_\chi\sqrt{1-2wr+r^2}(-1)(w-1)\\
&\quad+4\sqrt{1-c_L^2}(1+c_L)\sqrt{1-c_V^2}c_Vc_\chi\sqrt{1-2wr+r^2}(-1)(w-1)\\
&\quad+2G_5A_2+G_6A_1\\
G_1 &= (1-c_L)^2(1-c_V^2)(1-2wr+r^2)\\
&\quad+(1+c_L)^2(1-c_V^2)(1-2wr+r^2)\\
&\quad+4(1-c_L^2)c_V^2(w-r)^2\\
&\quad+(-2)(1-c_L^2)(1-c_V^2)(2c_\chi^2-1)(1-2wr+r^2)\\
&\quad+(-4)\sqrt{1-c_L^2}(1-c_L)\sqrt{1-c_V^2}c_Vc_\chi\sqrt{1-2wr+r^2}(w-r)\\
&\quad+4\sqrt{1-c_L^2}(1+c_L)\sqrt{1-c_V^2}c_Vc_\chi\sqrt{1-2wr+r^2}(w-r)\\
&\quad+(G_2-2G_4A_1-G_6A_2)A_1-(G_3-2G_5A_2-G_6A_1)A_2+G_4A_1^2+G_5A_2^2+G_6A_1A_2
\end{aligned}
\tag{306}
$$

where

$$
\begin{aligned}
A_1 &= -0.12(w-1)+0.05(w-1)^2\\
A_2 &= 0.11(w-1)-0.06(w-1)^2
\end{aligned}
\tag{307}
$$

Thus, same as previous section, we can, first, make 18 histograms corresponding to the 18 terms in the above $\mathcal{J}_{FF}(R_1,R_2,\rho^2)$. Then we can calculate the number of events N

$$\begin{aligned}
N = [&N_1 - N_2\rho^2 + N_3(\rho^2)^2 \\
&+N_4R_1 - N_5R_1\rho^2 + N_6R_1(\rho^2)^2 \\
&+N_7R_2 - N_8R_2\rho^2 + N_9R_2(\rho^2)^2 \\
&+N_{10}R_1^2 - N_{11}R_1^2\rho^2 + N_{12}R_1^2(\rho^2)^2 \\
&+N_{13}R_2^2 - N_{14}R_2^2\rho^2 + N_{15}R_2^2(\rho^2)^2 \\
&+N_{16}R_1R_2 - N_{17}R_1R_2\rho^2 + N_{18}R_1R_2(\rho^2)^2]\, R_N
\end{aligned} \tag{308}$$

The square of statistical uncertainty can also be calculated in the same way.

$$\begin{aligned}
&[F_1 - F_2\rho^2 + F_3(\rho^2)^2]^2\, [G_1 + G_2R_1 + G_3R_2 + G_4R_1^2 + G_5R_2^2 + G_6R_1R_2]^2 \\
&= [F_1^2 - 2F_1F_2\rho^2 + (2F_1F_3 + F_2^2)(\rho^2)^2 - 2F_2F_3(\rho^2)^3 + F_3^2(\rho^2)^4] \\
&\quad [G_1^2 + 2G_1G_2R_1 + 2G_1G_3R_2 \\
&\quad +(2G_1G_4 + G_2^2)R_1^2 + (2G_1G_5 + G_3^2)R_2^2 + 2(G_1G_6 + G_2G_3)R_1R_2 \\
&\quad +2G_2G_4R_1^3 + 2G_3G_5R_2^3 + 2(G_2G_6 + G_3G_4)R_1^2R_2 + 2(G_2G_5 + G_3G_6)R_1R_2^2 \\
&\quad +G_4^2R_1^4 + G_5^2R_2^4 + 2G_4G_6R_1^3R_2 + 2G_5G_6R_1R_2^3 + (2G_4G_5 + G_6^2)R_1^2R_2^2]
\end{aligned} \tag{309}$$

Thus, we need $5 \times 15 = 75$ histograms to calculate the statistical uncertainty.

11 Validation of the fitting method

We validate our fit as described in the following subsections.
We have chosen the parameters to fit for based on validation studies, especailly on toy MC study, which is explained below. Validation shows that we have reasonable sensitivity to the parameters and that they aren not too highly correlated with each other. We also find that floating additional parameters (e.g. D decay BFs) leads to larger biases.

11.1 Toy MC study

11.1.1 Method of toy MC study

To validate our fitting method, we perform toy MC study. The procedure of toy MC study is the following

1. We create fake (OnPeak - OffPeak) data from $B\bar{B}$ MC, wth input values shown in Table 18.
2. Fluctuate the entry of each bin of the fake data using a Gaussian random number based on the uncertainty of each bin.
3. Fit for the fluctuated fake OnPeak data.
4. Iterate 2 and 3 for approximately 1,000 times.
5. Plot pull distributions and get the mean and the standard deviation of each distribution.

In Tablee 18, Set b has different BF values than Set a, Set c has different background coefficients and Set d has different FF parameters.

11.1.2 Pull results.

Pulls are calculated by

$$\text{pull} = \frac{\text{fitted value} - \text{true value}}{\text{fitted uncertainty}} \tag{310}$$

The mean and standard deviation (r.m.s.) of these pull distributions are listed in Table 19. In the bottom line of the Table 19, the uncertainty on mean and standard deviation are listed. These are calculated with the number of succeeded fit $N = 960$. Assuming the standard deviation is $\sigma = 1$, the uncertainty on mean is

$$\frac{\sigma}{\sqrt{N}} = \frac{1}{\sqrt{1000}} = 0.0316 \tag{311}$$

and the uncertainty on standard deviation is

$$\frac{\sigma}{\sqrt{2N}} = \frac{1}{\sqrt{2 \times 1000}} = 0.0224 \tag{312}$$

The χ^2 and the pull plots are shown in Figure 74 - 77 only for parameter Set a.

Parameters	Set a	Set b	Set c	Set d
ρ_D^2	1.17	1.17	1.17	1.3
ρ^2	1.23	1.23	1.23	1.3
R_1	1.417	1.417	1.417	1.5
R_2	0.836	0.836	0.836	0.6
$\mathcal{B}(B^+ \to \bar{D}^0\ell^+\nu)$	0.0233	0.0215	0.0233	0.0233
$\mathcal{B}(B^+ \to \bar{D}^{*0}\ell^+\nu)$	0.0583	0.065	0.0583	0.0583
$\mathcal{BT}(B^+ \to \bar{D}^{**0}/(D\pi)^0\ell^+\nu)$	0.018	0.0215	0.018	0.018
f_{+0}	1.037	1.037	1.037	1.037
$C^{D^0}_{UncorDL}$	1.0	1.0	0.9	0.9
$C^{D^0}_{UncorCL}$	1.0	1.0	0.8	0.8
$C^{D^0}_{CascL}$	1.0	1.0	0.9	0.9
$C^{D^+}_{UncorDL}$	1.0	1.0	0.9	0.9
$C^{D^+}_{UncorCL}$	1.0	1.0	0.8	0.8
$C^{D^+}_{CascL}$	1.0	1.0	1.2	1.2

Table 18: [**Parameters of fake data**] The parameter values used to create fake data. Set b has different BF values than Set a, Set c has different background coefficients and Set d has different FF parameters.

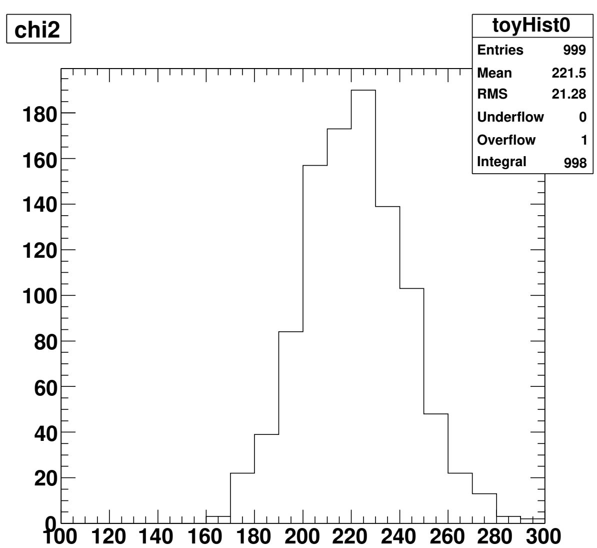

Figure 74: [**Toy MC χ^2 (Set a)**] Toy MC χ^2 plot for parameter Set a.

f_{+0} floated	Set a		Set b		Set c		Set d	
Parameters	Mean	r.m.s.	Mean	r.m.s.	Mean	r.m.s.	Mean	r.m.s.
ρ_D^2	+0.0219	1.006	+0.0255	1.005	-0.0207	1.004	-0.0267	1.007
ρ^2	-0.0022	1.005	-0.0113	1.005	-0.0558	0.950	-0.0332	0.949
R_1	-0.0132	1.028	-0.0172	1.027	-0.0162	0.973	+0.0040	0.975
R_2	+0.0341	1.005	+0.0410	1.005	+0.0584	0.953	+0.0298	0.955
$\mathcal{B}(B^+ \to \bar{D}^0\ell^+\nu)$	+0.0202	1.004	+0.0175	1.002	-0.0107	0.978	-0.0135	0.982
$\mathcal{B}(B^+ \to \bar{D}^{*0}\ell^+\nu)$	-0.0653	1.009	-0.0648	1.009	-0.0551	1.005	-0.0425	1.006
$\mathcal{BT}(B^+ \to \bar{D}^{**0}/(D\pi)^0\ell^+\nu)$	+0.0693	1.002	+0.0708	1.002	+0.0713	0.983	+0.0690	0.983
f_{+0}	+0.0895	0.999	+0.0856	1.000	+0.0482	1.008	+0.0485	1.008
$C^{D^0}_{UncorDL}$	-0.0286	1.023	-0.0307	1.022	+0.0195	1.050	+0.0369	1.051
$C^{D^0}_{UncorCL}$	+0.0237	0.994	+0.0235	0.992	+0.0357	0.979	+0.0350	0.984
$C^{D^0}_{CascL}$	-0.0417	0.974	-0.0412	0.973	-0.0760	0.980	-0.0785	0.980
$C^{D^+}_{UncorDL}$	+0.0238	0.996	+0.0215	0.994	+0.0426	1.009	+0.0457	1.010
$C^{D^+}_{UncorCL}$	+0.0560	1.051	+0.0585	1.050	+0.0227	0.976	+0.0222	0.977
$C^{D^+}_{CascL}$	+0.0001	0.975	-0.0018	0.977	-0.0540	1.003	-0.0542	1.003
Uncertainty	0.0316	0.0224	0.0316	0.0224	0.0317	0.0224	0.0317	0.0224

Table 19: [**Toy MC : Mean and Standard Deviation**] Mean and standard deviation (r.m.s.) of pull distributions of toy MC fits. The uncertainty on mean and standard deviation are also listed in the bottom line. Pulls are calculated from the difference to nominal fit results.

f_{+0} Fixed	Set a		Set b		Set c		Set d	
Parameters	Mean	r.m.s.	Mean	r.m.s.	Mean	r.m.s.	Mean	r.m.s.
ρ^2_D	-0.0303	0.998	-0.0271	1.000	-0.0290	0.999	-0.0344	1.002
ρ^2	-0.0628	0.945	-0.0709	0.946	-0.0633	0.946	-0.0407	0.945
R_1	-0.0201	0.971	-0.0241	0.972	-0.0211	0.972	-0.0014	0.974
R_2	+0.0589	0.952	+0.0656	0.953	+0.0596	0.953	+0.0330	0.953
$\mathcal{B}(B^+ \to \bar{D}^0\ell^+\nu)$	-0.0283	0.966	-0.0313	0.967	-0.0271	0.967	-0.0297	0.970
$\mathcal{B}(B^+ \to \bar{D}^{*0}\ell^+\nu)$	-0.0363	0.981	-0.0384	0.982	-0.0365	0.981	-0.0230	0.981
$\mathcal{BT}(B^+ \to \bar{D}^{**0}/(D\pi)^0\ell^+\nu)$	+0.0631	0.981	+0.0674	0.981	+0.0639	0.982	+0.0613	0.982
$C^{D^0}_{UncorDL}$	+0.0227	1.050	+0.0220	1.050	+0.0211	1.050	+0.0294	1.051
$C^{D^0}_{UncorCL}$	+0.0444	0.978	+0.0453	0.978	+0.0424	0.978	+0.0421	0.984
$C^{D^0}_{CascL}$	-0.0748	0.979	-0.0785	0.979	-0.0744	0.979	-0.0771	0.980
$C^{D^+}_{UncorDL}$	+0.0316	1.007	+0.0312	1.008	+0.0306	1.008	+0.0331	1.007
$C^{D^+}_{UncorCL}$	+0.0217	0.974	+0.0228	0.974	+0.0206	0.976	+0.0193	0.975
$C^{D^+}_{CascL}$	-0.0604	1.002	-0.0622	1.002	-0.0584	1.003	-0/0586	1.002
Uncertainty	0.0317	0.0224	0.0317	0.0224	0.0317	0.0224	0.0317	0.0224

Table 20: [**Toy MC : Mean and Standard Deviation (f_{+0} Fixed)**] Mean and standard deviation (r.m.s.) of pull distributions of toy MC by fixing $f_{+0} = 1.037$. The uncertainty on mean and standard deviation are also listed in the bottom line. Pulls are calculated from the difference to nominal fit results.

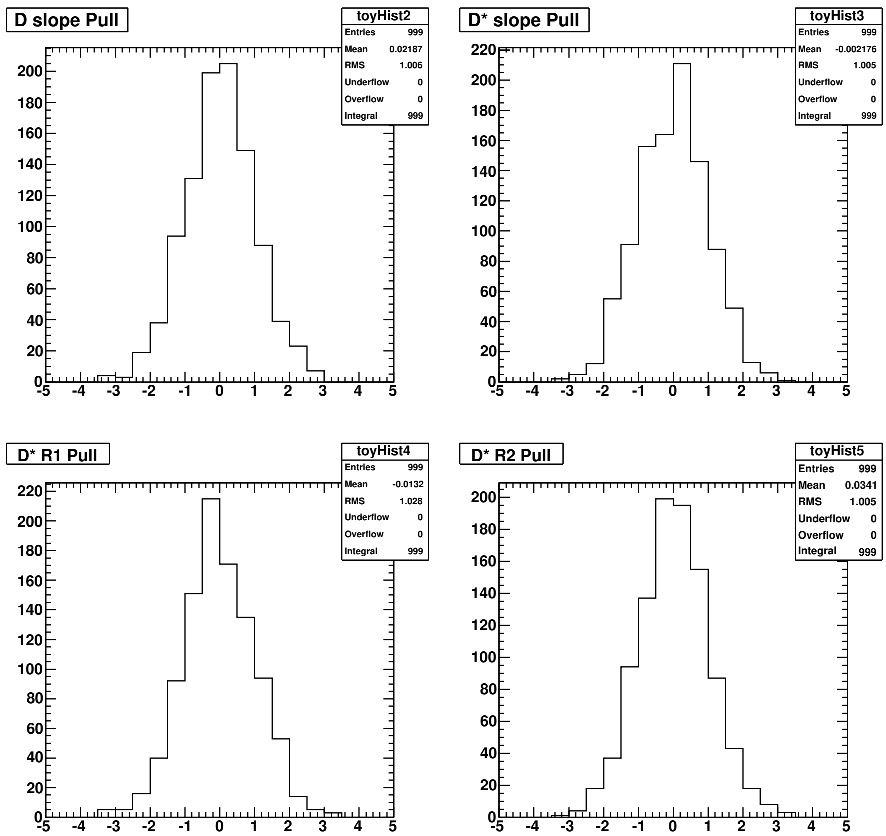

Figure 75: [**Toy MC Pull FF (Set a)**] Toy MC pull plots for FF parameters for parameter Set a.

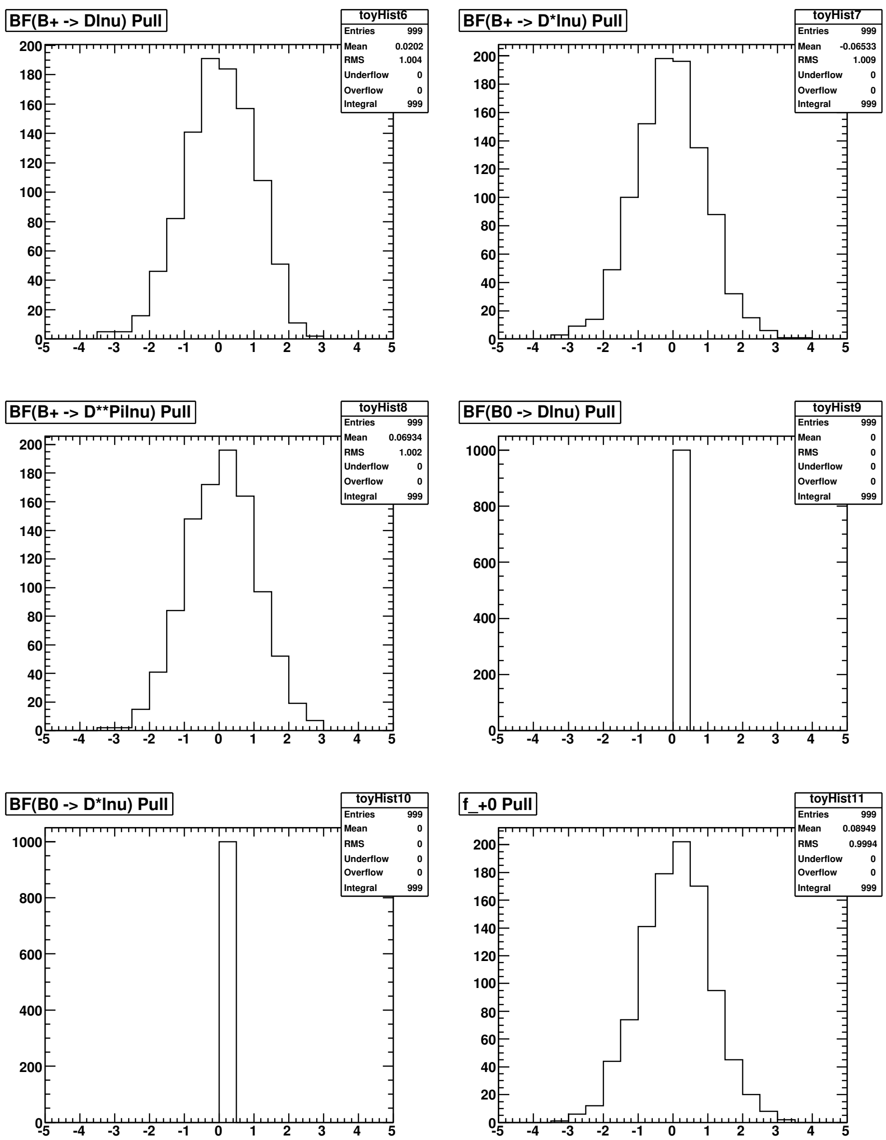

Figure 76: [**Toy MC Pull BF (Set a)**] Toy MC pull plots for BF and f_{+0} for parameter Set a.

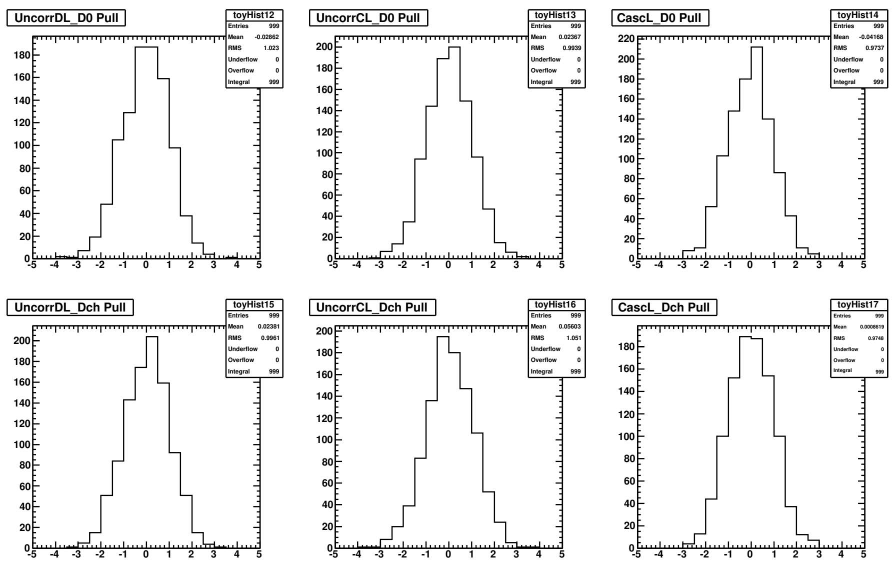

Figure 77: [**Toy MC Pull Bkg (Set a)**] Toy MC pull plots for background components for parameter Set a.

11.2 Validation fits by splitted MC

11.2.1 Validation fit method

To validate our fitting method, we construct fake (OnPeak - OffPeak) data from $B\bar{B}$ MC. We split MC into two halves. We use one half to construct fake data. We, then, create component histograms from the other half, and fit the fake data by the histograms. We can construct fake data with any branching fractions and form factor parameters we want. We then perform fitting to see if our method produce reasonable fitting results.
We use four different parameter sets to create fake data which are shown in Tables 18. The same values are listed as input values in the following tables. We split MC by four different ways

- Split A : Separate even number events and odd number events.
- Split B : Separate events using a set of random nombers.
- Split C : Separate events using another set of random nombers.
- Split D : Separate events using a different set of random nombers.

Thus, there are 16 different validation fittings need to be done.

11.2.2 Validation fit results

We performed fits by either floating or fxing f_{+0}. Fit results are given in Tables 21 - 28. As an index of agreement, we calculate pulls as defined in the above Equation (310). We also caluculate overall χ^2 between input and fitted parameter values, namely

$$\chi^2_{Val} = (\Delta_1, \Delta_2, ..., \Delta_k) \begin{pmatrix} \text{Invers} \\ \text{covariance} \\ \text{matrix} \end{pmatrix} \begin{pmatrix} \Delta_1 \\ \Delta_2 \\ . \\ . \\ . \\ \Delta_k \end{pmatrix} \tag{313}$$

where Δ_i is the differnce between fitted and input values of i-th parameter :

$$\Delta_i = \text{fitted value} - \text{true value} \tag{314}$$

For example, we expect the r.m.s. of a χ^2 distribution with 218 dof to be about 21.

f_{+0} floated	Input	Split A		Split B		Split C		Split D	
	(Set a)	fit result	pulls	fit result	pulls	fit result	pulls	fit result	pulls
ρ_D^2	1.17	1.132 ± 0.027	-1.38	1.184 ± 0.025	+0.94	1.161 ± 0.026	-0.33	1.173 ± 0.026	+0.13
ρ^2	1.23	1.256 ± 0.021	+1.24	1.240 ± 0.021	+0.46	1.204 ± 0.021	-1.27	1.256 ± 0.021	+1.23
R_1	1.417	1.455 ± 0.029	+1.32	1.411 ± 0.028	-0.23	1.376 ± 0.026	-1.55	1.453 ± 0.029	+1.23
R_2	0.836	0.794 ± 0.025	-1.69	0.829 ± 0.025	-0.27	0.865 ± 0.023	+1.23	0.804 ± 0.025	-1.28
$\mathcal{B}(B^+ \to \bar{D}^0 \ell^+ \nu)$	0.0233	0.02318 ± 0.00019	-0.65	0.02360 ± 0.00019	+1.61	0.02336 ± 0.00019	+0.29	0.02340 ± 0.00019	+0.52
$\mathcal{B}(B^+ \to \bar{D}^{*0} \ell^+ \nu)$	0.0583	0.05854 ± 0.00027	+0.92	0.05791 ± 0.00027	-1.46	0.05836 ± 0.00027	+0.23	0.05800 ± 0.00027	-1.15
$\mathcal{BT}(B^+ \to \bar{D}^{**0} \ell^+ \nu)$	0.018	0.01805 ± 0.00028	+0.19	0.01810 ± 0.00028	+0.36	0.01808 ± 0.00028	+0.28	0.01805 ± 0.00028	+0.18
f_{+0}	1.037	1.0147 ± 0.0076	-2.94	1.0470 ± 0.0078	+1.28	1.0300 ± 0.0077	-0.91	1.0491 ± 0.0078	+1.54
$C_{UncorDL}^{D^0}$	1.0	1.009 ± 0.015	+0.57	1.020 ± 0.015	+1.31	0.990 ± 0.015	-0.67	1.016 ± 0.015	+1.02
$C_{UncorCL}^{D^0}$	1.0	1.024 ± 0.017	+1.42	0.970 ± 0.017	-1.77	0.965 ± 0.017	-2.08	0.975 ± 0.016	-1.50
$C_{CascL}^{D^0}$	1.0	0.982 ± 0.023	-0.78	1.013 ± 0.024	+0.55	1.028 ± 0.024	+1.18	1.024 ± 0.024	+0.99
$C_{UncorDL}^{D^+}$	1.0	1.007 ± 0.042	+0.17	0.988 ± 0.042	-0.28	0.974 ± 0.042	-0.62	1.104 ± 0.042	+2.48
$C_{UncorCL}^{D^+}$	1.0	1.003 ± 0.035	+0.09	0.969 ± 0.036	-0.86	0.970 ± 0.036	-0.84	0.979 ± 0.036	-0.59
$C_{CascL}^{D^+}$	1.0	0.989 ± 0.058	-0.20	1.033 ± 0.059	+0.56	0.996 ± 0.058	-0.07	0.963 ± 0.058	-0.64
χ^2/ndof (P-value)		204/220 (0.77)		250/219 (0.07)		192/221 (0.92)		218/220 (0.53)	
χ^2_{Val}			18.4		11.7		12.1		14.5

Table 21: [**MC vs MC (Parameter set a)**] Validation fit results using parameter set a.

f_{+0} floated	Input	Split A		Split B		Split C		Split D	
	(Set b)	fit result	pulls	fit result	pulls	fit result	pulls	fit result	pulls
ρ_D^2	1.17	1.126 ± 0.027	-1.65	1.198 ± 0.027	+1.03	1.160 ± 0.028	-0.38	1.174 ± 0.026	+0.17
ρ^2	1.23	1.258 ± 0.020	+1.40	1.237 ± 0.020	+0.34	1.207 ± 0.019	-1.22	1.254 ± 0.019	+1.21
R_1	1.417	1.455 ± 0.027	+1.40	1.408 ± 0.026	-0.34	1.380 ± 0.025	-1.50	1.450 ± 0.027	+1.20
R_2	0.836	0.793 ± 0.024	-1.83	0.831 ± 0.023	-0.20	0.862 ± 0.022	+1.20	0.806 ± 0.024	-1.28
$\mathcal{B}(B^+ \to \bar{D}^0 \ell^+ \nu)$	0.0215	0.02136 ± 0.00017	-0.83	0.02156 ± 0.00018	+0.30	0.02180 ± 0.00019	+1.58	0.02160 ± 0.00017	+0.60
$\mathcal{B}(B^+ \to \bar{D}^{*0} \ell^+ \nu)$	0.065	0.06530 ± 0.00028	+1.08	0.06462 ± 0.00028	-1.35	0.06506 ± 0.00028	+0.23	0.06467 ± 0.00028	-1.18
$\mathcal{BT}(B^+ \to \bar{D}^{**0} \ell^+ \nu)$	0.0215	0.02156 ± 0.00027	+0.21	0.02162 ± 0.00029	+0.40	0.02157 ± 0.00027	+0.24	0.02157 ± 0.00024	+0.30
f_{+0}	1.037	1.0135 ± 0.0076	-3.09	1.0458 ± 0.0080	+1.09	1.0295 ± 0.0076	-0.99	1.0496 ± 0.0080	+1.58
$C^{D^0}_{UncorDL}$	1.0	1.008 ± 0.016	+0.55	1.020 ± 0.016	+1.31	0.990 ± 0.016	-0.66	1.016 ± 0.016	+1.02
$C^{D^0}_{UncorCL}$	1.0	1.024 ± 0.016	+1.53	0.970 ± 0.017	-1.81	0.965 ± 0.017	-2.13	0.979 ± 0.015	-1.68
$C^{D^0}_{CascL}$	1.0	0.981 ± 0.022	-0.88	1.013 ± 0.024	+0.55	1.028 ± 0.023	+1.25	1.023 ± 0.018	+1.27
$C^{D^+}_{UncorDL}$	1.0	1.005 ± 0.035	+0.15	0.985 ± 0.042	-0.35	0.974 ± 0.037	-0.70	1.105 ± 0.042	+2.50
$C^{D^+}_{UncorCL}$	1.0	1.004 ± 0.034	+0.13	0.969 ± 0.036	-0.87	0.970 ± 0.031	-0.98	0.979 ± 0.034	-0.62
$C^{D^+}_{CascL}$	1.0	0.988 ± 0.057	-0.21	1.029 ± 0.059	+0.50	0.997 ± 0.052	-0.05	0.962 ± 0.053	-0.71
χ^2/ndof (P-value)		203/220 (0.79)		245/219 (0.08)		195/222 (0.91)		220/220 (0.48)	
χ^2_{Val}			19.2		11.1		12.5		17.5

Table 22: [**MC vs MC (Parameter set b)**] Validation fit results using parameter set b.

f_{+0} floated	Input	Split A		Split B		Split C		Split D	
	(Set c)	fit result	pulls	fit result	pulls	fit result	pulls	fit result	pulls
ρ_D^2	1.17	1.133 ± 0.027	-1.38	1.194 ± 0.024	+1.00	1.160 ± 0.026	-0.37	1.173 ± 0.026	+0.11
ρ^2	1.23	1.258 ± 0.021	+1.33	1.238 ± 0.021	+0.40	1.204 ± 0.021	-1.27	1.255 ± 0.021	+1.21
R_1	1.417	1.457 ± 0.029	+1.40	1.408 ± 0.028	-0.30	1.375 ± 0.026	-1.59	1.453 ± 0.029	+1.25
R_2	0.836	0.792 ± 0.025	-1.77	0.831 ± 0.024	-0.21	0.865 ± 0.023	+1.26	0.805 ± 0.025	-1.24
$\mathcal{B}(B^+ \to \bar{D}^0 \ell^+ \nu)$	0.0233	0.02319 ± 0.00019	-0.61	0.02361 ± 0.00018	+1.67	0.02335 ± 0.00019	+0.25	0.02340 ± 0.00019	+0.52
$\mathcal{B}(B^+ \to \bar{D}^{*0} \ell^+ \nu)$	0.0583	0.05855 ± 0.00026	+0.94	0.05791 ± 0.00026	-1.49	0.05837 ± 0.00027	+0.25	0.05797 ± 0.00026	-1.26
$\mathcal{BT}(B^+ \to \bar{D}^{**0} \ell^+ \nu)$	0.018	0.01804 ± 0.00027	+0.15	0.01809 ± 0.00027	+0.33	0.01807 ± 0.00027	+0.25	0.01806 ± 0.00027	+0.23
f_{+0}	1.037	1.0151 ± 0.0076	-2.90	1.0471 ± 0.0076	+1.33	1.0299 ± 0.0077	-0.93	1.0491 ± 0.0078	+1.55
$C_{UncorDL}^{D^0}$	0.9	0.909 ± 0.015	+0.58	0.920 ± 0.014	+1.38	0.889 ± 0.015	-0.73	0.916 ± 0.015	+1.04
$C_{UncorCL}^{D^0}$	0.8	0.823 ± 0.016	+1.44	0.770 ± 0.016	-1.89	0.767 ± 0.016	-2.02	0.779 ± 0.016	-1.33
$C_{CascL}^{D^0}$	0.9	0.882 ± 0.023	-0.77	0.913 ± 0.023	+0.58	0.927 ± 0.023	+1.18	0.920 ± 0.023	+0.88
$C_{UncorDL}^{D^+}$	0.9	0.909 ± 0.042	+0.22	0.887 ± 0.042	-0.39	0.875 ± 0.042	-0.60	1.004 ± 0.042	+2.48
$C_{UncorCL}^{D^+}$	0.8	0.804 ± 0.035	+0.12	0.769 ± 0.032	-0.96	0.768 ± 0.035	-0.91	0.777 ± 0.035	-0.64
$C_{CascL}^{D^+}$	1.2	1.189 ± 0.058	-0.19	1.234 ± 0.057	+0.60	1.200 ± 0.058	-0.01	1.163 ± 0.058	-0.63
χ^2/ndof (P-value)		207/219 (0.72)		249/219 (0.08)		192/221 (0.92)		217/220 (0.54)	
χ^2_{Val}			18.5		13.5		12.1		14.2

Table 23: [**MC vs MC (Parameter set c)**] Validation fit results using parameter set c.

f_{+0} floated	Input	Split A		Split B		Split C		Split D	
	(Set d)	fit result	pulls	fit result	pulls	fit result	pulls	fit result	pulls
ρ_D^2	1.3	1.267 ± 0.023	-1.43	1.321 ± 0.021	+0.97	1.290 ± 0.023	-0.43	1.301 ± 0.023	+0.04
ρ^2	1.3	1.330 ± 0.023	+1.27	1.313 ± 0.024	+0.56	1.275 ± 0.023	-1.06	1.333 ± 0.024	+1.38
R_1	1.5	1.543 ± 0.034	+1.28	1.494 ± 0.033	-0.17	1.455 ± 0.031	-1.42	1.550 ± 0.036	+1.40
R_2	0.6	0.553 ± 0.030	-1.54	0.588 ± 0.030	-0.40	0.631 ± 0.029	+1.08	0.555 ± 0.032	-1.42
$\mathcal{B}(B^+ \to \bar{D}^0 \ell^+ \nu)$	0.0233	0.02342 ± 0.00019	-0.51	0.02362 ± 0.00019	+1.73	0.02333 ± 0.00019	+0.19	0.02341 ± 0.00019	+0.60
$\mathcal{B}(B^+ \to \bar{D}^{*0} \ell^+ \nu)$	0.0583	0.05850 ± 0.00025	+0.77	0.05787 ± 0.00025	-1.72	0.05838 ± 0.00026	+0.32	0.05798 ± 0.00026	-1.26
$\mathcal{BT}(B^+ \to \bar{D}^{**0} \ell^+ \nu)$	0.018	0.01802 ± 0.00027	+0.09	0.01812 ± 0.00027	+0.43	0.01807 ± 0.00027	+0.24	0.01805 ± 0.00027	+0.17
f_{+0}	1.037	1.0156 ± 0.0074	-2.91	1.0482 ± 0.0077	+1.46	1.0298 ± 0.0077	-0.93	1.0484 ± 0.0079	+1.45
$C_{UncorDL}^{D^0}$	0.9	0.909 ± 0.015	+0.57	0.920 ± 0.015	+1.31	0.889 ± 0.015	-0.70	0.918 ± 0.015	+1.14
$C_{UncorCL}^{D^0}$	0.8	0.820 ± 0.015	+1.36	0.771 ± 0.016	-1.84	0.767 ± 0.016	-1.97	0.777 ± 0.016	-1.48
$C_{CascL}^{D^0}$	0.9	0.887 ± 0.023	-0.58	0.912 ± 0.023	+0.52	0.926 ± 0.023	+1.15	0.922 ± 0.023	+0.94
$C_{UncorDL}^{D^+}$	0.9	0.910 ± 0.042	+0.23	0.888 ± 0.042	-0.28	0.876 ± 0.042	-0.59	1.004 ± 0.042	+2.49
$C_{UncorCL}^{D^+}$	0.8	0.805 ± 0.032	+0.16	0.771 ± 0.035	-0.84	0.769 ± 0.035	-0.88	0.774 ± 0.035	-0.72
$C_{CascL}^{D^+}$	1.2	1.186 ± 0.056	-0.25	1.229 ± 0.057	+0.50	1.194 ± 0.058	-0.11	1.171 ± 0.058	-0.50
χ^2/ndof (P-value)		208/219 (0.69)		249/219 (0.08)		194/221 (0.91)		217/220 (0.54)	
χ^2_{Val}			19.2		13.4		11.7		14.1

Table 24: [**MC vs MC (Parameter set d)**] Validation fit results using parameter set d.

f_{+0} fixed	Input	Split A		Split B		Split C		Split D	
	(Set a)	fit result	pulls	fit result	pulls	fit result	pulls	fit result	pulls
ρ_D^2	1.17	1.145 ± 0.026	-0.94	1.189 ± 0.025	+0.75	1.165 ± 0.026	-0.19	1.167 ± 0.026	-0.11
ρ^2	1.23	1.264 ± 0.021	+1.64	1.236 ± 0.021	+0.28	1.206 ± 0.021	-1.15	1.252 ± 0.021	+1.04
R_1	1.417	1.464 ± 0.029	+1.60	1.407 ± 0.028	-0.36	1.378 ± 0.026	-1.46	1.449 ± 0.029	+1.09
R_2	0.836	0.792 ± 0.025	-1.75	0.830 ± 0.025	-0.24	0.864 ± 0.023	+1.20	0.805 ± 0.025	-1.26
$\mathcal{B}(B^+ \to \bar{D}^0 \ell^+ \nu)$	0.0233	0.02335 ± 0.00018	+0.28	0.02353 ± 0.00018	+1.28	0.02341 ± 0.00018	+0.61	0.02331 ± 0.00018	+0.04
$\mathcal{B}(B^+ \to \bar{D}^{*0} \ell^+ \nu)$	0.0583	0.05821 ± 0.00024	-0.36	0.05805 ± 0.00024	-1.02	0.05826 ± 0.00024	-0.17	0.05817 ± 0.00024	-0.54
$\mathcal{BT}(B^+ \to \bar{D}^{**0} \ell^+ \nu)$	0.018	0.01817 ± 0.00027	+0.61	0.01805 ± 0.00027	+0.19	0.01811 ± 0.00027	+0.41	0.01799 ± 0.00027	-0.03
f_{+0}	1.037	1.037 (fixed)	0	1.037 (fixed)	0	1.037 (fixed)	0	1.037 (fixed)	0
$C^{D^0}_{UncorDL}$	1.0	1.007 ± 0.015	+0.46	1.021 ± 0.015	+1.36	0.989 ± 0.015	-0.71	1.017 ± 0.015	+1.08
$C^{D^0}_{UncorCL}$	1.0	1.018 ± 0.016	+1.07	0.973 ± 0.017	-1.63	0.964 ± 0.016	-2.21	0.979 ± 0.016	-1.31
$C^{D^0}_{CascL}$	1.0	0.980 ± 0.023	-0.86	1.014 ± 0.024	+0.59	1.027 ± 0.024	+1.15	1.024 ± 0.024	+1.03
$C^{D^+}_{UncorDL}$	1.0	1.040 ± 0.040	+0.98	0.974 ± 0.040	-0.64	0.984 ± 0.040	-0.40	1.086 ± 0.040	+2.14
$C^{D^+}_{UncorCL}$	1.0	1.010 ± 0.036	+0.27	0.966 ± 0.035	-0.95	0.972 ± 0.036	-0.78	0.975 ± 0.036	-0.69
$C^{D^+}_{CascL}$	1.0	1.002 ± 0.058	+0.03	1.027 ± 0.058	+0.46	1.000 ± 0.058	-0.004	0.956 ± 0.057	-0.76
χ^2/ndof (P-value)		213/221 (0.64)		252/220 (0.07)		193/222 (0.92)		220/221 (0.50)	
χ^2_{Val}			10.1		10.1		11.3		12.2

Table 25: [**MC vs MC (Parameter set a) f_{+0} fixed**] Validation fit results using parameter set a.

f_{+0} fixed	Input	Split A		Split B		Split C		Split D	
	(Set b)	fit result	pulls	fit result	pulls	fit result	pulls	fit result	pulls
ρ^2_D	1.17	1.141 ± 0.029	-1.00	1.193 ± 0.027	+0.85	1.164 ± 0.027	-0.22	1.167 ± 0.028	-0.10
ρ^2	1.23	1.265 ± 0.020	+1.77	1.234 ± 0.020	+0.20	1.209 ± 0.018	-1.20	1.250 ± 0.020	+1.03
R_1	1.417	1.463 ± 0.027	+1.67	1.405 ± 0.026	-0.46	1.382 ± 0.024	-1.42	1.446 ± 0.027	+1.07
R_2	0.836	0.792 ± 0.023	-1.88	0.832 ± 0.023	-0.18	0.862 ± 0.021	+1.23	0.806 ± 0.023	-1.27
$\mathcal{B}(B^+ \to \bar{D}^0 \ell^+ \nu)$	0.0215	0.02154 ± 0.00018	+0.22	0.02173 ± 0.00018	+1.29	0.02161 ± 0.00017	+0.68	0.02151 ± 0.00018	+0.05
$\mathcal{B}(B^+ \to \bar{D}^{*0} \ell^+ \nu)$	0.065	0.06494 ± 0.00025	-0.24	0.06475 ± 0.00025	-0.98	0.06495 ± 0.00023	-0.21	0.06486 ± 0.00025	-0.55
$\mathcal{BT}(B^+ \to \bar{D}^{**0} \ell^+ \nu)$	0.0215	0.02168 ± 0.00029	+0.64	0.02157 ± 0.00028	+0.25	0.02160 ± 0.00028	+0.38	0.02151 ± 0.00029	+0.02
f_{+0}	1.037	1.037 (fixed)	0	1.037 (fixed)	0	1.037 (fixed)	0	1.037 (fixed)	0
$C^{D^0}_{UncorDL}$	1.0	1.006 ± 0.016	+0.39	1.021 ± 0.015	+1.37	0.989 ± 0.015	-0.71	1.017 ± 0.016	+1.08
$C^{D^0}_{UncorCL}$	1.0	1.018 ± 0.017	+1.10	0.972 ± 0.017	-1.68	0.963 ± 0.016	-2.30	0.978 ± 0.016	-1.31
$C^{D^0}_{CascL}$	1.0	0.979 ± 0.024	-0.90	1.014 ± 0.024	+0.58	1.028 ± 0.023	+1.18	1.024 ± 0.024	+1.01
$C^{D^+}_{UncorDL}$	1.0	1.039 ± 0.041	+0.97	0.973 ± 0.040	-0.67	0.984 ± 0.040	-0.39	1.086 ± 0.040	+2.14
$C^{D^+}_{UncorCL}$	1.0	1.011 ± 0.036	+0.30	0.966 ± 0.035	-0.95	0.972 ± 0.036	-0.78	0.975 ± 0.036	-0.69
$C^{D^+}_{CascL}$	1.0	1.002 ± 0.058	+0.03	1.024 ± 0.058	+0.41	1.002 ± 0.057	+0.03	0.956 ± 0.058	-0.77
χ^2/ndof (P-value)		212/221 (0.66)		251/220 (0.07)		195/223 (0.91)		123/221 (0.46)	
χ^2_{Val}			10.1		9.9		12.5		12.3

Table 26: [**MC vs MC (Parameter set b) f_{+0} fixed**] Validation fit results using parameter set b.

f_{+0} fixed	Input	Split A		Split B		Split C		Split D	
	(Set c)	fit result	pulls	fit result	pulls	fit result	pulls	fit result	pulls
ρ_D^2	1.17	1.145 ± 0.026	-0.97	1.190 ± 0.025	+0.80	1.164 ± 0.026	-0.24	1.167 ± 0.026	-0.12
ρ^2	1.23	1.265 ± 0.021	+1.72	1.235 ± 0.021	+0.22	1.206 ± 0.020	-1.16	1.251 ± 0.021	+1.02
R_1	1.417	1.465 ± 0.029	+1.67	1.405 ± 0.028	-0.44	1.378 ± 0.026	-1.50	1.449 ± 0.029	+1.12
R_2	0.836	0.791 ± 0.025	-1.83	0.832 ± 0.024	-0.17	0.865 ± 0.023	+1.24	0.806 ± 0.025	-1.21
$\mathcal{B}(B^+ \to \bar{D}^0 \ell^+ \nu)$	0.0233	0.02335 ± 0.00018	+0.30	0.02353 ± 0.00018	+1.30	0.02340 ± 0.00018	+0.56	0.02331 ± 0.00018	+0.04
$\mathcal{B}(B^+ \to \bar{D}^{*0} \ell^+ \nu)$	0.0583	0.05822 ± 0.00024	-0.32	0.05805 ± 0.00024	-1.04	0.05826 ± 0.00024	-0.16	0.05814 ± 0.00024	-0.66
$\mathcal{BT}(B^+ \to \bar{D}^{**0} \ell^+ \nu)$	0.018	0.01815 ± 0.00027	+0.56	0.01804 ± 0.00027	+0.15	0.01810 ± 0.00027	+0.38	0.01801 ± 0.00027	+0.02
f_{+0}	1.037	1.037 (fixed)	0	1.037 (fixed)	0	1.037 (fixed)	0	1.037 (fixed)	0
$C_{UncorDL}^{D^0}$	0.9	0.907 ± 0.015	+0.46	0.920 ± 0.015	+1.38	0.888 ± 0.015	-0.77	0.917 ± 0.015	+1.11
$C_{UncorCL}^{D^0}$	0.8	0.818 ± 0.016	+1.10	0.773 ± 0.016	-1.72	0.766 ± 0.016	-2.14	0.782 ± 0.016	-1.14
$C_{CascL}^{D^0}$	0.9	0.881 ± 0.023	-0.85	0.914 ± 0.023	+0.61	0.926 ± 0.023	+1.16	0.921 ± 0.023	+0.91
$C_{UncorDL}^{D^+}$	0.9	0.941 ± 0.040	+1.01	0.873 ± 0.040	-0.67	0.885 ± 0.040	-0.37	0.986 ± 0.040	+2.15
$C_{UncorCL}^{D^+}$	0.8	0.809 ± 0.035	+0.24	0.767 ± 0.035	-0.94	0.769 ± 0.035	-0.87	0.775 ± 0.035	-0.72
$C_{CascL}^{D^+}$	1.2	1.204 ± 0.058	+0.07	1.227 ± 0.057	+0.47	1.204 ± 0.058	+0.07	1.156 ± 0.057	-0.77
χ^2/ndof (P-value)		215/220 (0.59)		251/220 (0.08)		193/222 (0.92)		220/221 (0.51)	
χ^2_{Val}			10.0		11.4		11.2		11.8

Table 27: [**MC vs MC (Parameter set c) f_{+0} fixed**] Validation fit results using parameter set c.

f_{+0} fixed	Input	Split A		Split B		Split C		Split D	
	(Set d)	fit result	pulls	fit result	pulls	fit result	pulls	fit result	pulls
ρ^2_D	1.3	1.277 ± 0.022	-1.06	1.316 ± 0.022	+0.75	1.293 ± 0.022	-0.31	1.296 ± 0.021	-0.17
ρ^2	1.3	1.338 ± 0.023	+1.65	1.309 ± 0.024	+0.36	1.278 ± 0.023	-0.95	1.329 ± 0.023	+1.25
R_1	1.5	1.554 ± 0.035	+1.54	1.488 ± 0.034	-0.34	1.459 ± 0.031	-1.32	1.544 ± 0.033	+1.34
R_2	0.6	0.548 ± 0.031	-1.69	0.591 ± 0.031	-0.30	0.630 ± 0.029	+1.03	0.558 ± 0.030	-1.40
$\mathcal{B}(B^+ \to \bar{D}^0 \ell^+ \nu)$	0.0233	0.02337 ± 0.00018	+0.37	0.02354 ± 0.00018	+1.34	0.02339 ± 0.00018	+0.50	0.02333 ± 0.00018	+0.17
$\mathcal{B}(B^+ \to \bar{D}^{*0} \ell^+ \nu)$	0.0583	0.05819 ± 0.00023	-0.50	0.05802 ± 0.00023	-1.19	0.05828 ± 0.00023	-0.09	0.05814 ± 0.00023	-0.71
$\mathcal{BT}(B^+ \to \bar{D}^{**0} \ell^+ \nu)$	0.018	0.01813 ± 0.00027	+0.48	0.01806 ± 0.00027	+0.24	0.01810 ± 0.00027	+0.38	0.01799 ± 0.00025	-0.02
f_{+0}	1.037	1.037 (fixed)	0	1.037 (fixed)	0	1.037 (fixed)	0	1.037 (fixed)	0
$C^{D^0}_{UncorDL}$	0.9	0.908 ± 0.015	+0.49	0.920 ± 0.015	+1.35	0.889 ± 0.016	-0.72	0.918 ± 0.014	+1.28
$C^{D^0}_{UncorCL}$	0.8	0.815 ± 0.016	+0.92	0.774 ± 0.016	-1.66	0.767 ± 0.016	-2.11	0.780 ± 0.015	-1.36
$C^{D^0}_{CascL}$	0.9	0.886 ± 0.023	-0.63	0.913 ± 0.023	+0.55	0.926 ± 0.023	+1.13	0.922 ± 0.023	+0.98
$C^{D^+}_{UncorDL}$	0.9	0.941 ± 0.040	+1.01	0.872 ± 0.040	-0.69	0.886 ± 0.040	-0.35	0.988 ± 0.040	+2.20
$C^{D^+}_{UncorCL}$	0.8	0.809 ± 0.035	+0.27	0.768 ± 0.035	-0.90	0.770 ± 0.035	-0.84	0.772 ± 0.035	-0.80
$C^{D^+}_{CascL}$	1.2	1.201 ± 0.057	+0.02	1.221 ± 0.057	+0.36	1.198 ± 0.057	-0.03	1.164 ± 0.056	-0.65
χ^2/ndof (P-value)		216/220 (0.57)		251/220 (0.07)		195/222 (0.91)		219/221 (0.52)	
χ^2_{Val}			9.7		11.0		11.0		12.4

Table 28: [**MC vs MC (Parameter set d)** f_{+0} **fixed**] Validation fit results using parameter set d.

D^0	Linear	Quadratic
Peak yield	719.9	719.1
Combinatrial yield	693.9	694.7
D^0	Linear	Quadratic
Peak yield	450.3	448.6
Combinatrial yield	2602.7	2604.7

Table 29: [**Toy MC : Mean and Standard Deviation (f_{+0} Fixed)**] Mean and standard deviation (r.m.s.) of pull distributions of toy MC by fixing $f_{+0} = 1.037$. The uncertainty on mean and standard deviation are also listed in the bottom line. Pulls are calculated from the difference to nominal fit results.

11.3 D mass sideband subtraction

We assume D mass sideband is flat when we do sideand subtraction. Here we check this assumption.

11.3.1 D mass fit

We try to fit OnPeak D mass plot with the following two combinations :

- 2 Gaussian + a linear function
- 2 Gaussina + a quadratic function

We use two Gaussinas with different width for the peak : one for signal and the other for peaking backgroud. We compare the yeild of sideband from linear and quadratic functions to make sure we get the similar results in both cases. Fitted plots are shown in Figure 78 for D^0 and in Figure 79 for D^+. Yeldsare given in Table 29. Yeilds difference is very small.

11.3.2 Sideband linearlity check

The linearlity of the sideband region may depend on kinematic variables : lepton momentum, D momentum and $\cos\Theta_{B-D\ell}$. To check the linearlity, we do the following.

1. Fit the sideband region with a linear function, $N(m_D) = am_D + b$, to get a and b
2. This allows to calculate a Poisson probability for i-th D candidate

$$p(m_k) = (am_k + b)e^{-(am_k+b)} \tag{315}$$

and a log likelifood

$$-\ln L = \sum_k [(am_k + b) - \ln(am_k + b)] \tag{316}$$

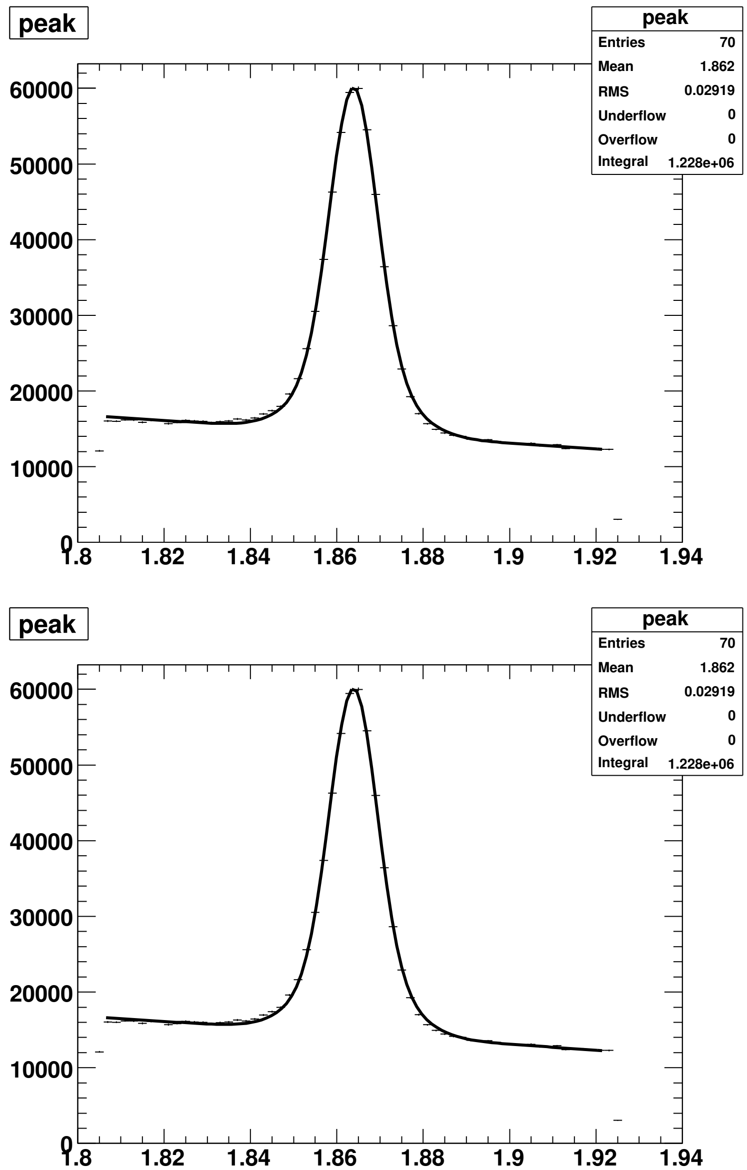

Figure 78: [D^0 **mass fit**] D^0 mass fit with linear function (top) and quadratic function (bottom).

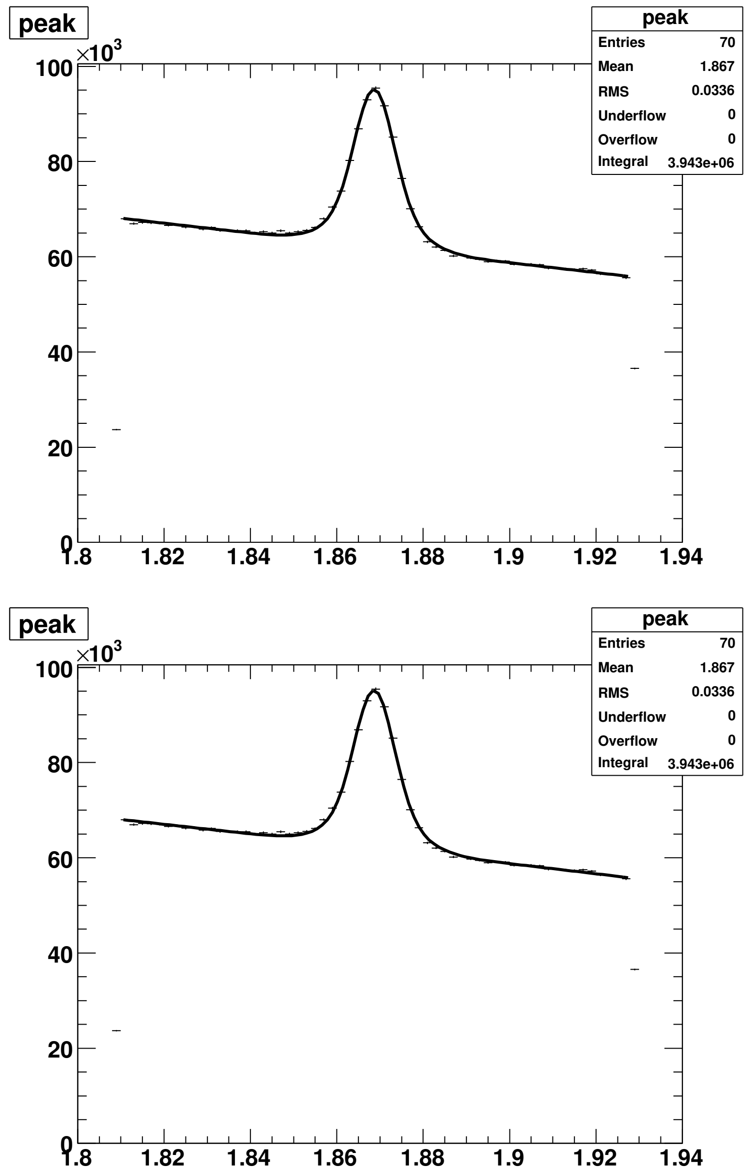

Figure 79: [D^0 **mass fit**] D^0 mass fit with linear function (top) and quadratic function (bottom).

3. If we assume the data is Gaussian, χ^2 is give by

$$\chi^2 = -2\ln L = 2\sum_k [(am_k + b) - \ln(am_k + b)] \tag{317}$$

4. We calculate P-value for each bin of $(p^*_\ell,\, p^*_D,\, \cos\Theta_{B-D\ell})$ and plot them.

12 Run by Run Differences

We compare "OnPeak - OffPeak" data with $B\bar{B}$ MC. $B\bar{B}$ MC is constructed using the parameters of nominal fit of Run2.

12.1 Electron only

12.1.1 RunX vs Run2

Run1 vs Run2 comparison is given in Figures 80-85.
Run3 vs Run2 comparison is given in Figures 86-91.
Run4 vs Run2 comparison is given in Figures 92-97.

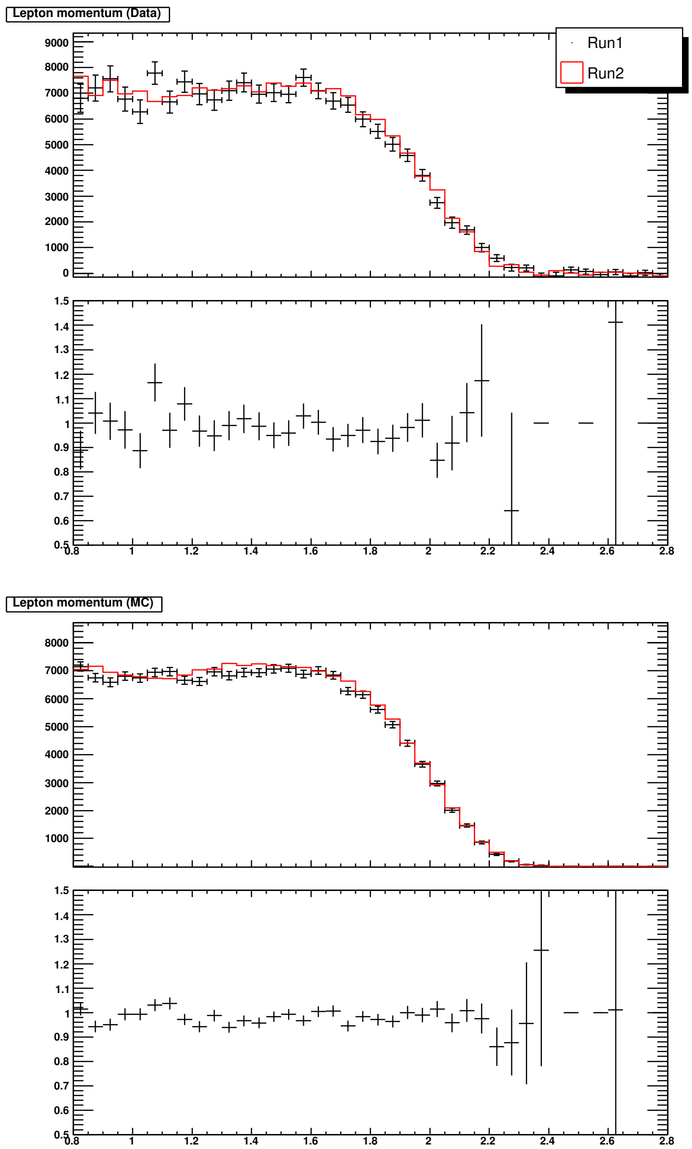

Figure 80: [**Run1 vs Run2 (Electron)** p_ℓ D^0] Run1 vs Run2 lepton momentum plot for (OnPeak - OffPeak) data (top) and $B\bar{B}$ MC (bottom) of D^0 (Electron only). Black lines with uncertainties are Run1 and red histograms are Run2.

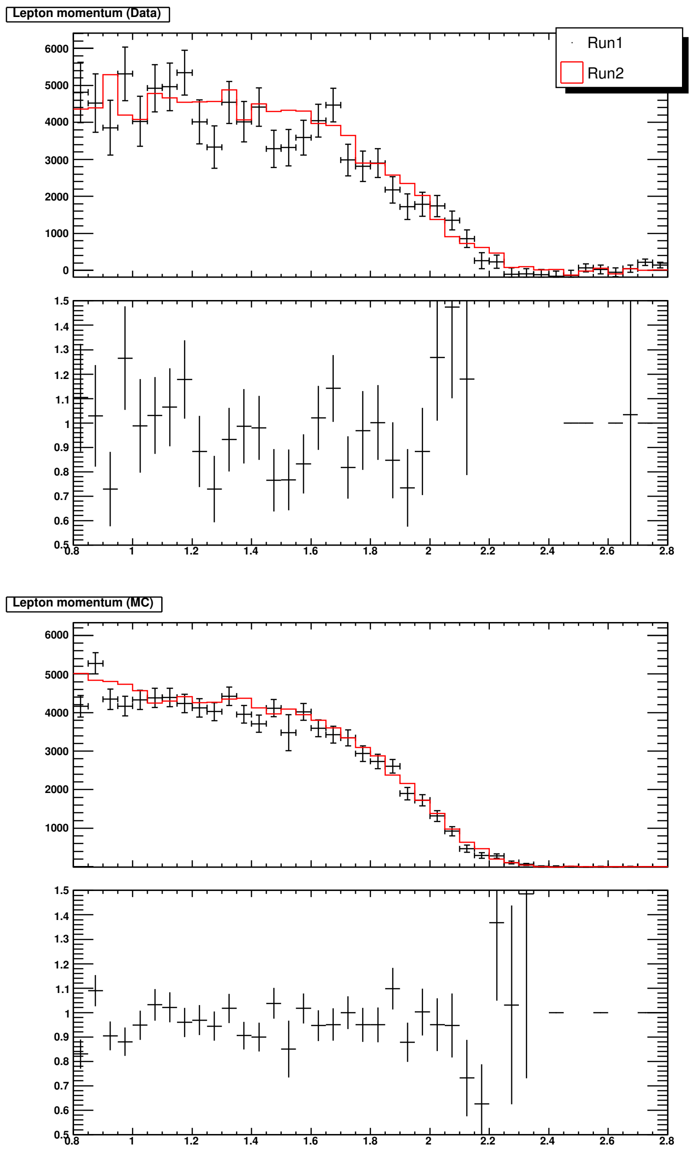

Figure 81: [**Run1 vs Run2 (Electron)** p_ℓ D^+] Run1 vs Run2 lepton momentum plot for (OnPeak - OffPeak) data (top) and $B\bar{B}$ MC (bottom) of D^+ (Electron only). Black lines with uncertainties are Run1 and red histograms are Run2.

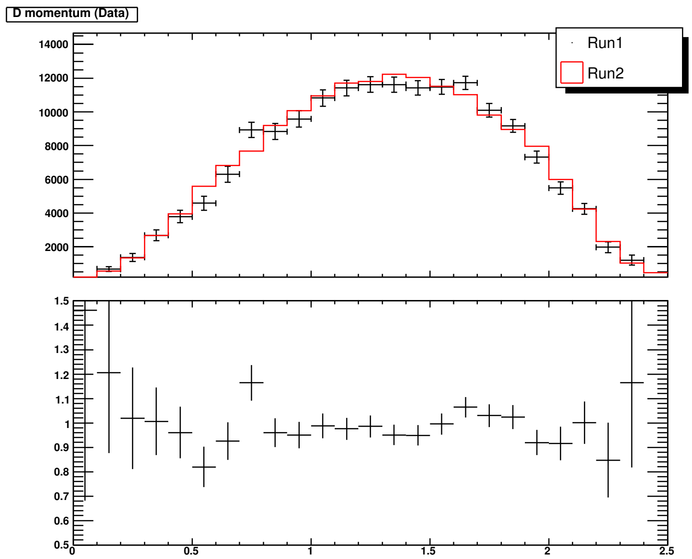

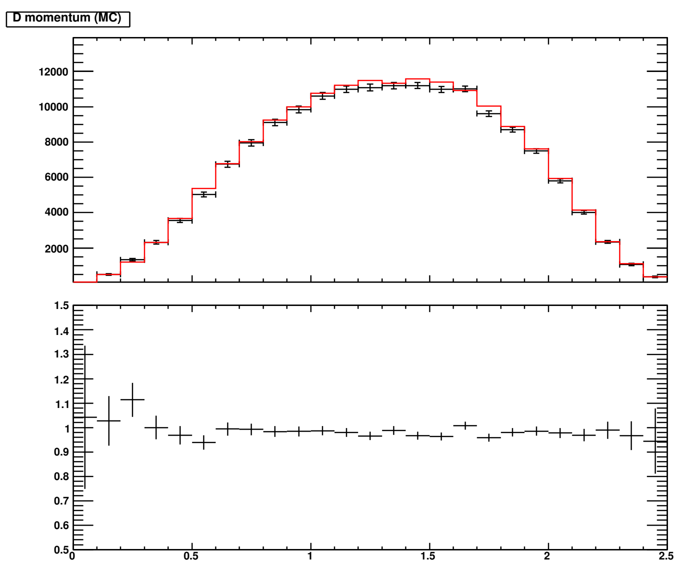

Figure 82: [**Run1 vs Run2 (Electron)** p_D D^0] Run1 vs Run2 D momentum plot for (OnPeak - OffPeak) data (top) and $B\bar{B}$ MC (bottom) of D^0 (Electron only). Black lines with uncertainties are Run1 and red histograms are Run2.

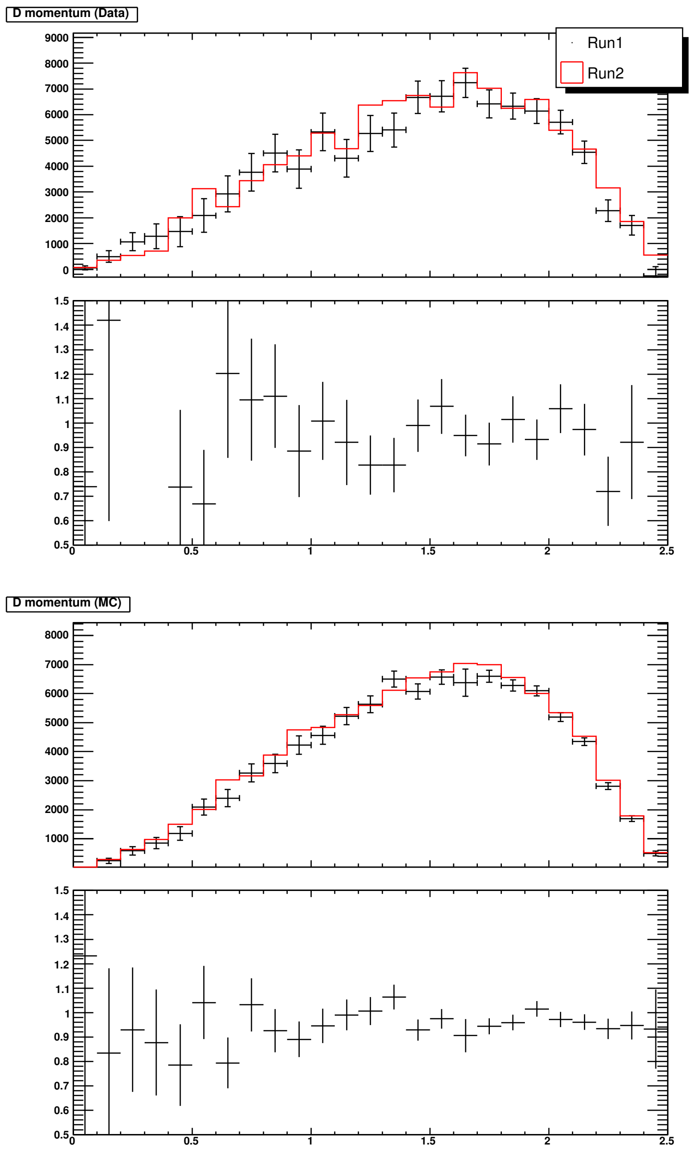

Figure 83: [**Run1 vs Run2 (Electron)** p_D D^+] Run1 vs Run2 D momentum plot for (OnPeak - OffPeak) data (top) and $B\bar{B}$ MC (bottom) of D^+ (Electron only). Black lines with uncertainties are Run1 and red histograms are Run2.

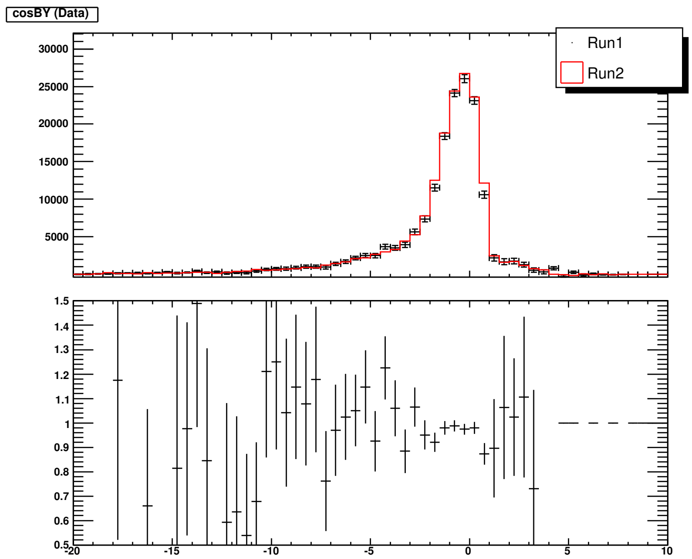

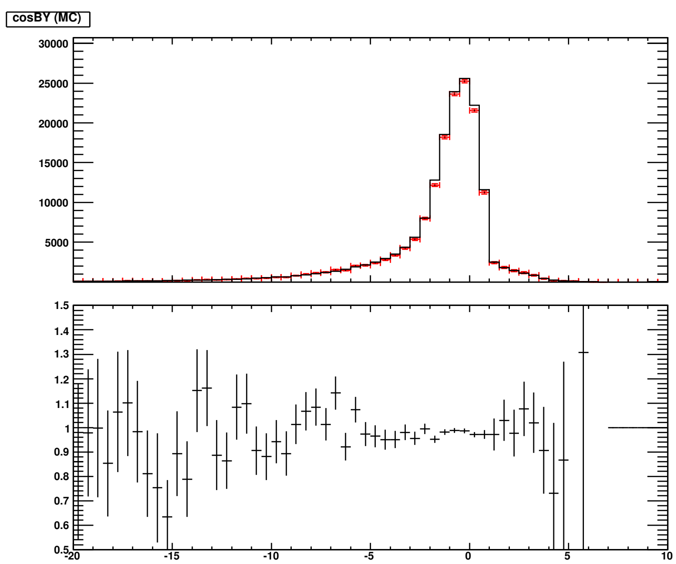

Figure 84: [**Run1 vs Run2 (Electron)** $\cos\Theta_{B-D\ell}$ D^0] Run1 vs Run2 $\cos\Theta_{B-D\ell}$ plot for (OnPeak - OffPeak) data (top) and $B\bar{B}$ MC (bottom) of D^0 (Electron only). Black lines with uncertainties are Run1 and red histograms are Run2.

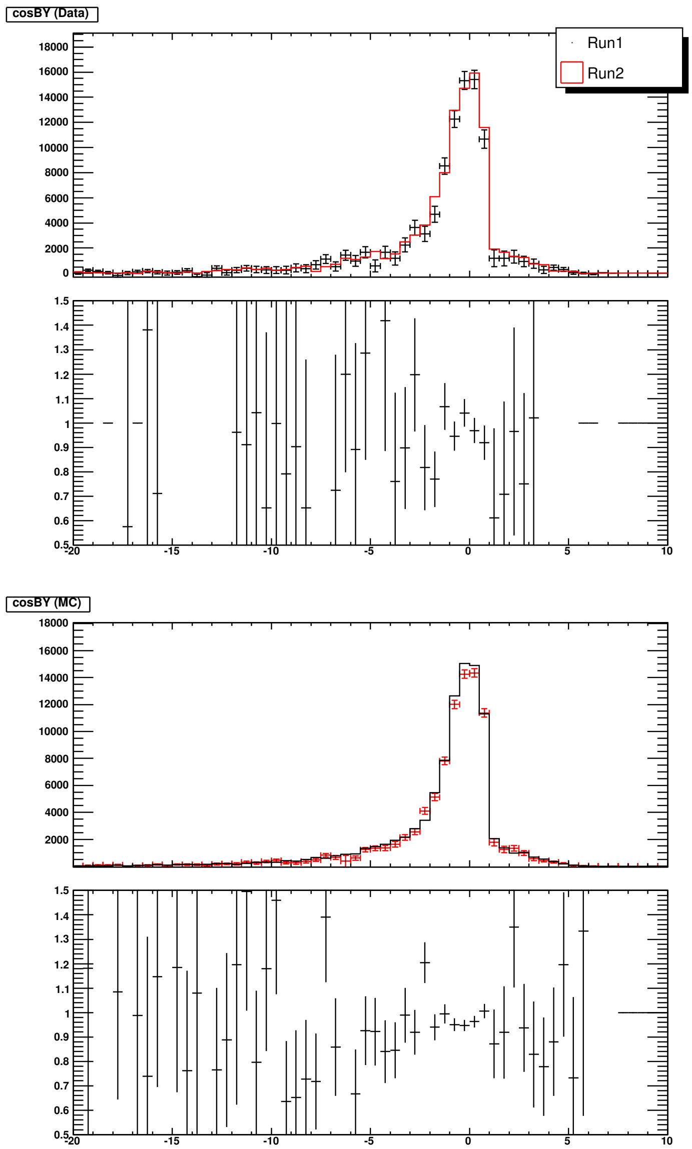

Figure 85: [**Run1 vs Run2 (Electron)** $\cos\Theta_{B-D\ell}$ D^+] Run1 vs Run2 $\cos\Theta_{B-D\ell}$ plot for (OnPeak - OffPeak) data (top) and $B\bar{B}$ MC (bottom) of D^+ (Electron only). Black lines with uncertainties are Run1 and red histograms are Run2.

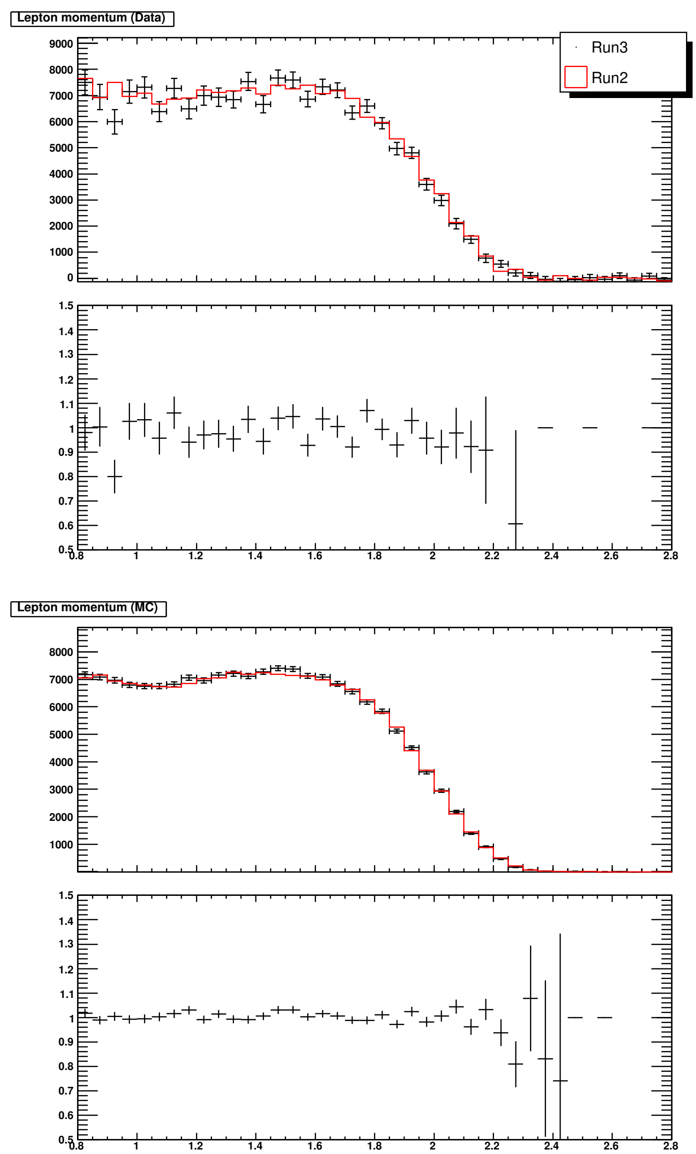

Figure 86: [**Run3 vs Run2 (Electron)** p_ℓ D^0] Run3 vs Run2 lepton momentum plot for (OnPeak - OffPeak) data (top) and $B\bar{B}$ MC (bottom) of D^0 (Electron only). Black lines with uncertainties are Run3 and red histograms are Run2.

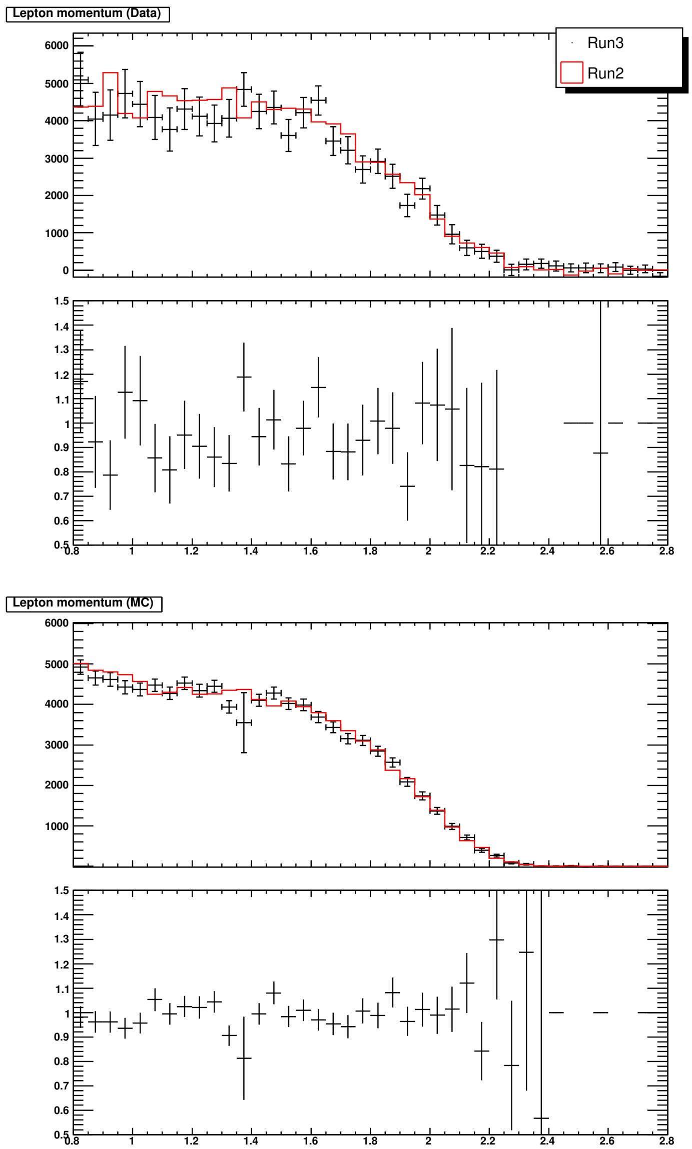

Figure 87: [**Run3 vs Run2 (Electron)** p_ℓ D^+] Run3 vs Run2 lepton momentum plot for (OnPeak - OffPeak) data (top) and $B\bar{B}$ MC (bottom) of D^+ (Electron only). Black lines with uncertainties are Run3 and red histograms are Run2.

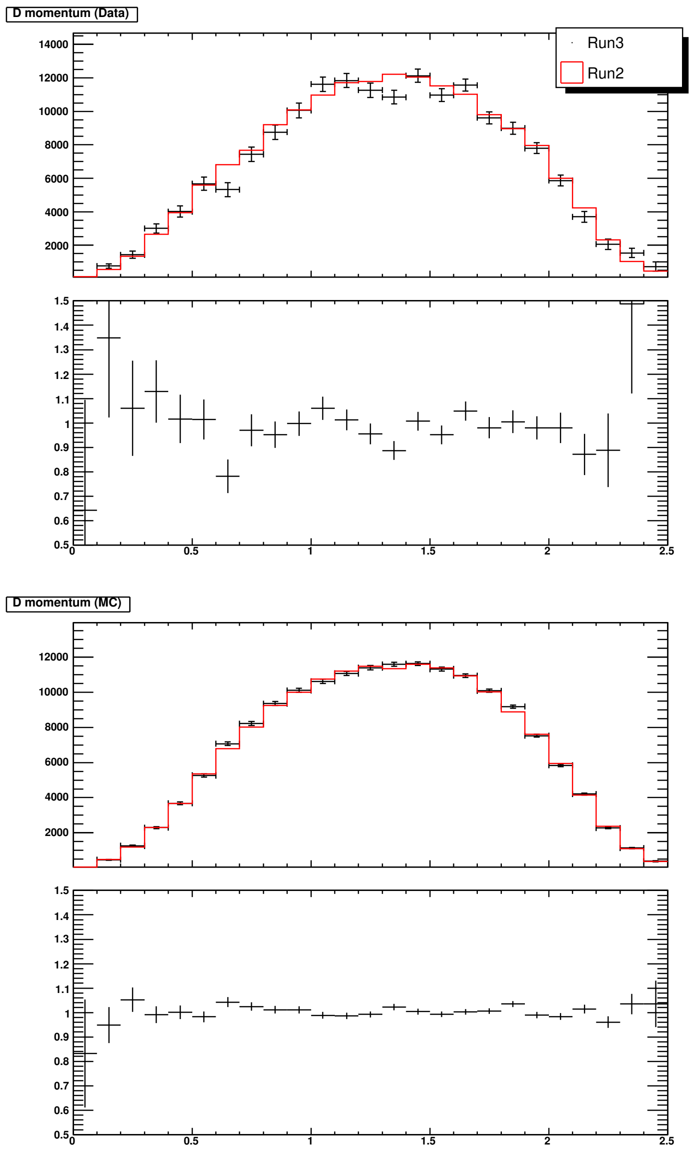

Figure 88: [**Run3 vs Run2 (Electron)** p_D D^0] Run3 vs Run2 D momentum plot for (OnPeak - OffPeak) data (top) and $B\bar{B}$ MC (bottom) of D^0 (Electron only). Black lines with uncertainties are Run3 and red histograms are Run2.

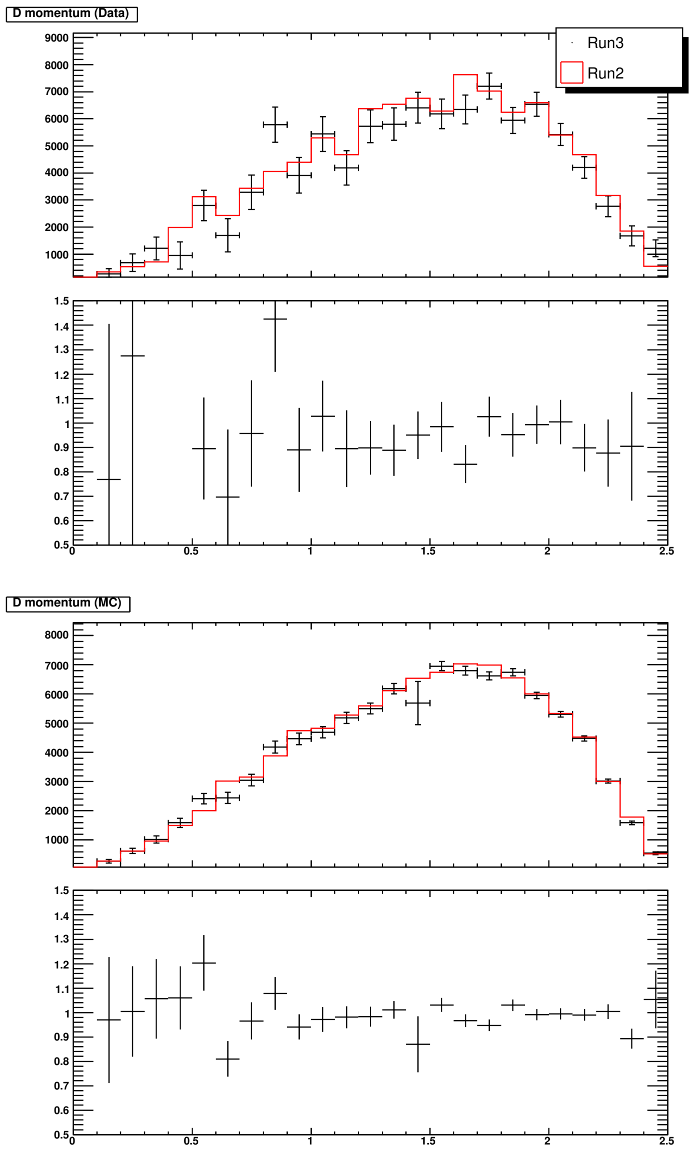

Figure 89: [**Run3 vs Run2 (Electron)** p_D D^+] Run3 vs Run2 D momentum plot for (OnPeak - OffPeak) data (top) and $B\bar{B}$ MC (bottom) of D^+ (Electron only). Black lines with uncertainties are Run3 and red histograms are Run2.

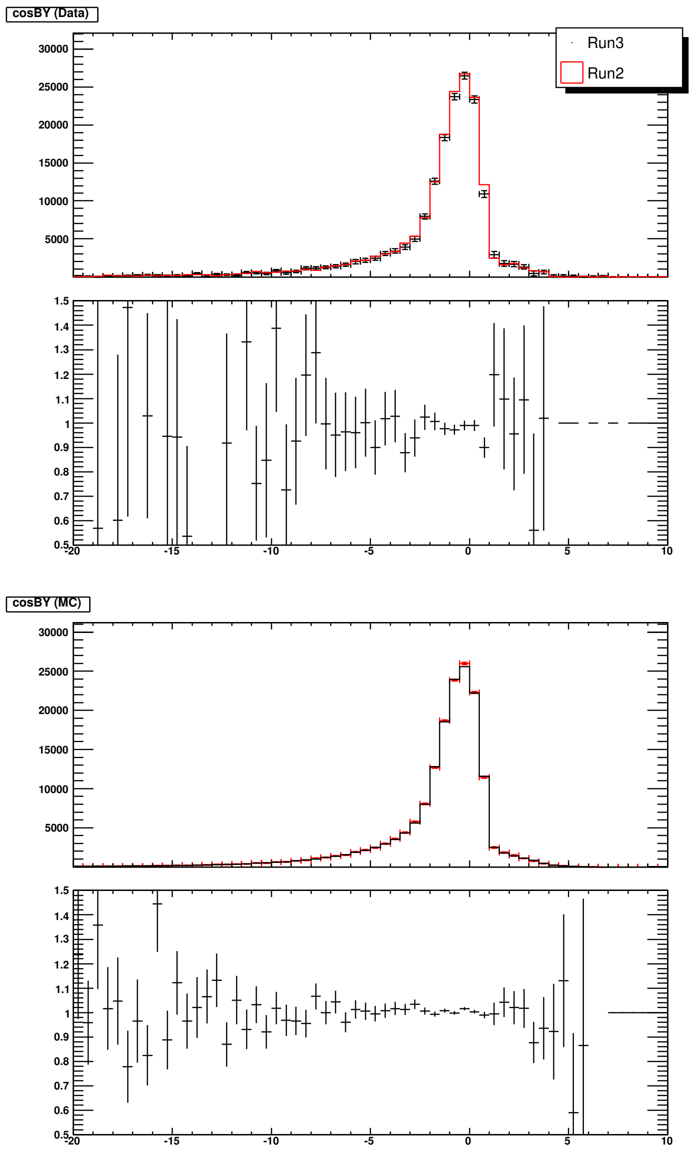

Figure 90: [**Run3 vs Run2 (Electron)** $\cos\Theta_{B-D\ell}$ D^0] Run3 vs Run2 $\cos\Theta_{B-D\ell}$ plot for (OnPeak - OffPeak) data (top) and $B\bar{B}$ MC (bottom) of D^0 (Electron only). Black lines with uncertainties are Run3 and red histograms are Run2.

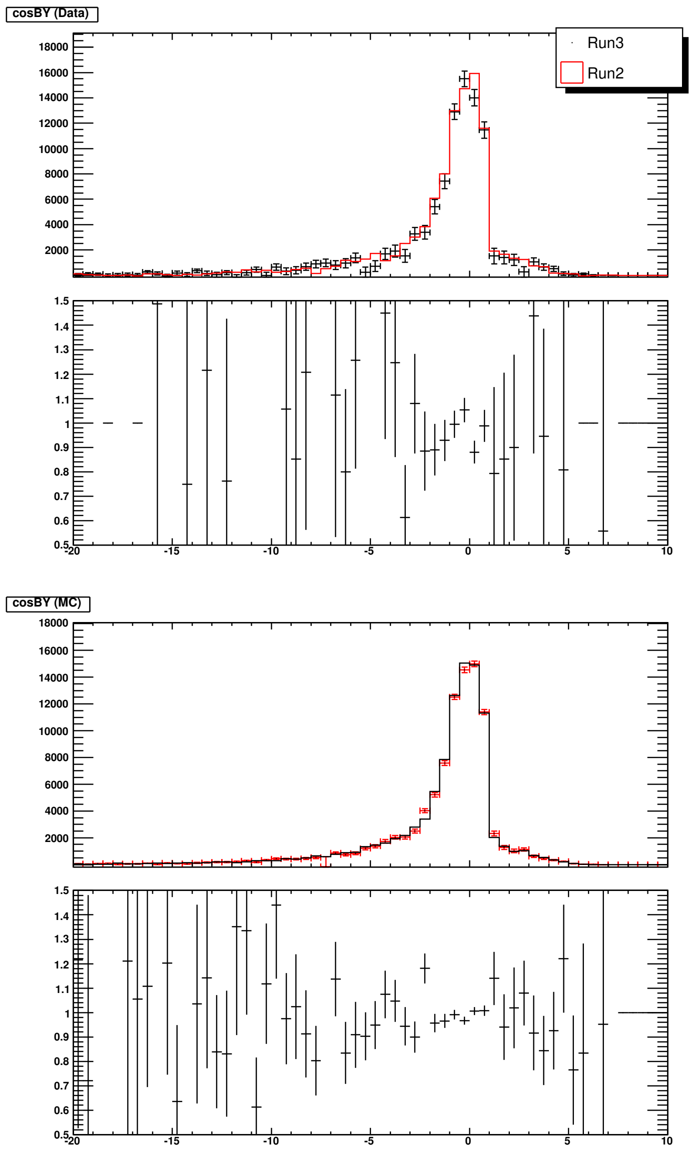

Figure 91: [**Run3 vs Run2 (Electron)** $\cos\Theta_{B-D\ell}$ D^{+}] Run3 vs Run2 $\cos\Theta_{B-D\ell}$ plot for (OnPeak - OffPeak) data (top) and $B\bar{B}$ MC (bottom) of D^{+} (Electron only). Black lines with uncertainties are Run3 and red histograms are Run2.

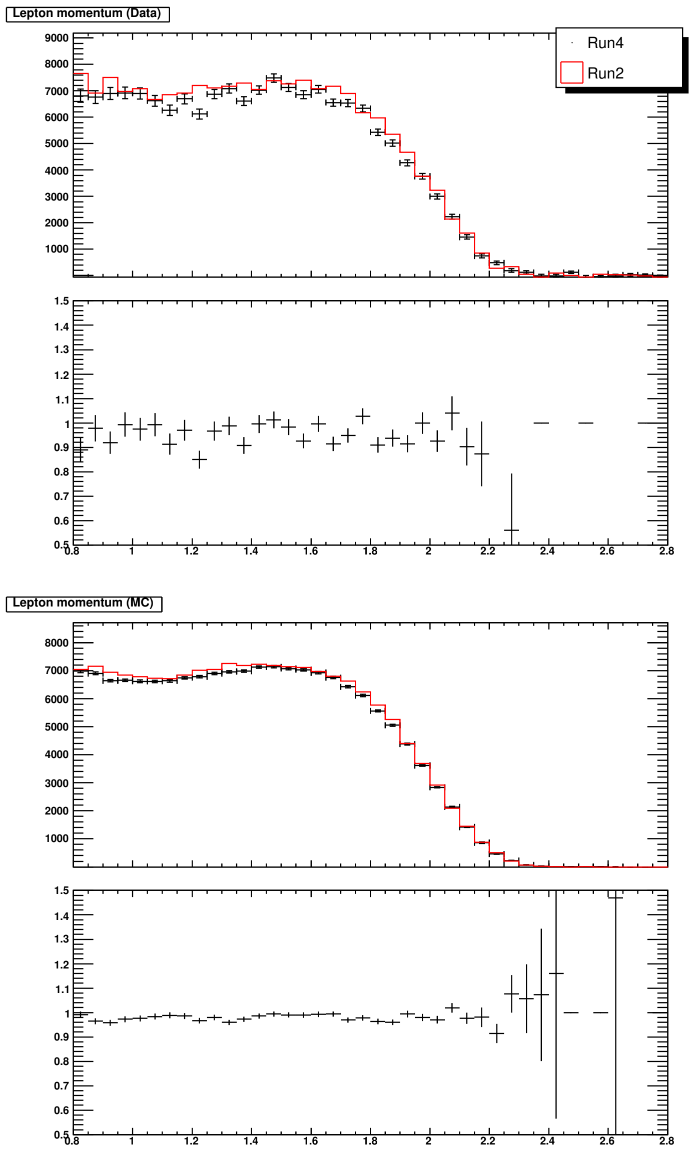

Figure 92: [**Run4 vs Run2 (Electron)** p_ℓ D^0] Run4 vs Run2 lepton momentum plot for (OnPeak - OffPeak) data (top) and $B\bar{B}$ MC (bottom) of D^0 (Electron only). Black lines with uncertainties are Run4 and red histograms are Run2.

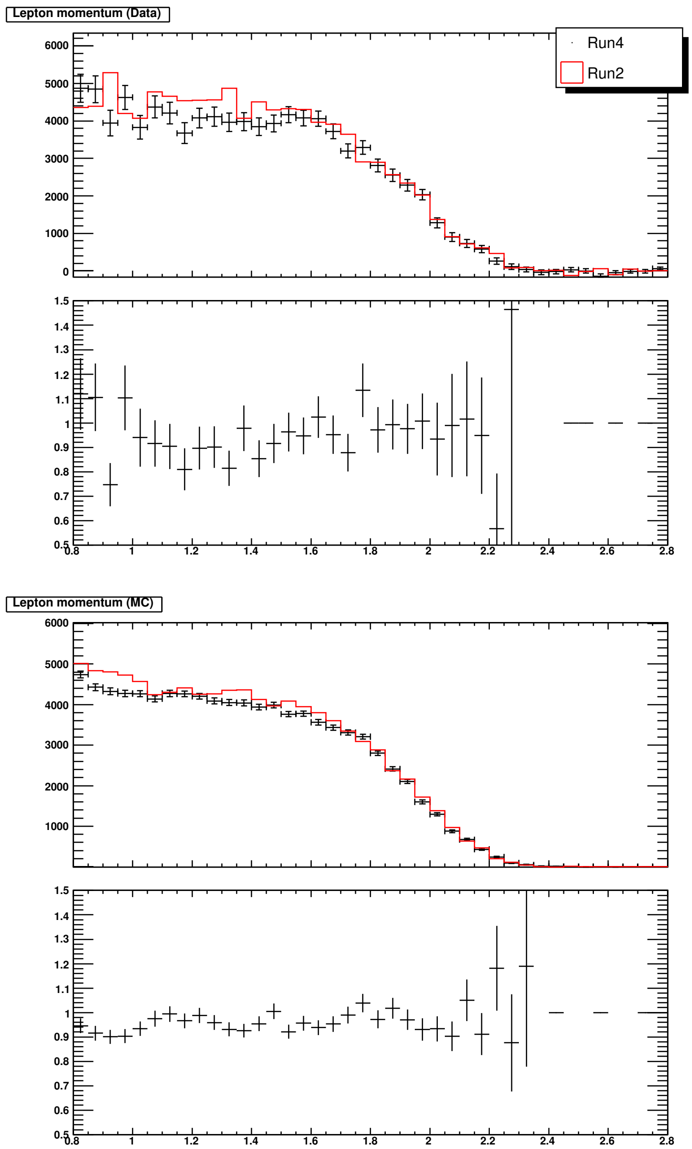

Figure 93: [**Run4 vs Run2 (Electron)** p_ℓ D^+] Run4 vs Run2 lepton momentum plot for (OnPeak - OffPeak) data (top) and $B\bar{B}$ MC (bottom) of D^+ (Electron only). Black lines with uncertainties are Run4 and red histograms are Run2.

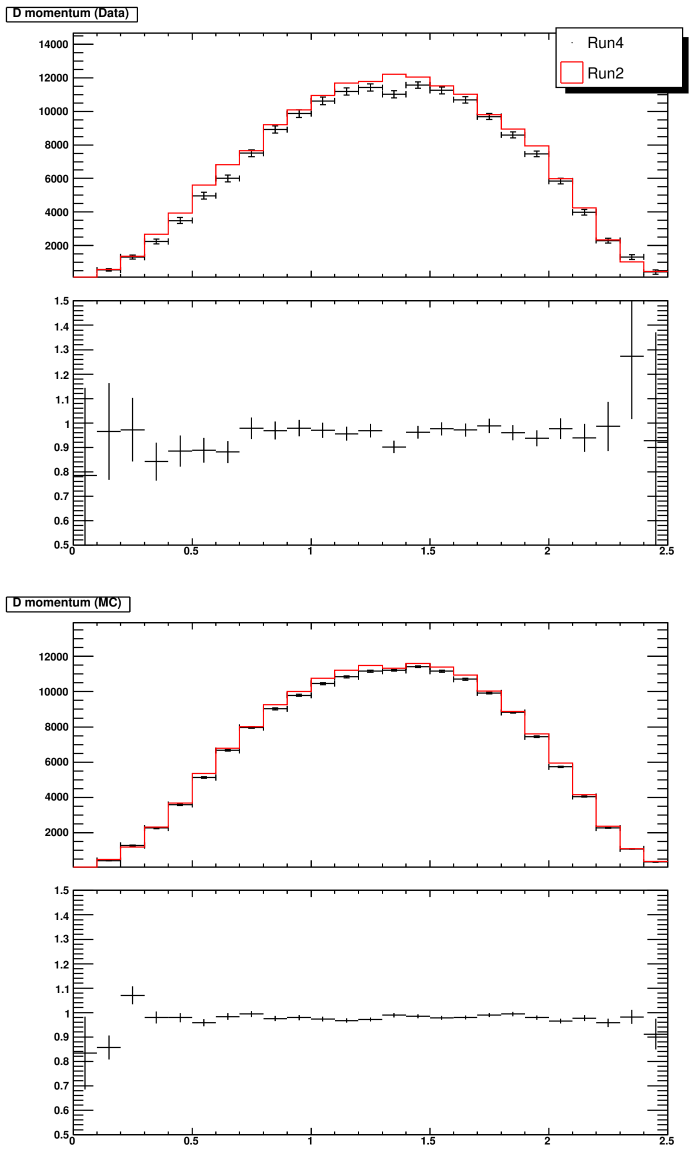

Figure 94: [**Run4 vs Run2 (Electron)** p_D D^0] Run4 vs Run2 D momentum plot for (OnPeak - OffPeak) data (top) and $B\bar{B}$ MC (bottom) of D^0 (Electron only). Black lines with uncertainties are Run4 and red histograms are Run2.

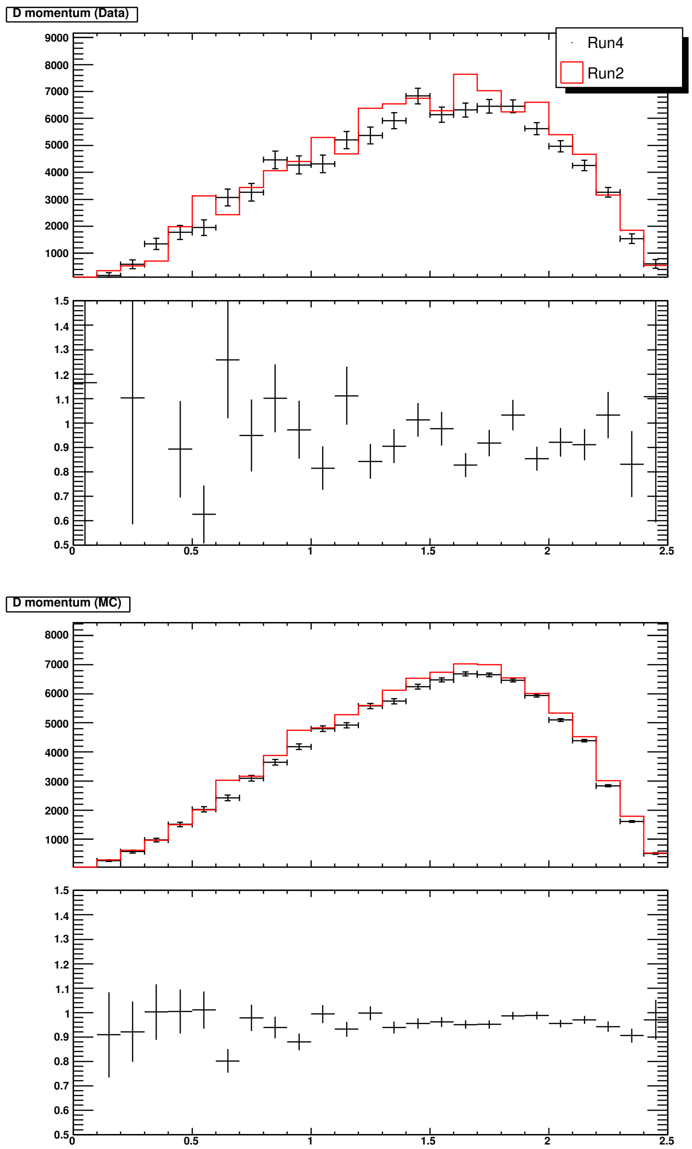

Figure 95: [**Run4 vs Run2 (Electron)** p_D D^+] Run4 vs Run2 D momentum plot for (OnPeak - OffPeak) data (top) and $B\bar{B}$ MC (bottom) of D^+ (Electron only). Black lines with uncertainties are Run4 and red histograms are Run2.

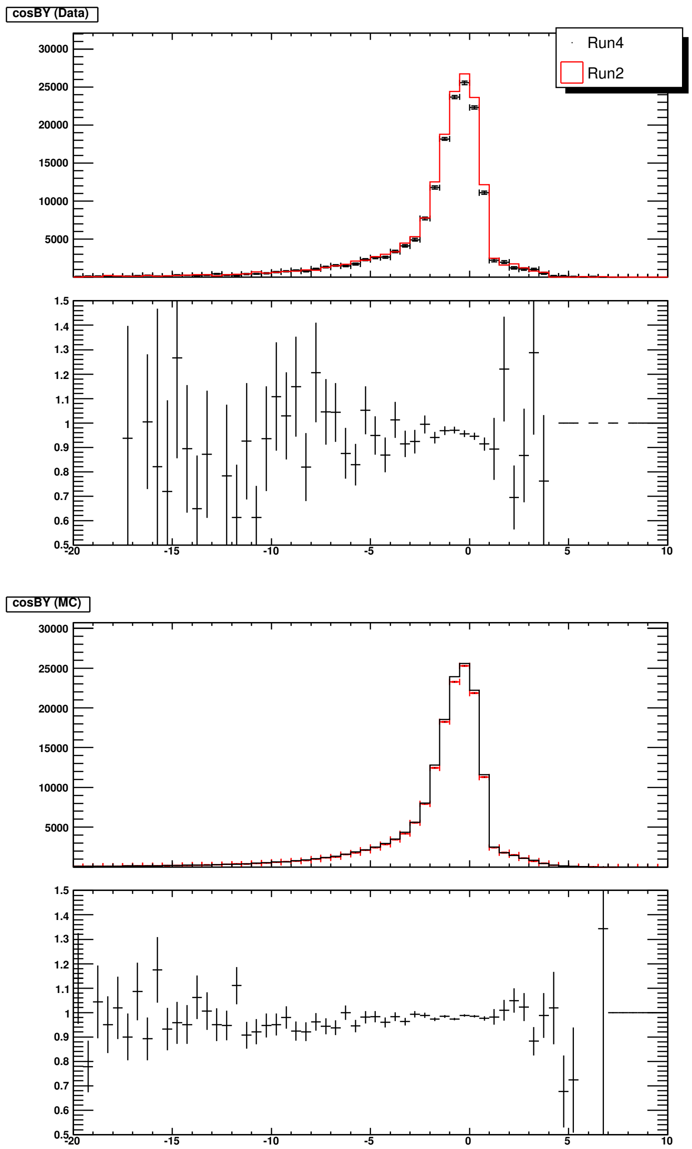

Figure 96: [**Run4 vs Run2 (Electron)** $\cos\Theta_{B-D\ell}$ D^0] Run4 vs Run2 $\cos\Theta_{B-D\ell}$ plot for (OnPeak - OffPeak) data (top) and $B\bar{B}$ MC (bottom) of D^0 (Electron only). Black lines with uncertainties are Run4 and red histograms are Run2.

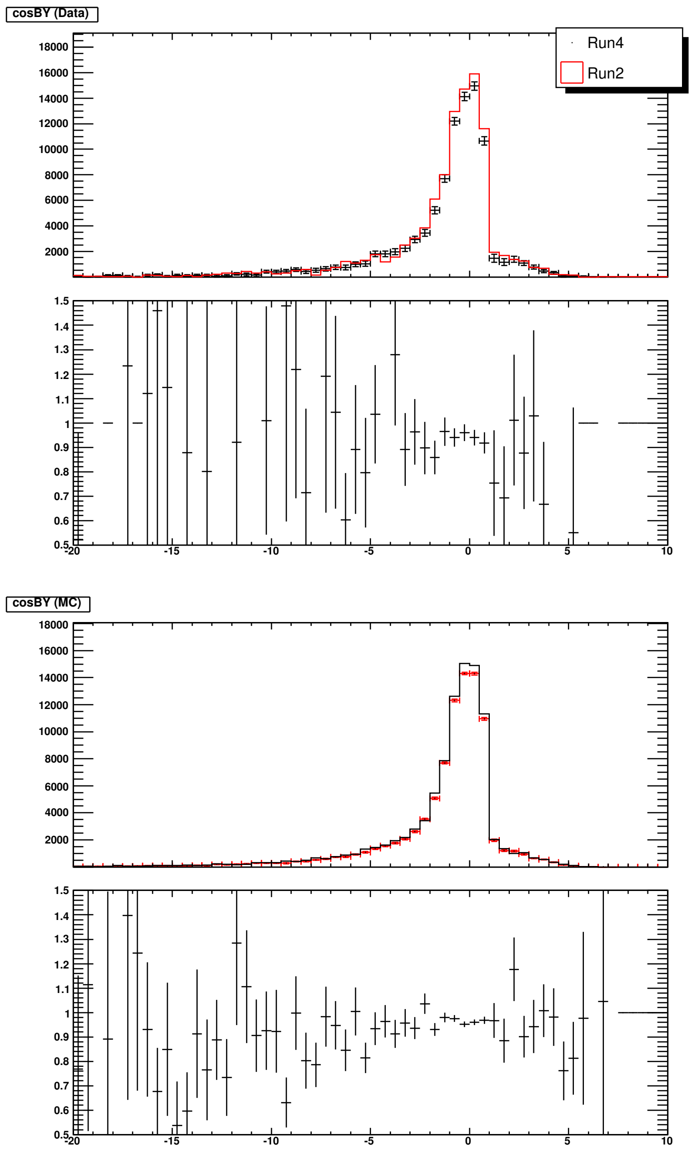

Figure 97: [**Run4 vs Run2 (Electron)** $\cos\Theta_{B-D\ell}$ D^{+}] Run4 vs Run2 $\cos\Theta_{B-D\ell}$ plot for (OnPeak - OffPeak) data (top) and $B\bar{B}$ MC (bottom) of D^{+} (Electron only). Black lines with uncertainties are Run4 and red histograms are Run2.

12.1.2 Data vs MC

Run1 Data MC comparisons are given in Figures 98-100.
Run2 Data MC comparisons are given in Figures 101-103.
Run3 Data MC comparisons are given in Figures 104-106.
Run1-3 Data MC comparisons are given in Figures 107-109.
Run4 Data MC comparisons are given in Figures 110-112.

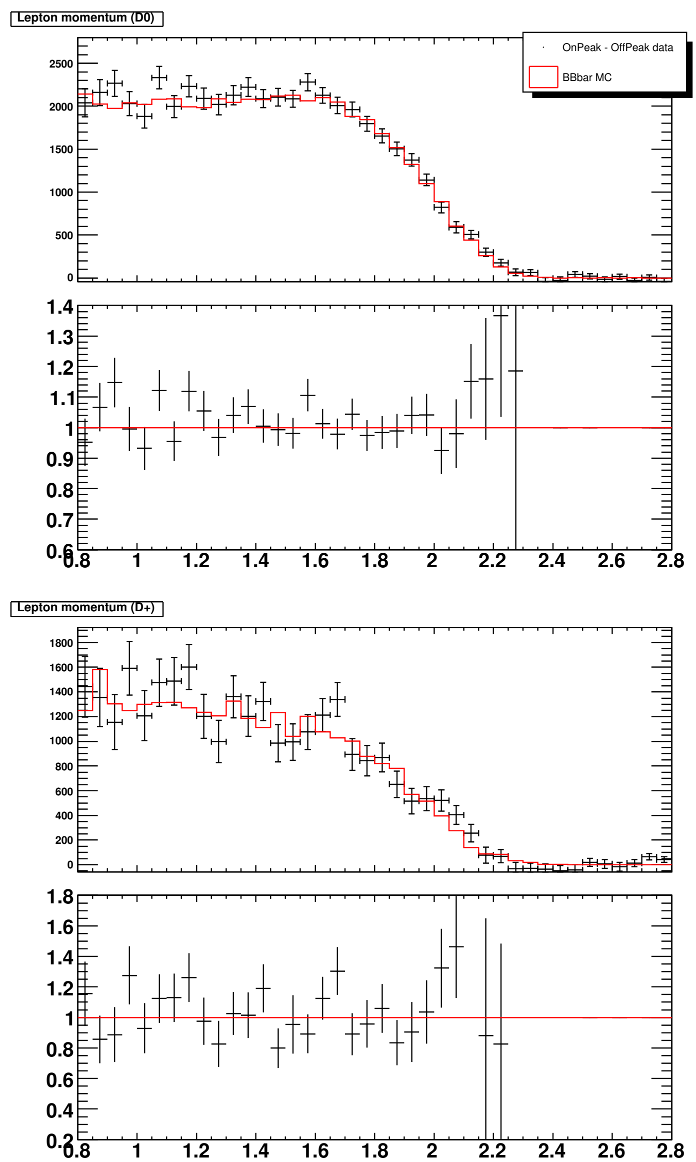

Figure 98: [**Run1 Data vs MC (Electron)** p_ℓ] Run1 Data vs MC lepton momentum plot for D^0 (top) and D^+ (bottom). Black lines with uncertainties (OnPeak - OffPeak) data and red histograms are $B\bar{B}$ MC.

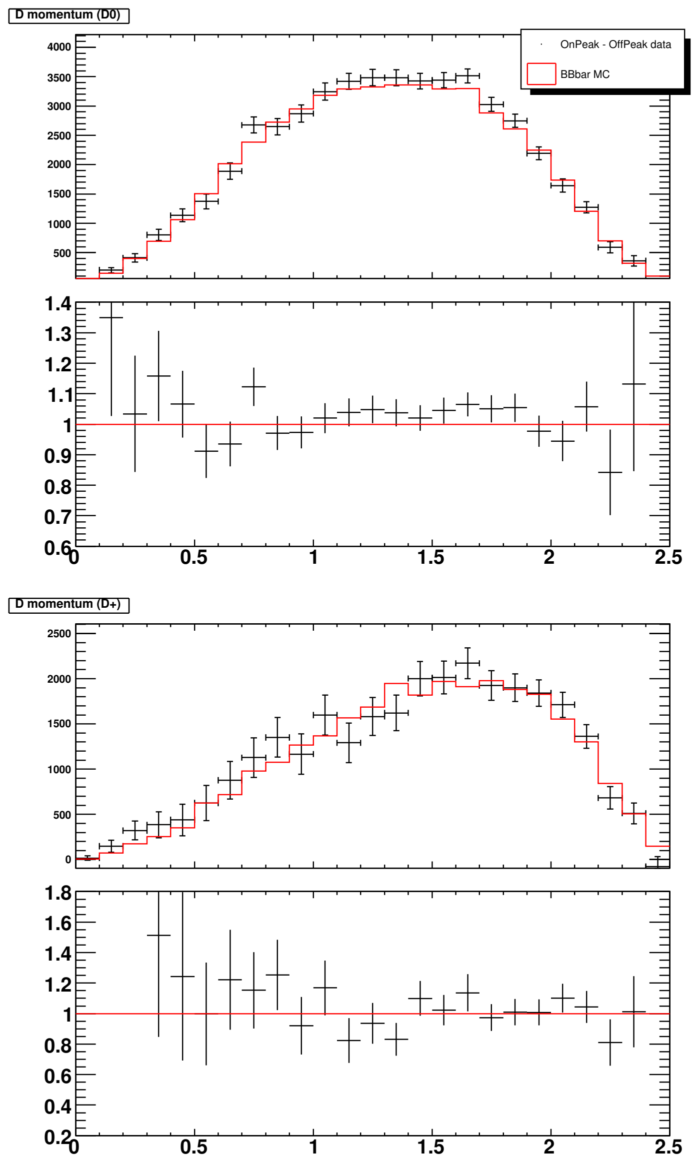

Figure 99: [**Run1 Data vs MC (Electron)** p_D] Run1 Data vs MC D momentum plot for D^0 (top) and D^+ (bottom). Black lines with uncertainties (OnPeak - OffPeak) data and red histograms are $B\bar{B}$ MC.

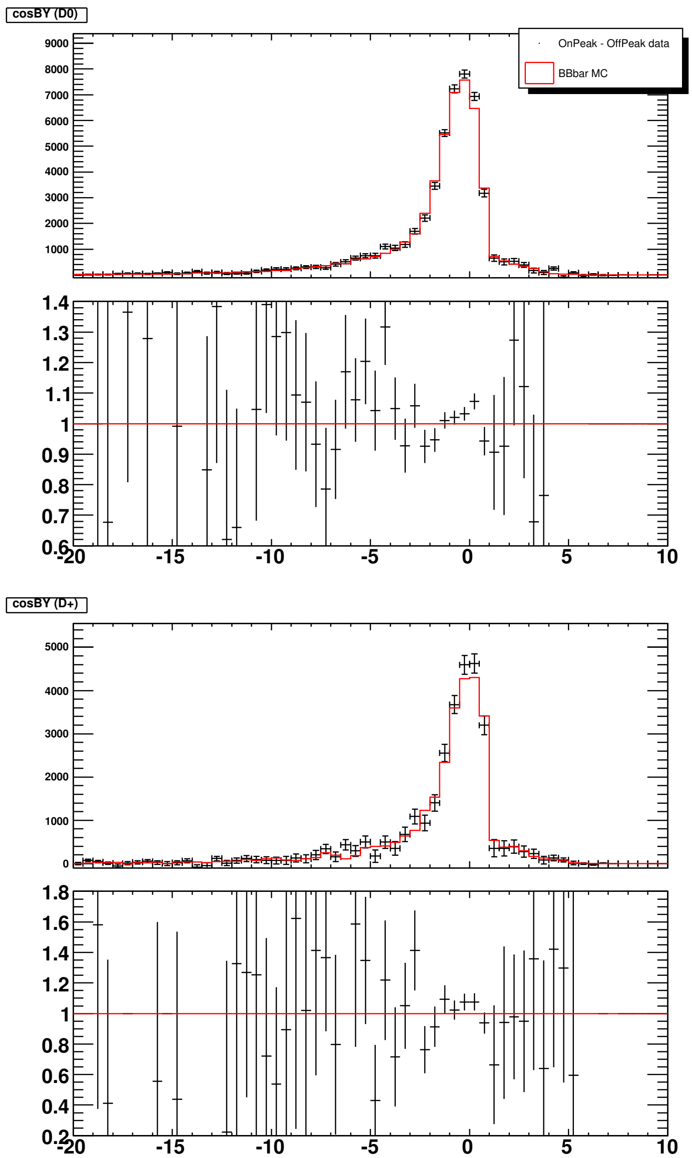

Figure 100: [**Run1 Data vs MC (Electron)** $\cos\Theta_{B-D\ell}$] Run1 Data vs MC $\cos\Theta_{B-D\ell}$ plot for D^0 (top) and D^+ (bottom). Black lines with uncertainties (OnPeak - OffPeak) data and red histograms are $B\bar{B}$ MC.

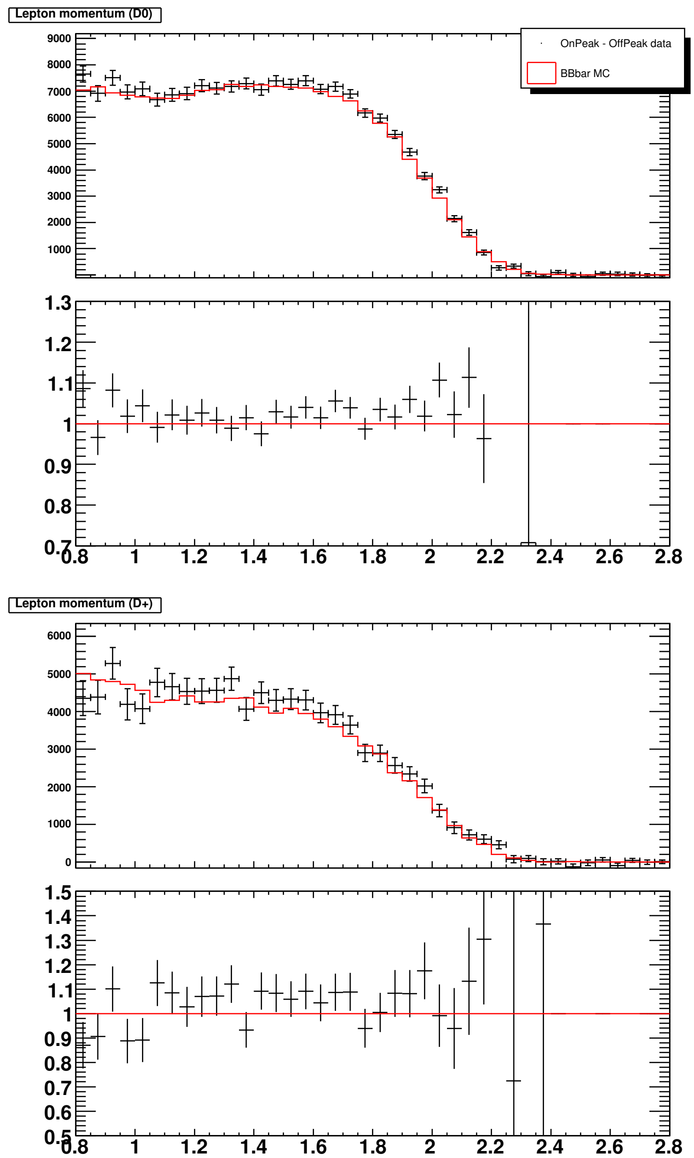

Figure 101: [**Run2 Data vs MC (Electron)** p_ℓ] Run2 Data vs MC lepton momentum plot for D^0 (top) and D^+ (bottom). Black lines with uncertainties (OnPeak - OffPeak) data and red histograms are $B\bar{B}$ MC.

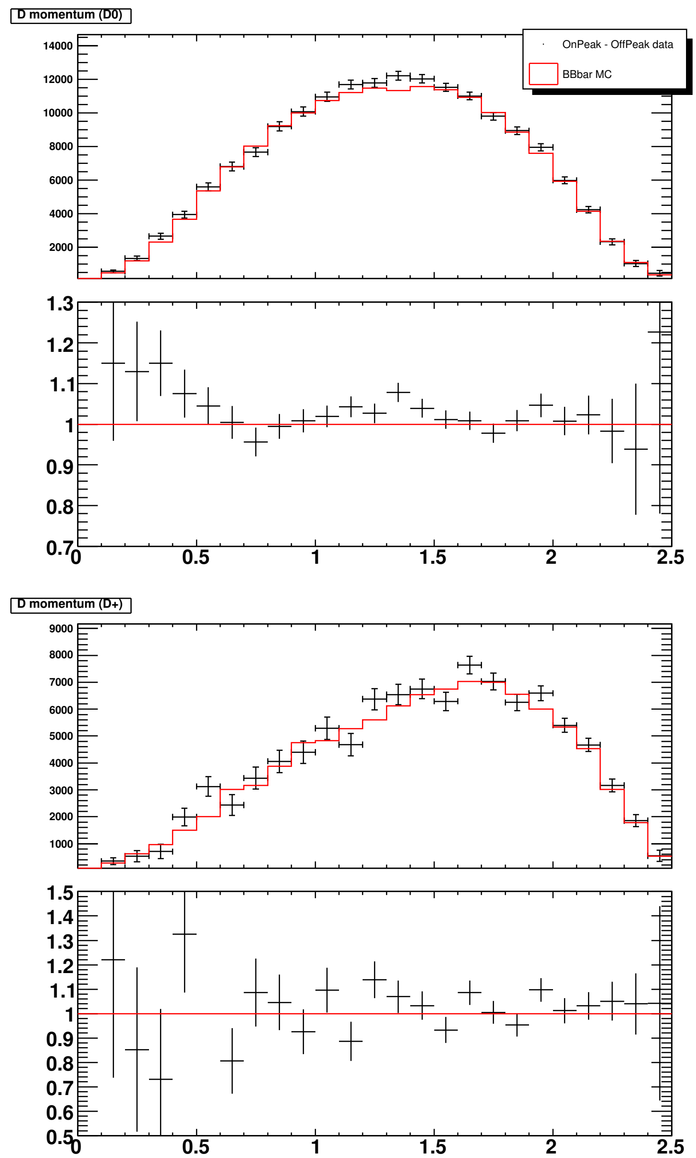

Figure 102: [**Run2 Data vs MC (Electron)** p_D] Run2 Data vs MC D momentum plot for D^0 (top) and D^+ (bottom). Black lines with uncertainties (OnPeak - OffPeak) data and red histograms are $B\bar{B}$ MC.

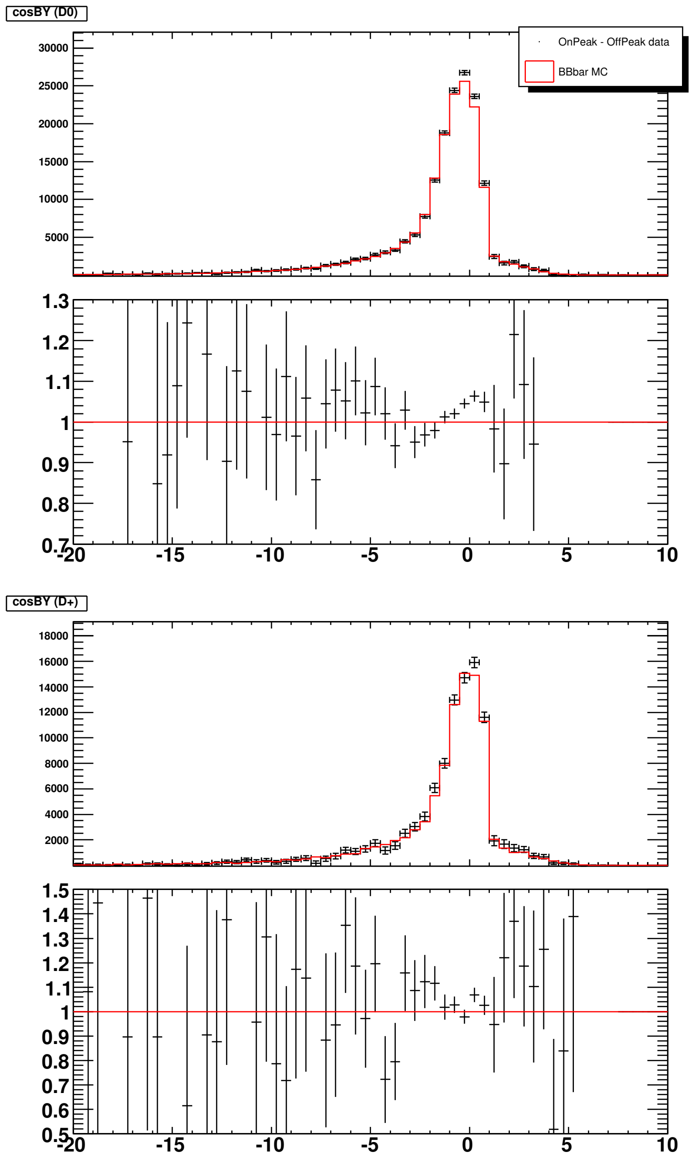

Figure 103: [**Run2 Data vs MC (Electron)** $\cos\Theta_{B-D\ell}$] Run2 Data vs MC $\cos\Theta_{B-D\ell}$ plot for D^0 (top) and D^+ (bottom). Black lines with uncertainties (OnPeak - OffPeak) data and red histograms are $B\bar{B}$ MC.

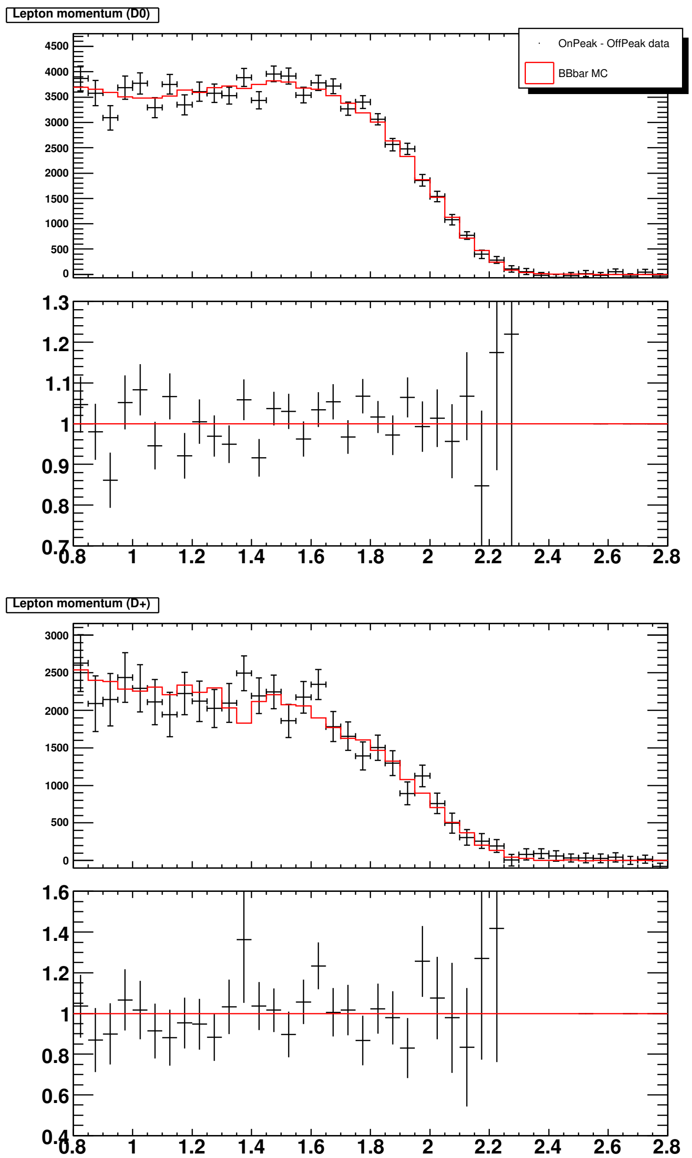

Figure 104: [**Run3 Data vs MC (Electron)** p_ℓ] Run3 Data vs MC lepton momentum plot for D^0 (top) and D^+ (bottom). Black lines with uncertainties (OnPeak - OffPeak) data and red histograms are $B\bar{B}$ MC.

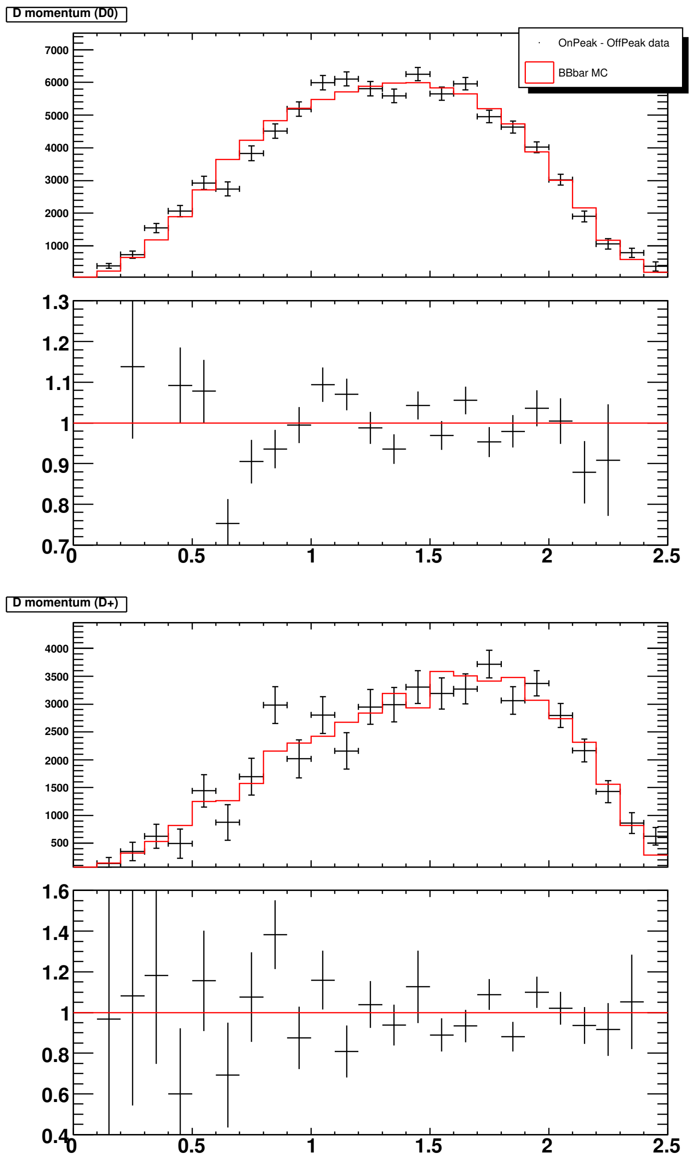

Figure 105: [**Run3 Data vs MC (Electron)** p_D] Run3 Data vs MC D momentum plot for D^0 (top) and D^+ (bottom). Black lines with uncertainties (OnPeak - OffPeak) data and red histograms are $B\bar{B}$ MC.

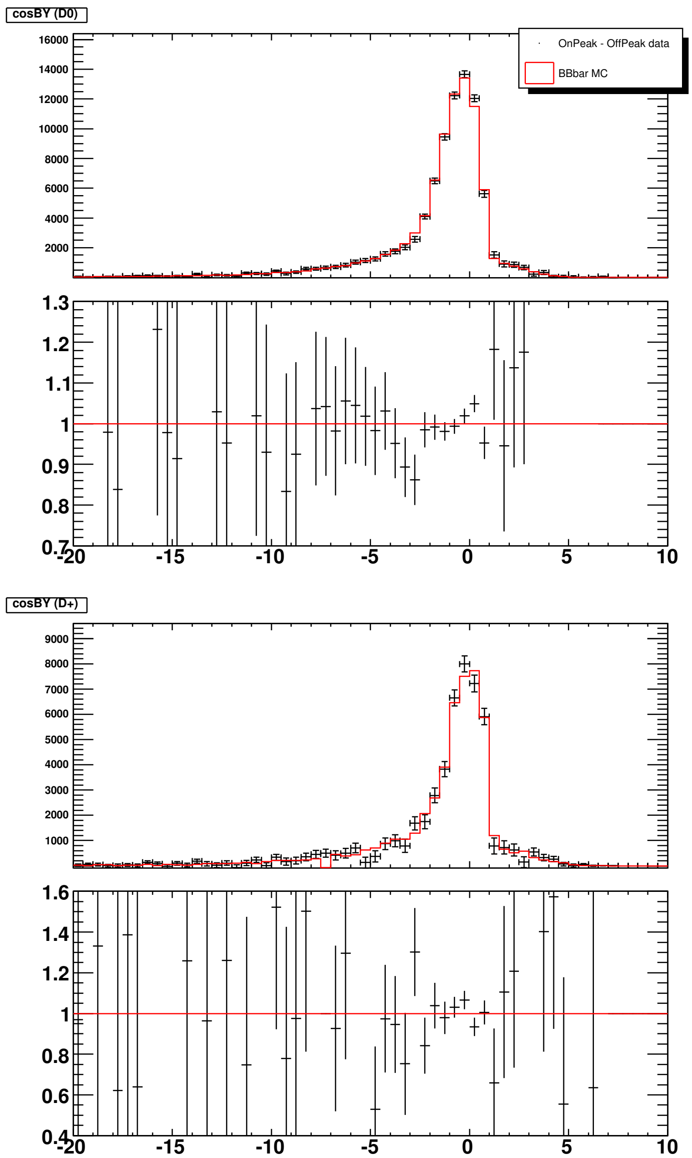

Figure 106: [**Run3 Data vs MC (Electron)** $\cos\Theta_{B-D\ell}$] Run3 Data vs MC $\cos\Theta_{B-D\ell}$ plot for D^0 (top) and D^+ (bottom). Black lines with uncertainties (OnPeak - OffPeak) data and red histograms are $B\bar{B}$ MC.

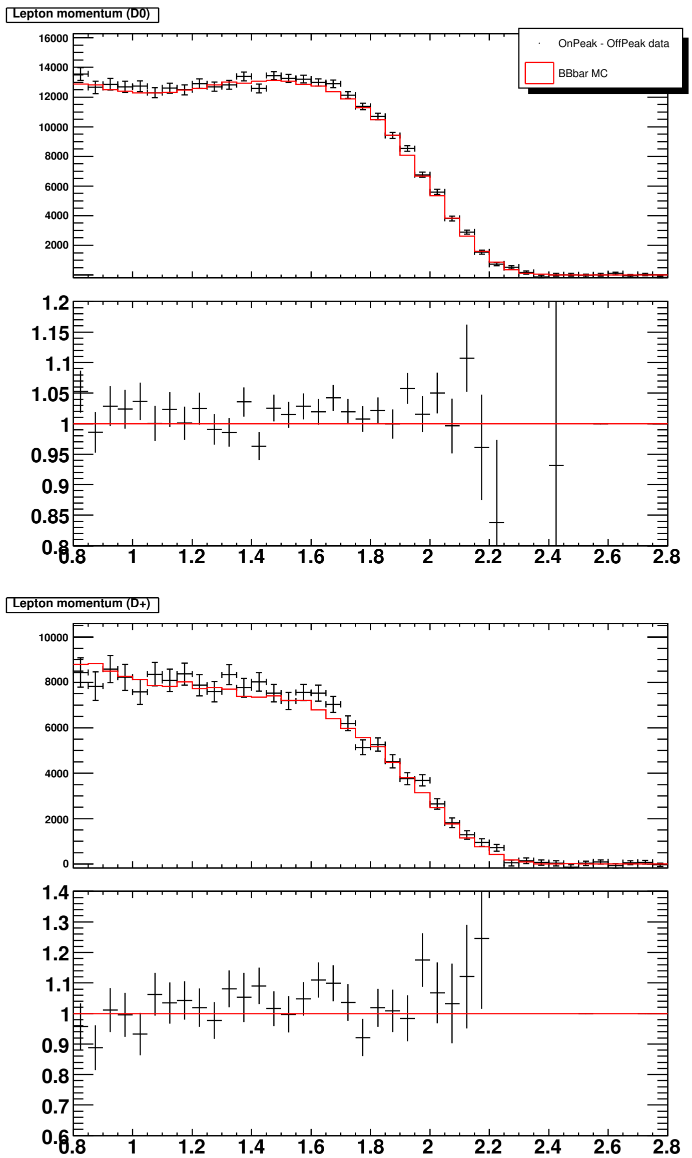

Figure 107: [**Run123 Data vs MC (Electron)** p_ℓ] Run123 Data vs MC lepton momentum plot for D^0 (top) and D^+ (bottom). Black lines with uncertainties (OnPeak - OffPeak) data and red histograms are $B\bar{B}$ MC.

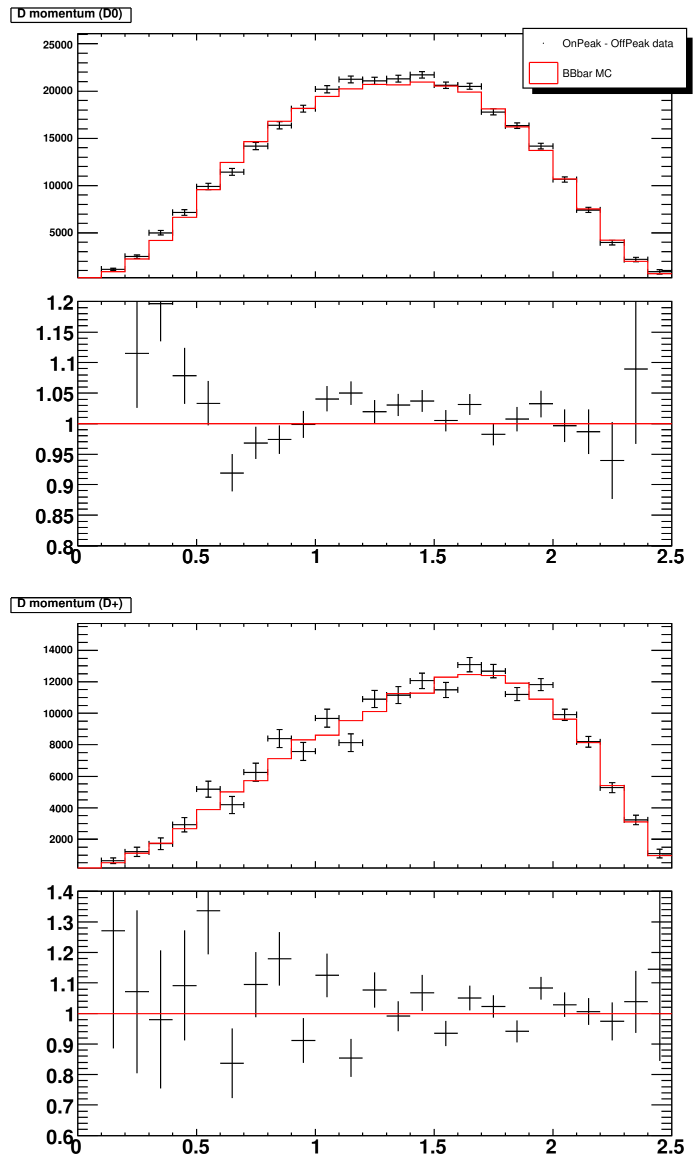

Figure 108: [**Run123 Data vs MC (Electron)** p_D] Run123 Data vs MC D momentum plot for D^0 (top) and D^+ (bottom). Black lines with uncertainties (OnPeak - OffPeak) data and red histograms are $B\bar{B}$ MC.

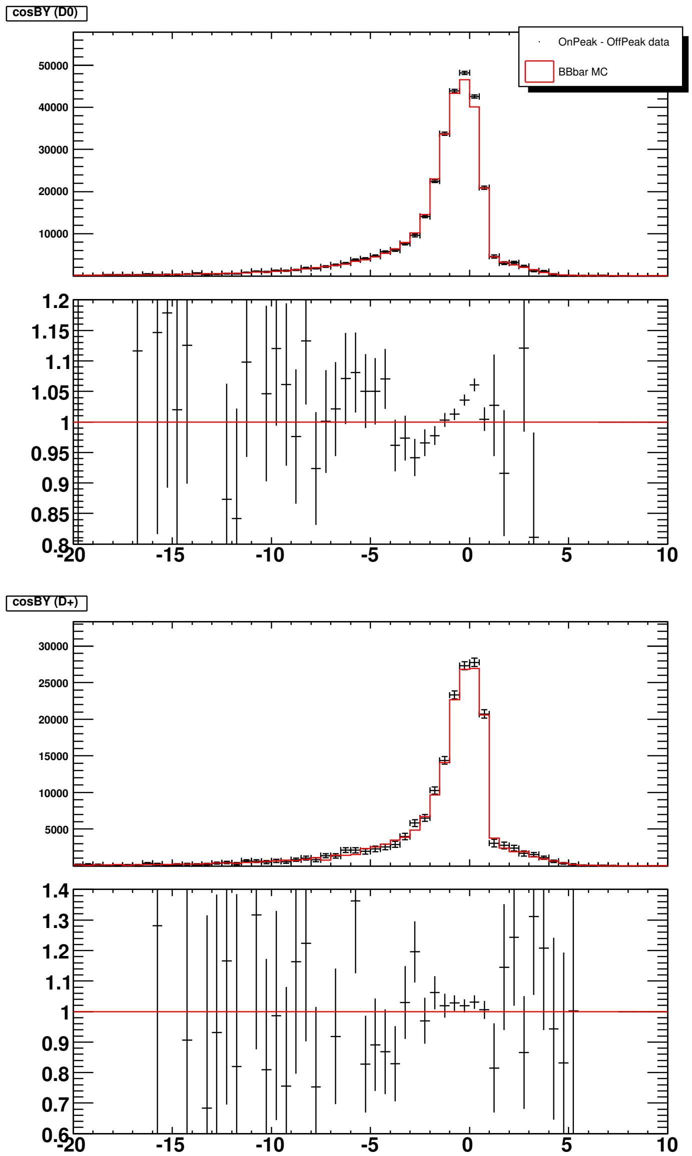

Figure 109: [**Run123 Data vs MC (Electron)** $\cos\Theta_{B-D\ell}$] Run123 Data vs MC $\cos\Theta_{B-D\ell}$ plot for D^0 (top) and D^+ (bottom). Black lines with uncertainties (OnPeak - OffPeak) data and red histograms are $B\bar{B}$ MC.

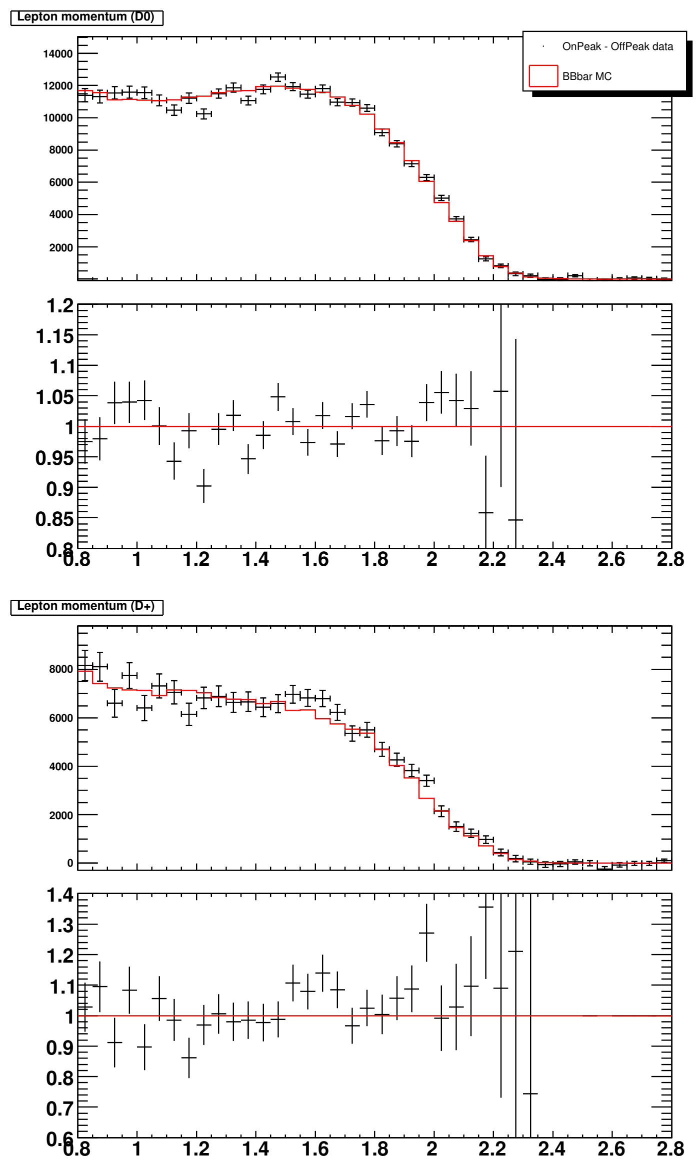

Figure 110: [**Run4 Data vs MC (Electron)** p_ℓ] Run4 Data vs MC lepton momentum plot for D^0 (top) and D^+ (bottom). Black lines with uncertainties (OnPeak - OffPeak) data and red histograms are $B\bar{B}$ MC.

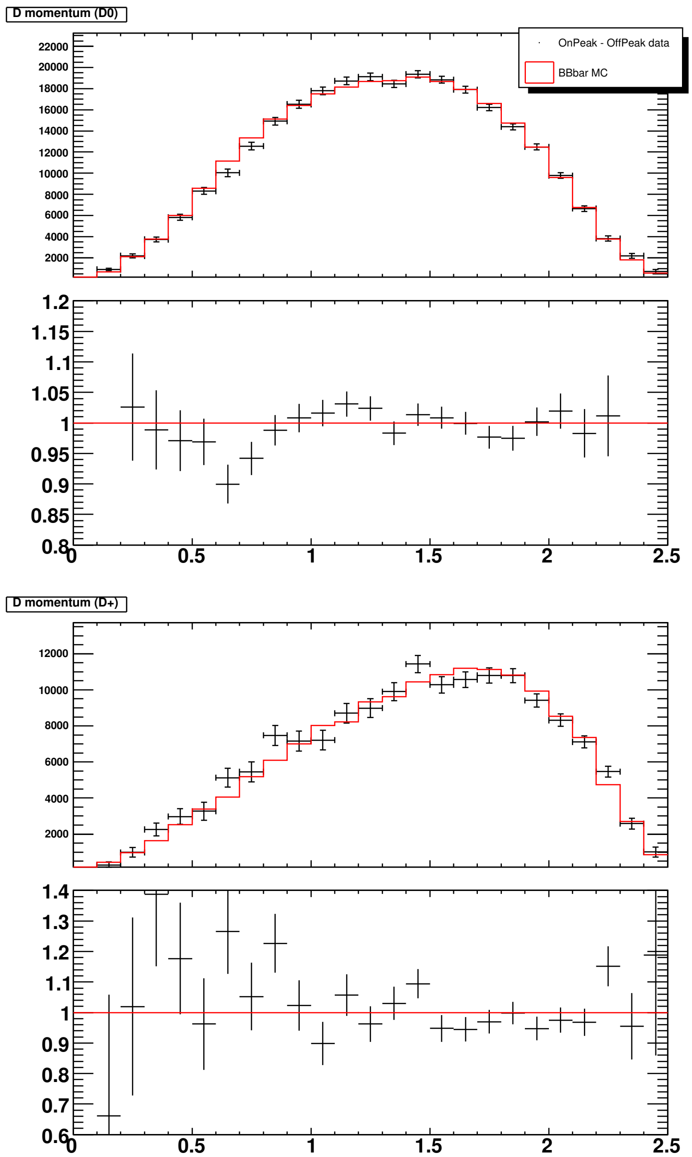

Figure 111: [**Run4 Data vs MC (Electron)** p_D] Run4 Data vs MC D momentum plot for D^0 (top) and D^+ (bottom). Black lines with uncertainties (OnPeak - OffPeak) data and red histograms are $B\bar{B}$ MC.

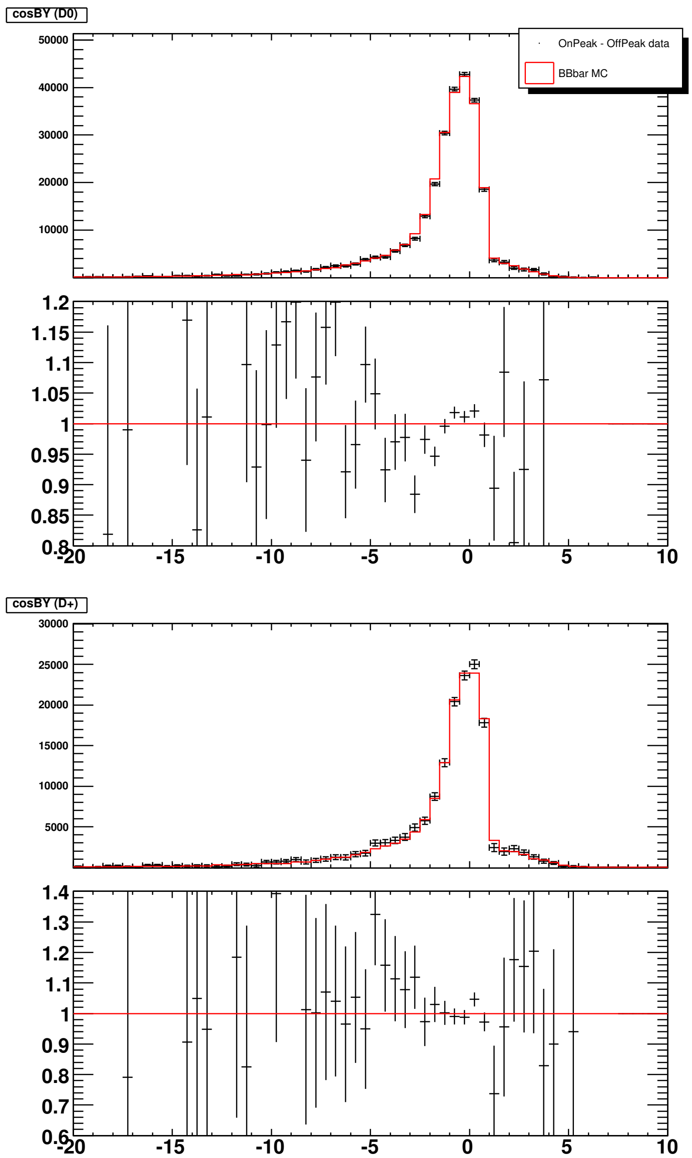

Figure 112: [**Run4 Data vs MC (Electron)** $\cos\Theta_{B-D\ell}$] Run4 Data vs MC $\cos\Theta_{B-D\ell}$ plot for D^0 (top) and D^+ (bottom). Black lines with uncertainties (OnPeak - OffPeak) data and red histograms are $B\bar{B}$ MC.

12.2 Muon only

12.2.1 RunX vs Run2

Run1 vs Run2 comparison is given in Figures 113-118.
Run3 vs Run2 comparison is given in Figures 119-124.
Run4 vs Run2 comparison is given in Figures 125-130.

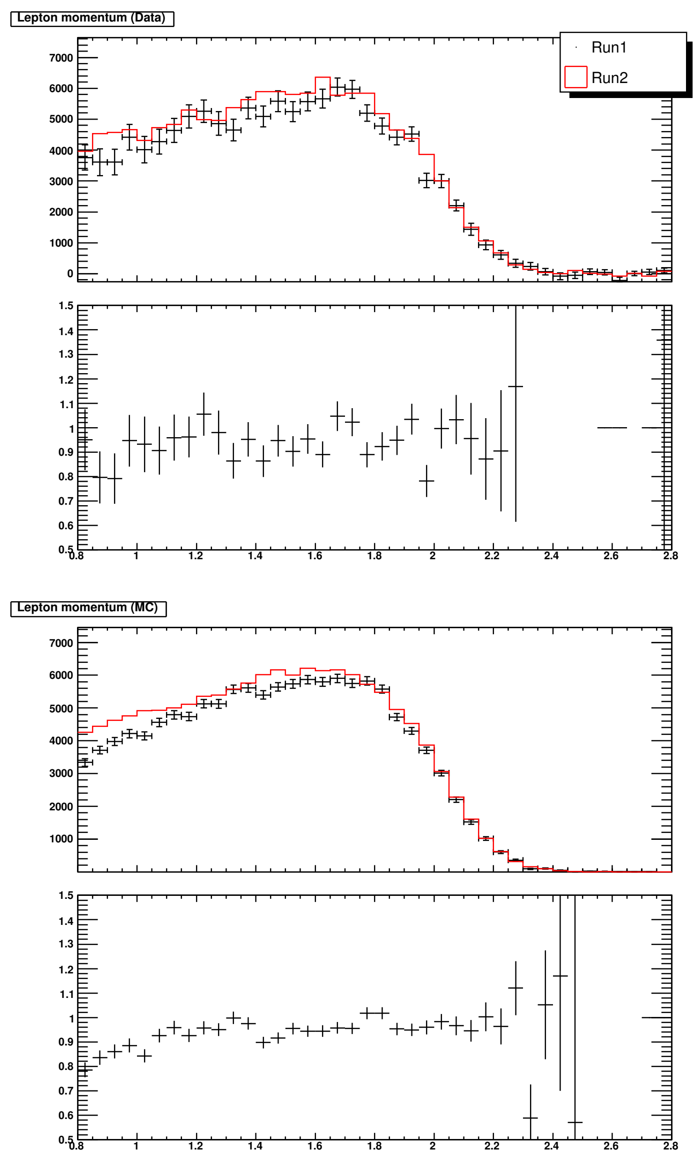

Figure 113: [**Run1 vs Run2 (Muon)** p_ℓ D^0] Run1 vs Run2 lepton momentum plot for (OnPeak - OffPeak) data (top) and $B\bar{B}$ MC (bottom) of D^0 (Muon only). Black lines with uncertainties are Run1 and red histograms are Run2.

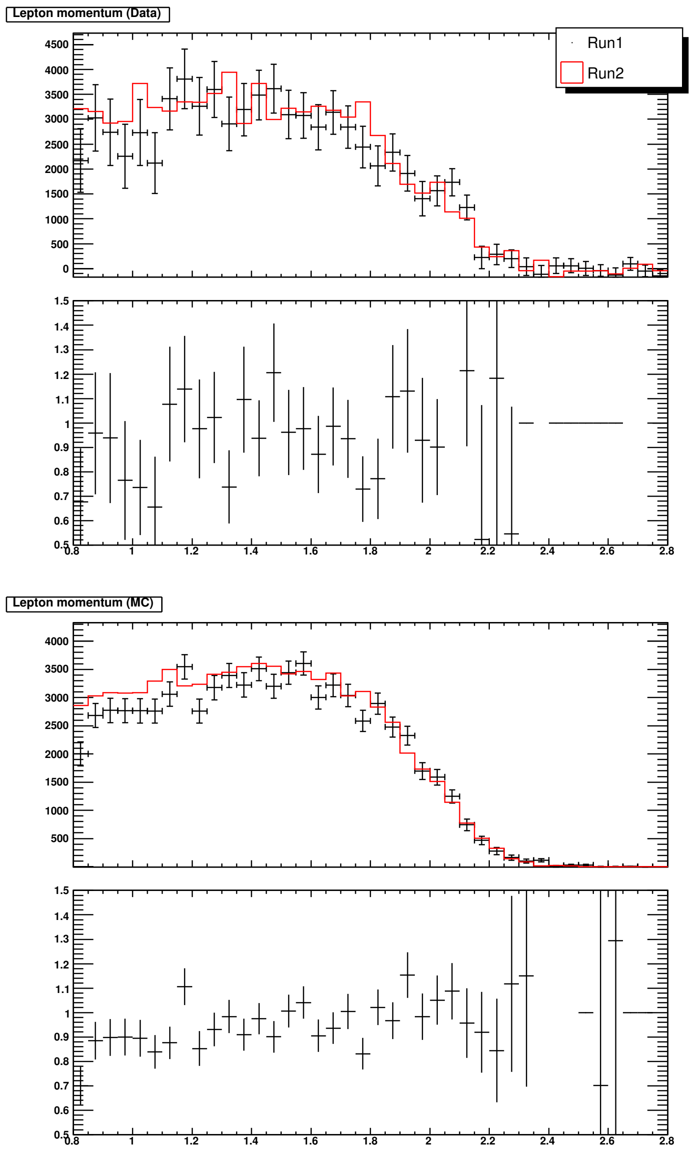

Figure 114: [**Run1 vs Run2 (Muon)** p_ℓ D^+] Run1 vs Run2 lepton momentum plot for (OnPeak - OffPeak) data (top) and $B\bar{B}$ MC (bottom) of D^+ (Muon only). Black lines with uncertainties are Run1 and red histograms are Run2.

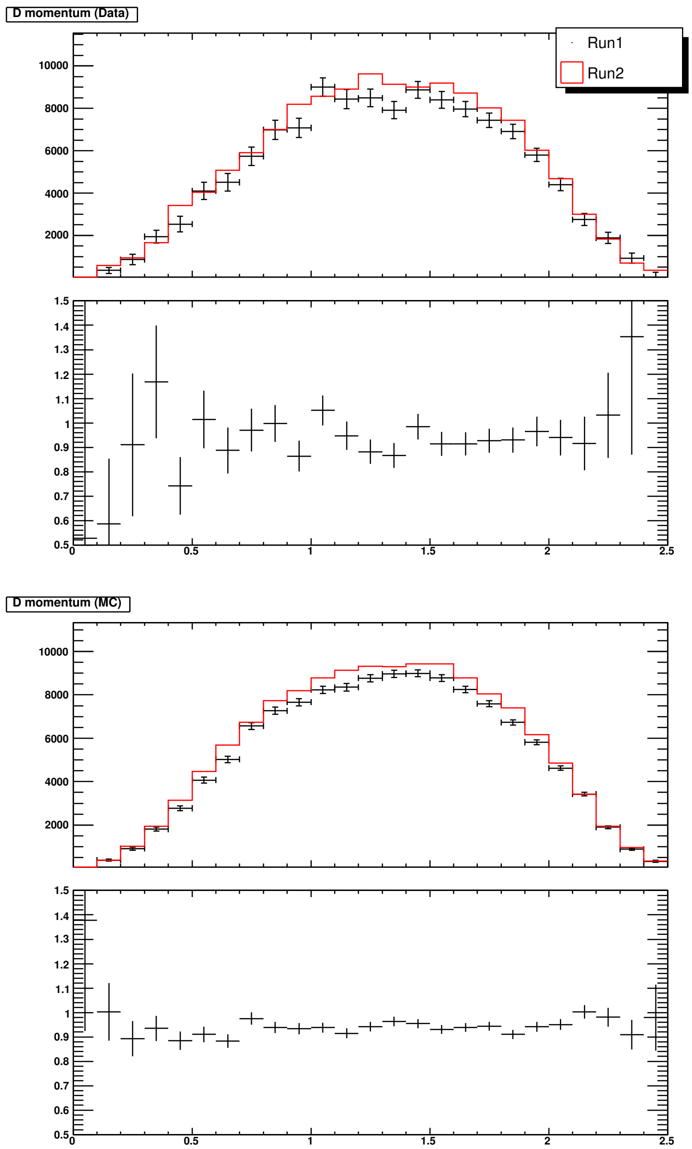

Figure 115: [**Run1 vs Run2 (Muon)** p_D D^0] Run1 vs Run2 D momentum plot for (OnPeak - OffPeak) data (top) and $B\bar{B}$ MC (bottom) of D^0 (Muon only). Black lines with uncertainties are Run1 and red histograms are Run2.

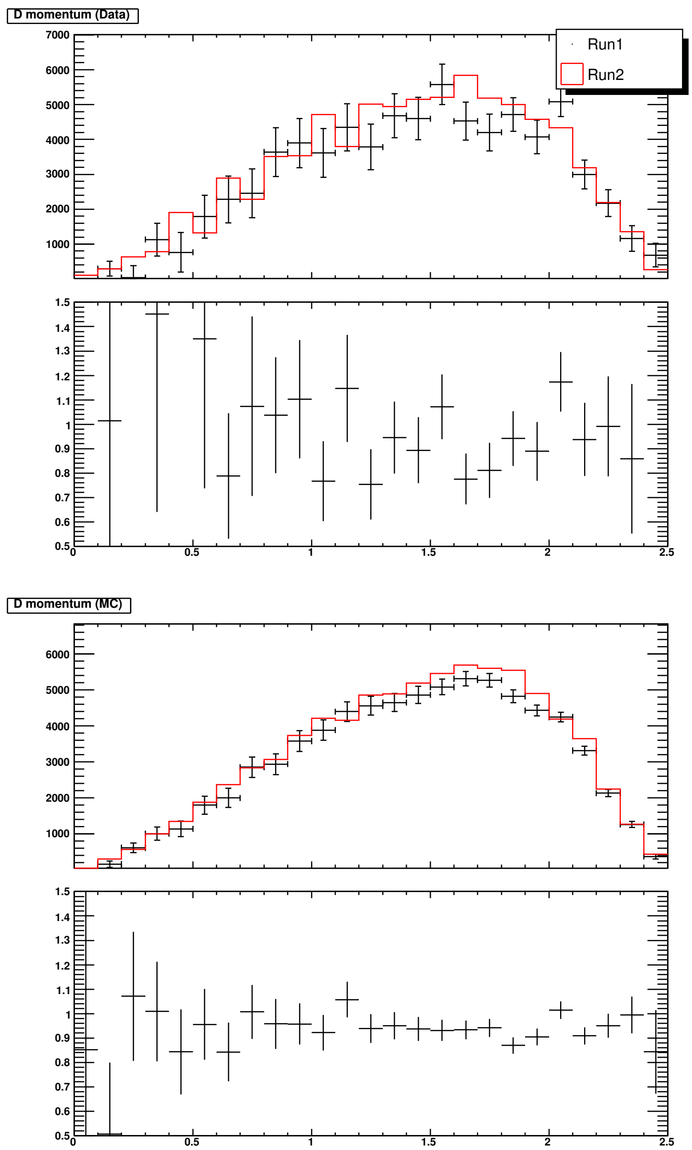

Figure 116: [**Run1 vs Run2 (Muon)** p_D D^+] Run1 vs Run2 D momentum plot for (OnPeak - OffPeak) data (top) and $B\bar{B}$ MC (bottom) of D^+ (Muon only). Black lines with uncertainties are Run1 and red histograms are Run2.

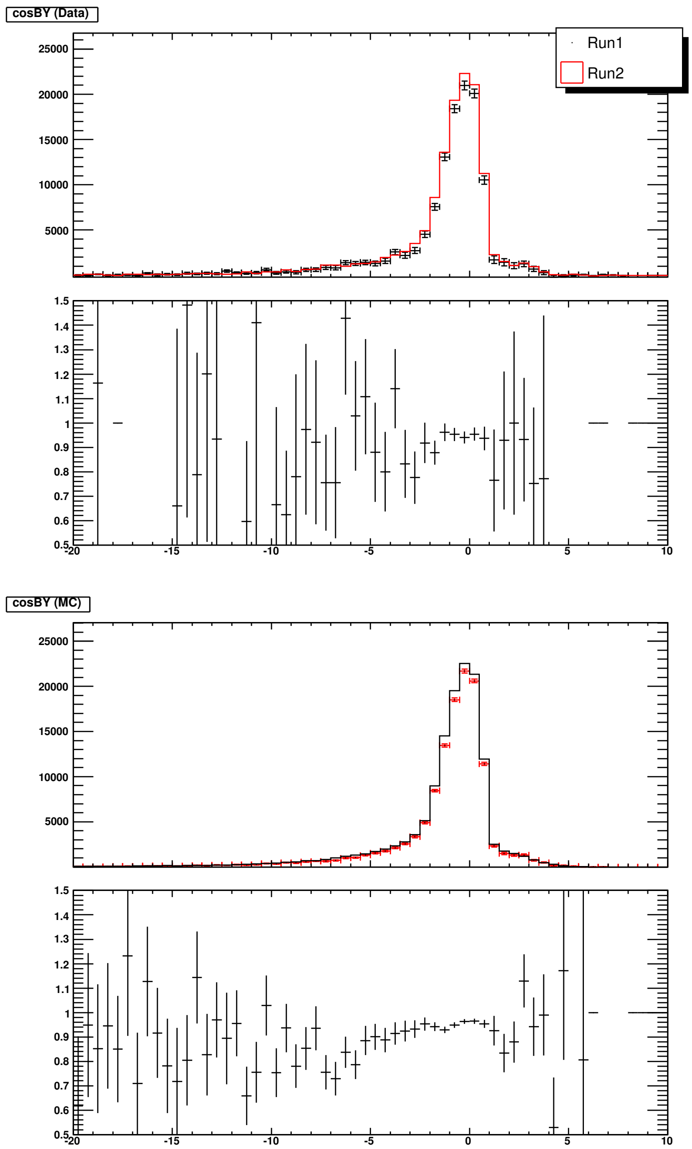

Figure 117: [**Run1 vs Run2 (Muon)** $\cos\Theta_{B-D\ell}$ D^0] Run1 vs Run2 $\cos\Theta_{B-D\ell}$ plot for (OnPeak - OffPeak) data (top) and $B\bar{B}$ MC (bottom) of D^0 (Muon only). Black lines with uncertainties are Run1 and red histograms are Run2.

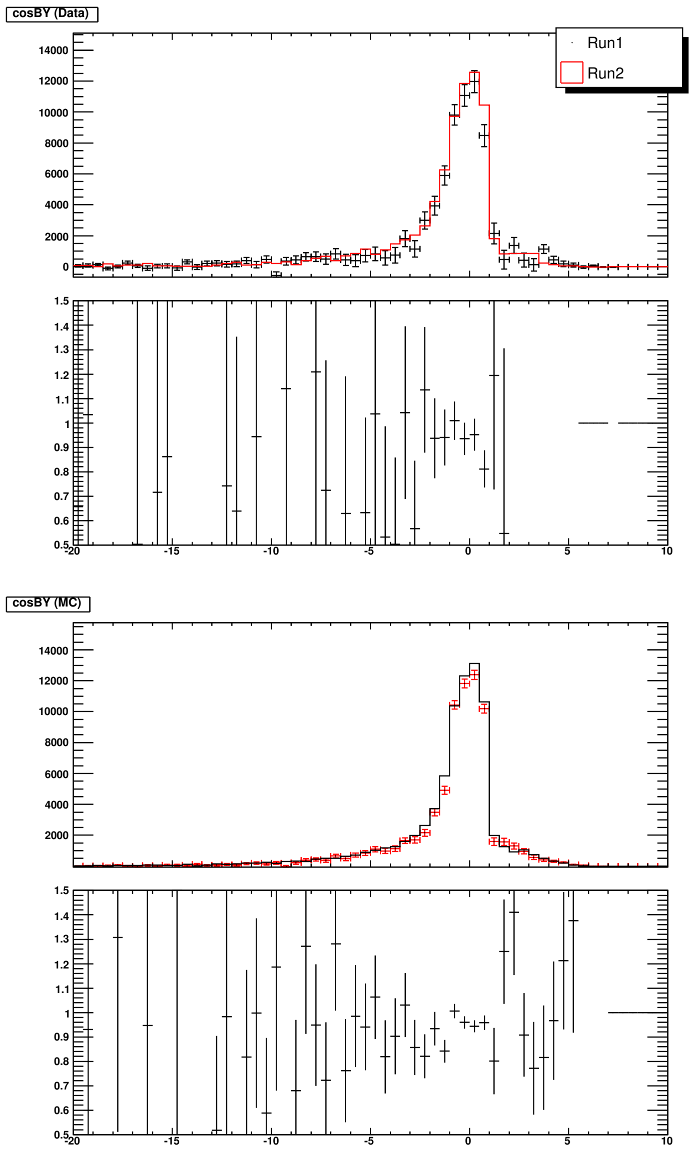

Figure 118: [**Run1 vs Run2 (Muon)** $\cos\Theta_{B-D\ell}$ D^+] Run1 vs Run2 $\cos\Theta_{B-D\ell}$ plot for (OnPeak - OffPeak) data (top) and $B\bar{B}$ MC (bottom) of D^+ (Muon only). Black lines with uncertainties are Run1 and red histograms are Run2.

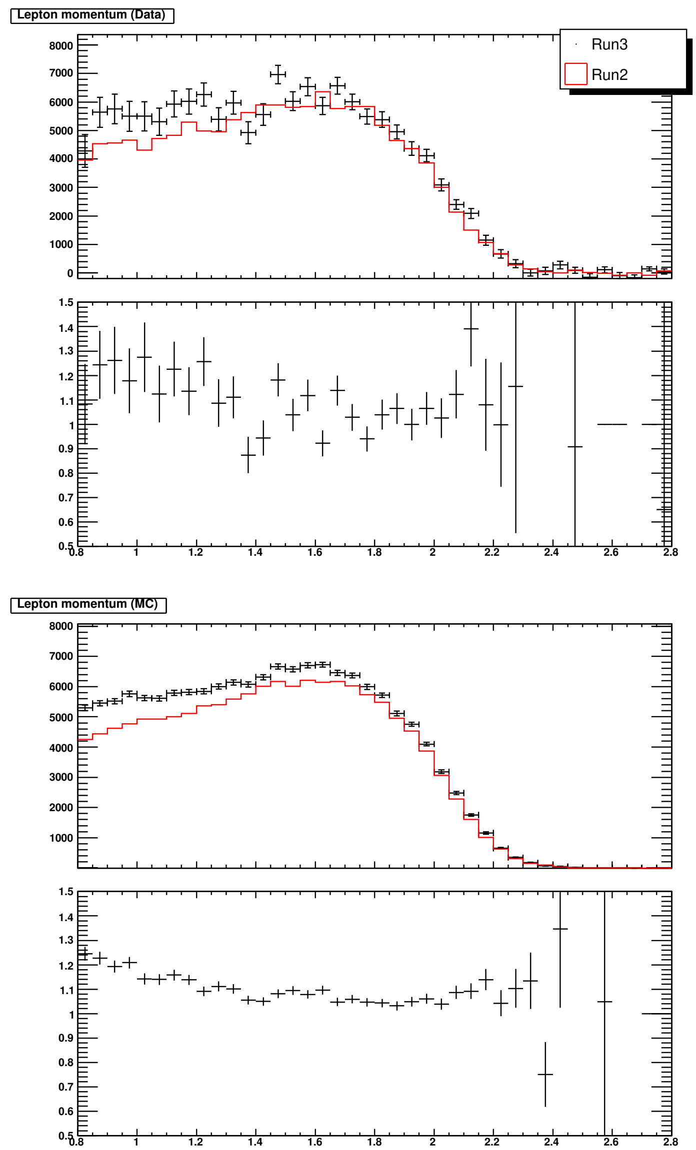

Figure 119: [**Run3 vs Run2 (Muon)** p_ℓ D^0] Run3 vs Run2 lepton momentum plot for (OnPeak - OffPeak) data (top) and $B\bar{B}$ MC (bottom) of D^0 (Muon only). Black lines with uncertainties are Run3 and red histograms are Run2.

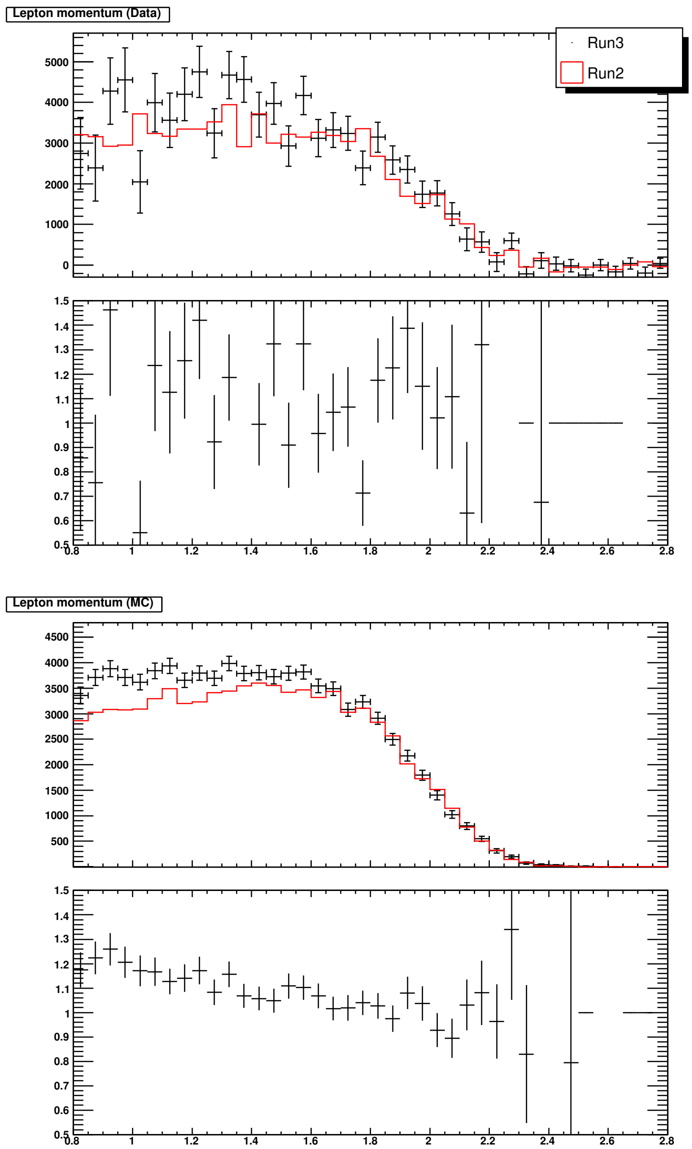

Figure 120: [**Run3 vs Run2 (Muon)** p_ℓ D^+] Run3 vs Run2 lepton momentum plot for (OnPeak - OffPeak) data (top) and $B\bar{B}$ MC (bottom) of D^+ (Muon only). Black lines with uncertainties are Run3 and red histograms are Run2.

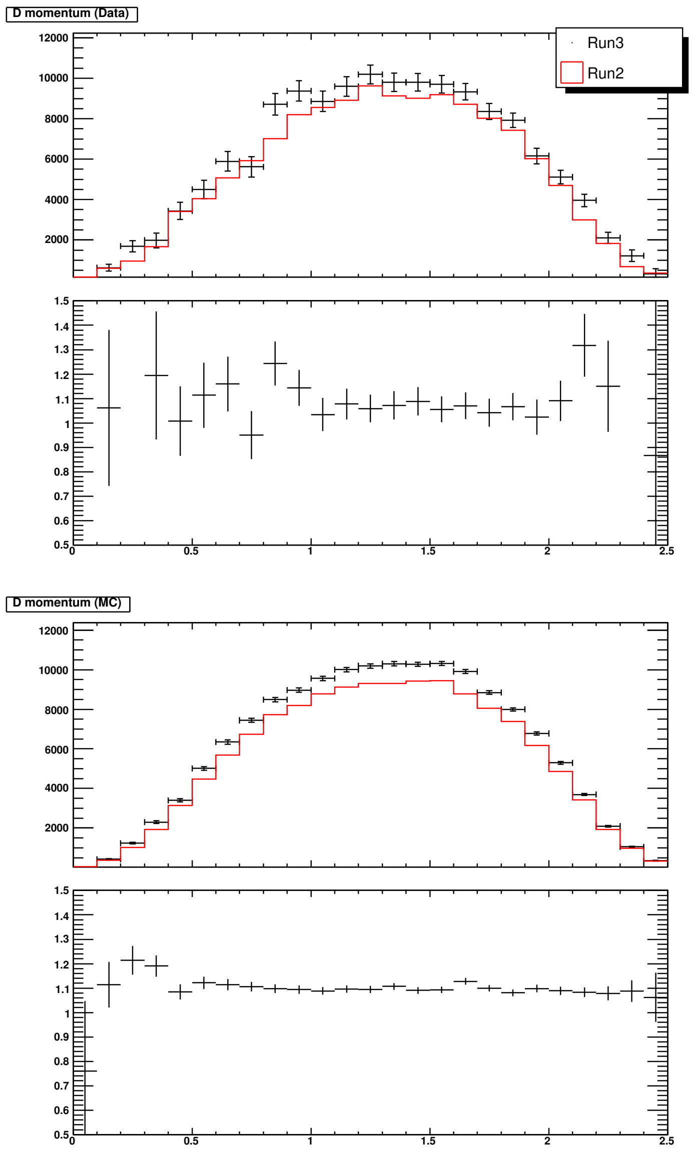

Figure 121: [**Run3 vs Run2 (Muon)** p_D D^0] Run3 vs Run2 D momentum plot for (OnPeak - OffPeak) data (top) and $B\bar{B}$ MC (bottom) of D^0 (Muon only). Black lines with uncertainties are Run3 and red histograms are Run2.

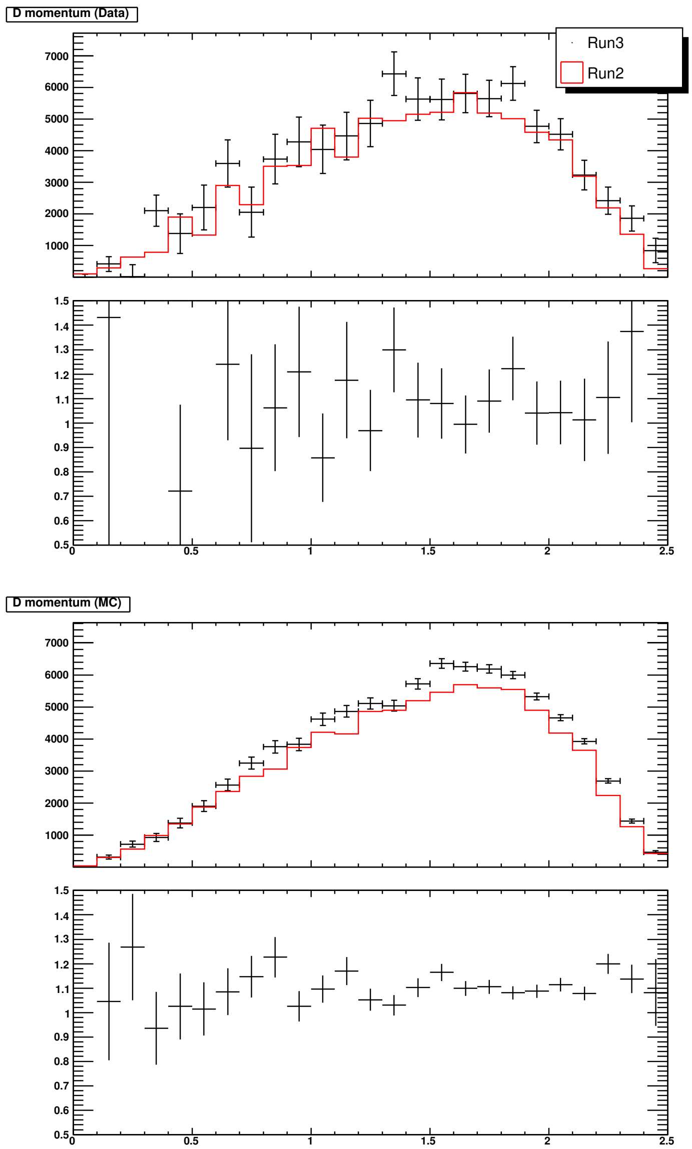

Figure 122: [**Run3 vs Run2 (Muon)** p_D D^+] Run3 vs Run2 D momentum plot for (OnPeak - OffPeak) data (top) and $B\bar{B}$ MC (bottom) of D^+ (Muon only). Black lines with uncertainties are Run3 and red histograms are Run2.

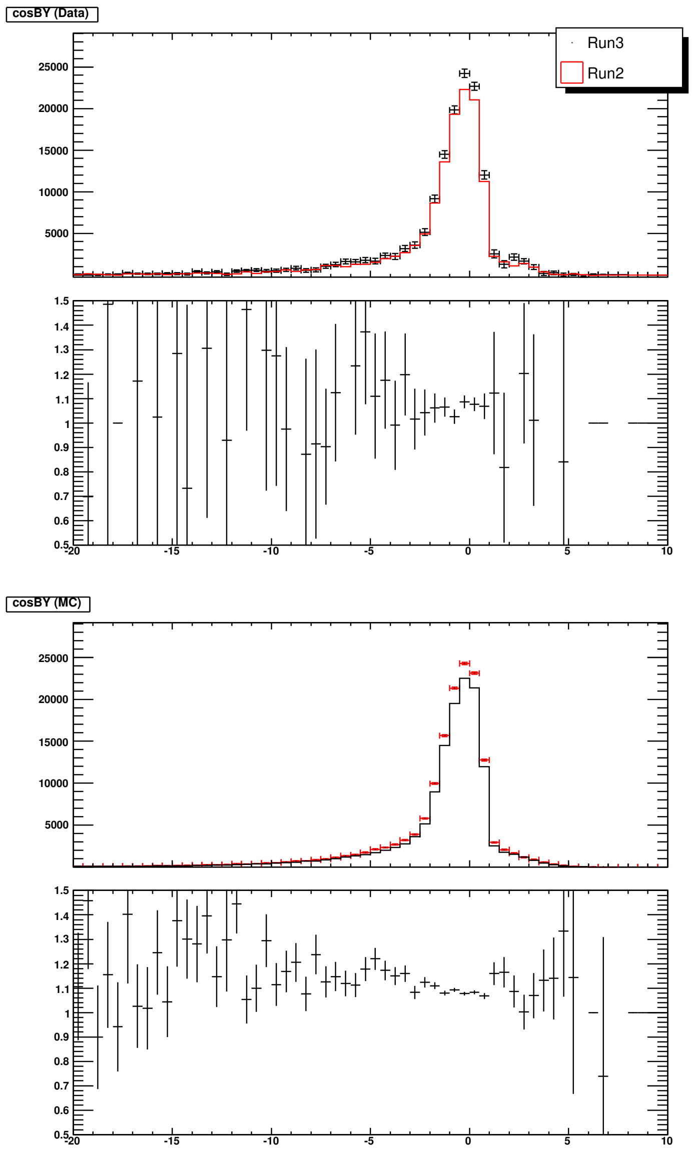

Figure 123: [**Run3 vs Run2 (Muon)** $\cos\Theta_{B-D\ell}$ D^0] Run3 vs Run2 $\cos\Theta_{B-D\ell}$ plot for (OnPeak - OffPeak) data (top) and $B\bar{B}$ MC (bottom) of D^0 (Muon only). Black lines with uncertainties are Run3 and red histograms are Run2.

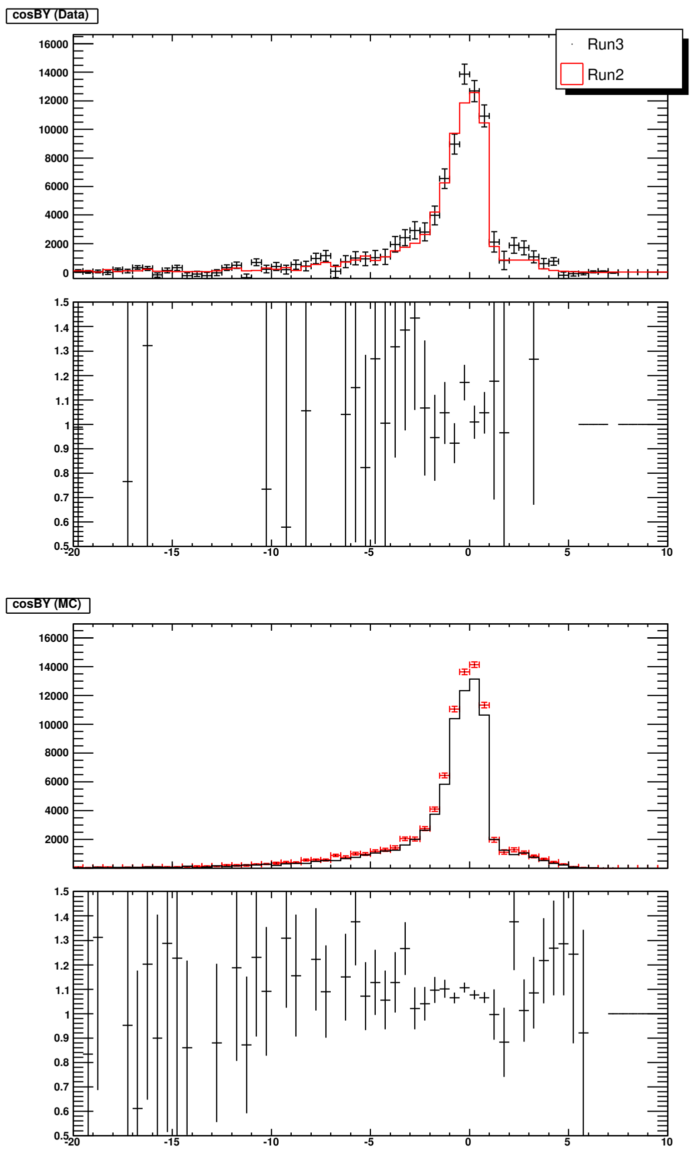

Figure 124: [**Run3 vs Run2 (Muon)** $\cos\Theta_{B-D\ell}$ D^+] Run3 vs Run2 $\cos\Theta_{B-D\ell}$ plot for (OnPeak - OffPeak) data (top) and $B\bar{B}$ MC (bottom) of D^+ (Muon only). Black lines with uncertainties are Run3 and red histograms are Run2.

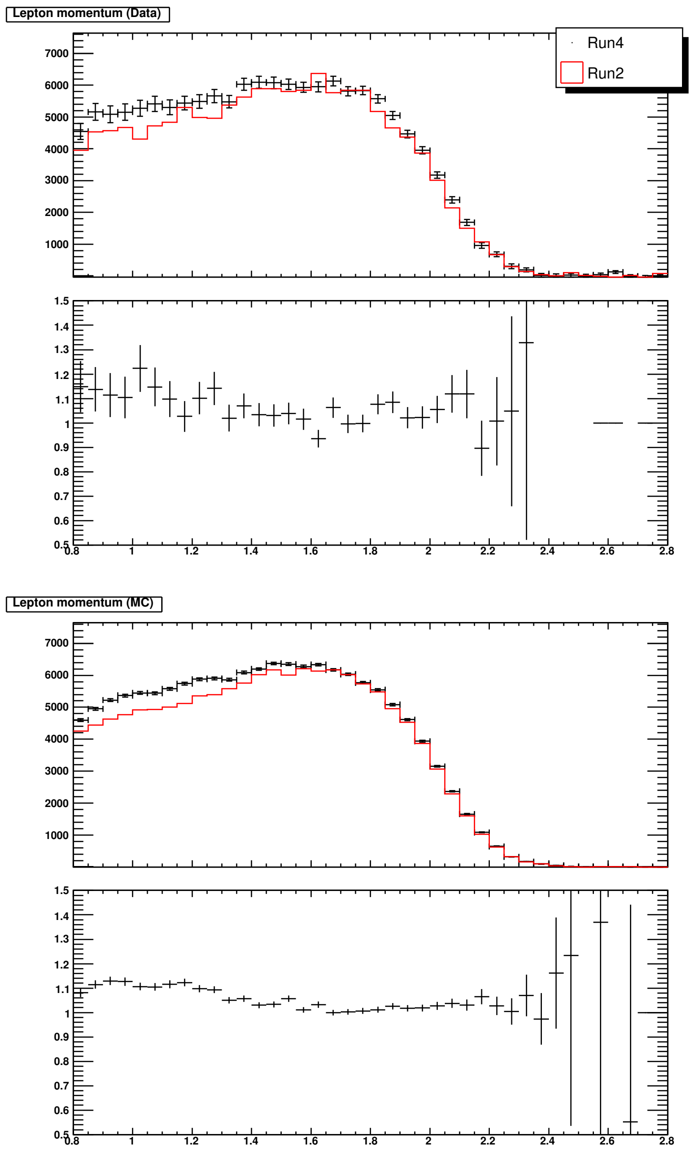

Figure 125: [**Run4 vs Run2 (Muon)** p_ℓ D^0] Run4 vs Run2 lepton momentum plot for (OnPeak - OffPeak) data (top) and $B\bar{B}$ MC (bottom) of D^0 (Muon only). Black lines with uncertainties are Run4 and red histograms are Run2.

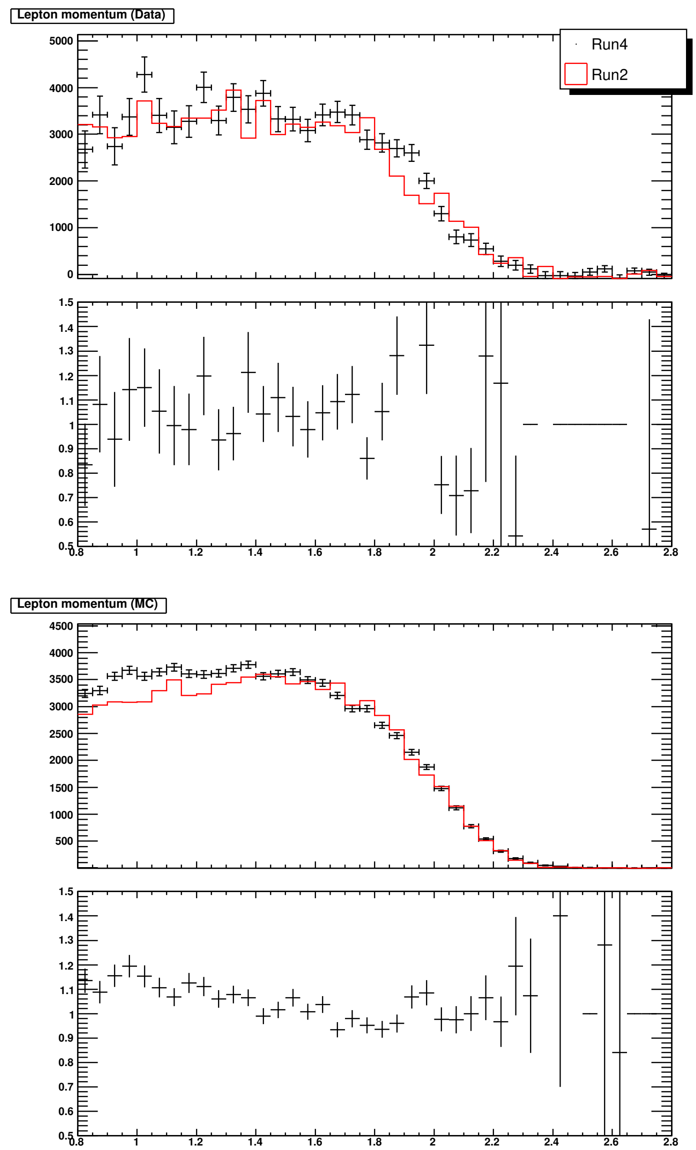

Figure 126: [**Run4 vs Run2 (Muon)** p_ℓ D^+] Run4 vs Run2 lepton momentum plot for (OnPeak - OffPeak) data (top) and $B\bar{B}$ MC (bottom) of D^+ (Muon only). Black lines with uncertainties are Run4 and red histograms are Run2.

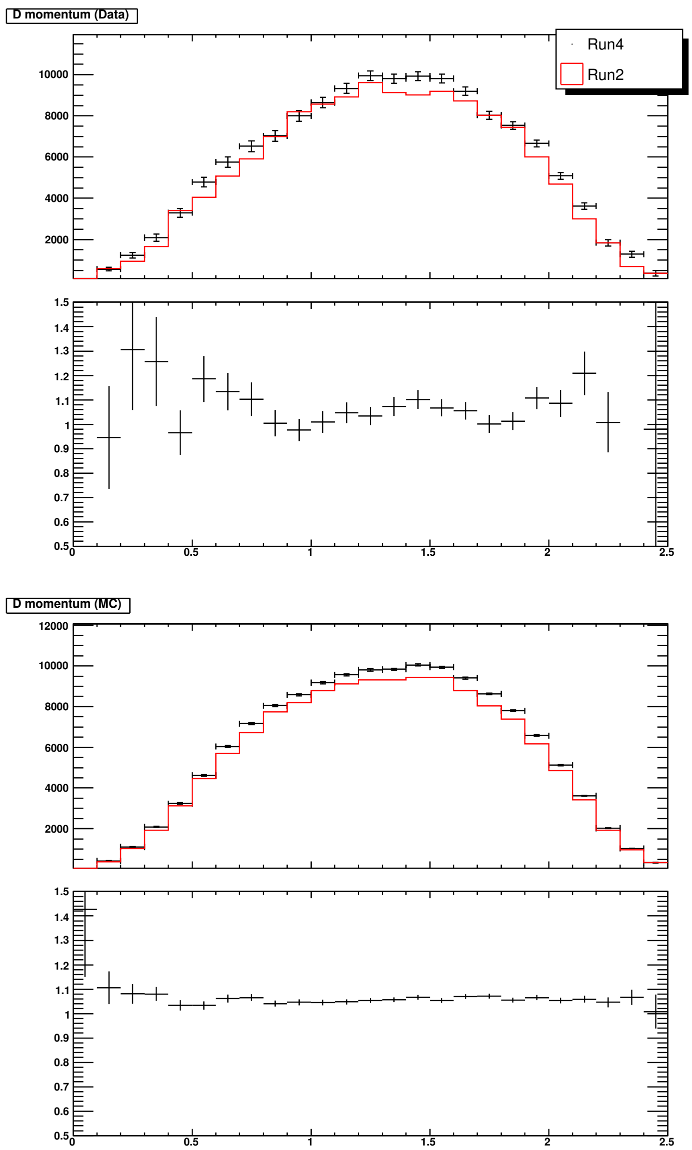

Figure 127: [**Run4 vs Run2 (Muon)** p_D D^0] Run4 vs Run2 D momentum plot for (OnPeak - OffPeak) data (top) and $B\bar{B}$ MC (bottom) of D^0 (Muon only). Black lines with uncertainties are Run4 and red histograms are Run2.

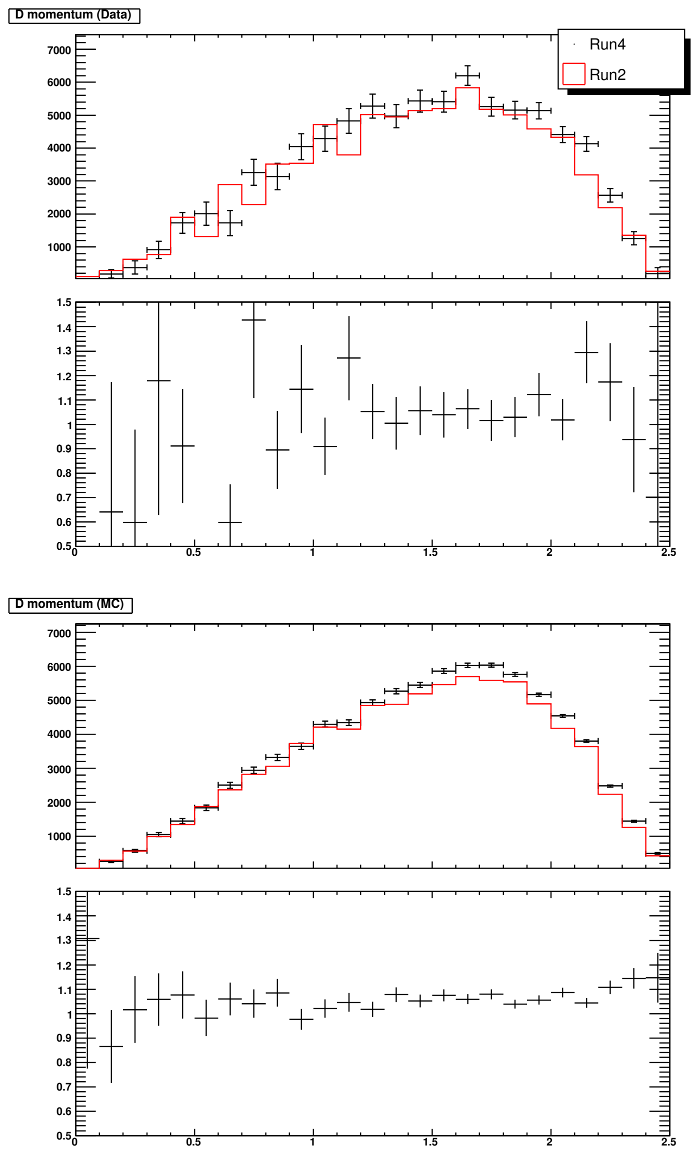

Figure 128: [**Run4 vs Run2 (Muon)** p_D D^+] Run4 vs Run2 D momentum plot for (OnPeak - OffPeak) data (top) and $B\bar{B}$ MC (bottom) of D^+ (Muon only). Black lines with uncertainties are Run4 and red histograms are Run2.

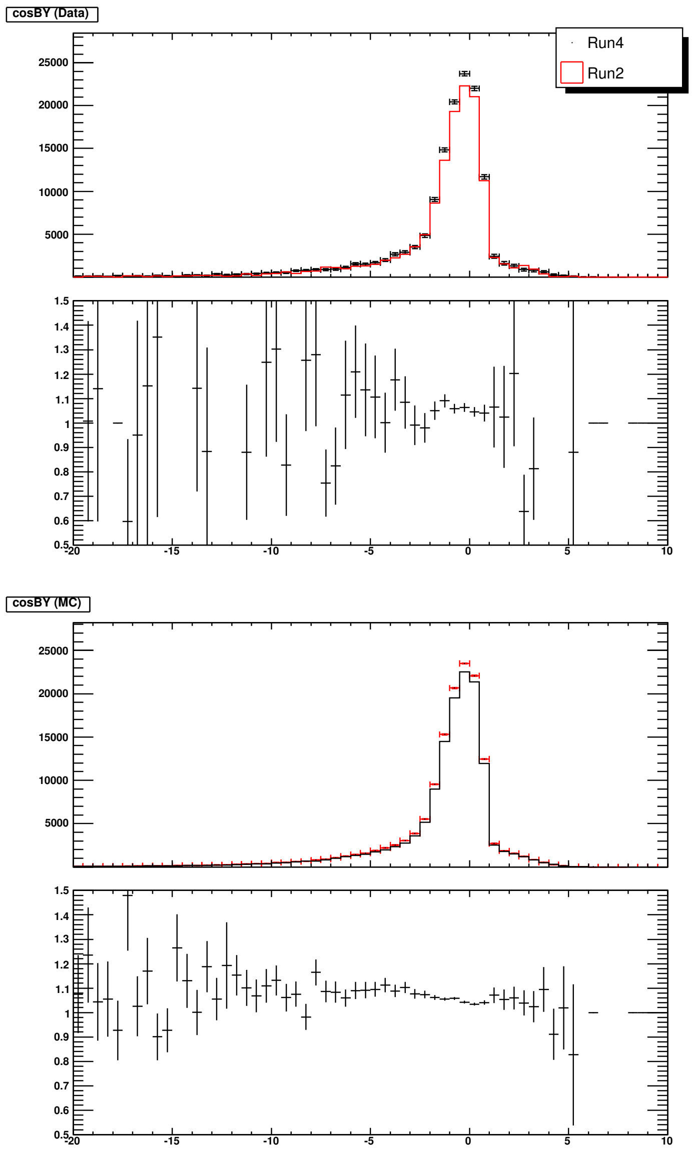

Figure 129: [**Run4 vs Run2 (Muon)** $\cos\Theta_{B-D\ell}$ D^0] Run4 vs Run2 $\cos\Theta_{B-D\ell}$ plot for (OnPeak - OffPeak) data (top) and $B\bar{B}$ MC (bottom) of D^0 (Muon only). Black lines with uncertainties are Run4 and red histograms are Run2.

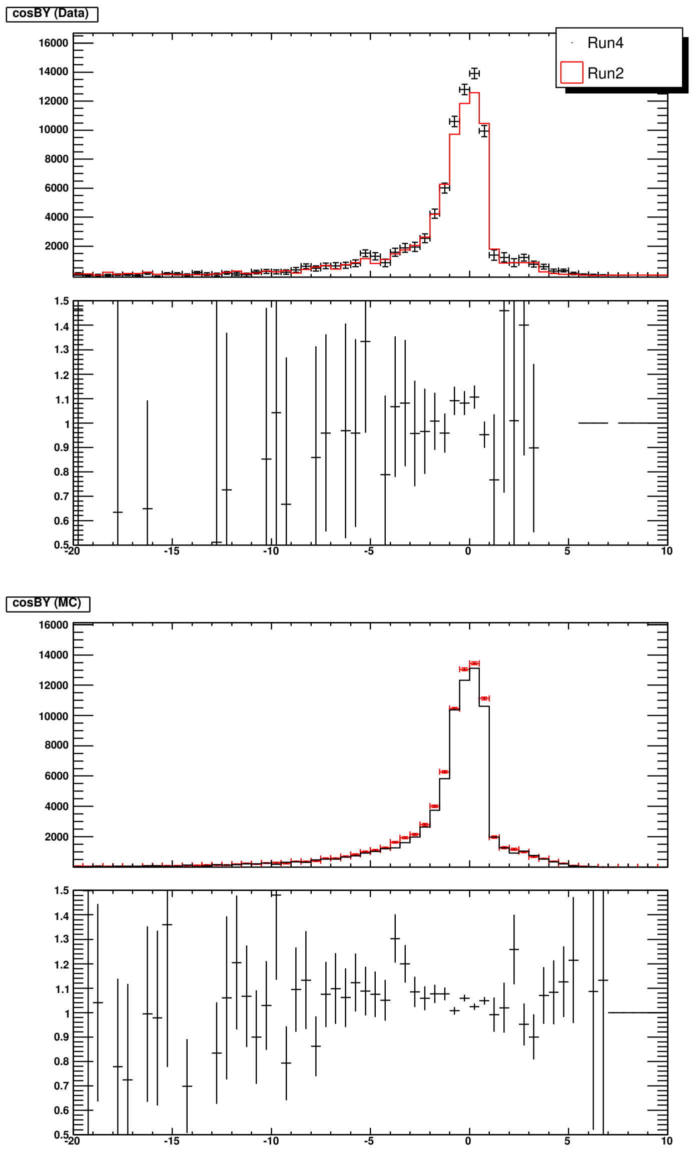

Figure 130: [**Run4 vs Run2 (Muon)** $\cos\Theta_{B-D\ell}$ D^+] Run4 vs Run2 $\cos\Theta_{B-D\ell}$ plot for (OnPeak - OffPeak) data (top) and $B\bar{B}$ MC (bottom) of D^+ (Muon only). Black lines with uncertainties are Run4 and red histograms are Run2.

12.2.2 Data vs MC

Run1 Data MC comparisons are given in Figures 131-133.
Run2 Data MC comparisons are given in Figures 134-136.
Run3 Data MC comparisons are given in Figures 137-139.
Run1-3 Data MC comparisons are given in Figures 140-142.
Run4 Data MC comparisons are given in Figures 143-145.

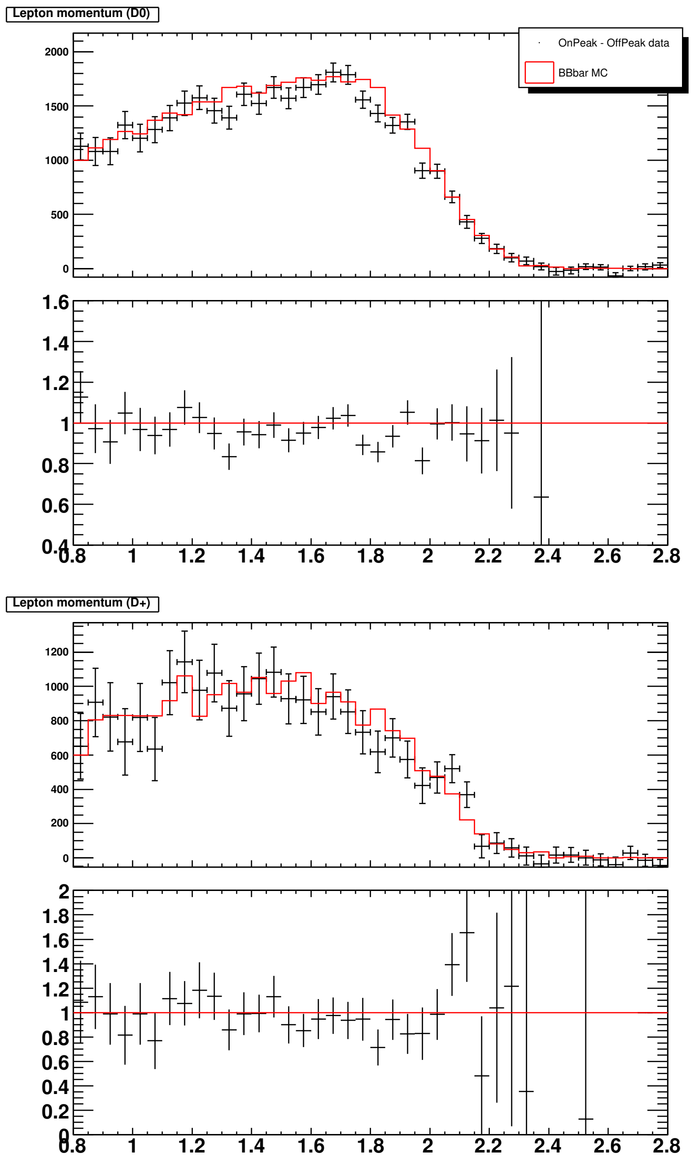

Figure 131: [**Run1 Data vs MC (Muon)** p_ℓ] Run1 Data vs MC lepton momentum plot for D^0 (top) and D^+ (bottom). Black lines with uncertainties (OnPeak - OffPeak) data and red histograms are $B\bar{B}$ MC.

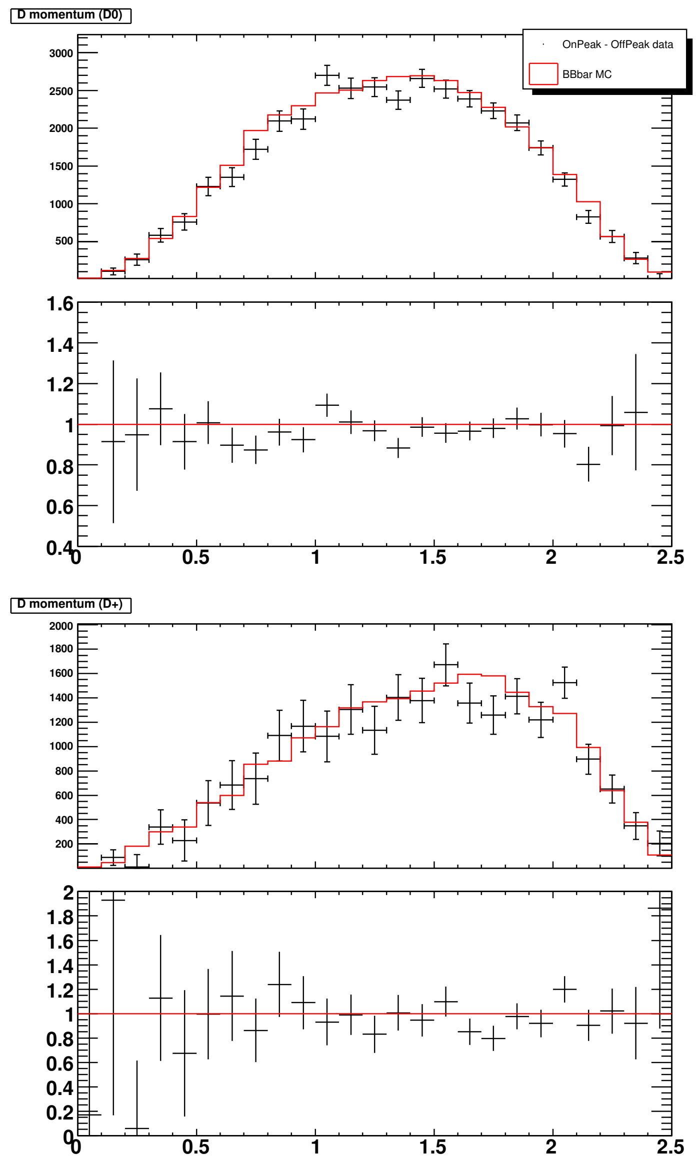

Figure 132: [**Run1 Data vs MC (Muon)** p_D] Run1 Data vs MC D momentum plot for D^0 (top) and D^+ (bottom). Black lines with uncertainties (OnPeak - OffPeak) data and red histograms are $B\bar{B}$ MC.

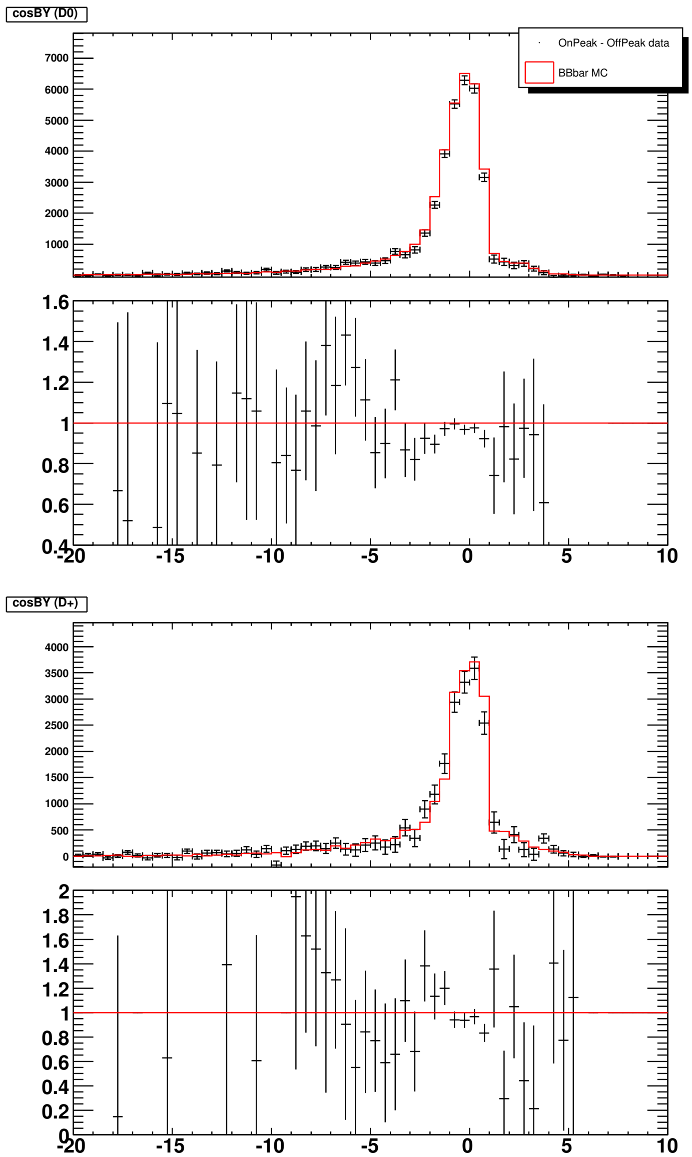

Figure 133: [**Run1 Data vs MC (Muon)** $\cos\Theta_{B-D\ell}$] Run1 Data vs MC $\cos\Theta_{B-D\ell}$ plot for D^0 (top) and D^+ (bottom). Black lines with uncertainties (OnPeak - OffPeak) data and red histograms are $B\bar{B}$ MC.

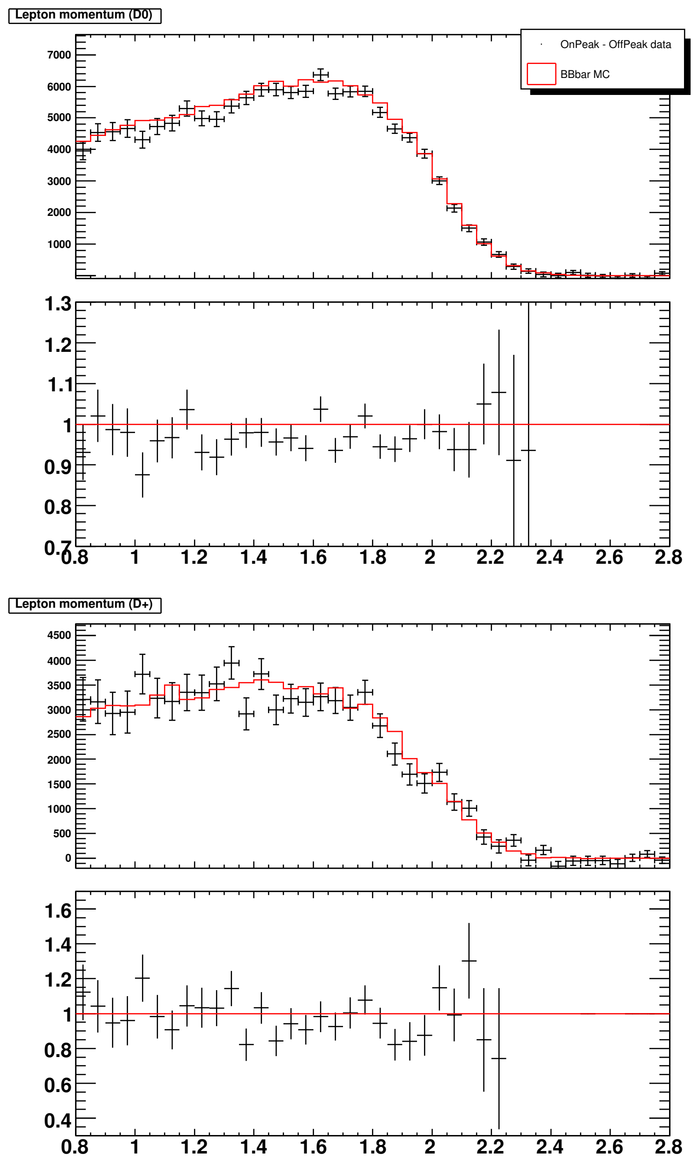

Figure 134: [**Run2 Data vs MC (Muon)** p_ℓ] Run2 Data vs MC lepton momentum plot for D^0 (top) and D^+ (bottom). Black lines with uncertainties (OnPeak - OffPeak) data and red histograms are $B\bar{B}$ MC.

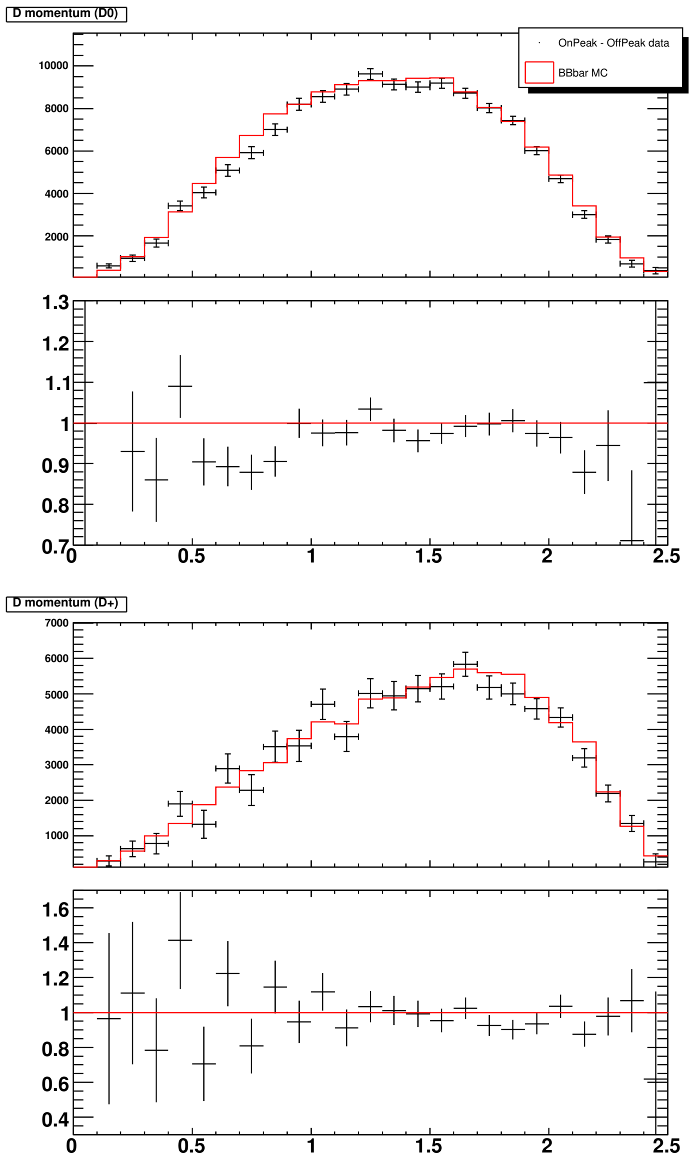

Figure 135: [**Run2 Data vs MC (Muon)** p_D] Run2 Data vs MC D momentum plot for D^0 (top) and D^+ (bottom). Black lines with uncertainties (OnPeak - OffPeak) data and red histograms are $B\bar{B}$ MC.

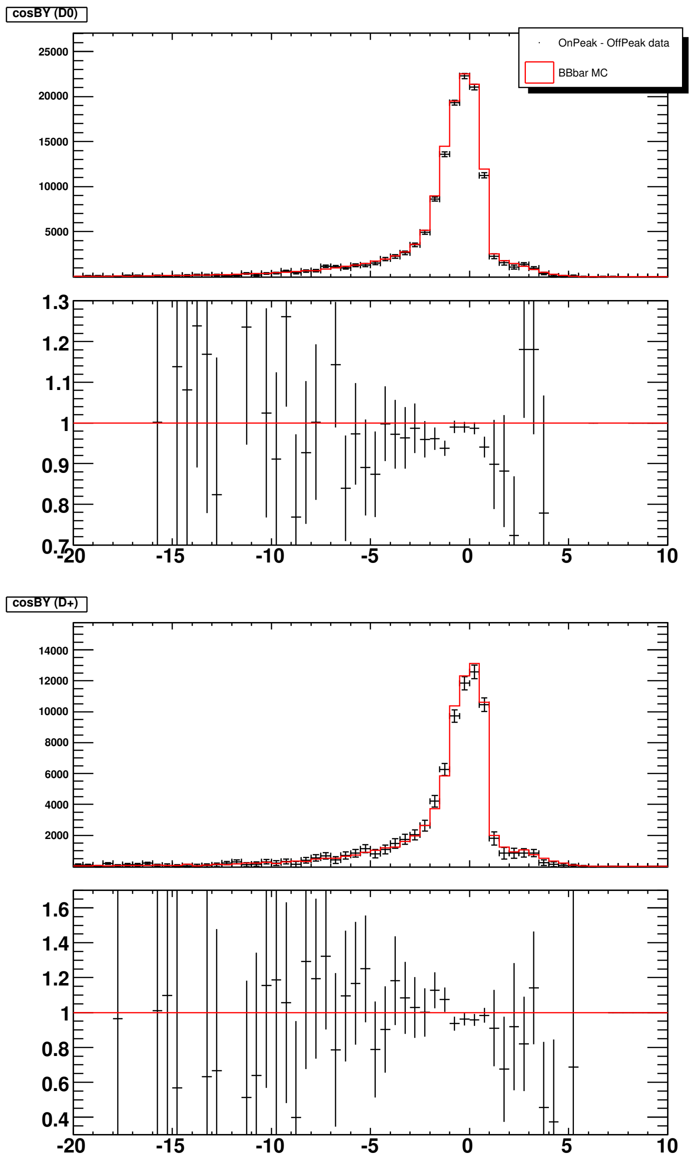

Figure 136: [**Run2 Data vs MC (Muon)** $\cos\Theta_{B-D\ell}$] Run2 Data vs MC $\cos\Theta_{B-D\ell}$ plot for D^0 (top) and D^+ (bottom). Black lines with uncertainties (OnPeak - OffPeak) data and red histograms are $B\bar{B}$ MC.

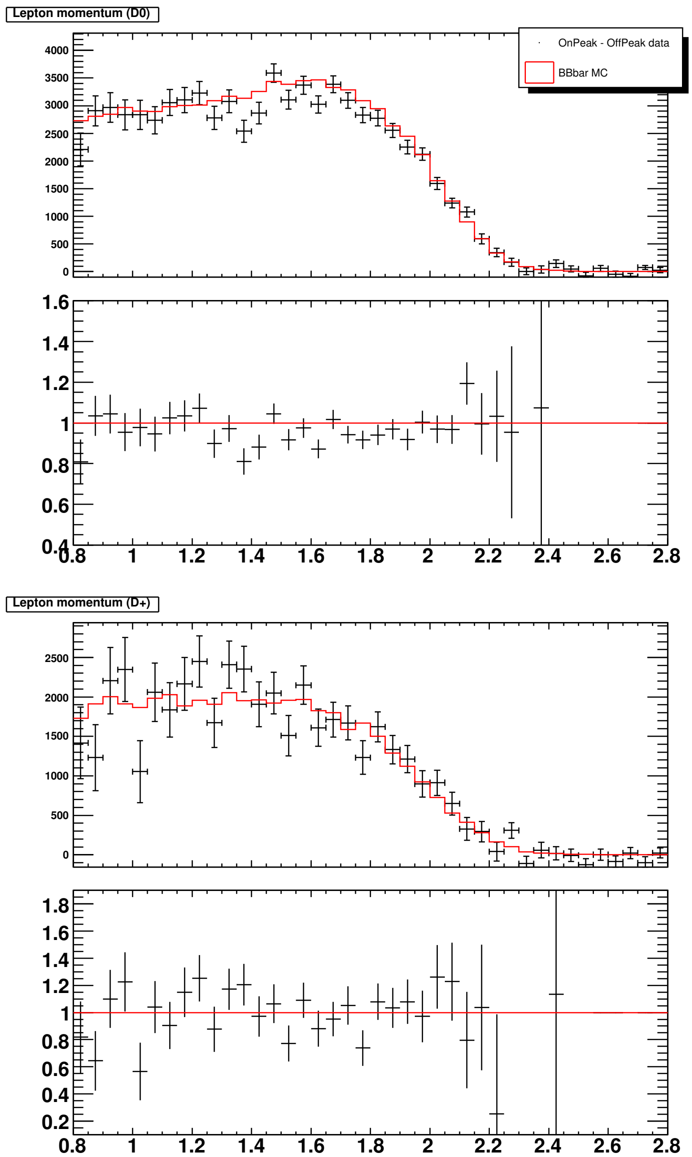

Figure 137: [**Run3 Data vs MC (Muon)** p_ℓ] Run3 Data vs MC lepton momentum plot for D^0 (top) and D^+ (bottom). Black lines with uncertainties (OnPeak - OffPeak) data and red histograms are $B\bar{B}$ MC.

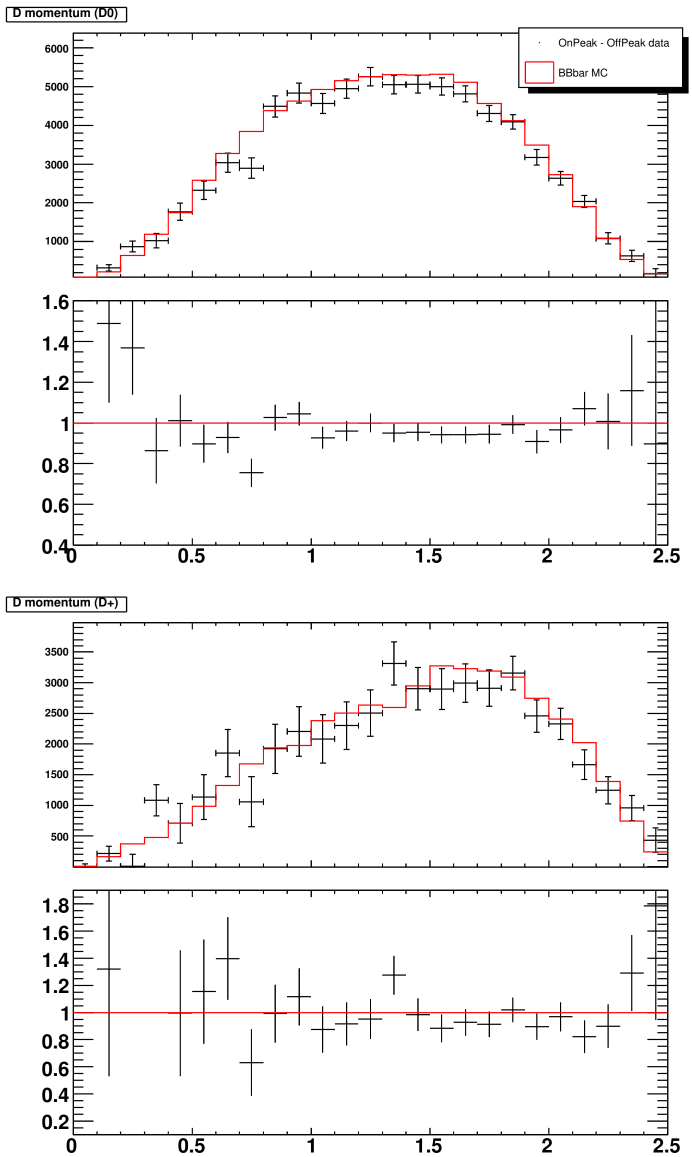

Figure 138: [**Run3 Data vs MC (Muon)** p_D] Run3 Data vs MC D momentum plot for D^0 (top) and D^+ (bottom). Black lines with uncertainties (OnPeak - OffPeak) data and red histograms are $B\bar{B}$ MC.

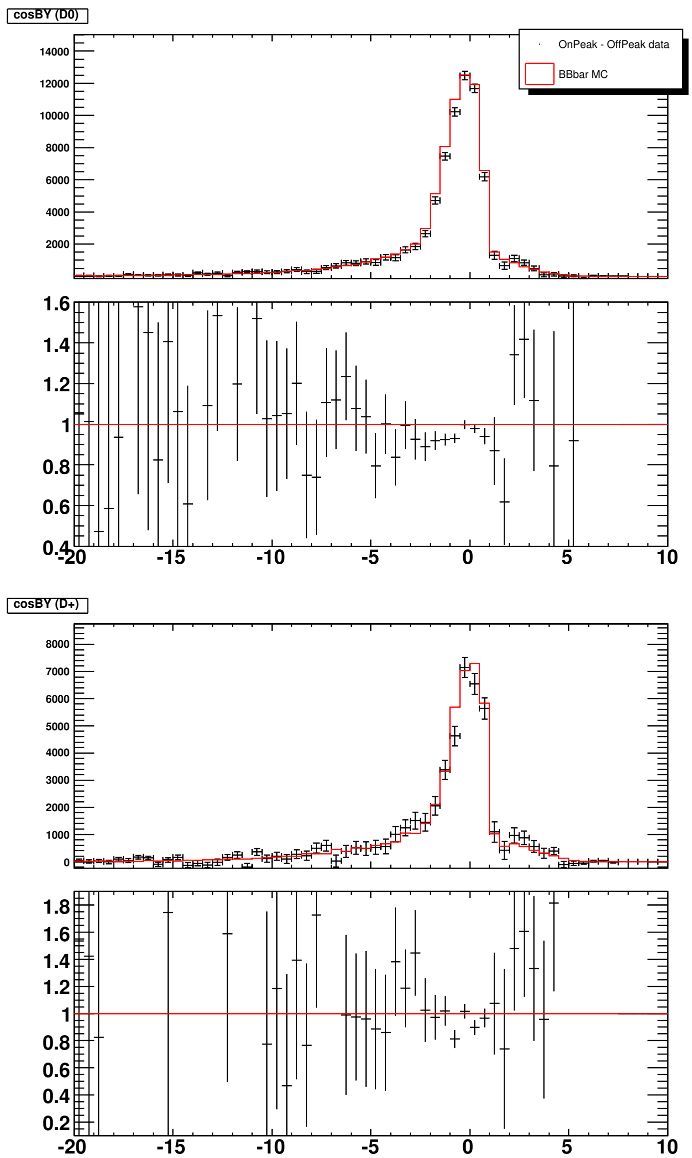

Figure 139: [**Run3 Data vs MC (Muon)** $\cos\Theta_{B-D\ell}$] Run3 Data vs MC $\cos\Theta_{B-D\ell}$ plot for D^0 (top) and D^+ (bottom). Black lines with uncertainties (OnPeak - OffPeak) data and red histograms are $B\bar{B}$ MC.

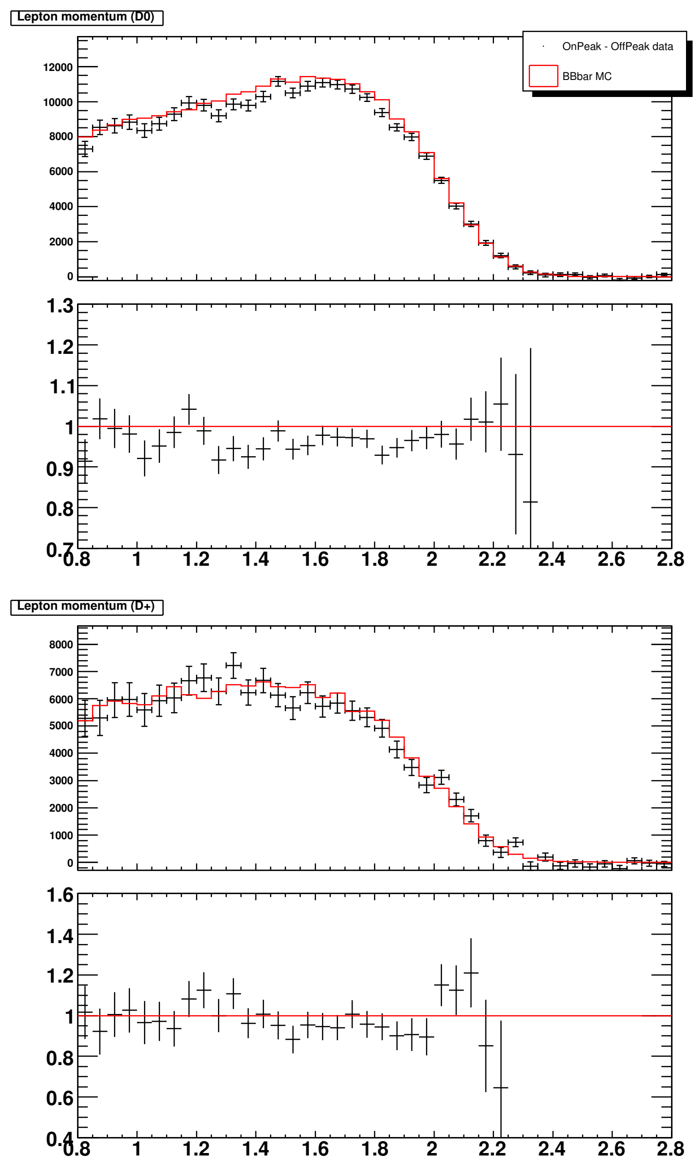

Figure 140: [**Run123 Data vs MC (Muon)** p_ℓ] Run123 Data vs MC lepton momentum plot for D^0 (top) and D^+ (bottom). Black lines with uncertainties (OnPeak - OffPeak) data and red histograms are $B\bar{B}$ MC.

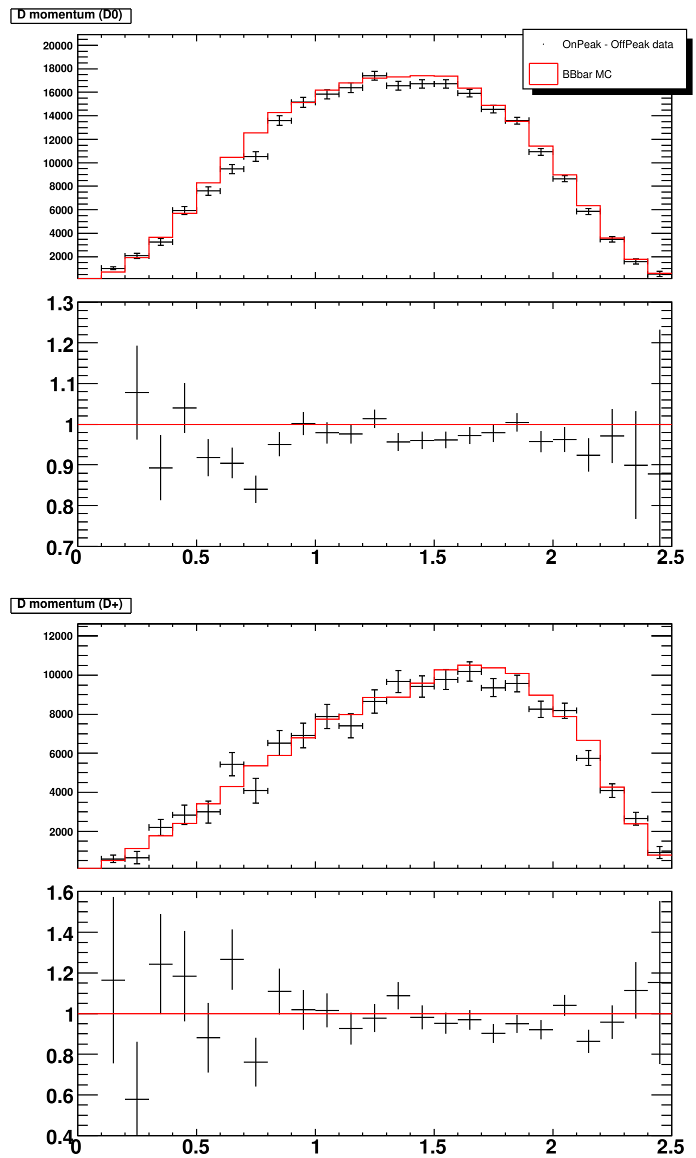

Figure 141: [**Run123 Data vs MC (Muon)** p_D] Run123 Data vs MC D momentum plot for D^0 (top) and D^+ (bottom). Black lines with uncertainties (OnPeak - OffPeak) data and red histograms are $B\bar{B}$ MC.

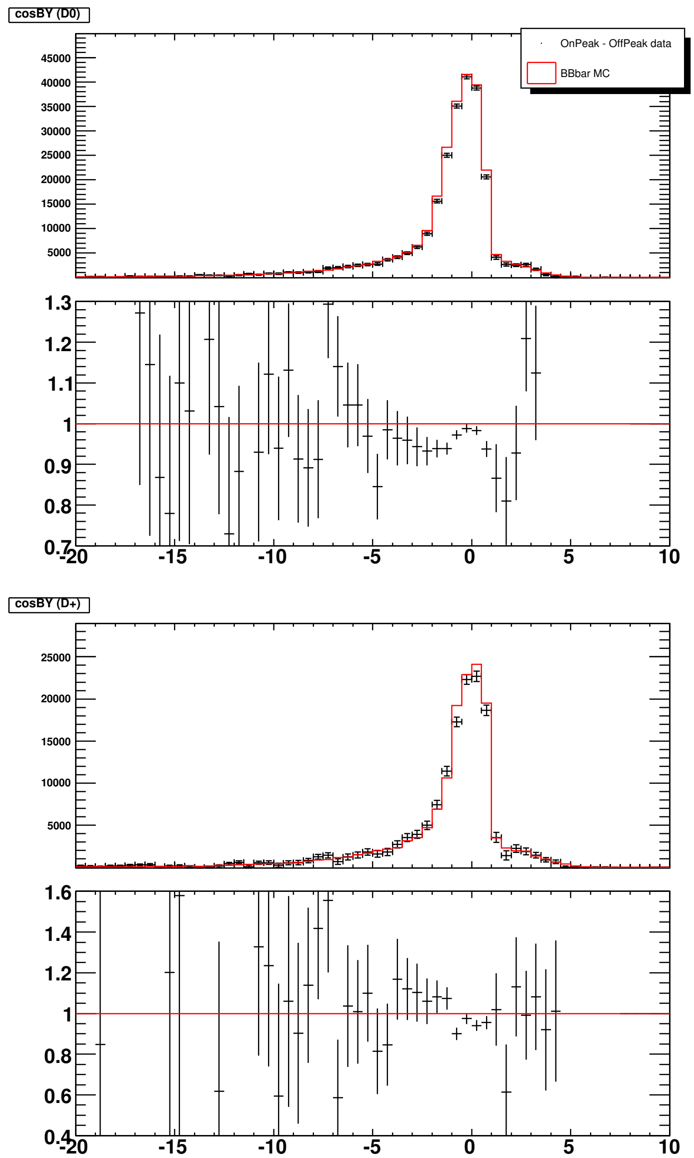

Figure 142: [**Run123 Data vs MC (Muon)** $\cos\Theta_{B-D\ell}$] Run123 Data vs MC $\cos\Theta_{B-D\ell}$ plot for D^0 (top) and D^+ (bottom). Black lines with uncertainties (OnPeak - OffPeak) data and red histograms are $B\bar{B}$ MC.

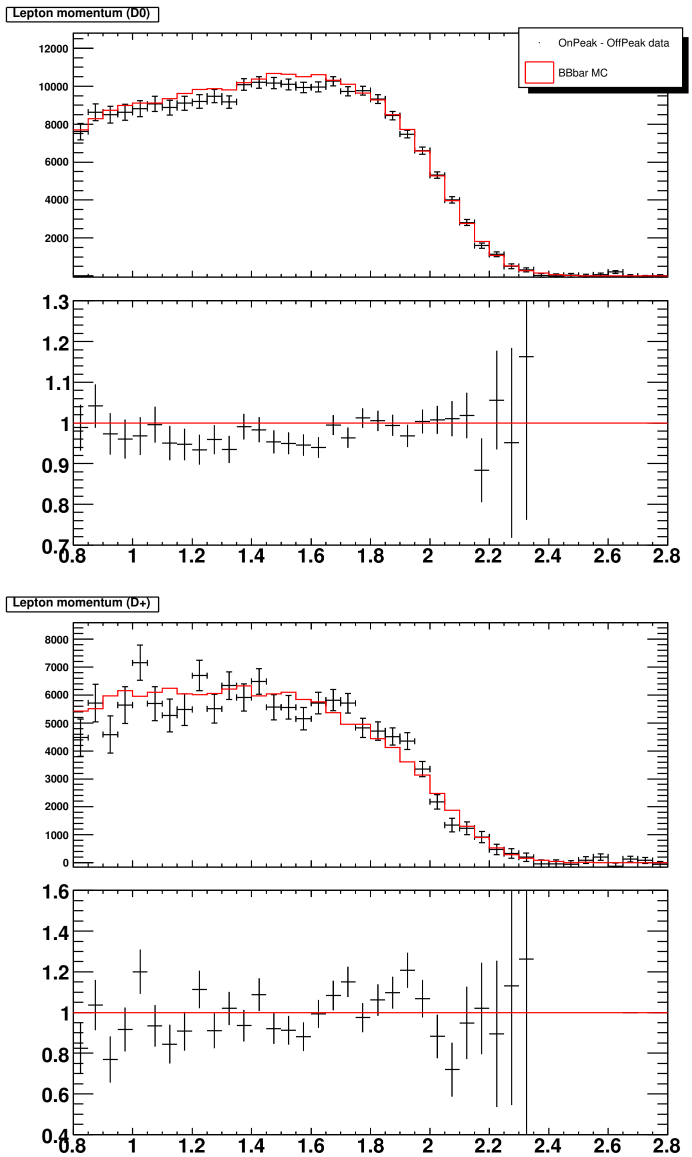

Figure 143: [**Run4 Data vs MC (Muon)** p_ℓ] Run4 Data vs MC lepton momentum plot for D^0 (top) and D^+ (bottom). Black lines with uncertainties (OnPeak - OffPeak) data and red histograms are $B\bar{B}$ MC.

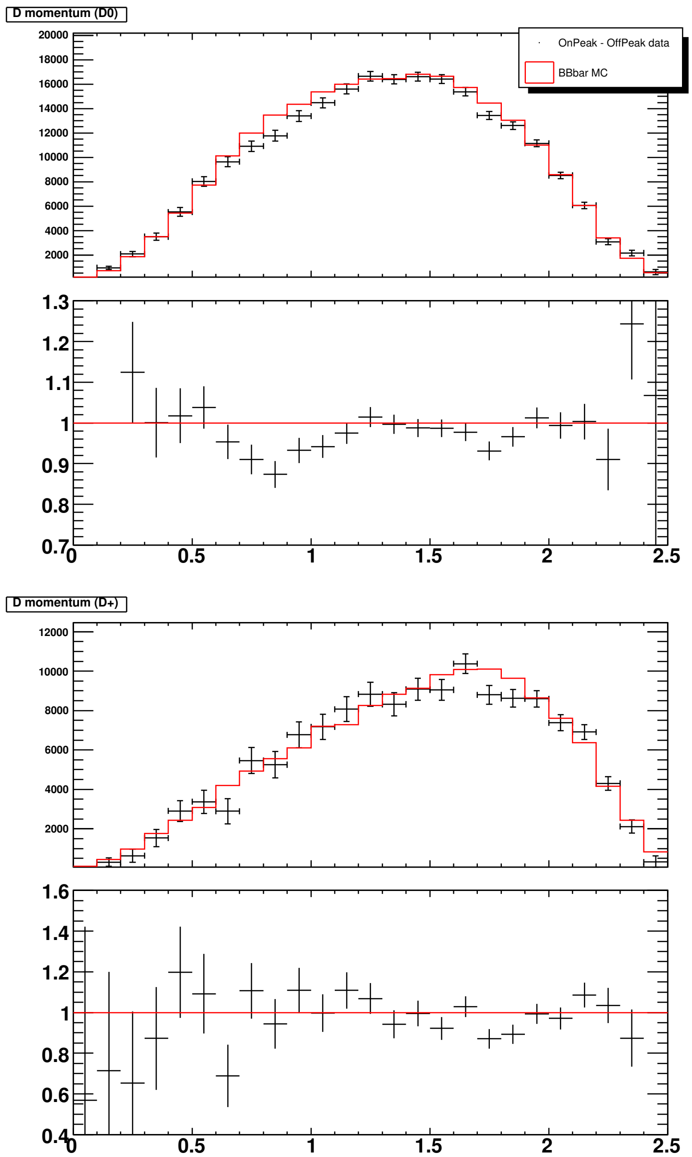

Figure 144: [**Run4 Data vs MC (Muon)** p_D] Run4 Data vs MC D momentum plot for D^0 (top) and D^+ (bottom). Black lines with uncertainties (OnPeak - OffPeak) data and red histograms are $B\bar{B}$ MC.

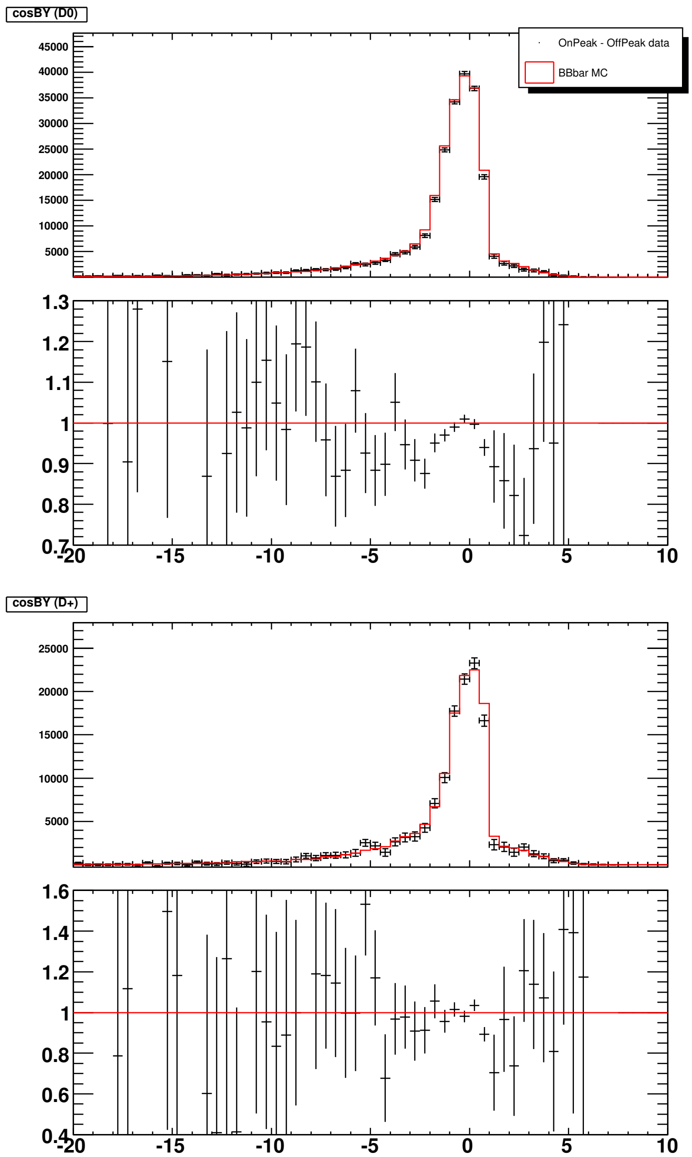

Figure 145: [**Run4 Data vs MC (Muon)** $\cos\Theta_{B-D\ell}$] Run4 Data vs MC $\cos\Theta_{B-D\ell}$ plot for D^0 (top) and D^+ (bottom). Black lines with uncertainties (OnPeak - OffPeak) data and red histograms are $B\bar{B}$ MC.

13 Fit Results

13.1 Summary of the fitting method

As described in section 5, we are trying to fit for three branching fractions and $\Upsilon(4S)$ decay BF ratio

- $\mathcal{B}(B^+ \to \bar{D}^0 \ell^+ \nu)$
- $\mathcal{B}(B^+ \to \bar{D}^{*0} \ell^+ \nu)$
- $\mathcal{BT}(B^+ \to \bar{D}^{**0}/(D\pi)^0 \ell^+ \nu)$
- f_{+0}

with isospin constraints

- $\mathcal{B}(B^+ \to \bar{D}^0 \ell^+ \nu) = t_{+0}\mathcal{B}(B^0 \to D^- \ell^+ \nu)$
- $\mathcal{B}(B^+ \to \bar{D}^{*0} \ell^+ \nu) = t_{+0}\mathcal{B}(B^0 \to D^{*-} \ell^+ \nu)$
- $\mathcal{B}(B^+ \to \bar{D}_0^{*0} \ell^+ \nu) = t_{+0}\mathcal{B}(B^0 \to D_0^{*-} \ell^+ \nu)$
- $\mathcal{B}(B^+ \to \bar{D}_1^0 \ell^+ \nu) = t_{+0}\mathcal{B}(B^0 \to D_1^- \ell^+ \nu)$
- $\mathcal{B}(B^+ \to \bar{D}_1^{*0} \ell^+ \nu) = t_{+0}\mathcal{B}(B^0 \to D_1'^- \ell^+ \nu)$
- $\mathcal{B}(B^+ \to \bar{D}_2^{*0} \ell^+ \nu) = t_{+0}\mathcal{B}(B^0 \to D_2^{*-} \ell^+ \nu)$
- $\mathcal{B}(B^+ \to D^- \pi^+ \ell^+ \nu) = 2\mathcal{B}(B^+ \to \bar{D}^0 \pi^0 \ell^+ \nu)$
  $= t_{+0}\mathcal{B}(B^0 \to \bar{D}^0 \pi^- \ell^+ \nu) = 2t_{+0}\mathcal{B}(B^0 \to D^- \pi^0 \ell^+ \nu)$
- $\mathcal{B}(B^+ \to D^{*-} \pi^+ \ell^+ \nu) = 2\mathcal{B}(B^+ \to \bar{D}^{*0} \pi^0 \ell^+ \nu)$
  $= t_{+0}\mathcal{B}(B^0 \to \bar{D}^{*0} \pi^- \ell^+ \nu) = 2t_{+0}\mathcal{B}(B^0 \to D^{*-} \pi^0 \ell^+ \nu)$

and constraints on relative branching fractions

- $f_{D_2^*/D_1} \equiv \frac{\mathcal{B}(B^+ \to \bar{D}_2^{*0} \ell^+ \nu)}{\mathcal{B}(B^+ \to \bar{D}_1^0 \ell^+ \nu)} = 0.78 \pm 0.17$
- $f_{D_0^* D\pi T/D_1 D_2^* T} \equiv \frac{\mathcal{BT}(B^+ \to \bar{D}_0^{*0}/(D\pi)^0 \ell^+ \nu)}{\mathcal{BT}(B^+ \to \bar{D}_1^0/\bar{D}_2^{*0} \ell^+ \nu)} = 0.77 \pm 0.19$
- $f_{D_1' D^*\pi T/D_1 D_2^* T} \equiv \frac{\mathcal{BT}(B^+ \to \bar{D}_1^{*0}/(D^*\pi)^0 \ell^+ \nu)}{\mathcal{BT}(B^+ \to \bar{D}_1^0/\bar{D}_2^{*0} \ell^+ \nu)} = 0.98 \pm 0.24$
- $f_{D\pi/D_0^*} \equiv \frac{\mathcal{B}(B^+ \to D^- \pi^+ \ell^+ \nu)}{\mathcal{B}(B^+ \to \bar{D}_0^{*0} \ell^+ \nu)} = 0.42 \pm 0.28$
- $f_{D^*\pi/D_1'} \equiv \frac{\mathcal{B}(B^+ \to D^{*-} \pi^+ \ell^+ \nu)}{\mathcal{B}(B^+ \to \bar{D}_1^{*0} \ell^+ \nu)} = 0.071 \pm 0.050$

and by floating background components

- $C^{D^0}_{UncorDL}$

- $C^{D^0}_{UncorCL}$
- $C^{D^0}_{CascL}$
- $C^{D^+}_{UncorDL}$
- $C^{D^+}_{UncorCL}$
- $C^{D^+}_{CascL}$

but fixing background components

- $C^{D^0}_{FakeL} = 1$
- $C^{D^+}_{FakeL} = 1$

In addition, we are fitting for form factor parameters

- $B \to D\ell\nu$ decay FF slope : ρ^2_D
- $B \to D^*\ell\nu$ decay FF slope : ρ^2
- $B \to D^*\ell\nu$ decay FF ratio : R_1
- $B \to D^*\ell\nu$ decay FF ratio : R_2

by fixing

- $B \to D^{**}\ell\nu$ decay FF slope : $\hat{\tau}' = -1.5 \pm 0.5$
- Approximation B1 : $\tau_1 = 0, \tau_2 = 0$
  for systematics, Approximation B2 : $\tau_1 = \bar{\Lambda}\tau, \tau_2 = -\bar{\Lambda}'\tau$
  (see details of $B \to D^{**}\ell\nu$ decay FF in Appendix H)

Note that we tried to float other parameters such as D decay BF in our fit, but toy MC study (see section 11.1) revealed large biases. So we resulted in the above combination of free parameters.

13.2 Fit results

Fit results are shown in Table 30 and correlations between parameters are given in Table 31. Plots of lepton momentum, D momentum and $\cos\theta_{B-Dl}$ after fitting are given in Figure 146 - 148. Figure 149 - 151 show the same variables with fitted binning. Bin by bin plots after fitting are also shown in Figure 152 and 153.

Parameters	Fit results
ρ^2_D	1.354 ± 0.066 (4.9 %)
ρ^2	1.338 ± 0.076 (5.7 %)
R_1	1.443 ± 0.123 (7.8 %)
R_2	0.680 ± 0.099 (14.5 %)
$\mathcal{B}(B^+ \to \bar{D}^0 \ell^+ \nu)$	0.02522 ± 0.00063 (2.4 %)
$\mathcal{B}(B^+ \to \bar{D}^{*0} \ell^+ \nu)$	0.05156 ± 0.00083 (1.6 %)
$\mathcal{BT}(B^+ \to \bar{D}^{**0}/(D\pi)^0 \ell^+ \nu)$	0.02197 ± 0.00096 (4.4 %)
f_{+0}	1.100 ± 0.031 (2.8 %)
$C^{D^0}_{UncorDL}$	0.996 ± 0.051 (5.1 %)
$C^{D^0}_{UncorCL}$	0.818 ± 0.063 (7.7 %)
$C^{D^0}_{CascL}$	0.798 ± 0.092 (11.5 %)
$C^{D^+}_{UncorDL}$	1.098 ± 0.126 (11.5 %)
$C^{D^+}_{UncorCL}$	0.815 ± 0.136 (16.7 %)
$C^{D^+}_{CascL}$	1.351 ± 0.224 (16.6 %)
χ^2/ndof (P-value)	237/215 (0.15)

Table 30: **(Run2 only)** [**Nominal fit results**] Fit results.

	ρ_D^2	ρ^2	R_1	R_2	$\mathcal{B}(D)$	$\mathcal{B}(D^*)$	Other	f_{+0}	$C^{D^0}_{UDL}$	$C^{D^0}_{UL}$	$C^{D^0}_{Cas}$	$C^{D^+}_{UDL}$	$C^{D^+}_{UCL}$	$C^{D^+}_{Cas}$
ρ_D^2	1													
ρ^2	-0.304	1												
R_1	-0.190	0.821	1											
R_2	0.260	-0.900	-0.900	1										
$\mathcal{B}(D\ell\nu)$	0.447	0.094	0.094	0.043	1									
$\mathcal{B}(D^*\ell\nu)$	-0.402	0.216	0.018	-0.260	-0.593	1								
$\mathcal{B}$(Oter)	0.090	-0.146	-0.125	0.146	0.087	-0.487	1							
f_{+0}	0.152	0.111	0.081	-0.005	0.393	-0.518	0.160	1						
$C^{D^0}_{UncDL}$	-0.029	0.090	0.351	-0.299	-0.028	-0.196	-0.080	-0.048	1					
$C^{D^0}_{UncCL}$	-0.189	0.110	0.183	-0.123	-0.194	0.078	0.060	-0.141	-0.212	1				
$C^{D^0}_{CascL}$	0.079	-0.022	-0.112	0.014	0.102	0.160	-0.551	-0.021	-0.080	-0.452	1			
$C^{D^+}_{UncDL}$	-0.160	0.092	0.111	-0.108	-0.151	-0.017	-0.097	0.286	0.084	0.012	0.016	1		
$C^{D^+}_{UncCL}$	-0.061	0.010	0.011	-0.007	-0.068	0.007	0.044	0.053	-0.014	0.022	-0.039	-0.399	1	
$C^{D^+}_{CascL}$	0.039	0.025	0.012	0.003	0.041	0.049	-0.295	0.076	0.013	-0.045	0.188	0.027	-0.350	1

Table 31: **(Run2 only)** [**Correlation coefficients**] Correlations between parameters.

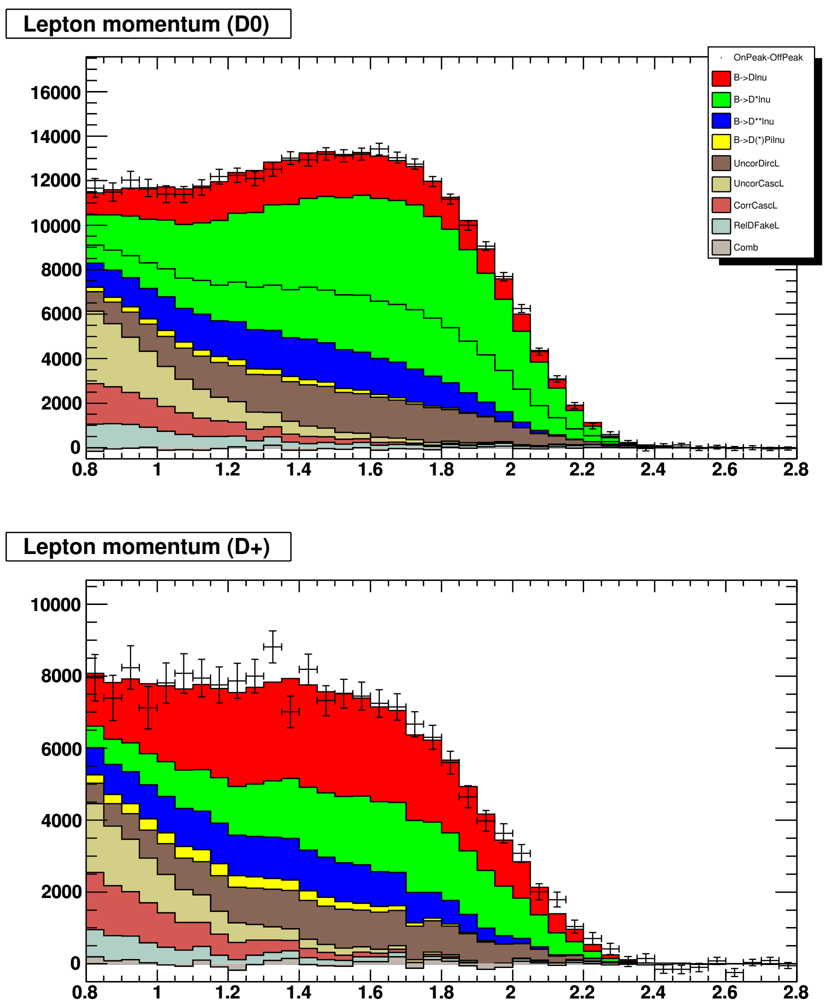

Figure 146: **(Run2 only)** [p_ℓ **after fitting**] Lepton momentum plot after fitting. The top is D^0 and the bottom is D^+. Black is OnPeak - OffPeak data. Red is $B \to D\ell\nu$, green is $B \to D^*\ell\nu$, blue is $B \to D^{**}\ell\nu$, yellow is non-resonant $B \to D^{(*)}\pi\ell\nu$, and the rest is background. Dark brown is UncorrDL, light brown is UncorrCL, dark red is CascL, blue gray is FakeL, and light gray is Comb. Comb is almost disappeared after D mass sideband subtraction.

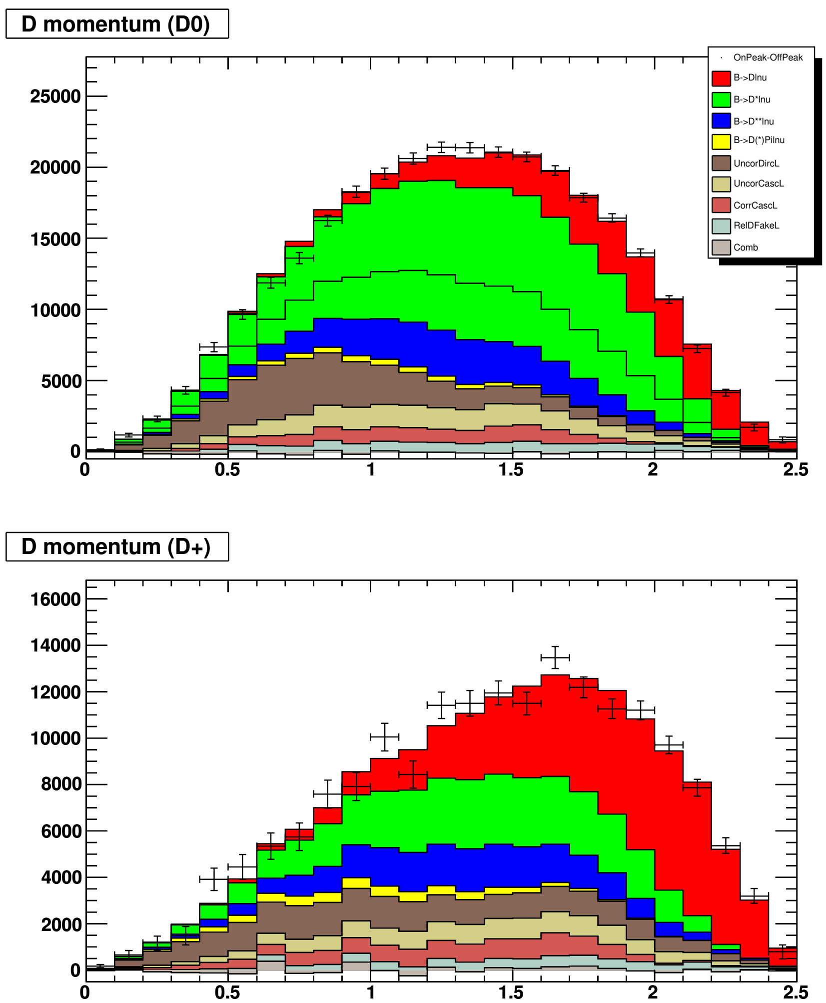

Figure 147: **(Run2 only)** [p_D **after fitting**] D momentum plot after fitting. The top is D^0 and the bottom is D^+. Black is OnPeak - OffPeak data. Red is $B \to D\ell\nu$, green is $B \to D^*\ell\nu$, blue is $B \to D^{**}\ell\nu$, yellow is non-resonant $B \to D^{(*)}\pi\ell\nu$, and the rest is background. Dark brown is UncorrDL, light brown is UncorrCL, dark red is CascL, blue gray is FakeL, and light gray is Comb. Comb is almost disappeared after D mass sideband subtraction.

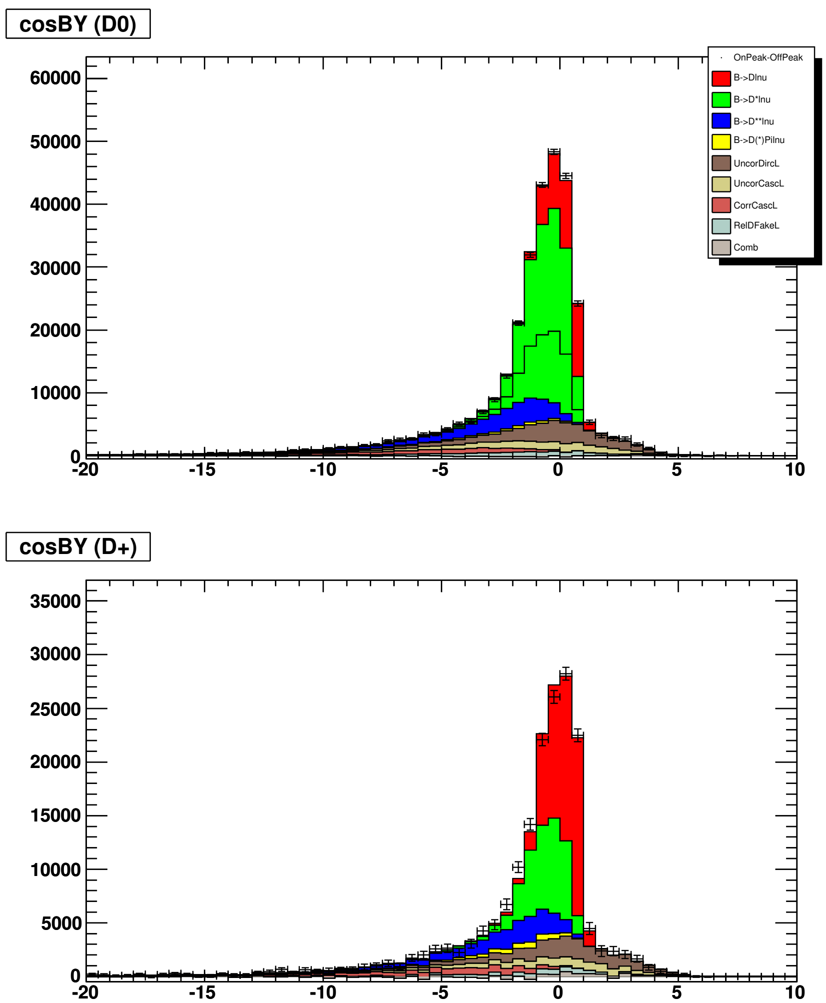

Figure 148: **(Run2 only)** [$\cos\theta_{B-Dl}$ **after fitting**] $\cos\theta_{B-Dl}$ plot after fitting. The top is D^0 and the bottom is D^+. Black is OnPeak - OffPeak data. Red is $B \to D\ell\nu$, green is $B \to D^*\ell\nu$, blue is $B \to D^{**}\ell\nu$, yellow is non-resonant $B \to D^{(*)}\pi\ell\nu$, and the rest is background. Dark brown is UncorrDL, light brown is UncorrCL, dark red is CascL, blue gray is FakeL, and light gray is Comb. Comb is almost disappeared after D mass sideband subtraction.

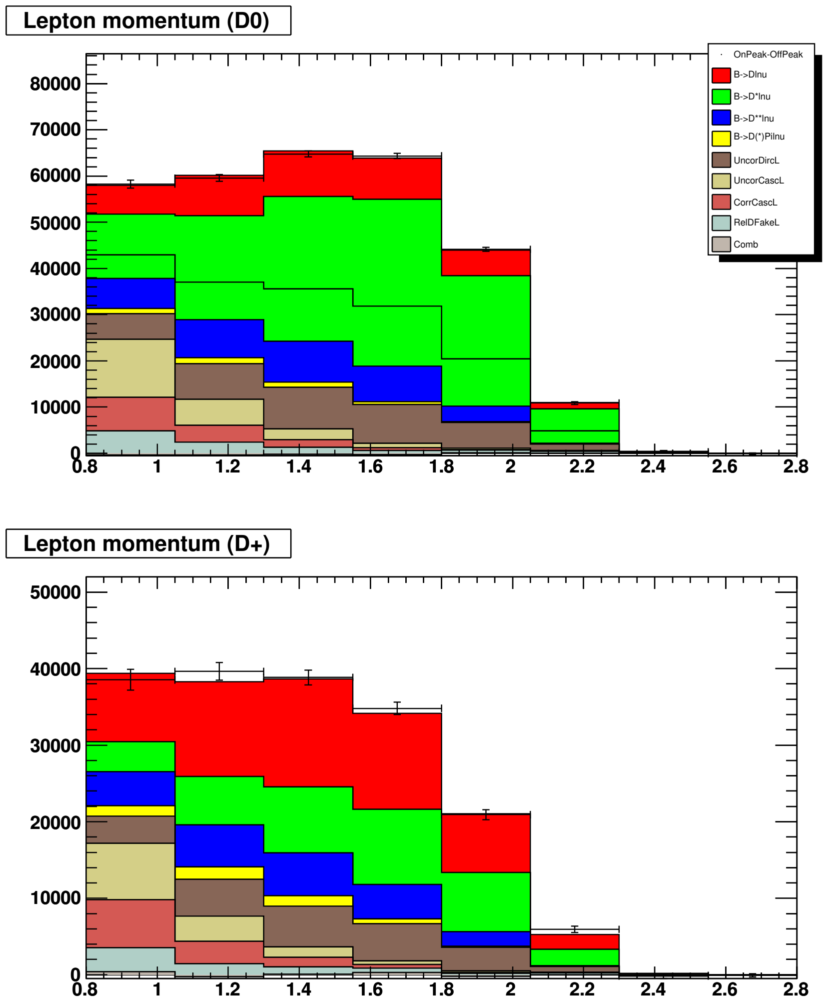

Figure 149: **(Run2 only)** [p_ℓ **with fitted binning**] Lepton momentum plot with fitted binning after fitting. The top is D^0 and the bottom is D^+. Black is OnPeak - OffPeak data. Red is $B \to D\ell\nu$, green is $B \to D^*\ell\nu$, blue is $B \to D^{**}\ell\nu$, yellow is non-resonant $B \to D^{(*)}\pi\ell\nu$, and the rest is background. Dark brown is UncorrDL, light brown is UncorrCL, dark red is CascL, blue gray is FakeL, and light gray is Comb. Comb is almost disappeared after D mass sideband subtraction.

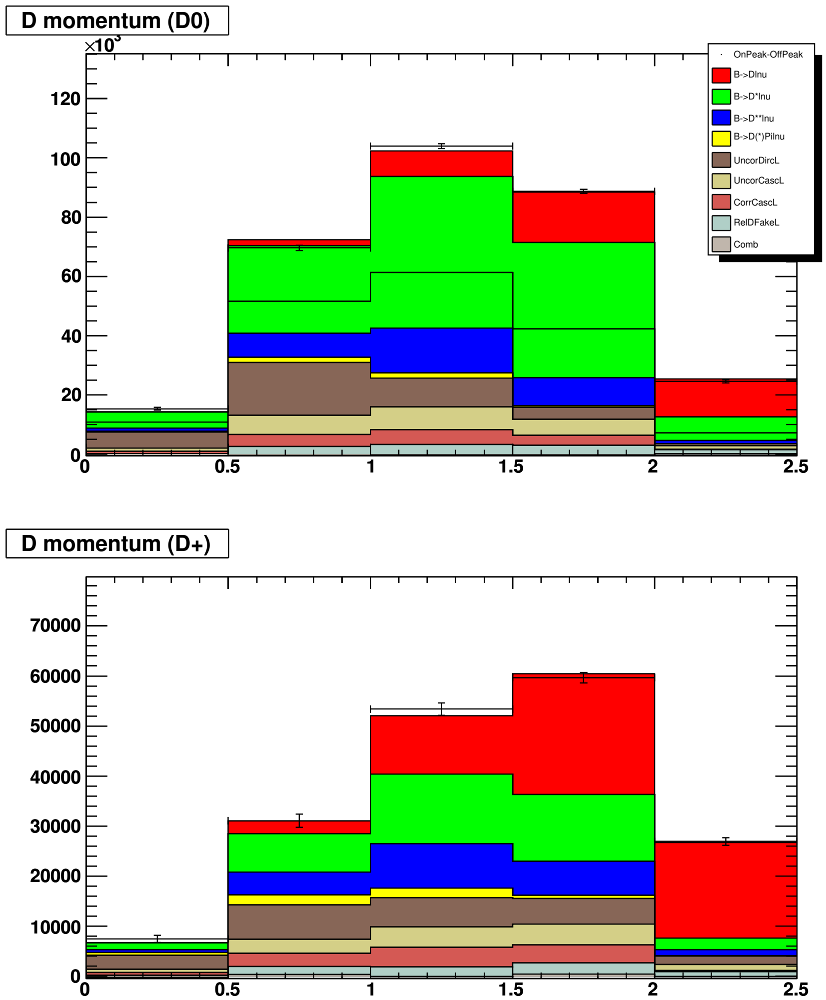

Figure 150: **(Run2 only)** [p_D **with fitted binning**] D momentum plot with fitted binning after fitting. The top is D^0 and the bottom is D^+. Black is OnPeak - OffPeak data. Red is $B \to D\ell\nu$, green is $B \to D^*\ell\nu$, blue is $B \to D^{**}\ell\nu$, yellow is non-resonant $B \to D^{(*)}\pi\ell\nu$, and the rest is background. Dark brown is UncorrDL, light brown is UncorrCL, dark red is CascL, blue gray is FakeL, and light gray is Comb. Comb is almost disappeared after D mass sideband subtraction.

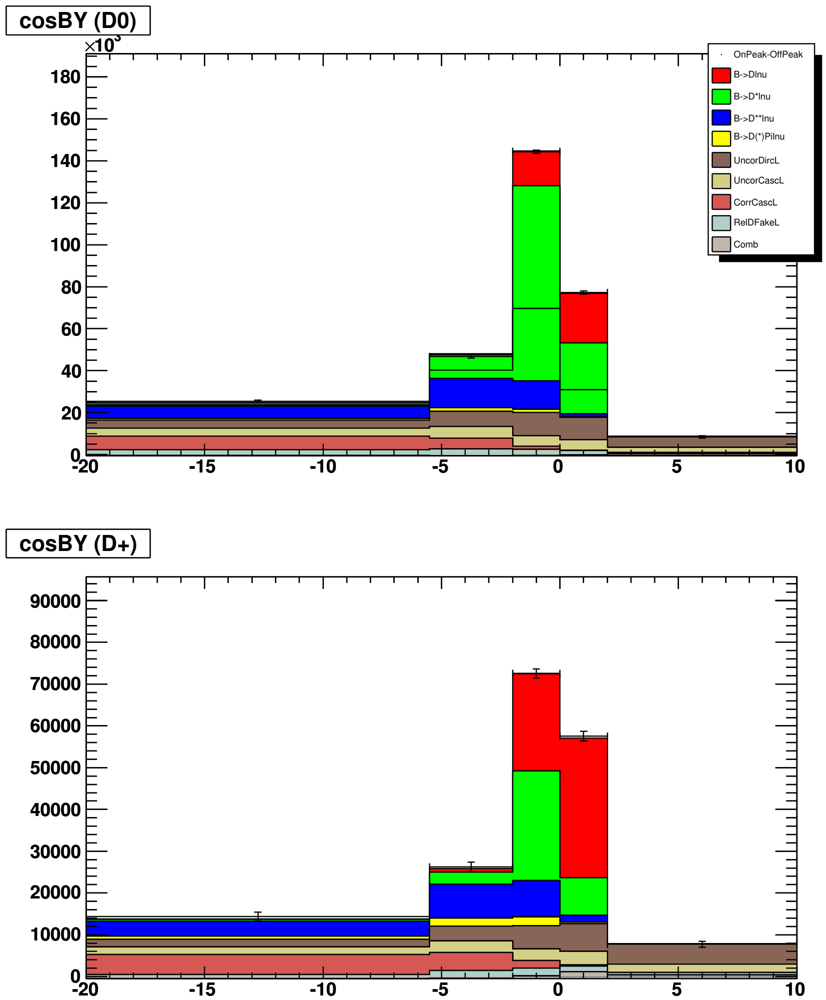

Figure 151: **(Run2 only)** [$\cos\theta_{B-Dl}$ **with fitted binning**] $\cos\theta_{B-Dl}$ plot with fitted binning after fitting. The top is D^0 and the bottom is D^+. Black is OnPeak - OffPeak data. Red is $B \to D\ell\nu$, green is $B \to D^*\ell\nu$, blue is $B \to D^{**}\ell\nu$, yellow is non-resonant $B \to D^{(*)}\pi\ell\nu$, and the rest is background. Dark brown is UncorrDL, light brown is UncorrCL, dark red is CascL, blue gray is FakeL, and light gray is Comb. Comb is almost disappeared after D mass sideband subtraction.

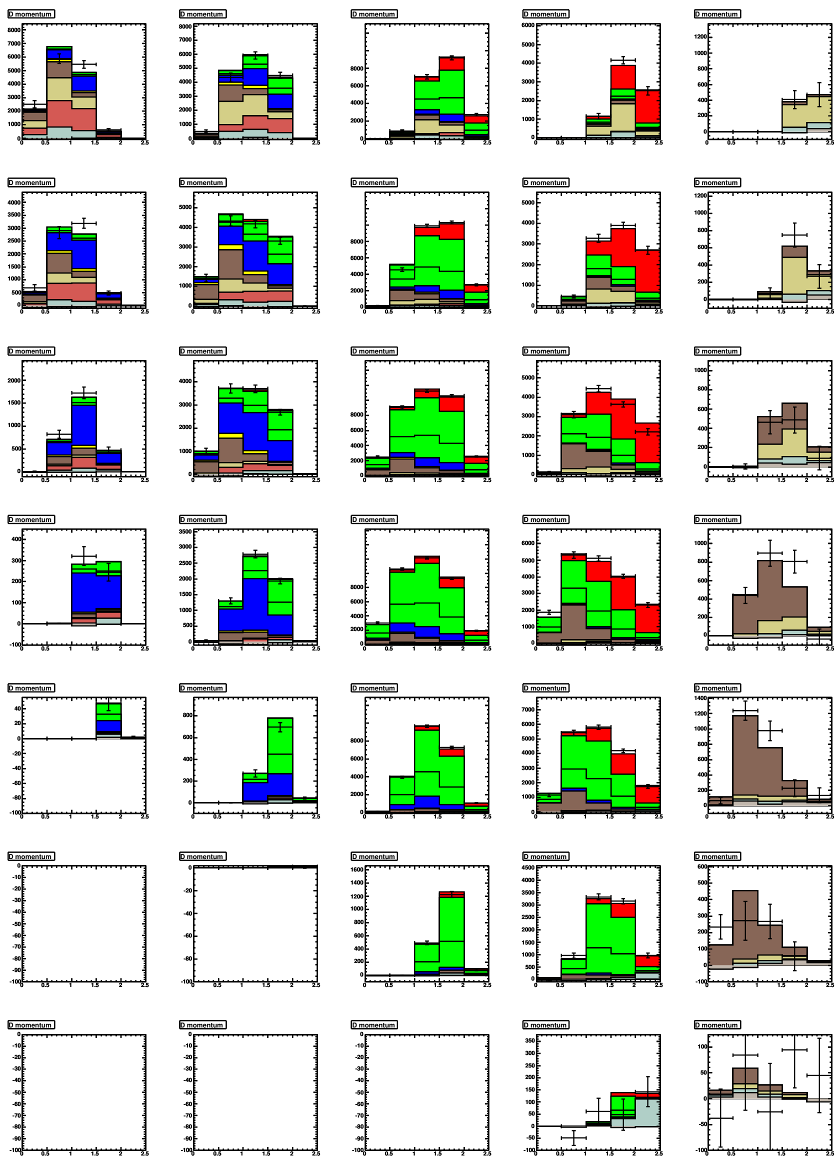

Figure 152: **(Run2 only)** [D^0 **bin by bin after fitting**] D^0 momentum plots showing all bins after fitting. From top to bottom, lepton momentum bin changes from the lowest to the highest, and from left to right, cosBY bin changes from negative to positive. In each plots, colors are the same as other plots. Black is OnPeak - OffPeak data. Red is $B \to D\ell\nu$, green is $B \to D^*\ell\nu$, blue is $B \to D^{**}\ell\nu$, yellow is non-resonant $B \to D^{(*)}\pi\ell\nu$, and the rest is background. Dark brown is UncorrDL, light brown is UncorrCL, dark red is CascL, blue gray is FakeL, and light gray is Comb. Comb is almost disappeared after D mass sideband subtraction.

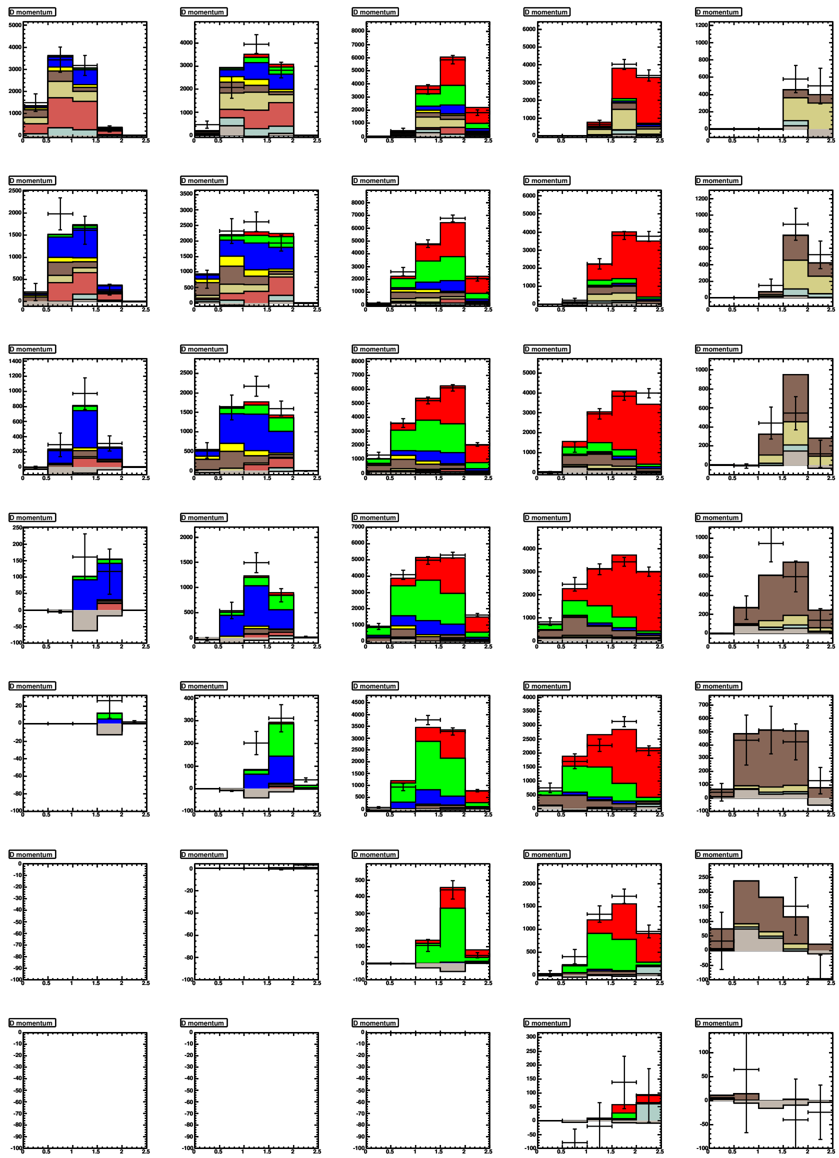

Figure 153: **(Run2 only)** [D^+ **bin by bin after fitting**] D^+ momentum plots showing all bins after fitting. From top to bottom, lepton momentum bin changes from the lowest to the highest, and from left to right, cosBY bin charger's from negative to positive. In each plots, colors are the same as other plots. Black is OnPeak - OffPeak data. Red is $B \to D\ell\nu$, green is $B \to D^{*}\ell\nu$, blue is $B \to D^{**}\ell\nu$, yellow is non-resonant $B \to D^{(*)}\pi\ell\nu$, and the rest is background. Dark brown is UncorrDL, light brown is UncorrCL, dark red is CascL, blue gray is FakeL, and light gray is Comb. Comb is almost disappeared after D mass sideband subtraction.

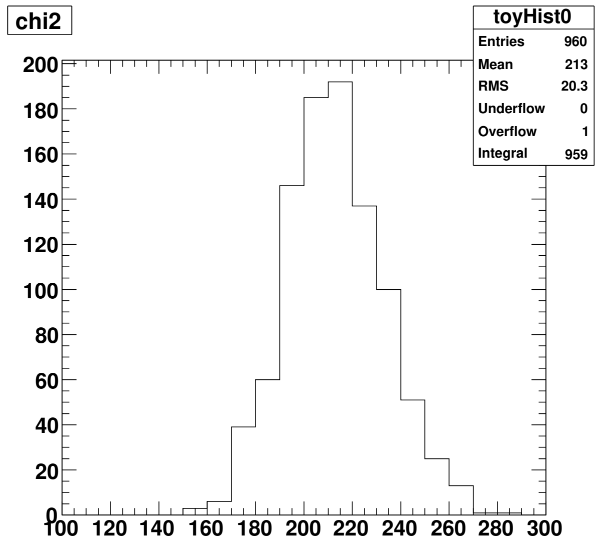

Figure 154: **(Run2 only)** [**Toy MC** χ^2 **: Nominal**] Toy MC χ^2 plot.

13.3 Toy MC study for nominal fit

13.3.1 Pull results.

Pulls are calculated by Equation (310). The χ^2 and the pull plots are shown in Figure 154 - 157 only for parameter Set a. The mean and standard deviation of these pull distributions are listed in Table 32. In the bottom line of the Table 32, the uncertainty on mean and standard deviation are listed. These are calculated with the number of succeeded fit $N = 960$. Assuming the standard deviation is $\sigma = 1$, the uncertainty on mean is

$$\frac{\sigma}{\sqrt{N}} = \frac{1}{\sqrt{960}} = 0.0323 \tag{318}$$

and the uncertainty on standard deviation is

$$\frac{\sigma}{\sqrt{2N}} = \frac{1}{\sqrt{2 \times 960}} = 0.0228 \tag{319}$$

The mean of the pulls of R_1, R_2, $\mathcal{B}(B^+ \to \bar{D}^0\ell^+\nu)$and $\mathcal{BT}(B^+ \to \bar{D}^{**0}/(D\pi)^0\ell^+\nu)$ are 2 - 3 times the uncertainty listed in the bottom line. Certain biases, while statistically significant, are numerically small (no more than 0.1 σ bais in the mean and no more than a few percent bias in the r.m.s.). **We may apply corrections to fitted results based on these toy MC studies.**

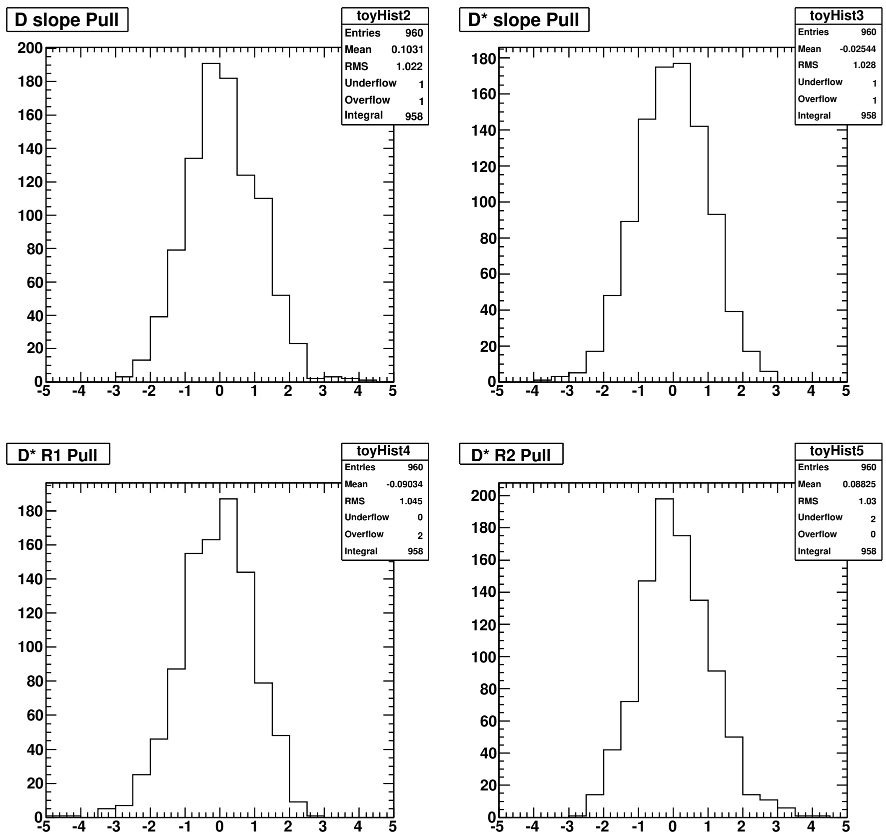

Figure 155: **(Run2 only)** [**Toy MC Pull FF : Nominal**] Toy MC pull plots for FF parameters.

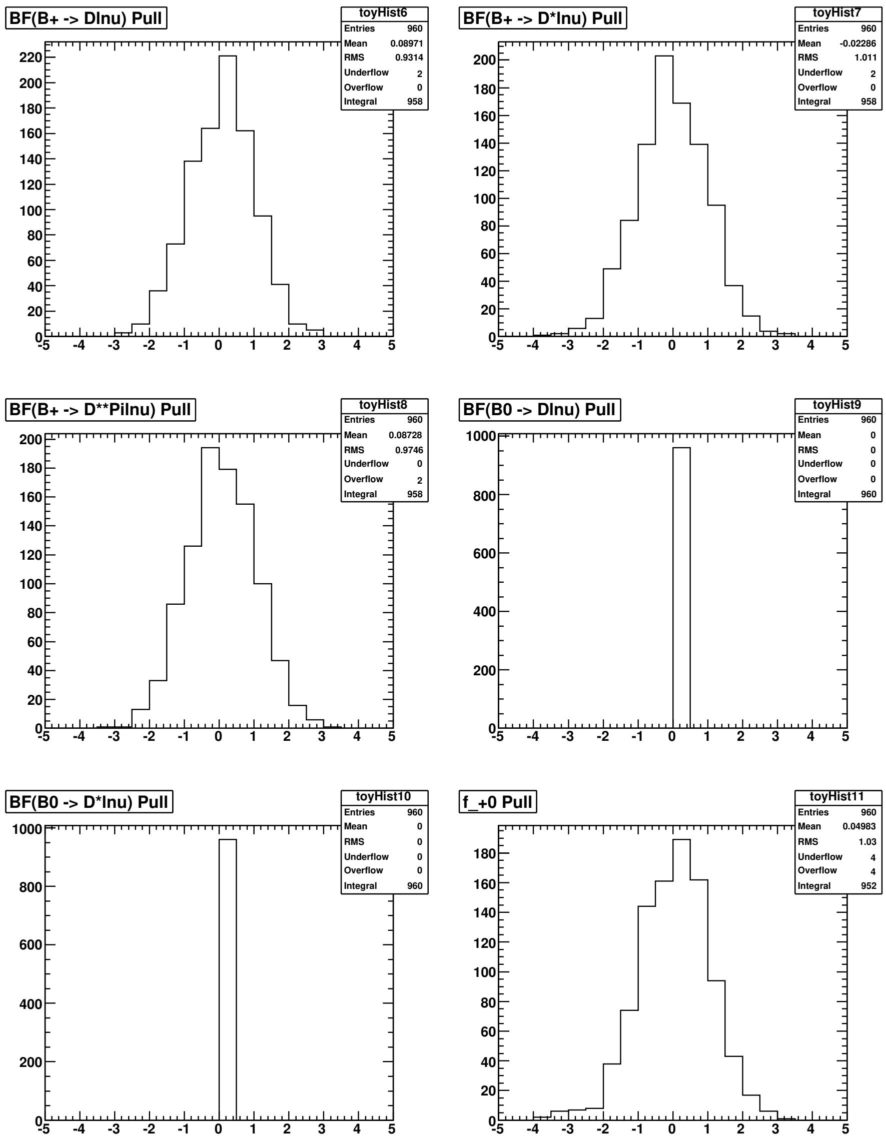

Figure 156: **(Run2 only)** [**Toy MC Pull BF : Nominal**] Toy MC pull plots for BF and f_{+0}.

Parameters	Mean	Standard Deviation
ρ_D^2	0.1031	1.022
ρ^2	-0.0254	1.028
R_1	-0.0903	1.045
R_2	0.0883	1.030
$\mathcal{B}(B^+ \to \bar{D}^0 \ell^+ \nu)$	0.0897	0.931
$\mathcal{B}(B^+ \to \bar{D}^{*0} \ell^+ \nu)$	-0.0229	1.011
$\mathcal{BT}(B^+ \to \bar{D}^{**0}/(D\pi)^0 \ell^+ \nu)$	0.0873	0.975
f_{+0}	0.0498	1.030
$C_{UncorDL}^{D^0}$	-0.0060	1.030
$C_{UncorCL}^{D^0}$	-0.0254	1.007
$C_{CascL}^{D^0}$	-0.0191	0.991
$C_{UncorDL}^{D^+}$	0.0169	1.040
$C_{UncorCL}^{D^+}$	0.0432	1.025
$C_{CascL}^{D^+}$	-0.0490	1.019
Uncertainty	0.0323	0.0228

Table 32: **(Run2 only)** [**Toy MC Nominal : Mean and Standard Deviation**] Mean and standard deviation of pull distributions of toy MC fits (Figures 155-157). The uncertainty on mean and standard deviation are also listed in the bottom line. Pulls are calculated from the difference to nominal fit results.

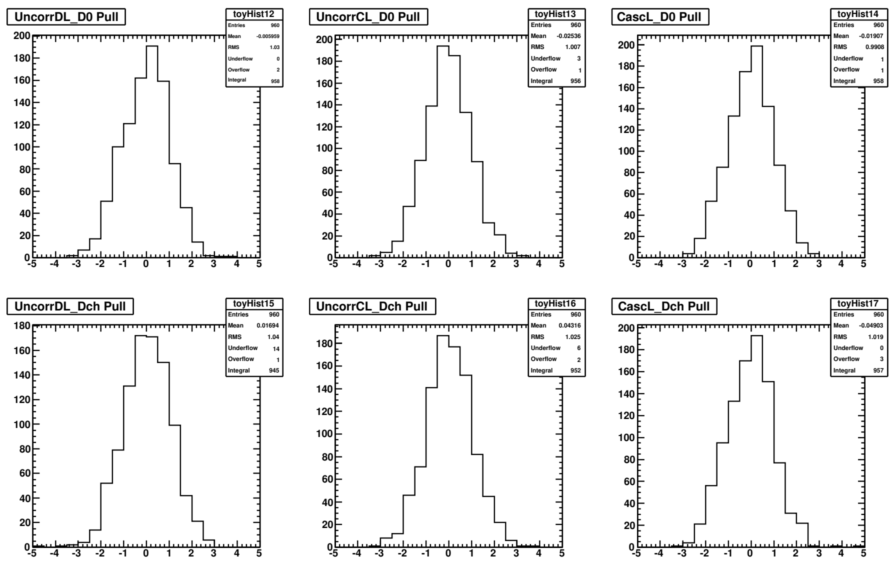

Figure 157: **(Run2 only)** [**Toy MC Pull Bkg : Nominal**] Toy MC pull plots for background components.

14 Cross Checks

14.1 Lepton momentum cut

In previous analysis of Babar, lepton momentum cuts were applied in one of the event selection cuts. For example, a cut such as $p^*_\ell > 1.2$ GeV was applied (see section 19), where p^*_ℓ is the lepton momentum in the CM frame. This cut is to reduce background because signal/bckground ratio is poor at lower p^*_ℓ, and to remove low qualty lepton tracks because both charged track reconstruction and particle identification are not efficient for low momentum tracks. We apply this cut to see how it affect on our fit. The results are given in Table 33. The normalized residuals (NR) in the Table is defined by

$$\mathrm{NR} = \frac{\text{(Fitted value)} - \text{(Nominal value)}}{\text{(Statistical uncertainty on the fitted value)}} \tag{320}$$

We also apply a cut on LAB frame lepton momentum, p^{LAB}_ℓ

$$p^{LAB}_\ell > 1.2\mathrm{GeV} \tag{321}$$

because

- To remove low quality tracks, LAB frame momentum are more appropriate than CM frame momentum.
- We can retain some part of $p^*_\ell < 1.2$ GeV candidates.

We apply the cut and compare the results with nominal fit. The results are also shown in Table 33. Plots after fitting are also given in Figures 158 to 160. No systematic uncertainty is assigned based on this.

Parameters	$p_\ell^* > 1.2$ GeV		$p_\ell^{LAB} > 1.2$ GeV	
	Fit results	NR	Fit results	NR
ρ_D^2	$\pm$		$\pm$	
ρ^2	$\pm$		$\pm$	
R_1	$\pm$		$\pm$	
R_2	$\pm$		$\pm$	
$\mathcal{B}(B^+ \to \bar{D}^0\ell^+\nu)$	$\pm$		$\pm$	
$\mathcal{B}(B^+ \to \bar{D}^{*0}\ell^+\nu)$	$\pm$		$\pm$	
$\mathcal{BT}(B^+ \to \bar{D}^{**0}/(D\pi)^0\ell^+\nu)$	$\pm$		$\pm$	
f_{+0}	$\pm$		$\pm$	
$C^{D^0}_{UncorDL}$	$\pm$		$\pm$	
$C^{D^0}_{UncorCL}$	$\pm$		$\pm$	
$C^{D^0}_{CascL}$	$\pm$		$\pm$	
$C^{D^+}_{UncorDL}$	$\pm$		$\pm$	
$C^{D^+}_{UncorCL}$	$\pm$		$\pm$	
$C^{D^+}_{CascL}$	$\pm$		$\pm$	
χ^2/ndof (P-value)	234/215 (0.18)			

Table 33: **(Run2 only)** [p_ℓ **cut**] Results and normaliaed residuals (NR) for the fit with p_ℓ >1.2 GeV cut.

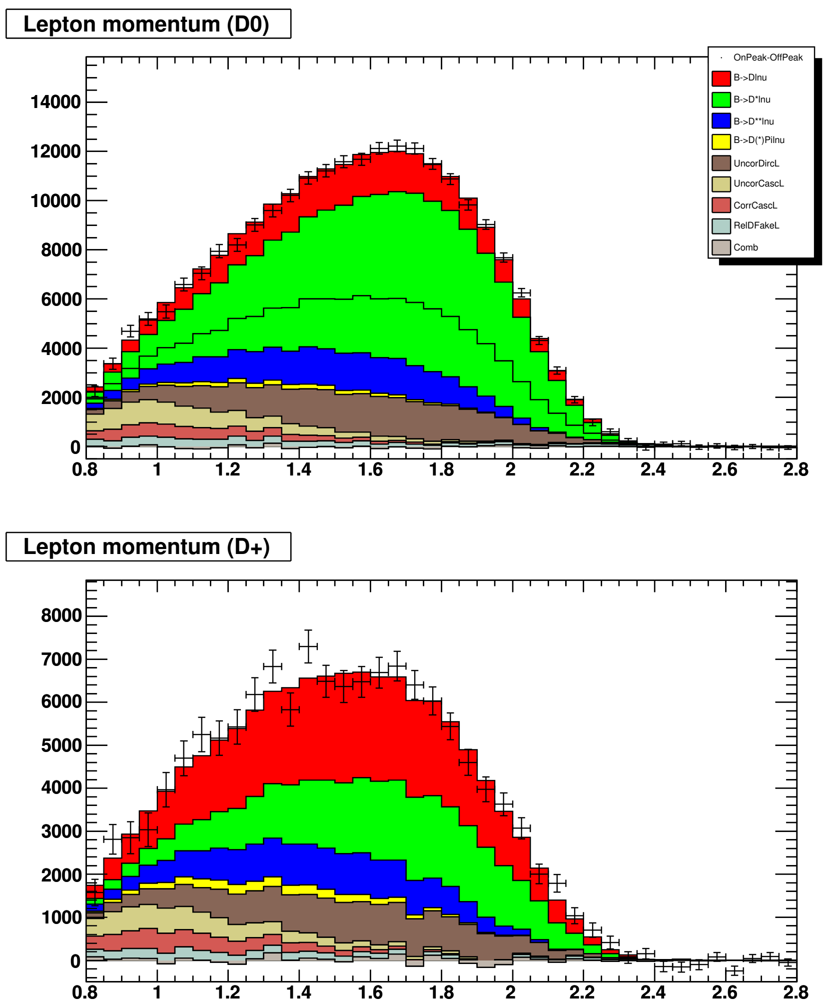

Figure 158: **(Run2 only)** [p_ℓ **with** p_ℓ^{LAB} **cut**] Lepton momentum plot with p_ℓ^{LAB} cut. The top is D^0 and the bottom is D^+. Black is OnPeak - OffPeak data. Red is $B \to D\ell\nu$, green is $B \to D^*\ell\nu$, blue is $B \to D^{**}\ell\nu$, yellow is non-resonant $B \to D^{(*)}\pi\ell\nu$, and the rest is background. Dark brown is UncorrDL, light brown is UncorrCL, dark red is CascL, blue gray is FakeL, and light gray is Comb. Comb is almost disappeared after D mass sideband subtraction.

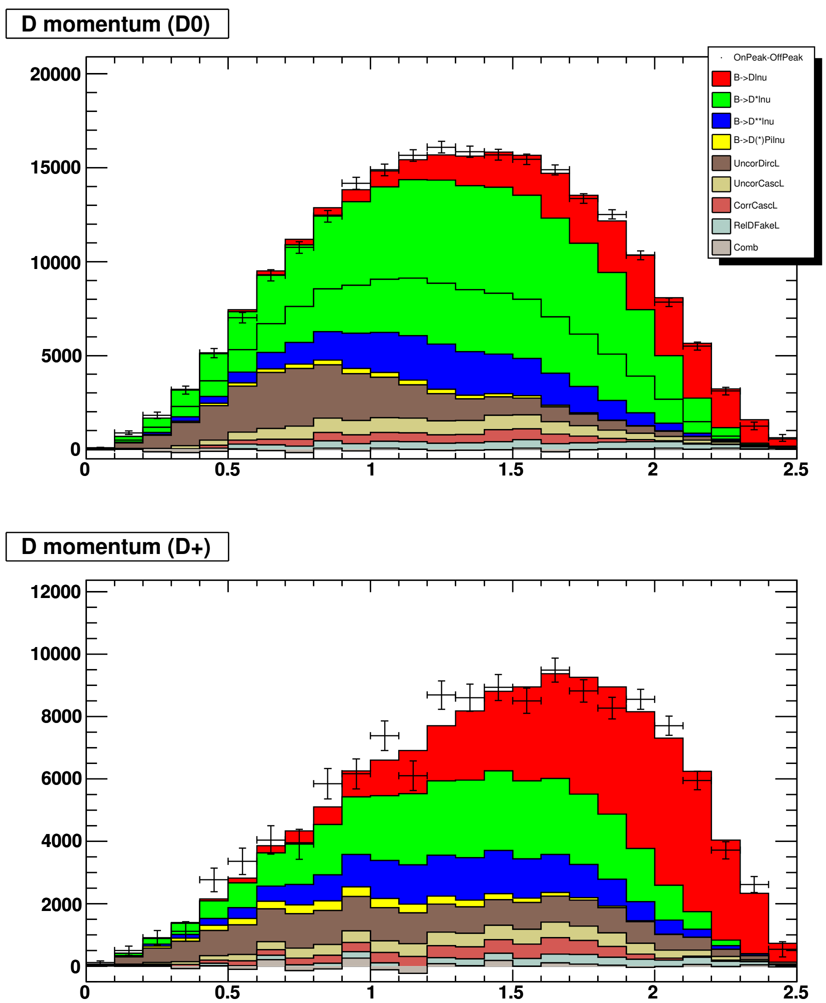

Figure 159: **(Run2 only)** [p_D **with** p_ℓ^{LAB} **cut**] D momentum plot with p_ℓ^{LAB} cut. The top is D^0 and the bottom is D^+. Black is OnPeak - OffPeak data. Red is $B \to D\ell\nu$, green is $B \to D^*\ell\nu$, blue is $B \to D^{**}\ell\nu$, yellow is non-resonant $B \to D^{(*)}\pi\ell\nu$, and the rest is background. Dark brown is UncorrDL, light brown is UncorrCL, dark red is CascL, blue gray is FakeL, and light gray is Comb. Comb is almost disappeared after D mass sideband subtraction.

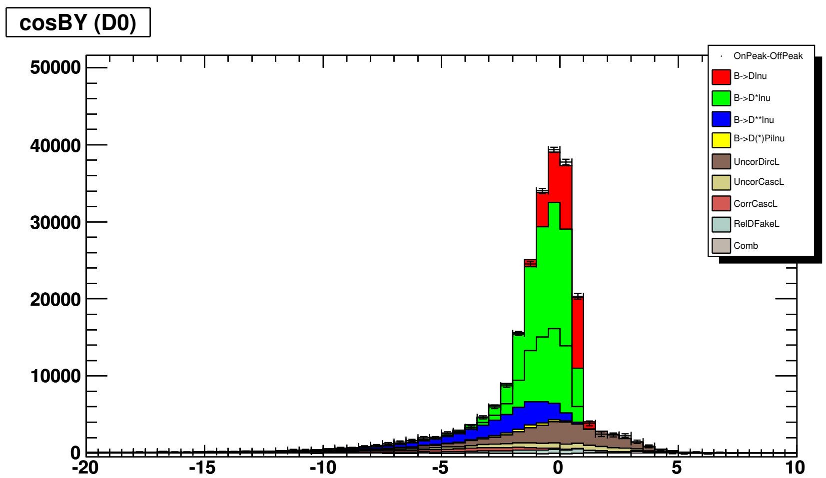

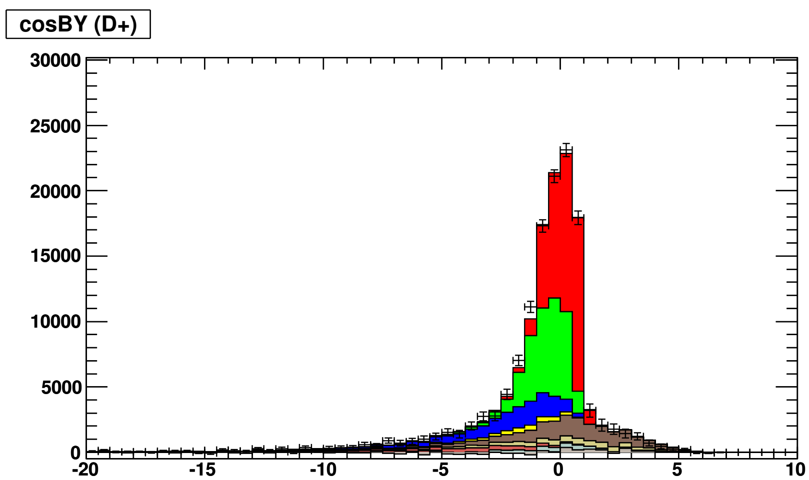

Figure 160: **(Run2 only)** [$\cos\theta_{B-Dl}$ **with** p_ℓ^{LAB} **cut**] $\cos\theta_{B-Dl}$ plot with p_ℓ^{LAB} cut. The top is D^0 and the bottom is D^+. Black is OnPeak - OffPeak data. Red is $B \to D\ell\nu$, green is $B \to D^*\ell\nu$, blue is $B \to D^{**}\ell\nu$, yellow is non-resonant $B \to D^{(*)}\pi\ell\nu$, and the rest is background. Dark brown is UncorrDL, light brown is UncorrCL, dark red is CascL, blue gray is FakeL, and light gray is Comb. Comb is almost disappeared after D mass sideband subtraction.

Parameters	Electron result	Muon result	NR
ρ_D^2	$\pm$	$\pm$	-0.002
ρ^2	$\pm$	$\pm$	-0.001
R_1	$\pm$	$\pm$	-0.001
R_2	$\pm$	$\pm$	0.004
$\mathcal{B}(B \to D\ell\nu)$	$\pm$	$\pm$	-0.813
$\mathcal{B}(B \to D^*\ell\nu)$	$\pm$	$\pm$	-0.457
$\mathcal{B}(B \to D^{**}/D^{(*)}\pi\ell\nu)$	$\pm$	$\pm$	0.049
f_{+0}	$\pm$	$\pm$	-0.054
$C^{D^0}_{UncorDL}$	$\pm$	$\pm$	-0.001
$C^{D^0}_{UncorCL}$	$\pm$	$\pm$	0.002
$C^{D^0}_{CascL}$	$\pm$	$\pm$	-0.025
$C^{D^+}_{UncorDL}$	$\pm$	$\pm$	-1.404
$C^{D^+}_{UncorCL}$	$\pm$	$\pm$	0.217
$C^{D^+}_{CascL}$	$\pm$	$\pm$	1.002
χ^2/ndof (P-value)	212/205 (0.35)	209/206 (0.43)	

Table 34: **(Run2 only)** [**Electron only and muon only fits**] Electrons and muons separated fit results and normaliaed residuals (NR).

14.2 Electron vs muon

We compare the two cases of leptons, namely electrons and muons. We separate the $D\ell$ candidate into two by selecting $\ell = e$ and $\ell = \mu$. Then we perform fitting separately. The results are give in Table 34. The normalized residuals (NR) in the Table is defined by

$$\mathrm{NR} = \frac{(\text{Muon fitted value}) - (\text{Elctron fitted value})}{\sqrt{\sigma_e^2 + \sigma_\mu^2}} \tag{322}$$

Plots from fit results are also shown in Figures 161-166. No systematic uncertainty is assigned based on this.

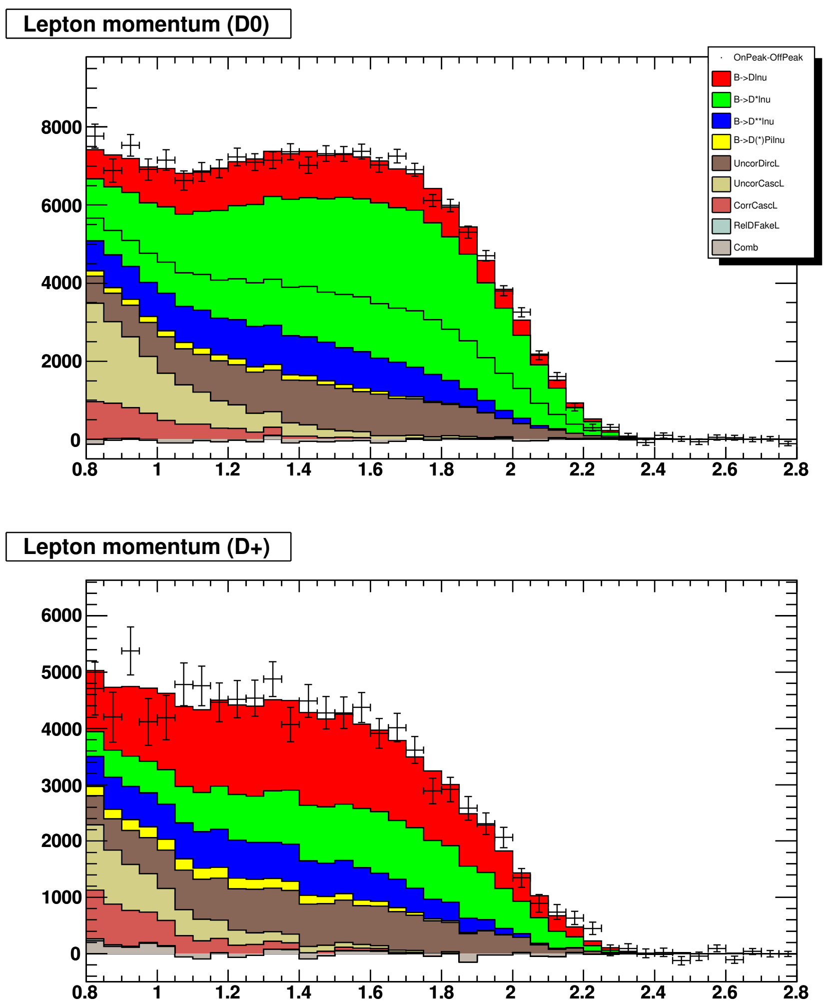

Figure 161: **(Run2 only)** [**Electron** p_ℓ] $\ell = e$. Lepton momentum plot after fitting. The top is D^0 and the bottom is D^+. Black is OnPeak - OffPeak data. Red is $B \to D\ell\nu$, green is $B \to D^*\ell\nu$, blue is $B \to D^{**}\ell\nu$, yellow is non-resonant $B \to D^{(*)}\pi\ell\nu$, and the rest is background. Dark brown is UncorrDL, light brown is UncorrCL, dark red is CascL, blue gray is FakeL, and light gray is Comb. Comb is almost disappeared after D mass sideband subtraction.

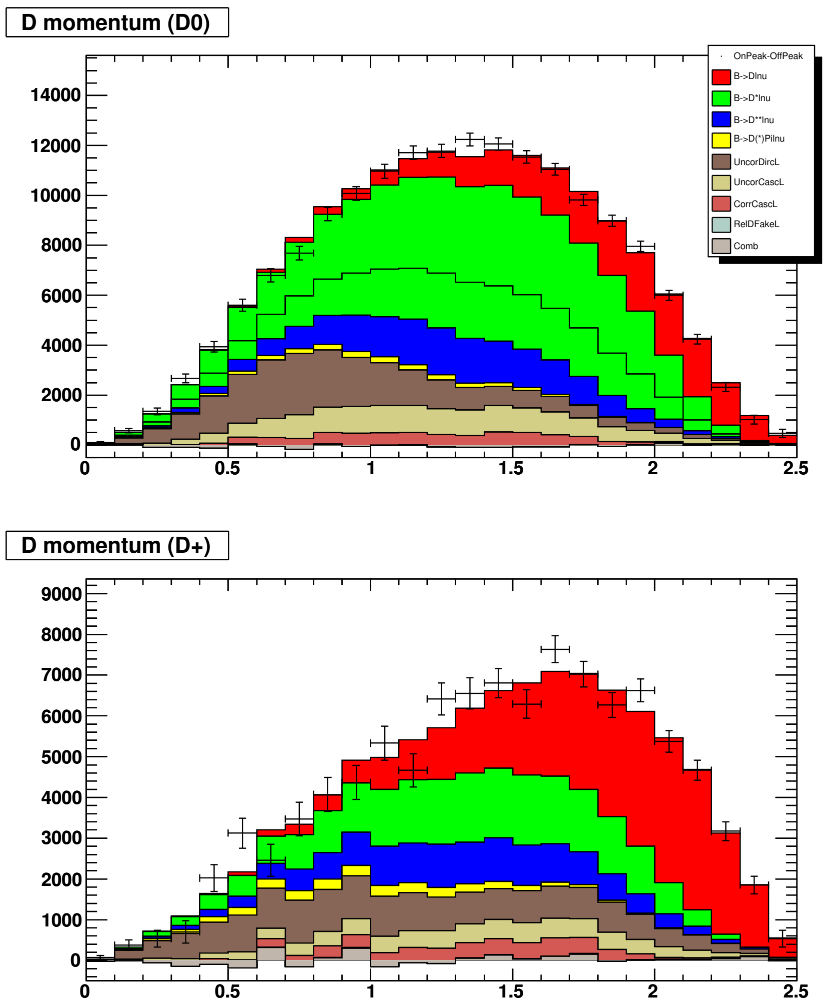

Figure 162: **(Run2 only)** [**Electron** p_D] $\ell = e$. D momentum plot after fitting. The top is D^0 and the bottom is D^+. Black is OnPeak - OffPeak data. Red is $B \to D\ell\nu$, green is $B \to D^*\ell\nu$, blue is $B \to D^{**}\ell\nu$, yellow is non-resonant $B \to D^{(*)}\pi\ell\nu$, and the rest is background. Dark brown is UncorrDL, light brown is UncorrCL, dark red is CascL, blue gray is FakeL, and light gray is Comb. Comb is almost disappeared after D mass sideband subtraction.

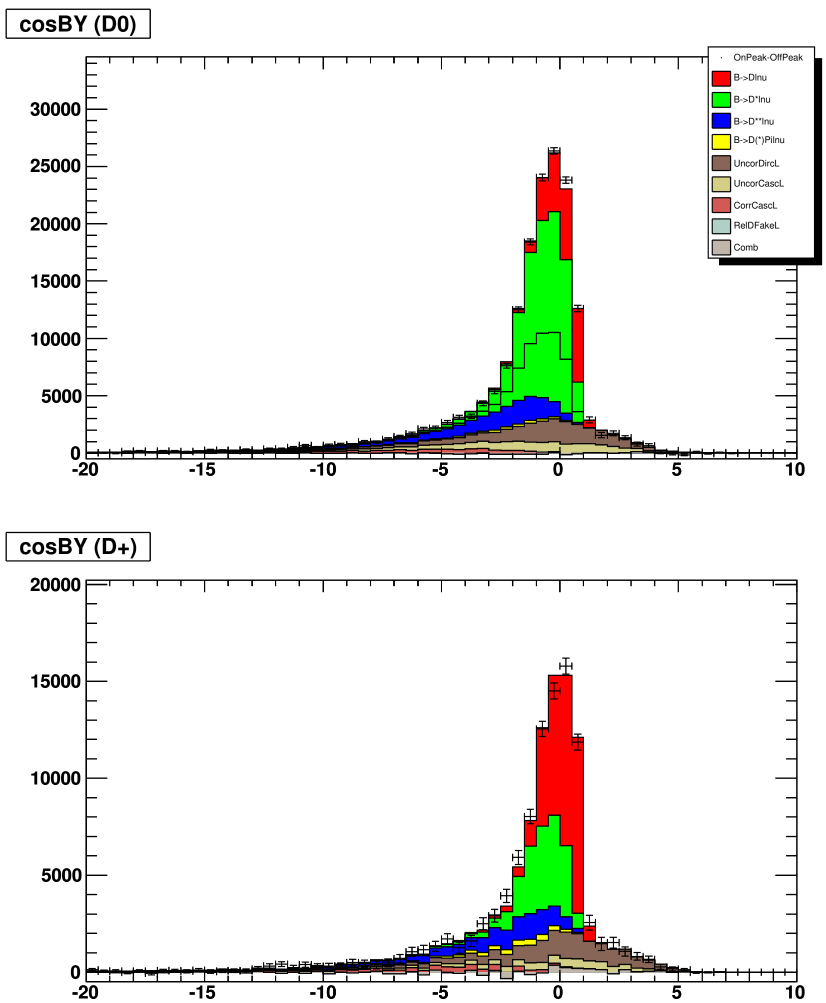

Figure 163: **(Run2 only)** [**Electron** $\cos\theta_{B-Dl}$] $\ell = e$. $\cos\theta_{B-Dl}$ plot after fitting. The top is D^0 and the bottom is D^+. Black is OnPeak - OffPeak data. Red is $B \to D\ell\nu$, green is $B \to D^*\ell\nu$, blue is $B \to D^{**}\ell\nu$, yellow is non-resonant $B \to D^{(*)}\pi\ell\nu$, and the rest is background. Dark brown is UncorrDL, light brown is UncorrCL, dark red is CascL, blue gray is FakeL, and light gray is Comb. Comb is almost disappeared after D mass sideband subtraction.

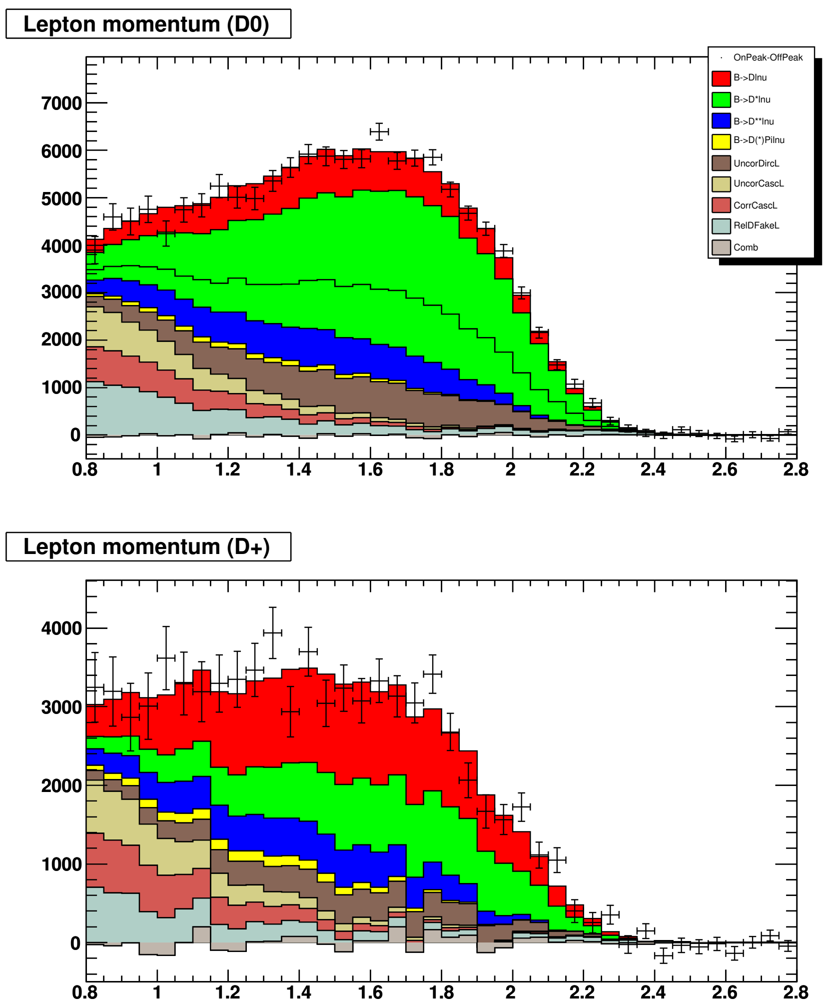

Figure 164: **(Run2 only)** [**Muon** p_ℓ] $\ell = \mu$. Lepton momentum plot after fitting. The top is D^0 and the bottom is D^+. Black is OnPeak - OffPeak data. Red is $B \to D\ell\nu$, green is $B \to D^*\ell\nu$, blue is $B \to D^{**}\ell\nu$, yellow is non-resonant $B \to D^{(*)}\pi\ell\nu$, and the rest is background. Dark brown is UncorrDL, light brown is UncorrCL, dark red is CascL, blue gray is FakeL, and light gray is Comb. Comb is almost disappeared after D mass sideband subtraction.

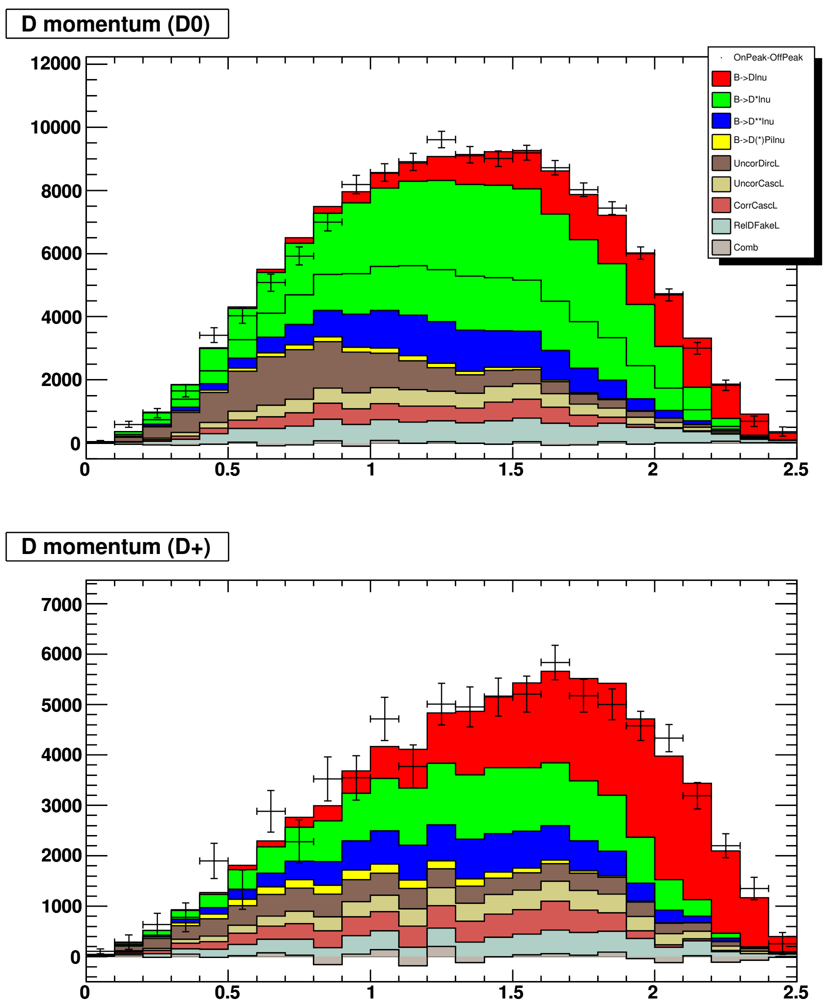

Figure 165: **(Run2 only)** [**Muon** p_D] $\ell = \mu$. D momentum plot after fitting. The top is D^0 and the bottom is D^+. Black is OnPeak - OffPeak data. Red is $B \to D\ell\nu$, green is $B \to D^*\ell\nu$, blue is $B \to D^{**}\ell\nu$, yellow is non-resonant $B \to D^{(*)}\pi\ell\nu$, and the rest is background. Dark brown is UncorrDL, light brown is UncorrCL, dark red is CascL, blue gray is FakeL, and light gray is Comb. Comb is almost disappeared after D mass sideband subtraction.

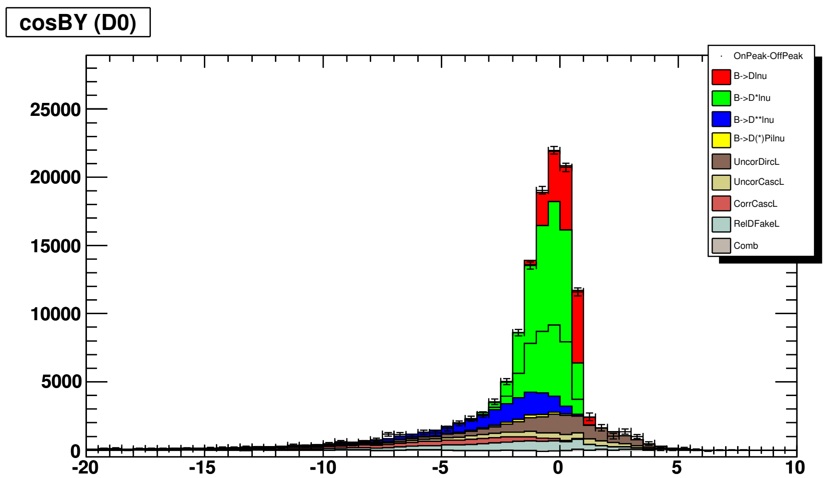

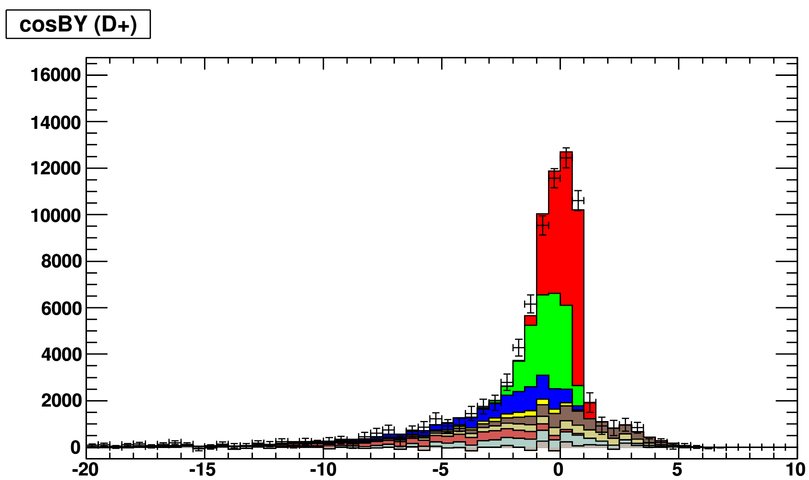

Figure 166: **(Run2 only)** [**Muon** $\cos\theta_{B-Dl}$] $\ell = \mu$. $\cos\theta_{B-Dl}$ plot after fitting. The top is D^0 and the bottom is D^+. Black is OnPeak - OffPeak data. Red is $B \to D\ell\nu$, green is $B \to D^*\ell\nu$, blue is $B \to D^{**}\ell\nu$, yellow is non-resonant $B \to D^{(*)}\pi\ell\nu$, and the rest is background. Dark brown is UncorrDL, light brown is UncorrCL, dark red is CascL, blue gray is FakeL, and light gray is Comb. Comb is almost disappeared after D mass sideband subtraction.

Parameters	D^0 result	D^+ result	NR
ρ_D^2	$\pm$	$\pm$	-1.259
ρ^2	$\pm$	$\pm$	-0.019
R_1	$\pm$	$\pm$	0.485
R_2	$\pm$	$\pm$	-0.181
$\mathcal{B}(B \to D\ell\nu)$	$\pm$	$\pm$	0.827
$\mathcal{B}(B \to D^*\ell\nu)$	$\pm$	$\pm$	0.610
$\mathcal{B}(B \to D^{**}/D^{(*)}\pi\ell\nu)$	$\pm$	$\pm$	1.394
f_{+0}	$\pm$	$\pm$	0.999
$C^{D^0}_{UncorDL}$	$\pm$	n/a	n/a
$C^{D^0}_{UncorCL}$	$\pm$	n/a	n/a
$C^{D^0}_{CascL}$	$\pm$	n/a	n/a
$C^{D^+}_{UncorDL}$	n/a	$\pm$	n/a
$C^{D^+}_{UncorCL}$	n/a	$\pm$	n/a
$C^{D^+}_{CascL}$	n/a	$\pm$	n/a
χ^2/ndof (P-value)	131/103 (0.03)	92/98 (0.65)	

Table 35: **(Run2 only)** [D^0 **only and** D^+ **only fits**] D^0 only and D^+ only fit results and normaliaed residuals (NR).

14.3 D^0 only vs D^+ only

We fit separately only for D^0 and only for D^+. In this fit we fixed $f_{+0} = 1.037$ because otherwise f_{+0} results in far from 1.037 and we get unreasonable fit results. The results are give in Table 35. The normalized residuals (NR) in the Table is defined by

$$\mathrm{NR} = \frac{(D^+ \text{ fitted value}) - (D^0 \text{ fitted value})}{\sqrt{\sigma^2_{D^+} + \sigma^2_{D^0}}} \tag{323}$$

Plots from fit results are also shown in Figures 167-172. No systematic uncertainty is assigned based on this.

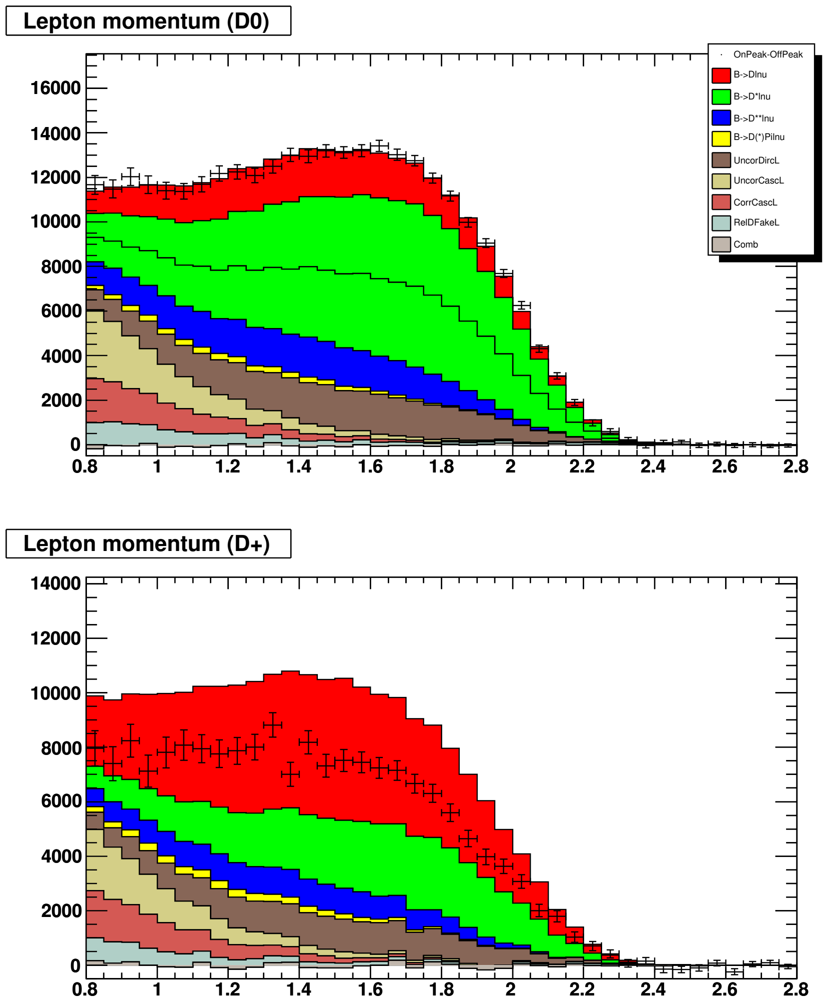

Figure 167: **(Run2 only)** [D^0 **only** p_ℓ] Lepton momentum plot after D^0 only fitting. The top is D^0 and the bottom is D^+. The bottom plot has no contribution to fitting. Black is OnPeak - OffPeak data. Red is $B \to D\ell\nu$, green is $B \to D^*\ell\nu$, blue is $B \to D^{**}\ell\nu$, yellow is non-resonant $B \to D^{(*)}\pi\ell\nu$, and the rest is background. Dark brown is UncorrDL, light brown is UncorrCL, dark red is CascL, blue gray is FakeL, and light gray is Comb. Comb is almost disappeared after D mass sideband subtraction.

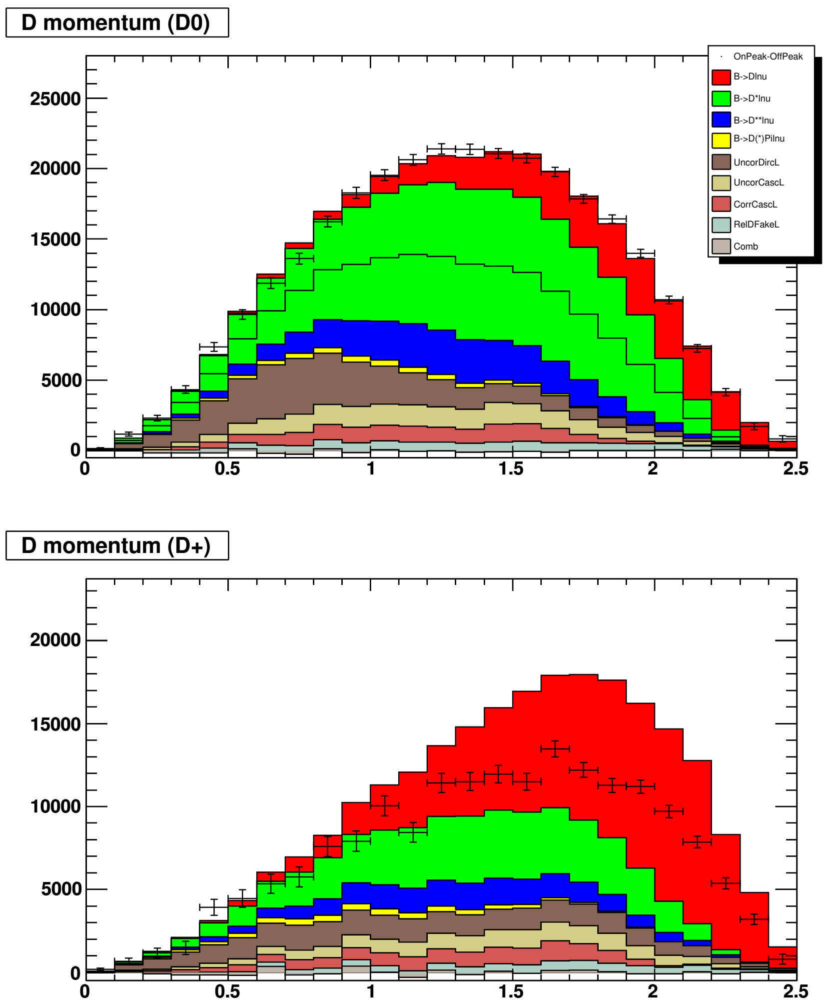

Figure 168: **(Run2 only)** [D^0 **only** p_D] D momentum plot after D^0 only fitting. The top is D^0 and the bottom is D^+. The bottom plot has no contribution to fitting. Black is OnPeak - OffPeak data. Red is $B \to D\ell\nu$, green is $B \to D^*\ell\nu$, blue is $B \to D^{**}\ell\nu$, yellow is non-resonant $B \to D^{(*)}\pi\ell\nu$, and the rest is background. Dark brown is UncorrDL, light brown is UncorrCL, dark red is CascL, blue gray is FakeL, and light gray is Comb. Comb is almost disappeared after D mass sideband subtraction.

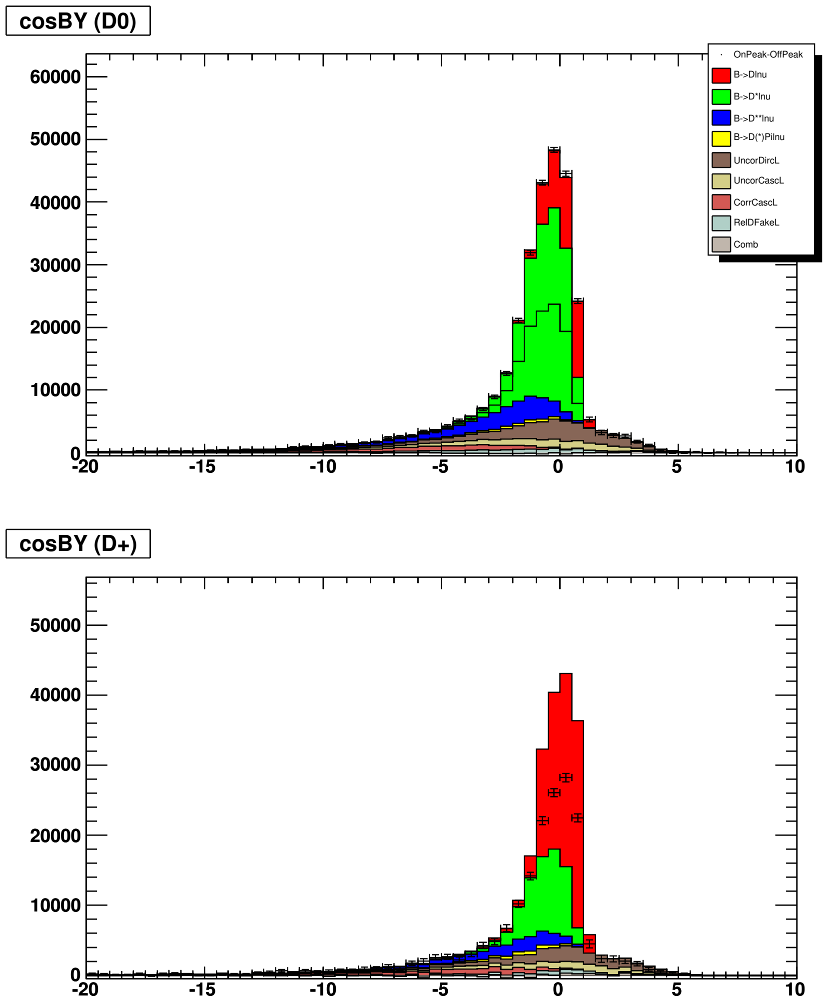

Figure 169: **(Run2 only)** [D^0 **only** $\cos\theta_{B-Dl}$] $\cos\theta_{B-Dl}$ plot after D^0 only fitting. The top is D^0 and the bottom is D^+. The bottom plot has no contribution to fitting. Black is OnPeak - OffPeak data. Red is $B \to D\ell\nu$, green is $B \to D^*\ell\nu$, blue is $B \to D^{**}\ell\nu$, yellow is non-resonant $B \to D^{(*)}\pi\ell\nu$, and the rest is background. Dark brown is UncorrDL, light brown is UncorrCL, dark red is CascL, blue gray is FakeL, and light gray is Comb. Comb is almost disappeared after D mass sideband subtraction.

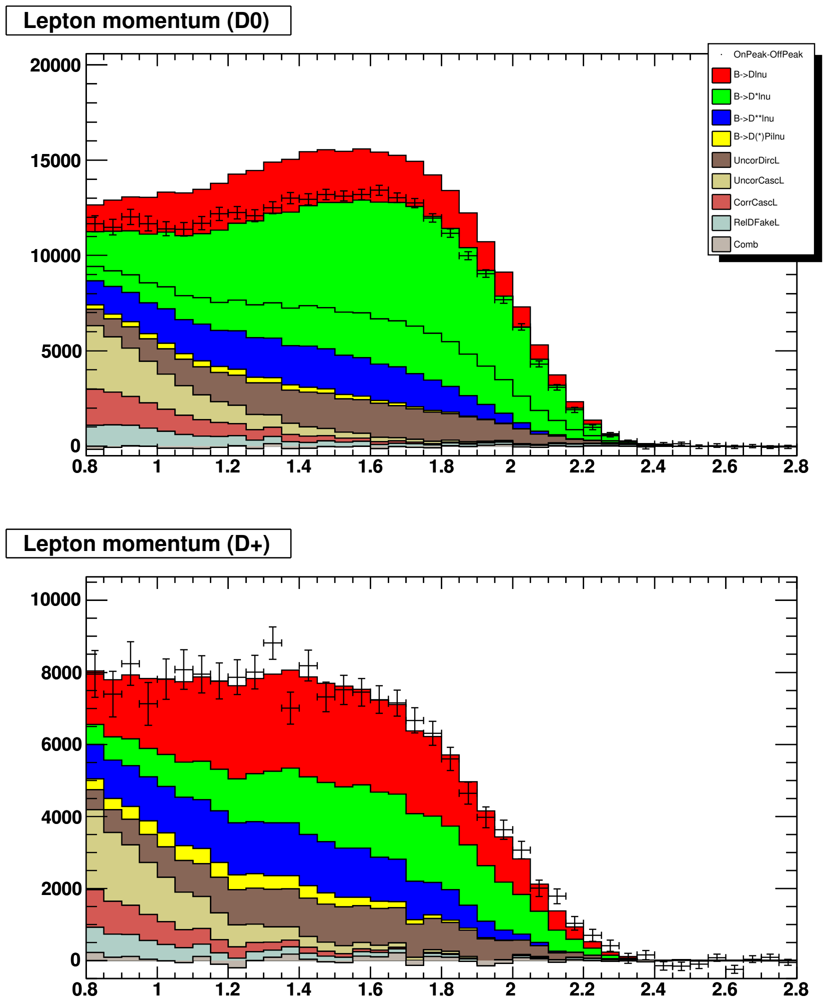

Figure 170: **(Run2 only)** [D^+ **only** p_ℓ] Lepton momentum plot after D^+ only fitting. The top is D^0 and the bottom is D^+. The top plot has no contribution to fitting. Black is OnPeak - OffPeak data. Red is $B \to D\ell\nu$, green is $B \to D^*\ell\nu$, blue is $B \to D^{**}\ell\nu$, yellow is non-resonant $B \to D^{(*)}\pi\ell\nu$, and the rest is background. Dark brown is UncorrDL, light brown is UncorrCL, dark red is CascL, blue gray is FakeL, and light gray is Comb. Comb is almost disappeared after D mass sideband subtraction.

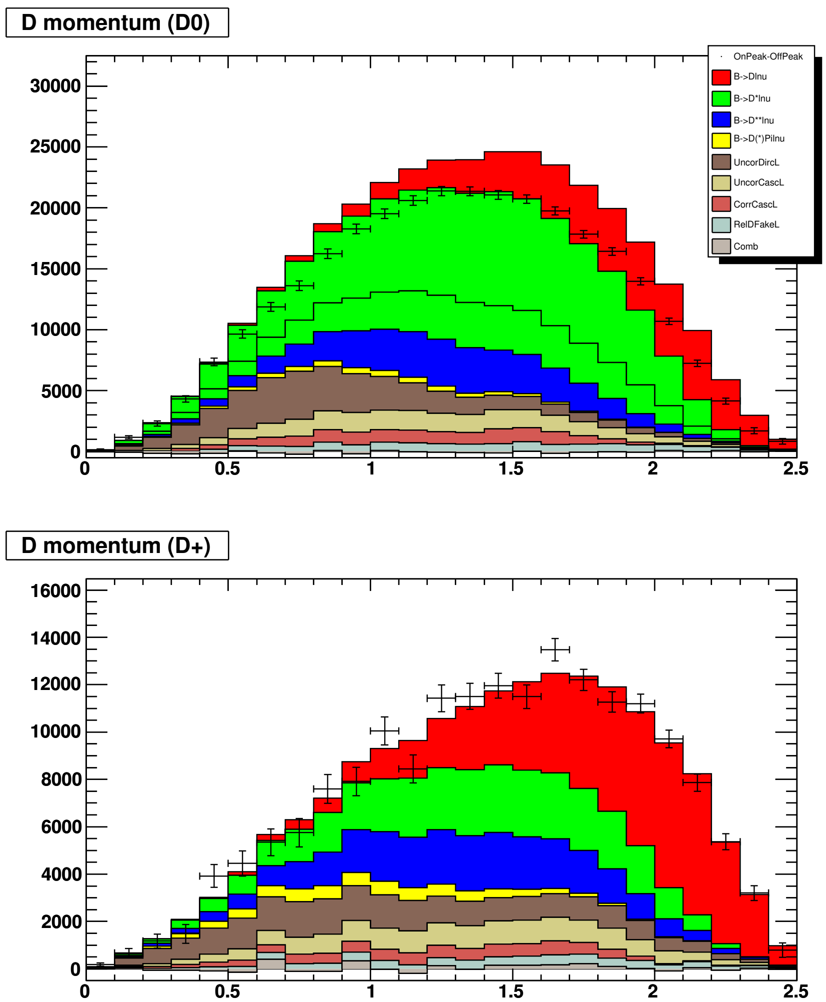

Figure 171: **(Run2 only)** [D^+ **only** p_D] D momentum plot after D^+ only fitting. The top is D^0 and the bottom is D^+. The top plot has no contribution to fitting. Black is OnPeak - OffPeak data. Red is $B \to D\ell\nu$, green is $B \to D^*\ell\nu$, blue is $B \to D^{**}\ell\nu$, yellow is non-resonant $B \to D^{(*)}\pi\ell\nu$, and the rest is background. Dark brown is UncorrDL, light brown is UncorrCL, dark red is CascL, blue gray is FakeL, and light gray is Comb. Comb is almost disappeared after D mass sideband subtraction.

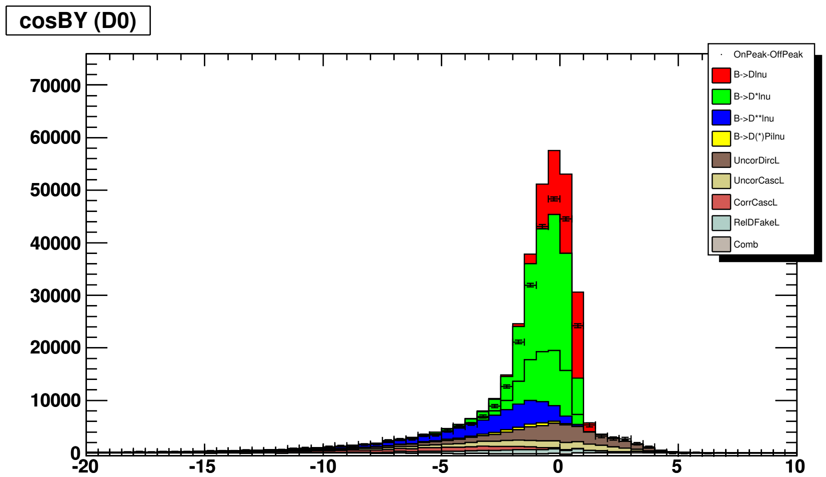

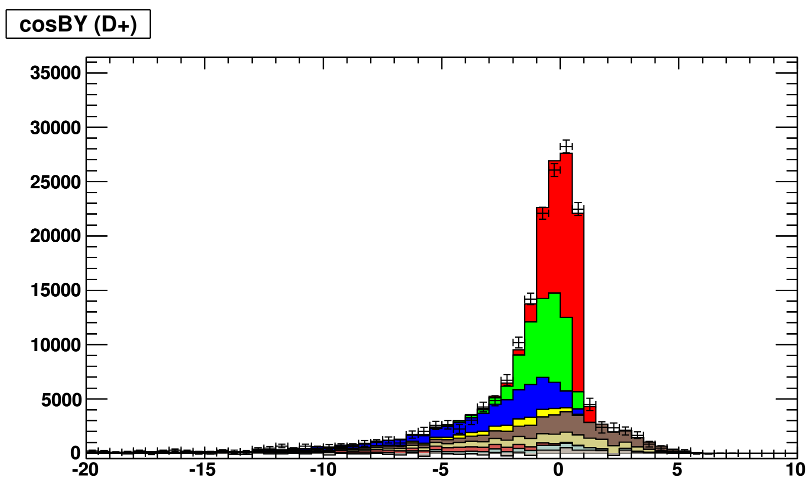

Figure 172: **(Run2 only)** [D^+ **only** $\cos\theta_{B-Dl}$] $\cos\theta_{B-Dl}$ plot after D^+ only fitting. The top is D^0 and the bottom is D^+. The top plot has no contribution to fitting. Black is OnPeak - OffPeak data. Red is $B \to D\ell\nu$, green is $B \to D^*\ell\nu$, blue is $B \to D^{**}\ell\nu$, yellow is non-resonant $B \to D^{(*)}\pi\ell\nu$, and the rest is background. Dark brown is UncorrDL, light brown is UncorrCL, dark red is CascL, blue gray is FakeL, and light gray is Comb. Comb is almost disappeared after D mass sideband subtraction.

14.4 Binning

14.4.1 $\cos\theta_{B-Dl}$ binning

$\cos\theta_{B-Dl}$ after the beam energy correction is shown in Figure 51. To avoid the data-MC difference based on the beam energy simulation, we take larger $\cos\theta_{B-Dl}$ bins. Especially, since the sharp edges of $B \to D\ell\nu$ at $\cos\theta_{B-Dl} = \pm 1$ are not well simulated, we widen the bins to ± 2. There are also tails at lower side of $B \to D\ell\nu$ and $B \to D^*\ell\nu$ due to missing pions because we do not explicitly reconstruct D^* or D^{**}. Thus, we set a boundary at $\cos\theta_{B-Dl} = -5.5$ to cover all $B \to D^*\ell\nu$ component.

14.4.2 Effect of binning

We change binning and see how fit results change. Nominal binnings are (section 3).

- lepton momentum in the CM frame p^*_ℓ
  (7 bins (GeV)) : 0.8, 1.05, 1.3, 1.55, 1.8, 2.05, 2.3, 2.55
- D momentum in the CM frame p^*_D
  (5 bins (GeV)) : 0, 0.5, 1, 1.5, 2.0, 2.5
- $\cos\theta_{B-Dl}$
  (5 bins) : -20, -5.5, -2, 0, 2, 10

First, we chcnage lepton momentum binning

- p^*_ℓ Binning 1
  (9 bins (GeV)) : 0.8, 1, 1.2, 1.4, 1.6, 1.8, 2, 2.2, 2.4, 2.6)
- p^*_ℓ Binning 2
  (4 bins (GeV)) : 0.8, 1.2, 1.6, 2, 2.4)
- p^*_ℓ Binning 3
  (4 bins (GeV)) : 0.8, 1.3, 1.8, 2.3, 2.8)

Results are given in Table 36. The normalized residuals (NR) in the Table is defined by

$$\mathrm{NR} = \frac{(\text{Fitted value}) - (\text{Nominal value})}{(\text{Statistical uncertainty on the fitted value})} \tag{324}$$

No systematic uncertainty is assigned based on this.
Next, we change D momentum binning

- p^*_D Binning 1
  (10 bins (GeV)) : 0, 0.25, 0.5, 0.75, 1, 1.25, 1.5, 1.75, 2.0, 2.25, 2.5
- p^*_D Binning 2
  (4 bins (GeV)) : 0, 0.6, 1.2, 1.8, 2.4

Results are given in Table 37. No systematic uncertainty is assigned based on this.
Finally, we change $\cos\theta_{B-Dl}$ bining

p_ℓ^* Parameters	Binning 1 results	Binning 1 NR	Binning 2 results	Binning 2 NR	Binning 3 results	Binning 3 NR
ρ_D^2	$\pm$	-0.083	$\pm$	-0.276	$\pm$	0.118
ρ^2	$\pm$	-0.600	$\pm$	-0.400	$\pm$	-0.843
R_1	$\pm$	-0.188	$\pm$	0.179	$\pm$	-0.515
R_2	$\pm$	+0.565	$\pm$	0.321	$\pm$	0.842
$\mathcal{B}(B \to D\ell\nu)$	$\pm$	-0.256	$\pm$	-0.388	$\pm$	-0.158
$\mathcal{B}(B \to D^*\ell\nu)$	$\pm$	+0.061	$\pm$	0.179	$\pm$	-0.286
$\mathcal{B}(B \to D^{**}/D^{(*)}\pi\ell\nu)$	$\pm$	-0.590	$\pm$	-0.799	$\pm$	-0.019
f_{+0}	$\pm$	-0.218	$\pm$	-0.309	$\pm$	-0.028
$C_{UncorDL}^{D^0}$	$\pm$	-0.103	$\pm$	-0.082	$\pm$	-0.154
$C_{UncorCL}^{D^0}$	$\pm$	+0.461	$\pm$	0.573	$\pm$	0.265
$C_{CascL}^{D^0}$	$\pm$	+0.195	$\pm$	0.259	$\pm$	-0.039
$C_{UncorDL}^{D^+}$	$\pm$	+0.200	$\pm$	0.141	$\pm$	-0.113
$C_{UncorCL}^{D^+}$	$\pm$	-0.211	$\pm$	-0.045	$\pm$	0.299
$C_{CascL}^{D^+}$	$\pm$	+0.316	$\pm$	0.442	$\pm$	-0.021
χ^2/ndof (P-value)	287/263 (0.15)		168/142 (0.07)		155/117 (0.01)	

Table 36: **(Run2 only)** [**Effect of p_ℓ binning**] Results and normaliaed residuals (NR) of the fits by changing the lepton momentum bining. Pulls are calculated from the difference to nominal fit results.

- $\cos\theta_{B-Dl}$ Binning 1
  (6 bins) : -20, -6, -2.5, -0.5, 0.5, 2, 10
- $\cos\theta_{B-Dl}$ Binning 2
  (5 bins) : -20, -4, -1.5, 0, 1.5, 10
- $\cos\theta_{B-Dl}$ Binning 3
  (4 bins) : -20, -3, -0.5, 1.5, 10

Results are given in Table 38. No systematic uncertainty is assigned based on this.

p_D^* Parameters	Binning 1 results	Binning 1 NR	Binning 2 results	Binning 2 NR
ρ_D^2	$\pm$	-0.679	$\pm$	0.113
ρ^2	$\pm$	-0.592	$\pm$	-0.314
R_1	$\pm$	-0.596	$\pm$	-0.069
R_2	$\pm$	0.682	$\pm$	0.124
$\mathcal{B}(B \to D\ell\nu)$	$\pm$	0.929	$\pm$	0.329
$\mathcal{B}(B \to D^*\ell\nu)$	$\pm$	-0.685	$\pm$	-0.014
$\mathcal{B}(B \to D^{**}/D^{(*)}\pi\ell\nu)$	$\pm$	0.152	$\pm$	-0.489
f_{+0}	$\pm$	1.265	$\pm$	-0.136
$C^{D^0}_{UncorDL}$	$\pm$	0.017	$\pm$	0.592
$C^{D^0}_{UncorCL}$	$\pm$	-0.538	$\pm$	-1.296
$C^{D^0}_{CascL}$	$\pm$	0.118	$\pm$	0.782
$C^{D^+}_{UncorDL}$	$\pm$	0.353	$\pm$	0.064
$C^{D^+}_{UncorCL}$	$\pm$	0.122	$\pm$	0.342
$C^{D^+}_{CascL}$	$\pm$	0.271	$\pm$	-0.030
χ^2/ndof (P-value)	468/407 (0.02)		220/179 (0.02)	

Table 37: **(Run2 only)** [**Effect of p_D binning**] Results and normaliaed residuals (NR) of the fits by changing the D momentum bining. Pulls are calculated from the difference to nominal fit results.

$\cos\theta_{B-Dl}$ Parameters	Binning 1		Binning 2		Binning 3	
	results	NR	results	NR	results	NR
ρ_D^2	$\pm$	0.065	$\pm$	-0.062	$\pm$	0.167
ρ^2	$\pm$	-0.071	$\pm$	0.428	$\pm$	-0.120
R_1	$\pm$	-0.136	$\pm$	0.540	$\pm$	-0.134
R_2	$\pm$	0.127	$\pm$	-0.336	$\pm$	0.765
$\mathcal{B}(B \to D\ell\nu)$	$\pm$	0.050	$\pm$	0.669	$\pm$	0.957
$\mathcal{B}(B \to D^*\ell\nu)$	$\pm$	0.285	$\pm$	-0.198	$\pm$	-0.735
$\mathcal{B}(B \to D^{**}/D^{(*)}\pi\ell\nu)$	$\pm$	0.356	$\pm$	-0.103	$\pm$	0.584
f_{+0}	$\pm$	-0.389	$\pm$	0.489	$\pm$	0.559
$C^{D^0}_{UncorDL}$	$\pm$	-0.537	$\pm$	$\pm$	-0.155	-0.976
$C^{D^0}_{UncorCL}$	$\pm$	0.457	$\pm$	$\pm$	-0.125	0.704
$C^{D^0}_{CascL}$	$\pm$	-0.447	$\pm$	$\pm$	0.248	-0.370
$C^{D^+}_{UncorDL}$	$\pm$	-0.199	$\pm$	$\pm$	0.121	-0.008
$C^{D^+}_{UncorCL}$	$\pm$	-0.045	$\pm$	$\pm$	-0.176	-0.264
$C^{D^+}_{CascL}$	$\pm$	-0.236	$\pm$	$\pm$	0.146	0.030
χ^2/ndof (P-value)	296/258 (0.05)		261/223 (0.04)		207/179 (0.07)	

Table 38: **(Run2 only)** [**Effect of** $\cos\theta_{B-Dl}$ **binning**] Results and normaliaed residuals (NR) of the fits by changing the $\cos\theta_{B-Dl}$ bining. Pulls are calculated from the difference to nominal fit results.

14.5 Minimum entry per bin

We change the requirement of minimum entries per bin to 5 and 20. In nominal fit it is set to 10. Results are shown in Table 39. The normalized residuals (NR) in the Table is defined by

$$\mathrm{NR} = \frac{(\text{Fitted value}) - (\text{Nominal value})}{(\text{Statistical uncertainty on the fitted value})} \tag{325}$$

No systematic uncertainty is assigned based on this.
When we change thie requirement, the number of bins goes into χ^2 changes as follows

- Minimum entry ber bin > 0 : number of bins goes into $\chi^2 = 260$ (100%)
- Minimum entry ber bin > 10 : number of bins goes into $\chi^2 = 229$ (88.1%)
- Minimum entry ber bin > 100 : number of bins goes into $\chi^2 = 197$ (76.2%)

Parameters	Minimum 5		Minimum 20	
	results	NR	results	NR
ρ_D^2	$\pm$	-0.00008	$\pm$	0.007
ρ^2	$\pm$	-0.002	$\pm$	0.048
R_1	$\pm$	-0.0002	$\pm$	0.020
R_2	$\pm$	-0.002	$\pm$	-0.022
$\mathcal{B}(B \to D\ell\nu)$	$\pm$	-0.005	$\pm$	0.047
$\mathcal{B}(B \to D^*\ell\nu)$	$\pm$	0.005	$\pm$	-0.034
$\mathcal{B}(B \to D^{**}/D^{(*)}\pi\ell\nu)$	$\pm$	0.00003	$\pm$	-0.015
f_{+0}	$\pm$	-0.002	$\pm$	0.079
$C_{UncorDL}^{D^0}$	$\pm$	0.002	$\pm$	-0.008
$C_{UncorCL}^{D^0}$	$\pm$	-0.002	$\pm$	-0.019
$C_{CascL}^{D^0}$	$\pm$	0.0003	$\pm$	0.022
$C_{UncorDL}^{D^+}$	$\pm$	0.0009	$\pm$	0.023
$C_{UncorCL}^{D^+}$	$\pm$	-0.0003	$\pm$	0.011
$C_{CascL}^{D^+}$	$\pm$	-0.001	$\pm$	-0.005
χ^2/ndof (P-value)	237/218 (0.18)		223/207 (0.22)	

Table 39: **(Run2 only)** [**Effect of minimum candidates per bin**] Results and normaliaed residuals (NR) of the fits by changing the requiremen of minimum candidates per bin.

15 Renormalization of Measured Branching Fractions

The fit starts with simulated distributions, normalized to the data luminosity, and determines multiplicative factors for each branching fraction. As such, we determine absolute branching fractions: $BF(fitted) = f \cdot BF(SP5MC)$, where f is the multiplicative factor. These absolute branching fractions are sensitive to the simulation of the efficiency, e.g. to lepton and kaon identification, tracking, vertexing, background modeling, etc., as well as to contributions from X_c states (such as $D^{(*)}\pi\pi\ell\nu$ and $D_sK\ell\nu$) that are not included in our fit. We can reduce the impact of the uncertainties in the simulation by re-normalizing the sum of the $b \to c\ell\nu$ fitted branching fractions to the measured inclusive $b \to c\ell\nu$ branching fraction, in which several of these error sources are either absent (kaon identification and vertexing) or reduced (tracking efficiency, background modeling). The method adopted for the renormalization is described in the next section.

15.1 Renormalization to inclusive BF

The fit determines branching fractions by adjusting the simulated spectra to the data in the 3-dimensional space. Once the fitted scale factors are determined, we can calculate partial BFs for each $B \to X_c\ell\nu$ fitted component in any desired kinematical region and compare their sum to the measured inclusive partial BF. We choose to do this in a region where the inclusive partial BF is well measured, and where the contribution from higher-mass X_c modes is small. To this end we consider the region $E_\ell^* \geq 1.5$ GeV. The residual contribution from the higher mass X_c states will be considered in evaluating systematic errors (see section 17).
We assume that

$$\begin{aligned}&\mathcal{B}(B^+ \to \bar{X}_c^0\ell^+\nu)\\&= \mathcal{B}(B^+ \to \bar{D}^0\ell^+\nu) + \mathcal{B}(B^+ \to \bar{D}^{*0}\ell^+\nu) + \mathcal{BT}(B^+ \to \bar{D}^{**0}/(D\pi)^0\ell^+\nu)\end{aligned} \tag{326}$$

and

$$\begin{aligned}&\mathcal{B}(B^0 \to X_c^-\ell^+\nu)\\&= \mathcal{B}(B^0 \to D^-\ell^+\nu) + \mathcal{B}(B^0 \to D^{*-}\ell^+\nu) + \mathcal{BT}(B^+ \to \bar{D}^{**0}/(D\pi)^0\ell^+\nu)\end{aligned} \tag{327}$$

We define partial branching fractions as follows

$$\begin{aligned}&\Delta\mathcal{B}(B^+ \to \bar{X}_c^0\ell^+\nu) \equiv \mathcal{B}(B^+ \to \bar{X}_c^0\ell^+\nu,\ \ E_\ell^* \geq 1.5\text{GeV})\\&= \Delta\mathcal{B}(B^+ \to \bar{D}^0\ell^+\nu) + \Delta\mathcal{B}(B^+ \to \bar{D}^{*0}\ell^+\nu) + \Delta\mathcal{BT}(B^+ \to \bar{D}^{**0}/(D\pi)^0\ell^+\nu)\end{aligned} \tag{328}$$

and

$$\begin{aligned}&\Delta\mathcal{B}(B^0 \to X_c^-\ell^+\nu) \equiv \mathcal{B}(B^0 \to X_c^-\ell^+\nu,\ \ E_\ell^* \geq 1.5\text{GeV}))\\&= \Delta\mathcal{B}(B^0 \to D^-\ell^+\nu) + \Delta\mathcal{B}(B^0 \to D^{*-}\ell^+\nu) + \Delta\mathcal{BT}(B^+ \to \bar{D}^{**0}/(D\pi)^0\ell^+\nu)\end{aligned} \tag{329}$$

The inclusive partial branching fraction measured by Babar is [45]

$$\Delta\mathcal{B}(B \to X_c \ell\nu) = 0.0454 \pm 0.0003 \pm 0.0008 = 0.0454 \pm 0.00085 \tag{330}$$

Combining this with lifetime ratio [13]

$$t_{+0} \equiv \frac{\tau_{B^+}}{\tau_{B^0}} = 1.071 \pm 0.009 \tag{331}$$

we can calculate B^+ and B^0 separately. By assuming B^+ and B^0 contributions are equal,

$$\Delta\mathcal{B}(B^+ \to \bar{X}_c^0 \ell^+\nu) + \Delta\mathcal{B}(B^0 \to X_c^- \ell^+\nu) = 2\Delta\mathcal{B}(B \to X_c \ell\nu) \tag{332}$$

From isospin symmetry

$$\Delta\mathcal{B}(B^+ \to \bar{X}_c^0 \ell^+\nu) = t_{+0}\Delta\mathcal{B}(B^0 \to X_c^- \ell^+\nu) \tag{333}$$

Thus

$$\Delta\mathcal{B}(B^+ \to \bar{X}_c^0 \ell^+\nu) = \frac{2t_{+0}}{1+t_{+0}}\Delta\mathcal{B}(B \to X_c \ell\nu) = 0.0470 \pm 0.00088 \tag{334}$$

and

$$\Delta\mathcal{B}(B^0 \to X_c^- \ell^+\nu) = \frac{2}{1+t_{+0}}\Delta\mathcal{B}(B \to X_c \ell\nu) = 0.0438 \pm 0.00082 \tag{335}$$

Here we have shown uncertainties only from measured $\Delta\mathcal{B}(B \to X_c\ell\nu)$. Since t_{+0} is included in many parts of our fit, the uncertainty originated from t_{+0} should be evaluated together with other parts. Thus, we need to treat these two sources of uncertainty separately.

15.2 Calculation of partial branching fractions

Using the above value, we can extract the normalization factor, F_N. But, first, we need to determine the ratio, P^{fitted}, of a partial branching fraction, $\Delta\mathcal{B}^{fitted}$, and a fitted branching fraction, $\mathcal{B}^{fitted}$. This ratio can be determined by applying the same weight, W_k, as we used in the fit and counting the number of candidates :

$$P^{fitted} \equiv \frac{\Delta\mathcal{B}^{fitted}}{\mathcal{B}^{fitted}} = \frac{\sum_{p_\ell^* \geq 1.5\mathrm{GeV}} W_k}{\sum_{p_\ell^* \geq 0\mathrm{GeV}} W_k} \tag{336}$$

For practical (not conceptual) reasons we evaluate this using generator-level MC. Note that the partial branching fractions determined by this method are partial branching fractions of fitted results because we apply weights calculated by fitted FF parameters. These are different from partial branching fractions of SP5/SP6 MC. The statistical uncertainty due to the number of events generated can be calculated by

$$\sigma_P = \frac{\sum_{p_\ell^* \geq 1.5\mathrm{GeV}} W_k}{\sum_{p_\ell^* \geq 0\mathrm{GeV}} W_k}\sqrt{\frac{\sum_{p_\ell^* \geq 1.5\mathrm{GeV}} W_k^2}{\left(\sum_{p_\ell^* \geq 1.5\mathrm{GeV}} W_k\right)^2} + \frac{\sum_{p_\ell^* \geq 0\mathrm{GeV}} W_k^2}{\left(\sum_{p_\ell^* \geq 0\mathrm{GeV}} W_k\right)^2}} \tag{337}$$

In this way, we can determine ratios

$$
\begin{aligned}
P^{fitted}_{D\ell\nu} &\equiv \tfrac{\Delta\mathcal{B}(B^0\to D^-\ell^+\nu)^{fitted}}{\mathcal{B}(B^0\to D^-\ell^+\nu)^{fitted}} \\
P^{fitted}_{D^*\ell\nu} &\equiv \tfrac{\Delta\mathcal{B}(B^0\to D^{*-}\ell^+\nu)^{fitted}}{\mathcal{B}(B^0\to D^{*-}\ell^+\nu)^{fitted}} \\
P^{fitted}_{D_0^*\ell\nu} &\equiv \tfrac{\Delta\mathcal{B}(B^0\to D_0^{*-}\ell^+\nu)^{fitted}}{\mathcal{B}(B^0\to D_0^{*-}\ell^+\nu)^{fitted}} \\
P^{fitted}_{D_1\ell\nu} &\equiv \tfrac{\Delta\mathcal{B}(B^0\to D_1^-\ell^+\nu)^{fitted}}{\mathcal{B}(B^0\to D_1^-\ell^+\nu)^{fitted}} \\
P^{fitted}_{D_1'\ell\nu} &\equiv \tfrac{\Delta\mathcal{B}(B^0\to D_1'^-\ell^+\nu)^{fitted}}{\mathcal{B}(B^0\to D_1'^-\ell^+\nu)^{fitted}} \\
P^{fitted}_{D_2^*\ell\nu} &\equiv \tfrac{\Delta\mathcal{B}(B^0\to D_2^{*-}\ell^+\nu)^{fitted}}{\mathcal{B}(B^0\to D_2^{*-}\ell^+\nu)^{fitted}} \\
P^{fitted}_{D\pi\ell\nu} &\equiv \tfrac{\Delta\mathcal{B}(B^0\to D^-\pi\ell^+\nu)^{fitted}}{\mathcal{B}(B^0\to D^-\pi\ell^+\nu)^{fitted}} \\
P^{fitted}_{D^*\pi\ell\nu} &\equiv \tfrac{\Delta\mathcal{B}(B^0\to D^{*-}\pi\ell^+\nu)^{fitted}}{\mathcal{B}(B^0\to D^{*-}\pi\ell^+\nu)^{fitted}}
\end{aligned}
\tag{338}
$$

We can also determine

$$
P^{fitted}_{Other} \equiv \frac{\Delta\mathcal{BT}(B^+ \to \bar{D}^{**0}/(D\pi)^0\ell^+\nu)^{fitted}}{\mathcal{BT}(B^+ \to \bar{D}^{**0}/(D\pi)^0\ell^+\nu)^{fitted}} \tag{339}
$$

using equations (137) - (144). From the definition of the ratio P^{fitted}

$$
\Delta B^{fitted} = P^{fitted} B^{fitted} = P^{fitted} \cdot \text{Factor} \cdot \mathcal{BT}(B^+ \to \bar{D}^{**0}/(D\pi)^0\ell^+\nu)^{fitted} \tag{340}
$$

where the "Factor" is given by equations (137) - (144).

$$
\text{Factor}(D_1) = \frac{1}{(1+f_{D_2^*/D_1})(1+f_{D_0^*D\pi T/D_1D_2^*T}+f_{D_1'D^*\pi T/D_1D_2^*T})} \tag{341}
$$

$$
\text{Factor}(D_2^*) = f_{D_2^*/D_1}\text{Factor}(D_1) \tag{342}
$$

$$
\text{Factor}(D_0^*) = \frac{2f_{D_0^*D\pi T/D_1D_2^*T}}{(2+3f_{D\pi/D_0^*})(1+f_{D_0^*D\pi T/D_1D_2^*T}+f_{D_1'D^*\pi T/D_1D_2^*T})} \tag{343}
$$

$$
\text{Factor}(D_1') = \frac{2f_{D_1'D^*\pi T/D_1D_2^*T}}{(2+3f_{D^*\pi/D_1'})(1+f_{D_0^*D\pi T/D_1D_2^*T}+f_{D_1'D^*\pi T/D_1D_2^*T})} \tag{344}
$$

$$
\text{Factor}(D\pi^+) = f_{D\pi/D_0^*}\text{Factor}(D_0^*) \tag{345}
$$

$$
\text{Factor}(D\pi^0) = \frac{\text{Factor}(D\pi^+)}{2} \tag{346}
$$

$$
\text{Factor}(D^*\pi^+) = f_{D^*\pi/D_1'}\text{Factor}(D_1') \tag{347}
$$

$$
\text{Factor}(D^*\pi^0) = \frac{\text{Factor}(D^*\pi^+)}{2} \tag{348}
$$

Thus

$$
\begin{aligned}
&P^{fitted}_{Other} \\
&= P^{fitted}_{D_0^*\ell\nu}\text{Factor}(D_0^*) + P^{fitted}_{D_1\ell\nu}\text{Factor}(D_1) + P^{fitted}_{D_1'\ell\nu}\text{Factor}(D_1') + P^{fitted}_{D_2^*\ell\nu}\text{Factor}(D_2^*) \\
&\qquad +P^{fitted}_{D\pi\ell\nu}\text{Factor}(D\pi^+) + P^{fitted}_{D\pi\ell\nu}\text{Factor}(D\pi^0) \\
&\qquad\quad +P^{fitted}_{D^*\pi\ell\nu}\text{Factor}(D^*\pi^+) + P^{fitted}_{D^*\pi\ell\nu}\text{Factor}(D^*\pi^0)
\end{aligned}
\tag{349}
$$

15.3 Determination of re-normalized BF

The normalization factor, F_N, is determined by the partial branching fractions :

$$\begin{aligned}&\Delta\mathcal{B}(B^+ \to \bar{X}_c^0 \ell^+ \nu)\\ &= F_N[\Delta\mathcal{B}(B^0 \to D^- \ell^+ \nu)^{fitted} + \Delta\mathcal{B}(B^0 \to D^{*-} \ell^+ \nu)^{fitted}\\ &\qquad + \Delta\mathcal{BT}(B^+ \to \bar{D}^{**0}/(D\pi)^0 \ell^+ \nu)^{fitted}]\end{aligned} \tag{350}$$

or,

$$\begin{aligned}&\Delta\mathcal{B}(B^+ \to \bar{X}_c^0 \ell^+ \nu)\\ &= F_N[P_{D\ell\nu}^{fitted}\mathcal{B}(B^0 \to D^- \ell^+ \nu)^{fitted} + P_{D^*\ell\nu}^{fitted}\mathcal{B}(B^0 \to D^{*-} \ell^+ \nu)^{fitted}\\ &\qquad + P_{Other}^{fitted}\mathcal{BT}(B^+ \to \bar{D}^{**0}/(D\pi)^0 \ell^+ \nu)^{fitted}]\end{aligned} \tag{351}$$

Using this F_N, re-normalized partial branching fractions are given by

$$\begin{aligned}&\Delta\mathcal{B}(B^+ \to \bar{D}^0 \ell^+ \nu) = F_N\ \Delta\mathcal{B}(B^+ \to \bar{D}^0 \ell^+ \nu)^{fitted}\\ &\Delta\mathcal{B}(B^+ \to \bar{D}^{*0} \ell^+ \nu) = F_N\ \Delta\mathcal{B}(B^+ \to \bar{D}^{*0} \ell^+ \nu)^{fitted}\\ &\Delta\mathcal{BT}(B^+ \to \bar{D}^{**0}/(D\pi)^0 \ell^+ \nu) = F_N\ \Delta\mathcal{BT}(B^+ \to \bar{D}^{**0}/(D\pi)^0 \ell^+ \nu)^{fitted}\end{aligned} \tag{352}$$

Hence, we can determine re-normalized branching fractions by

$$\begin{aligned}\tilde{\mathcal{B}}(B^+ \to \bar{D}^0 \ell^+ \nu) &= \frac{F_N\ \Delta\mathcal{B}(B^+ \to \bar{D}^0 \ell^+ \nu)^{fitted}}{P_{D\ell\nu}^{fitted}}\\ &= F_N\ \mathcal{B}(B^+ \to \bar{D}^0 \ell^+ \nu)^{fitted}\\ \tilde{\mathcal{B}}(B^+ \to \bar{D}^{*0} \ell^+ \nu) &= \frac{F_N\ \Delta\mathcal{B}(B^+ \to \bar{D}^{*0} \ell^+ \nu)^{fitted}}{P_{D^*\ell\nu}^{fitted}}\\ &= F_N\ \mathcal{B}(B^+ \to \bar{D}^{*0} \ell^+ \nu)^{fitted}\\ \tilde{\mathcal{BT}}(B^+ \to \bar{D}^{**0}/(D\pi)^0 \ell^+ \nu) &= \frac{F_N\ \Delta\mathcal{BT}(B^+ \to \bar{D}^{**0}/(D\pi)^0 \ell^+ \nu)^{fitted}}{P_{Other}^{fitted}}\\ &= F_N\ \mathcal{BT}(B^+ \to \bar{D}^{**0}/(D\pi)^0 \ell^+ \nu)^{fitted}\end{aligned} \tag{353}$$

Using the nominal fit results

$$\begin{aligned}&F_N = 1.093\\ &\tilde{\mathcal{B}}(B^+ \to \bar{D}^0 \ell^+ \nu) = 0.0276 \pm 0.0007\\ &\tilde{\mathcal{B}}(B^+ \to \bar{D}^{*0} \ell^+ \nu) = 0.0564 \pm 0.0009\\ &\tilde{\mathcal{BT}}(B^+ \to \bar{D}^{**0}/(D\pi)^0 \ell^+ \nu) = 0.0240 \pm 0.0011\end{aligned} \tag{354}$$

B^0 branching fractions can be determined in the same way.

16 Calculation of $\mathcal{G}(1)|V_{cb}|$ and $\mathcal{F}(1)|V_{cb}|$

16.1 $\mathcal{G}(1)|V_{cb}|$

Differential decay rate of $B \to D\ell\nu$ decays are given by

$$\frac{d\Gamma(B \to D\ell\nu)}{dw} = \frac{G_F^2|V_{cb}|^2 m_B^5}{48\pi^3} r^3 (w^2-1)^{3/2}\, \mathcal{J}_D(w) \tag{355}$$

where

$$\mathcal{J}_D(w) = [(1+r)h_+(w) - (1-r)h_-(w)]^2 \tag{356}$$

and

$$r = \frac{m_D}{m_B} \tag{357}$$

In HQET model, we can set

$$\begin{aligned} h_+(w) &= h_+(1)[1 - 8\rho_D^2 z + (51\rho_D^2 - 10)z^2 - (252\rho_D^2 - 84)z^3] \\ h_-(w) &= 0 \end{aligned} \tag{358}$$

where

$$z = \frac{\sqrt{w+1} - \sqrt{2}}{\sqrt{w+1} + \sqrt{2}} \tag{359}$$

Thus, differential decay rate is

$$\begin{aligned} &\frac{d\Gamma(B \to D\ell\nu)}{dw} \\ &= \frac{G_F^2 m_B^5}{48\pi^3} r^3 (w^2-1)^{3/2}\, (1+r)^2 [1 - 8\rho_D^2 z + (51\rho_D^2 - 10)z^2 - (252\rho_D^2 - 84)z^3]^2 \\ &\quad \times (\mathcal{G}(1)|V_{cb}|)^2 \end{aligned} \tag{360}$$

Note that $\mathcal{G}(1) = h_+(1)$. By integrating over w, we get

$$\begin{aligned} &\frac{\mathcal{B}(B \to D\ell\nu)}{\tau_B} \\ &= \frac{G_F^2 m_B^5}{48\pi^3} r^3 (1+r)^2 \int (w^2-1)^{3/2} [1 - 8\rho_D^2 z + (51\rho_D^2 - 10)z^2 - (252\rho_D^2 - 84)z^3]^2 dw \\ &\quad \times (\mathcal{G}(1)|V_{cb}|)^2 \end{aligned} \tag{361}$$

where τ_B the lifetime of the B meson. If we define

$$C^D \equiv \sqrt{\frac{48\pi^3}{G_F^2 m_B^5 \tau_B r^3 (1+r)^2}} \tag{362}$$

$$I_1^D \equiv \int (w^2-1)^{3/2} (1 - 10z^2 + 84z^3)^2 dw \tag{363}$$

$$I_2^D \equiv 2\int (w^2-1)^{3/2} (1 - 10z^2 + 84z^3)(8z - 51z^2 + 252z^3) dw \tag{364}$$

$$I_3^D \equiv \int (w^2-1)^{3/2} (8z - 51z^2 + 252z^3)^2 dw \tag{365}$$

then

$$\mathcal{G}(1)|V_{cb}| = C^D \mathcal{B}(B \to D\ell\nu)^{1/2}[I_1^D - \rho_D^2 I_2^D + (\rho_D^2)^2 I_3^D]^{-1/2} \tag{366}$$

Thus, using fit results $\mathcal{B}(B \to D\ell\nu)$ and ρ_D^2, we can calculate $\mathcal{G}(1)|V_{cb}|$. We use the following numerical values

$$\begin{aligned} \tau_{B^+} &= 1.638 \times 10^{-12}/6.58211915 \times 10^{-25} \quad \mathrm{GeV}^{-1} \\ m_{B^+} &= 5.2790 \quad \mathrm{GeV} \\ m_{D^0} &= 1.8645 \quad \mathrm{GeV} \\ G_F &= 1.166371 \times 10^{-5} \quad \mathrm{GeV}^{-2} \end{aligned} \tag{367}$$

16.2 $\mathcal{F}(1)|V_{cb}|^2$

Differential decay rate of $B \to D^*\ell\nu$ decays are given by

$$\frac{d\Gamma(B \to D^*\ell\nu)}{dw} = \frac{G_F^2 |V_{cb}|^2 m_B^5}{48\pi^3} r^3 (w^2-1)^{1/2} \mathcal{J}_{WD}(R_1, R_2, \rho^2) \tag{368}$$

where

$$\mathcal{J}_{WD}(R_1, R_2, \rho^2) = (w+1)^2 [h_{A_1}]^2 (\tilde{h}_+^2 + \tilde{h}_-^2 + \tilde{h}_0^2) \tag{369}$$

Here, the form factors are given by

$$\begin{aligned} &\tilde{h}_\pm(w) \equiv (1-r)\widetilde{H}_\pm(w) = \sqrt{1-2wr+r^2}\left(1 \mp \sqrt{\tfrac{w-1}{w+1}} R_1(w)\right) \\ &\tilde{h}_0(w) \equiv (1-r)\widetilde{H}_0(w) = (1-r) + (w-1)\,(1-R_2(w)) = (w-r) - (w-1)R_2(w) \\ &h_{A_1}(w) = h_{A_1}(1)\,[1 - 8\rho^2 z + (53\rho^2 - 15)z^2 - (231\rho^2 - 91)z^3] \end{aligned} \tag{370}$$

where

$$\begin{aligned} R_1(w) &= R_1 - 0.12(w-1) + 0.05(w-1)^2 \\ R_2(w) &= R_2 + 0.11(w-1) - 0.06(w-1)^2 \\ r &= \tfrac{m_{D^*}}{m_B} \\ z &= \tfrac{\sqrt{w+1}-\sqrt{2}}{\sqrt{w+1}+\sqrt{2}} \end{aligned} \tag{371}$$

Thus, the differential decay rate is

$$\begin{aligned} &\frac{d\Gamma(B \to D^*\ell\nu)}{dw} \\ &= \frac{G_F^2 |V_{cb}|^2 m_B^5}{48\pi^3} r^3 (w^2-1)^{1/2} (w+1)^2 \\ &\quad \times [\mathcal{F}(1)]^2 [1 - 8\rho^2 z + (53\rho^2 - 15)z^2 - (231\rho^2 - 91)z^3]^2 (\tilde{h}_+^2 + \tilde{h}_-^2 + \tilde{h}_0^2) \end{aligned} \tag{372}$$

Note that $\mathcal{F}(1) = h_{A_1}(1)$. By integrating over w, we get

$$\begin{aligned} \frac{\mathcal{B}(B \to D^*\ell\nu)}{\tau_B} &= \frac{G_F^2 m_B^5}{48\pi^3} r^3 \left(\mathcal{F}(1)|V_{cb}|\right)^2 \\ &\int (w^2-1)^{1/2} (w+1)^2 (\tilde{h}_+^2 + \tilde{h}_-^2 + \tilde{h}_0^2) \\ &\quad \times [1 - 8\rho^2 z + (53\rho^2 - 15)z^2 - (231\rho^2 - 91)z^3]^2 dw \end{aligned} \tag{373}$$

where τ_B the lifetime of the B meson. Let us simplify this equation. By defining

$$\begin{aligned}
k_1 &\equiv -0.12(w-1) + 0.05(w-1)^2 \\
k_2 &\equiv 0.11(w-1) - 0.06(w-1)^2
\end{aligned} \tag{374}$$

we get

$$\begin{aligned}
&\tilde{h}_+^2 + \tilde{h}_-^2 + \tilde{h}_0^2 \\
&\quad = (1-2wr+r^2)\left[1 - 2\sqrt{\frac{w-1}{w+1}}(R_1+k_1) + \frac{w-1}{w+1}(R_1+k_1)^2\right] \\
&\qquad +(1-2wr+r^2)\left[1 + 2\sqrt{\frac{w-1}{w+1}}(R_1+k_1) + \frac{w-1}{w+1}(R_1+k_1)^2\right] \\
&\qquad +(w-r)^2 - 2(w-r)(w-1)(R_2+k_2) + (w-1)^2(R_2+k_2)^2 \\
&\quad = (2+w^2-6wr+3r^2) + 2(1-2wr+r^2)\frac{w-1}{w+1}(R_1^2+2k_1R_1+k_1^2) \\
&\qquad -2(w-r)(w-1)(R_2+k_2) + (w-1)^2(R_2^2+2k_2R_2+k_2^2)
\end{aligned} \tag{375}$$

Thus, if we define

$$\begin{aligned}
A &\equiv (2+w^2-6wr+3r^2) + 2(1-2wr+r^2)\frac{w-1}{w+1}k_1^2 \\
&\qquad -2(w-r)(w-1)k_2 + (w-1)^2k_2^2
\end{aligned} \tag{376}$$

$$B_1 \equiv 4(1-2wr+r^2)\frac{w-1}{w+1}k_1 \tag{377}$$

$$D_1 \equiv 2(1-2wr+r^2)\frac{w-1}{w+1} \tag{378}$$

$$B_2 \equiv -2(w-r)(w-1) + 2k_2(w-1)^2 \tag{379}$$

$$D_2 \equiv (w-1)^2 \tag{380}$$

then

$$\tilde{h}_+^2 + \tilde{h}_-^2 + \tilde{h}_0^2 = A + B_1R_1 + D_1R_1^2 + B_2R_2 + D_2R_2^2 \tag{381}$$

If we further define

$$\begin{aligned}
E_1 &\equiv (w^2-1)^{1/2}(w+1)^2(1-15z^2+91z^3)^2 \\
E_2 &\equiv 2(w^2-1)^{1/2}(w+1)^2(1-15z^2+91z^3)(8z-53z^2+231z^3) \\
E_3 &\equiv (w^2-1)^{1/2}(w+1)^2(8z-53z^2+231z^3)^2
\end{aligned} \tag{382}$$

and

$$I_1 \equiv \int AE_1 dw \tag{383}$$

$$I_2 \equiv \int AE_2 dw \tag{384}$$

$$I_3 \equiv \int AE_3 dw \tag{385}$$

$$I_4 \equiv \int B_1 E_1 dw \tag{386}$$

$$I_5 \equiv \int B_1 E_2 dw \tag{387}$$

$$I_6 \equiv \int B_1 E_3 dw \tag{388}$$

$$I_7 \equiv \int C_1 E_1 dw \tag{389}$$

$$I_8 \equiv \int C_1 E_2 dw \tag{390}$$

$$I_9 \equiv \int C_1 E_3 dw \tag{391}$$

$$I_{10} \equiv \int B_2 E_1 dw \tag{392}$$

$$I_{11} \equiv \int B_2 E_2 dw \tag{393}$$

$$I_{12} \equiv \int B_2 E_3 dw \tag{394}$$

$$I_{13} \equiv \int C_2 E_1 dw \tag{395}$$

$$I_{14} \equiv \int C_2 E_2 dw \tag{396}$$

$$I_{15} \equiv \int C_2 E_3 dw \tag{397}$$

and also

$$C \equiv \sqrt{\frac{48\pi^3}{G_F^2 m_B^5 \tau_B r^3}} \tag{398}$$

$$\begin{aligned}\mathcal{F}(1)|V_{cb}| = C\mathcal{B}(B \to D^*\ell\nu)^{1/2}[&I_1 - I_2\rho^2 + I_3(\rho^2)^2 \\ &+I_4R_1 - I_5R_1\rho^2 + I_6R_1(\rho^2)^2 \\ &+I_7R_1^2 - I_8R_1^2\rho^2 + I_9R_1^2(\rho^2)^2 \\ &+I_{10}R_2 - I_{11}R_2\rho^2 + I_{12}R_2(\rho^2)^2 \\ &+I_{13}R_2^2 - I_{14}R_2^2\rho^2 + I_{15}R_2^2(\rho^2)^2]^{-1/2}\end{aligned} \tag{399}$$

Thus, using fit results $\mathcal{B}(B \to D^*\ell\nu)$, R_1, R_2 and ρ^2, we can calculate $\mathcal{F}(1)|V_{cb}|$. We use the following numerical values

$$\begin{aligned}
\tau_{B^+} &= 1.638 \times 10^{-12}/6.58211915 \times 10^{-25} \quad \text{GeV}^{-1} \\
m_{B^+} &= 5.2790 \quad \text{GeV} \\
m_{D^{*0}} &= 2.0067 \quad \text{GeV} \\
G_F &= 1.166371 \times 10^{-5} \quad \text{GeV}^{-2}
\end{aligned} \tag{400}$$

16.3 Results and statistical uncertainties

Using the fit results presented in the section 13, $\mathcal{G}(1)|V_{cb}|$ and $\mathcal{F}(1)|V_{cb}|$ are calculated to be

$$\begin{aligned}
\mathcal{G}(1)|V_{cb}| &= 0.04818 \\
\mathcal{F}(1)|V_{cb}| &= 0.03505
\end{aligned} \tag{401}$$

To calculate statistical uncertainties and correlation, for simplicity, we define

$$\begin{aligned}
y_1 &\equiv \mathcal{G}(1)|V_{cb}| \\
y_2 &\equiv \mathcal{F}(1)|V_{cb}| \\
y_3 &\equiv \rho^2 \\
y_4 &\equiv \rho_D^2 \\
y_5 &\equiv R_1 \\
y_6 &\equiv R_2 \\
x_1 &\equiv \rho_D^2 \\
x_2 &\equiv \rho^2 \\
x_3 &\equiv R_1 \\
x_4 &\equiv R_2 \\
x_5 &\equiv \mathcal{B}(B \to D\ell\nu) \\
x_6 &\equiv \mathcal{B}(B \to D^*\ell\nu)
\end{aligned} \tag{402}$$

then, Equation (366) becomes

$$y_1 = C^D x_5^{1/2} (I_1^D - I_2^D x_1 + I_3^D x_1^2)^{-1/2} \tag{403}$$

and Equation (399) becomes

$$\begin{aligned}
y_2 = C x_6^{1/2} [& I_1 - I_2 x_2 + I_3 x_2^2 \\
& + I_4 x_3 - I_5 x_3 x_2 + I_6 x_3 x_2^2 \\
& + I_7 x_3^2 - I_8 x_3^2 x_2 + I_9 x_3^2 x_2^2 \\
& + I_{10} x_4 - I_{11} x_4 x_2 + I_{12} x_4 x_2^2 \\
& + I_{13} x_4^2 - I_{14} x_4^2 x_2 + I_{15} x_4^2 x_2^2]^{-1/2}
\end{aligned} \tag{404}$$

The error matrix M(y) of y_1 - y_6 is determined by

$$M(y) = \left(\frac{\partial y_i}{\partial x_j}\right) M(x) \left(\frac{\partial y_i}{\partial x_j}\right) \tag{405}$$

where $M(x)$ the error matrix of x_1 - x_6

$$M(x) = \begin{pmatrix} 4.379\times10^{-3} & -1.559\times10^{-3} & -1.617\times10^{-3} & 1.789\times10^{-3} & 2.015\times10^{-5} & -2.288\times10^{-5} \\ -1.559\times10^{-3} & 5.841\times10^{-3} & 7.817\times10^{-3} & -7.167\times10^{-3} & 4.054\times10^{-6} & 1.244\times10^{-5} \\ -1.617\times10^{-3} & 7.817\times10^{-3} & 1.534\times10^{-2} & -1.183\times10^{-2} & 4.659\times10^{-6} & -2.025\times10^{-6} \\ 1.789\times10^{-3} & -7.167\times10^{-3} & -1.183\times10^{-2} & 1.067\times10^{-2} & 1.559\times10^{-6} & -1.887\times10^{-5} \\ 2.015\times10^{-5} & 4.054\times10^{-6} & 4.659\times10^{-6} & 1.559\times10^{-6} & 6.755\times10^{-7} & -3.001\times10^{-9} \\ -2.288\times10^{-5} & 1.244\times10^{-5} & -2.025\times10^{-6} & -1.887\times10^{-5} & -3.001\times10^{-9} & 1.498\times10^{-6} \end{pmatrix} \tag{406}$$

and

$$\frac{\partial y_1}{\partial x_1} = \frac{C}{2} x_5^{1/2} (I_2^D - 2I_3^D x_1)(I_1^D - I_2^D x_1 + I_3^D x_1^2)^{-3/2} \tag{407}$$

$$\frac{\partial y_1}{\partial x_5} = \frac{C}{2} x_5^{-1/2} (I_1^D - I_2^D x_1 + I_3^D x_1^2)^{-1/2} \tag{408}$$

$$\begin{aligned}\frac{\partial y_2}{\partial x_2} = -\frac{C}{2} x_6^{1/2} (&-I_2 + 2I_3 x_2 - I_5 x_3 + 2I_6 x_3 x_2 - I_8 x_3^2 + 2I_9 x_3^2 x_2 \\ &-I_{11} x_6 + 2I_{12} x_6 x_2 - I_{14} x_6^2 + 2I_{15} x_6^2 x_2) F^{-3/2}\end{aligned} \tag{409}$$

$$\frac{\partial y_2}{\partial x_3} = -\frac{C}{2} x_6^{1/2} (I_4 - I_5 x_2 + I_6 x_2^2 + 2I_7 x_3 - 2I_8 x_3 x_2 + 2I_9 x_3 x_2^2) F^{-3/2} \tag{410}$$

$$\frac{\partial y_2}{\partial x_4} = -\frac{C}{2} x_6^{1/2} (I_{10} - I_{11} x_2 + I_{12} x_2^2 + 2I_{13} x_4 - 2I_{14} x_4 x_2 + 2I_{15} x_4 x_2^2) F^{-3/2} \tag{411}$$

$$\frac{\partial y_2}{\partial x_6} = \frac{C}{2} x_6^{-1/2} F^{-1/2} \tag{412}$$

$$\frac{\partial y_3}{\partial x_1} = 1 \tag{413}$$

$$\frac{\partial y_4}{\partial x_2} = 1 \tag{414}$$

$$\frac{\partial y_5}{\partial x_3} = 1 \tag{415}$$

$$\frac{\partial y_6}{\partial x_4} = 1 \tag{416}$$

where

$$\begin{aligned} F = I_1 - I_2 x_2 + I_3 x_2^2 + I_4 x_3 - I_5 x_3 x_2 + I_6 x_3 x_2^2 + I_7 x_3^2 - I_8 x_3^2 x_2 + I_9 x_3^2 x_2^2 \\ +I_{10} x_4 - I_{11} x_4 x_2 + I_{12} x_4 x_2^2 + I_{13} x_4^2 - I_{14} x_4^2 x_2 + I_{15} x_4^2 x_2^2 \end{aligned} \tag{417}$$

and all other partial derivatives are zero.
Hence, with statistical uncertainty

$$\begin{aligned} \mathcal{G}(1)|V_{cb}| &= 0.04818 \pm 0.00185 \\ \mathcal{F}(1)|V_{cb}| &= 0.03505 \pm 0.00049 \end{aligned} \tag{418}$$

If we use re-normalized branching fractions

$$\begin{aligned}\tilde{\mathcal{G}}(1)|V_{cb}| &= 0.05038 \pm 0.00193 \\ \tilde{\mathcal{F}}(1)|V_{cb}| &= 0.03665 \pm 0.00051\end{aligned} \tag{419}$$

The correlation coefficient between these can be calculated to be

$$\frac{\mathrm{cov}(y_1, y_2)}{\sigma_{y_1}\sigma_{y_2}} = -0.228. \tag{420}$$

17 Systematic Uncertainties

Systematic uncertainties are shown in Tables 40-44. Numbers are negative when the corresponding fitted values decrease as a input parameter increases. Details are given in the following subsections. Note that the break down of background BF correction systematics are given in separate tables : Tables 45-49.

17.1 Form factors

17.1.1 w dependence of R_1 and R_2

We use the CLN parametrization of $B \to D^{(*)}\ell\nu$ decay form factors [37] (see section 9). Thus, we use

$$\begin{aligned} R_1(w) &= R_1 - 0.12(w-1) + 0.05(w-1)^2 \\ R_2(w) &= R_2 + 0.11(w-1) - 0.06(w-1)^2 \end{aligned} \tag{421}$$

Since there are different parametrization [38][39] and we cannot decide which is the best, we remove w dependence from R_1 and R_2 and consider the deviation as a systematic uncertainty.

17.1.2 $B \to D^{**}\ell\nu$ decay form factors

There are two sources of systematic uncertainty of D^{**} form factors :

- One is the FF slope $\tilde{\tau}' = -1.5$
- The other is the Approximation B_1 ($\tau_1 = 0$ and $\tau_2 = 0$).

To estimate systematic uncertainties,

- We change slope to -2.0 and -1.0, and take larger deviation.
- We use the Approximation B_2 ($\tau_1 \neq 0$ and $\tau_2 \neq 0$).

17.2 $B \to D^{**}/D^{(*)}\pi\ell\nu$ decay branching fraction ratios

We have five BF ratios as input :

- $f_{D_2^*/D_1} \equiv \frac{\mathcal{B}(B^+\to\bar{D}_2^{*0}\ell^+\nu)}{\mathcal{B}(B^+\to\bar{D}_1^0\ell^+\nu)} = 0.78 \pm 0.17$
- $f_{D_0^* D\pi T/D_1 D_2^* T} \equiv \frac{\mathcal{BT}(B^+\to\bar{D}_0^{*0}/(D\pi)^0\ell^+\nu)}{\mathcal{BT}(B^+\to\bar{D}_1^0/\bar{D}_2^{*0}\ell^+\nu)} = 0.77 \pm 0.19$
- $f_{D_1' D^*\pi T/D_1 D_2^* T} \equiv \frac{\mathcal{BT}(B^+\to\bar{D}_1^{*0}/(D^*\pi)^0\ell^+\nu)}{\mathcal{BT}(B^+\to\bar{D}_1^0/\bar{D}_2^{*0}\ell^+\nu)} = 0.98 \pm 0.24$
- $f_{D\pi/D_0^*} \equiv \frac{\mathcal{B}(B^+\to D^-\pi^+\ell^+\nu)}{\mathcal{B}(B^+\to\bar{D}_0^{*0}\ell^+\nu)} = 0.42 \pm 0.28$
- $f_{D^*\pi/D_1'} \equiv \frac{\mathcal{B}(B^+\to D^{*-}\pi^+\ell^+\nu)}{\mathcal{B}(B^+\to\bar{D}_1^{*0}\ell^+\nu)} = 0.071 \pm 0.050$

We change these ratios to $\pm$ one standard deviation and take larger deviation as systematic uncertainties.

item	ρ_D^2	ρ^2	R_1	R_2	f_{+0}
$R_1(w)$ and $R_2(w)$	0.11	1.42	-1.38	3.18	0.12
D^{**} slope	-0.58	-2.77	1.67	-1.54	-0.56
D^{**} B$_2$	-0.62	1.21	1.15	-0.19	0.09
FF total	**0.85**	**3.34**	**2.45**	**3.54**	**0.58**
$f_{D_2^*/D_1}$	-0.02	0.03	0.09	0.10	0.26
$f_{D_0^* D\pi/D_1 D_2^*}$	-0.37	0.86	2.15	-1.49	0.77
$f_{D_1^* D^*\pi/D_1 D_2^*}$	0.16	-0.53	-1.56	0.12	-0.75
$f_{D\pi/D_0^*}$	-0.60	0.25	2.32	-4.21	-0.61
$f_{D^*\pi/D_1^*}$	-0.02	0.00	0.56	-0.70	0.04
BF ratios total	**0.72**	**1.04**	**3.58**	**4.53**	**1.26**
$f_{D_2^*}$	-0.12	0.13	0.17	-0.34	0.31
D^{*+} BF	0.49	-0.37	-0.39	0.73	-0.83
D^0 BF	-0.32	0.33	0.39	-0.75	2.71
D^+ BF	0.24	-0.11	-0.16	0.30	-1.54
t_{+0}	-0.00	-0.03	-0.06	0.10	-0.82
Luminosity	0.05	0.07	0.06	-0.12	-0.01
Input parms total	**0.64**	**0.53**	**0.61**	**1.15**	**3.34**
Bkg BF total	**2.58**	**1.34**	**2.51**	**4.37**	**1.27**
Lepton PID	-0.45	-0.26	4.02	0.86	0.32
Kaon PID	0.01	0.91	0.41	-0.91	-0.31
Tracking eff.	-0.05	0.37	0.26	-0.52	1.14
PHOTOS	not yet	not yet	not yet	not yet	not yet
Corrections total	**0.46**	**1.01**	**4.05**	**1.35**	**1.23**
$D^{(*)}\pi\pi\ell\nu$	**1.12**	**1.50**	**0.99**	**5.37**	**1.76**
Grand total	**3.12**	**4.20**	**6.55**	**9.16**	**4.40**

Table 40: **(Run2 only)** [**Systematics : FF parms**] Systematic uncertainties on form factor parameters. Numbers are given in %. Numbers are negative when fitted value decrease as input parameter increase.

item	$\mathcal{B}(B \to D\ell\nu)$	$\mathcal{B}(B \to D^*\ell\nu)$	$\mathcal{B}(B \to D^{**}/D^{(*)}\pi\ell\nu)$
$R_1(w)$ and $R_2(w)$	0.16	-1.54	0.05
D^{**} slope	0.04	0.33	-3.69
D^{**} B$_2$	0.07	-0.12	1.09
FF total	**0.17**	**1.58**	**3.84**
$f_{D_2^*/D_1}$	-0.20	-0.07	0.38
$f_{D_0^* D\pi/D_1 D_2^*}$	-0.19	-0.34	3.47
$f_{D_1^* D^*\pi/D_1 D_2^*}$	0.35	0.27	-3.37
$f_{D\pi/D_0^*}$	0.62	0.07	1.67
$f_{D^*\pi/D_1^*}$	-0.08	0.11	1.32
BF ratios total	**0.77**	**0.46**	**5.30**
$f_{D_2^*}$	-0.08	-0.01	0.41
D^{*+} BF	0.22	-0.17	0.05
D^0 BF	-1.28	-0.28	-0.43
D^+ BF	-0.54	-1.10	-0.97
t_{+0}	0.39	0.40	0.43
Luminosity	-1.12	-1.12	-1.08
Input parms total	**1.85**	**1.65**	**1.63**
Bkg BF total	**0.93**	**0.42**	**1.49**
Lepton PID	-3.17	-3.91	-1.99
Kaon PID	-0.08	0.18	-0.31
Tracking eff.	-1.85	-1.50	-1.62
PHOTOS	not yet	not yet	not yet
Corrections total	**3.67**	**4.19**	**2.59**
$D^{(*)}\pi\pi\ell\nu$	**0.55**	**2.69**	**13.63**
Grand total	**4.33**	**5.52**	**15.50**

Table 41: **(Run2 only)** [**Systematics : BF**] Systematic uncertainties on branching fractions. Numbers are given in %. Numbers are negative when fitted value decrease as input parameter increase.

item	$\tilde{\mathcal{B}}(B \to D\ell\nu)$	$\tilde{\mathcal{B}}(B \to D^*\ell\nu)$	$\tilde{\mathcal{B}}(B \to D^{**}/D^{(*)}\pi\ell\nu)$
$R_1(w)$ and $R_2(w)$	0.91	-0.79	0.81
D^{**} slope	0.48	0.80	-3.23
D^{**} B_2	-0.17	-0.36	0.85
FF total	**1.04**	**1.18**	**3.44**
$f_{D_2^*/D_1}$	-0.15	-0.03	0.42
$f_{D_0^*D\pi/D_1D_2^*}$	-0.28	-0.44	3.38
$f_{D_1^*D^*\pi/D_1D_2^*}$	0.59	0.51	-3.12
$f_{D\pi/D_0^*}$	0.56	0.06	1.60
$f_{D^*\pi/D_1^*}$	-0.15	0.05	1.26
BF ratios total	**0.88**	**0.68**	**5.05**
$f_{D_2^*}$	-0.11	-0.04	0.38
D^{*+} BF	0.27	-0.13	0.10
D^0 BF	-0.75	0.25	0.11
D^+ BF	0.40	-0.15	-0.02
t_{+0}	0.40	0.41	0.43
Luminosity	-0.01	-0.01	0.03
Input parms total	**0.98**	**0.52**	**0.60**
Bkg BF total	**0.71**	**0.53**	**1.26**
Lepton PID	-0.05	-0.81	1.17
Kaon PID	-0.16	0.10	-0.39
Tracking eff.	-0.27	0.09	-0.04
PHOTOS	not yet	not yet	not yet
Corrections total	**0.31**	**0.82**	**1.23**
Inclusive BF	1.87	1.87	1.87
Higher $D^{(*)}\pi\pi\ell\nu$	-1.73	1.47	-14.66
Higher $D_sK\ell\nu$	not yet	not yet	not yet
BF renormalization total	**1.87**	**1.87**	**1.87**
Grand total	**2.63**	**2.57**	**6.66**

Table 42: **(Run2 only)** [**Systematics : Renormalized BF**] Systematic uncertainties on re-normalized branching fractions. Numbers are given in %. Numbers are negative when fitted value decrease as input parameter increase.

item	$\mathcal{G}(1)V_{cb}$	$\mathcal{F}(1)V_{cb}$
$R_1(w)$ and $R_2(w)$	0.15	0.34
D^{**} slope	-0.36	-1.22
D^{**} B$_2$	-0.36	0.29
FF total	**0.53**	**1.30**
$f_{D_2^*/D_1}$	-0.11	-0.02
$f_{D_0^* D\pi/D_1 D_2^*}$	-0.33	-0.22
$f_{D_1^* D^*\pi/D_1 D_2^*}$	0.27	0.06
$f_{D\pi/D_0^*}$	-0.07	-0.68
$f_{D^*\pi/D_1^*}$	-0.06	-0.09
BF ratios total	**0.45**	**0.72**
$f_{D_2^*}$	-0.11	-0.02
D^{*+} BF	0.42	-0.09
D^0 BF	-0.84	-0.15
D^+ BF	-0.13	-0.53
t_{+0}	0.19	0.21
Luminosity	-0.53	-0.56
Input parms total	**1.11**	**0.82**
Bkg BF total	**2.00**	**0.46**
Lepton PID	-1.88	-2.22
Kaon PID	-0.03	0.27
Tracking eff.	-0.96	-0.71
PHOTOS	not yet	not yet
Corrections total	**2.11**	**2.34**
$D^{(*)}\pi\pi\ell\nu$	**0.98**	**1.05**
Grand total	**3.34**	**3.11**

Table 43: **(Run2 only)** [**Systematics :** $\mathcal{G}(1)V_{cb}$ **and** $\mathcal{F}(1)V_{cb}$] Systematic uncertainties on $\mathcal{G}(1)V_{cb}$ and $\mathcal{F}(1)V_{cb}$. Numbers are given in %. Numbers are negative when fitted value decrease as input parameter increase.

item	$\tilde{\mathcal{G}}(1)V_{cb}$	$\tilde{\mathcal{F}}(1)V_{cb}$
$R_1(w)$ and $R_2(w)$	0.53	0.72
D^{**} slope	-0.13	-0.99
D^{**} B_2	-0.48	0.17
FF total	**0.72**	**1.23**
$f_{D_2^*/D_1}$	-0.09	0.01
$f_{D_0^* D\pi/D_1 D_2^*}$	-0.37	-0.27
$f_{D_1^* D^*\pi/D_1 D_2^*}$	0.40	0.18
$f_{D\pi/D_0^*}$	-0.10	-0.71
$f_{D^*\pi/D_1^*}$	-0.09	-0.12
BF ratios total	**0.57**	**0.79**
$f_{D_2^*}$	-0.13	-0.04
D^{*+} BF	0.45	-0.07
D^0 BF	-0.58	0.11
D^+ BF	0.35	-0.06
t_{+0}	0.20	0.21
Luminosity	0.03	0.00
Input parms total	**0.84**	**0.26**
Bkg BF total	**1.89**	**0.51**
Lepton PID	-0.31	-0.65
Kaon PID	-0.07	0.23
Tracking eff.	-0.16	0.09
PHOTOS	0.00	0.00
Corrections total	**0.36**	**0.70**
Inclusive BF	0.94	0.94
Higher X_c	0.00	0.00
BF renormalization total	**0.94**	**0.94**
Grand total	**2.48**	**1.96**

Table 44: **(Run2 only)** [**Systematics : $\tilde{\mathcal{G}}(1)V_{cb}$ and $\tilde{\mathcal{F}}(1)V_{cb}$**] Systematic uncertainties on $\tilde{\mathcal{G}}(1)V_{cb}$ and $\tilde{\mathcal{F}}(1)V_{cb}$ with re-normalized BF. Numbers are given in %. Numbers are negative when fitted value decrease as input parameter increase.

17.3 Input parameters

17.3.1 D_2^* decay branching fractions

As described in section 8.2, we have one parameter,

- $f_{D_2^*} = 2.1 \pm 0.644$

to calculate D_2^* decay branching fractions. We change $f_{D_2^*}$ to $\pm$ one standard deviation and take larger deviation as systematic uncertainties.

17.3.2 $D^{(*)}$ decay branching fractions

The $D^{(*)}$ decay branching fractions

- $\mathcal{B}(D^{*+} \to D^0\pi^+) = 0.677 \pm 0.005$
- $\mathcal{B}(D^0 \to K^-\pi^+) = 0.03912 \pm 0.00048$
- $\mathcal{B}(D^+ \to K^-\pi^+\pi^+) = 0.0915 \pm 0.0020$

are also input parameters of our fitting. We change these BFs to $\pm$ one standard deviation and take larger deviation as systematic uncertainties.

17.3.3 t_{+0}

Another input parameter of our fitting is lifetime ratio

- $t_{+0} \equiv \frac{\tau_{B^+}}{\tau_{B^0}} = 1.071 \pm 0.009$

We change t_{+0} to $\pm$ one standard deviation and take larger deviation as systematic uncertainties.

17.3.4 Luminosity normalization : B counting

There is 1.1 % uncertainty (statistical + systematic) on B counting. Thus we change luminosity normalization factors by $\pm$ 1.1 % and take larger deviation as systematic uncertainties. .

17.4 Background BF re-weighting

As describe in section 8, we re-weight branching fractions of background components.

17.4.1 BF re-weighting

The branching fractions we re-weight are semileptonic D decays

- $D^0 \to K^{*-}\ell\nu$
- $D^0 \to K^-\ell\nu$

- $D^0 \to \pi^- \ell \nu$
- $D^0 \to \rho^- \ell \nu$
- $D^+ \to K^{*0} \ell \nu$
- $D^+ \to K^0 \ell \nu$
- $D^+ \to \pi^0 \ell \nu$
- $D^+ \to \rho^0 \ell \nu$
- $D^+ \to \omega \ell \nu$
- $D_s^+ \to \phi \ell \nu$
- $D_s^+ \to \eta \ell \nu$
- $D_s^+ \to \eta' \ell \nu$

$B \to D^{(*)} \tau \nu$ decays

- $B^+ \to \bar{D}^0 \tau^+ \nu$
- $B^+ \to \bar{D}^{*0} \tau^+ \nu$
- $B^0 \to D^- \tau^+ \nu$
- $B^0 \to D^{*-} \tau^+ \nu$

inclusive $B \to X \ell \nu$ decays

- $B^+ \to \bar{X}^0 \ell^+ \nu$
- $B^0 \to X^- \ell^+ \nu$

and inclusive $B \to D_s$ decays

- $B^- \to D_s^+$
- $B^+ \to D_s^+$
- $\bar{B}^0 \to D_s^+$
- $B^0 \to D_s^+$

We change these BF to $\pm$ one standard deviation and take larger deviation as systematic uncertainties. We use different method for inclusive $B \to D$ decays as explained in the following subsection.

17.4.2 D momentum dependent inclusive $B \to D$ BF re-weighting

As described in section 8.1.4, we fit for D momentum dependent weight by a combination of a Gaussian ans 3rd order polynomial, and we use the fitted function to re-weight MC. To estimate the systematic uncertainty of this re-weighting, we do the following procedure :

1. We deviate each weight using Gaussian random numbers.
2. We fit the distribution of weight vs. D momentum using 3rd order polynomial.
3. We re-weight MC by the fitted functions to create 3D histograms.
4. Using the histograms, we perform fitting.
5. We iterate the above 1 to 4 400 times.
6. We make distributions of the deviations from the 400 fit results.
7. We take the standard deviation of each distribution as a systematic uncertainty.

where we us only 3rd order polynomial to fit for weights because if we use Gaussian + polynomial, the fit does not converge in most of the cases. This may change the mean of the distribution of the deviation, but the effect on the standard deviation should be small.

17.5 Various corrections

17.5.1 Lepton PID correction

We compare the fit results with and without lepton (electron or muon) PID correction. **Plan for the next version** : We can use the results of a systematic study done by PID group [48]. They got the folloeing sistematic uncertainties :

- PidLHElectron
  - 1.03 % for e^-
  - 0.69 % for e^+
- TightMuon
  - 4.53 % for μ^-
  - 3.99 % for μ^+

We cam evaluate systematic uncertainty as follows :

1. Average the positive and negative uncertainties.
2. Add the above uncertainties to the uncertainties of PID correction factors, which is the statistical uncertainties given in the PID table, by quadrature.

item	ρ_D^2	ρ^2	R_1	R_2	f_{+0}
$D^0 \to K^{*-}\ell\nu$	0.04	-0.01	0.00	-0.04	-0.02
$D^0 \to K^-\ell\nu$	-0.04	0.01	0.01	-0.05	-0.03
$D^0 \to \pi^-\ell\nu$	-0.03	0.01	-0.00	-0.01	-0.02
$D^0 \to \rho^-\ell\nu$	0.03	0.01	-0.00	-0.02	-0.02
$D^+ \to K^{*0}\ell\nu$	0.03	-0.01	-0.00	-0.02	0.03
$D^+ \to K^0\ell\nu$	-0.04	-0.05	-0.06	0.07	-0.02
$D^+ \to \pi^0\ell\nu$	-0.03	0.00	-0.01	-0.02	-0.02
$D^+ \to \rho^0\ell\nu$	-0.03	0.01	0.00	-0.01	0.02
$D^+ \to \omega\ell\nu$	0.03	0.01	-0.00	-0.01	0.02
$D_s^+ \to \phi\ell\nu$	-0.09	0.02	-0.04	0.05	0.03
$D_s^+ \to \eta\ell\nu$	-0.05	-0.14	-0.15	0.56	0.03
$D_s^+ \to \eta'\ell\nu$	-0.04	-0.03	0.01	0.02	-0.03
$B^+ \to \bar{D}^0\tau^+\nu$	0.03	-0.05	0.09	0.40	0.03
$B^+ \to \bar{D}^{*0}\tau^+\nu$	-0.04	0.09	0.13	-0.39	-0.03
$B^0 \to D^-\tau^+\nu$	-0.03	-0.00	-0.00	-0.01	-0.02
$B^0 \to D^{*-}\tau^+\nu$	-0.03	-0.00	-0.00	-0.01	-0.02
$B^+ \to \bar{X}^0\ell^+\nu$	-0.04	0.02	0.08	-0.12	0.02
$B^0 \to X^-\ell^+\nu$	-0.04	-0.06	-0.12	0.23	-0.03
$B^- \to D_s^+$	-0.03	0.01	-0.00	-0.01	0.02
$B^+ \to D_s^+$	0.03	0.01	-0.00	-0.02	0.02
$\bar{B}^0 \to D_s^+$	0.03	0.01	-0.00	-0.03	0.02
$B^0 \to D_s^+$	0.04	0.01	0.00	-0.02	-0.02
Sub total	**0.19**	**0.20**	**0.27**	**0.84**	**0.11**
$B \to D$	2.58	1.32	2.49	4.28	1.27
Grand total	**2.58**	**1.34**	**2.51**	**4.37**	**1.27**

Table 45: **(Run2 only)** [**Bkg BF Systematics : FF parms**] Systematic uncertainties on form factor parameters. Numbers are given in %. Numbers are negative when fitted value decrease as input parameter increase.

item	$\mathcal{B}(B \to D\ell\nu)$	$\mathcal{B}(B \to D^*\ell\nu)$	$\mathcal{B}(B \to D^{**}/D^{(*)}\pi\ell\nu)$
$D^0 \to K^{*-}\ell\nu$	0.02	-0.00	0.06
$D^0 \to K^-\ell\nu$	-0.03	0.00	0.07
$D^0 \to \pi^-\ell\nu$	-0.02	0.00	0.03
$D^0 \to \rho^-\ell\nu$	-0.02	0.00	0.03
$D^+ \to K^{*0}\ell\nu$	-0.02	-0.00	0.05
$D^+ \to K^0\ell\nu$	-0.04	0.00	0.14
$D^+ \to \pi^0\ell\nu$	-0.02	0.00	0.03
$D^+ \to \rho^0\ell\nu$	-0.02	-0.00	0.03
$D^+ \to \omega\ell\nu$	0.02	-0.00	0.03
$D_s^+ \to \phi\ell\nu$	-0.04	-0.01	-0.02
$D_s^+ \to \eta\ell\nu$	0.06	-0.05	0.09
$D_s^+ \to \eta'\ell\nu$	0.02	-0.02	0.16
$B^+ \to \bar{D}^0\tau^+\nu$	0.10	-0.08	-0.18
$B^+ \to \bar{D}^{*0}\tau^+\nu$	0.02	0.09	-0.45
$B^0 \to D^-\tau^+\nu$	-0.02	-0.00	-0.02
$B^0 \to D^{*-}\tau^+\nu$	-0.02	-0.00	-0.02
$B^+ \to \bar{X}^0\ell^+\nu$	0.02	-0.02	0.06
$B^0 \to X^-\ell^+\nu$	-0.05	0.02	0.08
$B^- \to D_s^+$	0.02	0.00	0.03
$B^+ \to D_s^+$	0.02	0.00	0.02
$\bar{B}^0 \to D_s^+$	0.02	0.00	0.04
$B^0 \to D_s^+$	0.03	0.00	-0.02
Sub total	**0.16**	**0.14**	**0.57**
$B \to D$	0.92	0.39	1.38
Grand total	**0.93**	**0.42**	**1.49**

Table 46: **(Run2 only)** [**Bkg BF Systematics : BF**] Systematic uncertainties on branching fractions. Numbers are given in %. Numbers are negative when fitted value decrease as input parameter increase.

item	$\tilde{\mathcal{B}}(B \to D\ell\nu)$	$\tilde{\mathcal{B}}(B \to D^*\ell\nu)$	$\tilde{\mathcal{B}}(B \to D^{**}/D^{(*)}\pi\ell\nu)$
$D^0 \to K^{*-}\ell\nu$	-0.02	-0.01	0.06
$D^0 \to K^-\ell\nu$	-0.03	-0.00	0.07
$D^0 \to \pi^-\ell\nu$	-0.02	0.00	0.03
$D^0 \to \rho^-\ell\nu$	-0.02	-0.00	0.03
$D^+ \to K^{*0}\ell\nu$	-0.02	-0.01	0.05
$D^+ \to K^0\ell\nu$	-0.05	-0.01	0.13
$D^+ \to \pi^0\ell\nu$	-0.02	0.00	0.03
$D^+ \to \rho^0\ell\nu$	-0.02	-0.00	0.03
$D^+ \to \omega\ell\nu$	0.02	-0.00	0.03
$D_s^+ \to \phi\ell\nu$	-0.02	0.00	0.03
$D_s^+ \to \eta\ell\nu$	0.05	-0.06	0.09
$D_s^+ \to \eta'\ell\nu$	-0.03	-0.03	0.16
$B^+ \to \bar{D}^0\tau^+\nu$	0.13	-0.05	-0.16
$B^+ \to \bar{D}^{*0}\tau^+\nu$	0.04	0.11	-0.43
$B^0 \to D^-\tau^+\nu$	-0.02	-0.00	-0.02
$B^0 \to D^{*-}\tau^+\nu$	-0.02	-0.00	-0.02
$B^+ \to \bar{X}^0\ell^+\nu$	0.03	-0.01	0.07
$B^0 \to X^-\ell^+\nu$	-0.06	0.01	0.07
$B^- \to D_s^+$	0.02	-0.00	0.03
$B^+ \to D_s^+$	0.02	-0.00	0.02
$\bar{B}^0 \to D_s^+$	-0.02	-0.00	0.04
$B^0 \to D_s^+$	0.02	-0.00	-0.03
Sub total	**0.19**	**0.14**	**0.54**
$B \to D$	0.68	0.51	1.14
Grand total	**0.71**	**0.53**	**1.26**

Table 47: **(Run2 only)** [**Bkg BF Systematics : Renormalized BF**] Systematic uncertainties on re-normalized branching fractions. Numbers are given in %. Numbers are negative when fitted value decrease as input parameter increase.

item	$\mathcal{G}(1)V_{cb}$	$\mathcal{F}(1)V_{cb}$
$D^0 \to K^{*-}\ell\nu$	0.04	-0.01
$D^0 \to K^-\ell\nu$	-0.04	-0.00
$D^0 \to \pi^-\ell\nu$	-0.03	0.00
$D^0 \to \rho^-\ell\nu$	0.03	-0.00
$D^+ \to K^{*0}\ell\nu$	0.03	-0.00
$D^+ \to K^0\ell\nu$	-0.05	-0.00
$D^+ \to \pi^0\ell\nu$	-0.03	0.00
$D^+ \to \rho^0\ell\nu$	-0.03	0.00
$D^+ \to \omega\ell\nu$	0.03	-0.00
$D_s^+ \to \phi\ell\nu$	-0.08	0.01
$D_s^+ \to \eta\ell\nu$	0.03	0.02
$D_s^+ \to \eta'\ell\nu$	-0.04	-0.02
$B^+ \to \bar{D}^0\tau^+\nu$	0.07	-0.00
$B^+ \to \bar{D}^{*0}\tau^+\nu$	-0.04	0.01
$B^0 \to D^-\tau^+\nu$	-0.03	-0.00
$B^0 \to D^{*-}\tau^+\nu$	-0.03	-0.00
$B^+ \to \bar{X}^0\ell^+\nu$	-0.03	-0.03
$B^0 \to X^-\ell^+\nu$	-0.05	0.03
$B^- \to D_s^+$	-0.03	0.00
$B^+ \to D_s^+$	0.03	0.00
$\bar{B}^0 \to D_s^+$	0.03	0.00
$B^0 \to D_s^+$	0.04	0.00
Sub total	**0.19**	**0.05**
$B \to D$	1.99	0.46
Grand total	**2.00**	**0.46**

Table 48: **(Run2 only)** [**Bkg BF Systematics :** $\mathcal{G}(1)V_{cb}$ **and** $\mathcal{F}(1)V_{cb}$] Systematic uncertainties on $\mathcal{G}(1)V_{cb}$ and $\mathcal{F}(1)V_{cb}$. Numbers are given in %. Numbers are negative when fitted value decrease as input parameter increase.

item	$\tilde{\mathcal{G}}(1)V_{cb}$	$\tilde{\mathcal{F}}(1)V_{cb}$
$D^0 \to K^{*-}\ell\nu$	0.04	-0.01
$D^0 \to K^-\ell\nu$	-0.04	-0.01
$D^0 \to \pi^-\ell\nu$	-0.03	0.00
$D^0 \to \rho^-\ell\nu$	0.03	-0.00
$D^+ \to K^{*0}\ell\nu$	0.03	-0.00
$D^+ \to K^0\ell\nu$	-0.05	-0.01
$D^+ \to \pi^0\ell\nu$	-0.03	0.00
$D^+ \to \rho^0\ell\nu$	-0.03	0.00
$D^+ \to \omega\ell\nu$	0.03	-0.00
$D_s^+ \to \phi\ell\nu$	-0.07	0.01
$D_s^+ \to \eta\ell\nu$	0.03	0.02
$D_s^+ \to \eta'\ell\nu$	-0.04	-0.02
$B^+ \to \bar{D}^0\tau^+\nu$	0.08	0.02
$B^+ \to \bar{D}^{*0}\tau^+\nu$	0.03	0.02
$B^0 \to D^-\tau^+\nu$	-0.02	-0.00
$B^0 \to D^{*-}\tau^+\nu$	-0.02	-0.00
$B^+ \to \bar{X}^0\ell^+\nu$	-0.03	-0.02
$B^0 \to X^-\ell^+\nu$	-0.06	0.02
$B^- \to D_s^+$	-0.03	-0.00
$B^+ \to D_s^+$	0.03	-0.00
$\bar{B}^0 \to D_s^+$	0.03	-0.00
$B^0 \to D_s^+$	0.03	-0.00
Sub total	**0.19**	**0.05**
$B \to D$	1.88	0.50
Grand total	**1.89**	**0.51**

Table 49: **(Run2 only)** [**Bkg BF Systematics :** $\tilde{\mathcal{G}}(1)V_{cb}$ **and** $\tilde{\mathcal{F}}(1)V_{cb}$] Systematic uncertainties on $\tilde{\mathcal{G}}(1)V_{cb}$ and $\tilde{\mathcal{F}}(1)V_{cb}$. Numbers are given in %. Numbers are negative when fitted value decrease as input parameter increase.

3. Deviate the PID correction factors by $\pm$ the added uncertainties; then perform fiting.

4. The deviations (%) of the above fit results from nominal values are the PID systemactics.

17.5.2 Kaon PID correction

We compare the fit results with and without kaon PID correction.
Plan for the next version : For the D^0 channel the BToDlnu skim does not require Kaon PID. We can therefore check the PID efficiency, independently data and MC, by making the following ratio

$$r = \frac{\text{Number of } D^0 \text{ with } K \text{ PID}}{\text{Number of } D^0 \text{ without } K \text{ PID}} \tag{422}$$

We can calculate r_{data} and r_{MC} in bins of kaon momentum and $\cos\theta$. By conparing the ratio

$$f = \frac{r_{data}}{r_{MC}} \tag{423}$$

with kaon PID correction factors, we can validate kaon PID correction and we can also get a meaningful way of assigning an uncertainty to the PID corrections.

17.5.3 Tracking efficiency correction

We compare the fit results with and without tracking efficiency correction.

17.5.4 Radiative corrections : PHOTOS

This has not yet done. The following is a plan for the next version.
We study the effect of radiation correction in generator level by comparing MC generated with PHOTOS on and off and seeing how the fit results change. Since we do not have fully simulated MC with PHOTOS off, we need to consrruct efficiency matrices for D^0 and D^+ as explained below. Once we have the efficiency matrices, we can take the D^0 and D^+ 3D histograms from generator-level MC, multiply them by the efficiency matrices, and do fits with and without PHOTOS; we can take the difference between the fits as an estimate of the systematic uncertainty.
Now, we explain about the efficiency matrix. This is a 3D matrix which can be constructed by the following procedure

1. We generate full MC with PHOTOS on.

2. We produce 3D histograms using MC truth as we do in our analysis, but we do not apply any event selection cuts or corrections.

3. We devide the above histograms, bin by bin, by the corresponding histograms which we use for the nominal fitting. Normalization can be done by the genarated number of events.

4. Then, we get 3D efficiency matrices/histograms, one for each MC mode.

17.6 Bremssrtrahlung

This has not yet done. The following is a plan for the next version.
Due to emission of bremsstrahlung photons, the electron loses energy when traveling through the detector material. This effect was studied in a previous Babar analysis [47]. They get an empilical formula for the electron energy loss

$$\Delta E = \mp 0.0125 \frac{E}{\text{GeV}} \pm 0.00425 \ \text{GeV} \tag{424}$$

We apply this correction and take the deviation as a systematic uncertainty.

17.7 Vertexing

The vertexing cut is described in the event selection section 6. We change the cuts on $P^D(\chi^2, dof)$ and $P^B(\chi^2, dof)$ to see the effect of vertexing on the fit results. Nonimal cuts are

$$\begin{aligned} P^D(\chi^2, dof) &> 0.001 \\ P^B(\chi^2, dof) &> 0.01 \end{aligned} \tag{425}$$

We did fit with the following conditions

- Looser B vertex : $P^B(\chi^2, dof) > 0.001$
- Looser B and D vertex : $P^B(\chi^2, dof) > 0.001$ and $P^D(\chi^2, dof) > 0.0001$
- Tighter D vertex : $P^D(\chi^2, dof) > 0.01$

Results are given in Table 50. There is no systematic effect on the fit results.

17.8 Effect of higher X_c states

17.8.1 $B \to D^{(*)}\pi\pi\ell\nu$ decays

The generic $B\bar{B}$ samples do not contain decays of the type $B \to X_c\ell\nu$ where X_c is a charm system that produces a $D^{(*)}$ and two pions. These decays must be modeled separately using EVTGEN and their impact on the fitted parameters must be determined. To do this we proceed as follows.

- The X_c systems studied cover a range of spin states and decay mechanisms. They are listed in Table 51. The decay $B \to X_c\ell\nu$ is performed using the HQET matrix element, i.e. the X_c system is treated as a heavier D or D^* according to the spin. The mass and spin of the X_c state therefore determine the lepton momentum spectrum. The D momentum and the $\cos\theta_{D\ell}$ depend on the decay dynamics as well. The Xc states are decayed into D or D* (with equal branching fractions) and two pions according to phase space; the Xc* states are decayed the same way. The Yc and Yc* states, on the other hand, are decayed as two-body $D^{(*)}\rho$ states (the Yc(*) mass was chosen to be just above threshold for this decay). These various choices of spin, mass and decay mode serve as a reasonable sample of the potential $B \to D^{(*)}\pi\pi$ decay modes.

Parameters	Looser B vtx	Loosed B and D vtx	Tighter D vtx
ρ_D^2	0.430	0.390	0.149
ρ^2	0.133	0.134	-0.014
R_1	0.216	0.250	0.036
R_2	-0.080	-0.129	-0.043
$\mathcal{B}(B \to D\ell\nu)$	1.117	1.129	-0.163
$\mathcal{B}(B \to D^*\ell\nu)$	-0.176	-0.049	0.061
$\mathcal{B}(B \to D^{**}/D^{(*)}\pi\ell\nu)$	0.079	0.080	-0.202
f_{+0}	0.540	0.037	-0.118
$C_{UncorDL}^{D^0}$	0.216	0.257	-0.055
$C_{UncorCL}^{D^0}$	0.077	0.116	-0.123
$C_{CascL}^{D^0}$	0.330	0.393	0.134
$C_{UncorDL}^{D^+}$	-0.059	-0.178	0.021
$C_{UncorCL}^{D^+}$	0.012	0.053	-0.093
$C_{CascL}^{D^+}$	0.039	-0.048	-0.053
χ^2/ndof (P-value)	246/215 (0.07)	248/215 (0.06)	243/215 (0.09)

Table 50: **(Run2 only)** [**Effect of vertex cuts**] Pulls of the fits with different vertex cuts. Pulls are calculated from the difference to nominal fit results.

name	mass	width	$\max_D m$	charge	spin
Xc0	2.61	0.3	0.3	0	0
anti-Xc0	2.61	0.3	0.3	0	0
Xc+	2.61	0.3	0.3	+1	0
Xc-	2.61	0.3	0.3	-1	0
Xc*0	2.61	0.3	0.3	0	1
anti-Xc*0	2.61	0.3	0.3	0	1
Xc*+	2.61	0.3	0.3	+1	1
Xc*-	2.61	0.3	0.3	-1	1
Yc0	2.87	0.1	0.1	0	0
anti-Yc0	2.87	0.1	0.1	0	0
Yc+	2.87	0.1	0.1	+1	0
Yc-	2.87	0.1	0.1	-1	0
Yc*0	2.87	0.1	0.1	0	1
anti-Yc*0	2.87	0.1	0.1	0	1
Yc*+	2.87	0.1	0.1	+1	1
Yc*-	2.87	0.1	0.1	-1	1

Table 51: **(Run2 only)** [X_c **systems**] X_c systems studied for systematic study.

- Each sample is used in turn, with its yield fixed by the difference in branching fraction between the inclusive $b \to c\ell\nu$ branching fraction and the sum over the exclusive decays to $D\ell\nu$, $D^*\ell\nu$ and $D^{**}\ell\nu$. With this component fixed the fit is performed as usual, and differences with respect to the nominal fit are used to estimate systematic errors.

17.9 BF renormalization

17.9.1 Inclusive BF

We use measured inclusive BF [45] as an input

$$\Delta\mathcal{B}(B \to X_c\ell\nu) = 0.0454 \pm 0.0003 \pm 0.0008 = 0.0454 \pm 0.00085 \tag{426}$$

We change this to $\pm$ one standard deviation and take larger deviation as systematic uncertainties.

Parameters	Fit results	Nominal fit
ρ_D^2	1.331 ± 0.068	1.346 ± 0.067
ρ^2	1.373 ± 0.075	1.353 ± 0.076
R_1	1.418 ± 0.075	1.405 ± 0.109
R_2	0.632 ± 0.107	0.668 ± 0.099
$\mathcal{B}(B^+ \to \bar{D}^0 \ell^+ \nu)$	0.02511 ± 0.00063	0.02525 ± 0.00063
$\mathcal{B}(B^+ \to \bar{D}^{*0} \ell^+ \nu)$	0.05434 ± 0.00099	0.05291 ± 0.00083
$\mathcal{BT}(B^+ \to \bar{D}^{**0}/(D\pi)^0 \ell^+ \nu)$	0.01693 ± 0.00136	0.01961 ± 0.00090
$\mathcal{BT}(B^+ \to \bar{D}^{(*)}\pi\pi \ell^+ \nu)$	0.00487 ± 0.00189	n/a
f_{+0}	1.061 ± 0.030	1.080 ± 0.030
$C^{D^0}_{UncorDL}$	0.932 ± 0.052	0.968 ± 0.050
$C^{D^0}_{UncorCL}$	0.874 ± 0.063	0.859 ± 0.064
$C^{D^0}_{CascL}$	0.671 ± 0.098	0.762 ± 0.092
$C^{D^+}_{UncorDL}$	1.053 ± 0.126	1.092 ± 0.126
$C^{D^+}_{UncorCL}$	0.838 ± 0.135	0.815 ± 0.136
$C^{D^+}_{CascL}$	1.168 ± 0.234	1.377 ± 0.222
χ^2/ndof (P-value)	234/217 (0.20)	240/217 (0.13)
B^+ BF sum	0.1013 ± 0.0026	0.0978 ± 0.0014

Table 52: **(Run2 only)** [$B \to D^{(*)}\pi\pi\ell\nu$ **fit results (Total)**] Fit results including $B \to D^{(*)}\pi\pi\ell\nu$ decays as a mix of Xc, Xc*, Yc and Yc*. The branching fraction of $B \to D^{(*)}\pi\pi\ell\nu$ component is floated.

Parameters	Xc	Xc*	Yc	Yc*	D_1
ρ^2_D	1.315 ± 0.071	1.338 ± 0.068	1.330 ± 0.069	1.342 ± 0.067	1.341 ± 0.068
ρ^2	1.392 ± 0.077	1.370 ± 0.076	1.368 ± 0.075	1.360 ± 0.075	1.368 ± 0.079
R_1	1.447 ± 0.113	1.421 ± 0.110	1.416 ± 0.108	1.403 ± 0.108	1.412 ± 0.111
R_2	0.608 ± 0.104	0.628 ± 0.102	0.639 ± 0.099	0.657 ± 0.098	0.645 ± 0.104
$\mathcal{B}(B^+ \to \bar{D}^0 \ell^+ \nu)$	0.02505 ± 0.00064	0.02517 ± 0.00063	0.02508 ± 0.00064	0.02519 ± 0.00063	0.02524 ± 0.00063
$\mathcal{B}(B^+ \to \bar{D}^{*0} \ell^+ \nu)$	0.05452 ± 0.00101	0.05444 ± 0.00104	0.05396 ± 0.00092	0.05366 ± 0.00093	0.05332 ± 0.00096
$\mathcal{BT}(B^+ \to \bar{D}^{**}/D\pi \ell^+ \nu)$	0.01611 ± 0.00158	0.01595 ± 0.00178	0.01818 ± 0.00107	0.01844 ± 0.00111	0.01838 ± 0.00172
$\mathcal{BT}(B^+ \to \bar{D}^{(*)} \pi\pi \ell^+ \nu)$	0.00614 ± 0.00229	0.00497 ± 0.00210	0.00409 ± 0.00165	0.00215 ± 0.00120	0.00138 ± 0.00165
f_{+0}	1.058 ± 0.030	1.061 ± 0.030	1.064 ± 0.030	1.070 ± 0.030	1.076 ± 0.030
$C^{D^0}_{UncorDL}$	0.957 ± 0.051	0.930 ± 0.053	0.945 ± 0.051	0.938 ± 0.053	0.966 ± 0.051
$C^{D^0}_{UncorCL}$	0.887 ± 0.064	0.860 ± 0.064	0.881 ± 0.064	0.863 ± 0.064	0.856 ± 0.064
$C^{D^0}_{CascL}$	0.617 ± 0.107	0.769 ± 0.092	0.607 ± 0.111	0.730 ± 0.094	0.779 ± 0.094
$C^{D^+}_{UncorDL}$	1.077 ± 0.125	1.045 ± 0.126	1.066 ± 0.126	1.063 ± 0.126	1.089 ± 0.126
$C^{D^+}_{UncorCL}$	0.850 ± 0.135	0.832 ± 0.135	0.838 ± 0.135	0.823 ± 0.135	0.820 ± 0.136
$C^{D^+}_{CascL}$	1.057 ± 0.249	1.309 ± 0.222	1.091 ± 0.248	1.299 ± 0.225	1.373 ± 0.221
χ^2/ndof (P-value)	234/217 (0.21)	235/217 (0.19)	235/217 (0.19)	238/217 (0.16)	240/216 (0.13)
B^+ BF sum	0.1018 ± 0.0030	0.1005 ± 0.0030	0.1013 ± 0.0026	0.0994 ± 0.0020	0.0983 ± 0.0026

Table 53: **(Run2 only)** [$B \to D^{(*)}\pi\pi\ell\nu$ **fit results (Component)**] Fit results including $B \to D^{(*)}\pi\pi\ell\nu$ decays in cases only Xc, Xc*, Yc or Yc* component is included. The last column include $D_1 \to D^{(*)}\pi\pi$ decays. The branching fraction of $B \to D^{(*)}\pi\pi\ell\nu$ component is floated.

Parameters	Fit results	Nominal fit
ρ_D^2	1.315 ± 0.070	1.346 ± 0.067
ρ^2	1.395 ± 0.074	1.353 ± 0.076
R_1	1.434 ± 0.108	1.405 ± 0.109
R_2	0.594 ± 0.100	0.668 ± 0.099
$\mathcal{B}(B^+ \to \bar{D}^0 \ell^+ \nu)$	0.02511 ± 0.00063	0.02525 ± 0.00063
$\mathcal{B}(B^+ \to \bar{D}^{*0} \ell^+ \nu)$	0.05434 ± 0.00099	0.05291 ± 0.00082
$\mathcal{BT}(B^+ \to \bar{D}^{**0}/(D\pi)^0 \ell^+ \nu)$	0.01409 ± 0.00090	0.01961 ± 0.00090
$\mathcal{BT}(B^+ \to \bar{D}^{(*)} \pi\pi \ell^+ \nu)$	0.01 (Fixed)	n/a
f_{+0}	1.043 ± 0.030	1.080 ± 0.030
$C_{UncorDL}^{D^0}$	0.895 ± 0.050	0.968 ± 0.050
$C_{UncorCL}^{D^0}$	0.888 ± 0.064	0.859 ± 0.064
$C_{CascL}^{D^0}$	0.577 ± 0.092	0.762 ± 0.092
$C_{UncorDL}^{D^+}$	1.014 ± 0.125	1.092 ± 0.126
$C_{UncorCL}^{D^+}$	0.861 ± 0.134	0.815 ± 0.136
$C_{CascL}^{D^+}$	0.954 ± 0.219	1.377 ± 0.222
χ^2/ndof (P-value)	264/219 (0.02)	234/217 (0.20)
B^+ BF sum	0.1049 ± 0.0014	0.0978 ± 0.0014

Table 54: **(Run2 only)** [$B \to D^{(*)}\pi\pi\ell\nu$ **fit results (Total), BF=0.001**] Fit results including $B \to D^{(*)}\pi\pi\ell\nu$ decays as a mix of Xc, Xc*, Yc and Yc*. The branching fraction of $B \to D^{(*)}\pi\pi\ell\nu$ component is fixed to 0.01.

Parameters	Xc	Xc*	Yc	Yc*	D_1
ρ_D^2	1.295 ± 0.071	1.328 ± 0.069	1.307 ± 0.071	1.328 ± 0.069	1.307 ± 0.069
ρ^2	1.416 ± 0.074	1.389 ± 0.076	1.390 ± 0.074	1.386 ± 0.073	1.467 ± 0.076
R_1	1.473 ± 0.113	1.437 ± 0.111	1.431 ± 0.107	1.398 ± 0.103	1.462 ± 0.111
R_2	0.571 ± 0.103	0.586 ± 0.102	0.599 ± 0.099	0.618 ± 0.096	0.493 ± 0.107
$\mathcal{B}(B^+ \to \bar{D}^0 \ell^+ \nu)$	0.02492 ± 0.00063	0.02509 ± 0.00063	0.02486 ± 0.00063	0.02503 ± 0.00063	0.02523 ± 0.00062
$\mathcal{B}(B^+ \to \bar{D}^{*0} \ell^+ \nu)$	0.05557 ± 0.00082	0.05606 ± 0.00082	0.05539 ± 0.00082	0.05629 ± 0.00082	0.05579 ± 0.00080
$\mathcal{BT}(B^+ \to \bar{D}^{**}/D\pi \ell^+ \nu)$	0.01384 ± 0.00090	0.01208 ± 0.00090	0.01617 ± 0.00090	0.01425 ± 0.00090	0.01069 ± 0.00088
$\mathcal{BT}(B^+ \to \bar{D}^{(*)} \pi\pi \ell^+ \nu)$	0.01 (Fixed)	0.01 (Fixed)	0.01 (Fixed)	0.01 (Fixed)	0.01 (Fixed)
f_{+0}	1.044 ± 0.029	1.041 ± 0.028	1.045 ± 0.029	1.040 ± 0.028	1.056 ± 0.027
$C^{D^0}_{UncorDL}$	0.950 ± 0.051	0.887 ± 0.051	0.914 ± 0.050	0.833 ± 0.050	0.958 ± 0.037
$C^{D^0}_{UncorCL}$	0.904 ± 0.063	0.860 ± 0.063	0.913 ± 0.064	0.875 ± 0.064	0.834 ± 0.063
$C^{D^0}_{CascL}$	0.523 ± 0.092	0.782 ± 0.092	0.390 ± 0.092	0.616 ± 0.092	0.892 ± 0.093
$C^{D^+}_{UncorDL}$	1.064 ± 0.125	0.995 ± 0.125	1.033 ± 0.125	0.960 ± 0.124	1.075 ± 0.123
$C^{D^+}_{UncorCL}$	0.874 ± 0.134	0.860 ± 0.134	0.869 ± 0.134	0.854 ± 0.134	0.853 ± 0.130
$C^{D^+}_{CascL}$	0.835 ± 0.219	1.229 ± 0.220	0.710 ± 0.219	1.035 ± 0.219	1.344 ± 0.216
χ^2/ndof (P-value)	237/218 (0.18)	281/220 (0.003)	264/219 (0.02)	344/220 (6.0×10^{-8})	268/217 (0.01)
B^+ BF sum	0.1043 ± 0.0014	0.1032 ± 0.0014	0.1064 ± 0.0014	0.1056 ± 0.0014	0.1017 ± 0.0014

Table 55: **(Run2 only)** [$B \to D^{(*)}\pi\pi\ell\nu$ **fit results (Component), BF=0.001**] Fit results including $B \to D^{(*)}\pi\pi\ell\nu$ decays in cases only Xc, Xc*, Yc or Yc* component is included. The last column include $D_1 \to D^{(*)}\pi\pi$ decays. The branching fraction of $B \to D^{(*)}\pi\pi\ell\nu$ component is fixed to 0.01.

17.9.2 Effect of $B \to D_s^{(*)} K\ell\nu$ decays

Decays of the type $B \to D_s^{(*)} K\ell\nu$ do not result in a $D\ell\nu X$ final state and therefore do not enter our reconstructed distributions. These states therefore have no impact on the parameters determined in the fit. They do, however, impact the renormalization, since they contribute to the inclusive $b \to c\ell\nu$ partial branching fraction for $E_\ell >$ 1.5GeV. To estimate the impact on the renormalization of these states we generate samples where the the pseudo-particle that gives rise to the $D_s K$ or $D_s^* K$ system is just above kinematic threshold, namely 2.50GeV or 2.63GeV. Samples are generated with total spin zero or one. The fraction of the lepton spectrum above 1.5GeV is recorded. These fractions, along with the measured upper limit on the $B \to D_s K\ell\nu$ branching fraction [49], bound the contribution of these states to the inclusive partial branching fraction. We take, as a systematic error, one-half of the maximum deviation.

18 Full Covariance Matrix

We construct full covariance matrices to keep track of correlation. For statistical uncertainty, if the statistical uncertainty of the i-th parameter is Δ_i^{stat}, the ij element of a statistical error correlation matrix is given by

$$\mathrm{cov}_{ij}^{stat} = \Delta_i^{stat} \cdot \Delta_j^{stat} \tag{427}$$

When we estimate systematic uncertainty, we vary the value of a quantity (k-th source of systematic uncertainty) and take differences, Δ^{sys}, between fitted values and nominal values of parameters. For i-th parameter

$$\Delta_{ik}^{sys} = \text{(fitted value - nominal value) of } i\text{-th parameter} \tag{428}$$

Then, the ij element of a systematic error correlation matrix is given by

$$\mathrm{cov}_{ij}^{sys} = \sum_k \Delta_{ik}^{sys} \cdot \Delta_{jk}^{sys} \tag{429}$$

In cases where we do two fits (one with a + variation and the other with a - variation), we calculate the two covariances (one for each fit) and average them.
Total error is given by the sum of these two matrices : cov_{ij}^{stat} and cov_{ij}^{sys}

19 Discussions

19.1 $B \to D^*\ell\nu$ form factors

We compare our results with previous Babar measurements [39][40]. The [39] reconstruct the decays

- $B^0 \to D^{*-}\ell^+\nu$, $D^{*-} \to D^0\pi_s^-$

Thus,

- $D^{*-} \to D^-\pi^0$ and $D^{*-} \to D^-\gamma$

are not included. They also use the cuts

$$\begin{aligned} &p_T(\pi_s^-) > 50 \ \text{GeV} \\ &p_\ell^* > 1.2 \ \text{GeV} \end{aligned} \tag{430}$$

where p_ℓ^* is the lepton momentum in the CM frame ($\Upsilon(4S)$ rest frame). The results are

$$\begin{aligned} &\rho^2 = 1.179 \pm 0.048 \pm 0.028 \\ &R_1 = 1.417 \pm 0.061 \pm 0.044 \\ &R_2 = 0.836 \pm 0.037 \pm 0.022 \\ &\mathcal{B}(B^0 \to D^{*-}\ell^+\nu) = 0.0477 \pm 0.0004 \pm 0.0039 \\ &\mathcal{F}(1)|V_{cb}| = 0.03468 \pm 0.00032 \pm 0.00115 \end{aligned} \tag{431}$$

The analysis in Ref.[40] use the decay mode

- $B^- \to D^{*0}\ell^-\bar{\nu}$, $D^{*0} \to D^0\pi_s^0$

Thus,

- $D^{*0} \to D^0\gamma$

is not included. They also apply the cuts

$$\begin{aligned} &E_\gamma(\text{from } \pi_s^0) > 30 \ \text{GeV} \\ &p_\ell^* > 1.2 \ \text{GeV} \end{aligned} \tag{432}$$

They use R_1 and R_2 from the above measurement. The results are

$$\begin{aligned} &\rho^2 = 1.15 \pm 0.06 \pm 0.08 \\ &\mathcal{B}(B^+ \to \bar{D}^{*0}\ell^+\nu) = 0.0571 \pm 0.0008 \pm 0.0041 \\ &\mathcal{F}(1)|V_{cb}| = 0.0363 \pm 0.0006 \pm 0.00148 \end{aligned} \tag{433}$$

Our results are

$$\begin{aligned} &\rho^2 = 1.338 \pm 0.076 \pm 0.057 \\ &R_1 = 1.443 \pm 0.123 \pm 0.108 \\ &R_2 = 0.680 \pm 0.099 \pm 0.064 \end{aligned} \tag{434}$$

19.1.1 Soft pion reconstruction

We do not apply any cuts on soft pion since we do not explicitly reconstruct D^*. This is the biggest difference between other measurements and our method. Figure 173 shows the transverse momentum distribution of soft pion in our analysis. These plots are made using MC truth info. Three modes are plotted separately :

- $B^+ \to \bar{D}^{*0}\ell^+\nu,\ D^{*0} \to D^0\pi_s^0$
- $B^0 \to D^{*-}\ell^+\nu,\ D^{*+} \to D^0\pi_s^+$
- $B^0 \to D^{*-}\ell^+\nu,\ D^{*+} \to D^+\pi_s^0$

The lines with error bars are based on our nominal fit results and the green histograms are based on previous Babar FF parameters [39]. The bottom plot of each mode is the ratio ($p_T(\pi_s)$ of previous FF)/($p_T(\pi_s)$ of our FF). In our analysis, the transverse momentum is well populated under the cut of previous measurements.
The acceptance of soft pions in out analysis is larger and more uniform than previous measurements. Figure 174 shows the population of soft pion as a function of their transverse momentum and $\cos\theta$, where θ is the angle with respect to the beam axis. Soft pions are most populated in the low θ region where SVT and DCH does not cover.
Plan for the next version : We can look at the efficiency matrix/histogram, explained in section 17.5.4, to see how uniform our efficiency is.

19.1.2 R_1 and R_2

We requested the author of the paper [39] to perform a fit by fixing R_1 and R_2 to

$$\begin{aligned} R_1 &= 1.542 \\ R_2 &= 0.584 \end{aligned} \tag{435}$$

Then their slope came out to be

$$\rho^2 = 1.331 \pm 0.0033 \tag{436}$$

In theanalysis in Ref. [40],

$$\begin{aligned} \frac{\partial rho^2}{\partial R_1} &= 0.0303, \quad \frac{\partial \mathcal{B}}{\partial R_1} = 0.00382 \\ \frac{\partial rho^2}{\partial R_2} &= -1.22, \quad \frac{\partial \mathcal{B}}{\partial R_2} = 0.00551 \end{aligned} \tag{437}$$

are given. Thus, if we change R_1 and R_2 to our fit results

$$\rho^2 = 1.15 + 0.0303 \times (1.443 - 1.417) - 1.22 \times (0.680 - 0.836) = 1.341 \tag{438}$$

In both cases, slopes are consistent with our results. This means that the real difference lies in the difference of R_2.
If we fix R_1 and R_2 to previous values, our fit results are the values shown in Table 56.

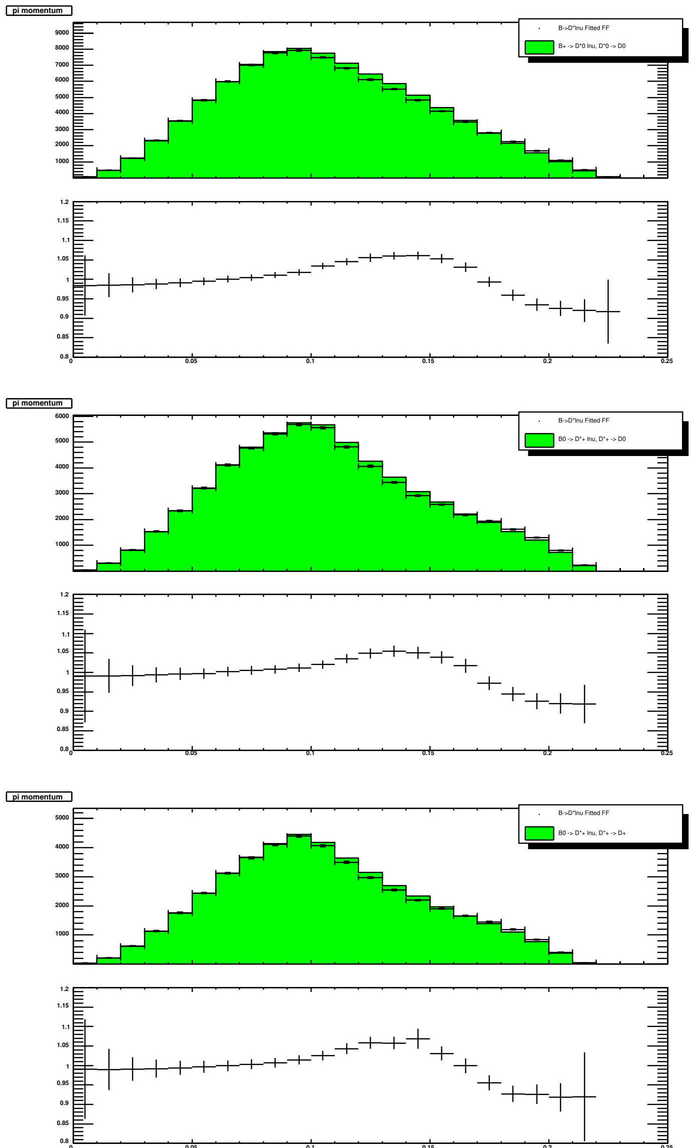

Figure 173: **(Run2 only)** [**Soft pi** p_T] The transverse momentum distribution of soft pion. From top to bottom : $B^+ \to \bar{D}^{*0}\ell^+\nu$ with $D^{*0} \to D^0\pi_s^0$, $B^0 \to D^{*-}\ell^+\nu$ with $D^{*+} \to D^0\pi_s^+$ and $B^0 \to D^{*-}\ell^+\nu$ with $D^{*+} \to D^+\pi_s^0$. The lines with error bars are based on our nominal fit results and the green histograms are based on previous Babar FF parameters [39]. The bottom plot of each mode is the ratio ($p_T(\pi_s)$ of our FF)/($p_T(\pi_s)$ of previous FF). These plots are made using MC truth info.

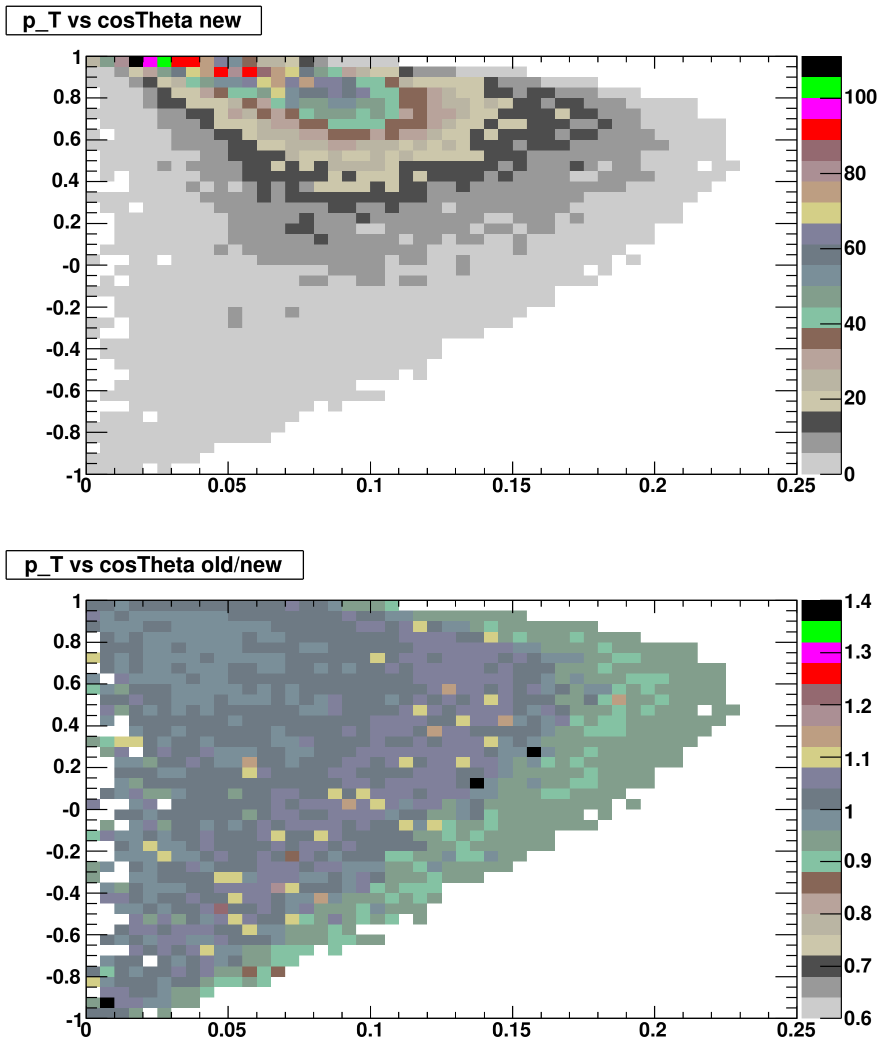

Figure 174: **(Run2 only)** [**Soft pi** p_T **vs** $\cos\theta$**;** $B^0 \to D^-$] The transverse momentum distribution vs $cos\theta$ of soft pion for the decay mode $B^0 \to D^{*-}\ell^+\nu$ with $D^{*+} \to D^+\pi^0_s$. The bottom plot is the ratio (based on our FF)/(based on previous FF). These plots are made using MC truth info.

Parameters	Fit results	Pull
ρ_D^2	1.399 ± 0.059	0.775
ρ^2	1.239 ± 0.036	-2.766
R_1	1.417 (Fixed)	n/a
R_2	0.836 (Fixed)	n/a
$\mathcal{B}(B^+ \to \bar{D}^0 \ell^+ \nu)$	0.02587 ± 0.00059	1.092
$\mathcal{B}(B^+ \to \bar{D}^{*0} \ell^+ \nu)$	0.04983 ± 0.00067	-2.568
$\mathcal{BT}(B^+ \to \bar{D}^{**0}/(D\pi)^0 \ell^+ \nu)$	0.02231 ± 0.00095	0.356
f_{+0}	1.119 ± 0.030	0.622
$C^{D^0}_{UncorDL}$	0.998 ± 0.048	0.039
$C^{D^0}_{UncorCL}$	0.833 ± 0.062	0.245
$C^{D^0}_{CascL}$	0.802 ± 0.091	0.046
$C^{D^+}_{UncorDL}$	1.089 ± 0.126	-0.079
$C^{D^+}_{UncorCL}$	0.818 ± 0.137	0.020
$C^{D^+}_{CascL}$	1.372 ± 0.225	0.093
χ^2/ndof (P-value)	248/215 (0.06)	

Table 56: **(Run2 only)** [R_1 **and** R_2 **fixed fit results**] Fit results with fixed R_1 and R_2. Pulls are calculated from the difference to nominal fit results.

19.2 Branching fractions

In addition to the above two previous measurements, Babar also measured [4]

$$\begin{aligned}
\mathcal{B}(B^+ \to \bar{D}^0\ell^+\nu) &= 0.0233 \pm 0.0009 \pm 0.0009 \\
\mathcal{B}(B^0 \to D^-\ell^+\nu) &= 0.0221 \pm 0.0011 \pm 0.0012 \\
\mathcal{B}(B^+ \to \bar{D}^{*0}\ell^+\nu) &= 0.0583 \pm 0.0015 \pm 0.0030 \\
\mathcal{B}(B^0 \to D^{*-}\ell^+\nu) &= 0.0549 \pm 0.0016 \pm 0.0025
\end{aligned} \tag{439}$$

If we take isospin average using $t_{+0} = 1.071 \pm 0.009$ and assuming these are independent, we get

$$\begin{aligned}
\mathcal{B}(B^+ \to \bar{D}^0\ell^+\nu) &= 0.0235 \pm 0.0010 \\
\mathcal{B}(B^+ \to \bar{D}^{*0}\ell^+\nu) &= 0.0585 \pm 0.0023
\end{aligned} \tag{440}$$

The avobe mesurement used PDG 2006 value of inclusive BF $\mathcal{B}(\bar{B} \to X\ell^-\bar{\nu}_\ell) = (10.78 \pm 0.18)\%$. Thus we correct the vale using PDG 2007 value of inclusive BF $\mathcal{B}(\bar{B} \to X\ell^-\bar{\nu}_\ell) = (10.24 \pm 0.15)\%$.

$$\begin{aligned}
\mathcal{B}(B^+ \to \bar{D}^0\ell^+\nu) &= 0.0223 \pm 0.0009 \\
\mathcal{B}(B^+ \to \bar{D}^{*0}\ell^+\nu) &= 0.0556 \pm 0.0022
\end{aligned} \tag{441}$$

Our results after re-normalization are

$$\begin{aligned}
\tilde{\mathcal{B}}(D^{*+} \to D^0\pi^+) &= 0.02757 \pm 0.00068 \pm 0.00073 \\
\tilde{\mathcal{B}}(B^+ \to \bar{D}^{*0}\ell^+\nu) &= 0.05637 \pm 0.00091 \pm 0.00145 \\
\tilde{\mathcal{BT}}(B^+ \to \bar{D}^{**0}/(D\pi)^0\ell^+\nu) &= 0.02402 \pm 0.00105 \pm 0.00160
\end{aligned} \tag{442}$$

Thus, if we devide the above Babar results by our results, for $B^+ \to \bar{D}^0\ell^+\nu$, we get

$$0.809 \pm 0.045 \tag{443}$$

and, for $B^+ \to \bar{D}^{*0}\ell^+\nu$, we get

$$0.987 \pm 0.049 \tag{444}$$

Thus $\mathcal{B}(B^+ \to \bar{D}^0\ell^+\nu)$ is 4.3σ off, but $\mathcal{B}(B^+ \to \bar{D}^{*0}\ell^+\nu)$ is consistent.
We also fit with ISGW2 model for $B \to D\ell\nu$ decays because in past mesurements including the above Baba analysis, for $B \to D\ell\nu$ decays, ISGW2 model was used in MC. Results are in Table 57. Renormalized BF are

$$\begin{aligned}
\tilde{\mathcal{B}}(D^{*+} \to D^0\pi^+) &= 0.02510 \pm 0.00056(stat.) \\
\tilde{\mathcal{B}}(B^+ \to \bar{D}^{*0}\ell^+\nu) &= 0.05891 \pm 0.00091(stat.) \\
\tilde{\mathcal{BT}}(B^+ \to \bar{D}^{**0}/(D\pi)^0\ell^+\nu) &= 0.02332 \pm 0.00105(stat.)
\end{aligned} \tag{445}$$

Both $\mathcal{B}(B^+ \to \bar{D}^0\ell^+\nu)$ and $\mathcal{B}(B^+ \to \bar{D}^{*0}\ell^+\nu)$ are colser to previous mesurements and f_{+0} is closer to PDG value $f_{+0} = 1.071 \pm 0.009$.

Parameters	Fit results	Pull
ρ^2	1.471 ± 0.075	1.775
R_1	1.574 ± 0.128	1.024
R_2	0.505 ± 0.112	-1.553
$\mathcal{B}(B^+ \to \bar{D}^0 \ell^+ \nu)$	0.02300 ± 0.00052	-4.302
$\mathcal{B}(B^+ \to \bar{D}^{*0} \ell^+ \nu)$	0.05398 ± 0.00073	3.293
$\mathcal{BT}(B^+ \to \bar{D}^{**0}/(D\pi)^0 \ell^+ \nu)$	0.02137 ± 0.00096	-0.628
f_{+0}	1.063 ± 0.030	-1.248
$C^{D^0}_{UncorDL}$	1.009 ± 0.052	0.235
$C^{D^0}_{UncorCL}$	0.893 ± 0.062	1.222
$C^{D^0}_{CascL}$	0.750 ± 0.091	-0.529
$C^{D^+}_{UncorDL}$	1.239 ± 0.126	1.140
$C^{D^+}_{UncorCL}$	0.873 ± 0.134	0.435
$C^{D^+}_{CascL}$	1.292 ± 0.221	-0.266
χ^2/ndof (P-value)	277/216 (0.003)	

Table 57: **(Run2 only)** [$B \to D\ell\nu$ **ISGW2 model fit results**] Fit results using ISGW2 model for $B \to D\ell\nu$ decays. Pulls are calculated from the difference to nominal fit results.

19.3 $B \to D^{(*)}\ell\nu$ isospin symmetry

We perform fitting by relaxing the isospin constraints on $B \to D\ell\nu$ and $B \to D^*\ell\nu$ decays. Fit results and correlations are shown in Table 58 and 59. The correlations between $\mathcal{B}(B^+ \to \bar{D}^0\ell^+\nu)$, $\mathcal{B}(B^0 \to D^-\ell^+\nu)$, $\mathcal{B}(B^+ \to \bar{D}^{*0}\ell^+\nu)$, $\mathcal{B}(B^0 \to D^{*-}\ell^+\nu)$ and f_{+0} are too big. This shows that we need to keep isospin constraints to get reliable fit results.
In order to reduce the above correlation, we did fits by

1. putting Gaussian constraint on f_{+0} to PDG value

$$\frac{(f_{+0} - 1.037)^2}{0.029^2} \tag{446}$$

2. fixing f_{+0} to PDG value 1.037

Fit results and mean and rms of toy MC pulls are given in Tables 60 - 63. Fit results are consistent with nominal fit. We check isospin symmetry of the results with Gaussian constraints. From Table 60,

$$\frac{\mathcal{B}(B^+ \to \bar{D}^0\ell^+\nu)}{\mathcal{B}(B^0 \to D^-\ell^+\nu)} = 1.1393 \pm 0.0578 \tag{447}$$

and

$$\frac{\mathcal{B}(B^+ \to \bar{D}^{*0}\ell^+\nu)}{\mathcal{B}(B^0 \to D^{*-}\ell^+\nu)} = 1.1066 \pm 0.0685 \tag{448}$$

If we devide these by $t_{+0} = 1.071 \pm 0.009$, we get

$$1.064 \pm 0.055 \tag{449}$$

and

$$1.033 \pm 0.065 \tag{450}$$

respectively. Thus, isospin symmetry holds.

Parameters	Fit results	Pull
ρ_D^2	1.354 ± 0.068	0.007
ρ^2	1.344 ± 0.078	0.076
R_1	1.453 ± 0.117	0.087
R_2	0.670 ± 0.102	-0.099
$\mathcal{B}(B^+ \to \bar{D}^0 \ell^+ \nu)$	0.0230 ± 0.0026	-0.849
$\mathcal{B}(B^0 \to D^- \ell^+ \nu)$	0.0264 ± 0.0040	0.699
$\mathcal{B}(B^+ \to \bar{D}^{*0} \ell^+ \nu)$	0.0474 ± 0.0046	-0.900
$\mathcal{B}(B^0 \to D^{*-} \ell^+ \nu)$	0.0532 ± 0.0068	0.739
$\mathcal{BT}(B^+ \to \bar{D}^{**0}/(D\pi)^0 \ell^+ \nu)$	0.0218 ± 0.0010	-0.161
f_{+0}	1.339 ± 0.320	0.747
$C^{D^0}_{UncorDL}$	1.012 ± 0.055	0.289
$C^{D^0}_{UncorCL}$	0.811 ± 0.062	-0.110
$C^{D^0}_{CascL}$	0.784 ± 0.092	-0.146
$C^{D^+}_{UncorDL}$	1.130 ± 0.141	0.223
$C^{D^+}_{UncorCL}$	0.906 ± 0.189	0.485
$C^{D^+}_{CascL}$	1.363 ± 0.241	0.052
χ^2/ndof (P-value)	236/215 (0.16)	

Table 58: **(Run2 only)** [**No isospin constraints**] Fit results without isospin constraints on $B \to D\ell\nu$ and $B \to D^*\ell\nu$, by floating f_{+0}. Pulls are calculated from the difference to nominal fit results.

	ρ_D^2	ρ^2	R_1	R_2	$\mathcal{B}(D^0)$	$\mathcal{B}(D^+)$	$\mathcal{B}(D^{*0})$	$\mathcal{B}(D^{*+})$	Other	f_{+0}
ρ_D^2	1									
ρ^2	-0.324	1								
R_1	-0.210	0.828	1							
R_2	0.268	-0.903	-0.904	1						
$\mathcal{B}(D^0\ell\nu)$	0.016	-0.021	-0.044	0.099	1					
$\mathcal{B}(D^+\ell\nu)$	0.161	0.055	0.077	-0.081	-0.923	1				
$\mathcal{B}(D^{*0}\ell\nu)$	-0.047	-0.070	-0.113	0.087	0.861	-0.897	1			
$\mathcal{B}(D^{*+}\ell\nu)$	-0.075	0.140	0.124	-0.164	-0.883	0.853	-0.960	1		
$\mathcal{B}$(Other)	0.099	-0.170	-0.151	0.170	0.179	-0.142	0.122	-0.259	1	
f_{+0}	0.076	0.073	0.089	-0.104	-0.951	0.980	-0.943	0.918	-0.155	1

Table 59: **(Run2 only)** [**Correlation coefficients : No isospin**] Correlations between parameters. Background components are not shown because those are not relevant.

Parameters	Fit results	Pull
ρ_D^2	1.385 ± 0.069 (5.1 %)	-0.073
ρ^2	1.338 ± 0.077 (5.7 %)	0.004
R_1	1.443 ± 0.114 (7.9 %)	-0.003
R_2	0.680 ± 0.099 (14.5 %)	0.004
$\mathcal{B}(B^+ \to \bar{D}^0 \ell^+ \nu)$	0.02592 ± 0.00096 (3.7 %)	0.733
$\mathcal{B}(B^0 \to D^- \ell^+ \nu)$	0.02275 ± 0.00079 (3.5 %)	-1.010
$\mathcal{B}(B^+ \to \bar{D}^{*0} \ell^+ \nu)$	0.05252 ± 0.00184 (3.5 %)	0.526
$\mathcal{B}(B^0 \to D^{*-} \ell^+ \nu)$	0.04746 ± 0.00242 (5.1 %)	-0.280
$\mathcal{BT}(B^+ \to \bar{D}^{**0}/(D\pi)^0 \ell^+ \nu)$	0.02197 ± 0.00097 (4.4 %)	0.003
f_{+0}	1.040 ± 0.029 (2.8 %)	-2.083
$C_{UncorDL}^{D^0}$	0.994 ± 0.051 (5.1 %)	0.054
$C_{UncorCL}^{D^0}$	0.821 ± 0.063 (7.7 %)	0.038
$C_{CascL}^{D^0}$	0.804 ± 0.093 (11.5 %)	0.061
$C_{UncorDL}^{D^+}$	1.080 ± 0.126 (11.6 %)	-0.144
$C_{UncorCL}^{D^+}$	0.798 ± 0.137 (17.1 %)	-0.123
$C_{CascL}^{D^+}$	1.338 ± 0.222 (16.6 %)	-0.060
χ^2/ndof (P-value)	237/215 (0.14)	

Table 60: **(Run2 only)** [**No isospin constraints, Gaussian constraint on** f_{+0}] Fit results without isospin constraints on $B \to D\ell\nu$ and $B \to D^*\ell\nu$, by floating f_{+0} with Gaussian constraint to PDG. Pulls are calculated from the difference to nominal fit results.

Parameters	Mean	Standard Deviation
ρ_D^2	0.0845	1.013
ρ^2	-0.0290	1.031
R_1	-0.0983	1.050
R_2	0.0994	1.037
$\mathcal{B}(B^+ \to \bar{D}^0 \ell^+ \nu)$	0.1111	1.017
$\mathcal{B}(B^0 \to D^- \ell^+ \nu)$	-0.0776	1.000
$\mathcal{B}(B^+ \to \bar{D}^{*0} \ell^+ \nu)$	-0.0503	0.988
$\mathcal{B}(B^0 \to D^{*-} \ell^+ \nu)$	-0.0294	1.011
$\mathcal{BT}(B^+ \to \bar{D}^{**0}/(D\pi)^0 \ell^+ \nu)$	0.0775	1.029
f_{+0}	-0.1108	1.026
$C_{UncorDL}^{D^0}$	-0.0202	1.030
$C_{UncorCL}^{D^0}$	-0.0281	1.015
$C_{CascL}^{D^0}$	-0.0136	1.014
$C_{UncorDL}^{D^+}$	0.0037	1.050
$C_{UncorCL}^{D^+}$	0.0470	1.018
$C_{CascL}^{D^+}$	-0.0697	1.016
Uncertainty	0.0322	0.0228

Table 61: **(Run2 only)** [**Toy MC no-isospin const, f_{+0} Gaussian**] Mean and standard deviation of pull distributions of toy MC fits without isospin constraints with Gaussian constrint on f_{+0}. The uncertainty on mean and standard deviation are also listed in the bottom line. Pulls are calculated from the difference to the fit results listed in Table 60.

Parameters	Fit results	Pull
ρ_D^2	1.349 ± 0.069	-0.074
ρ^2	1.338 ± 0.077	0.003
R_1	1.443 ± 0.114	-0.004
R_2	0.680 ± 0.099	0.005
$\mathcal{B}(B^+ \to \bar{D}^0\ell^+\nu)$	0.02597 ± 0.00090	0.835
$\mathcal{B}(B^0 \to D^-\ell^+\nu)$	0.02271 ± 0.00071	-1.183
$\mathcal{B}(B^+ \to \bar{D}^{*0}\ell^+\nu)$	0.05260 ± 0.00173	0.602
$\mathcal{B}(B^0 \to D^{*-}\ell^+\nu)$	0.04740 ± 0.00236	-0.315
$\mathcal{BT}(B^+ \to \bar{D}^{**0}/(D\pi)^0\ell^+\nu)$	0.02198 ± 0.00097	0.005
f_{+0}	1.037 (Fixed)	n/a
$C^{D^0}_{UncorDL}$	0.993 ± 0.051	-0.059
$C^{D^0}_{UncorCL}$	0.821 ± 0.063	0.040
$C^{D^0}_{CascL}$	0.804 ± 0.093	0.063
$C^{D^+}_{UncorDL}$	1.080 ± 0.125	-0.149
$C^{D^+}_{UncorCL}$	0.797 ± 0.136	-0.132
$C^{D^+}_{CascL}$	1.337 ± 0.222	-0.062
χ^2/ndof (P-value)	237/215 (0.14)	

Table 62: **(Run2 only)** [**No isospin constraints, Fix** f_{+0}] Fit results without isospin constraints on $B \to D\ell\nu$ and $B \to D^*\ell\nu$, by fixing f_{+0} to PDG. Pulls are calculated from the difference to nominal fit results.

Parameters	Mean	Standard Deviation
ρ_D^2	0.0777	1.010
ρ^2	-0.0076	1.033
R_1	-0.0793	1.050
R_2	0.0787	1.037
$\mathcal{B}(B^+ \to \bar{D}^0 \ell^+ \nu)$	0.0629	0.994
$\mathcal{B}(B^0 \to D^- \ell^+ \nu)$	-0.0237	0.963
$\mathcal{B}(B^+ \to \bar{D}^{*0} \ell^+ \nu)$	-0.0707	0.983
$\mathcal{B}(B^0 \to D^{*-} \ell^+ \nu)$	-0.0010	1.002
$\mathcal{BT}(B^+ \to \bar{D}^{**0}/(D\pi)^0 \ell^+ \nu)$	0.0639	1.014
$C_{UncorDL}^{D^0}$	-0.0123	1.025
$C_{UncorCL}^{D^0}$	-0.0278	1.006
$C_{CascL}^{D^0}$	-0.0159	0.995
$C_{UncorDL}^{D^+}$	0.0159	1.026
$C_{UncorCL}^{D^+}$	0.0464	1.013
$C_{CascL}^{D^+}$	-0.0563	1.018
Uncertainty	0.0321	0.0227

Table 63: **(Run2 only)** [**Toy MC no-isospin const, f_{+0} Fixed**] Mean and standard deviation of pull distributions of toy MC fits without isospin constraints by fixing f_{+0}. The uncertainty on mean and standard deviation are also listed in the bottom line. Pulls are calculated from the difference to the fit results listed in Table 62.

20 Conclusion

We measured form factor parameters

$$\begin{aligned}
\rho_D^2 &= 1.354 \pm 0.066(\text{stat.}, 4.9\%) \pm 0.040(\text{syst.}, 2.92\%) \\
\rho^2 &= 1.338 \pm 0.076(\text{stat.}, 5.7\%) \pm 0.052(\text{syst.}, 3.92\%) \\
R_1 &= 1.443 \pm 0.123(\text{stat.}, 7.8\%) \pm 0.093(\text{syst.}, 6.47\%) \\
R_2 &= 0.680 \pm 0.099(\text{stat.}, 14.5\%) \pm 0.051(\text{syst.}, 7.43\%)
\end{aligned} \tag{451}$$

production ratio

$$f_{+0} = 1.100 \pm 0.031(\text{stat.}, 2.8\%) \pm 0.044(\text{syst.}, 4.03\%) \tag{452}$$

branching fractions

$$\begin{aligned}
&\mathcal{B}(D^{*+} \to D^0\pi^+) = 0.02522 \pm 0.00063(\text{stat.}, 2.4\%) \pm 0.00108(\text{syst.}, 4.29\%) \\
&\mathcal{B}(B^+ \to \bar{D}^{*0}\ell^+\nu) = 0.05156 \pm 0.00083(\text{stat.}, 1.6\%) \pm 0.00249(\text{syst.}, 4.82\%) \\
&\mathcal{BT}(B^+ \to \bar{D}^{**0}/(D\pi)^0\ell^+\nu) = 0.02197 \pm 0.00096(\text{stat.}, 4.4\%) \pm 0.00162(\text{syst.}, 7.38\%)
\end{aligned} \tag{453}$$

and

$$\begin{aligned}
\mathcal{G}(1)|V_{cb}| &= 0.04818 \pm 0.00185(\text{stat.}, 3.8\%) \pm 0.00154(\text{syst.}, 3.19\%) \\
\mathcal{F}(1)|V_{cb}| &= 0.03505 \pm 0.00049(\text{stat.}, 1.4\%) \pm 0.00103(\text{syst.}, 2.93\%)
\end{aligned} \tag{454}$$

re-normalized branching fractions

$$\begin{aligned}
&\tilde{\mathcal{B}}(D^{*+} \to D^0\pi^+) = 0.02757 \pm 0.00068(\text{stat.}, 2.5\%) \pm 0.00073(\text{syst.}, 2.63\%) \\
&\tilde{\mathcal{B}}(B^+ \to \bar{D}^{*0}\ell^+\nu) = 0.05637 \pm 0.00091(\text{stat.}, 1.7\%) \pm 0.00145(\text{syst.}, 2.57\%) \\
&\tilde{\mathcal{BT}}(B^+ \to \bar{D}^{**0}/(D\pi)^0\ell^+\nu) = 0.02402 \pm 0.00105(\text{stat.}, 4.4\%) \pm 0.00160(\text{syst.}, 6.66\%)
\end{aligned} \tag{455}$$

with re-normalized branching fractions

$$\begin{aligned}
\mathcal{G}(1)|V_{cb}| &= 0.05038 \pm 0.00193(\text{stat.}, 3.8\%) \pm 0.00125(\text{syst.}, 2.48\%) \\
\mathcal{F}(1)|V_{cb}| &= 0.03665 \pm 0.00051(\text{stat.}, 1.4\%) \pm 0.00072(\text{syst.}, 1.96\%)
\end{aligned} \tag{456}$$

Run2 only. These are not final!!

21 Acknowledgements

A Decay modes to consider

A.1 Semileptonic $B \to D^{(*,**)}\ell\nu$ decays

A.1.1 Semileptonic B^+ decays

There are three types of decay modes (Figure 175).

- $B^+ \to \bar{D}^{(*,**)0}\ell^+\nu_\ell$
- $B^+ \to \bar{D}^{(*)0}\pi^0\ell^+\nu_\ell$
- $B^+ \to D^{(*)-}\pi^+\ell^+\nu_\ell$

A.1.2 Semileptonic B^0 decays

There are three types of decay modes (Figure 176).

- $B^0 \to D^{(*,**)-}\ell^+\nu_\ell$
- $B^0 \to D^{(*)-}\pi^0\ell^+\nu_\ell$
- $B^0 \to \bar{D}^{(*)0}\pi^-\ell^+\nu_\ell$

A.2 D^* and D^{**} decays

A.2.1 $D^{*,**+}$ decays

There are three types of decay modes (Figure 177).

- $D^{*,**+} \to D^{(*)0}\pi^+$
- $D^{*,**+} \to D^{(*)+}\pi^0$
- $D^{*,**+} \to D^{(*)+}\gamma$

Note that $D^{**+} \to D^{*+}\gamma$ is an electromagnetic process. Thus, it is negligible compared to strong processes. In case of $D^{*+} \to D^{*+}\gamma$, because strong processes are suppressed by phase space, the EM process amplitude has comparable size to strong processes.

A.2.2 $D^{*,**0}$ decays

There are three types of decay modes (Figure 178).

- $D^{*,**0} \to D^{(*)+}\pi^-$
- $D^{*,**0} \to D^{(*)0}\pi^0$
- $D^{*,**0} \to D^{(*)0}\gamma$

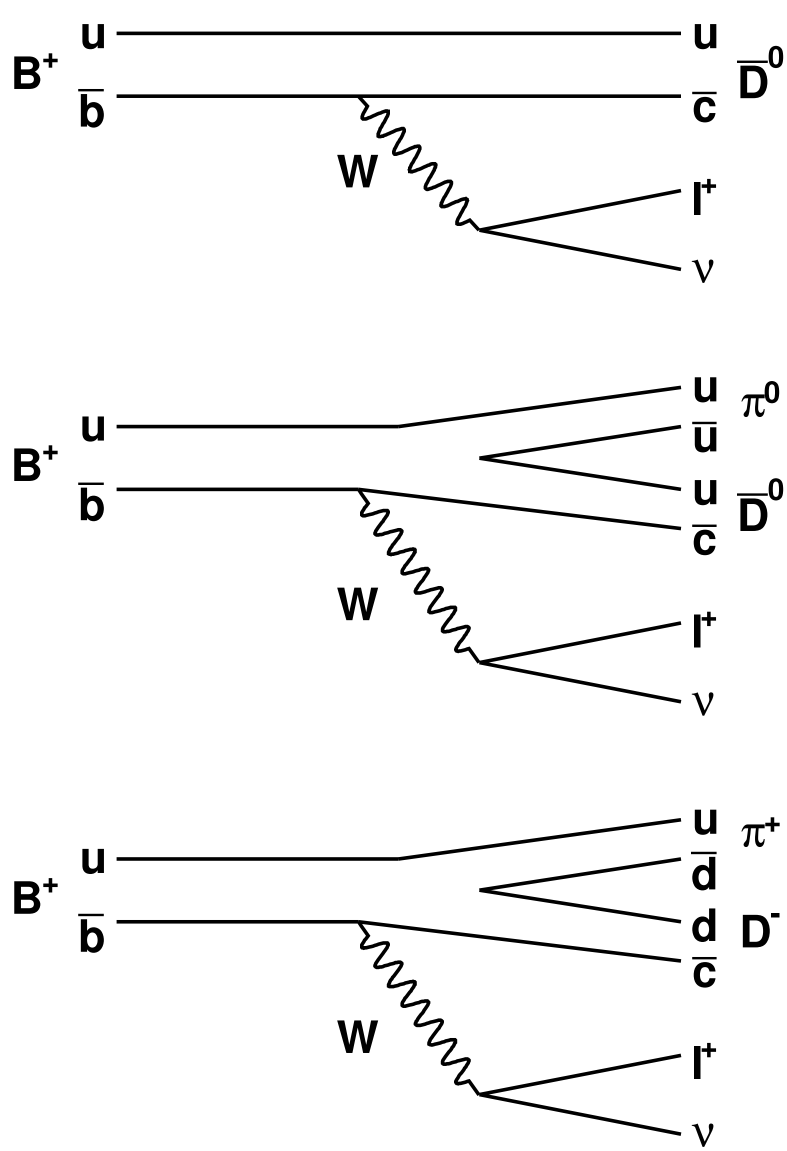

Figure 175: Feynman diagrams of semileptonic $B^+ \to D^{(*,**)}\ell\nu$ decays

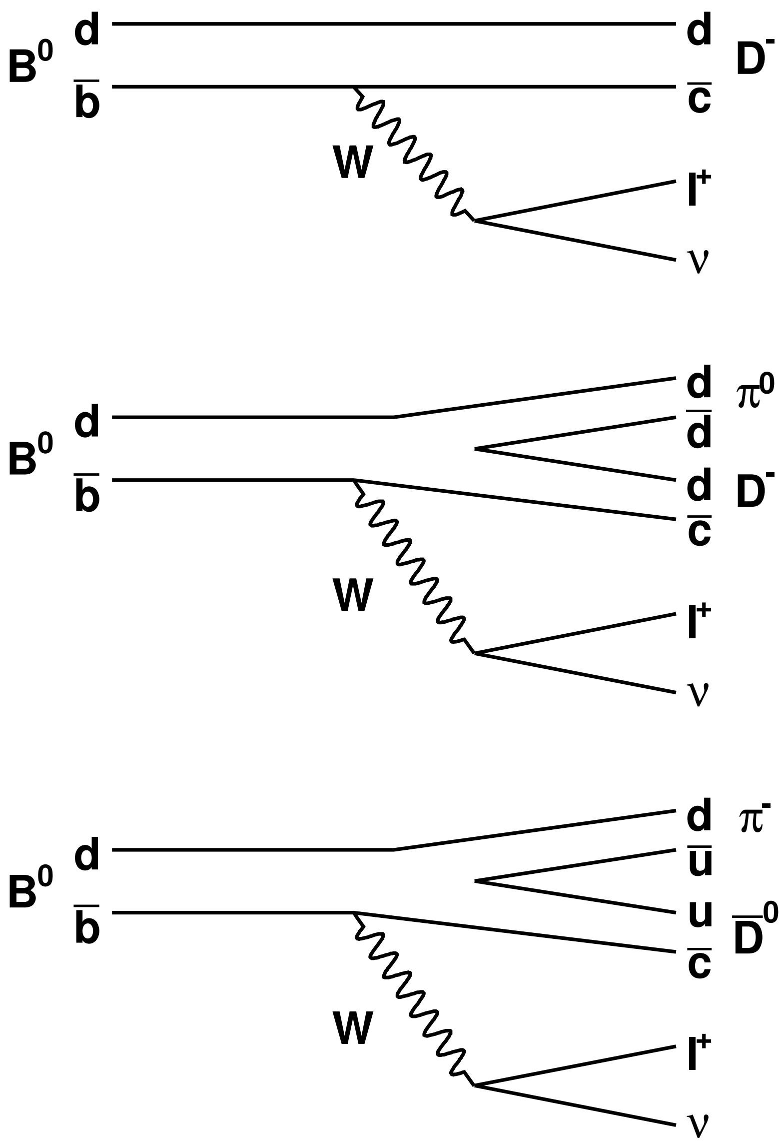

Figure 176: Feynman diagrams of semileptonic $B^0 \to D^{(*,**)}\ell\nu$ decays

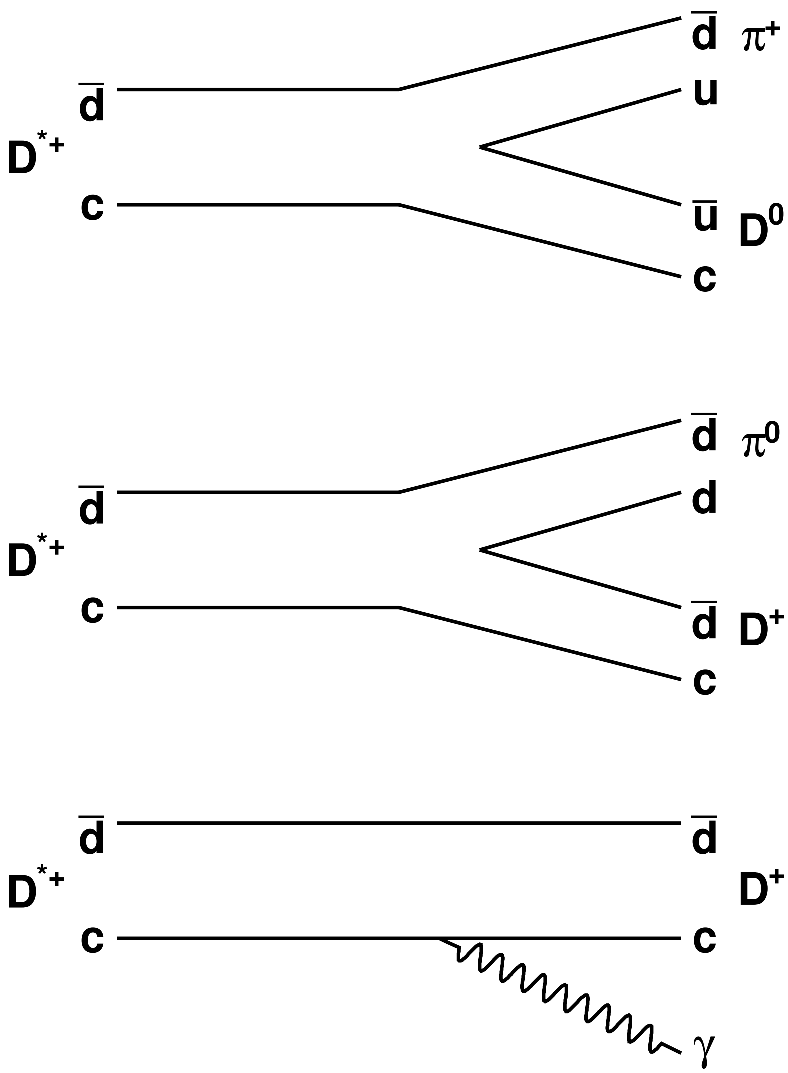

Figure 177: Feynman diagrams of $D^{*,**+}$ decays

Note that

- $D^{*0} \to D^+\pi^-$ is not allowed
  because $m_{D^{*0}} < m_{D^+} + m_{\pi^-}$
- $D^{**0} \to D^{*0}\gamma$ is negligible

A.3 D^0 and D^+ decays

A.3.1 D^0 decays

There are four decay modes used in the reconstruction of D^0 (Figure 179).

- $D^0 \to K^-\pi^+$
- $D^0 \to K^-\pi^+\pi^+\pi^-$
- $D^0 \to K^-\pi^+\pi^0$
- $D^0 \to K_s^0\pi^+\pi^-$

A.3.2 D^+ decays

There are two decay modes used in the reconstruction of D^+ (Figure 180).

- $D^+ \to K^-\pi^+\pi^+$
- $D^+ \to \bar{K}_s^0\pi^+$

A.3.3 π^0 and K_s^0

π^0 is reconstructed from 2γ.
K_s^0 is reconstructed from $\pi^0\pi^0$ or $\pi^+\pi^-$.

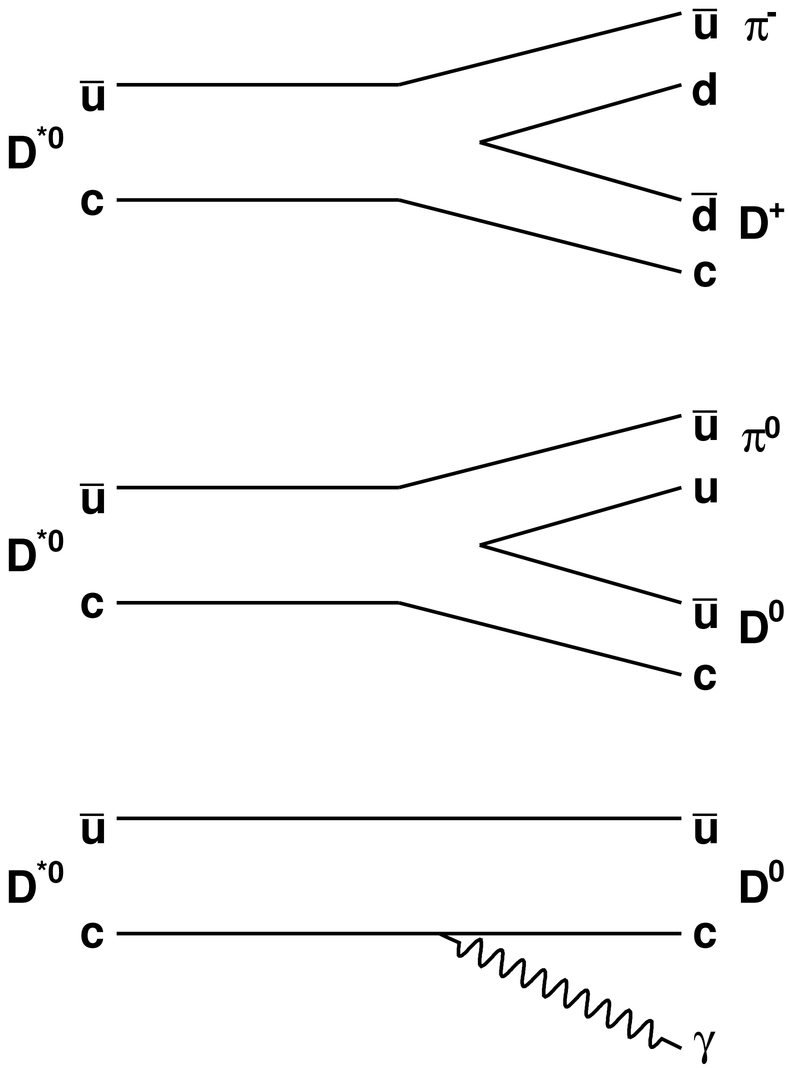

Figure 178: Feynman diagrams of $D^{*,**0}$ decays

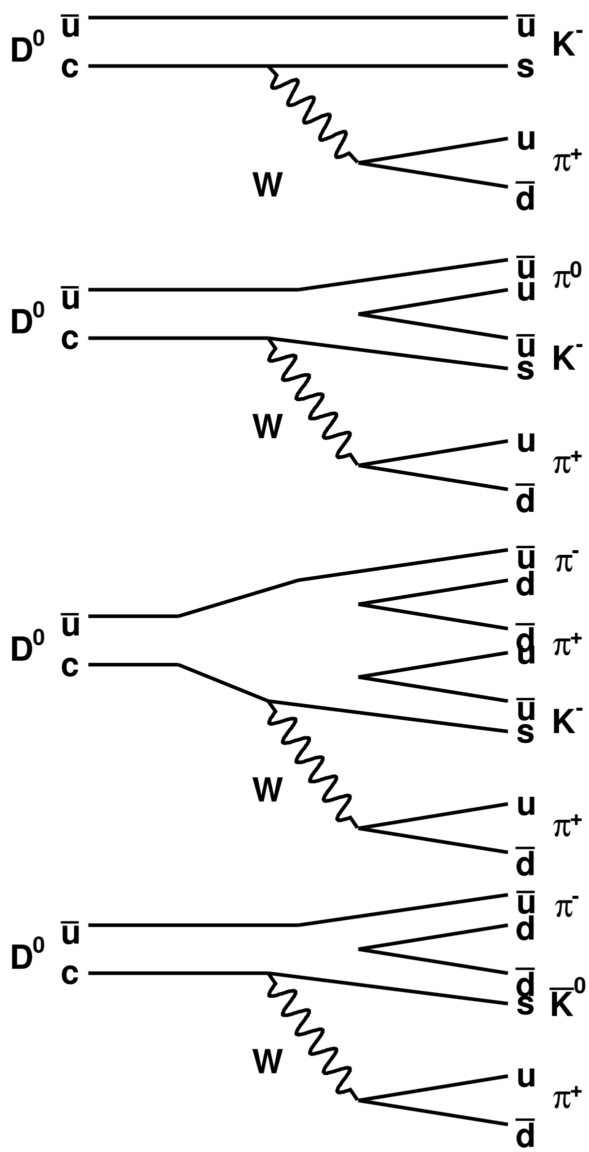

Figure 179: Feynman diagrams of D^0 decays

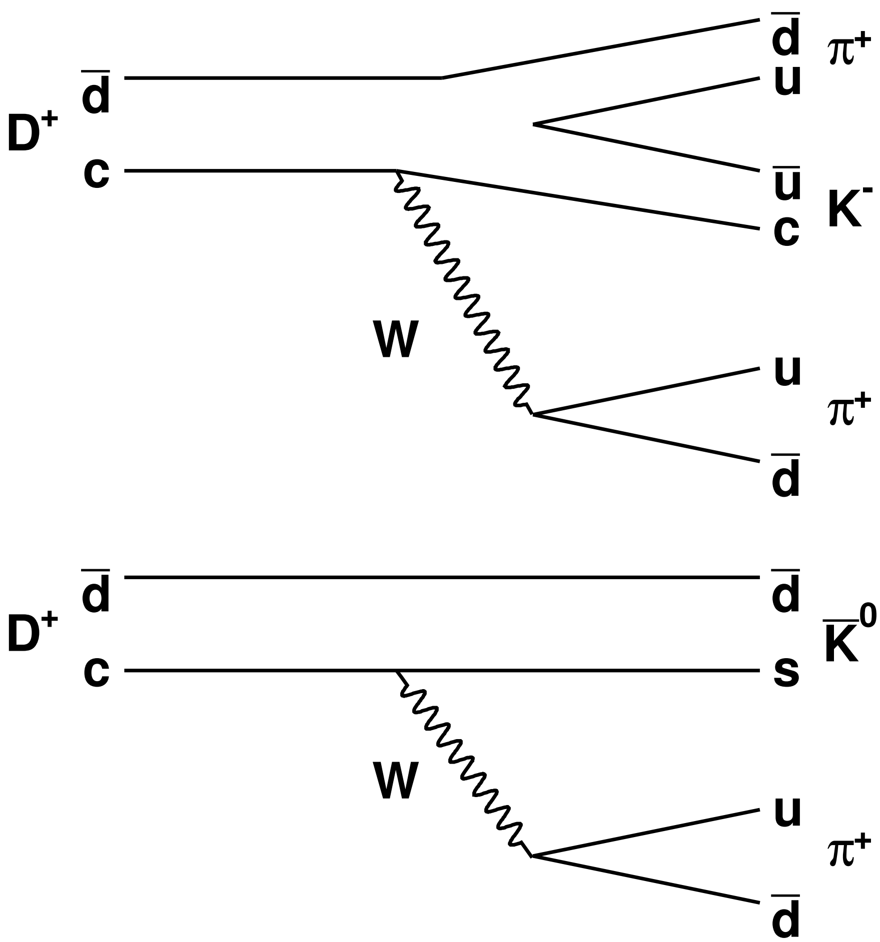

Figure 180: Feynman diagrams of D^+ decays

A.4 Decay chain

A.4.1 B^+ decay chain

1. $B^+ \to \bar{D}^0 \ell^+ \nu_\ell$ (D^0)
2. $B^+ \to \bar{D}^{*0} \ell^+ \nu_\ell$
    - $\to D^- \pi^+$ (not possible)
    - $\to \bar{D}^0 \pi^0$ (D^0)
    - $\to \bar{D}^0 \gamma$ (D^0)
3. $B^+ \to \bar{D}^{**0} \ell^+ \nu_\ell$
    - $\to D^- \pi^+$ (D^+)
    - $\to \bar{D}^0 \pi^0$ (D^0)
    - $\to \bar{D}^0 \gamma$ (D^0)
    - $\to D^{*-} \pi^+$
        - $\to \bar{D}^0 \pi^-$ (D^0)
        - $\to D^- \pi^0$ (D^+)
        - $\to D^- \gamma$ (D^+)
    - $\to \bar{D}^{*0} \pi^0$
        - $\to D^- \pi^+$ (D^+)
        - $\to \bar{D}^0 \pi^0$ (D^0)
        - $\to \bar{D}^0 \gamma$ (D^0)
    - $\to \bar{D}^{*0} \gamma$ (negligible)
4. $B^+ \to \bar{D}^0 \pi^0 \ell^+ \nu_\ell$ (D^0)
5. $B^+ \to D^- \pi^+ \ell^+ \nu_\ell$ (D^+)

6. $B^+ \to \bar{D}^{*0}\pi^0\ell^+\nu_\ell$
   - $\to D^-\pi^+$ (not possible)
   - $\to \bar{D}^0\pi^0$ (D^0)
   - $\to \bar{D}^0\gamma$ (D^0)
7. $B^+ \to D^{*-}\pi^+\ell^+\nu_\ell$
   - $\to \bar{D}^0\pi^-$ (D^0)
   - $\to D^-\pi^0$ (D^+)
   - $\to D^-\gamma$ (D^+)

A.4.2 B^0 decay chain

1. $B^0 \to D^-\ell^+\nu_\ell$ (D^0)
2. $B^0 \to D^{*-}\ell^+\nu_\ell$
   - $\to \bar{D}^0\pi^-$ (D^0)
   - $\to D^-\pi^0$ (D^+)
   - $\to D^-\gamma$ (D^+)

3. $B^0 \to D^{**-}\ell^+\nu_\ell$
   - $\bar{D}^0\pi^-$ (D^0)
   - $D^-\pi^0$ (D^+)
   - $D^-\gamma$ (D^+)
   - $D^{*-}\pi^0$
     - $\bar{D}^0\pi^-$ (D^0)
     - $D^-\pi^0$ (D^+)
     - $D^-\gamma$ (D^+)
   - $\bar{D}^{*0}\pi^-$
     - $D^-\pi^+$ (not possible)
     - $\bar{D}^0\pi^0$ (D^0)
     - $\bar{D}^0\gamma$ (D^0)
   - $\bar{D}^{*-}\gamma$ (negligible)
4. $B^0 \to D^-\pi^0\ell^+\nu_\ell$ (D^+)
5. $B^0 \to \bar{D}^0\pi^-\ell^+\nu_\ell$ (D^0)
6. $B^0 \to D^{*-}\pi^0\ell^+\nu_\ell$
   - $\bar{D}^0\pi^-$ (D^0)
   - $D^-\pi^0$ (D^+)
   - $D^-\gamma$ (D^+)
7. $B^0 \to \bar{D}^{*0}\pi^-\ell^+\nu_\ell$
   - $D^-\pi^+$ (not possible)
   - $\bar{D}^0\pi^0$ (D^0)
   - $\bar{D}^0\gamma$ (D^0)

B Classification of D^{**}

B.1 Angular momentum of a meson

In atomic spectroscopy, there are two useful schemes to add angular momentum: LS-coupling and jj-coupling.

- LS-coupling

$$\begin{aligned}\vec{S} &= \vec{s}_1 + \vec{s}_2 \\ \vec{J} &= \vec{L} + \vec{S}\end{aligned} \tag{457}$$

- jj-coupling

$$\begin{aligned}\vec{j}_1 &= \vec{L} + \vec{s}_1 \\ \vec{J} &= \vec{j}_1 + \vec{s}_2\end{aligned} \tag{458}$$

where s, l and j are the spin, orbital angular momentum and total angular momentum of individual particles, and S, L and J are the spin, orbital angular momentum and total angular momentum of the system.

B.2 Parity of a meson ($Q\bar{q}$-system) : $P = (-1)^{L+1}$

The parity of

- Quark [3] : $P_Q = +1$
- Anti-quark : $P_{\bar{q}} = -1$
- Orbital angular momentum L : $(-1)^L$

Thus, the parity of a $Q\bar{q}$-system is given by

$$P = (P_Q)(P_{\bar{q}})(-1)^L = (+1)(-1)(-1)^L = (-1)^{L+1} \tag{459}$$

Hence, $P = (-)$ for $L = 0$ and $P = (+)$ for $L = 1$.

B.3 Standard classification of mesons

For equal-mass meson system, it is traditional to couple the orbital angular momentum, $\vec{L}$, with the total spin of the quark and anti-quark, $\vec{S}$ (LS-coupling scheme).

$$\begin{aligned}\vec{S} &= \vec{s}_1 + \vec{s}_2 \\ \vec{J} &= \vec{L} + \vec{S}\end{aligned} \tag{460}$$

This is the standard practice for light mesons and heavy quarkonium ($c\bar{c}$ and $b\bar{b}$). The good quantum numbers are then S, L and J.
There are spin-singlet and spin-triplet levels because S is always $S = 0$ or $S = 1$.

[3] One could define the parity of quark to be (-1). Then its of anti-quark is (+1). But, as far as P(quark) = - P(anti-quark), the final result won't change.

	Particle	J^P
$^1S_0$	D	0^-
$^3S_1$	D^*	1^-
$^1P_1$	D_1	1^+
$^3P_0$	D_0^*	0^+
$^3P_1$	D_1^*	1^+
$^3P_2$	D_2^*	2^+

Table 64: Traditional spectroscopic notation of D, D^* and D^{**} mesons.

- For $L = 0$ and $S = 0$, $J = 0$: $^1S_0$
- For $L = 0$ and $S = 1$, $J = 1$: $^3S_1$
- For $L = 1$ and $S = 0$, $J = 1$: $^1P_1$
- For $L = 1$ and $S = 1$, $J = 0, 1, 2$: $^3P_0$, $^3P_1$ or $^3P_2$

In general, for $S = 0$ and $S = 1$

$$^1L_L \quad \text{and} \quad ^3L_{L-1,L,L+1} \tag{461}$$

We may apply this classification to D, D^* and D^{**} mesons. It is summarized in Table 64. In this classification D^{**} consists of one singlet (D_1) and a triplet (D_0^*, D_1^* and D_2^*).

B.4 Heavy Quark Effective Theory (HQET) and D, D^* and D^{**} mesons

In HQET, the spin symmetry suggests that the spin of heavy quark is conserved. Thus, for the mesons consist of heavy and light quarks, we can apply jj coupling scheme. First, we can add the angular momentum (L) and the spin of the light quark (s_l) to get the angular momentum of light constituent (j_l). Then we can add the spin of the heavy quark (s_h) to j_l.

$$\begin{aligned} \vec{j_l} &= \vec{L} + \vec{s_l} \\ \vec{J} &= \vec{j_l} + \vec{s_h} \end{aligned} \tag{462}$$

For $L = 0$ and $s_l = 1/2$, $j_l = 1/2$ only, and for $L = 1$ and $s_l = 1/2$, $j_l = 1/2$ or $j_l = 3/2$. Hence,

- $L = 0$, $j_l = 1/2 \rightarrow J = 0$ (D) or 1 (D^*)
- $L = 1$, $j_l = 1/2 \rightarrow J = 0$ (D_0^*) or 1 (D_1')

j_l^P	Particles	J^P	mass (GeV)
$\frac{1}{2}^+$	$D,\ D^*$	$0^-,\ 1^-$	1.971
$\frac{1}{2}^+$	$D_0^*,\ D_1'$	$0^+,\ 1^+$	2.40
$\frac{3}{2}^+$	$D_1,\ D_2^*$	$1^+,\ 2^+$	2.445

Table 65: Spin parity of charmed meson doublets

Initial state	Final state	ΔL	description
D_0^*	$D\pi$	0	broad S-wave transition
	$D^*\pi$	1	parity violation
D_1'	$D\pi$	1	parity violation
	$D^*\pi$	0	broad S-wave transition
		2	heavy quark spin symmetry violation
D_1	$D\pi$	1	parity violation
	$D^*\pi$	0	heavy quark spin symmetry violation
		2	narrow D-wave transition
D_2^*	$D\pi$	2	narrow D-wave transition
	$D^*\pi$	2	narrow D-wave transition

Table 66: D^{**} decay modes.

- $L = 1,\ j_l = 3/2 \to J = 1$ (D_1) or 2 (D_2^*)

These are summarized in Table 65. In this classification, D^{**} consists of two doublets : (D_0^*, D_1') and (D_1, D_2^*).

B.5 Decay modes of D^{**}

The HQET based classification implies that the $j = 3/2$ states will decay only through the d-wave ($D_1 \to D^*$ and $D_2^* \to D$) and so will be narrow. The $j = 1/2$ states can decay through the s-wave ($D_0^* \to D$ and $D_1' \to D^*$) and, in general, will be broad. This is shown in Figure 181 and summarized in Table 66. We consider this in detail.

Spin-parity of $D\pi$ system is

- Since $D : S = 0, P = (-)$ and $\pi : S = 0, P = (-)$
- if $L = 0,\ J = 0$ and $P = (-)(-)(-)^0 = (+)$, then $J^P = 0^+$
- if $L = 1,\ J = 1$ and $P = (-)(-)(-)^1 = (-)$, then $J^P = 1^-$

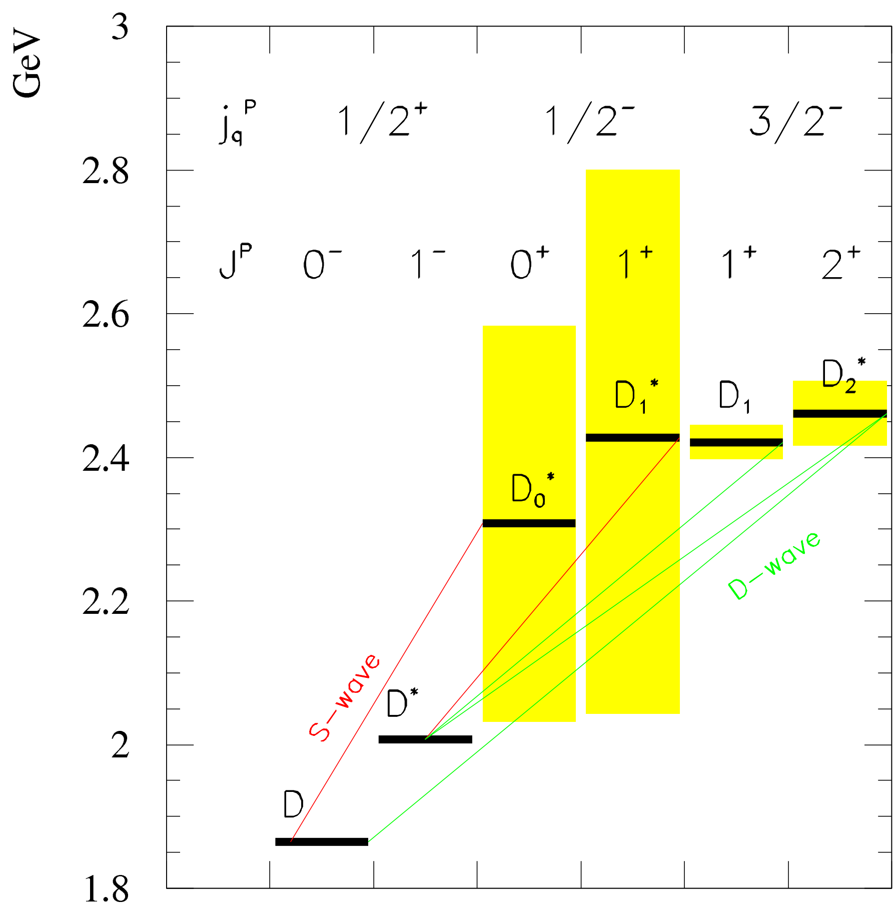

Figure 181: Charmed meson levels and transitions. $j_q = j_l$ in the text. The yellow bands show the width of each D^{**} state [16]

.

- if $L = 2,\ J = 2$ and $P = (-)(-)(-)^2 = (+)$, then $J^P = 2^+$

Note that $P = (-)^L$ for a orbital angular momentum L system. Spin-parity of $D^*\pi$ system is

- Since $D^* : S = 1, P = (-)$ and $\pi : S = 0, P = (-)$
- if $L = 0,\ J = 1$ and $P = (-)(-)(-)^0 = (+)$, then $J^P = 1^+$
- if $L = 1,\ J = 2, 1, 0$ and $P = (-)(-)(-)^1 = (-)$, then $J^P = 0^-, 1^-, 2^-$
- if $L = 2,\ J = 3, 2, 1$ and $P = (-)(-)(-)^2 = (+)$, then $J^P = 1^+, 2^+, 3^+$

Thus,

- $J^P = 0^+$ state (D_0^*) can decay only to $D\pi$ and $\Delta L = 0$
- $J^P = 1^+$ state (D_1 and D_1') can decay only to $D^*\pi$ and $\Delta L = 0, 2$
- $J^P = 2^+$ state (D_2^*) can decay both to $D\pi$ and to $D^*\pi$ and $\Delta L = 2$

Next, we consider angular momentum of D_1 and D_1' decays.

- $D_1(L = +1, s_l = +1/2, j_l = +3/2; s_h = -1/2, J = +1)$
  $\rightarrow D^*(s_l = +1/2, s_h = +1/2, j_D = +1) + \pi(j_\pi = 0) + (L = 0); J = +1$
  This violates heavy quark spin symmetry ($s_h = -1/2 \rightarrow s_h = +1/2$)
- $D_1(L = +1, s_l = +1/2, j_l = +3/2; s_h = -1/2, J = +1)$
  $\rightarrow D^*(s_l = -1/2, s_h = -1/2, j_D = -1) + \pi(j_\pi = 0) + (L = +2); J = +1$
  This conserves heavy quark spin symmetry ($s_h = -1/2 \rightarrow s_h = -1/2$)
- $D_1'(L = +1, s_l = -1/2, j_l = +1/2; s_h = +1/2, J = +1)$
  $\rightarrow D^*(s_l = +1/2, s_h = +1/2, j_D = +1) + \pi(j_\pi = 0) + (L = 0); J = +1$
  This conserves heavy quark spin symmetry ($s_h = +1/2 \rightarrow s_h = +1/2$)
- $D_1'(L = +1, s_l = -1/2, j_l = +1/2; s_h = +1/2, J = +1)$
  $\rightarrow D^*(s_l = -1/2, s_h = -1/2, j_D = -1) + \pi(j_\pi = 0) + (L = +2); J = +1$
  This violates heavy quark spin symmetry ($s_h = +1/2 \rightarrow s_h = -1/2$)

C Isospin Symmetry

C.1 Semileptonic B decays

From isospin symmetry, these B decay rates are identical

$$\begin{aligned}
\Gamma(B^+ \to \bar{D}^0\ell^+\nu) &= \Gamma(B^0 \to D^-\ell^+\nu) \\
\Gamma(B^+ \to \bar{D}^{*0}\ell^+\nu) &= \Gamma(B^0 \to D^{*-}\ell^+\nu) \\
\Gamma(B^+ \to \bar{D}^{**0}\ell^+\nu) &= \Gamma(B^0 \to D^{**-}\ell^+\nu)
\end{aligned} \tag{463}$$

Isospin symmetry may be applied to non-resonant $B \to D^{(*)}\pi\ell\nu$ decays.

$$\begin{aligned}
\Gamma(B^+ \to D^-\pi^+\ell^+\nu) &= \Gamma(B^0 \to \bar{D}^0\pi^-\ell^+\nu) \\
\Gamma(B^+ \to D^{*-}\pi^+\ell^+\nu) &= \Gamma(B^0 \to \bar{D}^{*0}\pi^-\ell^+\nu)
\end{aligned} \tag{464}$$

$$\begin{aligned}
\Gamma(B^+ \to D^-\pi^+\ell^+\nu) &= 2\Gamma(B^+ \to \bar{D}^0\pi^0\ell^+\nu) \\
\Gamma(B^0 \to \bar{D}^0\pi^-\ell^+\nu) &= 2\Gamma(B^0 \to D^-\pi^0\ell^+\nu) \\
\Gamma(B^+ \to D^{*-}\pi^+\ell^+\nu) &= 2\Gamma(B^+ \to \bar{D}^{*0}\pi^0\ell^+\nu) \\
\Gamma(B^0 \to \bar{D}^{*0}\pi^-\ell^+\nu) &= 2\Gamma(B^0 \to D^{*-}\pi^0\ell^+\nu)
\end{aligned} \tag{465}$$

The origin of the factor 2 is, for example,

$$\begin{aligned}
& B^+(u\bar{b}) : |1/2, 1/2> \\
& D^-(d\bar{c}) : |1/2, -1/2> \\
& \pi^+(u\bar{d}) : |1, 1> \\
& D^-\pi^+ : |1, 1> \times |1/2, -1/2> = \sqrt{\tfrac{1}{3}}|3/2, 1/2> + \sqrt{\tfrac{2}{3}}|1/2, 1/2> \\
& \bar{D}^0(u\bar{c}) : |1/2, 1/2> \\
& \pi^0(u\bar{u} \text{ or } d\bar{d}) : |1, 0> \\
& \bar{D}^0\pi^0 : |1, 0> \times |1/2, 1/2> = \sqrt{\tfrac{2}{3}}|3/2, 1/2> - \sqrt{\tfrac{1}{3}}|1/2, 1/2>
\end{aligned} \tag{466}$$

hence

$$\Gamma(B^+ \to D^-\pi^+\ell^+\nu) : \Gamma(B^+ \to \bar{D}^0\pi^0\ell^+\nu) = \frac{2}{3} : \frac{1}{3} = 2 : 1 \tag{467}$$

Branching fractions are not same because of the difference in total rate (Γ) or life time (τ) of B^+ and B^0. We define

$$t_{+0} \equiv \frac{\tau_{B^+}}{\tau_{B^0}} = \frac{\Gamma_{B^0}}{\Gamma_{B^+}} \tag{468}$$

and

$$t_{0+} \equiv \frac{\tau_{B^0}}{\tau_{B^+}} = \frac{\Gamma_{B^+}}{\Gamma_{B^0}} \tag{469}$$

So branching fractions are, for example,

$$\frac{\mathcal{B}(B^+ \to \bar{D}^{*0}\ell^+\nu)}{\mathcal{B}(B^0 \to D^{*-}\ell^+\nu)} = \frac{\Gamma(B^+ \to D^*\ell\nu)}{\Gamma(B^0 \to D^*\ell\nu)}\frac{\Gamma_{B^0}}{\Gamma_{B^+}} = t_{+0} \tag{470}$$

Thus, due to isospin symmetry, we have the following relations between branching fractions of semileptonic B decays.

$$\begin{aligned}
&\mathcal{B}(B^+ \to \bar{D}^0\ell^+\nu) = t_{+0}\mathcal{B}(B^0 \to D^-\ell^+\nu)\\
&\mathcal{B}(B^+ \to \bar{D}^{*0}\ell^+\nu) = t_{+0}\mathcal{B}(B^0 \to D^{*-}\ell^+\nu)\\
&\mathcal{B}(B^+ \to \bar{D}^{**0}\ell^+\nu) = t_{+0}\mathcal{B}(B^0 \to D^{**-}\ell^+\nu)\\
&\mathcal{B}(B^+ \to D^-\pi^+\ell^+\nu) = 2\mathcal{B}(B^+ \to \bar{D}^0\pi^0\ell^+\nu)\\
&= t_{+0}\mathcal{B}(B^0 \to \bar{D}^0\pi^-\ell^+\nu) = 2t_{+0}\mathcal{B}(B^0 \to D^-\pi^0\ell^+\nu)\\
&\mathcal{B}(B^+ \to D^{*-}\pi^+\ell^+\nu) = 2\mathcal{B}(B^+ \to \bar{D}^{*0}\pi^0\ell^+\nu)\\
&= t_{+0}\mathcal{B}(B^0 \to \bar{D}^{*0}\pi^-\ell^+\nu) = 2t_{+0}\mathcal{B}(B^0 \to D^{*-}\pi^0\ell^+\nu)
\end{aligned} \tag{471}$$

C.2 D^{**} decays

Isospin symmetry may be applied to D^{**} decays as well.

$$\begin{aligned}
\Gamma(D^{**0} \to D^+\pi^-) &= \Gamma(D^{**+} \to D^0\pi^+)\\
\Gamma(D^{**0} \to D^0\pi^0) &= \Gamma(D^{**+} \to D^+\pi^0)\\
\Gamma(D^{**0} \to D^{*+}\pi^-) &= \Gamma(D^{**+} \to D^{*0}\pi^+)\\
\Gamma(D^{**0} \to D^{*0}\pi^0) &= \Gamma(D^{**+} \to D^{*+}\pi^0)
\end{aligned} \tag{472}$$

And also

$$\begin{aligned}
\Gamma(D^{**0} \to D^+\pi^-) &= 2\Gamma(D^{**0} \to D^0\pi^0)\\
\Gamma(D^{**+} \to D^0\pi^+) &= 2\Gamma(D^{**+} \to D^+\pi^0)\\
\Gamma(D^{**0} \to D^{*+}\pi^-) &= 2\Gamma(D^{**0} \to D^{*0}\pi^0)\\
\Gamma(D^{**+} \to D^{*0}\pi^+) &= 2\Gamma(D^{**+} \to D^{*+}\pi^0)
\end{aligned} \tag{473}$$

This factor 2 has the same origin as B decay case. For example,

$$\begin{aligned}
&D^{**+} : |1/2, 1/2>\\
&D^0 : |1/2, -1/2>\\
&\pi^+ : |1, 1>\\
&D^0\pi^+ : |1, 1> \times |1/2, -1/2> = \sqrt{\tfrac{1}{3}}|3/2, 1/2> + \sqrt{\tfrac{2}{3}}|1/2, 1/2>\\
&D^+ : |1/2, 1/2>\\
&\pi^0 : |1, 0>\\
&D^+\pi^0 : |1, 0> \times |1/2, 1/2> = \sqrt{\tfrac{2}{3}}|3/2, 1/2> - \sqrt{\tfrac{1}{3}}|1/2, 1/2>
\end{aligned} \tag{474}$$

hence

$$\Gamma(D^{**+} \to D^0\pi^+) : \Gamma(D^{**+} \to D^+\pi^0) = \frac{2}{3} : \frac{1}{3} = 2:1 \tag{475}$$

Supposing total rates or lifetimes of D^{**0} and D^{**+} are same, branching fractions for D^{**} decays are

$$\begin{aligned}
&\mathcal{B}(D^{**0} \to D^+\pi^-) = 2\mathcal{B}(D^{**0} \to D^0\pi^0) = \mathcal{B}(D^{**+} \to D^0\pi^+) = 2\mathcal{B}(D^{**+} \to D^+\pi^0) \\
&\mathcal{B}(D^{**0} \to D^{*+}\pi^-) = 2\mathcal{B}(D^{**0} \to D^{*0}\pi^0) = \mathcal{B}(D^{**+} \to D^{*0}\pi^+) = 2\mathcal{B}(D^{**+} \to D^{*+}\pi^0)
\end{aligned} \tag{476}$$

D Values used in SP5/SP6 MC and related to our fit

The values used in SP5/SP6 MC are given in Tables 67-74. Calculated and used values are given in relevant sections in the text.

D.1 Definition of total or summed branching fractions, and branching fraction ratios

In section 5, we define the following total or summed branching fractions.

1. $\mathcal{BT}(B^+ \to \bar{D}^{**0}\ell^+\nu)$
$\equiv \mathcal{B}(B^+ \to \bar{D}_0^{*0}\ell^+\nu) + \mathcal{B}(B^+ \to \bar{D}_1^0\ell^+\nu) + \mathcal{B}(B^+ \to \bar{D}_1^{\prime 0}\ell^+\nu) + \mathcal{B}(B^+ \to \bar{D}_2^{*0}\ell^+\nu)$

2. $\mathcal{BT}(B^0 \to D^{**-}\ell^+\nu)$
$\equiv \mathcal{B}(B^0 \to D_0^{*-}\ell^+\nu) + \mathcal{B}(B^0 \to D_1^-\ell^+\nu) + \mathcal{B}(B^0 \to D_1^{\prime -}\ell^+\nu) + \mathcal{B}(B^0 \to D_2^{*-}\ell^+\nu)$

3. $\mathcal{BT}(B^+ \to \bar{D}_1^0/\bar{D}_2^{*0}\ell^+\nu) \equiv \mathcal{B}(B^+ \to \bar{D}_1^0\ell^+\nu) + \mathcal{B}(B^+ \to \bar{D}_2^{*0}\ell^+\nu)$

4. $\mathcal{BT}(B^0 \to D_1^-/D_2^{*-}\ell^+\nu) \equiv \mathcal{B}(B^0 \to D_1^-\ell^+\nu) + \mathcal{B}(B^0 \to D_2^{*-}\ell^+\nu)$

5. $\mathcal{BT}(B^+ \to D^-\pi^+\ell^+\nu)$
$\equiv \mathcal{B}(B^+ \to \bar{D}_2^{*0}\ell^+\nu)\mathcal{B}(\bar{D}_2^{*0} \to D^-\pi^+) + \mathcal{B}(B^+ \to \bar{D}_0^{*0}\ell^+\nu)\mathcal{B}(\bar{D}_0^{*0} \to D^-\pi^+)$
$+\mathcal{B}(B^+ \to D^-\pi^+\ell^+\nu)$

6. $\mathcal{BT}(B^0 \to \bar{D}^0\pi^-\ell^+\nu)$
$\equiv \mathcal{B}(B^0 \to D_2^{*-}\ell^+\nu)\mathcal{B}(D_2^{*-} \to \bar{D}^0\pi^-) + \mathcal{B}(B^0 \to D_0^{*-}\ell^+\nu)\mathcal{B}(D_0^{*-} \to \bar{D}^0\pi^-)$
$+\mathcal{B}(B^0 \to \bar{D}^0\pi^-\ell^+\nu)$

7. $\mathcal{BT}(B^+ \to \bar{D}_0^{*0}/(D\pi)^0\ell^+\nu)$
$\equiv \mathcal{B}(B^+ \to \bar{D}_0^{*0}\ell^+\nu) + \mathcal{B}(B^+ \to D^-\pi^+\ell^+\nu) + \mathcal{B}(B^+ \to \bar{D}^0\pi^0\ell^+\nu)$

8. $\mathcal{BT}(B^0 \to D_0^{*-}/(D\pi)^-\ell^+\nu)$
$\equiv \mathcal{B}(B^0 \to D_0^{*-}\ell^+\nu) + \mathcal{B}(B^0 \to \bar{D}^0\pi^-\ell^+\nu) + \mathcal{B}(B^0 \to D^-\pi^0\ell^+\nu)$

9. $\mathcal{BT}(B^+ \to D^{*-}\pi^+\ell^+\nu)$
$\equiv \mathcal{B}(B^+ \to \bar{D}_1^0\ell^+\nu)\mathcal{B}(\bar{D}_1^0 \to D^{*-}\pi^+) + \mathcal{B}(B^+ \to \bar{D}_2^{*0}\ell^+\nu)\mathcal{B}(\bar{D}_2^{*0} \to D^{*-}\pi^+)$
$+\mathcal{B}(B^+ \to \bar{D}_1^{\prime 0}\ell^+\nu)\mathcal{B}(\bar{D}_1^{\prime 0} \to D^{*-}\pi^+) + \mathcal{B}(B^+ \to D^{*-}\pi^+\ell^+\nu)$

10. $\mathcal{BT}(B^0 \to \bar{D}^{*0}\pi^-\ell^+\nu)$
$\equiv \mathcal{B}(B^0 \to D_1^-\ell^+\nu)\mathcal{B}(D_1^- \to \bar{D}^{*0}\pi^-) + \mathcal{B}(B^0 \to D_2^{*-}\ell^+\nu)\mathcal{B}(D_2^{*-} \to \bar{D}^{*0}\pi^-)$
$+\mathcal{B}(B^0 \to D_1^{\prime -}\ell^+\nu)\mathcal{B}(D_1^{\prime -} \to \bar{D}^{*0}\pi^-) + \mathcal{B}(B^0 \to \bar{D}^{*0}\pi^-\ell^+\nu)$

11. $\mathcal{BT}(B^+ \to \bar{D}_1^{\prime 0}/(D^*\pi)^0\ell^+\nu)$
$\equiv \mathcal{B}(B^+ \to \bar{D}_1^{\prime 0}\ell^+\nu) + \mathcal{B}(B^+ \to D^{*-}\pi^+\ell^+\nu) + \mathcal{B}(B^+ \to \bar{D}^{*0}\pi^0\ell^+\nu)$

12. $\mathcal{BT}(B^0 \to D_1^{\prime -}/(D^*\pi)^-\ell^+\nu)$
$\equiv \mathcal{B}(B^0 \to D_1^{\prime -}\ell^+\nu) + \mathcal{B}(B^0 \to \bar{D}^{*0}\pi^-\ell^+\nu) + \mathcal{B}(B^0 \to D^{*-}\pi^0\ell^+\nu)$

13. $\mathcal{BT}(B^+ \to \bar{D}^{**0}/(D\pi)^0\ell^+\nu)$
$\equiv \mathcal{B}(B^+ \to \bar{D}_0^{*0}\ell^+\nu)+\mathcal{B}(B^+ \to \bar{D}_1^0\ell^+\nu)+\mathcal{B}(B^+ \to \bar{D}_1^{\prime 0}\ell^+\nu)+\mathcal{B}(B^+ \to \bar{D}_2^{*0}\ell^+\nu)$
$+\mathcal{B}(B^+ \to D^-\pi^+\ell^+\nu) + \mathcal{B}(B^+ \to \bar{D}^0\pi^0\ell^+\nu)$
$+\mathcal{B}(B^+ \to D^{*-}\pi^+\ell^+\nu) + \mathcal{B}(B^+ \to \bar{D}^{*0}\pi^0\ell^+\nu)$

14. $\mathcal{BT}(B^0 \to D^{**-}/(D\pi)^-\ell^+\nu)$
$\equiv \mathcal{B}(B^0 \to D_0^{*-}\ell^+\nu)+\mathcal{B}(B^0 \to D_1^-\ell^+\nu)+\mathcal{B}(B^0 \to D_1^{\prime -}\ell^+\nu)+\mathcal{B}(B^0 \to D_2^{*-}\ell^+\nu)$
$+\mathcal{B}(B^0 \to \bar{D}^0\pi^-\ell^+\nu) + \mathcal{B}(B^0 \to D^-\pi^0\ell^+\nu)$
$+\mathcal{B}(B^0 \to \bar{D}^{*0}\pi^-\ell^+\nu) + \mathcal{B}(B^0 \to D^{*-}\pi^0\ell^+\nu)$

We also define the following branching fraction ratios :

1. $f_{D_2^*} \equiv \frac{\mathcal{B}(D_2^{*+}\to D^0\pi^+)}{\mathcal{B}(D_2^{*+}\to D^{*0}\pi^+)}$

2. $f_{D_2^*/D_1} \equiv \frac{\mathcal{B}(B^+\to\bar{D}_2^{*0}\ell^+\nu)}{\mathcal{B}(B^+\to\bar{D}_1^0\ell^+\nu)}$

3. $f_{D\pi/D_0^*} \equiv \frac{\mathcal{B}(B^+\to D^-\pi^+\ell^+\nu)}{\mathcal{B}(B^+\to\bar{D}_0^{*0}\ell^+\nu)}$

4. $f_{D^*\pi/D_1'} \equiv \frac{\mathcal{B}(B^+\to D^{*-}\pi^+\ell^+\nu)}{\mathcal{B}(B^+\to\bar{D}_1^{\prime 0}\ell^+\nu)}$

5. $f_{D_0^*D\pi T/D_1D_2^*T} \equiv \frac{\mathcal{BT}(B^+\to\bar{D}_0^{*0}/(D\pi)^0\ell^+\nu)}{\mathcal{BT}(B^+\to\bar{D}_1^0/\bar{D}_2^{*0}\ell^+\nu)}$

6. $f_{D_1'D^*\pi T/D_1D_2^*T} \equiv \frac{\mathcal{BT}(B^+\to\bar{D}_1^{\prime 0}/(D^*\pi)^0\ell^+\nu)}{\mathcal{BT}(B^+\to\bar{D}_1^0/\bar{D}_2^{*0}\ell^+\nu)}$

D.2 Measured $B \to D^{(*)}\pi^+\ell^+\nu$ branching fractions

$B \to D^{(*)}\pi^+\ell^+\nu$ branching fractions given in Table 67 and 68 includes not only non-resonant contribution but also $B \to D^{(*)}\pi^+\ell^+\nu$ contributions. Thus,

$$\begin{aligned}&\mathcal{BT}(B^+ \to D^-\pi^+\ell^+\nu)\\ &\quad = \mathcal{B}(B^+ \to \bar{D}_0^{*0}\ell^+\nu)\mathcal{B}(D_0^{*0} \to D^+\pi^-) + \mathcal{B}(B^+ \to \bar{D}_2^{*0}\ell^+\nu)\mathcal{B}(D_2^{*0} \to D^+\pi^-) + \mathcal{B}(B^+ \to D^-\pi^+\ell^+\nu)\end{aligned} \tag{477}$$

$$\begin{aligned}\mathcal{BT}(B^+ \to D^{*-}\pi^+\ell^+\nu) &= \mathcal{B}(B^+ \to \bar{D}_1^0\ell^+\nu)\mathcal{B}(D_1^0 \to D^{*+}\pi^-) + \mathcal{B}(B^+ \to \bar{D}_1^{\prime 0}\ell^+\nu)\mathcal{B}(D_1^{\prime 0} \to D^{*+}\pi^-)\\ &+\mathcal{B}(B^+ \to \bar{D}_2^{*0}\ell^+\nu)\mathcal{B}(D_2^{*0} \to D^{*+}\pi^-) + \mathcal{B}(B^+ \to D^{*-}\pi^+\ell^+\nu)\end{aligned} \tag{478}$$

$$\begin{aligned}&\mathcal{BT}(B^0 \to \bar{D}^0\pi^-\ell^+\nu)\\ &\quad = \mathcal{B}(B^0 \to D_0^{*-}\ell^+\nu)\mathcal{B}(D_0^{*+} \to D^0\pi^+) + \mathcal{B}(B^0 \to D_2^{*-}\ell^+\nu)\mathcal{B}(D_2^{*+} \to D^0\pi^+) + \mathcal{B}(B^0 \to \bar{D}^0\pi^-\ell^+\nu)\end{aligned} \tag{479}$$

$$\begin{aligned}\mathcal{BT}(B^0 \to \bar{D}^{*0}\pi^-\ell^+\nu) &= \mathcal{B}(B^0 \to D_1^-\ell^+\nu)\mathcal{B}(D_1^+ \to D^{*0}\pi^+) + \mathcal{B}(B^0 \to D_1^{\prime -}\ell^+\nu)\mathcal{B}(D_1^{\prime +} \to D^{*0}\pi^+)\\ &+\mathcal{B}(B^0 \to D_2^{*-}\ell^+\nu)\mathcal{B}(D_2^{*+} \to D^{*0}\pi^+) + \mathcal{B}(B^0 \to \bar{D}^{*0}\pi^-\ell^+\nu)\end{aligned} \tag{480}$$

Thus, using SP5/SP6 MC values

$$\begin{aligned}\mathcal{BT}(B^+ \to D^-\pi^+\ell^+\nu) &= 0.0020 \times 0.6667 + 0.0037 \times 0.459 + 0.0060 \\ &= 0.00903\end{aligned} \tag{481}$$

$$\begin{aligned}\mathcal{BT}(B^+ \to D^{*-}\pi^+\ell^+\nu) &= 0.0056 \times 0.6667 + 0.0037 \times 0.6667 \\ &\quad +0.0037 \times 0.209 + 0.0020 \\ &= 0.00897\end{aligned} \tag{482}$$

$$\begin{aligned}\mathcal{BT}(B^0 \to \bar{D}^0\pi^-\ell^+\nu) &= 0.0020 \times 0.6667 + 0.0037 \times 0.459 + 0.0060 \\ &= 0.00903\end{aligned} \tag{483}$$

$$\begin{aligned}\mathcal{BT}(B^0 \to \bar{D}^{*0}\pi^-\ell^+\nu) &= 0.0056 \times 0.6667 + 0.0037 \times 0.6667 \\ &\quad +0.0037 \times 0.209 + 0.0020 \\ &= 0.00897\end{aligned} \tag{484}$$

D.3 Inclusive $\mathcal{B}(B \to X_c\ell\nu)$

Inclusive branching fractions in SP5/SP6 MC are given by the sum of exclusive branching fractions :

$$\mathcal{B}(B^+ \to \bar{D}^0\ell^+\nu)+\mathcal{B}(B^+ \to \bar{D}^{*0}\ell^+\nu)+\mathcal{BT}(B^+ \to \bar{D}^{**0}/(D\pi)^0\ell^+\nu) = \mathcal{B}(B^+ \to X_c\ell^+\nu) \tag{485}$$

and

$$\mathcal{B}(B^0 \to D^-\ell^+\nu)+\mathcal{B}(B^0 \to D^{*-}\ell^+\nu)+\mathcal{BT}(B^0 \to D^{**-}/(D\pi)^-\ell^+\nu) = \mathcal{B}(B^0 \to X_c\ell^+\nu) \tag{486}$$

In SP5/SP6 the following value is used :

$$\mathcal{B}(B^+ \to X_c\ell\nu) = \mathcal{B}(B^0 \to X_c\ell\nu) = 0.104 \tag{487}$$

Measured values form PDG [13] are

$$\begin{aligned}\mathcal{B}(B \to X\ell\nu) &= 0.1081 \pm 0.0014 \\ \mathcal{B}(B \to X_u\ell\nu) &= 0.00233 \pm 0.00022\end{aligned} \tag{488}$$

Thus,

$$\begin{aligned}\mathcal{B}(B \to X_c\ell\nu) &= (0.1081 \pm 0.0014) - (0.00233 \pm 0.00022) \\ &= 0.10577 \pm 0.001417\end{aligned} \tag{489}$$

Combining this with lifetime ratio [13]

$$t_{+0} \equiv \frac{\tau_{B^+}}{\tau_{B^0}} = 1.071 \pm 0.009 \tag{490}$$

Branching fraction	SP5/SP6	Measurement [reference]
$\mathcal{B}(B^+ \to \bar{D}^0 \ell^+ \nu)$	0.0210	0.0215 ± 0.0022 [13] $0.0233 \pm 0.0009 \pm 0.0008$ [4]
$\mathcal{B}(B^+ \to \bar{D}^{*0} \ell^+ \nu)$	0.0560	0.065 ± 0.005 [13] $0.0583 \pm 0.0015 \pm 0.0028$ [4]
$\mathcal{B}(B^+ \to \bar{D}_0^{*0} \ell^+ \nu)$	0.0020	
$\mathcal{B}(B^+ \to \bar{D}_1^0 \ell^+ \nu)$	0.0056	0.0056 ± 0.0016 [13] $0.00448 \pm 0.00026 \pm 0.00035$ [16]
$\mathcal{B}(B^+ \to \bar{D}_1^{\prime 0} \ell^+ \nu)$	0.0037	
$\mathcal{B}(B^+ \to \bar{D}_2^{*0} \ell^+ \nu)$	0.0037	$0.00354 \pm 0.00032 \pm 0.00054$ [16]
$\mathcal{B}(B^+ \to D^- \pi^+ \ell^+ \nu)$	0.0060	
$\mathcal{B}(B^+ \to \bar{D}^0 \pi^0 \ell^+ \nu)$	0.0030	
$\mathcal{B}(B^+ \to D^{*-} \pi^+ \ell^+ \nu)$	0.0020	
$\mathcal{B}(B^+ \to \bar{D}^{*0} \pi^0 \ell^+ \nu)$	0.0010	
$\mathcal{B}\mathcal{T}(B^+ \to D^- \pi^+ \ell^+ \nu)$	0.00903	0.0052 ± 0.0010 [13] $0.0042 \pm 0.0006 \pm 0.0003$ [4]
$\mathcal{B}\mathcal{T}(B^+ \to D^{*-} \pi^+ \ell^+ \nu)$	0.00897	0.0063 ± 0.0015 [13] $0.0059 \pm 0.0005 \pm 0.0004$ [4]

Table 67: B^+ decay branching fractions.

we can calculate B^+ and B^0 separately. By assuming B^+ and B^0 contributions are equal,

$$\mathcal{B}(B^+ \to \bar{X}_c^0 \ell^+ \nu) + \mathcal{B}(B^0 \to X_c^- \ell^+ \nu) = 2\mathcal{B}(B \to X_c \ell \nu) \tag{491}$$

From isospin symmetry

$$\mathcal{B}(B^+ \to \bar{X}_c^0 \ell^+ \nu) = t_{+0} \mathcal{B}(B^0 \to X_c^- \ell^+ \nu) \tag{492}$$

Thus

$$\mathcal{B}(B^+ \to \bar{X}_c^0 \ell^+ \nu) = \frac{2t_{+0}}{1 + t_{+0}} \mathcal{B}(B \to X_c \ell \nu) = 0.1094 \pm 0.0014 \tag{493}$$

and

$$\mathcal{B}(B^+ \to \bar{X}_c^0 \ell^+ \nu) = \frac{2}{1 + t_{+0}} \mathcal{B}(B \to X_c \ell \nu) = 0.1021 \pm 0.0014 \tag{494}$$

Branching fraction	SP5/SP6	Measurement [reference]
$\mathcal{B}(B^0 \to D^- \ell^+ \nu)$	0.0210	0.0208 ± 0.0018 [13]
		$0.0221 \pm 0.0011 \pm 0.0009$ [4]
$\mathcal{B}(B^0 \to D^{*-} \ell^+ \nu)$	0.0560	0.0529 ± 0.0019 [13]
		$0.0549 \pm 0.0016 \pm 0.0023$ [4]
$\mathcal{B}(B^0 \to D_0^{*-} \ell^+ \nu)$	0.0020	$0.0042 \pm 0.0033 \pm 0.022$ [17]
$\mathcal{B}(B^0 \to D_1^- \ell^+ \nu)$	0.0056	$0.00364 \pm 0.00032 \pm 0.00049$ [16]
$\mathcal{B}(B^0 \to D_1^{\prime -} \ell^+ \nu)$	0.0037	$0.0124 \pm 0.0025 \pm 0.027$ [17]
$\mathcal{B}(B^0 \to D_2^{*-} \ell^+ \nu)$	0.0037	$0.00270 \pm 0.00035 \pm 0.00043$ [16]
$\mathcal{BT}(B^0 \to D^{**-} \ell^+ \nu)$	0.0150	$0.027 \pm 0.007 \pm 0.002$ [17]
$\mathcal{B}(B^0 \to \bar{D}^0 \pi^- \ell^+ \nu)$	0.0060	
$\mathcal{B}(B^0 \to D^- \pi^0 \ell^+ \nu)$	0.0030	
$\mathcal{B}(B^0 \to \bar{D}^{*0} \pi^- \ell^+ \nu)$	0.0020	
$\mathcal{B}(B^+ \to \bar{D}^{*0} \pi^0 \ell^+ \nu)$	0.0010	
$\mathcal{BT}(B^0 \to \bar{D}^0 \pi^- \ell^+ \nu)$	0.00903	0.0032 ± 0.0010 [13]
		$0.0043 \pm 0.0008 \pm 0.0003$ [4]
$\mathcal{BT}(B^0 \to \bar{D}^{*0} \pi^- \ell^+ \nu)$	0.00897	0.0065 ± 0.0015 [13]
		$0.0048 \pm 0.0008 \pm 0.0004$ [4]

Table 68: B^0 decay branching fractions.

Branching fraction	SP5/SP6	AWG average
$\mathcal{B}(B^+ \to \bar{D}_1^0 \ell^+ \nu)$	0.0056	0.0054 ± 0.0006
$\mathcal{B}(B^+ \to \bar{D}_2^{*0} \ell^+ \nu)$	0.0037	0.0042 ± 0.0008
$\mathcal{BT}(B^+ \to \bar{D}_1^0/\bar{D}_2^{*0} \ell^+ \nu)$	0.0093	
$\mathcal{B}(B^+ \to \bar{D}_0^{*0} \ell^+ \nu)$	0.0020	0.0085 ± 0.0020
$\mathcal{B}(B^+ \to D^- \pi^+ \ell^+ \nu)$	0.0060	0.0019 ± 0.0012
$\mathcal{B}(B^+ \to \bar{D}^0 \pi^0 \ell^+ \nu)$	0.0030	0.0010 ± 0.0006
$\mathcal{BT}(B^+ \to \bar{D}_0^{*0}/(D\pi)^0 \ell^+ \nu)$	0.0110	
$\mathcal{B}(B^+ \to \bar{D}_1^{\prime 0} \ell^+ \nu)$	0.0037	0.0045 ± 0.0009
$\mathcal{B}(B^+ \to D^{*-} \pi^+ \ell^+ \nu)$	0.0020	0.0006 ± 0.0004
$\mathcal{B}(B^+ \to \bar{D}^{*0} \pi^0 \ell^+ \nu)$	0.0010	0.0003 ± 0.0002
$\mathcal{BT}(B^+ \to \bar{D}_1^{*0}/(D^*\pi)^0 \ell^+ \nu)$	0.0067	
$\mathcal{BT}(B^+ \to \bar{D}^{**0}/(D\pi)^0 \ell^+ \nu)$	0.0270	
$f_{D_2^*/D_1}$	$37/56 = 0.66$	
$f_{D\pi/D_0^*}$	$60/20 = 3.0$	
$f_{D^*\pi/D_1^*}$	$20/37 = 0.54$	
$f_{D_0^* D\pi T/D_1 D_2^* T}$	$110/93 = 1.18$	
$f_{D_1^* D^*\pi T/D_1 D_2^* T}$	$67/93 = 0.72$	

Table 69: $B^+ \to D^{**}\ell\nu$ and $B^+ \to D^{(*)}\pi\ell\nu$ decay branching fractions and ratios defined in section 5.

Branching fraction	SP5/SP6	Measurement [reference]
$\mathcal{B}(B^+ \to X \ell^+ \nu)$		0.1099 ± 0.0028 [13]
$\mathcal{B}(B^+ \to \bar{X}_c^0 \ell^+ \nu)$	0.1040	0.108 ± 0.004 [13]
$\mathcal{B}(B^0 \to X \ell^+ \nu)$		0.1033 ± 0.0028 [13]
$\mathcal{B}(B^0 \to X_c^- \ell^+ \nu)$	0.1040	0.101 ± 0.004 [13]
$\mathcal{B}(B \to X \ell^+ \nu)$		0.1024 ± 0.0015 [13]
$\mathcal{B}(B \to X_c \ell \nu)$	0.1040	0.1057 ± 0.0015 [13]
$\mathcal{B}(B \to X_u \ell \nu)$		0.00233 ± 0.00022 [13]
$\mathcal{B}(B \to X_c e \nu(\gamma), E_e > 1.5\mathrm{GeV})$		$0.0454 \pm 0.0003 \pm 0.0008$ [45]

Table 70: Inclusive B decay branching fractions.

Branching fraction	SP5/SP6	Measurement [reference]
$\mathcal{B}(D_0^{*+} \to D^0\pi^+)$	0.6667	
$\mathcal{B}(D_0^{*+} \to D^+\pi^0)$	0.3333	
$\mathcal{B}(D_0^{*0} \to D^+\pi^-)$	0.6667	
$\mathcal{B}(D_0^{*0} \to D^0\pi^0)$	0.3333	
$\mathcal{B}(D_1^{+} \to D^{*0}\pi^+)$	0.6667	
$\mathcal{B}(D_1^{+} \to D^{*+}\pi^0)$	0.3333	
$\mathcal{B}(D_1^{0} \to D^{*+}\pi^-)$	0.6667	
$\mathcal{B}(D_1^{0} \to D^{*0}\pi^0)$	0.3333	
$\mathcal{B}(D_1^{\prime +} \to D^{*0}\pi^+)$	0.6667	
$\mathcal{B}(D_1^{\prime +} \to D^{*+}\pi^0)$	0.3333	
$\mathcal{B}(D_1^{\prime 0} \to D^{*+}\pi^-)$	0.6667	
$\mathcal{B}(D_1^{\prime 0} \to D^{*0}\pi^0)$	0.3333	
$f_{D_2^*}$	$459/209 = 2.2$	$\frac{\mathcal{B}(D_2^{*+} \to D^0\pi^+)}{\mathcal{B}(D_2^{*+} \to D^{*0}\pi^+)} = 1.9 \pm 1.1 \pm 0.3$ [13] $\frac{\mathcal{B}(D_2^{*0} \to D^+\pi^-)}{\mathcal{B}(D_2^{*0} \to D^{*+}\pi^-)} = 2.3 \pm 0.6$ [13]
$\mathcal{B}(D_2^{*+} \to D^0\pi^+)$	0.4590	
$\mathcal{B}(D_2^{*+} \to D^+\pi^0)$	0.2290	
$\mathcal{B}(D_2^{*+} \to D^{*0}\pi^+)$	0.2090	
$\mathcal{B}(D_2^{*+} \to D^{*+}\pi^0)$	0.1030	
$\mathcal{B}(D_2^{*0} \to D^+\pi^-)$	0.4590	
$\mathcal{B}(D_2^{*0} \to D^0\pi^0)$	0.2290	
$\mathcal{B}(D_2^{*0} \to D^{*+}\pi^-)$	0.2090	
$\mathcal{B}(D_2^{*0} \to D^{*0}\pi^0)$	0.1030	

Table 71: D^{**} decay branching fractions.

Branching fraction	SP5/SP6	Measurement [reference]
$\mathcal{B}(D^{*+} \to D^0\pi^+)$	0.6830	0.677 ± 0.005 [13]
$\mathcal{B}(D^{*+} \to D^+\pi^0)$	0.3060	0.307 ± 0.005 [13]
$\mathcal{B}(D^{*+} \to D^+\gamma)$	0.0110	0.016 ± 0.004 [13]
$\mathcal{B}(D^{*0} \to D^0\pi^0)$	0.6190	0.619 ± 0.029 [13]
$\mathcal{B}(D^{*0} \to D^0\gamma)$	0.3810	0.381 ± 0.029 [13]
$\mathcal{B}(D^0 \to K^-\pi^+)$	0.0383	0.0382 ± 0.0007 [13]
		$0.04007 \pm 0.00037 \pm 0.00070$ [30]
		$0.03891 \pm 0.00035 \pm 0.00059 \pm 0.00035$ [31]
$\mathcal{B}(D^+ \to K^-\pi^+\pi^+)$	0.0900	0.0951 ± 0.0034 [13]
		$0.0915 \pm 0.0010 \pm 0.0016 \pm 0.0007$ [31]

Table 72: $D^{(*)}$ decay branching fractions.

Constant	SP5/SP6	Measurement [reference]
t_{+0}	1	1.071 ± 0.009 [13]
f_{+0}	1	1.037 ± 0.029 [13]

Table 73: Constants.

Parameter	SP5/SP6	Measurement [reference]
R_1	1.18	$1.396 \pm 0.060 \pm 0.035 \pm 0.027$ [38]
R_2	0.72	$0.885 \pm 0.040 \pm 0.022 \pm 0.013$ [38]
ρ^2	0.92	$1.145 \pm 0.059 \pm 0.030 \pm 0.035$ [38]
R_1	1.18	$1.417 \pm 0.061 \pm 0.044$ [39]
R_2	0.72	$0.836 \pm 0.037 \pm 0.022$ [39]
ρ^2	0.92	$1.179 \pm 0.048 \pm 0.028$ [39]
$\mathcal{F}(1)\|V_{cb}\|$		$(34.68 \pm 0.32 \pm 1.15) \times 10^{-3}$ [39]
$\mathcal{B}(B^0 \to D^{*-}\ell^+\nu)$	0.0560	$0.0477 \pm 0.0004 \pm 0.0039$ [39]
ρ^2	0.92	$1.15 \pm 0.06 \pm 0.08$ [40]
$\mathcal{F}(1)\|V_{cb}\|$		$(34.3 \pm 0.6 \pm 1.4) \times 10^{-3}$ [40]
$\mathcal{B}(B^- \to D^{*0}e^-\bar{\nu}_e)$	0.0560	$0.0571 \pm 0.0008 \pm 0.0041$ [40]

Table 74: $B \to D^*\ell\nu$ FF parameters. “Measurement” is the most recent measured value and “Used” is the used value in the fit. Definition of these parameters are given in Appendix H. Note that different parametrizations of ρ^2 was used in SP5/SP6 MC and [38]. See details in section 9

E BToDlnu skim rates and luminosities

The event selection rates and luminosities of R16b BToDlnu skims of data and MC is summarized in Table 76 and 77.
The luminosities of BpBm and B0B0bar MC are calculated by the generated number of events and B counting number in the OnPeak table 76. For example, in case of BpBm MC Run2, the generated number of events is 146536000. The B counting number for Run2 OnPeak is 65697538.1 ± 723956.4, which corresponds to the luminosity of 59.402357 fb^{-1}. We assume the half of the $B\bar{B}$ is B^+B^-. Thus, the luminosity is

$$\frac{146536000}{(65697538.1 \pm 723956.4)/2} \times 59.402357 = 264.99 \pm 2.92 \ \text{fb}^{-1}$$

The luminosities of ccbar, uds and tautau MC are calculated by the generated number of events and their cross section. Cross sections are taken from the Babar Physics Book [50] and given in Table 75. The luminosities are calculated based on the cross sections and the number of events before skimming. For example, in case of ccbar Run4 MC, as the number of events before skimming is 188718626, its luminosity is

$$\frac{188718626}{1.30 \times 10^3} = 1.452 \times 10^5 \text{pb}^{-1} = 145.2 \ \text{fb}^{-1}$$

Type of MC	Cross section (nb)
$B\bar{B}$	1.05
$c\bar{c}$	1.30
uds	2.09
$\tau^+\tau^-$	0.94

Table 75: Cross sections used to calculate MC luminosities.

Data set	Selection rate	Luminosity (fb^{-1})	Number of BBbar
OnPeak Run1	8792976/245552690	17.807136	19411539.8 ± 214782.8
Run2	31374579/852649140	59.402357	65697538.1 ± 723956.4
Run3	17527801/438622047	30.630558	33754342.8 ± 372583.9
Run4	57952809/1448776065	99.405417	$109449337.9 \pm 1205214.0$
Total		207.245468	
OffPeak Run1	515760/28946433	2.330076	
Run2	1674989/90665305	6.833280	
Run3	659867/31451100	2.394734	
Run4	2878531/132941301	9.929434	
Total		21.487524	

Table 76: BToDlnu Data skims event selection rates and luminosities.

Data set	Selection rate	Luminosity (fb^{-1})
BpBm Run1	6920906/27176000	49.86 ± 0.55
Run2	39029539/146536000	264.99 ± 2.92
Run3	23854196/86492000	156.98 ± 1.73
Run4	89759580/323822000	588.21 ± 6.48
Total		1060.04 ± 7.34
B0B0bar Run1	7421839/28762000	52.77 ± 0.58
Run2	30164526/111924000	202.40 ± 2.23
Run3	17081965/61158000	111.00 ± 1.23
Run4	90093404/321150000	583.36 ± 6.42
Total		949.53 ± 6.93
ccbar Run1	1897239/21346000	16.420
Run2	9838664/99972000	76.708
Run3	6127861/57700000	44.385
Run4	25956105/246602000	189.69
Total		327.20
uds Run1	948025/30168000	14.434
Run2	6799899/176242000	84.326
Run3	5639210/124040000	59.349
Run4	15259514/346551000	165.81
Total		323.919
tautau Run1	135022/22098000	23.509
Run2	695973/99806000	106.18
Run3	544465/69852000	74.311
Run4	1472037/154900000	164.79
Total		368.79

Table 77: BToDlnu MC skims event selection rates and luminosities.

F $\cos\theta_{BY}$

F.1 $B \to D\ell\nu$ decays

In the decay of $B \to Dl + \nu$, 4-momentum conservation gives

$$p_B = p_{Dl} + p_\nu \tag{495}$$

As the mass of neutrino is equal to zero

$$0 = p_\nu^2 = (p_B - p_{Dl})^2 = p_B^2 + p_{Dl}^2 - 2p_B \cdot p_{Dl} = m_B^2 + m_{Dl}^2 - 2p_B \cdot p_{Dl} \tag{496}$$

Here,

$$p_B \cdot p_{Dl} = E_B E_{Dl} - \vec{p}_B \cdot \vec{p}_{Dl} = E_B E_{Dl} - |\vec{p}_B||\vec{p}_{Dl}| \cos\Theta_{B-Dl} \tag{497}$$

Hence

$$\begin{aligned} 0 &= m_B^2 + m_{Dl}^2 - 2(E_B E_{Dl} - |\vec{p}_B||\vec{p}_{Dl}| \cos\Theta_{B-Dl}) \\ \Rightarrow m_B^2 + m_{Dl}^2 &= 2E_B E_{Dl} - 2|\vec{p}_B||\vec{p}_{Dl}| \cos\Theta_{B-Dl} \end{aligned} \tag{498}$$

Therefore

$$\cos\Theta_{B-Dl} = \frac{2E_B E_{Dl} - m_B^2 - m_{Dl}^2}{2|\vec{p}_B||\vec{p}_{Dl}|} \tag{499}$$

In practice, E_B is given by the half of the beam energy in the CM frame. $|\vec{p}_B|$ is given by

$$|\vec{p}_B| = \sqrt{E_B^2 - m_B^2} \tag{500}$$

F.2 With an additional pion

If there are additional particles, $\cos\Theta_{B-Dl} < -1$ is possible. Let us consider an additional pion, for example, from D^*. Conservation of 4-momentum is

$$p_B = p_{Dl} + p_\pi + p_\nu \tag{501}$$

Then,

$$\begin{aligned} &(p_\nu + p_\pi)^2 = (p_B - p_{Dl})^2 \\ &\Rightarrow p_\nu^2 + p_\pi^2 + 2p_\nu \cdot p_\pi = p_B^2 + p_{Dl}^2 - 2p_B \cdot p_{Dl} \\ &\Rightarrow 0 + m_\pi^2 + 2p_\nu \cdot p_\pi = m_B^2 + m_{Dl}^2 - 2p_B \cdot p_{Dl} \end{aligned} \tag{502}$$

Since $m_\pi \ll m_B$,

$$0 + 0 + 2p_\nu \cdot p_\pi = m_B^2 + m_{Dl}^2 - 2p_B \cdot p_{Dl} \tag{503}$$

and also

$$\begin{aligned} p_\nu \cdot p_\pi &= E_\nu E_\pi - \vec{p}_\nu \cdot \vec{p}_\pi = E_\nu E_\pi - |\vec{p}_\nu||\vec{p}_\pi| \cos\Theta_{\nu-\pi} \\ &= E_\nu E_\pi - E_\nu E_\pi \cos\Theta_{\nu-\pi} = E_\nu E_\pi (1 - \cos\Theta_{\nu-\pi}) \geq 0 \end{aligned} \tag{504}$$

Let the angle between B and Dl be Θ'_{B-Dl}. Then,

$$p_B \cdot p_{Dl} = E_B E_{Dl} - \vec{p}_B \cdot \vec{p}_{Dl} = E_B E_{Dl} - |\vec{p}_B||\vec{p}_{Dl}| \cos\Theta'_{B-Dl} \tag{505}$$

Hence,

$$\begin{aligned}\cos\Theta'_{B-Dl} &= \tfrac{2E_B E_{Dl} - m_B^2 - m_{Dl}^2}{2|\vec{p}_B||\vec{p}_{Dl}|} + \tfrac{2p_\nu \cdot p_\pi}{2|\vec{p}_B||\vec{p}_{Dl}|} \\ &= \cos\Theta_{B-Dl} + \alpha\end{aligned} \tag{506}$$

where

$$\alpha = \frac{2p_\nu \cdot p_\pi}{2|\vec{p}_B||\vec{p}_{Dl}|} \geq 0 \tag{507}$$

Considering

$$-1 \leq \cos\Theta'_{B-Dl} \leq 1 \tag{508}$$

$\cos\Theta_{B-Dl} = \cos\Theta'_{B-Dl} - \alpha$ is

$$-1 - \alpha \leq \cos\Theta_{B-Dl} \leq 1 - \alpha \leq 1 \tag{509}$$

Since $\alpha \geq 0$, the lower end of $\cos\Theta_{B-Dl}$ can be smaller than -1, whereas the upper end remains to 1.

F.3 If D and l come from different B

In the case that D and l came from different B, $\cos\Theta_{B-Dl} > 1$ is possible. The p_{Dl} is

$$p_{Dl} = p_D + p_l = (E_D + E_l, -\vec{p}_D - \vec{p}_l) = (E_{Dl}, -\vec{p}_{Dl}) \tag{510}$$

Hence

$$\begin{aligned}&E_{Dl} = E_D + E_l = \sqrt{m_D^2 + |\vec{p}_D|^2} + \sqrt{m_l^2 + |\vec{p}_l|^2} = \sqrt{m_D^2 + |\vec{p}_D|^2} + |\vec{p}_l| \\ &|\vec{p}_{Dl}|^2 = |\vec{p}_D + \vec{p}_l|^2 = |\vec{p}_D|^2 + |\vec{p}_l|^2 + 2|\vec{p}_D||\vec{p}_l|\cos\theta\end{aligned} \tag{511}$$

and

$$\begin{aligned}m_{Dl}^2 &= p_{Dl}^2 = E_{Dl}^2 - |\vec{p}_{Dl}|^2 \\ &= m_D^2 + |\vec{p}_D|^2 + |\vec{p}_l|^2 + 2|\vec{p}_l|\sqrt{m_D^2 + |\vec{p}_D|^2} - |\vec{p}_D|^2 - |\vec{p}_l|^2 - 2|\vec{p}_D||\vec{p}_l|\cos\theta \\ &= m_D^2 + 2|\vec{p}_l|\sqrt{m_D^2 + |\vec{p}_D|^2} - 2|\vec{p}_D||\vec{p}_l|\cos\theta \\ &= m_D^2 + |\vec{p}_l|(2\sqrt{m_D^2 + |\vec{p}_D|^2} - 2|\vec{p}_D|\cos\theta)\end{aligned} \tag{512}$$

If D and l come from different B, p_D and p_l are not restricted by energy momentum conservation. The $|\vec{p}_D|$ and $|\vec{p}_l|$ can be any value. If $|\vec{p}_l|$ is very large, E_{Dl} is very large but m_{Dl}^2 can be as small as m_D^2 if

$$2\sqrt{m_D^2 + |\vec{p}_D|^2} \simeq 2|\vec{p}_D|\cos\theta \tag{513}$$

Hence

$$\cos\Theta_{B-Dl} = \frac{2E_B E_{Dl} - m_B^2 - m_{Dl}^2}{2|\vec{p}_B||\vec{p}_{Dl}|} \tag{514}$$

can be larger than 1.

G Velocity transfer w

G.1 w and q^2

In the framework of Heavy Quark Effective Theory (HQET) it is convenient to use the velocity transfer w instead of momentum transfer q^2. In semileptonic $B \to D^{(*)}\ell\nu$ decays, w is defined as the product of 4-velocities of B and $D^{(*)}$

$$w \equiv v_B \cdot v_{D^{(*)}} = \frac{p_B \cdot p_{D^{(*)}}}{m_B m_{D^{(*)}}} \tag{515}$$

The momentum transfer q from B to $D^{(*)}$ (or the invariant mass of the virtual W) is given by

$$q = p_\ell + p_\nu = p_B - p_{D^{(*)}} \tag{516}$$

Thus

$$\begin{aligned} & q^2 = (p_B - p_{D^{(*)}})^2 = p_B^2 + p_{D^{(*)}}^2 - 2p_B \cdot p_{D^{(*)}} = m_B^2 + m_{D^{(*)}}^2 - 2p_B \cdot p_{D^{(*)}} \\ & \Rightarrow p_B \cdot p_{D^{(*)}} = \frac{m_B^2 + m_{D^{(*)}}^2 - q^2}{2} \end{aligned} \tag{517}$$

Hence

$$w = \frac{m_B^2 + m_{D^{(*)}}^2 - q^2}{2m_B m_{D^{(*)}}} \tag{518}$$

w is a Lorentz invariant and linearly related to q^2.
w corresponds to the relativistic boost γ of the $D^{(*)}$ in the B rest frame.

$$\gamma_{D^{(*)}} = \frac{E_{D^{(*)}}}{m_{D^{(*)}}} \tag{519}$$

G.2 $1 \leq w \lesssim 1.5$

The range of w and q^2 are restricted by kinematics of the decay. When $q^2 = 0$, w is maximum

$$w_{\max} = \frac{m_B^2 + m_{D^{(*)}}^2}{2m_B m_{D^{(*)}}} \tag{520}$$

Using $m_B = 5279$, $m_D = 1867$ and $m_{D^*} = 2008$ MeV,

$$\frac{m_B^2 + m_D^2}{2m_B m_D} = 1.590, \quad \frac{m_B^2 + m_{D^*}^2}{2m_B m_{D^*}} = 1.504 \tag{521}$$

Using $m_{D_0^*} = 2400$, $m_{D_1'} = 2430$, $m_{D_1} = 2420$ and $m_{D_2^*} = 2460$ MeV,

$$\begin{aligned} \frac{m_B^2 + m_{D_0^*}^2}{2m_B m_{D_0^*}} = 1.327, \quad \frac{m_B^2 + m_{D_1'}^2}{2m_B m_{D_1'}} = 1.316, \\ \frac{m_B^2 + m_{D_1}^2}{2m_B m_{D_1}} = 1.320, \quad \frac{m_B^2 + m_{D_2^*}^2}{2m_B m_{D_2^*}} = 1.306 \end{aligned} \tag{522}$$

The minimum of the w is

$$w_{\text{min}} = 1 \tag{523}$$

which corresponds to

$$q^2_{\text{max}} = (m_B - m_{D^{(*)}})^2 \tag{524}$$

where

$$(m_B - m_D)^2 = 11.64, \quad (m_B - m_{D^*})^2 = 10.69 \ (\text{GeV}/c^2)^2 \tag{525}$$

and

$$(m_B - m_{D_0^*})^2 = 8.29, \quad (m_B - m_{D_1'})^2 = 8.12 \ (\text{GeV}/c^2)^2, \tag{526}$$

$$(m_B - m_{D_1})^2 = 8.17, \quad (m_B - m_{D_2^*})^2 = 7.95 \ (\text{GeV}/c^2)^2 \tag{527}$$

G.3 Practical calculation of w

We can calculate w by the following formula

$$w = \frac{p_B \cdot p_{D^{(*)}}}{m_B m_{D^{(*)}}} = \frac{E_B E_{D^{(*)}} - |\vec{P}_B||\vec{P}_{D^{(*)}}| \cos\theta_{B-D}}{m_B m_{D^{(*)}}} \tag{528}$$

In practice, E_B is the half of the beam energy, and $|\vec{P}_B|$ is given by

$$|\vec{P}_B| = \sqrt{E_B^2 - m_B^2} \tag{529}$$

$\cos\theta_{B-D}$ can be calculated from $\cos\theta_{B-Dl}$ (see Appendix F and Figure 57).

H Form Factors (FF) of $B \to D^{(*,**)} X \ell \nu$ decays

H.1 Matrix elements, form factors and decay rates

The amplitude of $B \to D^{(*,**)} \ell \nu$ decay is given by

$$\mathcal{M} = -i \frac{G_F}{\sqrt{2}} V_{cb} L^\mu H_\mu \tag{530}$$

where the leptonic current can be written in terms of Dirac spinors u_l and v_ν

$$L^\mu = \bar{u}_l \gamma^\mu (1 - \gamma_5) v_\nu \tag{531}$$

The hadronic current H_μ can be written in terms of quark spinors b and c

$$H^\mu = < D|\bar{c}\gamma^\mu (1-\gamma_5) b|B > = < D|V^\mu|B > - < D|A^\mu|B > \tag{532}$$

where

$$\begin{aligned} V^\mu &= \bar{c}\gamma^\mu b \quad \text{(vector current)} \\ A^\mu &= \bar{c}\gamma^\mu \gamma_5 b \quad \text{(axial-vector current)} \end{aligned} \tag{533}$$

The matrix elements $< D|V^\mu|B >$ and $< D|A^\mu|B >$ can be expressed by form factors. In constituent quark models such as ISGW2 model [32][33], form factors are functions of momentum transfer q^2, whereas in HQET (Heavy Quark Effective Theory) models, it is more natural to express form factors as functions of the velocity transfer w

$$w = v \cdot v' = v_B \cdot v_D = \frac{p_B \cdot p_D}{m_B m_D} \tag{534}$$

We also use the following mass ratios

$$r = \frac{m_D}{m_B}, \;\; R = \frac{2\sqrt{m_B m_D}}{m_B + m_D} \tag{535}$$

where D in the v_D, p_D and m_D may be D^*, D_0^*, D_1', D_1 or D_2^* depending on the final state.

H.1.1 $B \to D \ell \nu$

In the ISGW2 model, the matrix elements are given by

$$< D(p')|V^\mu|B(p) > = f_+(q^2)(p+p')^\mu + f_-(q^2)(p-p')^\mu \tag{536}$$

$$< D(p')|A^\mu|B(p) > = 0 \tag{537}$$

In HQET models,

$$\frac{< D(v')|V^\mu|B(v) >}{\sqrt{m_D m_B}} = h_+ (v+v')^\mu + h_-(v-v')^\mu \tag{538}$$

$$\frac{< D(v')|A^\mu|B(v) >}{\sqrt{m_D m_B}} = 0 \tag{539}$$

We can relate ISGW2 form factors with HQET form factors using $p = m_B v$ and $p' = m_D v'$. By comparing the coefficients of v^μ and v'^μ,

$$f_+ m_B + f_- m_B = \sqrt{m_D m_B}(h_+ + h_-) \tag{540}$$
$$f_+ m_D - f_- m_D = \sqrt{m_D m_B}(h_+ - h_-) \tag{541}$$

Thus

$$h_+ = \frac{m_B + m_D}{2\sqrt{m_D m_B}}\left(f_+ + \frac{m_B - m_D}{m_B + m_D} f_-\right) \tag{542}$$
$$h_- = \frac{m_B + m_D}{2\sqrt{m_D m_B}}\left(\frac{m_B - m_D}{m_B + m_D} f_+ + f_-\right) \tag{543}$$

Hence,

$$h_+ = \frac{1}{R}\left(f_+ + \frac{1-r}{1+r} f_-\right) \tag{544}$$
$$h_- = \frac{1}{R}\left(\frac{1-r}{1+r} f_+ + f_-\right) \tag{545}$$

The differential decay rate is given by

$$\frac{d\Gamma(B \to D\ell\nu)}{dw} = \frac{G_F^2 |V_{cb}|^2 m_B^5}{48\pi^3} r^3 (w^2-1)^{3/2} \mathcal{J}_D(w) \tag{546}$$

where

$$\mathcal{J}_D(w) = [(1+r)h_+ - (1-r)h_-]^2 \tag{547}$$

H.1.2 $B \to D^*\ell\nu$

In the ISGW2 model, the matrix elements are given by

$$< D^*(p', \varepsilon)|V^\mu|B(p) >= -ig(q^2)\epsilon^{\mu\nu\alpha\beta}\varepsilon^*_\nu (p+p')_\alpha (p-p')_\beta \tag{548}$$

$$< D^*(p', \varepsilon)|A^\mu|B(p) >= f(q^2)\varepsilon^{*\mu} + a_+(q^2)(\varepsilon^* \cdot p)(p+p')^\mu + a_-(q^2)(\varepsilon^* \cdot p)(p-p')^\mu \tag{549}$$

In HQET models,

$$\frac{< D^*(v', \varepsilon)|V^\mu|B(v) >}{\sqrt{m_{D^*} m_B}} = ih_V \epsilon^{\mu\nu\alpha\beta}\varepsilon^*_\nu v'_\alpha v_\beta \tag{550}$$

$$\frac{< D^*(v', \varepsilon)|A^\mu|B(v) >}{\sqrt{m_{D^*} m_B}} = h_{A_1}(w+1)\varepsilon^{*\mu} - (h_{A_2} v^\mu + h_{A_3} v'^\mu)(\varepsilon^* \cdot v) \tag{551}$$

We can relate ISGW2 form factors with HQET form factors using $p = m_B v$ and $p' = m_D v'$. First, we use $< D^*(p', \varepsilon)|V^\mu|B(p) >$. We can simplify

$$\begin{aligned}&\epsilon^{\mu\nu\alpha\beta}\varepsilon^*_\nu(p+p')_\alpha(p-p')_\beta = \epsilon^{\mu\nu\alpha\beta}\varepsilon^*_\nu(m_B v + m_{D^*}v')_\alpha(m_B v - m_{D^*}v')_\beta \\ &= -2m_B m_{D^*}\epsilon^{\mu\nu\alpha\beta}\varepsilon^*_\nu v_\alpha v'_\beta\end{aligned} \tag{552}$$

where we used the fact that $\epsilon^{\mu\nu\alpha\beta}$ is antisymmetric but $v_\alpha v_\beta$ and $v'_\alpha v'_\beta$ are symmetric between α and β. Thus,

$$2m_B m_{D^*} g = \sqrt{m_{D^*}m_B}\, h_V \tag{553}$$

Hence

$$h_V = 2\sqrt{m_{D^*}m_B}\, g = m_B R(1+r)g \tag{554}$$

Next, we use $< D^*(p', \varepsilon)|A^\mu|B(p) >$. By comparing the coefficient of $\varepsilon^{*\mu}$,

$$f = \sqrt{m_{D^*}m_B} h_{A_1}(w+1) = \frac{m_B R(1+r)}{2}(w+1)h_{A_1} \tag{555}$$

Thus

$$h_{A_1} = \frac{2}{m_B R(1+r)(w+1)} f \tag{556}$$

By comparing the coefficients of v^μ and v'^μ,

$$m_B a_+ + m_B a_- = \sqrt{m_{D^*}m_B} h_{A_2} \tag{557}$$

$$m_{D^*} a_+ - m_{D^*} a_- = \sqrt{m_{D^*}m_B} h_{A_3} \tag{558}$$

Thus

$$h_{A_3} + r h_{A_2} = \frac{m_{D^*}m_B}{\sqrt{m_{D^*}m_B}} \cdot 2a_+ = m_B R(1+r)a_+ \tag{559}$$

The differential decay rate is given by

$$\frac{d\Gamma(B \to D^*\ell\nu)}{dw} = \frac{G_F^2|V_{cb}|^2 m_B^5}{48\pi^3} r^3(w^2-1)^{1/2}\mathcal{J}_{D^*}(w) \tag{560}$$

where

$$\begin{aligned}\mathcal{J}_{D^*}(w) = 2(1-2wr+r^2)&\left[(w+1)^2 h_{A_1}^2 + (w^2-1)h_V^2\right] \\ &+ \left[(w+1)(w-r)h_{A_1} - (w^2-1)(h_{A_3}+rh_{A_2})\right]^2\end{aligned} \tag{561}$$

H.1.3 $B \to D_0^*\ell\nu$

In the ISGW2 model, the matrix elements are given by

$$< D_0^*(p')|V^\mu|B(p) >= 0 \tag{562}$$

$$< D_0^*(p')|A^\mu|B(p) >= u_+(q^2)(p+p')^\mu + u_-(q^2)(p-p')^\mu \tag{563}$$

In HQET models,

$$\frac{< D_0^*(v')|V^\mu|B(v) >}{\sqrt{m_{D_0^*}m_B}} = 0 \tag{564}$$

$$\frac{< D_0^*(v')|A^\mu|B(v) >}{\sqrt{m_{D_0^*}m_B}} = g_+(v+v')^\mu + g_-(v-v')^\mu \tag{565}$$

We can relate the form factors as we did in the $B \to D\ell\nu$ case

$$g_+ = \frac{1}{R}\left(u_+ + \frac{1-r}{1+r}u_-\right) \tag{566}$$

$$g_- = \frac{1}{R}\left(\frac{1-r}{1+r}u_+ + u_-\right) \tag{567}$$

The differential decay rate is given by

$$\frac{d\Gamma(B \to D_0^*\ell\nu)}{dw} = \frac{G_F^2|V_{cb}|^2 m_B^5}{48\pi^3} r^3(w^2-1)^{3/2}\ \mathcal{J}_{D_0^*}(w) \tag{568}$$

where

$$\mathcal{J}_{D_0^*}(w) = [(1+r)g_+ - (1-r)g_-]^2 \tag{569}$$

H.1.4 $B \to D_1'\ell\nu$

In the ISGW2 model, the matrix elements are given by

$$< D_1'(p',\varepsilon)|V^\mu|B(p) > = l(q^2)\varepsilon^{*\mu} + c_+(q^2)(\varepsilon^*\cdot p)(p+p')^\mu + c_-(q^2)(\varepsilon^*\cdot p)(p-p')^\mu \tag{570}$$

$$< D_1'(p',\varepsilon)|A^\mu|B(p) > = -iq(q^2)\epsilon^{\mu\nu\alpha\beta}\varepsilon^*_\nu(p+p')_\alpha(p-p')_\beta \tag{571}$$

In HQET models,

$$\frac{< D_1'(v',\varepsilon)|V^\mu|B(v) >}{\sqrt{m_{D_1'}m_B}} = g_{V_1}\varepsilon^{*\mu} + (g_{V_2}v^\mu + g_{V_3}v'^\mu)(\varepsilon^*\cdot v) \tag{572}$$

$$\frac{< D_1(v',\varepsilon)|A^\mu|B(v) >}{\sqrt{m_{D_1}m_B}} = ig_A\epsilon^{\mu\nu\alpha\beta}\varepsilon^*_\nu v_\alpha v'_\beta \tag{573}$$

We can relate the form factors as we did in the $B \to D^*\ell\nu$ case

$$g_A = m_B R(1+r)q \tag{574}$$

and

$$g_{V_1} = \frac{2}{m_B R(1+r)} l \tag{575}$$

$$g_{V_3} + r g_{V_2} = m_B R(1+r)c_+ \tag{576}$$

The differential decay rate is given by

$$\frac{d\Gamma(B \to D_1'\ell\nu)}{dw} = \frac{G_F^2|V_{cb}|^2 m_B^5}{48\pi^3} r^3(w^2-1)^{1/2}\ \mathcal{J}_{D_1'}(w) \tag{577}$$

where

$$\begin{aligned}\mathcal{J}_{D_1'}(w) = &\left[(w-r)g_{V_1} + (w^2-1)(g_{V_3}+rg_{V_2})\right]^2 \\ &+2(1-2rw+r^2)[g_{V_1}^2 + (w^2-1)g_A^2]\end{aligned} \tag{578}$$

H.1.5 $B \to D_1\ell\nu$

In the ISGW2 model, the matrix elements are given by

$$< D_1'(p',\varepsilon)|V^\mu|B(p) >= r(q^2)\varepsilon^{*\mu} + s_+(q^2)(\varepsilon^*\cdot p)(p+p')^\mu + s_-(q^2)(\varepsilon^*\cdot p)(p-p')^\mu \quad (579)$$

$$< D_1'(p',\varepsilon)|A^\mu|B(p) >= -iv(q^2)\epsilon^{\mu\nu\alpha\beta}\varepsilon^*_\nu(p+p')_\alpha(p-p')_\beta \quad (580)$$

In HQET models,

$$\frac{< D_1(v',\varepsilon)|V^\mu|B(v) >}{\sqrt{m_{D_1}m_B}} = f_{V_1}\varepsilon^{*\mu} + (f_{V_2}v^\mu + f_{V_3}v'^\mu)(\varepsilon^*\cdot v) \quad (581)$$

$$\frac{< D_1(v',\varepsilon)|A^\mu|B(v) >}{\sqrt{m_{D_1}m_B}} = if_A\epsilon^{\mu\nu\alpha\beta}\varepsilon^*_\nu v_\alpha v'_\beta \quad (582)$$

We can relate the form factors as we did in the $B \to D^*\ell\nu$ case

$$f_A = m_B R(1+r)v \quad (583)$$

and

$$f_{V_1} = \frac{2}{m_B R(1+r)}r \quad (584)$$

$$f_{V_3} + rf_{V_2} = m_B R(1+r)s_+ \quad (585)$$

The differential decay rate is given by

$$\frac{d\Gamma(B\to D_1\ell\nu)}{dw} = \frac{G_F^2|V_{cb}|^2m_B^5}{48\pi^3}r^3(w^2-1)^{1/2}\,\mathcal{J}_{D_1}(w) \quad (586)$$

where

$$\begin{aligned}\mathcal{J}_{D_1}(w) = &\left[(w-r)f_{V_1} + (w^2-1)(f_{V_3}+rf_{V_2})\right]^2\\ &+2(1-2rw+r^2)[f_{V_1}^2 + (w^2-1)f_A^2]\end{aligned} \quad (587)$$

H.1.6 $B \to D_2^*\ell\nu$

In the ISGW2 model, the matrix elements are given by

$$< D_2^*(p',\varepsilon)|V^\mu|B(p) >= -ih(q^2)\epsilon^{\mu\nu\alpha\beta}\varepsilon^*_{\nu\sigma}p^\sigma(p+p')_\alpha(p-p')_\beta \quad (588)$$

$$\begin{aligned}&< D_2^*(p',\varepsilon)|A^\mu|B(p) >\\ &= k(q^2)\varepsilon^{*\mu\alpha}p_\alpha + b_+(q^2)\varepsilon^*_{\alpha\beta}p^\alpha p^\beta(p+p')^\mu + b_-(q^2)\varepsilon^*_{\alpha\beta}p^\alpha p^\beta(p-p')^\mu\end{aligned} \quad (589)$$

In HQET models,

$$\frac{< D_2^*(v',\varepsilon)|V^\mu|B(v) >}{\sqrt{m_{D_2^*}m_B}} = ik_V\epsilon^{\mu\nu\alpha\beta}\varepsilon^*_{\nu\sigma}v^\sigma v_\alpha v'_\beta \quad (590)$$

$$\frac{< D_2^*(v',\varepsilon)|A^\mu|B(v) >}{\sqrt{m_{D_2^*}m_B}} = k_{A_1}\varepsilon^{*\mu\alpha}v_\alpha + (k_{A_2}v^\mu + k_{A_3}v'^\mu)\varepsilon^{*\alpha\beta}v_\alpha v'_\beta \quad (591)$$

We can relate the form factors as we did in the $B \to D^*\ell\nu$ case. Notice that we pick up an extra m_B from $\varepsilon^{*\mu\alpha}p_\alpha$.

$$k_V = m_B^2 R(1+r)v \tag{592}$$

and

$$k_{A_1} = \frac{2}{R(1+r)} r \tag{593}$$

$$k_{A_3} + r k_{A_2} = m_B^2 R(1+r)s_+ \tag{594}$$

The differential decay rate is given by

$$\frac{d\Gamma(B \to D_2^*\ell\nu)}{dw} = \frac{G_F^2 |V_{cb}|^2 m_B^5}{48\pi^3} r^3 (w^2-1)^{3/2}\ \mathcal{J}_{D_2^*}(w) \tag{595}$$

where

$$\begin{aligned}\mathcal{J}_{D_2^*}(w) = \frac{2}{3}\left[(w-r)k_{A_1} + (w^2-1)(k_{A_3} + r k_{A_2})\right]^2 \\ +(1-2rw+r^2)[k_{A_1}^2 + (w^2-1)k_V^2]\end{aligned} \tag{596}$$

H.2 Traditional notation

We summarize a traditional notation of form factors and decay rates as a reference.

H.2.1 $B \to D\ell\nu$

Traditionally, the form factors $F_0(q^2)$ and $F_1(q^2)$ are used.

$$\begin{aligned}&< D(p')|V^\mu|B(p) > \\ &= F_1(q^2)\left[(p+p')^\mu - \tfrac{m_B^2 - m_D^2}{q^2} q^\mu\right] + F_0(q^2)\tfrac{m_B^2 - m_D^2}{q^2} q^\mu\end{aligned} \tag{597}$$

where

$$q^\mu = p^\mu - p'^\mu \tag{598}$$

We can relate these form factors with $f_+(q^2)$ and $f_-(q^2)$

$$\begin{aligned}F_1(q^2) &= f_+(q^2) \\ F_0(q^2) &= f_+(q^2) + \tfrac{q^2}{m_B^2 - m_D^2} f_-(q^2)\end{aligned} \tag{599}$$

The form factors $F_1(q^2)$ and $F_0(q^2)$ can be associated with the exchange of particles with quantum numbers $J^P = 1^-$ and $J^P = 0^+$, respectively. There is no singular behavior at $q^2 = 0$ because $F_1(0) = F_0(0)$. In practice the terms proportional to q^μ are nearly always negligible. Thus

$$< D(p')|V^\mu|B(p) >= F_1(q^2)(p+p')^\mu \tag{600}$$

or

$$< D(p')|V^\mu|B(p) >= f_+(q^2)(p+p')^\mu \tag{601}$$

The differential decay rate is given by

$$\begin{aligned}\frac{d\Gamma(B\to D\ell\nu)}{dq^2} &= \frac{G_F^2|V_{cb}|^2}{24\pi^3}|\vec{P}_D|^3|f_+(q^2)|^2 \\ &= \frac{G_F^2|V_{cb}|^2}{192\pi^3 m_B^3}\left[(q^2-m_B^2-m_D^2)^2-4m_B^2m_D^2\right]^{3/2}|f_+(q^2)|^2\end{aligned} \tag{602}$$

where we used the following calculation. In the B rest frame,

$$p=(m_B,\vec{0}), \quad p'=(\sqrt{m_D^2+|\vec{P}_D|^2},\vec{p}') \tag{603}$$

Thus

$$\begin{aligned}&q^2=(p-p')^2=p^2+p'^2-2p\cdot p'=m_B^2+m_D^2-2m_B\sqrt{m_D^2+|\vec{P}_D|^2} \\ &\Rightarrow 4m_B^2\left(m_D^2+|\vec{P}_D|^2\right)=(q^2-m_B^2-m_D^2)^2 \\ &\Rightarrow |\vec{P}_D|=\tfrac{1}{2m_B}\left[(q^2-m_B^2-m_D^2)^2-4m_B^2m_D^2\right]^{1/2}\end{aligned} \tag{604}$$

We can derive $\frac{d\Gamma(B\to D\ell\nu)}{dq^2}$ from $\frac{d\Gamma(B\to D\ell\nu)}{dw}$ (Equation (546)). Since

$$w=\frac{m_B^2+m_D^2-q^2}{2m_Bm_D} \quad\Rightarrow\quad dw=-\frac{dq^2}{2m_Bm_D} \tag{605}$$

the left-hand side is

$$\frac{d\Gamma(B\to D\ell\nu)}{dw}=2m_Bm_D\frac{d\Gamma(B\to D\ell\nu)}{dq^2} \tag{606}$$

where we removed a negative sign because it is not relevant to the decay rate, which is positive. The right-hand side is

$$\begin{aligned}&\frac{G_F^2|V_{cb}|^2m_B^5}{48\pi^3}r^3(w^2-1)^{3/2}|(1+r)h_+-(1-r)h_-|^2 \\ &\quad=\frac{G_F^2|V_{cb}|^2m_B^5}{48\pi^3}\left(\frac{m_D}{m_B}\right)^3\left[\left(\frac{m_B^2+m_D^2-q^2}{2m_Bm_D}\right)^2-1\right]^{3/2} \\ &\qquad\times\left|\left(1+\frac{m_D}{m_B}\right)h_+-\left(1-\frac{m_D}{m_B}\right)h_-\right|^2 \\ &=\frac{G_F^2|V_{cb}|^2}{48\pi^3}\frac{m_B^5m_D^3(m_B+m_D)^2}{m_B^3(8m_B^3m_D^3)m_B^2}[(m_B^2+m_D^2-q^2)^2-4m_B^2m_D^2]^{3/2} \\ &\qquad\times\left|h_+-\frac{m_B-m_D}{m_B+m_D}h_-\right|^2 \\ &=\frac{G_F^2|V_{cb}|^2}{192\pi^3m_B^3}\frac{(m_B+m_D)^2}{2}[(m_B^2+m_D^2-q^2)^2-4m_B^2m_D^2]^{3/2} \\ &\qquad\times\left|\frac{2\sqrt{m_Bm_D}}{m_B+m_D}f_+\right|^2 \\ &=2m_Bm_D\frac{G_F^2|V_{cb}|^2}{192\pi^3m_B^3}[(m_B^2+m_D^2-q^2)^2-4m_B^2m_D^2]^{3/2}|f_+|^2\end{aligned} \tag{607}$$

Thus, we recover

$$\frac{d\Gamma(B \to D\ell\nu)}{dq^2} = \frac{G_F^2|V_{cb}|^2}{192\pi^3 m_B^3}[(m_B^2 + m_D^2 - q^2)^2 - 4m_B^2 m_D^2]^{3/2}|f_+|^2 \tag{608}$$

H.2.2 $B \to D^*\ell\nu$

In this case

$$< D^*(p', \varepsilon)|V^\mu|B(p) >= \frac{2i\epsilon^{\mu\nu\alpha\beta}}{m_B + m_{D^*}}\varepsilon_\nu^* p'_\alpha p_\beta V(q^2) \tag{609}$$

and

$$\begin{aligned} < D^*(p', \varepsilon)|A^\mu|B(p) >= & -(m_B + m_{D^*})\varepsilon^{*\mu}A_1(q^2) \\ & + \frac{\varepsilon^* \cdot q}{m_B + m_{D^*}}(p + p')^\mu A_2(q^2) \\ & + 2m_{D^*}\frac{\varepsilon^* \cdot q}{q^2}q^\mu A_3(q^2) \\ & - 2m_{D^*}\frac{\varepsilon^* \cdot q}{q^2}q^\mu A_0(q^2) \end{aligned} \tag{610}$$

where

$$A_3(q^2) = \frac{m_B + m_{D^*}}{2m_{D^*}}A_1(q^2) - \frac{m_B - m_{D^*}}{2m_{D^*}}A_2(q^2) \tag{611}$$

with $A_0(0) = A_3(0)$. The form factors $A_1(q^2)$ and $A_2(q^2)$ can be associated with the exchange of particles with quantum numbers $J^P = 1^+$, whereas $V(q^2)$ is associated with $J^P = 1^-$.
We can relate these form factors with $g(q^2)$, $f(q^2)$, $a_+(q^2)$ and $a_-(q^2)$

$$\begin{aligned} V(q^2) &= (m_B + m_{D^*})g(q^2) \\ A_1(q^2) &= \tfrac{1}{m_B + m_{D^*}}f(q^2) \\ A_2(q^2) &= (m_B + m_{D^*})a_+(q^2) \\ A_3(q^2) - A_0(q^2) &= \tfrac{q^2}{2m_{D^*}}a_-(q^2) \end{aligned} \tag{612}$$

Here, we used

$$\begin{aligned} \epsilon^{\mu\nu\alpha\beta}p_\alpha p_\beta &= \epsilon^{\mu\nu\alpha\beta}p'_\alpha p'_\beta = 0 \\ \epsilon^{\mu\nu\alpha\beta}p_\alpha p'_\beta &= -\epsilon^{\mu\nu\alpha\beta}p'_\alpha p_\beta \end{aligned} \tag{613}$$

Again, terms proportional to q^μ only play an important role only for the case $l = \tau$. Thus those are negligible in our case

$$\begin{aligned} < D^*(p', \varepsilon)|A^\mu|B(p) >= & -(m_B + m_{D^*})\varepsilon^{*\mu}A_1(q^2) \\ & + \frac{\varepsilon^* \cdot q}{m_B + m_{D^*}}(p + p')^\mu A_2(q^2) \end{aligned} \tag{614}$$

or

$$< D^*(p', \varepsilon)|A^\mu|B(p) >= \varepsilon^{*\mu}f(q^2) + \varepsilon^* \cdot q(p + p')^\mu a_+(q^2) \tag{615}$$

H.3 ISGW2 model

ISGW2 model [32][33] is a quark model before the Heavy Quark Effective Theory (HQET) Form Factors (FF) are developed. It provides a method to calculate $B \to D^{(*,**)}\ell\nu$ decay FF. In this model, the quark-model B and D masses are defined as

$$\begin{aligned} \tilde{m}_B &= m_b + m_u = m_b + m_d \\ \tilde{m}_D &= m_c + m_u = m_c + m_d \end{aligned} \tag{616}$$

where m_u, m_d, m_c and m_b are u, d, c and b quark masses, respectively. In ISGW2 model,

$$\begin{aligned} m_d &= m_u = 0.33\text{GeV} \\ m_c &= 1.82\text{GeV} \\ m_b &= 5.20\text{GeV} \end{aligned} \tag{617}$$

are used. Using, these quark masses, ISGW2 define

$$\mu_\pm = \left(\frac{1}{m_c} \pm \frac{1}{m_b}\right)^{-1} \tag{618}$$

The hyperfine-averaged physical mass of a HQS multiplet with light degrees of freedom having angular momentum j_l is

$$\bar{m}_{j_l} = \frac{j_l+1}{2j_l+1} m_{J=j_l+\frac{1}{2}} + \frac{j_l}{2j_l+1} m_{J=j_l-\frac{1}{2}} \tag{619}$$

For example

$$\begin{aligned} \bar{m}_B &= \tfrac{3}{4}m_B + \tfrac{1}{4}m_{B^*} = 5.31 \\ \bar{m}_D &= \bar{m}_{D^*} = \tfrac{3}{4}m_D + \tfrac{1}{4}m_{D^*} \\ \bar{m}_{D_0^*} &= \bar{m}_{D_1{}'} = \tfrac{3}{4}m_{D_1'} + \tfrac{1}{4}m_{D_0^*} \\ \bar{m}_{D_1} &= \bar{m}_{D_2^*} = \tfrac{5}{8}m_{D_2^*} + \tfrac{3}{8}m_{D_1} \end{aligned} \tag{620}$$

where

$$\begin{aligned} m_B &= 5.27\text{GeV}, \quad & m_{B^*} &= 5.33\text{GeV} \\ m_D &= 1.87\text{GeV}, \quad & m_{D^*} &= 2.01\text{GeV} \\ m_{D_0^*} &= 2.40\text{GeV}, \quad & m_{D_1'} &= 2.49\text{GeV} \\ m_{D_1} &= 2.42\text{GeV}, \quad & m_{D_2^*} &= 2.46\text{GeV} \end{aligned} \tag{621}$$

There are also parameters β in the wave functions, and those values in the ISGW2 model are

$$\begin{aligned} \beta_B &= 0.431\text{GeV} \\ \beta_D &= 0.45\text{GeV} \\ \beta_{D^*} &= 0.38\text{GeV} \\ \beta_{D^{**}} &= 0.33\text{GeV} \end{aligned} \tag{622}$$

Also, β_{BX}^2 ($X = D$, D^* or D^{**}) is defined as

$$\beta_{BX}^2 \equiv \frac{1}{2}(\beta_B^2 + \beta_X^2) \tag{623}$$

The momentum transfer is

$$t = (p_B - p_D)^2 = q^2 \tag{624}$$

and the maximum momentum transfer is

$$t_m = (m_B - m_D)^2 \tag{625}$$

where m_D can be m_{D^*} or $m_{D^{**}}$.
In ISGW2 model, the factor $F_n^{(\alpha)}$ is defined as

$$F_n^{(\alpha)} = \left(\frac{\bar{m}_B}{\tilde{m}_B}\right)^{n_B(\alpha)} \left(\frac{\bar{m}_D}{\tilde{m}_D}\right)^{n_X(\alpha)} \left(\frac{\tilde{m}_D}{\tilde{m}_B}\right)^{1/2} \left(\frac{\beta_B \beta_D}{\beta_{BD}^2}\right)^{n/2} \left[1 + \frac{1}{6N} r^2 (t_m - t)\right]^{-N} \tag{626}$$

where $N = 2 + n + n'$. n and n' are the harmonic oscillator quantum numbers of the initial and final wave-functions. Therefore, $N = 2$ for S wave to S wave ($B \to D$ or D^*), and $N = 3$ for S wave to P wave ($B \to D^{**}$). $n_B(\alpha)$ and $n_X(\alpha)$ is given in the table

Form factors (α)	$n_B(\alpha)$	$n_X(\alpha)$
$f_+ + f_-$	-1/2	+1/2
$f_+ - f_-$	+1/2	-1/2
g	-1/2	-1/2
f	+1/2	+1/2
$a_+ + a_-$	-3/2	+1/2
$a_+ - a_-$	-1/2	-1/2
$u_+ + u_-$	-1/2	+1/2
$u_+ - u_-$	+1/2	-1/2
$l_{(3/2,1/2)}, r$	+1/2	+1/2
$c_{+(3/2,1/2)} + c_{-(3/2,1/2)}, s_+ + s_-$	-3/2	+1/2
$c_{+(3/2,1/2)} - c_{-(3/2,1/2)}, s_+ - s_-$	-1/2	-1/2
$q_{(3/2,1/2)}, v$	-1/2	-1/2
h	-3/2	-1/2
k	-1/2	+1/2
$b_+ + b_-$	-5/2	+1/2
$b_+ - b_-$	-3/2	-1/2

The form factors in this table are defined later. r^2 is

$$r^2 = \frac{3}{4 m_b m_c} + \frac{3 m_d^2}{2 \bar{m}_B \bar{m}_D \beta_{BD}^2} + \frac{1}{\bar{m}_B \bar{m}_D} \left(\frac{16}{33 - 2N_f}\right) \ln\left[\frac{\alpha_s(\mu_{QM})}{\alpha_s(m_c)}\right] \tag{627}$$

where, if a scale $\mu < 0.6$ GeV,

$$\alpha_s(\mu) = 0.6 \tag{628}$$

and if $\mu > 0.6$ GeV,

$$\alpha_s(\mu) = \frac{12\pi}{33-2N_f}\left[\ln\left(\frac{\mu^2}{\Lambda^2_{QCD}}\right)\right]^{-1} \tag{629}$$

where N_f is the number of active flavors below the scale μ. For $\mu = m_c$, $N_f = 3$, and for $\mu = m_b$, $N_f = 4$. Thus, $N_f = 3$ for $b \to c$ decays. The constants in the above equations are

$$\begin{aligned} \mu_{QM} &= 0.1\mathrm{GeV} \\ \Lambda^2_{QCD} &= 0.04\mathrm{GeV}^2 \end{aligned} \tag{630}$$

The factor $R^{(\alpha)}$ is defined as

$$R^{(\alpha)} = C_{cb}\left[f^{(\alpha)} + \tilde{\beta}^{(\alpha)}_{cb}(w)\frac{\alpha_s\left(\sqrt{m_b m_c}\right)}{\pi}\right] \tag{631}$$

where $f^{(\alpha)} = 0$ for $a_+ + a_-$ and $f^{(\alpha)} = 1$ for others.
Here

$$C_{cb} = \left[\frac{\alpha_s(m_b)}{\alpha_s(m_c)}\right]^{a_I}\left[\frac{\alpha_s(m_c)}{\alpha_s(\mu_{QM})}\right]^{a_L(w)} \tag{632}$$

is independent of α and has

$$a_I = -\frac{6}{33-2N_f} \tag{633}$$

and

$$a_L(w) = -\frac{8}{33-2N'_f}[wr(w)-1] \tag{634}$$

with

$$r(w) = \frac{1}{\sqrt{w^2-1}}\ln\left(w+\sqrt{w^2-1}\right) \tag{635}$$

and

$$w = 1 + \frac{t_m - t}{2m_B m_D} \tag{636}$$

where m_D may be m^*_D or m^{**}_D depending on the decay modes. N_f is the number of active flavors below the scale m_b and N'_f is the number of active flavors below the scale m_c. Thus, $N_f = 4$ and $N'_f = 3$. In ISGW2, $\tilde{w}$ is defined as

$$\tilde{w} = 1 + \frac{t_m - t}{2\bar{m}_B\bar{m}_D} \tag{637}$$

For w near 1

$$\left[\frac{\alpha_s(m_c)}{\alpha_s(\mu_{QM})}\right]^{a_L(w)} = 1 - \frac{2}{3}\left(\frac{8}{33-2N'_f}\right)\ln\left[\frac{\alpha_s(\mu_{QM})}{\alpha_s(m_c)}\right](w-1) \tag{638}$$

In SP5/SP6, $\left[\frac{\alpha_s(m_c)}{\alpha_s(\mu_{QM})}\right]^{a_L(w)} = 1$ was used.

At $w = 1$, $\tilde{\beta}_{cb}$ are

$$\begin{array}{l}
\tilde{\beta}_{cb}^{(f_+ + f_-)}(1) = \gamma_{cb} - \frac{2}{3}\chi_{cb} \\
\tilde{\beta}_{cb}^{(f_+ - f_-)}(1) = \gamma_{cb} + \frac{2}{3}\chi_{cb} \\
\tilde{\beta}_{cb}^{(g)}(1) = \gamma_{cb} + \frac{2}{3} \\
\tilde{\beta}_{cb}^{(f)}(1) = \gamma_{cb} - \frac{2}{3} \\
\tilde{\beta}_{cb}^{(a_+ + a_-)}(1) = -1 - \chi_{cb} + \frac{4}{3}\frac{1}{(1-z_{cb})} + \frac{2}{3}\frac{1+z_{cb}}{(1-z_{cb})^2}\gamma_{cb} \\
\tilde{\beta}_{cb}^{(a_+ - a_-)}(1) = -\frac{1}{3} - \chi_{cb} + \frac{4}{3}\frac{1}{(1-z_{cb})} + \left[1 - \frac{2}{3}\frac{1+z_{cb}}{(1-z_{cb})^2}\right]\gamma_{cb}
\end{array} \tag{639}$$

where

$$\gamma_{cb} = \frac{2z_{cb}}{1 - z_{cb}} \ln\left(\frac{1}{z_{cb}}\right) - 2 \tag{640}$$

and

$$\chi_{cb} = -1 - \frac{\gamma_{cb}}{1 - z_{cb}} \tag{641}$$

with

$$z_{cb} = \frac{m_c}{m_b} \tag{642}$$

w dependence of $\tilde{\beta}$ is weak and negligible.

In ISGW [33], LL-coupling was used, and ISGW2 [32] also follows the convention. But, ISGW2 aware that jj-coupling is a better representation of heavy-light mesons. Thus, ISGW2 also gives jj-coupling type of form factors for D_1 and D_1'.

H.3.1 $B \to D\ell\nu$ (1^2S_0)

Matrix element is

$$< D(p')|V^\mu|B(p) >= f_+(q^2)(p + p')^\mu + f_-(q^2)(p - p')^\mu \tag{643}$$

where f_+ and f_- are the form factors. These are calculated as follows :

$$f_+ + f_- = \left[2 - \frac{\tilde{m}_D}{m_c}\left(1 - \frac{m_d m_c}{2\mu_+ \tilde{m}_D}\frac{\beta_B^2}{\beta_{BD}^2}\right)\right] F_3^{(f_+ + f_-)} R^{(f_+ + f_-)} \tag{644}$$

and

$$f_+ - f_- = \frac{\tilde{m}_B}{m_c}\left(1 - \frac{m_d m_c}{2\mu_+ \tilde{m}_D}\frac{\beta_B^2}{\beta_{BD}^2}\right) F_3^{(f_+ - f_-)} R^{(f_+ - f_-)} \tag{645}$$

Thus, we get f_+ and f_- from these two equations. For example,

$$f_+ = \frac{(f_+ + f_-) + (f_+ - f_-)}{2} \tag{646}$$

H.3.2 $B \to D^* \ell\nu$ (1^3S_0)

Matrix element is

$$< D^*(p', \varepsilon)|V^\mu|B(p) >= i\epsilon^{\mu\nu\alpha\beta}\varepsilon^*_\nu(p+p')_\alpha(p-p')_\beta g(q^2) \tag{647}$$

and

$$< D^*(p', \varepsilon)|A^\mu|B(p) >= \varepsilon^{*\mu} f(q^2) + \varepsilon^* \cdot p(p+p')^\mu a_+(q^2) + \varepsilon^* \cdot p(p-p')^\mu a_-(q^2) \tag{648}$$

Form factors g, f, a_+ and a_- are given by the following equations.

$$f = C_f \tilde{m}_B \left[(1+\tilde{w}) + \frac{m_d(\tilde{w}-1)}{2\mu_+}\right] F_3^{(f)} R^{(f)} \tag{649}$$

where $C_f = 0.989$ for $B \to D^*$.

$$g = \frac{1}{2}\left[\frac{1}{m_c} - \frac{m_d \beta_B^2}{2\mu_- \tilde{m}_D \beta_{BD}^2}\right] F_3^{(g)} R^{(g)} \tag{650}$$

$$\begin{aligned} & a_+ + a_- \\ & = C_{cb}\left[\frac{m_d}{(1+\tilde{w})m_c m_b}\frac{\beta_D^2}{\beta_{BD}^2}\left(1 - \frac{m_d}{2\tilde{m}_B}\frac{\beta_D^2}{\beta_{BD}^2}\right) + \tilde{\beta}^{(a_+ + a_-)}\frac{\alpha_s}{\pi}\tilde{m}_B\right] \\ & \qquad F_3^{(a_+ + a_-)} \end{aligned} \tag{651}$$

$$\begin{aligned} & a_+ - a_- \\ & = -\frac{1}{\tilde{m}_D}\left[\frac{\tilde{m}_B}{m_b} - \frac{m_d}{2\mu_+}\frac{\beta_D^2}{\beta_{BD}^2} + \frac{\tilde{w} m_d \tilde{m}_B}{(1+\tilde{w})m_c m_b}\frac{\beta_D^2}{\beta_{BD}^2}\left(1 - \frac{m_d}{2\tilde{m}_B}\frac{\beta_D^2}{\beta_{BD}^2}\right)\right] \\ & \qquad F_3^{(a_+ - a_-)} R^{(a_+ - a_-)} \end{aligned} \tag{652}$$

H.3.3 $B \to D_0^* \ell\nu$ (1^3P_0)

Matrix element is

$$< D_0^*(p')|V^\mu|B(p) >= 0 \tag{653}$$

and

$$< D_0^*(p')|A^\mu|B(p) >= u_+(q^2)(p+p')^\mu + u_-(q^2)(p-p')^\mu \tag{654}$$

Form factors u_+ and u_- are given by the following two equations.

$$u_+ + u_- = -\sqrt{\frac{2}{3}}\frac{m_d}{\beta_B} F_5^{(u_+ + u_-)} \tag{655}$$

$$u_+ - u_- = \sqrt{\frac{2}{3}}\frac{m_d \tilde{m}_B}{\beta_B \tilde{m}_D} F_5^{(u_+ - u_-)} \tag{656}$$

H.3.4 $B \to D_1' \ell\nu$ (1^3P_1)

Matrix element is

$$< D_1'(p',\varepsilon)|V^\mu|B(p) >= \varepsilon^{*\mu} l(q^2) + \varepsilon^* \cdot p(p+p')^\mu c_+(q^2) + \varepsilon^* \cdot p(p-p')^\mu c_-(q^2) \quad (657)$$

and

$$< D_1'(p',\varepsilon)|A^\mu|B(p) >= i\epsilon^{\mu\nu\alpha\beta}\varepsilon^*_\nu (p+p')_\alpha (p-p')_\beta q(q^2) \quad (658)$$

Form factors l, c_+, c_- and q are given by the following equations.

$$q = -\frac{m_d}{2\tilde{m}_D\beta_B}\left(\frac{5+\tilde{w}}{6}\right) F_5^{(q)} \quad (659)$$

$$l = -\tilde{m}_B\beta_B\left[\frac{1}{\mu_-} + \frac{m_d\tilde{m}_D(\tilde{w}-1)}{\beta_B^2}\left(\frac{5+\tilde{w}}{6m_c} - \frac{1}{2\mu_-}\frac{m_d}{\tilde{m}_D}\frac{\beta_B^2}{\beta_{BD}^2}\right)\right] F_5^{(l)} \quad (660)$$

$$c_+ + c_- = -\frac{m_d\tilde{m}_D}{2m_c\tilde{m}_B\beta_B}\left(1 - \frac{m_d m_c}{2\tilde{m}_D\mu_-}\frac{\beta_B^2}{\beta_{BD}^2}\right) F_5^{(c_+ + c_-)} \quad (661)$$

$$c_+ - c_- = -\frac{m_d\tilde{m}_D}{2m_c\tilde{m}_B\beta_B}\left(\frac{\tilde{w}+2}{3} - \frac{m_d m_c}{2\tilde{m}_D\mu_-}\frac{\beta_B^2}{\beta_{BD}^2}\right) F_5^{(c_+ - c_-)} \quad (662)$$

H.3.5 $B \to D_1 \ell\nu$ (1^1P_1)

Matrix element is

$$< D_1'(p',\varepsilon)|V^\mu|B(p) >= \varepsilon^{*\mu} r(q^2) + \varepsilon^* \cdot p(p+p')^\mu s_+(q^2) + \varepsilon^* \cdot p(p-p')^\mu s_-(q^2) \quad (663)$$

and

$$< D_1'(p',\varepsilon)|A^\mu|B(p) >= i\epsilon^{\mu\nu\alpha\beta}\varepsilon^*_\nu (p+p')_\alpha (p-p')_\beta v(q^2) \quad (664)$$

Form factors r, s_+, s_- and v are given by the following equations.

$$v = \left[\frac{\tilde{m}_B\beta_B}{4\sqrt{2}m_b m_c\tilde{m}_D} + \frac{(\tilde{w}-1)}{6\sqrt{2}}\frac{m_d}{\tilde{m}_D\beta_B}\right] F_5^{(v)} \quad (665)$$

$$r = \frac{\tilde{m}_B\beta_B}{\sqrt{2}}\left[\frac{1}{\mu_+} + \frac{m_d\tilde{m}_D}{3m_c\beta_B^2}(\tilde{w}-1)^2\right] F_5^{(r)} \quad (666)$$

$$s_+ + s_- = \frac{m_d}{\sqrt{2}\tilde{m}_B\beta_B}\left(1 - \frac{m_d}{m_c} + \frac{m_d}{2\mu_+}\frac{\beta_B^2}{\beta_{BD}^2}\right) F_5^{(s_+ + s_-)} \quad (667)$$

$$s_+ - s_- = \frac{m_d}{\sqrt{2}m_c\beta_B}\left(\frac{4-\tilde{w}}{3} - \frac{m_d m_c}{2\tilde{m}_D\mu_+}\frac{\beta_B^2}{\beta_{BD}^2}\right) F_5^{(s_+ - s_-)} \quad (668)$$

H.3.6 $B \to D_2^*\ell\nu$ (1^3P_2)

Matrix element is

$$< D_2^*(p',\varepsilon)|V^\mu|B(p) >= i\epsilon^{\mu\nu\alpha\beta}\varepsilon^*_{\nu\sigma}p^\sigma(p+p')_\alpha(p-p')_\beta h(q^2) \tag{669}$$

and

$$\begin{aligned}&< D_2^*(p',\varepsilon)|A^\mu|B(p) >\\ &= \varepsilon^{*\mu\sigma}p_\sigma k(q^2) + \varepsilon^*_{\alpha\beta}p^\alpha p^\beta(p+p')^\mu b_+(q^2) + \varepsilon^*_{\alpha\beta}p^\alpha p^\beta(p-p')^\mu b_-(q^2)\end{aligned} \tag{670}$$

Form factors h, b_+, b_- and k are given by the following equations.

$$h = \frac{m_d}{2\sqrt{2}\tilde{m}_B\beta_B}\left[\frac{1}{m_c} - \frac{m_d\beta_B^2}{2\mu_-\tilde{m}_D\beta_{BD}^2}\right]F_5^{(h)} \tag{671}$$

$$k = \frac{m_d}{\sqrt{2}\beta_B}(1+\tilde{w})F_5^{(k)} \tag{672}$$

$$b_+ + b_- = \frac{m_d^2}{4\sqrt{2}m_c m_b\tilde{m}_B\beta_B}\frac{\beta_D^2}{\beta_{BD}^2}\left(1 - \frac{m_d}{2\tilde{m}_B}\frac{\beta_D^2}{\beta_{BD}^2}\right)F_5^{(b_++b_-)} \tag{673}$$

$$\begin{aligned}&b_+ - b_-\\ &= -\frac{m_d}{\sqrt{2}m_b\tilde{m}_D\beta_B}\left[1 - \frac{m_d m_b}{2\mu_+\tilde{m}_B}\frac{\beta_D^2}{\beta_{BD}^2} + \frac{m_d}{4m_c}\frac{\beta_D^2}{\beta_{BD}^2}\left(1 - \frac{m_d}{2\tilde{m}_B}\frac{\beta_D^2}{\beta_{BD}^2}\right)\right]\\ &\qquad F_5^{(b_+-b_-)}\end{aligned} \tag{674}$$

H.3.7 $B \to D_1^*\ell\nu$ $(\frac{1}{2}^+)$

Form factors are

$$q_{1/2} = \sqrt{\frac{1}{6}}\frac{m_d}{\tilde{m}_D\beta_B}\left(1 - \frac{\beta_B^2\tilde{m}_B}{4m_d m_c m_b}\right)F_5^{(q_{1/2})} \tag{675}$$

$$l_{1/2} = \sqrt{\frac{2}{3}}\tilde{m}_B\beta_B\left[\frac{1}{2m_c} - \frac{3}{2m_b} + \frac{m_d\tilde{m}_D(\tilde{w}-1)}{\beta_B^2}\left(\frac{1}{m_c} - \frac{1}{2\mu_-}\frac{m_d}{\tilde{m}_D}\frac{\beta_B^2}{\beta_{BD}^2}\right)\right]F_5^{(l_{1/2})} \tag{676}$$

$$c_{1/2+} + c_{1/2-} = \frac{m_d^2\beta_D^2}{\sqrt{6}m_c\tilde{m}_B\beta_B\beta_{BD}^2}F_5^{(c_{1/2+}+c_{1/2-})} \tag{677}$$

$$c_{1/2+} - c_{1/2-} = -\sqrt{\frac{2}{3}}\frac{m_d}{2\tilde{m}_D\beta_B}\left(1 + \frac{m_d}{2m_c}\frac{\beta_D^2}{\beta_{BD}^2}\right)F_5^{(c_{1/2+}-c_{1/2-})} \tag{678}$$

H.3.8 $B \to D_1\ell\nu$ $(\frac{3}{2}^+)$

Form factors are

$$q_{3/2} = -\frac{1}{2\sqrt{3}}\frac{m_d}{\tilde{m}_D\beta_B}\left(\frac{1+\tilde{w}}{2} + \frac{\beta_B^2\tilde{m}_B}{2m_d m_c m_b}\right)F_5^{(q_{3/2})} \tag{679}$$

$$l_{3/2} = -\frac{2}{\sqrt{3}}\tilde{m}_B\beta_B\left[\frac{1}{m_c} + \frac{m_d\tilde{m}_D(\tilde{w}-1)}{2\beta_B^2}\left(\frac{\tilde{w}+1}{2m_c} - \frac{1}{2\mu_-}\frac{m_d}{\tilde{m}_D}\frac{\beta_B^2}{\beta_{BD}^2}\right)\right]F_5^{(l_{3/2})} \tag{680}$$

$$c_{3/2+} + c_{3/2-} = -\frac{\sqrt{3}m_d}{2\tilde{m}_B\beta_B}\left[1 - \frac{m_d}{2m_c} - \frac{m_d}{3}\frac{\beta_B^2}{\beta_{BD}^2}\left(\frac{1}{2\mu_-} - \frac{1}{\mu_+}\right)\right]F_5^{(c_{3/2+}+c_{3/2-})} \tag{681}$$

$$c_{3/2+} - c_{3/2-} = -\frac{m_d}{2\sqrt{3}\tilde{m}_D\beta_B}\left[\frac{(2-\tilde{w})\tilde{m}_D}{m_c} + \frac{m_d\beta_B^2}{\beta_{BD}^2}\left(\frac{1}{2\mu_-} - \frac{1}{\mu_+}\right)\right]F_5^{(c_{3/2+}-c_{3/2-})} \tag{682}$$

H.4 HQET model

Details of HQET model is described in [34][35]. We will summarize the part which is related to our analysis.

H.4.1 $B \to D\ell\nu$

In heavy quark limit, the form factors $h_+(w)$ and $h_-(w)$ are

$$h_+(w) = \xi(w), \;\; h_-(w) = 0 \tag{683}$$

where $\xi(w)$ is the Isgur-Wise Function.

$$\xi(w) = \xi(1)[1 - \rho_D^2(w-1)] \tag{684}$$

where ρ_D^2 is the form factor slope. $h_+(1) = \xi(1)$ can be calculated by the Lattice QCD.

H.4.2 $B \to D^*\ell\nu$

The kinematic variables in $B \to D^*\ell\nu$ decays are shown in Figure 57.

- θ_ℓ : Angle between the directions of "the ℓ in the W rest frame" and "the W in the B rest frame".
- θ_V : Angle between the directions of "the D in the D^* rest frame" and "the D^* in the B rest frame".
- χ : Azimuthal angle between the planes formed by "W-ℓ system" and "$D^* - D$ system".

Form factors $V(q^2)$, $A_1(q^2)$ and $A_2(q^2)$ are related to helicity form factors $H_0(q^2)$, $H_+(q^2)$ and $H_-(q^2)$, which correspond to the three allowed polarization state of D^* (one longitudinal and two transverse). A_1 contributes to all three helicity components, A_2 contributes only to the helicity-zero component and V contributes only to the helicity ± 1 components

$$H_+(q^2) = (m_B + m_{D^*})A_1(q^2) - \frac{\sqrt{(q^2 - m_B^2 - m_{D^*}^2)^2 - 4m_B^2 m_{D^*}^2}}{m_B + m_{D^*}} V(q^2) \tag{685}$$

$$H_-(q^2) = (m_B + m_{D^*})A_1(q^2) + \frac{\sqrt{(q^2 - m_B^2 - m_{D^*}^2)^2 - 4m_B^2 m_{D^*}^2}}{m_B + m_{D^*}} V(q^2) \tag{686}$$

$$H_0(q^2) = \frac{1}{2m_{D^*}\sqrt{q^2}} \left[(m_B^2 - m_{D^*}^2 - q^2)(m_B + m_{D^*})A_1(q^2) - \frac{(q^2 - m_B^2 - m_{D^*}^2)^2 - 4m_B^2 m_{D^*}^2}{m_B + m_{D^*}} A_2(q^2) \right] \tag{687}$$

Differential decay rate is given in terms of the helicity form factors,

$$\begin{aligned}
\frac{d\Gamma(B \to D^*\ell\nu)}{dw d\cos\theta_V d\cos\theta_\ell d\chi} = & \frac{3G_F^2}{4(4\pi)^4}|V_{cb}|^2 m_B m_{D^*}^2 \sqrt{w^2-1}(1 - 2wr + r^2)\times \\
& [(1 - \cos\theta_\ell)^2 \sin^2\theta_V |H_+(w)|^2 \\
& +(1 + \cos\theta_\ell)^2 \sin^2\theta_V |H_-(w)|^2 \\
& +4\sin^2\theta_\ell \cos^2\theta_V |H_0(w)|^2 \\
& -4\sin\theta_\ell(1 - \cos\theta_\ell)\sin\theta_V\cos\theta_V\cos\chi H_+(w)H_0(w) \\
& +4\sin\theta_\ell(1 + \cos\theta_\ell)\sin\theta_V\cos\theta_V\cos\chi H_-(w)H_0(w) \\
& -2\sin^2\theta_\ell \sin^2\theta_V \cos 2\chi H_+(w)H_-(w)]
\end{aligned} \tag{688}$$

$H_i(w)$ are

$$H_i = -m_B \frac{R^*(1-r^2)(w+1)}{2\sqrt{1-2wr+r^2}} h_{A_1}(w)\widetilde{H}_i(w) \tag{689}$$

$h_{A_1}(w)$ is

$$h_{A_1}(w) = h_{A_1}(1)\left[1 - \rho^2(w-1)\right] \tag{690}$$

where ρ^2 is the form factor slope, and $\widetilde{H}_i(w)$ are

$$\begin{aligned}
\widetilde{H}_\pm(w) &= \frac{\sqrt{1-2wr+r^2}}{1-r}\left(1 \mp \sqrt{\frac{w-1}{w+1}}R_1(w)\right) \\
\widetilde{H}_0(w) &= 1 + \frac{w-1}{1-r}\left(1 - R_2(w)\right)
\end{aligned} \tag{691}$$

where R_1 and R_2 are the form factor ratios.

$$R_1 = \frac{h_V}{h_{A_1}}, \quad R_2 = \frac{h_{A_3} + r h_{A_2}}{h_{A_1}} \tag{692}$$

To make the notation simple, we define

$$
\begin{aligned}
&c_L \equiv \cos\theta_\ell \\
&c_V \equiv \cos\theta_V \\
&\tilde{h}_\pm(w) \equiv (1-r)\widetilde{H}_\pm(w) = \sqrt{1-2wr+r^2}\left(1 \mp \sqrt{\tfrac{w-1}{w+1}}R_1\right) \\
&\tilde{h}_0(w) \equiv (1-r)\widetilde{H}_0(w) = (1-r) + (w-1)(1-R_2)
\end{aligned}
\tag{693}
$$

then

$$
\frac{d\Gamma(B \to D^*\ell\nu)}{dw dc_V dc_L d\chi} = f(w) \;\; \left[h_{A_1}(w)\right]^2 g(w) \tag{694}
$$

where

$$
\begin{aligned}
f(w) &\equiv \frac{3G_F^2}{4(4\pi)^4}|V_{cb}|^2 m_B m_{D^*}^2 \sqrt{w^2-1}(1-2wr+r^2) \times \\
&\qquad \left[m_B \frac{2\sqrt{m_B m_{D^*}}}{m_B+m_{D^*}} \frac{(1-r^2)(w+1)}{2\sqrt{1-2wr+r^2}} \frac{1}{(1-r)}\right]^2 \\
&= \frac{3G_F^2}{4(4\pi)^4}|V_{cb}|^2 \frac{m_B^4 m_{D^*}^3}{(m_B+m_{D^*})^2}(1+r)^2(w+1)^2\sqrt{w^2-1} \\
&= \frac{3G_F^2|V_{cb}|^2}{1024\pi^4}\frac{m_B^5 r^3}{(1+r)^2}(1+r)^2(w+1)^2\sqrt{w^2-1} \\
&= \frac{G_F^2|V_{cb}|^2 m_B^5}{48\pi^3} r^3 (w^2-1)^{1/2} \times \frac{9}{64\pi}(w+1)^2
\end{aligned}
\tag{695}
$$

and

$$
\begin{aligned}
g(w) \;\; = \;\; &[(1-c_L)^2(1-c_V^2)\tilde{h}_+^2 + (1+c_L)^2(1-c_V^2)\tilde{h}_-^2 \\
&+4(1-c_L^2)c_V^2\tilde{h}_0^2 - 2(1-c_L^2)(1-c_V^2)\cos 2\chi \tilde{h}_+\tilde{h}_- \\
&-4\sqrt{1-c_L^2}(1-c_L)\sqrt{1-c_V^2}c_V\cos\chi\tilde{h}_+\tilde{h}_0 \\
&+4\sqrt{1-c_L^2}(1+c_L)\sqrt{1-c_V^2}c_V\cos\chi\tilde{h}_-\tilde{h}_0]
\end{aligned}
\tag{696}
$$

Integrating over c_L, c_V and χ

$$
\int_{-1}^{1} dc_L \int_{-1}^{1} dc_V \int_0^{2\pi} d\chi \;\; g(w) = \left[\frac{8}{3}\frac{4}{3}2\pi\tilde{h}_+^2 + \frac{8}{3}\frac{4}{3}2\pi\tilde{h}_-^2 + 4\frac{4}{3}\frac{2}{3}2\pi\tilde{h}_0^2\right] \tag{697}
$$

Thus

$$
\frac{d\Gamma(B \to D^*\ell\nu)}{dw} = \frac{G_F^2|V_{cb}|^2 m_B^5}{48\pi^3} r^3 (w^2-1)^{1/2}\mathcal{J}_{D^*}(w) \tag{698}
$$

where

$$
\begin{aligned}
\mathcal{J}_{D^*}(w) &= \frac{9}{64\pi}(w+1)^2\left[h_{A_1}\right]^2 \frac{64\pi}{9}\left[\tilde{h}_+^2 + \tilde{h}_-^2 + \tilde{h}_0^2\right] \\
&= (w+1)^2\left[h_{A_1}\right]^2\left[\tilde{h}_+^2 + \tilde{h}_-^2 + \tilde{h}_0^2\right] \\
&= (w+1)^2\left[h_{A_1}\right]^2\left[(1-2wr+r^2)\left(1 - \sqrt{\frac{w-1}{w+1}}\frac{h_V}{h_{A_1}}\right)^2\right.
\end{aligned}
$$

$$
\begin{aligned}
&+(1-2wr+r^2)\left(1+\sqrt{\frac{w-1}{w+1}}\frac{h_V}{h_{A_1}}\right)^2 \\
&+\left\{(1-r)+(w-1)\left(1-\frac{h_{A_3}+rh_{A_2}}{h_{A_1}}\right)\right\}^2\Bigg] \\
&=(1-2wr+r^2)\left[\left\{(w+1)h_{A_1}-\sqrt{w^2-1}\,h_V\right\}^2\right. \\
&\qquad\left.+\left\{(w+1)h_{A_1}+\sqrt{w^2-1}\,h_V\right\}^2\right] \\
&\quad+[(1-r)(w+1)h_{A_1} \\
&\qquad+(w^2-1)\{(h_{A_1}-(h_{A_3}+rh_{A_2})\}]^2 \\
&=2(1-2wr+r^2)\left[(w+1)^2h_{A_1}^2+(w^2-1)h_V^2\right] \\
&\quad+\left[(w-r)(w+1)h_{A_1}-(w^2-1)(h_{A_3}+rh_{A_2})\right]^2
\end{aligned} \tag{699}
$$

Thus, we recovered equation (561).

H.5 Leibovich Ligeti Stewart Wise (LLSW) model

Details of LLSW model is described in [41][42]. We will summarize the part which is related to our analysis.
Kinematic variables are w and θ. This θ is the angle between the charged lepton and the charmed meson in the rest frame of the virtual W boson. Thus $\theta = \pi - \theta_\ell$,

$$\cos\theta = \cos(\pi - \theta_\ell) = -\cos\theta_\ell \tag{700}$$

In the paper [42], they use different approximations : Approximation A and B. In Approximation A, they treat $w-1$ as order $\Lambda_{\mathrm{QCD}}/m_Q$ and expand decay rates in these parameters. In Approximation B, they keep the known order $\Lambda_{\mathrm{QCD}}/m_Q$ contributions to form factors as well as the full w-dependence of decay rates.
In the paper some parameters are defined as follows

$$\varepsilon_b \equiv \frac{1}{2m_b}, \quad \varepsilon_c \equiv \frac{1}{2m_c} \tag{701}$$

with numerical values

$$
\begin{aligned}
m_b &= 4.8\mathrm{GeV} \\
m_c &= 1.4\mathrm{GeV}
\end{aligned} \tag{702}
$$

The difference between a hadron mass and a heavy quark mass in the first order :

$$
\begin{aligned}
&\bar{\Lambda} \text{ for ground state doublet } (D \text{ and } D^*) \\
&\bar{\Lambda}' \text{ for exited } \tfrac{3}{2}^+ \text{ doublet } (D_1 \text{ and } D_2^*) \\
&\bar{\Lambda}^* \text{ for exited } \tfrac{1}{2}^+ \text{ doublet } (D_0^* \text{ and } D_1')
\end{aligned} \tag{703}
$$

with numerical values

$$\begin{aligned}
\bar{\Lambda} &= 0.4\text{GeV} \\
\bar{\Lambda}' - \bar{\Lambda} &= 0.39\text{GeV} \\
\bar{\Lambda}^* - \bar{\Lambda} &= 0.35\text{GeV}
\end{aligned} \tag{704}$$

In the paper, they also used the branching fraction

$$\mathcal{B}(B \to D_1 e\bar{\nu}_e) = 0.0060 \tag{705}$$

H.5.1 $B \to D_1\ell\nu$

The matrix elements are

$$\frac{< D_1(v',\varepsilon)|V^\mu|B(v) >}{\sqrt{m_{D_1}m_B}} = f_{V_1}\varepsilon^{*\mu} + (f_{V_2}v^\mu + f_{V_3}v'^\mu)(\varepsilon^* \cdot v) \tag{706}$$

$$\frac{< D_1(v',\varepsilon)|A^\mu|B(v) >}{\sqrt{m_{D_1}m_B}} = if_A\epsilon^{\mu\alpha\beta\gamma}\varepsilon^*_\alpha v_\beta v'_\gamma \tag{707}$$

The differential decay rate is

$$\begin{aligned}
\frac{d^2\Gamma_{D_1}}{dwd\cos\theta} = 3\Gamma_0 r_1^3\sqrt{w^2-1}\{&\sin^2\theta[(w-r_1)f_{V_1} + (w^2-1)(f_{V_3}+r_1f_{V_2})]^2 \\
&+(1-2r_1w+r_1^2)[(1+\cos^2\theta)(f_{V_1}^2+(w^2-1)f_A^2) \\
&-4\cos\theta\sqrt{w^2-1}f_{V_1}f_A]\}
\end{aligned} \tag{708}$$

where

$$\Gamma_0 = \frac{G_F^2|V_{cb}|^2m_B^5}{192\pi^3} \tag{709}$$

and

$$r_1 = \frac{m_{D_1}}{m_B} \tag{710}$$

In approximation B, the form factors are given by

$$\begin{aligned}
\sqrt{6}f_A &= -(w+1)\tau - \varepsilon_b\{(w-1)[(\bar{\Lambda}'+\bar{\Lambda})\tau - (2w+1)\tau_1 - \tau_2] + (w+1)\eta_b\} \\
&\quad -\varepsilon_c[4(w\bar{\Lambda}'-\bar{\Lambda})\tau - 3(w-1)(\tau_1-\tau_2) + (w+1)(\eta_{\text{ke}} - 2\eta_1 - 3\eta_3)] \\
\sqrt{6}f_{V_1} &= (1-w^2)\tau - \varepsilon_b(w^2-1)[(\bar{\Lambda}'+\bar{\Lambda})\tau - (2w+1)\tau_1 - \tau_2 + \eta_b] \\
&\quad -\varepsilon_c[4(w+1)(w\bar{\Lambda}'-\bar{\Lambda})\tau - (w^2-1)(3\tau_1 - 3\tau_2 - \eta_{\text{ke}} + 2\eta_1 + 3\eta_3)] \\
\sqrt{6}f_{V_2} &= -3\tau - 3\varepsilon_b[(\bar{\Lambda}'+\bar{\Lambda})\tau - (2w+1)\tau_1 - \tau_2 + \eta_b] \\
&\quad -\varepsilon_c[(4w-1)\tau_1 + 5\tau_2 + 3\eta_{\text{ke}} + 10\eta_1 + 4(w-1)\eta_2 - 5\eta_3)] \\
\sqrt{6}f_{V_3} &= (w-2)\tau + \varepsilon_b\{(2+w)[(\bar{\Lambda}'+\bar{\Lambda})\tau - (2w+1)\tau_1 - \tau_2] - (2-w)\eta_b\} \\
&\quad +\varepsilon_c[4(w\bar{\Lambda}'-\bar{\Lambda})\tau + (2+w)\tau_1 + (2+3w)\tau_2 \\
&\quad +(w-2)\eta_{\text{ke}} - 2(6+w)\eta_1 - 4(w-1)\eta_2 - (3w-2)\eta_3]
\end{aligned} \tag{711}$$

where τ is the leading $m_Q \to \infty$ Isgur-Wise function, which is assumed to be a linear form:

$$\tau(w) = \tau(1)[1 + \hat{\tau}'(w-1)] \tag{712}$$

where

$$\tau' = \frac{d\tau}{dw}, \quad \hat{\tau}' = \frac{\tau'}{\tau(1)} \tag{713}$$

The uncertainty in the $\Lambda_{\rm QCD}/m_Q$ corrections is parameterized by τ_1 and τ_2.
In Approximation B_1,

$$\begin{aligned} \tau_1 &= 0 \\ \tau_2 &= 0 \end{aligned} \tag{714}$$

In Approximation B_2,

$$\begin{aligned} \tau_1 &= \bar{\Lambda}\tau \\ \tau_2 &= -\bar{\Lambda}'\tau \end{aligned} \tag{715}$$

These are the two end values of τ_1 and τ_2. True τ_1 and τ_2 reside somewhere in between. η_i comes from the correction to the HQET Lagrangian. In Approximation B,

$$\eta_1 = \eta_2 = \eta_3 = 0 \tag{716}$$

Also, in this Approximation, $\eta_1^{(b)} = \eta_2^{(b)} = \eta_3^{(b)} = 0$. Thus

$$\eta_b \equiv \eta_{\rm ke}^{(b)} + 6\eta_1^{(b)} - 2(w-1)\eta_2^{(b)} + \eta_3^{(b)} = \eta_{\rm ke}^{(b)} \tag{717}$$

Hence, the form factors are

$$\begin{aligned}
\sqrt{6} f_A &= -(w+1)(\tau + \varepsilon_c \eta_{\rm ke} + \varepsilon_b \eta_{\rm ke}^{(b)}) - \varepsilon_b (w-1)[(\bar{\Lambda}' + \bar{\Lambda})\tau - (2w+1)\tau_1 - \tau_2] \\
&\quad -\varepsilon_c[4(w\bar{\Lambda}' - \bar{\Lambda})\tau - 3(w-1)(\tau_1 - \tau_2)] \\
\sqrt{6} f_{V_1} &= (1-w^2)(\tau + \varepsilon_c \eta_{\rm ke} + \varepsilon_b \eta_{\rm ke}^{(b)}) - \varepsilon_b (w^2-1)[(\bar{\Lambda}' + \bar{\Lambda})\tau - (2w+1)\tau_1 - \tau_2] \\
&\quad -\varepsilon_c[4(w+1)(w\bar{\Lambda}' - \bar{\Lambda})\tau - 3(w^2-1)(\tau_1 - \tau_2)] \\
\sqrt{6} f_{V_2} &= -3(\tau + \varepsilon_c \eta_{\rm ke} + \varepsilon_b \eta_{\rm ke}^{(b)}) - 3\varepsilon_b[(\bar{\Lambda}' + \bar{\Lambda})\tau - (2w+1)\tau_1 - \tau_2] \\
&\quad -\varepsilon_c[(4w-1)\tau_1 + 5\tau_2] \\
\sqrt{6} f_{V_3} &= (w-2)(\tau + \varepsilon_c \eta_{\rm ke} + \varepsilon_b \eta_{\rm ke}^{(b)}) + \varepsilon_b (2+w)[(\bar{\Lambda}' + \bar{\Lambda})\tau - (2w+1)\tau_1 - \tau_2] \\
&\quad +\varepsilon_c[4(w\bar{\Lambda}' - \bar{\Lambda})\tau + (2+w)\tau_1 + (2+3w)\tau_2]
\end{aligned} \tag{718}$$

$\eta_{\rm ke}$ and $\eta_{\rm ke}^{(b)}$ can be absorbed into τ by the replacement of τ by

$$\tilde{\tau} = \tau + \varepsilon_c \eta_{\rm ke} + \varepsilon_b \eta_{\rm ke}^{(b)} \tag{719}$$

Thus, the form factors are

$$\begin{aligned}
\sqrt{6} f_A &= -(w+1)\tilde{\tau} - \varepsilon_b (w-1)[(\bar{\Lambda}' + \bar{\Lambda})\tau - (2w+1)\tau_1 - \tau_2] \\
&\quad -\varepsilon_c [4(w\bar{\Lambda}' - \bar{\Lambda})\tau - 3(w-1)(\tau_1 - \tau_2)] \\
\sqrt{6} f_{V_1} &= (1-w^2)\tilde{\tau} - \varepsilon_b (w^2-1)[(\bar{\Lambda}' + \bar{\Lambda})\tau - (2w+1)\tau_1 - \tau_2] \\
&\quad -\varepsilon_c [4(w+1)(w\bar{\Lambda}' - \bar{\Lambda})\tau - 3(w^2-1)(\tau_1 - \tau_2)] \\
\sqrt{6} f_{V_2} &= -3\tilde{\tau} - 3\varepsilon_b [(\bar{\Lambda}' + \bar{\Lambda})\tau - (2w+1)\tau_1 - \tau_2] \\
&\quad -\varepsilon_c [(4w-1)\tau_1 + 5\tau_2] \\
\sqrt{6} f_{V_3} &= (w-2)\tilde{\tau} + \varepsilon_b (2+w)[(\bar{\Lambda}' + \bar{\Lambda})\tau - (2w+1)\tau_1 - \tau_2] \\
&\quad +\varepsilon_c [4(w\bar{\Lambda}' - \bar{\Lambda})\tau + (2+w)\tau_1 + (2+3w)\tau_2]
\end{aligned} \tag{720}$$

Other τ can also be replaced by $\tilde{\tau}$ in the same order of approximation. For simplicity, we omit $\tilde{}$, then

$$\begin{aligned}
\sqrt{6} f_A &= -(w+1)\tau - \varepsilon_b (w-1)[(\bar{\Lambda}' + \bar{\Lambda})\tau - (2w+1)\tau_1 - \tau_2] \\
&\quad -\varepsilon_c [4(w\bar{\Lambda}' - \bar{\Lambda})\tau - 3(w-1)(\tau_1 - \tau_2)] \\
\sqrt{6} f_{V_1} &= (1-w^2)\tau - \varepsilon_b (w^2-1)[(\bar{\Lambda}' + \bar{\Lambda})\tau - (2w+1)\tau_1 - \tau_2] \\
&\quad -\varepsilon_c [4(w+1)(w\bar{\Lambda}' - \bar{\Lambda})\tau - 3(w^2-1)(\tau_1 - \tau_2)] \\
\sqrt{6} f_{V_2} &= -3\tau - 3\varepsilon_b [(\bar{\Lambda}' + \bar{\Lambda})\tau - (2w+1)\tau_1 - \tau_2] \\
&\quad -\varepsilon_c [(4w-1)\tau_1 + 5\tau_2] \\
\sqrt{6} f_{V_3} &= (w-2)\tau + \varepsilon_b (2+w)[(\bar{\Lambda}' + \bar{\Lambda})\tau - (2w+1)\tau_1 - \tau_2] \\
&\quad +\varepsilon_c [4(w\bar{\Lambda}' - \bar{\Lambda})\tau + (2+w)\tau_1 + (2+3w)\tau_2]
\end{aligned} \tag{721}$$

In Approximation A, the differential decay rate can be expanded in powers of $w-1$

$$\begin{aligned}
\tfrac{d^2\Gamma_{D_1}}{dw\, d\cos\theta} &= \Gamma_0 \tau^2(1) r_1^3 \sqrt{w^2-1} \textstyle\sum_n (w-1)^n \\
&\quad \{\sin^2\theta\, s_1^{(n)} + (1 - 2r_1 w + r_1^2)[(1+\cos^2\theta) t_1^{(n)} - 4\cos\theta\sqrt{w^2-1}\, u_1^{(n)}]\}
\end{aligned} \tag{722}$$

where

$$\begin{aligned}
& s_1^{(0)} = 32\varepsilon_c^2 (1-r_1)^2 (\bar{\Lambda}' - \bar{\Lambda})^2 + ... \\
& s_1^{(1)} = 32\varepsilon_c (1-r_1^2)(\bar{\Lambda}' - \bar{\Lambda}) + ... \\
& s_1^{(2)} = 8(1+r_1)^2 + ... \\
& t_1^{(0)} = 32\varepsilon_c^2 (\bar{\Lambda}' - \bar{\Lambda})^2 + ... \\
& t_1^{(1)} = 4 + 8\varepsilon_c [4(\bar{\Lambda}' - \bar{\Lambda}) + \hat{\eta}_{\text{ke}} - 2\hat{\eta}_1 - 3\hat{\eta}_3] + 8\varepsilon_b \hat{\eta}_b + ... \\
& t_1^{(2)} = 8(1 + \hat{\tau}') + ... \\
& u_1^{(0)} = 8\varepsilon_c (\bar{\Lambda}' - \bar{\Lambda}) + ... \\
& u_1^{(1)} = 2 + ...
\end{aligned} \tag{723}$$

where

$$\hat{\eta}_i = \frac{\eta_i}{\tau(1)} \tag{724}$$

We use the same tricks for ηs, then

$$\begin{aligned}
s_1^{(0)} &= 32\varepsilon_c^2(1-r_1)^2(\bar{\Lambda}'-\bar{\Lambda})^2 \\
s_1^{(1)} &= 32\varepsilon_c(1-r_1^2)(\bar{\Lambda}'-\bar{\Lambda}) \\
s_1^{(2)} &= 8(1+r_1)^2 \\
t_1^{(0)} &= 32\varepsilon_c^2(\bar{\Lambda}'-\bar{\Lambda})^2 \\
t_1^{(1)} &= 4+8\varepsilon_c[4(\bar{\Lambda}'-\bar{\Lambda})] \\
t_1^{(2)} &= 8(1+\hat{\tau}')+... \\
u_1^{(0)} &= 8\varepsilon_c(\bar{\Lambda}'-\bar{\Lambda}) \\
u_1^{(1)} &= 2
\end{aligned} \tag{725}$$

The differential decay rate can be integrated over $\cos\theta$ to give

$$\frac{d^2\Gamma_{D_1}}{dw} = \Gamma_0\tau^2(1)r_1^3\sqrt{w^2-1}\sum_n (w-1)^n\left[\frac{4}{3}s_1^{(n)} + (1-2r_1w+r_1^2)\frac{8}{3}t_1^{(n)}\right] \tag{726}$$

$$\begin{aligned}
\frac{d^2\Gamma_{D_1}}{dw} &= \frac{G_F^2|V_{cb}|^2m_B^5}{192\pi^3}r_1^3(w^2-1)^{1/2}\,\tau^2(1)\sum_n (w-1)^n\left[\frac{4}{3}s_1^{(n)} + (1-2r_1w+r_1^2)\frac{8}{3}t_1^{(n)}\right] \\
&= \frac{G_F^2|V_{cb}|^2m_B^5}{48\pi^3}r^3(w^2-1)^{1/2}\,\mathcal{J}_{D_1}(w)
\end{aligned} \tag{727}$$

where

$$\mathcal{J}_{D_1}(w) = \frac{1}{3}\tau^2(1)\sum_n (w-1)^n\left[s_1^{(n)} + 2(1-2r_1w+r_1^2)t_1^{(n)}\right] \tag{728}$$

Numerical values used in the LLSW paper are

$$\begin{aligned}
\tau(1)\left[\frac{6.0\times10^{-3}}{\mathcal{B}(B\to D_1 e\bar{\nu}_e)}\right]^{1/2} &= 0.71 \text{ for Approximation B1} \\
&= 0.75 \text{ for Approximation B2} \\
&= 0.60 \text{ for Approximation A}
\end{aligned} \tag{729}$$

and

$$\hat{\tau}' = -1.5 \tag{730}$$

H.5.2 $B \to D_2^*\ell\nu$

The matrix elements are

$$\frac{< D_2^*(v',\varepsilon)|V^\mu|B(v) >}{\sqrt{m_{D_2^*}m_B}} = ik_V\epsilon^{\mu\alpha\beta\gamma}\varepsilon^*_{\alpha\sigma}v^\sigma v_\beta v'_\gamma \tag{731}$$

$$\frac{< D_2^*(v',\varepsilon)|A^\mu|B(v) >}{\sqrt{m_{D_2^*}m_B}} = k_{A_1}\varepsilon^{*\mu\alpha}v_\alpha + (k_{A_2}v^\mu + k_{A_3}v'^\mu)\varepsilon^*_{\alpha\beta}v^\alpha v^\beta \tag{732}$$

The differential decay rate is

$$\frac{d^2\Gamma_{D_2^*}}{dw d\cos\theta} = \frac{3}{2}\Gamma_0 r_2^3 (w^2-1)^{3/2}\{\frac{4}{3}\sin^2\theta[(w-r_2)k_{A_1} + (w^2-1)(k_{A_3}+r_2 k_{A_2})]^2 \\ +(1-2r_2 w + r_2^2)[(1+\cos^2\theta)(k_{A_1}^2 + (w^2-1)k_V^2) - 4\cos\theta\sqrt{w^2-1}k_{A_1}k_V]\} \tag{733}$$

where

$$r_2 = \frac{m_{D_2^*}}{m_B} \tag{734}$$

In Approximation B, the form factors are given by

$$\begin{aligned} k_V &= -\tau - \varepsilon_b[(\bar{\Lambda}'+\bar{\Lambda})\tau - (2w+1)\tau_1 - \tau_2 + \eta_b] - \varepsilon_c(\tau_1 - \tau_2 + \eta_{\rm ke} - 2\eta_1 + \eta_3) \\ k_{A_1} &= -(1+w)\tau - \varepsilon_b\{(w-1)[(\bar{\Lambda}'+\bar{\Lambda})\tau - (2w+1)\tau_1 - \tau_2] + (1+w)\eta_b\} \\ &\quad -\varepsilon_c[(w-1)(\tau_1-\tau_2) + (w+1)(\eta_{\rm ke} - 2\eta_1 + \eta_3)] \\ k_{A_2} &= -2\varepsilon_c(\tau_1+\eta_2) \\ k_{A_3} &= \tau + \varepsilon_b[(\bar{\Lambda}'+\bar{\Lambda})\tau - (2w+1)\tau_1 - \tau_2 + \eta_b] \\ &\quad -\varepsilon_c(\tau_1 + \tau_2 - \eta_{\rm ke} + 2\eta_1 - 2\eta_2 - \eta_3) \end{aligned} \tag{735}$$

We use the same tricks for ηs, then

$$\begin{aligned} k_V &= -\tau - \varepsilon_b[(\bar{\Lambda}'+\bar{\Lambda})\tau - (2w+1)\tau_1 - \tau_2] - \varepsilon_c(\tau_1-\tau_2) \\ k_{A_1} &= -(1+w)\tau - \varepsilon_b(w-1)[(\bar{\Lambda}'+\bar{\Lambda})\tau - (2w+1)\tau_1 - \tau_2] \\ &\quad -\varepsilon_c(w-1)(\tau_1-\tau_2) \\ k_{A_2} &= -2\varepsilon_c\tau_1 \\ k_{A_3} &= \tau + \varepsilon_b[(\bar{\Lambda}'+\bar{\Lambda})\tau - (2w+1)\tau_1 - \tau_2] - \varepsilon_c(\tau_1+\tau_2) \end{aligned} \tag{736}$$

In Approximation B_1,

$$\begin{aligned} \tau_1 &= 0 \\ \tau_2 &= 0 \end{aligned} \tag{737}$$

In Approximation B_2,

$$\begin{aligned} \tau_1 &= \bar{\Lambda}\tau \\ \tau_2 &= -\bar{\Lambda}'\tau \end{aligned} \tag{738}$$

These are the two end values of τ_1 and τ_2. True τ_1 and τ_2 reside somewhere in between. In Approximation A, the differential decay rate can be expanded in powers of $w-1$

$$\frac{d^2\Gamma_{D_2^*}}{dw d\cos\theta} = \frac{3}{2}\Gamma_0\tau^2(1) r_2^3 (w^2-1)^{3/2}\sum_n (w-1)^n \\ \{\frac{4}{3}\sin^2\theta s_2^{(n)} + (1-2r_2 w + r_2^2)[(1+\cos^2\theta)t_2^{(n)} - 4\cos\theta\sqrt{w^2-1}u_2^{(n)}]\} \tag{739}$$

where

$$\begin{aligned} s_2^{(0)} &= 4(1-r_2)^2[1+2\varepsilon_b\hat{\eta}_b + 2\varepsilon_c(\hat{\eta}_{\text{ke}} - 2\hat{\eta}_1 + \hat{\eta}_3)] + ... \\ s_2^{(1)} &= 4(1-r_2)^2(1+2\hat{\tau}') + ... \\ t_2^{(0)} &= 4 + 8\varepsilon_b\hat{\eta}_b + 8\varepsilon_c(\hat{\eta}_{\text{ke}} - 2\hat{\eta}_1 + \hat{\eta}_3) + ... \\ t_2^{(1)} &= 2(3+4\hat{\tau}') + ... \\ u_2^{(0)} &= 2 + ... \end{aligned} \tag{740}$$

We use the same tricks for ηs, then

$$\begin{aligned} s_2^{(0)} &= 4(1-r_2)^2 \\ s_2^{(1)} &= 4(1-r_2)^2(1+2\hat{\tau}') \\ t_2^{(0)} &= 4 \\ t_2^{(1)} &= 2(3+4\hat{\tau}') \\ u_2^{(0)} &= 2 \end{aligned} \tag{741}$$

The differential decay rate can be integrated over $\cos\theta$

$$\frac{d^2\Gamma_{D_2^*}}{dw} = \frac{3}{2}\Gamma_0\tau^2(1)r_2^3(w^2-1)^{3/2}\sum_n (w-1)^n\left[\frac{4}{3}\frac{4}{3}s_2^{(n)} + (1-2r_2w+r_2^2)\frac{8}{3}t_2^{(n)}\right] \tag{742}$$

Thus,

$$\begin{aligned} \frac{d^2\Gamma_{D_2^*}}{dw} &= \frac{3}{2}\frac{G_F^2|V_{cb}|^2m_B^5}{192\pi^3}r_2^3(w^2-1)^{3/2}\tau^2(1) \\ &\quad \sum_n (w-1)^n\left[\frac{16}{9}s_2^{(n)} + (1-2r_2w+r_2^2)\frac{8}{3}t_2^{(n)}\right] \\ &= \frac{G_F^2|V_{cb}|^2m_B^5}{48\pi^3}r^3(w^2-1)^{3/2}\,\mathcal{J}_{D_2^*}(w) \end{aligned} \tag{743}$$

where

$$\mathcal{J}_{D_2^*}(w) = \frac{1}{3}\tau^2(1)\sum_n (w-1)^n\left[2s_2^{(n)} + 3(1-2r_2w+r_2^2)t_2^{(n)}\right] \tag{744}$$

Numerical values used in the LLSW paper are

$$\begin{aligned} \tau(1)\left[\frac{6.0\times10^{-3}}{\mathcal{B}(B\to D_1 e\bar{\nu}_e)}\right]^{1/2} &= 0.71 \text{ for Approximation B1} \\ &= 0.75 \text{ for Approximation B2} \\ &= 0.60 \text{ for Approximation A} \end{aligned} \tag{745}$$

and

$$\hat{\tau}' = -1.5 \tag{746}$$

H.5.3 $B \to D_0^*\ell\nu$

The matrix elements are

$$\frac{< D_0^*(v',\varepsilon)|V^\mu|B(v) >}{\sqrt{m_{D_0^*}m_B}} = 0 \tag{747}$$

$$\frac{< D_0^*(v',\varepsilon)|A^\mu|B(v) >}{\sqrt{m_{D_0^*}m_B}} = g_+(v^\mu + v'^\mu) + g_-(v^\mu - v'^\mu) \tag{748}$$

The differential decay rate is

$$\frac{d^2\Gamma_{D_0^*}}{dw d\cos\theta} = 3\Gamma_0 r_0^{*3}(w^2-1)^{3/2}\sin^2\theta[(1+r_0^*)g_+ - (1-r_0^*)g_-]^2 \tag{749}$$

where

$$r_0^* = \frac{m_{D_0^*}}{m_B} \tag{750}$$

In Approximation B, the form factors are given by

$$\begin{array}{rcl} g_+ &=& \varepsilon_c\left[2(w-1)\zeta_1 - 3\zeta\frac{w\bar{\Lambda}^*-\bar{\Lambda}}{w+1}\right] - \varepsilon_b\left[\frac{\bar{\Lambda}^*(2w+1)-\bar{\Lambda}(w+2)}{w+1}\zeta - 2(w-1)\zeta_1\right] \\ g_- &=& \zeta + \varepsilon_c\left[\chi_{\rm ke} + 6\chi_1 - 2(w+1)\chi_2\right] + \varepsilon_b\chi_b \end{array} \tag{751}$$

We can use the same tricks for χs as ηs, then

$$\begin{array}{rcl} g_+ &=& \varepsilon_c\left[2(w-1)\zeta_1 - 3\zeta\frac{w\bar{\Lambda}^*-\bar{\Lambda}}{w+1}\right] - \varepsilon_b\left[\frac{\bar{\Lambda}^*(2w+1)-\bar{\Lambda}(w+2)}{w+1}\zeta - 2(w-1)\zeta_1\right] \\ g_- &=& \zeta \end{array} \tag{752}$$

where

$$\zeta(w) = \frac{w+1}{\sqrt{3}}\tau(w) \tag{753}$$

Thus,

$$\begin{array}{rl} \zeta(1)[1+\hat{\zeta}'(w-1)] = & \frac{2+(w-1)}{\sqrt{3}}\tau(1)[1+\hat{\tau}'(w-1)] \\ \simeq & \frac{1}{\sqrt{3}}\tau(1)[2+2\hat{\tau}'(w-1)+(w-1)] \\ = & \frac{2}{\sqrt{3}}\tau(1)\left[1+\left(\hat{\tau}'+\frac{1}{2}\right)(w-1)\right] \end{array} \tag{754}$$

Hence

$$\begin{array}{l} \zeta(1) = \frac{2}{\sqrt{3}}\tau(1) \\ \hat{\zeta}' = \frac{1}{2} + \hat{\tau}' = -1 \end{array} \tag{755}$$

In Approximation B_1,

$$\begin{array}{l} \zeta_1 = 0 \\ \zeta_2 = 0 \end{array} \tag{756}$$

In Approximation B_2,

$$\begin{array}{l} \zeta_1 = \bar{\Lambda}\zeta \\ \zeta_2 = -\bar{\Lambda}^*\zeta \end{array} \tag{757}$$

These are the two end values of ζ_1 and ζ_2. True ζ_1 and ζ_2 reside somewhere in between. In Approximation A, the differential decay rate can be expanded in powers of $w - 1$

$$\frac{d^2\Gamma_{D_0^*}}{dw d\cos\theta} = 3\Gamma_0 \zeta^2(1) r_0^{*3} (w^2 - 1)^{3/2} \sin^2\theta \sum_n (w-1)^n s_0^{(n)} \tag{758}$$

where

$$\begin{aligned} s_0^{(0)} &= (1 - r_0^*)^2 [1 + 2\varepsilon_c(\hat{\chi}_{\rm ke} + 6\hat{\chi}_1 - 4\hat{\chi}_2) + 4\varepsilon_b\hat{\chi}_b] \\ &\qquad + 3(\varepsilon_c + \varepsilon_b)(1 - r_0^{*2})(\bar{\Lambda}^* - \bar{\Lambda}) + ... \\ s_0^{(1)} &= 2(1 - r_0^*)^2 \hat{\zeta}' + ... \end{aligned} \tag{759}$$

We can use the same tricks for χs, then

$$\begin{aligned} s_0^{(0)} &= (1 - r_0^*)^2 + 3(\varepsilon_c + \varepsilon_b)(1 - r_0^{*2})(\bar{\Lambda}^* - \bar{\Lambda}) \\ s_0^{(1)} &= 2(1 - r_0^*)^2 \hat{\zeta}' \end{aligned} \tag{760}$$

The differential decay rate can be integrated over $\cos\theta$

$$\frac{d^2\Gamma_{D_0^*}}{dw} = 3\Gamma_0 \zeta^2(1) r_0^{*3} (w^2 - 1)^{3/2} \frac{4}{3} \sum_n (w-1)^n s_0^{(n)} \tag{761}$$

Thus

$$\begin{aligned} \frac{d^2\Gamma_{D_0^*}}{dw} &= 3\frac{G_F^2 |V_{cb}|^2 m_B^5}{192\pi^3} r_0^{*3} (w^2 - 1)^{3/2} \zeta^2(1) \frac{4}{3} \sum_n (w-1)^n s_0^{(n)} \\ &= \frac{G_F^2 |V_{cb}|^2 m_B^5}{48\pi^3} r^3 (w^2 - 1)^{3/2} \, \mathcal{J}_{D_0^*}(w) \end{aligned} \tag{762}$$

where

$$\mathcal{J}_{D_0^*}(w) = \zeta^2(1) \sum_n (w-1)^n s_0^{(n)} \tag{763}$$

Numerical values used in the LLSW paper are

$$\begin{aligned} \tau(1) \left[\frac{6.0 \times 10^{-3}}{\mathcal{B}(B \to D_1 e \bar{\nu}_e)} \right]^{1/2} &= 0.71 \text{ for Approximation B1} \\ &= 0.75 \text{ for Approximation B2} \\ &= 0.60 \text{ for Approximation A} \end{aligned} \tag{764}$$

and

$$\hat{\tau}' = -1.5 \tag{765}$$

H.5.4 $B \to D_1^*\ell\nu$

The matrix elements are

$$\frac{< D_1^*(v',\varepsilon)|V^\mu|B(v) >}{\sqrt{m_{D_1^*}m_B}} = g_{V_1}\varepsilon^{*\mu} + (g_{V_2}v^\mu + g_{V_3}v'^\mu)(\varepsilon^* \cdot v) \tag{766}$$

$$\frac{< D_1^*(v',\varepsilon)|A^\mu|B(v) >}{\sqrt{m_{D_1^*}m_B}} = ig_A\epsilon^{\mu\alpha\beta\gamma}\varepsilon^*_\alpha v_\beta v'_\gamma \tag{767}$$

The differential decay rate is

$$\begin{array}{l}\frac{d^2\Gamma_{D_1^*}}{dwd\cos\theta} = 3\Gamma_0 r_1^{*3}\sqrt{w^2-1}\{\sin^2\theta[(w-r_1^*)g_{V_1} + (w^2-1)(g_{V_3}+r_1^*g_{V_2})]^2 \\ +(1-2r_1^*w+r_1^{*2})[(1+\cos^2\theta)(g_{V_1}^2+(w^2-1)g_A^2) - 4\cos\theta\sqrt{w^2-1}g_{V_1}g_A]\}\end{array} \tag{768}$$

where

$$r_1^* = \frac{m_{D_1^*}}{m_B} \tag{769}$$

In Approximation B, the form factors are given by

$$\begin{array}{l}g_A = \zeta + \varepsilon_c\left[\frac{w\bar{\Lambda}^*-\bar{\Lambda}}{w+1}\zeta + \chi_{\rm ke} - 2\chi_1\right] - \varepsilon_b\left[\frac{\bar{\Lambda}^*(2w+1)-\bar{\Lambda}(w+2)}{w+1}\zeta - 2(w-1)\zeta_1 - \chi_b\right] \\ g_{V_1} = (w-1)\zeta + \varepsilon_c\left[(w\bar{\Lambda}^*-\bar{\Lambda})\zeta + (w-1)(\chi_{\rm ke}-2\chi_1)\right] \\ \qquad -\varepsilon_b\left[(\bar{\Lambda}^*(2w+1)-\bar{\Lambda}(w+2))\zeta - 2(w^2-1)\zeta_1 - (w-1)\chi_b\right] \\ g_{V_2} = 2\varepsilon_c(\zeta_1-\chi_2) \\ g_{V_3} = -\zeta - \varepsilon_c\left[\frac{w\bar{\Lambda}^*-\bar{\Lambda}}{w+1}\zeta + 2\zeta_1 + \chi_{\rm ke} - 2\chi_1 + 2\chi_2\right] \\ \qquad +\varepsilon_b\left[\frac{\bar{\Lambda}^*(2w+1)-\bar{\Lambda}(w+2)}{w+1}\zeta - 2(w-1)\zeta_1 - \chi_b\right]\end{array} \tag{770}$$

where

$$\zeta(w) = \frac{w+1}{\sqrt{3}}\tau(w) \tag{771}$$

We use the same tricks for χs, then

$$\begin{array}{l}g_A = \zeta + \varepsilon_c\left[\frac{w\bar{\Lambda}^*-\bar{\Lambda}}{w+1}\zeta\right] - \varepsilon_b\left[\frac{\bar{\Lambda}^*(2w+1)-\bar{\Lambda}(w+2)}{w+1}\zeta - 2(w-1)\zeta_1\right] \\ g_{V_1} = (w-1)\zeta + \varepsilon_c(w\bar{\Lambda}^*-\bar{\Lambda})\zeta \\ \qquad -\varepsilon_b\left[(\bar{\Lambda}^*(2w+1)-\bar{\Lambda}(w+2))\zeta - 2(w^2-1)\zeta_1\right] \\ g_{V_2} = 2\varepsilon_c\zeta_1 \\ g_{V_3} = -\zeta - \varepsilon_c\left[\frac{w\bar{\Lambda}^*-\bar{\Lambda}}{w+1}\zeta + 2\zeta_1\right] \\ \qquad +\varepsilon_b\left[\frac{\bar{\Lambda}^*(2w+1)-\bar{\Lambda}(w+2)}{w+1}\zeta - 2(w-1)\zeta_1\right]\end{array} \tag{772}$$

In Approximation B_1,

$$\begin{array}{l}\zeta_1 = 0 \\ \zeta_2 = 0\end{array} \tag{773}$$

In Approximation B$_2$,

$$\begin{aligned}\zeta_1 &= \bar{\Lambda}\zeta \\ \zeta_2 &= -\bar{\Lambda}^*\zeta\end{aligned} \tag{774}$$

These are the two end values of ζ_1 and ζ_2. True ζ_1 and ζ_2 reside somewhere in between. In Approximation A, the differential decay rate can be expanded in powers of $w-1$

$$\begin{aligned}&\tfrac{d^2\Gamma_{D_1^*}}{dwd\cos\theta} = 3\Gamma_0\zeta^2(1)r_1^{*3}\sqrt{w^2-1}\textstyle\sum_n(w-1)^n \\ &\{\sin^2\theta s_1^{(n)} + (1-2r_1^*w+r_1^{*2})[(1+\cos^2\theta)t_1^{(n)} - 4\cos\theta\sqrt{w^2-1}u_1^{(n)}]\}\end{aligned} \tag{775}$$

where

$$\begin{aligned}s_1^{(0)} &= (\varepsilon_c - 3\varepsilon_b)^2(1-r_1^*)^2(\bar{\Lambda}^*-\bar{\Lambda})^2 + ... \\ s_1^{(1)} &= -2(\varepsilon_c - 3\varepsilon_b)(1-r_1^{*2})(\bar{\Lambda}^*-\bar{\Lambda}) + ... \\ s_1^{(2)} &= (1+r_1^*)^2 + ... \\ t_1^{(0)} &= (\varepsilon_c - 3\varepsilon_b)^2(\bar{\Lambda}^*-\bar{\Lambda})^2 + ... \\ t_1^{(1)} &= 2 + 4(\varepsilon_c - 3\varepsilon_b)(\bar{\Lambda}^*-\bar{\Lambda}) + 4\varepsilon_c(\hat{\chi}_{\rm ke} - 2\hat{\chi}_1) + 4\varepsilon_b\hat{\chi}_b + ... \\ t_1^{(2)} &= 2(1+2\hat{\zeta}') + ... \\ u_1^{(0)} &= (\varepsilon_c - 3\varepsilon_b)(\bar{\Lambda}^*-\bar{\Lambda}) + ... \\ u_1^{(1)} &= 1 + ...\end{aligned} \tag{776}$$

We use the same tricks for χs, then

$$\begin{aligned}s_1^{(0)} &= (\varepsilon_c - 3\varepsilon_b)^2(1-r_1^*)^2(\bar{\Lambda}^*-\bar{\Lambda})^2 \\ s_1^{(1)} &= -2(\varepsilon_c - 3\varepsilon_b)(1-r_1^{*2})(\bar{\Lambda}^*-\bar{\Lambda}) \\ s_1^{(2)} &= (1+r_1^*)^2 \\ t_1^{(0)} &= (\varepsilon_c - 3\varepsilon_b)^2(\bar{\Lambda}^*-\bar{\Lambda})^2 \\ t_1^{(1)} &= 2 + 4(\varepsilon_c - 3\varepsilon_b)(\bar{\Lambda}^*-\bar{\Lambda}) \\ t_1^{(2)} &= 2(1+2\hat{\zeta}') \\ u_1^{(0)} &= (\varepsilon_c - 3\varepsilon_b)(\bar{\Lambda}^*-\bar{\Lambda}) \\ u_1^{(1)} &= 1\end{aligned} \tag{777}$$

The differential decay rate can be integrated over $\cos\theta$

$$\frac{d^2\Gamma_{D_1^*}}{dw} = 3\Gamma_0\zeta^2(1)r_1^{*3}\sqrt{w^2-1}\sum_n(w-1)^n\left[\frac{4}{3}s_1^{(n)} + (1-2r_1^*w+r_1^{*2})\frac{8}{3}t_1^{(n)}\right] \tag{778}$$

Thus

$$\begin{aligned}\frac{d^2\Gamma_{D_1^*}}{dw} &= \frac{G_F^2|V_{cb}|^2m_B^5}{192\pi^3}r_1^{*3}(w^2-1)^{1/2}\zeta^2(1) \\ &\quad \sum_n(w-1)^n\left[4s_1^{(n)} + 8(1-2r_1^*w+r_1^{*2})t_1^{(n)}\right] \\ &= \frac{G_F^2|V_{cb}|^2m_B^5}{48\pi^3}r^3(w^2-1)^{1/2}\ \mathcal{J}_{D_1'}(w)\end{aligned} \tag{779}$$

where

$$\mathcal{J}_{D_1'}(w) = \zeta^2(1)\sum_n (w-1)^n \left[s_1^{(n)} + 2(1-2r_1^* w + r_1^{*2})t_1^{(n)}\right] \quad (780)$$

Numerical values used in the LLSW paper are

$$\begin{aligned} \tau(1)\left[\frac{6.0\times 10^{-3}}{\mathcal{B}(B\to D_1 e\bar{\nu}_e)}\right]^{1/2} &= 0.71 \text{ for Approximation B1} \\ &= 0.75 \text{ for Approximation B2} \\ &= 0.60 \text{ for Approximation A} \end{aligned} \quad (781)$$

and

$$\hat{\tau}' = -1.5 \quad (782)$$

H.6 GoityRoberts model

In GoiryRoberts model [44], the "soft-pion" domain was studied in the framework of the chiral Lagrangian approach combined with the $1/m_Q$ expansion.

H.6.1 $B \to D\pi\ell\nu$

The amplitude for this process has the general form

$$T = \kappa j_\mu \Omega^\mu \quad (783)$$

Here j_μ is the V-A charged leptonic current and the Ω^μ is the hadronic part of the amplitude. To evaluate Ω^μ, these six diagrams are considered to get the amplitude (matrix element)

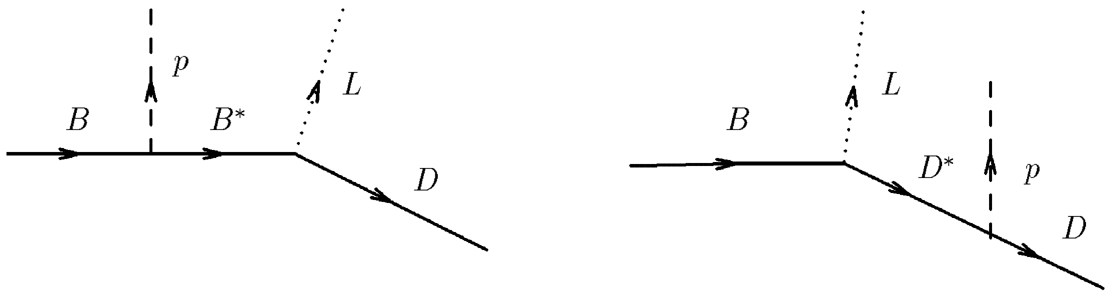

(a)

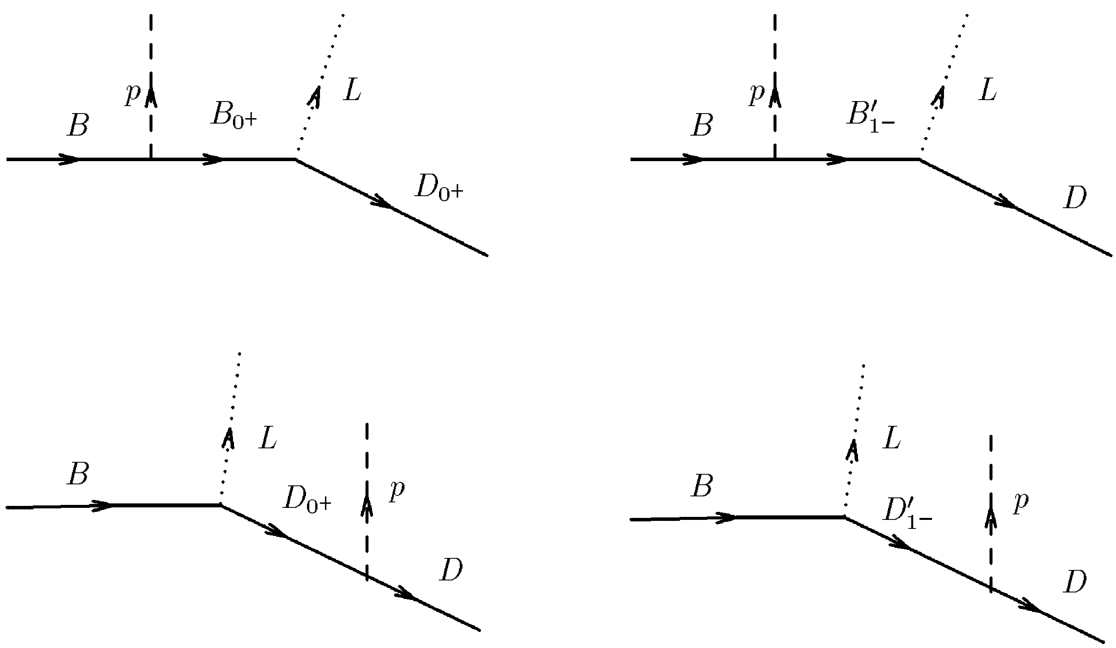

(b)

(a) shows two non-resonant decays , (b) shows four resonant decays. The non-resonant portion of Ω^μ is

$$\begin{aligned} \Omega_\mu^{NR} \;=\; & \tfrac{g}{F_0}\xi(\nu)p_\nu\Big\{\tfrac{\Theta^{\nu\rho}(v)}{-2(p\cdot v-\delta m_B)+i\varepsilon}\left[iv^\alpha v'^\beta\epsilon_{\mu\alpha\beta\rho}+g_{\mu\rho}(1+\nu)-v_\mu v'_\rho\right] \\ & +\tfrac{\Theta^{\nu\rho}(v')}{2(p\cdot v'-\delta m_D)+i\varepsilon}\left[iv^\alpha v'^\beta\epsilon_{\mu\alpha\beta\rho}+g_{\mu\rho}(1+\nu)-v_\rho v'_\mu\right]\Big\} \end{aligned} \tag{784}$$

where $\delta m_D = m_{D^*} - m_D$ and $\delta m_B = m_{B^*} - m_B$, and

$$\Theta^{\mu\nu}(v) = g^{\mu\nu} - v^\mu v^\nu \tag{785}$$

The resonant portion of Ω^μ is

$$
\begin{aligned}
\Omega^R_\mu \;=\;& \frac{\alpha_1}{F_0}\rho_1(\nu)(v-v')_\mu\left[-\frac{p\cdot v}{2(-p\cdot v-\delta\tilde{m}_1)}+\frac{p\cdot v'}{2(p\cdot v'-\delta\tilde{m}_1)}\right]\\
&+\frac{\alpha_2}{3F_0}\rho_2(\nu)p_\rho\Big\{\frac{\Theta^{\nu\rho}(v)}{2(-p\cdot v-\delta\tilde{m}_2)}\left[i\epsilon_{\mu\nu\alpha\beta}v^\alpha v'^\beta(\nu-1)+g_{\mu\nu}(\nu^2-1)\right.\\
&\qquad\qquad\left.-v'_\nu\left(v_\mu(2+\nu)-3v'_\mu\right)\right]\\
&+\frac{\Theta^{\nu\rho}(v')}{2(p\cdot v'-\delta\tilde{m}_2)}\left[i\epsilon_{\mu\nu\alpha\beta}v^\alpha v'^\beta(\nu-1)+g_{\mu\nu}(\nu^2-1)\right.\\
&\qquad\qquad\left.-v_\nu\left(v'_\mu(2+\nu)-3v_\mu\right)\right]\Big\}\\
&+\frac{\alpha_3}{F_0}\xi^{(1)}(\nu)p_\nu\Big\{\frac{\Theta^{\nu\rho}(v)}{-2p\cdot v-\delta\tilde{m}_3}\left[i\epsilon_{\mu\alpha\beta\rho}v^\alpha v'^\beta+g_{\mu\rho}(\nu+1)-v_\mu v'_\rho\right]\\
&+\frac{\Theta^{\nu\rho}(v')}{2p\cdot v'-\delta\tilde{m}_3}\left[i\epsilon_{\mu\alpha\beta\rho}v^\alpha v'^\beta+g_{\mu\rho}(\nu+1)-v_\rho v'_\mu\right]\Big\}
\end{aligned}
\tag{786}
$$

Here we denote $\delta\tilde{m}-j=\delta m_j-i\Gamma_j/2$, where Γ_j is the total width of the resonance. Contribution from other resonances are small. Isgur-Wise functions are given by

$$
\begin{aligned}
&\xi(\nu)=\exp\left[\tfrac{\bar{\Lambda}^2}{4\beta^2}(\nu^2-1)\right]\\
&\xi^{(1)}(\nu)=-\sqrt{\tfrac{2}{3}}\left[\tfrac{\bar{\Lambda}^2}{4\beta^2}(\nu^2-1)\right]\exp\left[\tfrac{\bar{\Lambda}^2}{4\beta^2}(\nu^2-1)\right]\\
&\rho_1(\nu)=\tfrac{1}{\sqrt{2}}\tfrac{\bar{\Lambda}}{\beta}\left(\tfrac{2\beta\beta'}{\beta^2+\beta'^2}\right)^{5/2}\exp\left[\tfrac{\bar{\Lambda}^2}{2(\beta^2+\beta'^2)}(\nu^2-1)\right]\\
&\rho_2(\nu)=\tfrac{1}{2\sqrt{2}}\left(\tfrac{\bar{\Lambda}}{\beta}\right)^2\left(\tfrac{2\beta\beta'}{\beta^2+\beta'^2}\right)^{7/2}\exp\left[\tfrac{\bar{\Lambda}^2}{2(\beta^2+\beta'^2)}(\nu^2-1)\right]
\end{aligned}
\tag{787}
$$

where β and β' are the harmonic oscillator parameters of the ground and excited states, respectively. $\bar{\Lambda}$ is defined by

$$M_{(0^-,1^-)}=m_Q+\bar{\Lambda} \tag{788}$$

Ω_μ can be, in general, expressed as

$$\Omega_\mu=-ihm_Bm_D\epsilon_{\mu\nu\rho\sigma}v^\nu v'^\rho p^\sigma_\pi+A_1p_{\pi\mu}+A_2m_Bv_\mu+A_3m_Dv'_{mu} \tag{789}$$

where h, A_1, A_2 and A_3 are the form factors and p_π is the 4-momentum of the pion. The non-resonant contribution to the form factors are

$$
\begin{aligned}
&h_{NR}=\tfrac{g}{2F_0}\tfrac{\xi(\nu)}{m_Bm_D}\left(\tfrac{1}{p_\pi\cdot v+\delta m_B-i\varepsilon}-\tfrac{1}{p_\pi\cdot v'-\delta m_D+i\varepsilon}\right)\\
&A_{1NR}=-\tfrac{g}{2F_0}\xi(\nu)(1+\nu)\left(\tfrac{1}{p_\pi\cdot v+\delta m_B-i\varepsilon}-\tfrac{1}{p_\pi\cdot v'-\delta m_D+i\varepsilon}\right)\\
&A_{2NR}=\tfrac{g}{2F_0}\tfrac{\xi(\nu)}{m_B}\left(\tfrac{p_\pi\cdot v+p_\pi\cdot v'}{p_\pi\cdot v+\delta m_B-i\varepsilon}\right)\\
&A_{3NR}=-\tfrac{g}{2F_0}\tfrac{\xi(\nu)}{m_D}\left(\tfrac{p_\pi\cdot v+p_\pi\cdot v'}{p_\pi\cdot v'-\delta m_D+i\varepsilon}\right)
\end{aligned}
\tag{790}
$$

In SP5/SP6, the contribution from $B \to D^*\ell\nu \to D\pi\ell\nu$ was removed. Hence

$$\begin{aligned}
h_{NR} &= \tfrac{g}{2F_0}\tfrac{\xi(\nu)}{m_B m_D}\left(\tfrac{1}{p_\pi\cdot v+\delta m_B - i\varepsilon}\right)\\
A_{1NR} &= -\tfrac{g}{2F_0}\xi(\nu)(1+\nu)\left(\tfrac{1}{p_\pi\cdot v+\delta m_B - i\varepsilon}\right)\\
A_{2NR} &= \tfrac{g}{2F_0}\tfrac{\xi(\nu)}{m_B}\left(\tfrac{p_\pi\cdot v+p_\pi\cdot v'}{p_\pi\cdot v+\delta m_B - i\varepsilon}\right)\\
A_{3NR} &= 0
\end{aligned} \tag{791}$$

The resonant contribution to the form factors are

$$\begin{aligned}
h_R &= \frac{\alpha_2\rho_2(\nu)}{6F_0 m_B m_D}(\nu-1)\left(\frac{1}{p_\pi\cdot v+\delta\tilde{m}_2}-\frac{1}{p_\pi\cdot v'-\delta\tilde{m}_2}\right)\\
&\quad+\frac{\alpha_3\xi^{(1)}(\nu)}{2F_0 m_B m_D}\left(\frac{1}{p_\pi\cdot v+\delta\tilde{m}_3}-\frac{1}{p_\pi\cdot v'-\delta\tilde{m}_3}\right)
\end{aligned} \tag{792}$$

$$\begin{aligned}
A_{1R} &= -\frac{\alpha_2\rho_2(\nu)}{6F_0}(\nu^2-1)\left(\frac{1}{p_\pi\cdot v+\delta\tilde{m}_2}-\frac{1}{p_\pi\cdot v'-\delta\tilde{m}_2}\right)\\
&\quad-\frac{\alpha_3\xi^{(1)}(\nu)}{2F_0}(1+\nu)\left(\frac{1}{p_\pi\cdot v+\delta\tilde{m}_3}-\frac{1}{p_\pi\cdot v'-\delta\tilde{m}_3}\right)
\end{aligned} \tag{793}$$

$$\begin{aligned}
A_{2R} &= \frac{\alpha_1\rho_1(\nu)}{2F_0 m_B}\left(\frac{p_\pi\cdot v}{p_\pi\cdot v+\delta\tilde{m}_1}+\frac{p_\pi\cdot v'}{p_\pi\cdot v'-\delta\tilde{m}_2}\right)\\
&\quad+\frac{\alpha_2\rho_2(\nu)}{F_0 m_B}\Big\{\frac{1}{p_\pi\cdot v+\delta\tilde{m}_2}\left[\frac{1}{6}(\nu p_\pi\cdot v'-p_\pi\cdot v)+\frac{1}{3}(p_\pi\cdot v'-\nu p_\pi\cdot v)\right]\\
&\quad+\frac{1}{2}\frac{1}{p_\pi\cdot v'-\delta\tilde{m}_2}(p_\pi\cdot v-\nu p_\pi\cdot v')\Big\}\\
&\quad+\frac{\alpha_3\xi^{(1)}(\nu)}{2F_0 m_B}\left(\frac{p_\pi\cdot(v+v')}{p_\pi\cdot v+\delta\tilde{m}_3}\right)
\end{aligned} \tag{794}$$

$$\begin{aligned}
A_{3R} &= -\frac{\alpha_1\rho_1(\nu)}{2F_0 m_D}\left(\frac{p_\pi\cdot v}{p_\pi\cdot v+\delta\tilde{m}_1}+\frac{p_\pi\cdot v'}{p_\pi\cdot v'-\delta\tilde{m}_1}\right)\\
&\quad-\frac{\alpha_2\rho_2(\nu)}{F_0 m_D}\Big\{\frac{1}{p_\pi\cdot v'-\delta\tilde{m}_2}\left[\frac{1}{6}(\nu p_\pi\cdot v-p_\pi\cdot v')+\frac{1}{3}(p_\pi\cdot v-\nu p_\pi\cdot v')\right]\\
&\quad+\frac{1}{2}\frac{1}{p_\pi\cdot v+\delta\tilde{m}_2}(p_\pi\cdot v'-\nu p_\pi\cdot v)\Big\}\\
&\quad-\frac{\alpha_3\xi^{(1)}(\nu)}{2F_0 m_D}\left(\frac{p_\pi\cdot(v+v')}{p_\pi\cdot v'-\delta\tilde{m}_3}\right)
\end{aligned} \tag{795}$$

In SP5/SP6 contributions from D^{**} was removed

$$\begin{aligned}
h_R &= \tfrac{\alpha_2\rho_2(\nu)}{6F_0 m_B m_D}(\nu-1)\left(\tfrac{1}{p_\pi\cdot v+\delta\tilde{m}_2}\right)+\tfrac{\alpha_3\xi^{(1)}(\nu)}{2F_0 m_B m_D}\left(\tfrac{1}{p_\pi\cdot v+\delta\tilde{m}_3}\right)\\
A_{1R} &= -\tfrac{\alpha_2\rho_2(\nu)}{6F_0}(\nu^2-1)\left(\tfrac{1}{p_\pi\cdot v+\delta\tilde{m}_2}\right)-\tfrac{\alpha_3\xi^{(1)}(\nu)}{2F_0}(1+\nu)\left(\tfrac{1}{p_\pi\cdot v+\delta\tilde{m}_3}\right)\\
A_{2R} &= \tfrac{\alpha_1\rho_1(\nu)}{2F_0 m_B}\left(\tfrac{p_\pi\cdot v}{p_\pi\cdot v+\delta\tilde{m}_1}\right)\\
&\quad+\tfrac{\alpha_2\rho_2(\nu)}{F_0 m_B}\left\{\tfrac{1}{p_\pi\cdot v+\delta\tilde{m}_2}\left[\tfrac{1}{6}(\nu p_\pi\cdot v'-p_\pi\cdot v)+\tfrac{1}{3}(p_\pi\cdot v'-\nu p_\pi\cdot v)\right]\right\}\\
&\quad+\tfrac{\alpha_3\xi^{(1)}(\nu)}{2F_0 m_B}\left(\tfrac{p_\pi\cdot(v+v')}{p_\pi\cdot v+\delta\tilde{m}_3}\right)\\
A_{3R} &= -\tfrac{\alpha_1\rho_1(\nu)}{2F_0 m_D}\left(\tfrac{p_\pi\cdot v}{p_\pi\cdot v+\delta\tilde{m}_1}\right)\\
&\quad-\tfrac{\alpha_2\rho_2(\nu)}{F_0 m_D}\left\{\tfrac{1}{2}\tfrac{1}{p_\pi\cdot v+\delta\tilde{m}_2}(p_\pi\cdot v'-\nu p_\pi\cdot v)\right\}
\end{aligned} \tag{796}$$

Numerical values used in SP5/SP6 are

$$\begin{aligned}
&g = 0.5\\
&\alpha_1 = -1.430\\
&\alpha_2 = -0.140\\
&\alpha_3 = 0.690\\
&F_0 = 0.093\\
&\delta m_B = 0.0460 - \tfrac{0.00001}{2}i\\
&\delta m_D = 0.1421 - \tfrac{0.00006}{2}i\\
&\delta\tilde{m}_1 = 0.392 - \tfrac{1.040}{2}i\\
&\delta\tilde{m}_2 = 0.709 - \tfrac{0.405}{2}i\\
&\delta\tilde{m}_3 = 0.563 - \tfrac{0.191}{2}i\\
&\beta = 0.285\\
&\beta' = 0.280 \quad \text{for} \quad \rho_1(\nu)\\
&\beta' = 0.260 \quad \text{for} \quad \rho_2(\nu)\\
&\bar{\Lambda} = 0.750
\end{aligned} \tag{797}$$

H.6.2 $B \to D^*\pi\ell\nu$

The amplitude for this process has the general form

$$T = \kappa j_\mu \Omega^{\mu\nu}\varepsilon_{D^*\nu} \tag{798}$$

where $\varepsilon_{D^*\nu}$ is the polarization vector of the D^*.

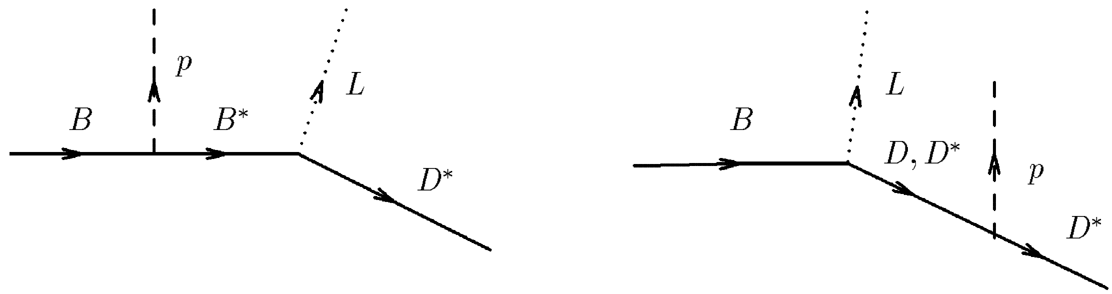

(a)

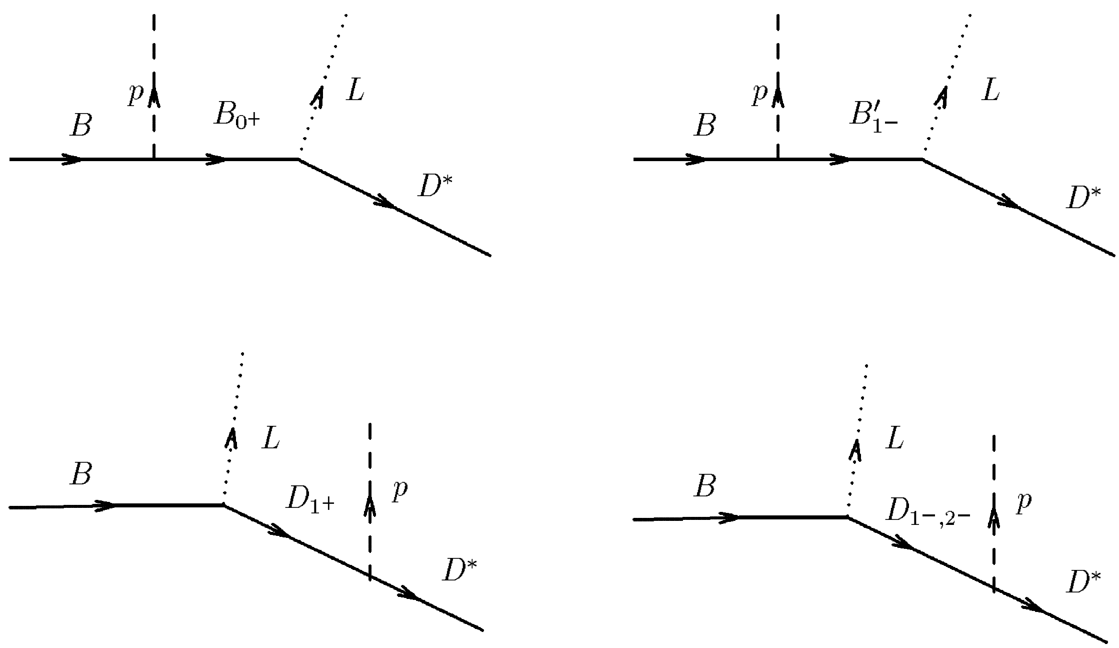

(b)

(a) shows two non-resonant decays , (b) shows four resonant decays. The non-resonant portion of $\Omega_{\mu\nu}$ is

$$\begin{aligned}\Omega^{NR}_{\mu\nu} \quad = \quad & \tfrac{g}{2F_0}\xi(\nu)\Big\{(v+v')_\mu \tfrac{p_\nu}{p\cdot v'+\delta m_D+i\varepsilon} \\ & -p^\rho \tfrac{\Theta_{\rho\sigma}(v)}{-(p\cdot v+\delta m_B)+i\varepsilon}\left[g_{\nu\sigma}(v+v')_\mu - g_{\mu\sigma}v_\nu - g_{\mu\nu}v'_\sigma + i\epsilon_{\mu\alpha\sigma\nu}(v+v')^\alpha\right] \\ & +\tfrac{\Theta_{\rho\delta}(v')}{p\cdot v'+i\varepsilon}\left[-i\epsilon_{\mu\rho\alpha\beta}v'^\alpha v^\beta + g_{\mu\rho}(1+\nu) - v_\rho v'_\mu\right] i\epsilon_{\omega\nu\gamma\delta}p^\gamma v'^\omega\Big\}\end{aligned} \tag{799}$$

The resonant portion of $\Omega_{\mu\nu}$ is

$$\begin{aligned}
\Omega^R_{\mu\nu} \;=\;& \tfrac{\alpha_1}{F_0}\rho_1(\nu)\left[-g_{\mu\nu}(\nu-1)+v'_\mu v_\nu - i\epsilon_{\mu\nu\alpha\beta}v^\alpha v'^\beta\right]\left[-\tfrac{p\cdot v}{2(-p\cdot v-\delta\tilde{m}_1)}+\tfrac{p\cdot v'}{2(p\cdot v'-\delta\tilde{m}_1)}\right]\\
&-\tfrac{\alpha_2}{3F_0}\rho_2(\nu)\Big\{p_\rho\tfrac{\Theta^{\rho\sigma}(v)}{2(-p\cdot v-\delta\tilde{m}_2)}\left[-g_{\nu\sigma}(v+v')_\mu(\nu-1)+3v_\nu v'_\mu v'_\sigma-2g_{\mu\nu}v'_\sigma(\nu-1)\right.\\
&\left.+g_{\mu\sigma}v_\nu(\nu-1)+i\epsilon_{\mu\sigma\alpha\nu}(v-v')^\alpha(1+\nu)+2i\epsilon_{\sigma\nu\alpha\beta}v'^\alpha v^\beta v'_\mu+i\epsilon_{\mu\nu\alpha\beta}v'_\sigma v'^\alpha v^\beta\right]\\
&+3p^\gamma\tfrac{\Theta^{\sigma\rho}_{\gamma\nu}(v')}{2(p\cdot v'-\delta\tilde{m}_2)+i\varepsilon}\left[v_\delta g_{\rho\mu}(\nu-1)-v_\delta v_\rho v'_\mu+i\epsilon_{\mu\delta\alpha\beta}v_\rho v^\alpha v'^\beta\right]\\
&+\tfrac{i}{2}\tfrac{\Theta^{\sigma\rho}(v)}{2(p\cdot v'-\delta\tilde{m}_2)}\epsilon_{\rho\delta\gamma\nu}p^\delta_\pi v'^\gamma\\
&\quad\times\left[i\epsilon_{\mu\sigma\alpha\beta}v^\alpha v'^\beta(\nu-1)+g_{\mu\sigma}(\nu^2-1)-v_\alpha\left(v'_\mu(2+\nu)-3v_\mu\right)\right]\Big\}\\
&+\tfrac{\alpha_3}{F_0}\xi^{(1)}(\nu)\Big\{(v+v')_\mu\tfrac{p_\nu}{2(p\cdot v'-\delta\tilde{m}_3)}\\
&+p^\rho\tfrac{\Theta_{\rho\sigma}(v)}{-2(-p\cdot v-\delta\tilde{m}_3)}\left[g_{\nu\sigma}(v+v')_\mu-g_{\mu\sigma}v_\nu-g_{\mu\nu}v'_\sigma+i\epsilon_{\mu\alpha\sigma\nu}(v+v')^\alpha\right]\\
&+\tfrac{\Theta_{\rho\delta}(v')}{2(p\cdot v'-\delta\tilde{m}_3)}\left[-i\epsilon_{\mu\rho\alpha\beta}v'^\alpha v^\beta+g_{\mu\rho}(1+\nu)-v_\rho v'_\mu\right]i\epsilon_{\omega\nu\gamma\delta}p^\gamma v'^\omega\Big\}
\end{aligned} \tag{800}$$

The tensor $\Omega_{\mu\nu}$ can be expressed as

$$\begin{aligned}
\Omega_{\mu\nu} \;=\;& \tfrac{i}{2}\epsilon_{\mu\nu\rho\sigma}\left[h_1 m_B m_D v^\rho v'^\sigma + h_2 m_B v^\rho p^\sigma_\pi + h_3 m_D v'^\rho p^\sigma_\pi\right]\\
&+f_1 m_B v_\mu p_{\pi\nu}+f_2 m_D v'_\mu p_{\pi\nu}+f_3 p_{\pi\mu}p_{\pi\nu}+f_4 m_B^2 v_\mu v_\nu\\
&+f_5 m_B m_D v'_\mu v_\nu + f_6 m_B p_{\pi\mu}v_\nu\\
&+k g_{\mu\nu}\\
&+\tfrac{i}{2}\epsilon_{\mu\delta\rho\sigma}v^\delta v'^\rho p^\sigma_\pi(g_1 p_{\pi\nu}+g_2 m_B v_\nu)\\
&+\tfrac{i}{2}\epsilon_{\nu\delta\rho\sigma}v^\delta v'^\rho p^\sigma_\pi(g_3 m_B v_\mu + g_4 m_D v'_\mu + g_5 p_{\pi\mu})
\end{aligned} \tag{801}$$

The non-resonant contribution to the form factors are

$$
\begin{aligned}
h_{1NR} &= -\tfrac{g\xi(\nu)}{F_0 m_B m_D}\tfrac{p_\pi\cdot v}{p_\pi\cdot v+\delta m_B - i\varepsilon}\\
h_{2NR} &= -\tfrac{g\xi(\nu)}{F_0 m_B}\tfrac{1}{p_\pi\cdot v+\delta m_B - i\varepsilon}\\
h_{3NR} &= -\tfrac{g\xi(\nu)}{F_0 m_D}\left(\tfrac{1}{p_\pi\cdot v+\delta m_B - i\varepsilon} - \tfrac{1+\nu}{p_\pi\cdot v'+i\varepsilon}\right)\\
f_{1NR} &= -\tfrac{g\xi(\nu)}{2F_0 m_B}\left(\tfrac{1}{p_\pi\cdot v+\delta m_B - i\varepsilon} - \tfrac{1}{p_\pi\cdot v'+\delta m_D+i\varepsilon}\right)\\
f_{2NR} &= \tfrac{m_B}{m_D} f_{1NR}\\
f_{3NR} &= 0\\
f_{4NR} &= 0\\
f_{5NR} &= -\tfrac{g\xi(\nu)}{2F_0 m_B m_D}\left(1+\tfrac{p_\pi\cdot v}{p_\pi\cdot v+\delta m_B - i\varepsilon}\right)\\
f_{6NR} &= -\tfrac{g\xi(\nu)}{2F_0 m_B}\left(\tfrac{1}{p_\pi\cdot v+\delta m_B - i\varepsilon} - \tfrac{1}{p_\pi\cdot v'+i\varepsilon}\right)\\
k_{NR} &= \tfrac{g\xi(\nu)}{2F_0}\left(\tfrac{p_\pi\cdot v' - \nu p_\pi\cdot v}{p_\pi\cdot v+\delta m_B - i\varepsilon} + \tfrac{p_\pi\cdot v - \nu p_\pi\cdot v'}{p_\pi\cdot v'+i\varepsilon}\right)\\
g_{1NR} &= 0\\
g_{2NR} &= 0\\
g_{3NR} &= 0\\
g_{4NR} &= \tfrac{g\xi(\nu)}{F_0 m_D}\tfrac{1}{p_\pi\cdot v'+i\varepsilon}\\
g_{5NR} &= 0
\end{aligned}
\tag{802}
$$

The resonant contribution to the form factors are

$$
\begin{aligned}
h_{1R} &= \frac{\alpha_1\rho_1(\nu)}{F_0 m_B m_D}\left(\frac{p_\pi\cdot v}{-p_\pi\cdot v-\delta\tilde{m}_1} - \frac{p_\pi\cdot v'}{p_\pi\cdot v'-\delta\tilde{m}_1}\right) \\
&\quad + \frac{\alpha_2\rho_2(\nu)}{3F_0 m_B m_D}\left(\frac{p_\pi\cdot v(1+2\nu)-p_\pi\cdot v'}{p_\pi\cdot v+\delta\tilde{m}_2} + \frac{3}{2}\frac{\nu p_\pi\cdot v'-p_\pi\cdot v}{p_\pi\cdot v'-\delta\tilde{m}_2}\right) \\
&\quad - \frac{\alpha_3\xi^{(1)}(\nu)}{F_0 m_B m_D}\frac{p_\pi\cdot v}{p_\pi\cdot v+\delta\tilde{m}_3} \\
h_{2R} &= \frac{\alpha_2(1+\nu)\rho_2(\nu)}{3F_0 m_B}\frac{1}{-p_\pi\cdot v-\delta\tilde{m}_2} - \frac{\alpha_3\xi^{(1)}(\nu)}{F_0 m_B}\frac{1}{p_\pi\cdot v+\delta\tilde{m}_3} \\
h_{3R} &= \frac{\alpha_2\rho_2(\nu)}{3F_0 m_D}\left(\frac{1+\nu}{p_\pi\cdot v+\delta\tilde{m}_2} - \frac{\nu^2-1}{2(p_\pi\cdot v'-\delta\tilde{m}_2)}\right) - \frac{\alpha_3\xi^{(1)}(\nu)}{F_0 m_D}\left(\frac{1}{p_\pi\cdot v+\delta\tilde{m}_3} - \frac{1+\nu}{p_\pi\cdot v'-\delta\tilde{m}_3}\right) \\
f_{1R} &= -\frac{\alpha_2\rho_2(\nu)(\nu-1)}{6F_0 m_B}\left(\frac{1}{p_\pi\cdot v+\delta\tilde{m}_2} - \frac{1}{p_\pi\cdot v'-\delta\tilde{m}_2}\right) - \frac{\alpha_3\xi^{(1)}(\nu)}{2F_0 m_B}\left(\frac{1}{p_\pi\cdot v+\delta\tilde{m}_3} - \frac{1}{p_\pi\cdot v'-\delta\tilde{m}_3}\right) \\
f_{2R} &= \frac{m_B}{m_D} f_{1R} \\
f_{3R} &= 0 \\
f_{4R} &= 0 \\
f_{5R} &= -\frac{\alpha_1\rho_1(\nu)}{2F_0 m_B m_D}\left(\frac{p_\pi\cdot v}{p_\pi\cdot v+\delta\tilde{m}_1} + \frac{p_\pi\cdot v'}{p_\pi\cdot v'-\delta\tilde{m}_1}\right) \\
&\quad + \frac{\alpha_2\rho_2(\nu)}{2F_0 m_B m_D}\left(\frac{p_\pi\cdot v'-\frac{1}{3}p_\pi\cdot v(1+2\nu)}{p_\pi\cdot v+\delta\tilde{m}_2} + \frac{p_\pi\cdot v-\frac{1}{3}p_\pi\cdot v'(1+2\nu)}{p_\pi\cdot v'-\delta\tilde{m}_2}\right) \\
&\quad + \frac{\alpha_3\xi^{(1)}(\nu)}{F_0 m_B m_D}\left(\frac{p_\pi\cdot v}{p_\pi\cdot v+\delta\tilde{m}_3} + \frac{p_\pi\cdot v'}{p_\pi\cdot v'-\delta\tilde{m}_3}\right) \\
f_{6R} &= \frac{\alpha_2\rho_2(\nu)(\nu-1)}{6F_0 m_B}\left(\frac{1}{p_\pi\cdot v+\delta\tilde{m}_2} - \frac{1}{p_\pi\cdot v'-\delta\tilde{m}_2}\right) + \frac{\alpha_3\xi^{(1)}(\nu)}{2F_0 m_B}\left(\frac{1}{p_\pi\cdot v+\delta\tilde{m}_3} - \frac{1}{p_\pi\cdot v'-\delta\tilde{m}_3}\right) \\
k_R &= -\frac{\alpha_1\rho_1(\nu)(\nu-1)}{2F_0}\left(\frac{p_\pi\cdot v}{p_\pi\cdot v+\delta\tilde{m}_1} + \frac{p_\pi\cdot v'}{p_\pi\cdot v'-\delta\tilde{m}_1}\right) \\
&\quad - \frac{\alpha_2\rho_2(\nu)(\nu-1)}{3F_0}\left(\frac{p_\pi\cdot v'-\nu p_\pi\cdot v}{p_\pi\cdot v+\delta\tilde{m}_2} + \frac{p_\pi\cdot v-\nu p_\pi\cdot v'}{p_\pi\cdot v'-\delta\tilde{m}_2}\right) \\
&\quad + \frac{\alpha_3\xi^{(1)}(\nu)}{2F_0}\left(\frac{p_\pi\cdot v'-\nu p_\pi\cdot v}{p_\pi\cdot v+\delta\tilde{m}_3} + \frac{p_\pi\cdot v-\nu p_\pi\cdot v'}{p_\pi\cdot v'-\delta\tilde{m}_3}\right) \\
g_{1R} &= 0 \\
g_{2R} &= -\frac{\alpha_2\rho_2(\nu)}{2F_0 m_B}\frac{1}{p_\pi\cdot v'-\delta\tilde{m}_2} \\
g_{3R} &= -g_{2R} \\
g_{4R} &= \frac{\alpha_2\rho_2(\nu)}{3F_0 m_D}\left(\frac{2}{p_\pi\cdot v+\delta\tilde{m}_2} - \frac{1+\frac{1}{2}\nu}{p_\pi\cdot v'-\delta\tilde{m}_2}\right) + \frac{\alpha_3\xi^{(1)}(\nu)}{F_0}\frac{1}{p_\pi\cdot v'-\delta\tilde{m}_3} \\
g_{5R} &= 0
\end{aligned}
\tag{803}
$$

In SP5/SP6 contributions from D^{**} was removed

$$
\begin{aligned}
h_{1R} &= \frac{\alpha_1\rho_1(\nu)}{F_0 m_B m_D}\left(\frac{p_\pi\cdot v}{-p_\pi\cdot v-\delta\tilde{m}_1}\right)+\frac{\alpha_2\rho_2(\nu)}{3F_0 m_B m_D}\left(\frac{p_\pi\cdot v(1+2\nu)-p_\pi\cdot v'}{p_\pi\cdot v+\delta\tilde{m}_2}\right)\\
&\quad -\frac{\alpha_3\xi^{(1)}(\nu)}{F_0 m_B m_D}\frac{p_\pi\cdot v}{p_\pi\cdot v+\delta\tilde{m}_3}\\
h_{2R} &= \frac{\alpha_2(1+\nu)\rho_2(\nu)}{3F_0 m_B}\frac{1}{-p_\pi\cdot v-\delta\tilde{m}_2}-\frac{\alpha_3\xi^{(1)}(\nu)}{F_0 m_B}\frac{1}{p_\pi\cdot v+\delta\tilde{m}_3}\\
h_{3R} &= \frac{\alpha_2\rho_2(\nu)}{3F_0 m_D}\left(\frac{1+\nu}{p_\pi\cdot v+\delta\tilde{m}_2}\right)-\frac{\alpha_3\xi^{(1)}(\nu)}{F_0 m_D}\left(\frac{1}{p_\pi\cdot v+\delta\tilde{m}_3}\right)\\
f_{1R} &= -\frac{\alpha_2\rho_2(\nu)(\nu-1)}{6F_0 m_B}\left(\frac{1}{p_\pi\cdot v+\delta\tilde{m}_2}\right)-\frac{\alpha_3\xi^{(1)}(\nu)}{2F_0 m_B}\left(\frac{1}{p_\pi\cdot v+\delta\tilde{m}_3}\right)\\
f_{2R} &= \frac{m_B}{m_D}f_{1R}\\
f_{3R} &= 0\\
f_{4R} &= 0\\
f_{5R} &= -\frac{\alpha_1\rho_1(\nu)}{2F_0 m_B m_D}\left(\frac{p_\pi\cdot v}{p_\pi\cdot v+\delta\tilde{m}_1}\right)+\frac{\alpha_2\rho_2(\nu)}{2F_0 m_B m_D}\left(\frac{p_\pi\cdot v'-\frac{1}{3}p_\pi\cdot v(1+2\nu)}{p_\pi\cdot v+\delta\tilde{m}_2}\right)\\
&\quad +\frac{\alpha_3\xi^{(1)}(\nu)}{F_0 m_B m_D}\left(\frac{p_\pi\cdot v}{p_\pi\cdot v+\delta\tilde{m}_3}\right)\\
f_{6R} &= \frac{\alpha_2\rho_2(\nu)(\nu-1)}{6F_0 m_B}\left(\frac{1}{p_\pi\cdot v+\delta\tilde{m}_2}\right)+\frac{\alpha_3\xi^{(1)}(\nu)}{2F_0 m_B}\left(\frac{1}{p_\pi\cdot v+\delta\tilde{m}_3}\right)\\
k_R &= -\frac{\alpha_1\rho_1(\nu)(\nu-1)}{2F_0}\left(\frac{p_\pi\cdot v}{p_\pi\cdot v+\delta\tilde{m}_1}\right)-\frac{\alpha_2\rho_2(\nu)(\nu-1)}{3F_0}\left(\frac{p_\pi\cdot v'-\nu p_\pi\cdot v}{p_\pi\cdot v+\delta\tilde{m}_2}\right)\\
&\quad +\frac{\alpha_3\xi^{(1)}(\nu)}{2F_0}\left(\frac{p_\pi\cdot v'-\nu p_\pi\cdot v}{p_\pi\cdot v+\delta\tilde{m}_3}\right)\\
g_{1R} &= 0\\
g_{2R} &= 0\\
g_{3R} &= -g_{2R}\\
g_{4R} &= \frac{\alpha_2\rho_2(\nu)}{3F_0 m_D}\left(\frac{2}{p_\pi\cdot v+\delta\tilde{m}_2}\right)\\
g_{5R} &= 0
\end{aligned}
\tag{804}
$$

Numerical values used in SP5/SP6 are

$$
\begin{aligned}
&g = 0.5 \\
&\alpha_1 = -1.430 \\
&\alpha_2 = -0.140 \\
&\alpha_3 = 0.690 \\
&F_0 = 0.093 \\
&\delta m_B = 0.0460 - \tfrac{0.00001}{2} i \\
&\delta m_D = 0.1421 - \tfrac{0.00006}{2} i \\
&\delta \tilde{m}_1 = 0.392 - \tfrac{1.040}{2} i \\
&\delta \tilde{m}_2 = 0.709 - \tfrac{0.405}{2} i \\
&\delta \tilde{m}_3 = 0.563 - \tfrac{0.191}{2} i \\
&\beta = 0.285 \\
&\beta' = 0.280 \quad \text{for} \quad \rho_1(\nu) \\
&\beta' = 0.260 \quad \text{for} \quad \rho_2(\nu) \\
&\bar{\Lambda} = 0.750
\end{aligned}
\tag{805}
$$

References

[1] N. Cabbibo, *"Unitary Symmetry and Leptonic Decays"*, Phys. Rev. Lett. **10**, 531 (1963).

[2] M. Kobayashi and T. Maskawa, *"CP-Violation in the Renormalizable Theory of Weak Interaction"*, Prog. Theor. Phys. **49**, 652 (1973).

[3] BABAR Collaboration, *"Measurement of the Relative Branching Fractions of $\bar{B} \to D/D^*/D^{**}\ell^-\bar{\nu}_\ell$ Decays in Events with a Fully Reconstructed B Meson"*, Phys. Rev. D, (2007), hep-ex/0703027.

[4] BABAR Collaboration, *"Measurement of the Branching Fractions of Exclusive $\bar{B} \to D/D^*/D^*\pi\ell^-\bar{\nu}_\ell$ Decays in Events tagged by a Fully Reconstructed B Meson"*, arXiv:0708.1738v1 [hep-ex], BAD1821.

[5] BABAR Collaboration, *"A Measurement of the Branching Fractions of Exclusive $\bar{B} \to D/D^*/D^{(*)}\pi\ell^-\bar{\nu}_\ell$ Decays in Events with a Fully Reconstructed B Meson"*, arXiv: [hep-ex], BAD1889.

[6] BELLE Collaboration, K. Abe *et al.*, *"Determination of $|V_{cb}|$ using the semileptonic decay $\bar{B}^0 \to D^{*+}e^-\bar{\nu}$"*, Phys. Lett. B**526**, 247 (2002), hep-ex/0111060.

[7] DELPHI Collaboration, P. Abreu *et al.*, *"Measurement of V_{cb} from the decay process $\bar{B}^0 \to D^{*+}\ell^-\bar{\nu}$"*, Phys. Lett. B**510**, 55 (2001), hep-ex/0104026.

[8] BABAR Collaboration, B. Aubert *et al.*, *"Measurement of the $\bar{B}^0 \to D^{*+}l^-\bar{\nu}_l$ Decay Rate and $|V_{cb}|$"*, Phys. Rev. D**71**, 051502 (2005), hep-ex/0408027.

[9] OPAL Collaboration, G. Abbiendi *et al.*, *"Measurement of $|V_{cb}|$ using $B^0 \to D^*l\nu$ decays"*, Phys. Lett. B**482**, 15 (2000), hep-ex/0003013.

[10] ALEPH Collaboration, D. Buskulic *et al.*, *"Measurements of $|V_{cb}|$, form-factors and branching fractions in the decays $\bar{B}^0 \to D^{*+}l^-\bar{\nu}_l$ and $\bar{B}^0 \to D^+l^-\bar{\nu}_l$"*, Phys. Lett. B**395**, 373 (1997).

[11] DELPHI Collaboration, J. Abdallah *et al.*, *"Measurement of $|V_cb|$ using the semileptonic decay $\bar{B}^0_d \to D^{*+}l^-\bar{\nu}_l$"*, European. Phys. J. C**33**, 213 (2004), hep-ex/0401023.

[12] CLEO Collaboration, N. E. Adam *et al.*, *"Determination of the $\bar{B} \to D^*l\bar{\nu}$ Decay Width and $|V_{cb}|$"*, Phys. Rev. D**67**, 032001 (2003), hep-ex/0210040.

[13] Particle Data Group, W. M. Yao *et al.*, *"Review of Particle Physics"*, J. Phys. G**33**, 1 (2006); URL: http://pdg.lbl.gov (2007).

[14] BELLE Collaboration, K. Abe *et al.*, *"Measurement of $\mathcal{B}(\bar{B} \to D^+l^-\bar{\nu})$ and Determination of $|V_{cb}|$"*, Phys. Lett. B**526**, 258 (2002), hep-ex/0111082.

[15] CLEO Collaboration, J. Bartelt *et al.*, *"Measurement of the $B \to D\ell\nu$ Branching Fractions and Form Factor"*, Phys. Rev. Lett.**82**, 3746 (2003), hep-ex/9811042.

[16] BABAR Collaboration, B. Aubert *et al.*, *"Measurement of Semileptonic B Decays into Orbitally-Excited Charmed Mesons with BaBar Detector at SLAC"*, BAD1565 (2006).

[17] DELPHI Collaboration, J. Abdallah *et al.*, *"Determination of heavy quark non-perturbative parameters from spectral moments in semileptonic B decays"*, European. Phys. J. C**45**, 35 (2006), hep-ex/0510024.

[18] BELLE Collaboration, Liventsev, D. *et al.*, *"Measurement of the branching fractions for $B^- \to D^{(*)+}\pi^- l^- \bar{\nu}$ and $\bar{B}^0 \to D^{(*)0}\pi^+ l^- \bar{\nu}$"*, Phys. Rev. D**72**, 051109 (2005), hep-ex/0507060.

[19] BABAR Collaboration, Semileptonic Analysis Working Group, http://www.slac.stanford.edu/BFROOT/www/Physics/Analysis/AWG/Semileptonic/Reweighting2007.html.

[20] BABAR Collaboration, B. Aubert *et al.*, *"The BABAR Detector"*, Nucl. Instrum. Meth. **A479**, 1 (2002), hep-ex/0105044.

[21] *"PEP-II Conceptual Design Report"*, SLAC-0418 (2002).

[22] D. J. Lange, *"The EvtGen particle decay simulation package"*, Nucl. Instrum. Meth. **A462**, 152 (2001).

[23] Geant 4 Collaboration, S. Agostinelli *et al.*, *"GEANT4: A Simulation toolkit"*, Nucl. Instrum. Meth. **A506**, 250 (2003).

[24] W. D. Hulsbergen, *"Decay Chain Fitting with a Kalman Filter"*, Nucl. Instrum. Meth. **A552**, 566 (2005).

[25] BABAR Collaboration, B. Aubert *et al.*, *"Observation of the Semileptonic Decays $B \to D^*\tau\bar{\nu}_\tau$ and Evidence for $B \to D\tau\bar{\nu}_\tau$"*, Phys. Rev. D **76**, 051104 (2007), arXiv:0709.1698v1 [hep-ex].

[26] BELLE Collaboration, A. Matyia *et al.*, *"Observation of $B^0 \to D^{*-}\tau^+\nu_\tau$ decay at Belle"*, arXiv:0706.4429 [hep-ex].

[27] Babar Collaboration, B. Barate*et al.*, *"Study of inclusive charm production in B meson decays with the BaBar experiment"*, Babar Analysis Document 1234, (2006).

[28] Babar Collaboration, B. Barate*et al.*, *"Study of Inclusive B^- and $\bar{B}^0$ Decays to Flavor-Tagged D, D_s and Λ_c^+"*, Phys. Rev. D **75**, 072002 (2007), hep-ex/0606026.

[29] BELLE Collaboration, K. Abe *et al.*, *"Observation of the $D_1(2420) \to D\pi^+\pi^-$ decays"*, Phys. Rev. Lett. **94**, 221805 (2005), hep-ex/0410091.

[30] Babar Collaboration, B. Aubert *et al.*, *"Measurement of the Absolute Branching Fraction of $D^0 \to K^-\pi^+$ Decays"*, Presented at Joint Meeting of Pacific Region Particle Physics Communities (DPF and JPS 2006), Honolulu, Hawaii, 29 Oct - 3 Nov 2006, arXiv:0704.2080v1 [hep-ex].

[31] CLEO Collaboration, S. Dobbs *et al.*, *"Measurement of Absolute Hadronic Branching Fractions of D Mesons and $e^+e^- \to D\bar{D}$ Cross Sections at the* $\psi(3770)$ ", Phys. Rev. D , (2007), arXiv:0709.3783v2[hep-ex].

[32] D. Scora and N. Isgur., Phys. Rev. D**52**, 2783 (1995), *"Semileptonic Meson Decays in the Quark Model: An Update"*, hep-ph/9503486.

[33] N. Isgur, D. Scora, B. Grinstein and M. B. Wise., *"Semileptonic Meson Decays in the Quark Model"*, Phys. Rev. D**39**, 2783 (1989).

[34] M. Neubert, *"Heavy Quark Symmetry"*, Phys. Rept. **245**, 259 (1994), hep-ph/9306320.

[35] J. D. Richman and P. R. Burchat., *"Leptonic and Semileptonic Decays of Charm and Bottom Hadrons"*, Rev. Mod. Phys. **67**, 893 (1995), hep-ph/9508250.

[36] M. Okamoto *et al.*, *"Semileptonic $D \to \pi/K$ and $B \to \pi/D$ decays in 2+1 flavor lattice QCD"*, Nucl. Phys. Proc. Suppl. **140**, 461 (2005), hep-lat/0409116.

[37] I. Caprini, L. Lellouch and M.Neubert., *"Dispersive Bounds on the Shape of $B \to D^{(*)}l\nu$ Form Factors"*, Nucl. Phys. B**530**, 153 (1998), hep-ph/9712417.

[38] BABAR Collaboration, B. Aubert *et al.*, *"Measurements of the B to D^* Form Factors Using the Decay $B^0 \to D^*e\nu_e$"*, Phys. Rev. D**74**, 092004 (2006), hep-ex/0602023; BAD 482.

[39] BABAR Collaboration, B. Aubert *et al.*, *"Determination of the Form Factors for the Decay $B^0 \to D^{*-}\ell^+\nu_\ell$ and of the CKM Matrix Element $|V_{cb}|$"*, 33^{rd} International Conference on High-Energy Physics, ICHEP 06, 2006, hep-ex/0607076.

[40] BABAR Collaboration, B. Aubert *et al.*, *"Measurements of the Decay $B^- \to D^{*0}e^-\bar{\nu}_e$"*, arXiv:0707.2655v1 [hep-ex]; BAD 1809.

[41] A. K. Leibovich, Z. Ligeti, I. W. Stewart, M. B. Wise., *"Model independent results for $B \to D_1(2420)\ell\bar{\nu}$ and $B \to D_2^*(2460)\ell\bar{\nu}$ at order $\Lambda_{QCD}/m_{c,b}$"*, Phys. Rev. Lett.**78**, 3995 (1997), hep-ph/9703213.

[42] A. K. Leibovich, Z. Ligeti, I. W. Stewart, M. B. Wise., *"Semileptonic B decays to excited charmed mesons"*, Phys. Rev. D**57**, 308 (1998), hep-ph/9705467.

[43] J. L. Goity, *"Chiral perturbation theory for SU(3) breaking in heavy meson systems"*, Phys. Rev. D**46**, 3929 (1992), hep-ph/9206230.

[44] J. L. Goity and W. Roberts., *"Soft Pion Emission in Semileptonic B-Meson Decays"*, Phys. Rev. D**51**, 3459 (1995), hep-ph/9406236.

[45] Babar Collaboration, B. Aubert *et al.*, *"Measurement of the Electron Energy Spectrum and its Moments in Inclusive $B \rightarrow Xe\nu$ Decays"*, Phys. Rev. D**69**, 111104 (2004), hep-ex/0403030.

[46] CLEO Collaboration, B. Bartelt *et al.*, *"Observation of the radiative decay $D^{*+} \rightarrow D^{+}\gamma$"*, Phys. Rev. Lett. **80**, 3919 (1998), hep-ex/9711011.

[47] Babar Analysis Document 664.

[48] Babar Analysis Document 1465.

[49] *"$B \rightarrow D_s K \ell \nu$"*.

[50] BABAR Collaboration, P. F. Harrison, ed. *et al.*, *"The BABAR Physics Book"*, (1997), SLAC-R-504.